SOME EFFECTS OF ESCARPMENTS ON THE ATMOSPHERIC BOUNDARY-LAYER

A thesis presented for the Degree of Doctor of Philosophy in Mechanical Engineering in the University of Canterbury

by

A.J. Bowen, M.E., C.Eng., M.I.Mech.E., M.N.Z.I.E.

Department of Mechanical Engineering,
University of Canterbury,
Christchurch,
New Zealand.

June, 1979

ABSTRACT

The project described in this thesis was undertaken in order to contribute to the understanding of the wind flow behaviour over complex terrain by making field and model measurements of the flow over two-dimensional, forward facing escarpments.

In achieving these objectives, two field studies over a low 2:1 and cliff escarpment are reported which used orthogonal arrays of fast response propeller anemometers to record the wind flow data. The development and performance of these anemometers together with the digital data acquisition system are discussed in detail and are shown to cope adequately with the longitudinal turbulence data. Both escarpments were situated in open rural terrain at oblique incidence angles to the recorded strong winds. Mean wind speeds and direction, turbulence intensities, Reynolds stresses, gust factors and some longitudinal power spectra are reported for positions at $^{1}/_{2}$ and 4 escarpment heights behind the crest, up to a height of nearly two escarpment heights. The data are compared with the conditions measured upstream in the undisturbed boundary-layer which are shown to be affected by the slightly non-neutral atmospheric conditions prevailing at the time.

Wind tunnel tests using accurate models of the two full scale situations and wind directions are also reported. In addition, two model test series using plain 2D escarpments are described which illustrate the effects of upwind hill slope and wind incidence on the flow over rough and smooth escarpments.

A comparison of the accumulated results from the model and field tests with the literature is made. The mean flow and turbulence close to the ground were dominated by the turbulent wakes generated by the sharp crests. Significant increases in mean wind speed were evident below 3 escarpment heights above local ground level. However little change in the turbulence characteristics was noticed outside the wake regions. No significant trends in gust factor were evident due to the presence of the escarpment. The variation of the recorded gust factor was fully explained in terms of instrument response, gust averaging time, record length and turbulence intensity using established methods.

ACKNOWLEDGEMENTS

I wish to record my grateful appreciation for the help and encouragement provided by a number of persons who have contributed to the successful completion of this project.

Firstly to Dr. D. Lindley who supervised the project until he left the University in 1978 and who provided a good deal of enthusiasm and discussion during the early stages. Secondly to Professor D.C. Stevenson as Head of Department of Mechanical Engineering for his continual interest and guidance throughout the project and as supervisor over the later stages.

The willing co-operation and skill of Mrs. J. Percival in typing this thesis to such a high standard is gratefully appreciated. Thanks are also due to Miss J. Shelton for her care and skill in draughting the large number of diagrams with the assistance of Mr. T. Bird and for her photographic work.

Many other members of the Department of Mechanical Engineering also provided assistance in the construction, servicing and operation of the field test equipment. In particular, thanks are due to Mr. L.N. Cheeseman, Mr. H.J. Anink and the workshop staff directed by Mr. E.D. Retallick.

The co-operation of the farm owners, Mr. R. James of Amberley and Mr. R.C. Hart of Rakaia in allowing the field equipment to be erected on their properties for some considerable time is gratefully acknowledged.

The financial support of the University Grants Committee and the New Zealand Electricity is also gratefully acknowledged.

Finally, the project could not have been successfully completed without the continual encouragement and support from my wife Betty. Together with our family, she showed enduring patience and understanding during the many long evenings and weekends spent in my absence.

LIST OF CONTENTS

CHAPTER PAGE

CHAPTER PAGE

CHAPTER PAGE

LIST OF FIGURES

FIGURE PAGE

LIST OF TABLES

LIST OF SYMBOLS

A	Pasquill atmospheric stability class - very unstable.
	Function of turbulence intensity used in gust analysis.
	Effective area of anemometer propeller blade.
	Ratio of standard deviation of the longitudinal velocity component to friction velocity, σ_u/V_*.
A_Z	Amplification factor, $\bar{V}_Z/_{REF}\bar{V}_Z$.
A_2	Constant in hill flow-prediction equation 3.17.
a	Scale factor in distribution of extreme values.
	Nondimensional height at reference upwind position, Z_{REF}/H.
B	Pasquill atmospheric stability class - unstable.
	Ratio of standard deviation of the lateral velocity component to friction velocity, σ_v/V_*
b	Number of anemometer propeller blades.
C	Pasquill atmospheric stability class - slightly unstable.
	Ratio of standard deviation of the vertical velocity component to friction velocity, σ_w/V_*.
C_D	Drag coefficient of the anemometer propeller blade elements.
C_L	Lift coefficient of the anemometer propeller blade elements.
C_P	Specific heat of air at constant pressure.
C_V	Specific heat of air at constant volume.
$C_{uu}(\tau)$	Auto-covariance function, $\overline{u(t).u(t+\tau)}$.
c	Weibull probability distribution constant.
D	Pasquill atmospheric stability class - neutral.
ΔD	Aerodynamic drag force on element of anemometer propeller blade.
d	Zero plane displacement above ground due to surrounding obstacles.
E	Pasquill atmospheric stability class - slightly stable.
e	Natural logarithmic base, 2.7183.

F Pasquill atmospheric stability class - strongly stable.

f Frequency, radians/second.

$f(\theta)$ Function describing the change in anemometer output with wind incidence angle, θ to the shaft.

g Gravitational constant.

H Height of escarpment or hill above surrounding terrain.

h Horizontal scaling factor for finite element grid size.
Height of building.

I Moment of inertia of rotating parts of propeller anemometer.

i,j Integers.

K_h Eddy conductivity coefficient.

K_m Eddy viscosity coefficient.

k Von Karman constant ≈ 0.4.
Vertical scaling factor for finite element grid size.
Weibull probability distribution constant.

L Hill half length. Horizontal upwind distance from hill crest to half height.
Distance constant of anemometer with an axial mean wind velocity.
Monin-Obukhov length scale.

L' $L' = (K_h/K_m)L$.

L_d Horizontal length of downwind hill slope.

L_u Horizontal length of upwind hill slope.

$L(\theta)$ Distance constant of anemometer with a mean wind angle of incidence, θ.

ΔL Aerodynamic lift force on a blade element of an anemometer propeller.

L_{ux}, L_{vx}, L_{wx} Length scales of turbulence in the longitudinal direction relating to the u, v and w components of turbulence respectively.

ℓ Thickness of inner layer.

m Source strength.

m_r $m_r = \int_0^\infty n^r \cdot S(n)\,dn$

N Number of samples in each data set.

n Frequency, Hz.
Number of blocks processed.

u^n_p, v^n_p, w^n_p Frequency at which the peak energy occurs in the velocity power spectral density function for the u, v and w components respectively.

P Pitch of anemometer propeller blades.

P(> V) Probability of a wind velocity occurring at a value greater than V.

PDF Probability density function.

$P(\tilde{x})$ Hill shape function.

p Constant in equation 10.10.

p(v) Probability density function of longitudinal velocity component.

p(u,v) Bivariate normal distribution of two normal mean velocity components $\bar{u}$, $\bar{v}$.

q Vertical heat flux.
Constant in equation 10.10.

R Ideal calibration constant of anemometer.

R_i Gradient Richardson number.

R_o Outer radius of anemometer propeller.

r Distance of blade element from anemometer axis of rotation.
Integer (Chapter 2).

S Speed-up factor, $\bar{V}_Z / {}_{REF}\bar{V}_{Z+H}$

$S_{uu}(n)$, $S_{vv}(n)$, $S_{ww}(n)$ — Single point velocity power spectral density functions for u, v and w components.

$S(n)$ — Longitudinal velocity power spectral density function (abbreviated symbol).

ΔS — Fractional speed-up factor, $(\bar{V}_Z - {}_{REF}\bar{V}_Z)/{}_{REF}\bar{V}_Z$.

s — Averaging time interval (Chapter 5).
Nondimensional height, Z/H.

T — Data sampling interval or gust averaging time.

T_A — Total aerodynamic torque on the anemometer propeller.

T_C — Dynamic response time-constant of anemometer.

T_E — Eulerian time-scale of turbulence. Area under autocorrelation - τ curve.

T_o — Length of time over which data is averaged or length of data file.

T_s — Friction torque of propeller anemometer.

T_Z — Absolute air temperature at height Z.

ΔT — Aerodynamic torque on blade element of anemometer propeller.

t — Time.

t' — Time origin (Chapter 5).

$U(t)$ — Instantaneous wind velocity in longitudinal direction along the mean wind direction, $\bar{V}_Z + u(t)$.

$u, u(t)$ — Instantaneous longitudinal wind velocity component.

u — Mean horizontal wind velocity component such that the total wind speed $= \sqrt{u^2 + v^2}$ (Chapter 2).

V_a, V_b, V_c — Mean wind velocity components aligned along the three anemometer axes of an orthogonal array.

V_G Mean wind velocity at the gradient height.

V_i Indicated wind velocity from anemometer shaft speed.

$\bar{V}_n$ Cumulative mean wind velocity for n data blocks.

V_{REL} Wind velocity relative to moving blade element of anemometer propeller.

$V_s(\theta)$ Stall velocity. Wind speed at an angle of incidence θ at which anemometer ceases to turn.

$V_t(\theta)$ Threshold velocity. Wind speed at an angle of incidence θ at which anemometer begins to turn.

$\bar{V}_Z$ Mean wind speed at height, Z.

$_{REF}\bar{V}_Z$ $\bar{V}_Z$ at reference position upwind of obstacle.

V_∞ Free stream velocity in wind tunnel.

V_* Friction velocity.

$\hat{V}$ Peak gust velocity.

ΔV Half amplitude of sinusoidal velocity input to analyse first order response of anemometer.

v,v(t) Instantaneous lateral wind velocity component.

v Mean horizontal wind velocity component such that the total wind speed = $\sqrt{u^2 + v^2}$ (Chapter 2).

w,w(t) Instantaneous vertical wind velocity component.

x Distance in the direction of the mean wind velocity.
Distance downwind of a change in roughness.

$\tilde{x}$ Nondimensional horizontal position over a hill.

y Horizontal distance perpendicular to the mean wind velocity.

Z Height above ground.

Z_G Gradient height.

Z_{REF} Reference height above ground.

Z_o Surface roughness length.

z Vertical distance perpendicular to the mean wind velocity.

ΔZ Increase in apparent height of building to allow for increase in exposure due to hill site (Chapter 10).

α Exponent in power-law wind velocity-height profile

Angle between mean wind direction and horizontal plane.

Angle between relative wind velocity, V_{REL} and blade element of anemometer propeller.

Constant used in the definition of hill shape (Chapter 3).

α_c, α_o Exponent in power-law wind velocity-height profile over crest (α_c) and upstream reference site (α_o).

β Empirical constant in stability term of logarithmic wind velocity-height profile.

Angle between mean horizontal wind component and axis of anemometer, a (Fig.5.6).

Constant used in the definition of hill shape (Chapter 3).

Γ Dry adiabatic lapse rate.

γ Absolute air temperature gradient with height.

δ Depth of boundary-layer in wind tunnel.

ξ Vorticity.

η $\eta = (V - \bar{V})/\sigma_v$.

$\hat{\eta}$ $\hat{\eta} = (\hat{V} - \bar{V})/\sigma_v$.

θ Angle between average upwind hill slope and horizontal.

Wind direction (Chapter 2)

Potential temperature.

Wind incidence angle to anemometer axis.

Height of interfacial layer after change in surface roughness.

θ_1 Lower level of boundary-layer generated upstream of transition.

θ_2 Upper level of boundary-layer generated downstream of transition.

θ_a, θ_b, θ_c Wind incidence angles between mean wind and three orthogonal anemometers.

λ Gust wavelength.

ν Kinematic viscosity.

Parameter indicating the average frequency of extreme gusts.

ρ Air density.

$\rho_{uu}(\tau)$ Autocorrelation function of the longitudinal wind velocity component.

σ_u, σ_v, σ_w Standard deviation of fluctuating wind velocity components, u, v and w.

τ Incremental time lag.

τ_o Surface shear stress at reference position over flat terrain.

τ_s Surface shear stress over hill.

τ_Z Shear stress ($-\rho\overline{uw}$) at height Z.

ϕ Wind incidence angle with normal to hill crest.

Pitch angle between anemometer axis and blade element of propeller.

Phase angle in anemometer first order response.

ϕ_M Dimensionless wind shear.

$\chi(n)$ Aerodynamic admittance factor.

ψ Stream function.

$\psi(Z/L)$ Universal function representing atmospheric stability in logarithmic wind velocity-height profile.

$\psi(T,T_o)$ Spectral filter function due to finite T,T_o.

ω Angular velocity of shaft.

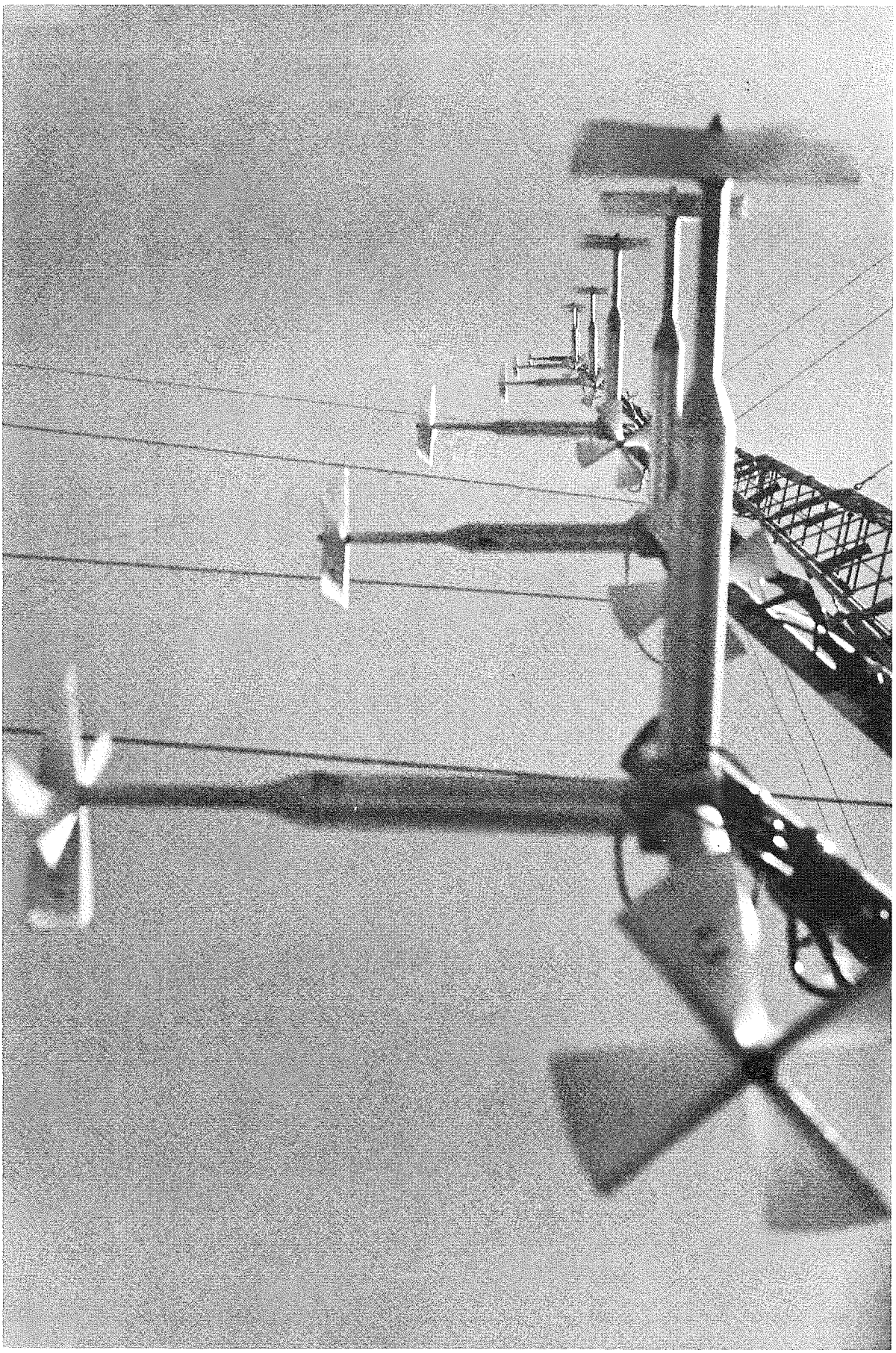

VIEW FROM BELOW OF PROPELLER ANEMOMETERS MOUNTED ON THE 20 m HIGH LATTICE MAST

CHAPTER 1

INTRODUCTION

1.1 WIND FLOW OVER COMPLEX TERRAIN

An understanding of the modification to the earth's boundary-layer caused by abrupt changes in local topography is essential if the local wind conditions at a site in hilly terrain are to be predicted. Wind speeds and turbulence data are well established for the neutral boundary-layer over homogeneous terrain such as that presented in ESDU (1972, 1974), but very little quantitative information exists on the effect of hills on the local wind characteristics. Existing meteorological data is mostly confined to airports and populated areas that are situated on flat even terrain and at present, any predictions of the wind flow over nearby hills are hazardous without extensive on-site measurements or model tests.

A major application of the understanding of topographical effects is in the estimation of wind loads on buildings and structures that are situated on exposed hill sites. In addition to the design of buildings in hilly urban areas, there are many other structures such as communication aerials, cable ways and electricity transmission lines and towers, which are often sited on exposed ridges and whose structural reliability is of the utmost importance. Some building codes such as the British Standard CP3 (1972) and the New Zealand Standard 4203 (1976), cover sites on uniform flat terrain and offer a simple wind speed exposure factor between 0.9 and 1.3 for hilly sites to allow for the increased exposure that is often experienced in these conditions. In addition, special consideration has been given to sites near the crest of an escarpment by increasing the effective height of the building for the purpose of choosing a more appropriate design wind speed. A building close to the crest of a steeply sloping escarpment would thus have an effective height equal to the building height plus a fraction of the escarpment height, resulting in the choice of a higher design wind speed. Recent theoretical studies, model and field tests by Jackson and Hunt (1975), Freeston (1974), Bowen and Lindley (1974, 1977) and others, have confirmed the inadequacy of these factors to cope with the modification to the mean wind speed by escarpments and showed that both the velocity increase and the extent of their influence downstream could be significantly greater than the ranges quoted in the above Codes.

In addition, there is very little guidance given in the literature on the prediction of the turbulence characteristics that might prevail over a particular hill and which would enable maximum gust speeds and dynamic loading effects to be accurately predicted for exposed sites.

A further application of topographical wind effects is in the optimum siting of wind turbines for the generation of power, where an increase in wind speed on a hill-top site compared with that on flat terrain could be used to advantage by enhancing the power output of a particular machine. A 50% increase in wind velocity results in over a 300% increase in available wind energy. Knowledge of the effects of hills on the wind flow would enable potential wind turbine sites to be located and instrumented for more detailed wind surveys. In addition, a better prediction of the maximum loads on the turbine tower and blades under a variety of wind conditions would also be possible.

Other important applications exist in the planning and management of farming and forestry developments where wind exposure can have an important influence on the economics of the project by affecting the welfare and rate of growth of the livestock, vegetation or trees. The planning and routing of roads and railways should also take into account the hazards associated with exposure to high winds. The generation of turbulence by hills and their effect on low flying aircraft near airports or during topdressing operations is also an important consideration. Finally, a major application of topographical wind effects is in the field of atmospheric diffusion and pollutant dispersal. There are an increasing number of chimneys situated near or amongst hilly terrain and the correct prediction of the plume behaviour under such conditions is of prime importance to the owner and the local authorities.

1.2 PROJECT BACKGROUND

New Zealand is situated in an isolated and wind swept part of the South Pacific between latitudes 34° and 47°S. The rugged mountain chain which dominates the two main islands lies across the path of the strong prevailing North West winds (N.Z. Meteorological Service, 1975) and is responsible for the wide range of climate and exposure throughout the country. In a recent survey of wind energy potential in New Zealand by Cherry (1976), it was noted that New Zealand was very well endowed with high winds, illustrated by the relatively large number of

"moderate" wind energy sites (3.2 - 5.2 m/s mean annual wind speed at 10 m height) with some exposed sites reaching annual mean wind speeds of over 9 m/s. Table 1.1 from NZS 4203 (1976) indicates the maximum 3 second gust speeds with return periods of 5, 25 and 50 years at some cities and towns in New Zealand and indicates the general high wind speeds expected in urban areas.

Widespread storm damage to afforested areas and superficial but extensive damage to buildings in suburban areas are a feature of the country's severe storms. In addition, the New Zealand Electricity Department has reported occasional damage to their inland high-country electricity transmission lines by unexpectedly high winds. The occasional disastrous storm such as the "Wahine Storm" of May, 1968 and the August 1975 storm have also caused damage worth many millions of dollars and occasionally a substantial loss of life.

It is therefore abundantly clear that the problem of wind effects over complex terrain is a practical problem of very real importance to New Zealand's development and general welfare, and it was with these thoughts in mind that the Mechanical Engineering Department began its research programme in wind engineering during 1969. The 4' x 4' (1.2 m x 1.2 m) atmospheric boundary-layer wind tunnel was designed and built by Raine (1974 a,b) and was first used to investigate the extent and nature of the wind protection by fences (Raine and Stevenson, 1977). It was also thought that a most effective way to contribute to wind engineering was to concentrate on field investigations backed by wind tunnel model studies. With the financial help of the University and the New Zealand Electricity Department, a unique field measurement facility was developed for this purpose. The development of the data acquisition unit and the propeller anemometer extended over a period of about 5 years and involved a good deal of effort and time. This facility was first used by Flay (1978) for the measurement of the atmospheric boundary-layer over rural terrain and was then employed for the field work in the present project. Allied work on the investigation of the wind flow over two-dimensional hill shapes in the wind tunnel to investigate the effects of hill shape and the flow characteristics was also commenced by J. Pearse and is still in progress. A model and full scale investigation of the Rakaia Gorge area was undertaken and reported by Meroney et al (1978), followed by a further complex terrain study of the Gebbies Pass area by D. Neal which is still in progress at the time of writing. It was hoped that

City or town	$\bar{V}_{10}$ (m/s) for return period of :		
	5 years	25 years	50 years
Auckland	28	31	33
Blenheim	28	31	33
Christchurch	33	38	40
Dunedin	32	36	38
Gisborne	29	33	35
Hokitika	31	35	37
Invercargill	36	40	42
Kaitaia	36	44	48
Napier	31	35	37
Nelson	29	35	37
New Plymouth	34	39	41
Palmerston North	31	35	36
Rotorua	28	32	34
Tauranga	27	30	32
Timaru	31	37	39
Wanganui	36	43	46
Wellington	40	47	50
Westport	30	34	36
Whangarei	32	41	44

TABLE 1.1 MAXIMUM 3 SECOND GUST SPEEDS AT 10 METRES HEIGHT FOR VARIOUS RETURN PERIODS OVER THE MAJOR URBAN AREAS IN NEW ZEALAND. (NZS 4203, 1976).

the work described above would complement each other and provide a better understanding of the flow over complex terrain for engineering purposes.

1.3 SCOPE AND OBJECTIVES OF PROJECT

The project described in this report was undertaken in order to contribute to the understanding of the wind flow over complex terrain which was shown above to be a significant engineering problem. The project was limited to the measurement and investigation in atmospheric conditions close to neutral stability, of the wind flow over several low forward-facing, two-dimensional escarpments of different slopes. This restriction was imposed in order to isolate the effect of hill slope and wind direction on the mean velocity and turbulence characteristics close to the ground and yet undertake a programme which could be completed in a reasonable time.

The main contribution of original work was seen as the field experimental programme which also involved a substantial amount of preparation in the development of suitable equipment. The wind tunnel model tests were undertaken to provide a comparison with the field data and to increase the scope of the results.

The information from this project concerning the extent and trends exhibited by the disturbed air flow was intended for engineering applications and a discussion on possible prediction methods for the mean wind speeds over a hill is included with this in mind.

1.4 SELECTION OF FIELD SITES

The choice of sites suitable for the present field measurements was limited by a number of major restrictive criteria which made the search for suitable sites a major operation involving a lot of time and travel. The search was carried out spasmodically over a period of one year and was greatly helped by the author's long association and familiarity with the country surrounding his home town.

It was decided for reasons given earlier, to confine the search to suitable two-dimensional, forward-facing escarpments. In order that the sites were not made unique by unusual features or obstructions nearby, they had to be set in exposed, open-country situations. A limit of between 10 to 20 metres was set on their height, H so that a sufficiently useful range of $^{Z}/H$ values could be covered using the

10 m and 20 m masts that were available. The sites had to be sufficiently close to Christchurch to enable day trips to be made for the frequent servicing of equipment and for taking the wind recordings on suitable days. The escarpment slopes had to face, as close to the normal as possible, a prevailing wind direction which was noted for its strength and frequency of occurrence to ensure a good chance of suitable strong wind conditions occurring during the time available. The measurements were to be taken during the Summer to ensure easier site access, working conditions and less anemometer wear and tear. For Canterbury, the prevailing Summer wind (Fig.1.1) is the sea breeze from the North to North East which is conveniently, stronger in the Summer than in the Winter. However strong winds from the North West and South West also occur, albeit less frequently. The sites had to have vehicle access but be sufficiently out of sight from the road to reduce the chance of vandalism and theft during the long periods when the equipment was left unattended. Lastly, the permission and co-operation from the owner of the farm on which the site was situated had to be obtained and the disturbance of their stock kept to a minimum.

It was found that the equipment required at least one week to erect and commission and that 1 to 2 months were necessary to obtain only five or six strong wind recordings. Because of other demands on the field equipment for other projects, the Summer of 1977-78 was allocated for the present field work and it soon became clear that only two sites could be investigated in the time available.

The two sites chosen for the field tests were a sloping escarpment near Amberley Beach and a cliff escarpment on the banks of the Rakaia River. Both site locations are shown on the map of New Zealand in Fig.1.1 which also shows the prevailing strong winds taken from N.Z. Meteorological Service (1975). It was considered that the two sites provided a good range of slope, with the cliff representing the most abrupt case involving separated flows whilst the sloping escarpment represented a substantial obstruction but possibly with attached flows.

1.5 LAYOUT OF REPORT

A description of the atmospheric boundary-layer over uniform terrain is given in Chapter 2 with emphasis on the parameters that are considered later in the experimental programme. The other well established characteristics of the atmospheric boundary-layer are fully

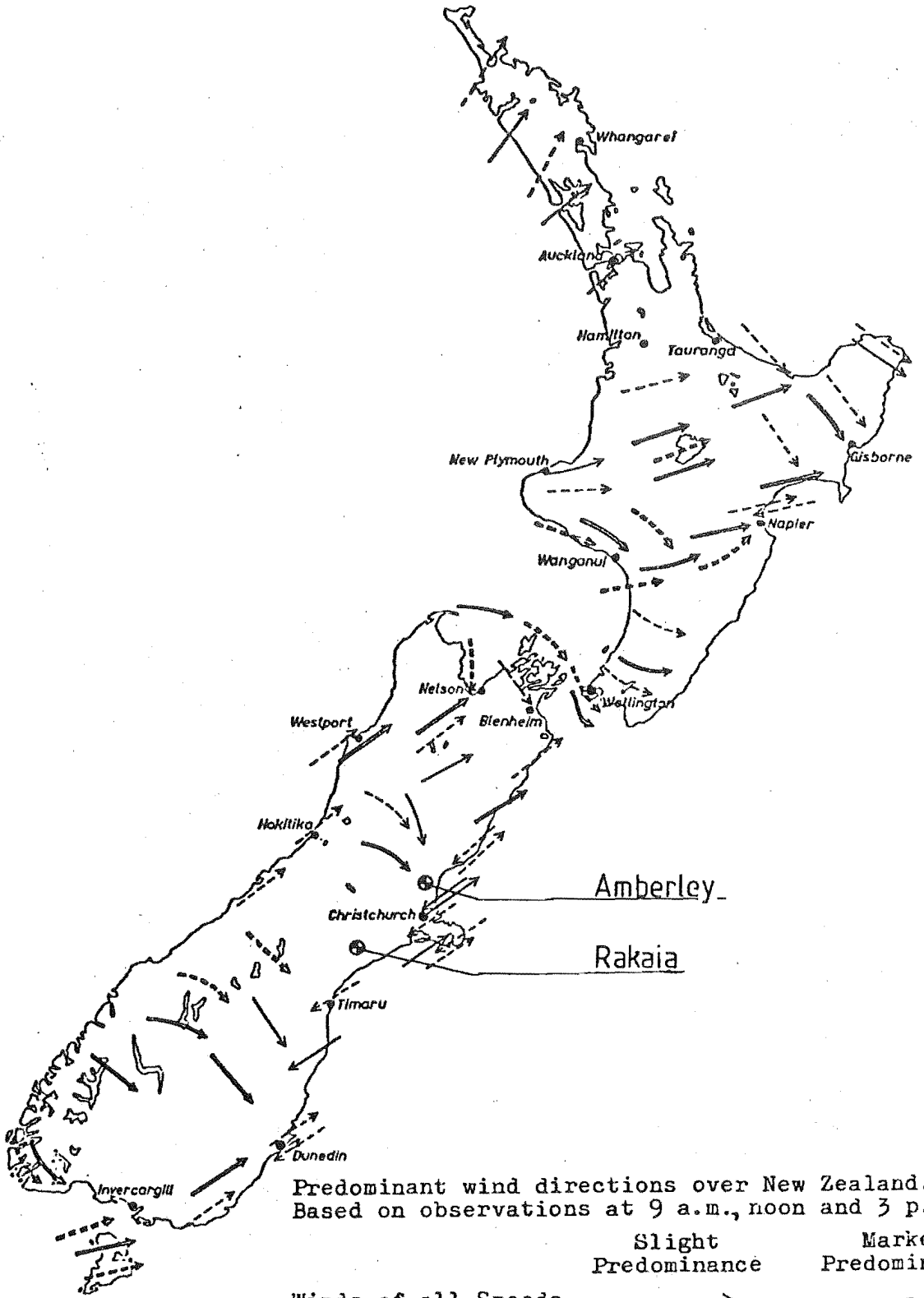

FIG 1·1 SITE LOCATIONS AND PREDOMINANT WINDS OVER NEW ZEALAND (N.Z. METEOROLOGICAL SERVICE 1975).

described in the literature and are not reported here. Chapter 3 continues with a review of the literature concerned with the modification of the wind flow by complex terrain.

The performance of the anemometers used in the field experimental work is discussed in Chapter 4, followed by the methods and logic employed in the sampling and processing of the anemometer data in Chapter 5. The two field investigations are described in Chapters 6 and 7, together with a presentation and discussion of the results obtained. Chapter 8 describes the wind tunnel model tests in a similar manner.

A comparison of the project results with the available literature on escarpment wind flows is undertaken in Chapter 9. This is followed by a discussion of currently proposed engineering prediction methods for the wind flow over hills and the relevant code rules in Chapter 10. Chapter 11 concludes the report with a summary of the principal conclusions from the project together with recommendations for future research work on the subject of wind flow over complex terrain.

CHAPTER 2

THE ATMOSPHERIC BOUNDARY-LAYER

Boundary-layer theory has been well established for some time and its various aspects have been fully discussed in such classic texts as Hinze (1959) and Schlichting (1960) and summarised in a less rigorous form by Launder and Spalding (1972), Bradshaw (1971) and others. The application of these concepts to the atmospheric boundary-layer has been complicated by the necessary consideration of the earth's rotation, radiation of heat from the sun, precipitation, non-uniform surface temperature and roughness, and topographic relief. These meteorological parameters have been dealt with by Sutton (1953) and more recently by Munn (1966), Haugen (1973), Pasquill (1974) and others, contributing greatly to the understanding of the earth's boundary-layer and the dispersion of wind-borne material.

With the more recent growth in interest in what is now generally called 'wind engineering' and provoked by the need to understand and predict the wind loading on structures, the attention of engineers has been drawn to the nature and values of the relevant meteorological parameters. The history of wind engineering has been well presented by Cermak (1974) and has shown an incredible growth in interest and activity over the last twenty years. Although various forms of dynamic wind loading occur at intermediate wind speeds, interest has mostly centred about strong winds in near neutrally stable conditions. However recently there has been a growing concern that a good deal of structural damage could be attributed to squalls, tornadoes and other unstable and statistically unpredictable wind events.

Statistical theory has been applied to the description of turbulence and turbulent diffusion for some time, but Davenport (1961) first applied statistical concepts to the description of wind loading of structures and subsequently formulated statistical methods with which to predict specific wind effects on structures in strong winds. Since then a good deal has been written about the wind loading of structures and the nature and behaviour of the significant parameters in the earth's boundary-layer (Cermak, 1974). The texts by Lumley and Panofsky (1964) and Plate (1971) and various recent review articles by Harris (1970), Raine (1974a), Jackson (1977), Panofsky (1977) and others have adequately defined the important boundary-layer parameters involved, although the

understanding of the statistical treatment of extreme wind speeds is still developing. Recent experimental projects involving extensive field tests have been reported by Elderkin (1966), Harris (1968), Teunissen (1970), Flay (1978) and others which have provided the engineer with information on the likely values that might be expected during strong winds over flat homogeneous terrain. Such experimental data except for the most recent contributions, have been exhaustively summarised by Counihan (1975) and the ESDU series (1972, 1974).

In view of the impressive array of talent involved and available literature on the atmospheric boundary-layer mentioned above, a further review was considered superfluous. This chapter therefore sets out only to define and clarify the parameters and methods utilised throughout the report and to comment on the values that might be expected to occur in neutral strong wind conditions over flat open rural terrain.

2.1 MEAN VELOCITY

If the continually changing wind speed U(t) at a height Z is averaged in the longitudinal direction over a length of time T_o, then the mean wind speed $\bar{V}_Z$ is expressed by

$$\bar{V}_Z = \lim_{T_o \to \infty} \frac{1}{T_o} \int_0^{T_o} U(t)\, dt \qquad 2.1$$

However due to changing diurnal weather patterns and the gustiness inherent in the natural wind illustrated by Van der Hoven's spectrum, the record length, T_o must be chosen with care. The mean wind speed is usually taken as the hourly mean wind speed because one hour is normally short enough to provide a stationary record and long enough to be independent of the wind turbulence. However there is sufficient evidence that little error is introduced if T_o is shortened to a value somewhere between 10 and 60 minutes.

2.1.1 Mean Velocity-Height Profiles

Between the earth's surface and the gradient wind height at the top of the boundary-layer usually taken as 600 m (Counihan, 1975), the wind is retarded by a shear stress τ_Z resulting from the exchange of momentum between successive layers of the atmosphere. The momentum exchange is given by the mean product of the vertical velocity, w and the horizontal momentum, ρu which is called the 'Reynolds stress', such that

$$\tau_z = -\rho\overline{uw} \qquad 2.2$$

This Reynolds stress is zero at the gradient height and increases to a maximum at the ground equal to the surface shear stress, τ_o created by the surface roughness. A friction velocity, V_* characteristic of the surface roughness may then be defined as

$$V_* = \sqrt{\frac{\tau_o}{\rho}} \qquad 2.3$$

In the surface layer within 30 to 150 m of the ground it may be assumed that the shear stress is almost constant and equal to the surface shear stress, τ_o so that

$$\tau_z = \tau_o = -\rho\overline{uw} = -\rho V_*^2 \qquad 2.4$$

For neutrally stable conditions over homogeneous terrain it can be shown that the above assumptions lead to a logarithmic velocity-height profile such as

$$\bar{V}_z = \frac{V_*}{k} \log_e \left(\frac{z-d}{z_o}\right) \qquad 2.5$$

where k is Von Karman's constant often take as 0.4, z_o is the surface roughness length and d the displacement depth. Since z_o and d determine the apparent height at which the mean velocity vanishes when extrapolated downwards, they are characteristic length scales of the surface roughness. Generally, the displacement depth can be ignored unless z is the same order of magnitude as d as is the case over urban, heavily vegetated areas or at low heights above the ground. Equation 2.5 may be written in a more practical form in terms of the natural logarithm as :

$$\bar{V}_z = 5.76\ V_* \log_{10} \left(\frac{z-d}{z_o}\right) \qquad 2.6$$

Traditionally however, engineers have used the more tractable power law profile :

$$\frac{\bar{V}_z}{\bar{V}_{REF}} = \left(\frac{z}{z_{REF}}\right)^{\alpha} \qquad 2.7$$

This law can be made to fit observed profiles over uniform terrain quite well but only over limited ranges of heights which are however, usually large enough for most practical applications. The advantage of the logarithmic profile is that the parameters involved have real physical relevance whilst the power law is largely empirical. Typical values of

Z_o and α may be obtained from ESDU (1972) or Counihan (1975) for various flat homogeneous terrains. For the open rural terrain characterising the two field sites, one may expect to find values of approximately Z_o = 0.05 m and α = 0.19 during neutrally stable atmospheric conditions.

2.1.2 Atmospheric Stability

The factors that determine the air temperature T_Z at a certain height Z may be classified into three groups (Munn 1966).

1) Radiation flux

2) Advection - horizontal motion of wind - only important in non-uniform surfaces say, warm land and cool sea interaction.

3) Convection a) Forced convection through turbulent transfer

   b) Free convection through buoyancy effects causing vertical motion

   c) Natural convection through buoyancy effects in otherwise still air, say over a heat island.

A rising bubble of air will move through levels of decreasing density and will expand and cool. If in the hypothetical case, there is no mixing or heat exchange, the cooling is said to occur at the dry adiabatic lapse rate,

Γ = 0.98°C/100 metres so that

$$\frac{dT_Z}{dZ} = -\Gamma \qquad 2.8$$

For saturated air, cooling will follow the moist adiabatic rate as the latent heat of condensation will reduce the rate of cooling.

During stable or inversion conditions, the value of dT_Z/dZ in the surrounding atmosphere is less negative than the adiabatic lapse rate or even positive. This occurs often at night when the air close to the ground is colder than the air higher above the ground. Under these conditions, any air displaced upwards will remain colder than the surrounding air and will experience a stabilising force downwards due to its greater density.

During unstable conditions, the value of dT_Z/dZ in the surrounding atmosphere is more negative than the adiabatic lapse rate, which is a common situation during a sunny day. Rising air will in this case find itself still hotter than the surrounding air and will continue to rise due to its lower density, causing instability. Greater turbulence levels

are present as a result of these unstable conditions.

In neutral conditions, the rising air remains at the same temperature and density as the surrounding air in accordance with equation 2.8. The adiabatic lapse rate is often used as an index of vertical stability which however, is an over-simplification due to the dependence of forced convection on the wind speed and the ground roughness.

The potential temperature, θ is the temperature that a parcel of air would have if it was brought adiabatically from its initial state to standard sea level. For an ideal gas,

$$\frac{1}{\theta}\frac{\partial\theta}{\partial z} = \frac{1}{T}\left[\frac{\partial T}{\partial z} + \Gamma\right] \qquad 2.9$$

For the atmospheric boundary-layer,

$$\theta \approx T_z + \Gamma.z \qquad 2.10$$

The turbulent energy required to displace a vertical movement of air is extracted from the mean flow through the Reynolds stresses. Whether the velocity fluctuations increase or decrease depends on whether the energy supply is greater or less than the rate at which work must be done in moving the bubble in the vertical direction.

The dimensionless gradient Richardson Number, R_i may be used to express the stability of the atmosphere and is usually defined as

$$R_i = \frac{\frac{g}{\theta}\cdot\frac{\partial\theta}{\partial z}}{\left(\frac{\partial\bar{V}}{\partial z}\right)^2} \qquad 2.11$$

With the help of equation 2.9, the Richardson number may be rewritten as

$$R_i = \frac{g}{T}\cdot\frac{(\Gamma - \gamma)}{\left(\frac{\partial\bar{V}}{\partial z}\right)^2} \quad \text{if } \gamma = \frac{\partial T}{\partial z} \qquad 2.12$$

When R_i or $\left(\frac{\partial\theta}{\partial z}\right)$ is negative, the air is unstable and considerable convective turbulence occurs in addition to the mechanical turbulence.

When $|R_i| < 0.01$ the air has near neutral stability and the turbulence is purely mechanical. It is often assumed that this condition occurs at low heights during strong winds. However, as the wind shear decreases rapidly with height, convective turbulence becomes progressively

more important with height causing the numerical value of the Richardson number to decrease upwards towards instability.

When R_i is positive, the air is stable with thermal stratification damping out mechanical turbulence.

For values larger than 0.2, the turbulence is essentially damped out altogether and winds at different heights become uncoupled.

The difference between observed and logarithmic velocity-height profiles depends then on the Richardson number, but unfortunately its variation with height cannot be readily predicted. However, the recent introduction of the Monin-Obukhov theory has clarified the behaviour of wind profiles in non-neutral conditions.

When $Z >> Z_o$ it is maintained that the turbulence characteristics will depend on only five quantities, four of which are approximately constant throughout the surface layer (Munn, 1966).

Height	Z
Density	ρ
Buoyancy parameter	g/T
Turbulent shear stress	Z or $V_* = \sqrt{\frac{\tau}{\rho}}$
Vertical heat flux	q or $q/c_p.\rho$

These may be combined using dimensional analysis to yield the dimensional paramter, Z/L where the Monin-Obukhov Length,

$$L = - \frac{V_*^3}{k \cdot \frac{g}{T_o} \cdot \frac{q}{c_p \rho_o}} \qquad 2.13$$

L is independent of height and defined to be negative with upward heat flux, as in the daytime. Thus L is positive in stable stratification and negative in unstable stratification. For small Z/L, mechanical turbulence dominates and for larger Z/L ($\gtrsim 0.1$), convection dominates. Z/L however, can only be measured if the vertical heat flux, q is known which rarely is the case. Alternatively, when the temperature gradients and wind shears are known then the Monin-Obukhov length may be redefined (Lumley and Panofsky, 1964) as $L' = \frac{K_h}{K_m} L$

so that $$L' = \frac{V_* \cdot \frac{\partial \bar{V}}{\partial Z} \cdot T}{k \cdot g \cdot \frac{\partial \theta}{\partial Z}} \qquad 2.14$$

The Monin-Obukhov theory predicted that $^{Z}/L$ is only dependent on R_i and research measurements summarised by Plate (1971) and shown in Fig.2.1, show that very nearly,

$$\frac{Z}{L} = R_i \qquad \text{for } R_i \leqslant 0$$

and

$$\frac{Z}{L} = \frac{R_i}{1 - 5R_i} \qquad \text{for } 0 \leqslant R_i < 0.2$$

Plate (1971) reported that the theory continued by expressing the wind shear in the dimensionless form

$$\phi_M = \left(\frac{kZ}{V_*}\right)\left(\frac{\partial \bar{V}}{\partial Z}\right) \qquad 2.15$$

The variation of ϕ_M with $^{Z}/L$ is shown in Fig.2.2. When $^{Z}/L = 0$, $\phi_M = 1$ which leads to the logarithmic profile for $Z >> Z_o$ under neutral conditions. For small values of $^{Z}/L$ only, ϕ_M is a function of $^{Z}/L$ which can be approximated using an empirical constant, β such that

$$\phi_M \approx 1 + \beta\left(\frac{Z}{L}\right)$$

$$\therefore \quad \frac{\partial \bar{V}}{\partial Z} \approx \frac{V_*}{kZ}\left[1 + \beta\left(\frac{Z}{L}\right)\right]$$

and

$$\bar{V} = \frac{V_*}{k}\left[\log_e\left(\frac{Z}{Z_o}\right) + \beta\left(\frac{Z}{L}\right)\right]$$

The empirical constant, β may be obtained from Fig.2.2 for positive values of $^{Z}/L$ only, as $\beta = 4.7$. However, for unstable conditions the situation is more complex and Panofsky (1977) replaced the term $\beta(^{Z}/L)$ by a universal function $\psi(^{Z}/L)$ so that

$$\bar{V}_Z = \frac{V_*}{k}\left[\log_e\left(\frac{Z}{Z_o}\right) - \psi\left(\frac{Z}{L}\right)\right] \qquad 2.16$$

For stable air then by comparison with $\beta = 4.7$,

$$\psi\left(\frac{Z}{L}\right) \approx -5\left(\frac{Z}{L}\right)$$

but for unstable conditions a rough value of $\psi\left(\frac{Z}{L}\right)$ may be obtained from the following table (Panofsky, 1977):

$\frac{Z}{L}$	-0.01	-0.02	-0.05	-0.1	-0.2	-0.5	-1.0	-2.0	-5.0
$\psi\left(\frac{Z}{L}\right)$	0.05	0.10	0.20	0.37	0.60	1.01	1.40	1.85	2.52

TABLE 2.1 VARIATION OF ψ WITH $^{Z}/L$ FOR UNSTABLE CONDITIONS

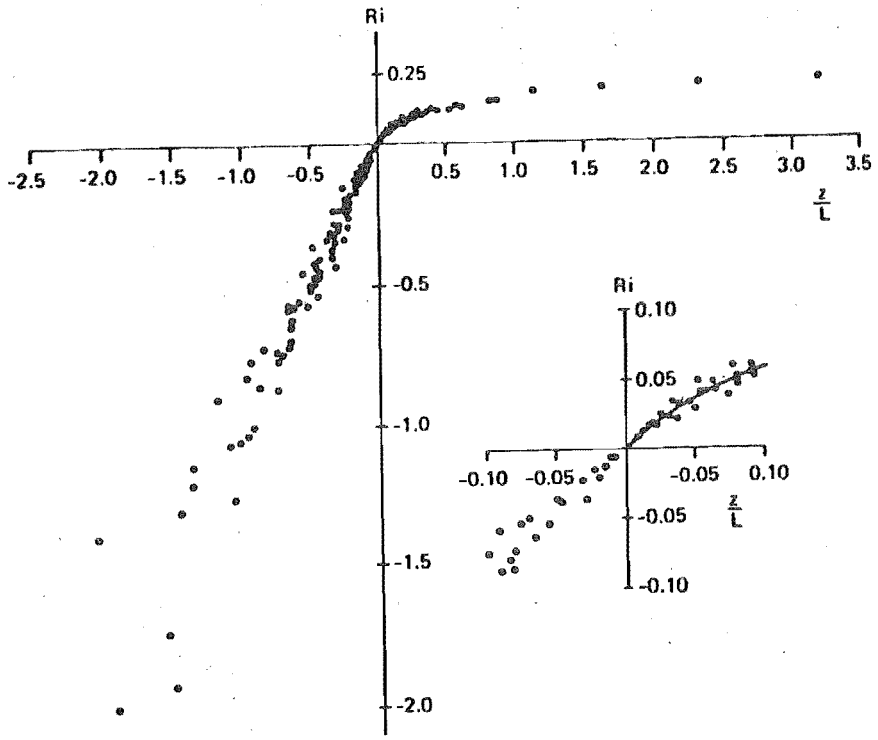

FIG 2·1 THE RELATION BETWEEN Z/L AND RICHARDSON No., Ri FOR THE WHOLE RANGE OF STABILITY FROM EXPERIMENTAL RESULTS. (PLATE 1971)

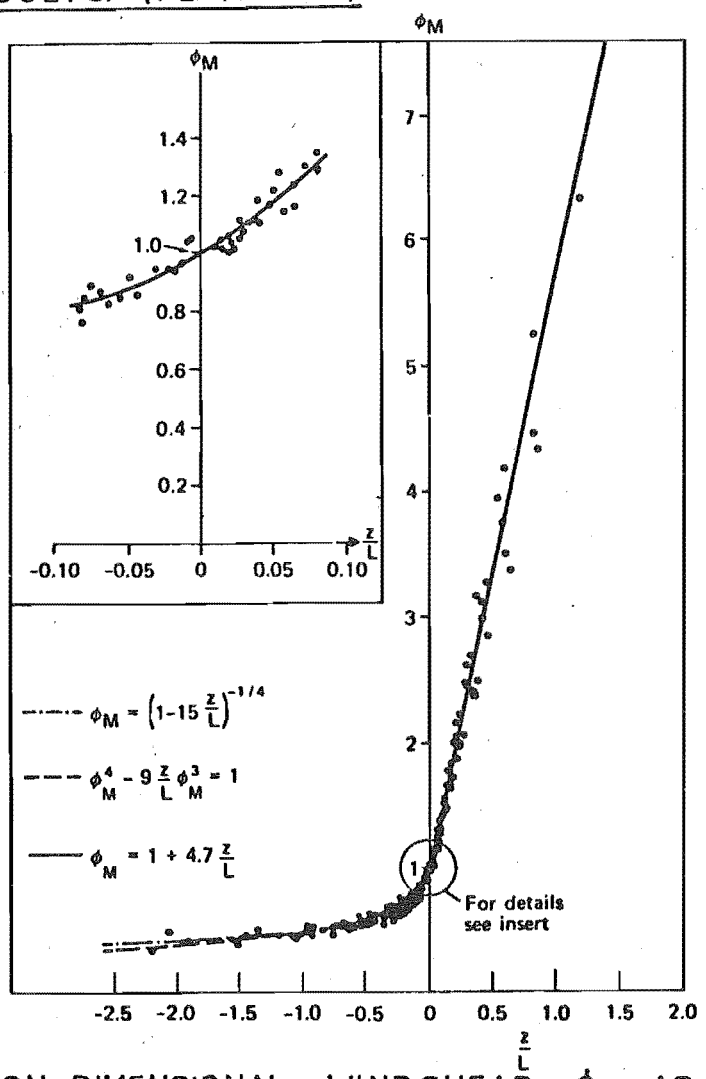

FIG 2·2 NON DIMENSIONAL WINDSHEAR, ϕm AS A FUNCTION OF Z/L FROM EXPERIMENTAL RESULTS (PLATE, 1971)

Thus for a certain stability condition, the correct velocity-profile from equation 2.16 may be estimated if a value can be assigned to the parameter $^{Z}/_{L}$. However the value of L is not normally known without taking elaborate measurements, but Panofsky (1977) has outlined an approximate method which is to be used later in the analysis of the field results.

Panofsky showed first that by combining equation 2.16 for two heights and comparing with equation 2.7, the family of curves in Fig.2.3a may be obtained, covering different conditions of stability with the range of $^{Z}/_{L}$. Fig.2.3b was also given which permits the estimation of L from the surface roughness length, Z_o and the Pasquill stability class which is in turn, defined in Fig.2.3c. Panofsky suggested that this information could be used in the following way.

1) Consider the terrain and estimate Z_o subjectively.

2) Decide on the Pasquill class from Fig.2.3c knowing the mean velocity at 10 m height, the degree of cloud cover and time of day.

3) Enter Fig.2.3b and determine L.

4) Estimate the expected power law α in Fig.2.3a.

The information in Fig.2.3 was used as "Panofsky's method' in an iterative fashion in conjunction with Table 2.1, to estimate the actual stability condition and Z_o value for the field tests when the power law and cloud cover were known. Discussions in Chapters 6 and 7 indicate that large variations from the neutral velocity-height profile may occur even in strong winds around 7 - 10 m/s.

2.1.3 Changes in Terrain Roughness

When sudden changes in surface roughness occur, the structure of the boundary-layer is complicated by the development of a new boundary-layer associated with the new roughness. Given a line normal to the wind flow marking the change in terrain roughness, the air downwind of this line may be divided into two parts by a sloping surface or interface; air that has felt the terrain change below the interface, and air that has not above. The interface rises with distance downstream in a transition zone until it reaches the gradient height and the boundary-layer is fully developed over the new roughness. The boundary-layer in the transition region can therefore be considered to have a profile below the interface appropriate to the new terrain and a profile above appropriate to the old terrain upwind. The thickness of this interfacial layer and the behaviour of the wind shear within it is still open to conjecture.

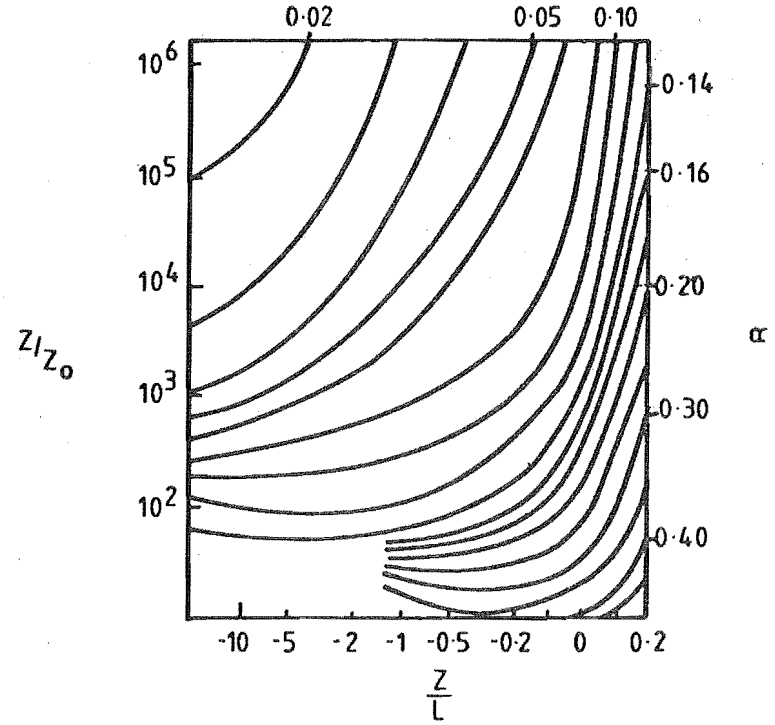

a) The power law exponent, α as a function of z/z_o and z/L

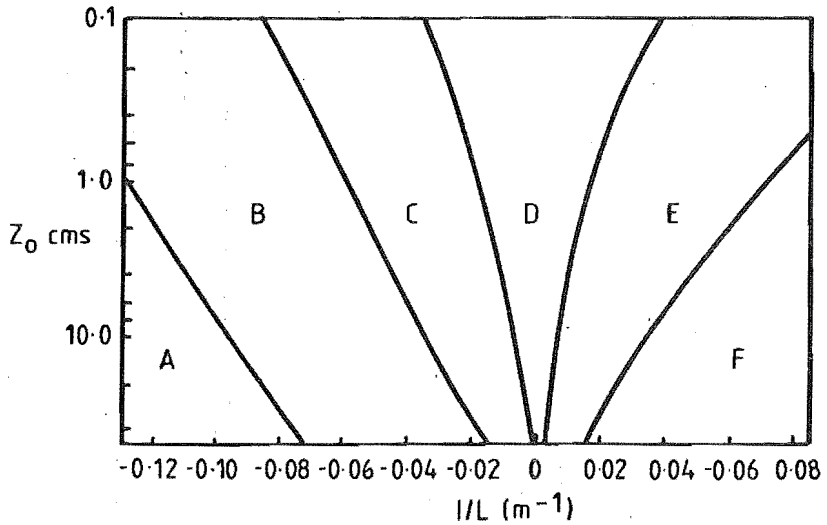

b) Relation between Monin—Obukhov length L, Pasquill stability class and roughness length z_o

surface wind speed (at 10m) m sec^{-1}	Day			Night	
	incoming solar radiation			thinly overcast or ≥4/8 low cloud	<3/8 cloud
	strong	moderate	light		
<2	A	A-B	B		
2-3	A-B	B	C	E	F
3-5	B	B-C	C	D	E
5-6	C	C-D	D	D	D
>6	C	D	D	D	D

The neutral class, D, should be assumed for thick overcast during day or night.

c) Pasquill stability class and the weather.

FIG. 2·3 INFORMATION FOR THE DETERMINATION OF THE VELOCITY—HEIGHT PROFILES IN CONDITIONS OF NON NEUTRAL STABILITY (PANOFSKY 1977)

The height of the interface with distance downstream is of great interest to engineers when the velocity-height profile is being defined near a change in roughness. ESDU(1972), Panofsky (1977), and Jackson (1977) agreed that no satisfactory general treatment of this situation was available and there was insufficient experimental evidence except from a few such as Antonia and Luxton (1971), to endorse any particular approach. ESDU (1972) reported that some theories predicted the height of the interfacial layer, θ as being about one tenth of the distance travelled by the wind from the change in roughness, x except near the change in roughness where a steeper slope could be expected. Jackson preferred the theoretical approach put forward by Townsend (1965) which resulted in the relation ,

$$\frac{\theta}{x}\left[\log_e\left(\frac{\theta}{Z_o}\right) - 1\right] = \text{constant} \qquad 2.17$$

Jackson continued to show that for a power law profile over rural terrain then,

$$\theta \propto x^{0.8} \qquad 2.18$$

A recent contribution by Biétry et al (1978) reported a similar practical approach (Method (1)) adopted by the Code of Practice for Wind loads for Denmark (presumably for smooth to rough transition) where, referring to Fig.2.4,

$$\theta_1 = 0.7\, Z_o \left(\frac{x}{Z_o}\right)^{0.8} \qquad 2.19$$

and

$$\theta_2 = \theta_1 \left(\frac{\theta_1}{200}\right)^3 + Z_o \qquad 2.20$$

Above θ_1, the profile was the same as that upwind of the roughness change and below θ_2, the profile was assumed to be the same as that over horizontally homogeneous terrain of the new roughness Z_o. Between θ_1 and θ_2 within the interfacial layer, the profile was assumed to be logarithmic and continuous at elevations θ_1 and θ_2 with the two profiles previously defined.

Biétry considered other theoretical and model studies which suggested that whilst the form of equation 2.19 was appropriate, the value of 0.7 was too large. He concluded that beyond a sufficient distance of about 500 m downwind of the transition where the upstream profile could still be assumed at all heights, the internal boundary-layer depth may be approximated by

$$\theta_1 = \frac{x}{12.5} \qquad 2.21$$

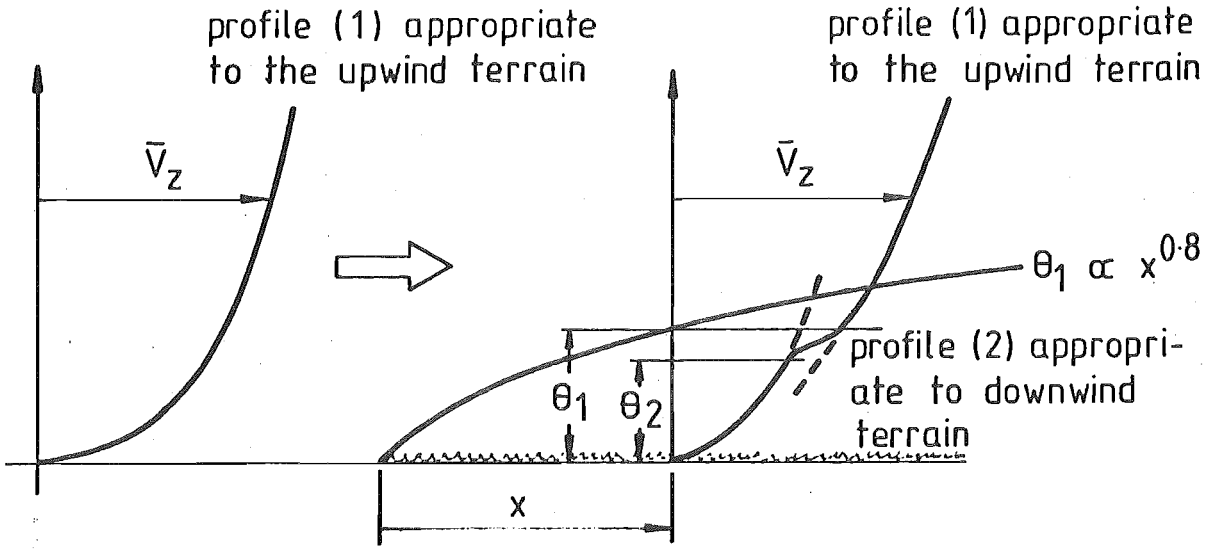

(a) method 1

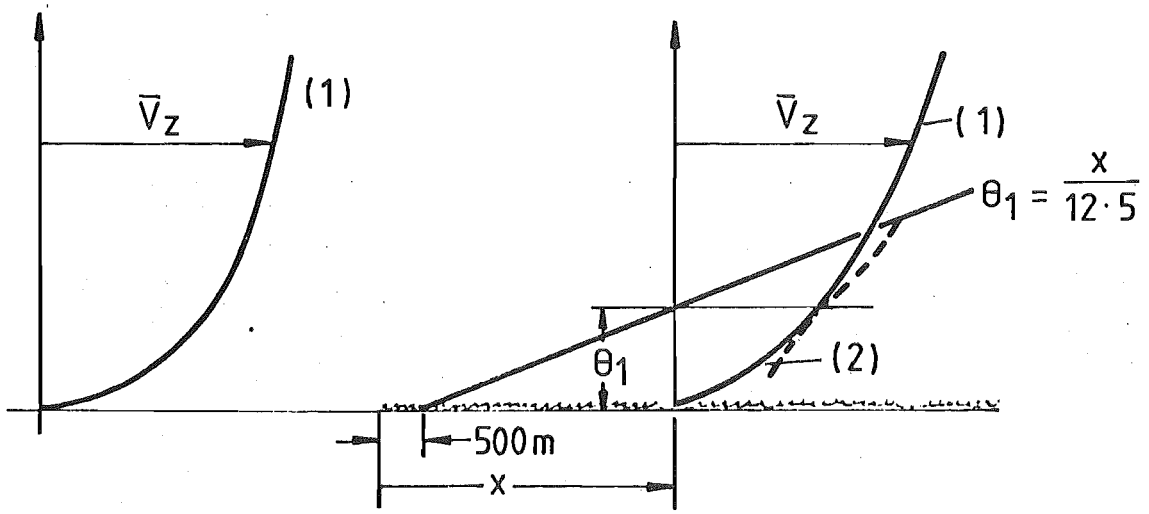

(b) preferred method 2

FIG 2·4 TWO METHODS OF PREDICTING THE VELOCITY-HEIGHT PROFILE OVER A CHANGE IN ROUGHNESS (Bietry, et al 1978)

It was also observed that the rate of growth of θ_2 was considerably smaller than that given by equation 2.20 and little error would be created if θ_2 was neglected altogether. This approach (method 2) together with the Denmark code and ESDU's approach (method 1) are illustrated in Fig.2.4. Beyond 5 km downwind of the change in roughness, Biétry (1978) concluded that the wind profile corresponding to the new roughness could be considered to be completely established. It was stated that by using method 2 and thus ignoring the influence of the new Z_o on the slope of the interfacial layer, an acceptable error of the order of 5% or less could be expected.

2.2 TURBULENCE

The fluctuations in wind velocity at a certain height, Z are usually considered in terms of three orthogonal components u(t) parallel to, and v(t), w(t) normal to the mean flow direction, so that in the longitudinal direction

$$U(t) = \bar{V}_Z + u(t) \qquad 2.22$$

In the lateral direction but still on the horizontal plane, the mean velocity component is zero which leaves only the fluctuating component v(t) at a time t. Similarly, in the direction normal to the plane in which u and v lie, only the fluctuating component w(t) will exist.

When the flow over flat homogeneous terrain is considered, the u(t) and v(t) components are horizontal and the w(t) component lies in the vertical direction, but this situation need not be so for flow over hills as illustrated in Fig.5.5. In this more general case, the components u(t) and w(t) may no longer be horizontal and vertical respectively. In the discussion that follows and during the report, the fluctuating velocity components u(t), v(t) and w(t) are more concisely referred to as u, v and w.

2.2.1 Turbulence Intensity

If the longitudinal velocity component, U(t) is recorded over a period of time T_o, then the mean square velocity in the longitudinal direction is

$$\overline{U^2(t)} = \lim_{T_o \to \infty} \frac{1}{T_o} \int_0^{T_o} U^2(t)\, dt \qquad 2.23$$

Assuming that T_o is sufficiently long for a stable average as discussed later in Chapter 5 then,

$$\overline{U^2(t)} = \frac{1}{T_o} \int_0^{T_o} (\bar{V}_Z + u)^2 \, dt$$

and

$$\overline{U^2(t)} = \bar{V}_Z^2 + \frac{1}{T_o} \int_0^{T_o} (u)^2 \, dt \qquad 2.24$$

The integral term in equation 2.24 is defined as the variance, σ_u^2 of the longitudinal component. The variances in the other two directions may also be defined in the same way. It follows that

$$\sigma_u^2 = \overline{U^2}(t) - \bar{V}_Z^2 \qquad 2.25$$

Alternatively, the variances may be defined as

$$\sigma_u^2 = \underset{T_o \to \infty}{\text{LIM}} \int_0^{T_o} (U(t) - \bar{V}_Z)^2 \, dt \qquad 2.26$$

The variances are usually presented as non-dimensional turbulence intensities $\sigma_u/\bar{V}_Z$, $\sigma_v/\bar{V}_Z$ and $\sigma_w/\bar{V}_Z$ or normalised by the friction velocity V_* to form the ratios

$$A = \sigma_u/V_*, \quad B = \sigma_v/V_* \text{ and } C = \sigma_w/V_* \; .$$

Counihan (1975) concluded that for rural terrain, A = 2.5, B = 1.875 and C = 1.25 from which $\sigma_v/\sigma_u = 0.75$ and $\sigma_w/\sigma_u = 0.50$, compared with the ESDU (1974) data of 0.69 and 0.43. In the constant shear layer, the decrease in longitudinal turbulence with height could be approximated to by assuming that σ_u was proportional to V_* which yields

$$\frac{\sigma_u}{\bar{V}_Z} \propto \frac{1}{\log_e(\frac{Z}{Z_o})} \qquad 2.27$$

ESDU (1974) gives values of the three turbulence intensities as functions of height and surface roughness from a summary of world wide sources of data, which showed that equation 2.27 was not strictly correct. For a surface roughness of $Z_o = 0.05$ m characterising an open rural terrain, ESDU data indicates that the turbulence intensities at 10 m height would be $\sigma_u/\bar{V}_Z = 0.21$, $\sigma_v/\bar{V}_Z = 0.15$ and $\sigma_w/\bar{V}_Z = 0.09$.

2.2.2 Reynolds Stresses

The Reynolds stress term, $-\rho\overline{uw}$ introduced earlier and defined by equation 2.4, determines the surface shear stress and velocity profile and is therefore an important quantity. It has however a reputation of

being very difficult to measure accurately and results in the literature vary significantly. The other two components $\overline{uv}$ and $\overline{vw}$ are usually small and may be ignored.

Values of $\overline{uw}/(\sigma_u \cdot \sigma_w) = -0.285$ are given by ESDU (1974) for a surface roughness length $Z_o = 0.05$ m and Counihan (1975) suggests a value between -0.002 and -0.003 for the ratio $\overline{uw}/\bar{V}_G^2$.

2.2.3 Velocity Power Spectra

The contribution to the longitudinal variance from u(t) by the velocity fluctuations at a frequency n and within a bandwidth Δn is termed the longitudinal velocity power spectral density, $S_{uu}(n)$ as $\Delta n \to 0$. It follows by definition that

$$S_{uu}(n) = \underset{\Delta n \to 0}{\text{LIM}} \frac{\left[\overline{u^2}\right]_n^{\Delta n}}{\Delta n} \qquad \text{for } 0 < n < \infty \qquad 2.28$$

The variance may then be defined as the total contribution from all frequencies, so that

$$\overline{u^2} = \sigma_u^2 = \int_0^\infty S_{uu}(n)\, d(n) \qquad 2.29$$

The area under the spectrum of S(n) versus n is equal to the variance, σ_u^2. The error in σ_u due to the use of a finite frequency range is discussed later in Chapter 5. Even so, the linear frequency scale cannot cope with the necessary frequency range, so normally a logarithmic frequency scale is used with the wave number parameter, $\frac{n}{\bar{V}_Z}$.

Let $m = \log_{10}\left(\frac{n}{\bar{V}_Z}\right)$

$\therefore \quad \log_e\left(\frac{n}{\bar{V}_Z}\right) = 2.303\ m$

and differentiating,

$$\frac{1}{n}\, dn = 2.303\ dm$$

so that $$dn = 2.303\ n\ d\left(\log_{10}\frac{n}{\bar{V}_Z}\right)$$

$\therefore$ equation 2.29 becomes

$$\sigma_u^2 = 2.303 \int_0^\infty n \cdot S_{uu}(n) \cdot d\left(\log_{10}\frac{n}{\bar{V}_Z}\right) \qquad 2.30$$

The power spectra may then be plotted in the non-dimensional form

$$\frac{n \cdot S_{uu}(n)}{\sigma_u^2} \quad \text{against } \log_{10}\left(\frac{n}{\bar{V}_Z}\right).$$

However the area under the spectrum is now only proportional to the variance.

Using data from the third octave spectral analyser, the individual readings represent the total contribution over a $^1/_3$ octave bandwidth, where $\frac{n}{\Delta n}$ = constant $\approx$ 4.34. The nondimensional spectrum may then be calculated directly from

$$\frac{n \cdot S(n)}{\sigma_u^2} = \frac{n}{\Delta n} \cdot \left[\bar{u}^2\right]_n^{1/3 \text{ oct.}} \cdot \sigma_u^{-2} \qquad 2.31$$

The readings in decibels with respect to 0.01 volts must however first be translated to a linear reading using the following relation :

$$\text{Power level reading in db} = 20 \log_{10}\left(\frac{\sigma_{\text{volts}}}{0.01}\right) \qquad 2.32$$

The statistical procedures and errors involved in the estimation of power spectral densities from digital data such as that obtained from the project field tests have been well covered by Flay (1978).

Standard power spectra for all three components of velocity are given in Fig.4.15 and the longitudinal spectrum with a logarithmic ordinate in Fig.6.10, taken from ESDU (1974) for flat open terrain at 10 m height. Very little energy is evident in the $S_{uu}(n)$ and $S_{vv}(n)$ spectra beyond the wavenumber band of $0.025 < \frac{n}{\bar{V}_Z} < 0.25$ ($0.25 < n < 2.5$ Hz for $\bar{V}_Z$ = 10 m/s) and $0.25 < \frac{n}{\bar{V}_Z} < 2.5$ for the vertical spectrum, $S_{ww}(n)$.

2.2.4 Autocorrelation Function

The covariance function is the mean product of one or two fluctuating velocity components measured at one or two points in the flow, either at the same time or with a time lag τ between them. In particular, the longitudinal autocovariance function is defined as

$$C_{uu}(\tau) = \overline{u(t) \cdot u(t+\tau)} = \underset{T_o \to \infty}{\text{LIM}} \int_0^{T_o} u(t) \cdot u(t+\tau)\, dt \qquad 2.33$$

When the time lag τ is zero, the autocovariance function reduces to the variance which may be used to non-dimensionalise the function to form the autocorrelation function $\rho_{uu}(\tau)$ namely

$$\rho_{uu}(\tau) = \frac{C_{uu}(\tau)}{C_{uu}(0)} = \frac{C_{uu}(\tau)}{\sigma_u^2} \qquad 2.34$$

A plot of $\rho_{uu}(\tau)$ against τ gives an indication of the extent in time of a passing gust. Integration of the area under the autocorrelation curve yields the Eulerian time-scale of the turbulence, T_E which provides an indication of the gust size in time

i.e. $$T_E = \int_0^\infty \rho_{uu}(\tau)\, d\tau \qquad 2.35$$

An important property of the autocorrelation function is that it forms a Fourier Transform pair with the power spectral density function so that

$$S_{uu}(n) = 4 \int_0^\infty C_{uu}(\tau) \cos(2\pi n\tau)\, d\tau$$

and $$C_{uu}(\tau) = \int_0^\infty S_{uu}(n) \cos(2\pi n\tau)\, dn \qquad 2.36$$

This pair may be used to obtain the autocorrelation function and the power spectral density function from the same data processing routine using Fourier Transforms, which was done in the program PSAUTCORS described by Flay (1978). However if the analogue output is analysed as was the case with the first test series in the present wind tunnel programme, a time delay/correlator is necessary to indicate the covariance function for a certain time delay τ secs.

2.2.5 Length Scales of Turbulence

The length scale of turbulence is a measure of the longest spacial separation between correlated velocities in a certain direction in the flow. A length scale may be defined for each of the three velocity components.

They may be obtained with the use of the Eulerian time scale, T_E obtained from the autocorrelation-time delay curves using equation 2.35. Assuming that Taylor's hypothesis is true, namely that for $\bar{V}_Z >> u(t)$, the turbulence field can be considered as frozen in space and convected past a point with velocity $\bar{V}_Z$, then

$$\Delta x = \bar{V}_Z\, \Delta t$$

and $$L_{ux} = \bar{V}_Z\, T_E \qquad 2.37$$

However difficulties often occur when the function $\rho_{uu}(\tau)$ does not converge to zero or oscillates about zero due to trends in the data or very low frequencies comparable with the record length. In this case the integration of equation 2.35 is either taken until $\rho_{uu}(\tau)$ falls to 5% or until the first zero crossing. Alternatively it may be assumed that the decay of $\rho_{uu}(\tau)$ with τ behaves as a negative exponential function and T_E is given by the time for the function to drop to a value of $1/e$ or 0.368.

Alternatively the length scales may be obtained from the location of the peak frequency, n_p of the appropriate velocity power spectrum at which the greatest turbulence energy is contained. It may be shown for the standard ESDU (1974) spectra based on the von Karman model, that

$$L_{ux} = \frac{0.146\ \bar{V}_Z}{n_{up}} \quad , \quad L_{vx} = \frac{0.106\ \bar{V}_Z}{n_{vp}} \quad , \quad L_{wx} = \frac{0.106\ \bar{V}_Z}{n_{wp}} \qquad 2.38$$

This method involves the selection of the peak frequencies from experimental velocity power spectra which often are characterised by a very flat peak. As a result, large errors of the order of 100% in the value of n_p are quite possible.

The length scales increase with distance above the ground and decrease with surface roughness. For homogeneous isotropic turbulence, theory predicts that $L_{vx} = L_{wx} = L_{ux}/2$, whilst for a typical open country boundary-layer with $Z_o = 0.05$ m and $Z = 10$ m ESDU (1974) predicts that

$$L_{ux} = 80 \text{ m}$$

$$L_{vx} = 25 \text{ m}$$

$$L_{wx} = 3.5 \text{ m}$$

Caution is expressed in the accuracy of length scales close to the ground, especially for the vertical component which is most affected by the presence of the ground surface.

2.2.6 Probability Distribution of Wind Velocity

If the range of longitudinal velocity encountered during a long recording is divided into a number of discrete cells and the number of occurrences in each cell is counted, the result constitutes a frequency histogram. If these counts are then divided by the cell

width, the result is a probability density histogram which tends to the probability density function, PDF as the cell width is reduced to zero.

There is strong evidence that all three components of wind velocity behave in a random Gaussian or Normal fashion characteristic of most turbulent motion. Considering the variation of the instantaneous longitudinal velocity component, U(t) during a stationary wind event, the PDF of velocity having a value between V and dV may be described by

$$p(V) = \frac{1}{\sigma_u \sqrt{2\pi}} \cdot e^{-x} \, dV \qquad 2.39$$

where $$x = \frac{(U(t) - \bar{V})^2}{2\sigma_u^2} = \frac{u^2}{2\sigma_u^2}$$

The PDF may be normalised using

$$\eta = \frac{U(t) - \bar{V}}{\sigma_u} = \frac{u}{\sigma_u}$$

so that $$p(V) = \frac{1}{\sqrt{2\pi}} \cdot e^{-\frac{\eta^2}{2}} \, d\eta \qquad 2.40$$

The PDF of the instantaneous velocity component is usually symmetrical about its hourly mean wind speed with very little skewness, defined by (Mean-Mode)/σ.

The frequency of occurrence of the hourly mean wind speeds during say a one year period, is also of interest to engineers and the PDF of mean velocity has been discussed by Davenport (1967) and Baynes (1974). Davenport showed that the simplest PDF model was the Rayleigh distribution by regarding the large scale atmospheric motions as two-dimensional isotropic turbulent motion with no prevailing wind direction. Assuming that the distributions of these two components u,v are uncorrelated Gaussian distributions, the probability of obtaining a mean velocity with components between u and (u+du) and v and (v+dv) is given by the bell shaped Bivariate Normal distribution,

$$p(u,v)\, du\, dv = p(u)\, du \cdot p(v)\, dv = \frac{1}{2\pi\sigma_u \sigma_v} e^{-\left[\frac{u^2}{2\sigma_u^2} + \frac{v^2}{2\sigma_v^2}\right]} du\, dv$$

Assuming that the wind is isotropic, $\sigma_u = \sigma_v = \sigma$,

$$p(u,v)\,du\,dv = \frac{1}{2\pi\sigma^2}\, e^{-\left[\frac{u^2+v^2}{2\sigma^2}\right]}\, du\, dv$$

Now, the magnitude of the wind speed is given by

$$V^2 = u^2 + v^2$$

If the distribution of wind speed in the region V and (V+dV) is taken in the direction sector θ and $(\theta+d\theta)$ and then integrated round the full circle, the probability of wind speed between V and (V+dV) is obtained regardless of direction, as

$$p(V)dV = \oint \frac{1}{2\pi\sigma^2}\, e^{-\left[\frac{u^2+v^2}{2\sigma^2}\right]}\, dudv = \frac{1}{2\pi\sigma^2} \oint e^{-\frac{V^2}{2\sigma^2}}\, dudv$$

Changing from cartesian to polar coordinates

$$dudv = V\, dV\, d\theta$$

so that

$$p(V)dV = \frac{1}{2\pi\sigma^2} \int_0^{2\pi} e^{-\frac{V^2}{2\sigma^2}}\, V\, dV\, d\theta = \frac{1}{2\pi\sigma^2}\, V\, e^{-\frac{V^2}{2\sigma^2}}\, dV \int_0^{2\pi} d\theta$$

$$\therefore \quad p(V)dV = \frac{V}{\sigma^2}\, e^{-\frac{V^2}{2\sigma^2}}\, dV \qquad 2.41$$

The probability of a velocity occurring at a value greater than V is

$P\ (>V)$ where

$$P\ (>V) = \int_V^{\infty} p(V)\, dV$$

$$\therefore \quad P\ (>V) = e^{-\frac{V^2}{2\sigma^2}} \qquad 2.42$$

This simple approach leading to the Rayleigh distribution of equation 2.42, is only applicable to fully developed temporate weather systems and does not include tropical cyclones or tornadoes. The peak is also likely to be shifted by a prevailing wind speed and the assumption of isotropy of the wind is not likely to occur due to the influences of local terrain.

An improved PDF for this application is the Weibull distribution of which the Rayleigh form is a special case when k = 2.

$$P(>V) = e^{-\left(\frac{V}{c}\right)^k} \qquad 2.43$$

Davenport (1967) gave various successful fits of wind data throughout the world to the Weibull PDF using values of k ranging between 1.7 and 2.5.

2.2.7 Peak Gusts

In the study of wind loading, a principal concern is for extreme loads that are associated with the extreme velocities indicated by the tails of the PDF. The maximum and minimum values of velocity encountered during each particular recording of a series, be it an hour or one year period, are variates in their own right for which PDFs may be formed from the data. It is therefore not the main body of data that describes the probability of an extreme velocity, but the behaviour of the maximum or minimum velocities of each data recording. A large number of recordings is therefore necessary to obtain an accurate distribution of these extreme events.

Davenport (1967) stated that if the parent distribution has the Weibull form as does the mean hourly wind speed data, then the distribution of the extreme values taken from a large number of data sets (say annual extremes) has a Fisher-Tippett, Type 1 form

$$P\ (>V) \quad = \quad e^{-e^{-a(V-u)}} \qquad 2.44$$

where $^{1}/_{a}$ is a scale factor measuring the dispersion of the data and u is the mode of the data. For the Rayleigh distribution,

$$^{1}/_{a} \quad = \quad \frac{\sigma}{\sqrt{2 \log_e N}}$$

and $$u = \sigma \sqrt{2 \log_e N}$$

where N is the number of samples in each data set. The extreme value theory employed assumes that the N sample values are independent of one another which in the case of wind, is not altogether true as adjacent samples are often correlated.

The Fisher-Tippett distribution is used extensively for the treatment of annual maximum mean wind speeds (Shellard 1963) and forms the basis for the analysis of the risk of occurrence of a certain extreme mean wind speed for structural design code purposes.

The maximum or peak gust speed averaged over a short period was also related to the mean wind speed by Davenport (1964) using extreme

value analysis. The distribution of the largest value from each of a large number of recordings of a stationary random function was derived, which might be for instance, the largest gust velocity during an hour. The mean value of this distribution of extreme events was shown to be approximately,

$$\text{Mean peak factor, } \hat{\eta} = (2 \log_e \nu\, T_o)^{\frac{1}{2}} + \gamma(2 \log_e \nu\, T_o)^{-\frac{1}{2}}$$

$$\text{where} \quad \eta = (V-\bar{V})/\sigma_V \qquad 2.45$$

$$\text{or} \quad \hat{V} = \bar{V} + \hat{\eta}\,\sigma_V$$

T_o = length of recording

γ = Eulers constant = 0.5772

The parameter ν is a measure of the average frequency of gusts and given by,

$$\nu = \left(\frac{m_2}{m_o}\right)^{\frac{1}{2}}$$

$$\text{where} \quad m_r = \int_0^\infty n^r\, S(n)\, dn \qquad 2.46$$

The parameter ν thus depends on the accuracy of the measured S(n) curve or in other words, the response of the data acquisition system and the selected averaging time of the data samples. The distribution of maxima about the mean largest value $\bar{\eta}_{max}$ was shown to be narrow in relation to the parent distribution with a standard deviation of

$$\sigma(\hat{\eta}) = \frac{\pi}{\sqrt{6}} \frac{1}{\sqrt{2 \log_e \nu\, T_o}} \qquad 2.47$$

As a result, the most likely gust velocity may be estimated using equation 2.45, although the actual peak gust velocity encountered during a one hour record may have a value anywhere on the extreme value PDF. Examples of the extreme PDF's resulting from Davenport's analysis are shown in Fig.2.5 for record lengths T_o defined by $\nu\, T_o$ = 100, 1000 and 10,000. The parameter ν is a measure of the average frequency of gusts and was said to have a typical value of 0.1 Hz for a standard Dynes pressure-tube anemometer. Values of $\nu\, T_o$ = 100, 1000 and 10,000 therefore correspond roughly to time intervals of 15 minutes, 3 hours and 30 hours respectively. It may therefore be estimated that the measured peak gust during a one hour period will exceed the mean value by about $3.5\sigma_v$. In open country at 10 m the turbulence intensity is

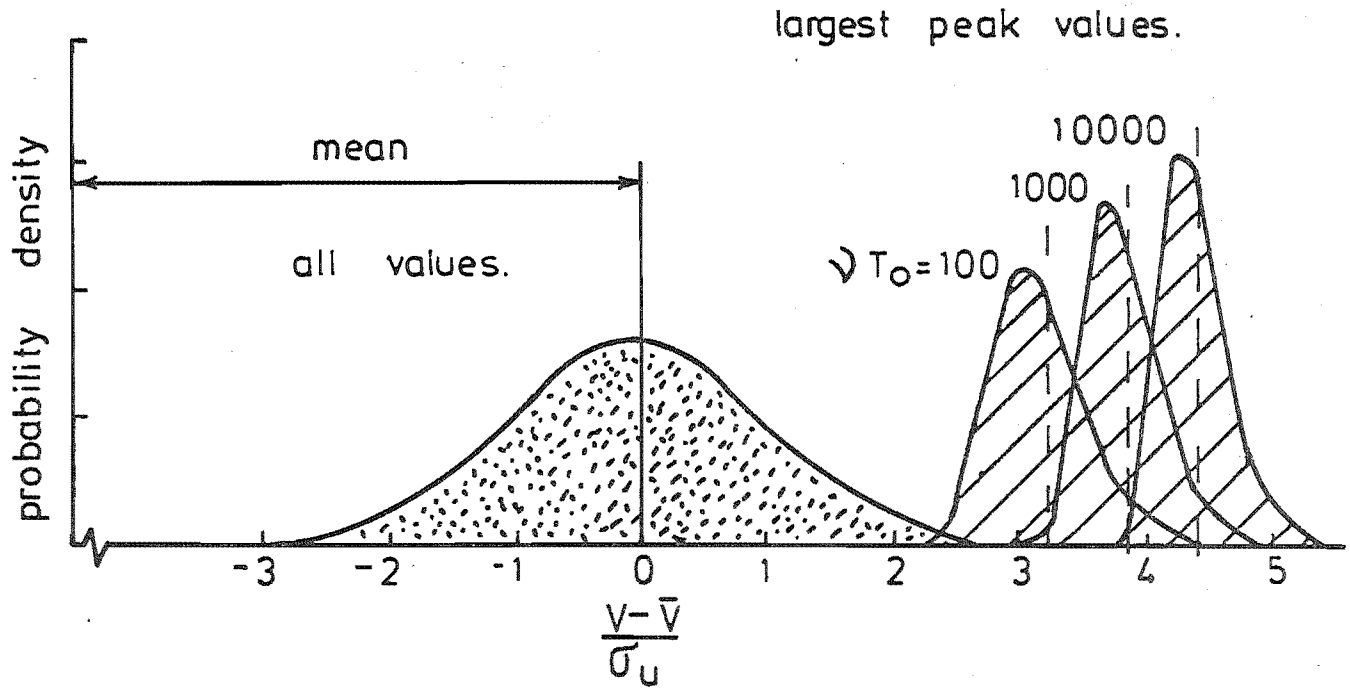

FIG. 2·5 GAUSSIAN PROBABILITY DISTRIBUTION OF WIND SPEED AND PEAK GUST SPEED. (DAVENPORT 1964)

about 0.15 giving an expected ratio of peak gust to mean speed of about 1.5.

The effect of the turbulence intensity, $\frac{\sigma_u}{\bar{V}}$ sample averaging time, T and record length, T_o has been considered by Mackey (1970) and the literature summarised by ESDU (1972) who adopted similar empirical models based directly on wind speed measurements. The suggested gust factor relationships were of the form

$$\frac{\hat{V}}{\bar{V}}(T,T_o) = 1 - A \log_{10}\left[\frac{T}{T_o}\right] \qquad 2.48$$

Although both sources agreed on the dependence of A on the turbulence intensity, disagreement on the empirical constants was apparent which was probably due to the different response characteristics of the instruments involved. Mackey (1970) suggested that

$$A = 0.6226 \left(\frac{\sigma_u}{\bar{V}}\right)^{1.2716} \qquad 2.49$$

whereas ESDU (1972) concluded that

$$A = 2.14 \left(\frac{\sigma_u}{\bar{V}}\right)^{1.33} \qquad 2.50$$

A similar expression was put forward by Wieringa (1973) which was shown to be as accurate as the available data with which it was compared. The effect of turbulence intensity was represented by the approximate empirical relation below assuming a constant ratio for $\sigma_u/V_* \approx 2.5$, as in equation 2.27 thus,

$$\frac{\sigma_u}{\bar{V}} = \frac{1.0}{\log_e(Z/Z_o)}$$

Wieringa (1973) suggested the following expression

$$\frac{\hat{V}}{\bar{V}}(T,3600) = 1.1 \frac{\hat{V}}{\bar{V}}(T,600) \qquad 2.51$$

and

$$\frac{\hat{V}}{\bar{V}}(T,600) = 1 + \frac{1.42 + 0.3013 \log_e\left[(^{990}/_{\bar{V}\cdot T}) - 4\right]}{\log_e\left[Z/Z_o\right]} \qquad 2.52$$

The relationship between the likely maximum gust speed averaged over a period of T seconds and the mean wind speed from a recording period of T_o seconds is important for a number of reasons. Simple wind loading calculations are often carried out using a T = 3, 5 or 15

second gust speed and ignoring the dynamic response of the structure. Field data providing these gust speeds are fragmented (Durst, 1960 and Wieringa, 1973) and furthermore, the anemometers used in the collection of these design wind speeds have differing response characteristics and would only provide accurate gust speeds if the so-called gust averaging time, T is correctly matched to the dynamic response of the instrument. However the relationship between the two is still unclear for anything but a single sinusoidal frequency input. (Wieringa, 1976).

A knowledge of the variation of maximum gust speed with averaging time would thus allow a means of standardising peak gust speeds obtained from different types of anemometers and in flows of different turbulence intensities. Conversely, the turbulence intensity could be estimated directly from the peak gust speeds recorded by conventional anemometers which otherwise would require more elaborate fast-response equipment.

2.3 CONCLUSIONS

* The characteristics of the air flow over flat homogeneous terrain is well understood for neutrally stable conditions and have been summarised above.

* Under neutral conditions over open rural terrain the main flow parameters may be expected to have values approximating to those listed below.

Surface roughness length	z_o	= 0.05 m
Power law exponent	α	= 0.19
Longitudinal turbulence intensity	$\frac{\sigma_u}{\bar{V}}$	= 0.21
Lateral " "	$\frac{\sigma_v}{\bar{V}}$	= 0.15
Vertical " "	$\frac{\sigma_w}{\bar{V}}$	= 0.09
RMS/friction velocity,	σ_u/V_*	= 2.5
" " "	σ_v/V_*	= 1.87
" " "	σ_w/V_*	= 1.25
RMS ratios	σ_v/σ_u	= 0.75 - 0.69
" "	σ_w/σ_u	= 0.50 - 0.43

Reynolds stress $\dfrac{\overline{uw}}{\sigma_u \cdot \sigma_w}$ = -0.285

Longitudinal Length scales L_{ux} = 80 m

Lateral " " L_{vx} = 25 m

Vertical " " L_{wx} = 3.5 m

Peak gust from Dines anemometer $\hat{V}/\bar{V}$ = 1.5

* Very little energy was evident in the longitudinal and lateral power spectra beyond the wave number band $0.025 < \frac{n}{\bar{V}_Z} < 0.25$ ($0.25 < n < 2.5$ Hz for $\bar{V}_Z$ = 10 m/s) and $0.25 < \frac{n}{\bar{V}_Z} < 2.5$ for the vertical spectrum.

* Thermal effects in the atmospheric boundary-layer can have a profound effect on the flow parameters in wind speeds even as high as 7 - 10 m/s.

CHAPTER 3

MODIFICATION OF THE WIND FLOW BY HILLS:- A REVIEW

The majority of interest in the effects of uneven topography on the wind flow close to the ground has been stimulated by the question of wind power potential at specific sites in hilly terrain. The most comprehensive earlier works on this subject have been produced by Putnam (1948) and Golding (1955). However these projects involved site situations which were unique in character which together with the inadequate record of the upwind atmospheric conditions, make it impossible to draw any generalised conclusions from the mass of accumulated data. A later review of current knowledge on wind power was contained in the WMO Technical Note No. 63 (1964). The section on topographical effects consisted mainly of a review of conventional meteorology as it applied to wind machines. According to Meroney (1976) which provides a useful and up to date historic background to wind turbine siting in hilly terrain, this WMO publication offered very little guidance and stimulus to research on this subject and coincided by chance with a waning in interest in wind power which extended into the early 1970's.

However, a number of model and field tests of wind flow over uneven topography have been completed for a variety of purposes from which a certain amount of information may be obtained. The more significant projects under this category have been listed by Meroney et al (1976). Shellard (1963) quoted from general meteorological experience to suggest a method of predicting the wind speed over an exposed ridge for the purposes of estimating the wind loads on structures, but very little in the literature has since been devoted to this problem. The main body of information available today has come during only the last five years since the recent revival of interest in wind energy. One of the most significant contributors to the recent research progress in the understanding of wind characteristics over complex terrain has been the Colorado State University which has published during 1977-78 a set of comprehensive reports of theoretical, field and model studies such as Bouwmeester et al (1978) for example.

The main parameters likely to be significant in determining the nature of the wind flow over complex terrain (Bowen, 1977) may be

summarised as

Geometric shape of the hill.

'Second order' surface features of the hill slopes such as the slope curvature at the crest and minor bumps.

Scale of the hill compared with the atmospheric boundary-layer depth.

Three-dimensional effects such as ridge length, nearby valley systems and shelter from upwind hills.

Angle of incidence between wind direction and crest line.

Surface roughness of the hill slopes.

Flow separation behind the hill crest and effect of the leeward slope.

Wind speed-height profile upwind of the hill.

Thermal stability of the atmospheric boundary-layer.

Local heating of the flow by sunny hill slopes.

The variety and obviously inter-related nature of the parameters involved make the task of accurately predicting a certain wind flow at a hilly site a very difficult one to accomplish. The purpose of this chapter is to review the more recent and significant literature on the subject and to gather information that would indicate the nature and relative importance of these parameters on the mean wind speed and turbulence characteristics close to the ground.

The modification to the mean wind speed at a particular height above local ground level over a hill may be expressed as the Amplification factor. This may be defined as the mean wind speed at a height Z above local ground level divided by the mean wind speed of the undisturbed flow at the same height above flat ground, upstream of the hill. Using the notation in Fig.3.1 then

$$A_Z = \frac{\bar{V}_Z}{\bar{V}_{REF\,Z}} \qquad 3.1$$

The amplification factor is then a direct measure of the increase in exposure of a structure due to its siting on a hill rather than on flat terrain. Alternatively, the local mean velocity $\bar{V}_Z$ may be expressed in terms of the upwind velocity at the same elevation, $\bar{V}_{Z+H}$ as recommended by Shellard (1963), forming the Speed-up factor S, so that

$$S = \frac{\bar{V}_Z}{\bar{V}_{REF\,Z+H}} \qquad 3.2$$

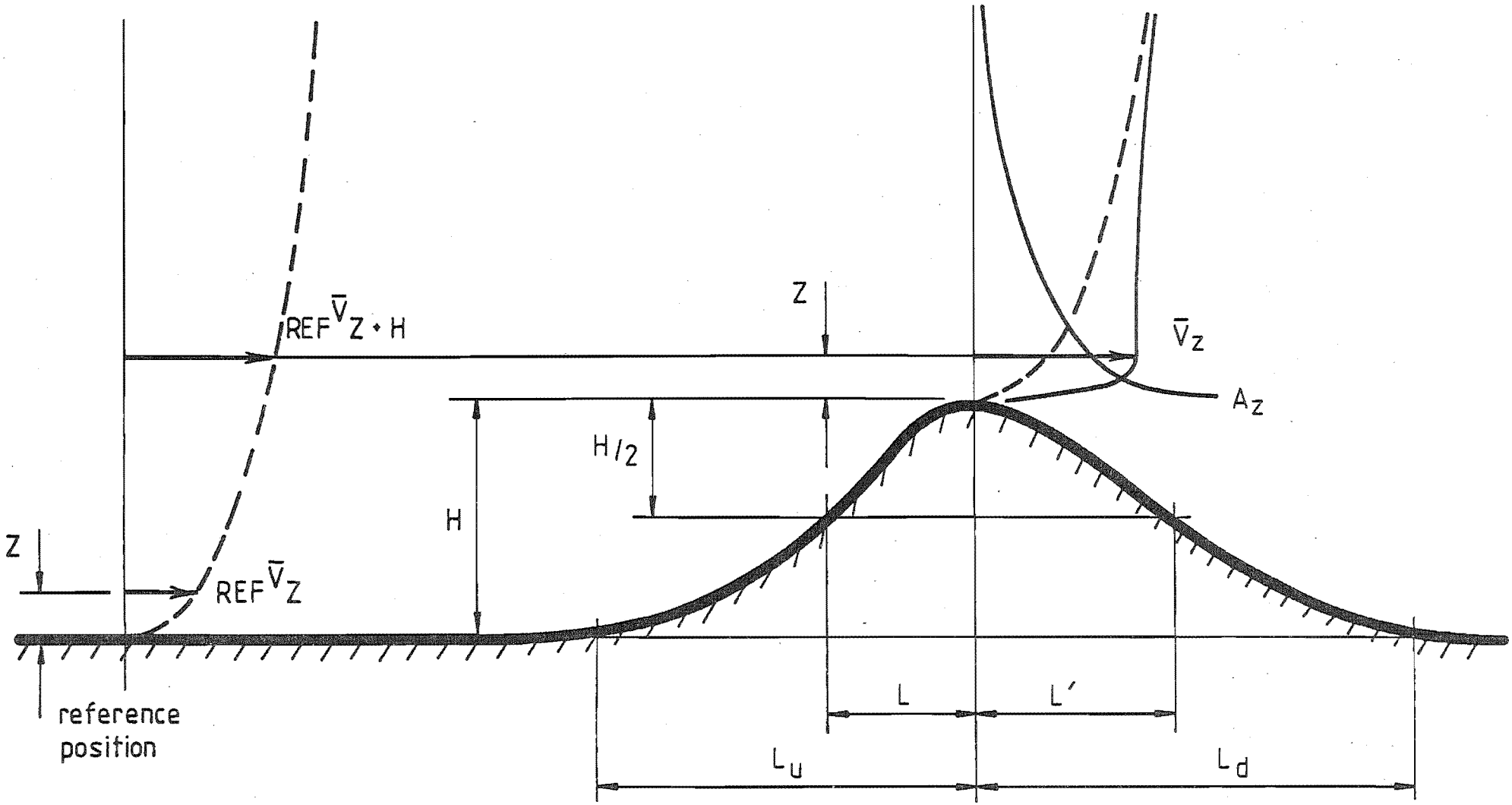

FIG 3·1 NOTATION DESCRIBING THE VARIATION IN MEAN VELOCITY OVER A HILL.

However the value of $_{REF}\bar{V}_{Z+H}$ is difficult to measure for anything but a low hill and extrapolation from measured velocity profiles at a lower height range is open to large errors. The Fractional speed-up factor, ΔS has found common use however, which is defined as

$$\Delta S = \frac{\bar{V}_Z - {}_{REF}\bar{V}_Z}{{}_{REF}\bar{V}_Z} \qquad 3.3$$

In this report ΔS and A_Z are used where convenient and may be considered to be interchangeable using the relation

$$\Delta S = A_Z - 1 \qquad 3.4$$

3.1 THEORETICAL SOLUTIONS

A number of theoretical solutions for the behaviour of the mean wind speed over a hill have been reported recently using numerical analysis techniques and analytical models with mixed success. The numerical solutions may prove to be the most efficient way of obtaining actual values from a wind flow problem but the analytical models have the great advantage of suggesting likely expressions for engineering predictions such as design code rules.

The accuracy of each solution remains largely unproven due to the lack of full scale information as to the magnitude and range of values encountered and due to the severe limitations that are inevitably placed on the solution during the analysis. Recent work by Jackson and Hunt (1975) indicated that the changes in shear stress were significant only in an inner layer close to the ground while outside, the flow behaved in an irrotational fashion predicted by simple potential flow theory. It was therefore felt necessary to include some of the more simple solutions in this discussion as accuracy in prediction is not always indicated by the degree of complexity of the solution.

3.1.1 Ideal Flow Solutions

Classical analytical solutions to a source and sink of equal strength in a uniform horizontal flow was used by Golding (1955) to predict the flow velocity near a two-dimensional semi-circular hill of height H (= a, radius of cylinder) placed normal to the flow. It may be shown that the resulting amplification factor above the crest of the hill is given by

$$A_Z = 1 + \frac{H^2}{(Z+H)^2} \qquad 3.5$$

A maximum value of $A_Z = 2.0$ therefore occurs on the surface of the hill at the crest. For more gradual hills, a streamline boundary say $\psi = P$ may be used to define the hill shape. Golding repeated the analysis for a hemispherical hill where now,

$$A_Z = 1 + \frac{H^3}{2(Z+H)^3} \qquad 3.6$$

A maximum value of $A_Z = 1.5$ occurs on the surface of this circular hill at the summit. By plotting out the streamlines over the long semi-circular and hemispherical (circular) hills and adopting certain streamline boundaries, the fractional speed-up ratios shown in Fig. 3.2 were obtained. Golding pointed out that when a wind was blowing across a ridge, the values of ΔS were greater than those over a circular hill and fell away more slowly with height above the summit. However circular hills would exhibit this value for all wind directions in contrast with the two-dimensional ridge. It may also be inferred that the greater ΔS values from a steep hill disappeared more quickly with increasing height above the summit than that produced by a more gradual slope.

A hill profile may also be generated using Rankine's method involving the stagnation streamline created by a source of strength, m in a uniform horizontal stream of velocity, V. If the ultimate height of the source ramp is $H = m/2V$, it was shown by Bartowski (1963) that the lines of constant velocity over this surface could be represented by a family of circles. It may also be shown that lines of equal A_Z are also represented by a family of circles which may be plotted as in Fig.3.3, giving a maximum surface value of $A_Z = 1.27$.

3.1.2 Frozen Vorticity Solutions for Rotational Flow

For a mean horizontal velocity, $\bar{u}$ and vertical velocity component, $\bar{w}$ in an incompressible two-dimensional, rotational flow, the voriticity ξ is defined as

$$\bar{\xi} = \frac{\partial \bar{w}}{\partial x} - \frac{\partial \bar{u}}{\partial z} \qquad 3.7$$

By introducing the stream function ψ which is defined by

$$\bar{u} = + \frac{\partial \bar{\psi}}{\partial z} \quad \text{and} \quad \bar{w} = - \frac{\partial \bar{\psi}}{\partial x} \qquad 3.8$$

equation 3.7 may be re-expressed as an elliptic Poisson equation,

$$\frac{\partial^2 \bar{\psi}}{\partial x^2} + \frac{\partial^2 \bar{\psi}}{\partial z^2} = \nabla^2 \bar{\psi} = - \bar{\xi} \qquad 3.9$$

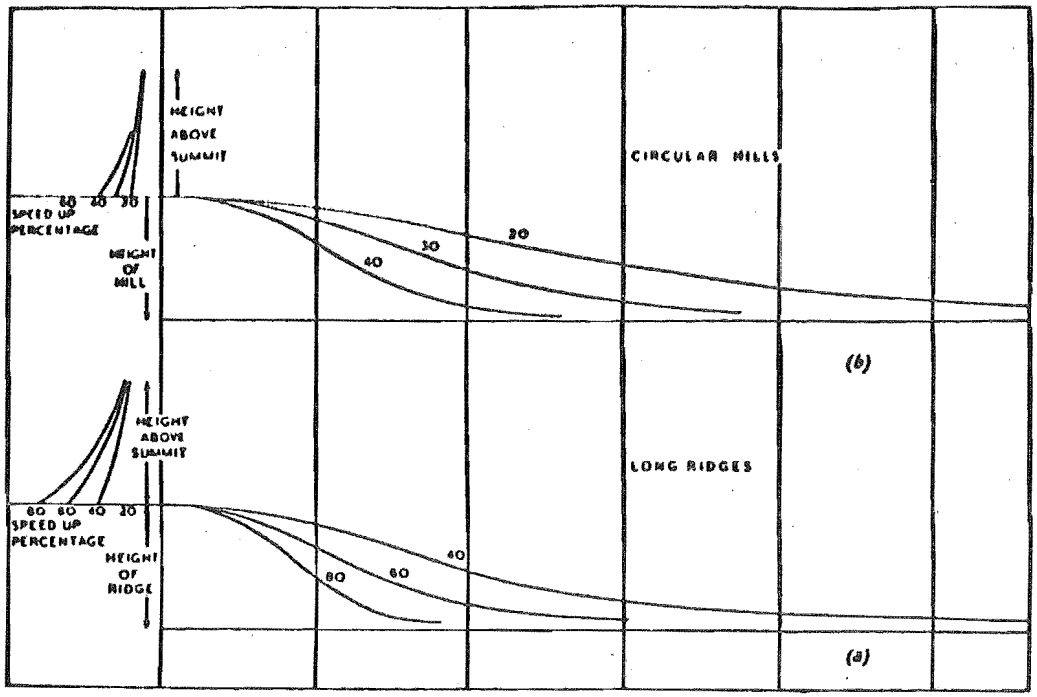

FIG 3·2 FRACTIONAL SPEED-UP CURVES FOR CIRCULAR HILLS AND LONG RIDGES OF VARIOUS SLOPES, GOLDING (1955)

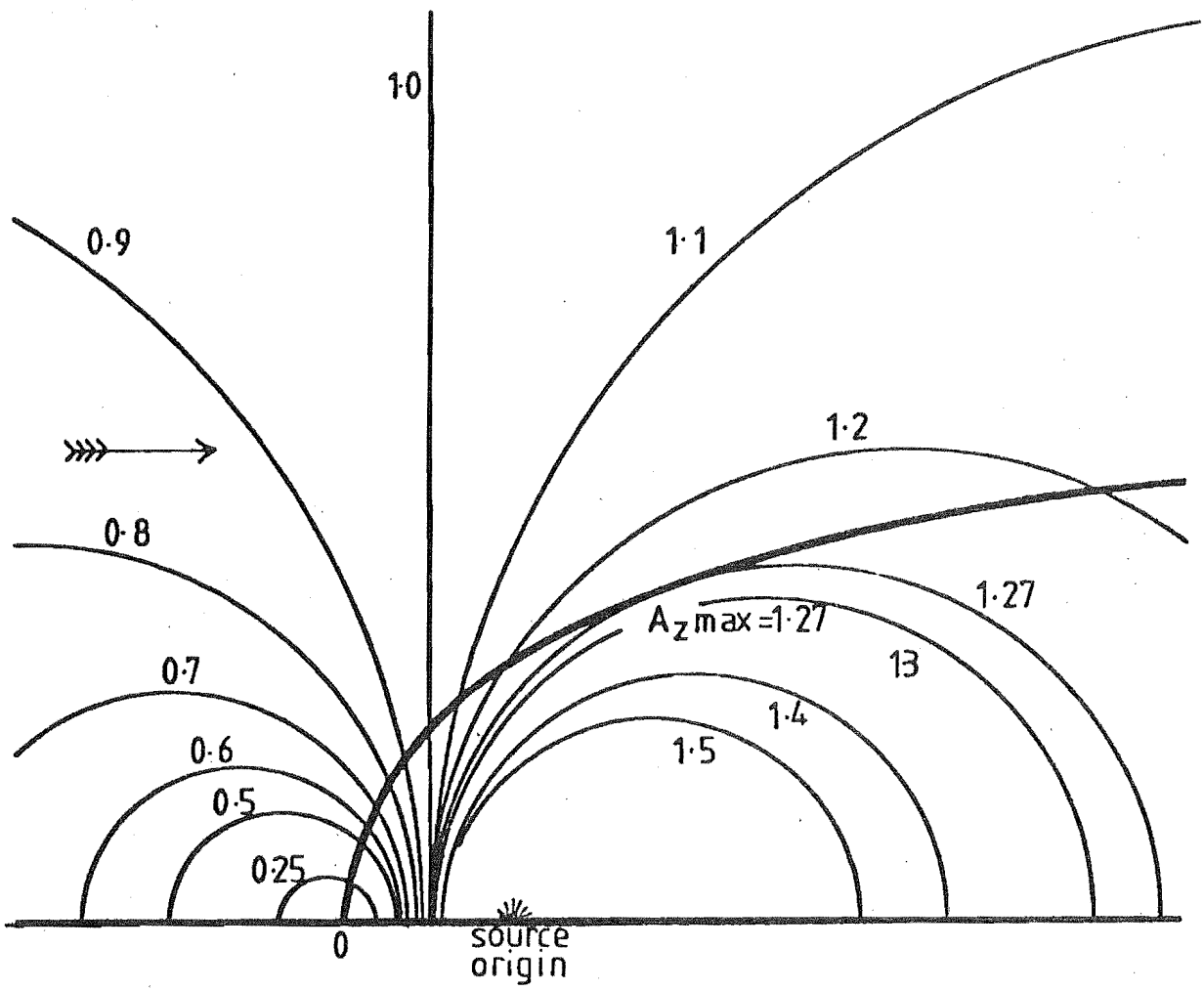

FIG. 3·3 CONTOURS OF EQUAL AMPLIFICATION FACTOR NEAR THE SURFACE CREATED BY A SOURCE IN A UNIFORM POTENTIAL FLOW.

Boundary-layer theory is normally used for the analysis of viscous flows to describe the relatively slow modification and development of the flow due to the vorticity diffusing action of viscosity. Techniques of this kind will be discussed later and are characteristicly confined to the accurate analysis of the flow close to the surface of small obstructions with gradual slopes. However for flows over large surface obstructions where the surface changes are relatively abrupt, the resulting effects on the flow are so sudden that the Reynolds stress terms have little effect on the flow apart from the flow in an inner layer close to the surface (Jackson and Hunt, 1975). The principal influences on the flow are due to the obstruction and the flow may be considered to be non-viscous near these boundary changes. Viscosity in this case may be considered to be only a generator of the initial vorticity and the velocity-height profile of the upstream flow. Once the oncoming flow is thus defined at a boundary which is considered far enough upstream to be uninfluenced by the boundary change in question, no further effects of viscosity need be considered and the vorticity is then assumed to remain the same along each streamline over the obstruction. The vorticity in the flow field is therefore considered to be 'frozen' along each streamline and is purely a function of the stream function, ψ which is defined by the velocity-height profile adopted at the upstream boundary. This approach has been justified by Robertson (1965) and has been used successfully by Walker (1957), Yih (1959) and others.

A matrix of simultaneous equations (3.9) may be set up at each grid point in the flow field and solved using matrix inversion techniques, but this method has the disadvantage of requiring a large computer memory if a large number of grid points is employed as is normally the case. Finite difference techniques may also be used assuming that $f(\psi)$ is a single valued, finite and continuous function. Using Taylor's theorem and neglecting second order and higher terms,

$$f'(\psi) = \frac{f(\psi+h) - f(\psi)}{h}$$

and

$$f''(\psi) = \frac{f(\psi+h) + f(\psi-h) - 2f(\psi)}{h^2} \qquad 3.10$$

The central difference equation 3.10 may be used in a two-dimensional mesh representing two independent variables x and z of which ψ is a function.

Let $x = ih$ and $z = jk$

then $\psi = \psi_{(ih,jk)}$ or $\psi_{(i,j)}$

$$\therefore \quad \frac{\partial^2\psi}{\partial x^2} = \frac{\psi_{(i+1,j)} + \psi_{(i-1,j)} - 2\psi_{(i,j)}}{h^2}$$

and $$\frac{\partial^2\psi}{\partial y^2} = \frac{\psi_{(i,j+1)} + \psi_{(i,j-1)} - 2\psi_{(i,j)}}{k^2}$$

Equation 3.9 describing the distribution of stream function can now be expressed in a finite difference form, which for a square grid becomes

$$4\psi_{(i,j)} \approx \psi_{(i+1,j)} + \psi_{(i-1,j)} + \psi_{(i,j+1)} + \psi_{(i,j-1)} + h^2\xi(\psi) \qquad 3.11$$

Various well established iterative methods such as the Jacobi and Gauss-Seidel methods (Smith, 1975) are available to solve equation 3.11 with various rates of convergence and computer efficiency.

As an example of this method and to obtain a 'first order approximation' of the flow velocity speed-up over an escarpment, the central-difference method just described was used to solve the flow field over four different escarpment slopes under uniform potential flow or zero vorticity. Nearly 500 grid points were used with a large square grid size equal to the escarpment height, H for a first approximate solution. The upper boundary was considered to be unchanged at 50 H above the step which gave only a 2% change in velocity due to continuity considerations. The inlet and outlet boundary conditions were uniform velocity profiles at ± 10 H away from the step and $\bar{w}_{in} = \bar{w}_{out} = 0$. After the large grid network had been solved, the calculated stream functions along the grid points 2H above the escarpment were used as the boundary conditions for the next smaller grid layout below that height, using escarpments of different slopes. The results from these calculations are summarised in Fig.3.4 which indicates the general behaviour and extent of the flow speed-up over the escarpment and shows in particular, only a weak trend of increasing A_z with slope angle.

The logical step from the uniform approach situation just described is to introduce a certain velocity profile at the inlet and outlet boundaries, thus defining the stream function and causing a real vorticity-height variation. Unfortunately the use of a logarithmic or power law profile produces infinite vorticities at ground level and subsequent convergency problems in the iterative solution.

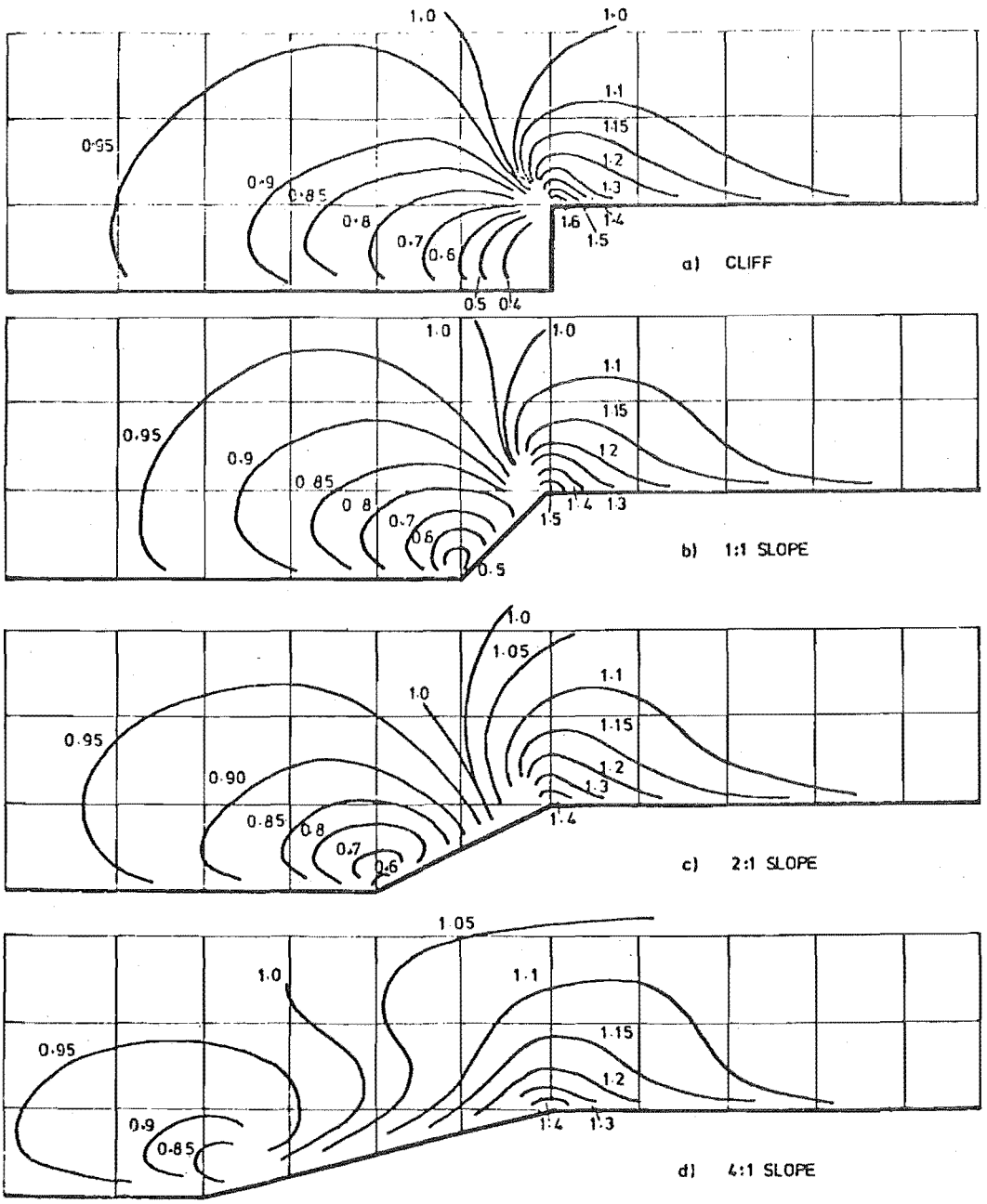

FIG 3·4 CONTOURS OF EQUAL AMPLIFICATION FACTOR, A_z FOR VARIOUS SLOPES CALCULATED FOR UNIFORM POTENTIAL FLOW.

However a sine velocity-height profile may be used (Yih, 1959) as it provides a simple expression for vorticity with finite values at the ground but it is not a profile that is found in practice. The other alternative adopted by Walker (1952) and others is to modify the profile close to the ground (say a linear variation with a wall velocity), to obtain a finite vorticity at the surface. Walker (1957) went on to solve the flow using a power law profile $\alpha = 0.12$ over a slender arc body normal to the flow ($^{H}/L = 0.48$). He found a maximum value of A_Z at 0.1 H of 1.57 ($\Delta S = 1.19\,^{H}/L$) which dropped in value quickly with increasing height to a value of 1.08 at 2 H above the crest. The peak velocities varied considerably with the hill height to boundary-layer height ratio. Similar results were also reported from his model experiments. Taulbee and Robertson (1972) found good agreement with model tests using this method when investigating the flow separation in front of a forward facing step, although the separated flow is sensitive to the arbitrary choice of wall velocity.

Astley (1977) solved equation 3.9 in the flow field over various hill shapes with a power law velocity profile using finite element techniques and obtained good agreement with the wind tunnel data from Bowen and Lindley (1977), except in areas of high turbulence downwind of the crests. Some of the results are shown in Fig.3.5 compared with wind tunnel data which used a power law profile, $\alpha = {}^{1}/6$ and demonstrate a very promising technique.

3.1.3 Solutions Using the Equations of Motion

Most attempts to predict the flow over hills have used numerical techniques to solve the equations of motion using a variety of closure assumptions to achieve an approximate solution and neglecting Coriolis and buoyancy effects. No models have yet accurately predicted the flow field near regions of flow separation but this may not be so important for the flow over hills where unique features or buildings could seriously affect the extent of separation anyway. The details of the various closure assumptions and the mathematical prediction procedures have recently been discussed by Bouwmeester et al (1978).

Alexander and Coles (1971) were one of the first to publish a theoretical study of the flow over a low two-dimensional hill using a rather unrealistic constant eddy-viscosity assumption. Results showed that the influence of the hill on the flow extended up to 4 H above the crest, with higher velocities at a certain height from upstream velocity profiles of lower exponent, α using the same gradient velocity.

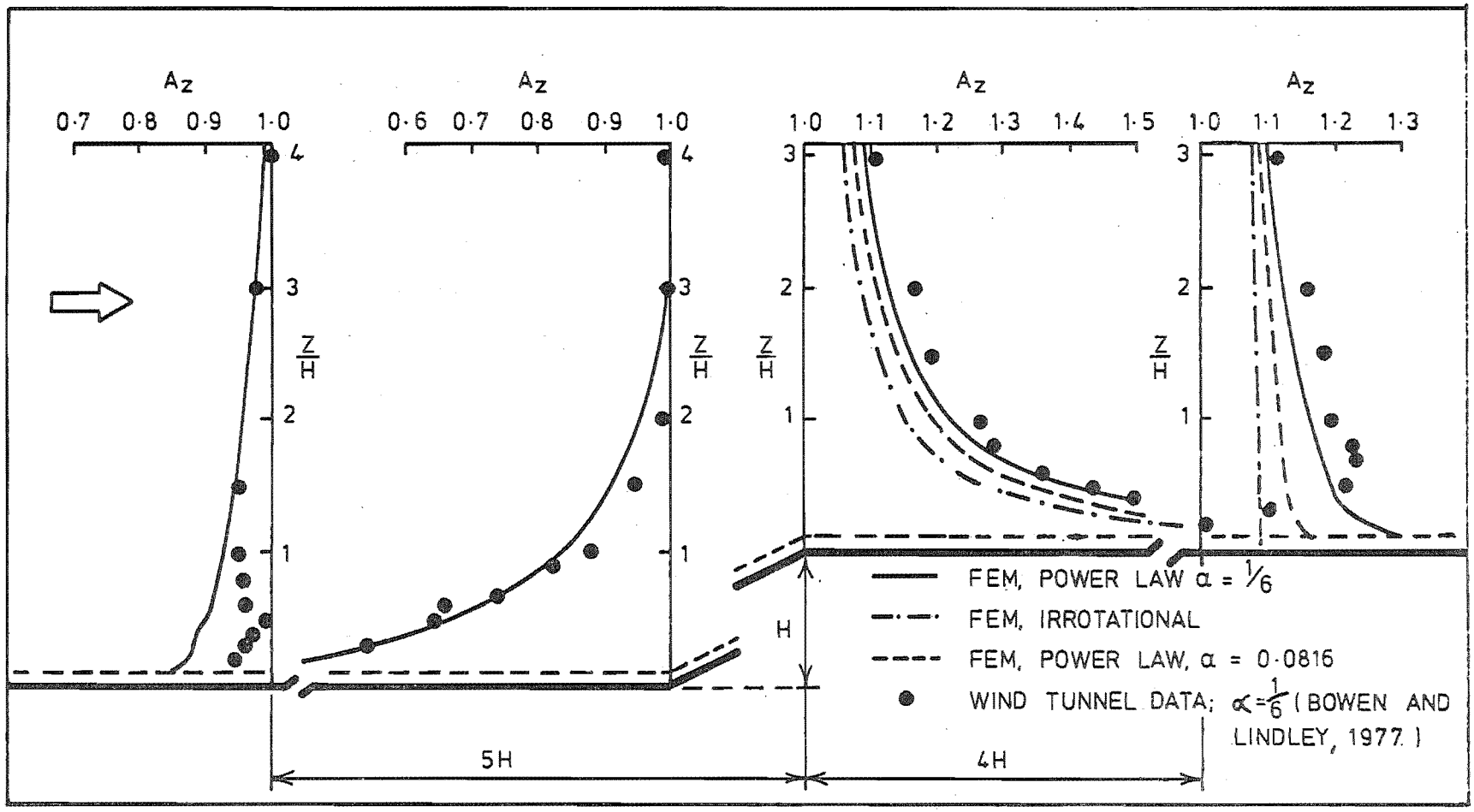

FIG. 3·5 THE VARIATION OF AMPLIFICATION FACTORS WITH HEIGHT OVER A 2:1 ESCARPMENT NORMAL TO THE FLOW, CALCULATED BY A FINITE ELEMENT FROZEN VORTICITY SOLUTION AND COMPARED WITH WIND TUNNEL DATA. (ASTLEY, 1977)

Taylor and Gent (1974) reported a theoretical study of unseparated flow over a low hill using conformal mapping of the flow region and two alternative models to close the equation, based on a mixing length model and a turbulent energy equation model. It was shown that the hill gave rise to an increase in the horizontal shear stress on the surface in a very shallow inner layer (200 Z_o) compared with the upper layer in which the shear stress was reduced. The extreme values of shear stress and surface pressure showed a rapid increase with hill height in a strongly nonlinear fashion. The results supported the conclusion of Jackson and Hunt (1974) that just above the top of the hill, (see Fig.3.1)

$$\Delta S_{max} \approx 2 \frac{H}{L} \qquad 3.12$$

However the values of ΔS were somewhat higher than that indicated by equation 3.12 for the larger hills considered, but the values always decreased rapidly with height above the ground.

In order to cope with prospective problems involving more complex topography, a further solution had been developed, (Taylor, 1977a) using a more sophisticated mapping technique and the preferred turbulent energy closure assumption. Results presented showing the variation in surface shear stress, surface pressure and velocity-height profiles over Gaussian shaped hills and valleys and smooth sloping escarpments compared well with his earlier method. It was noticed (Fig.3.6) that the detailed shape of the escarpment ramp had a pronounced effect on the distribution of surface shear stress to which the amplification factor was clearly related. The two escarpments considered were a $\tan^{-1}$ curve as used by Sacré (1975)

$$Z_b = \frac{\alpha}{\pi} \tan^{-1} \frac{x}{\beta} \qquad 3.13$$

and a sine ramp as used by de Bray (1975) and Freeston (1974)

$$\begin{aligned} Z_b &= -\frac{\alpha}{2} && \text{if } x \leqslant -\beta \\ &= \frac{\alpha}{2} \sin \frac{\pi x}{2\beta} && \text{if } -\beta < x < \beta \\ &= \frac{\alpha}{2} && \text{if } x \geqslant \beta \end{aligned} \qquad 3.14$$

Maximum velocities occurred near the top of the 4:1 sine ramp ($\frac{H}{L} = 0.5$) with a maximum amplification factor of 1.5 close to the ground so that for this case then, $\Delta S_{max} = 1.0\ ^{H}/L$.

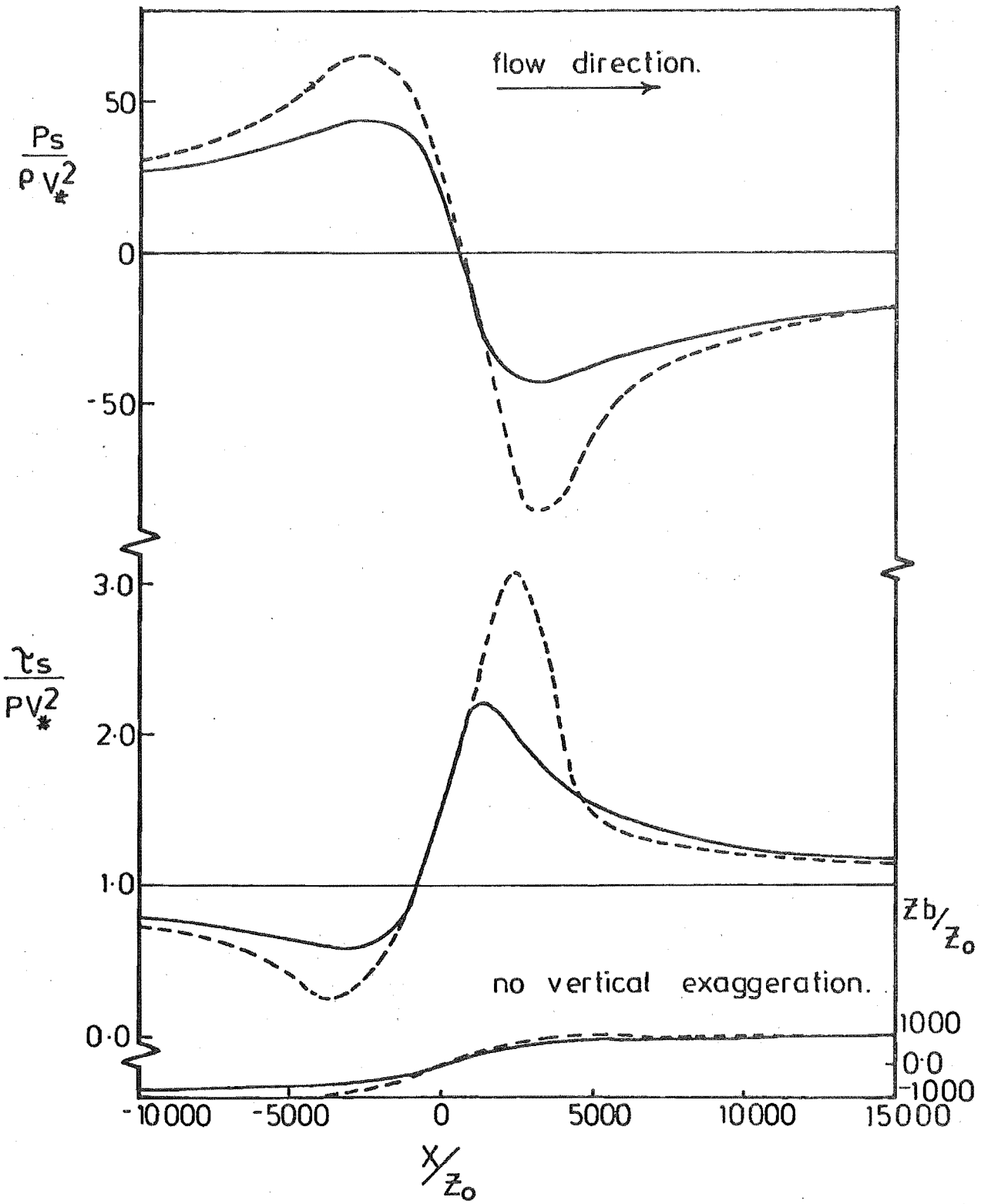

FIG. 3·6 SURFACE SHEAR-STRESS AND PRESSURE RESULTS FOR SLOPING ESCARPMENTS; ——— TAN-1 ESCARPMENT, $\alpha = 2000 z_o$, $\beta = 2000 z_o$; - - - - 1 IN 4 SINE RAMP, $a = 2000 z_o$, $\beta = 4000 z_o$. (TAYLOR, 1977$_a$)

A further extension of this technique was reported by Taylor (1977b) which was able to cope with larger horizontal hill scales of the order of 1 km by modifying the basic assumptions of the flow beyond the constant shear stress layer. A range of thermal conditions under which thermal effects could be neglected was also established. The results obtained were similar to those from the earlier models but with the inclusion of the cross wind velocity component, the effect of different wind angles to the ridge line could be investigated. It was shown for an oblique slope, that the wind direction turned to strike the hill at an angle closer to the normal than the overall wind direction (see Fig.3.7 for an oblique forward facing escarpment), with a corresponding readjustment in the other direction behind the summit. Changes in surface wind direction of up to 20 - 25° over the upwind slopes were predicted in some of the situations considered. The largest shear stress values and surface pressure changes occurred when the wind flow was approximately normal to the crest of the hill. Consequently, the impact of the topography on the flow would be lessened as the direction of the mean flow became more oblique to the ridge line.

Frost et al (1974) reported a numerical solution using a mixing-length closure assumption and later Frost et al (1975) reported a similar solution using a turbulence kinetic energy model for the flow over 2D semi-elliptical surface obstructions normal to the flow. The results offered for a 2:1 ($^{H}/L = 0.577$) and 4:1 ($^{H}/L = 0.289$) ellipse were similar and yielded approximate peak A_Z values at the crest of 2.3 ($^{Z_o}/H = 0.005$) and 2.14 ($^{Z_o}/H = 0.02$) for the 2:1 ellipse and 1.65 ($^{Z_o}/H = 0.005$) and 1.8 ($^{Z_o}/H = 0.02$) for the 4:1 ellipse. Therefore the value of $\Delta S/(^{H}/L)$ ranged from 2.25 - 1.98 for the 2:1 ellipse and 2.25 - 2.77 for the 4:1 ellipse. Above the crest, the peak velocity occurred at a height of $^{Z}/H = 0.3$ for the 2:1 ellipse and $^{Z}/H = 0.6$ for the 4:1 ellipse, below which the velocities were marginally greater above the windward slope in both cases. Although the accuracy of the model was in doubt in the vicinity of the stagnation regions, it was noticed that a decrease in the elliptical aspect ratio and an increase in the surface roughness caused larger separation regions.

The flow of air over a smooth two-dimensional surface obstruction, with no steep slopes likely to cause separation ($^{H}/L < 0.7$) and a height well below that of the boundary-layer depth has also been investigated by Sacré (1974,1975). The flow over an obstacle was first

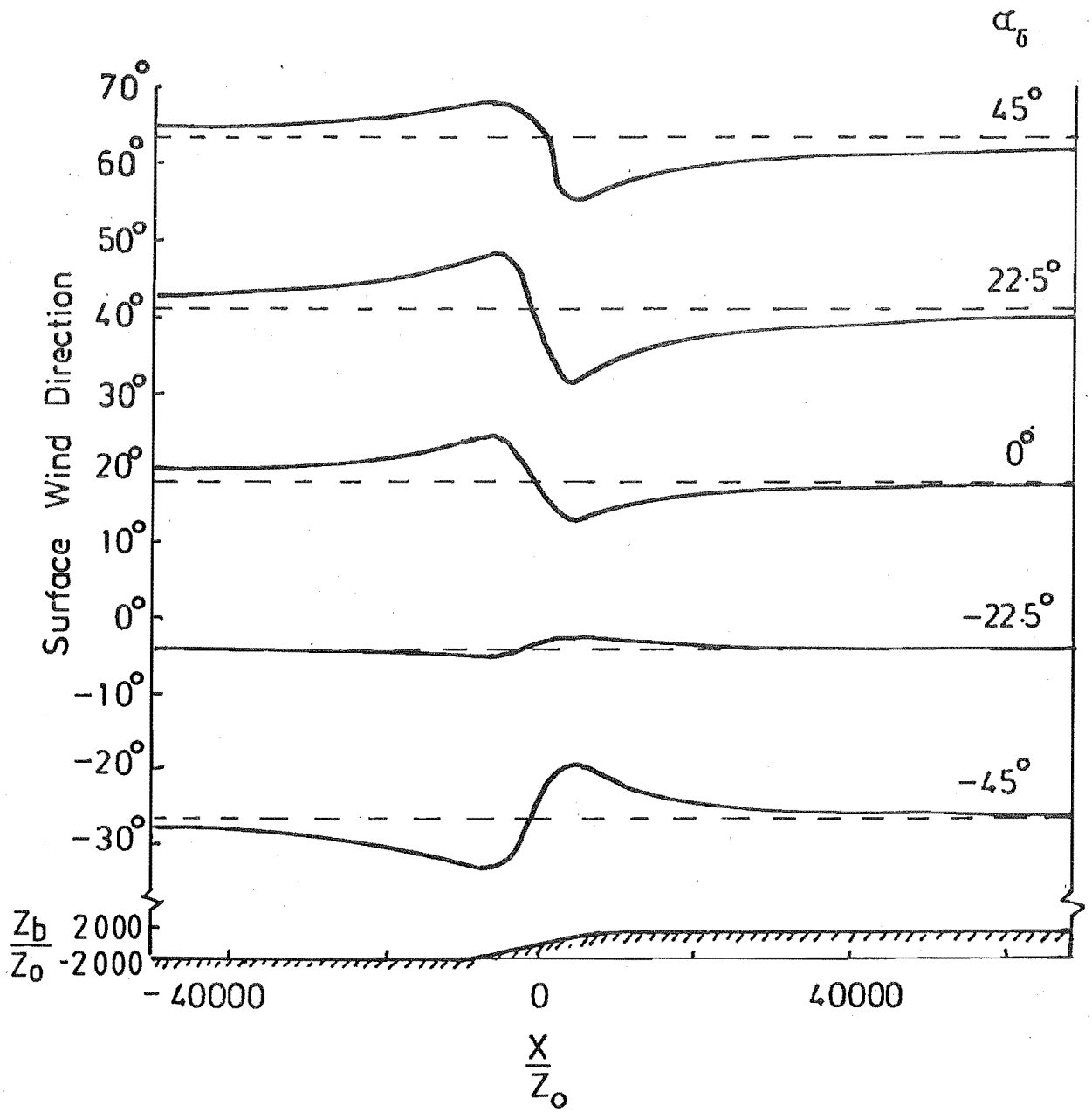

FIG 3·7 SURFACE WIND DIRECTION FOR FLOW AT DIFFERENT ANGLES TO A TAN^{-1} ESCARPMENT, $a = \beta = 4000\ Z_o$. (α_δ = DIRECTION OF GRADIENT WIND) (Taylor 1977b)

calculated analytically using small perturbation theory developed for mountain wave analysis and assuming that the obstacle could be defined by a series of sinusoids (Sacré, 1974). The introduction of turbulence effects was based on the assumptions that the shear stress was a linear function of the along-wind components of turbulent energy and that transfer of turbulent energy across the streamlines was negligible near the obstacle. The velocity distribution was obtained using Prandtl's mixing-length hypothesis and a non-zero ground velocity. This theoretical model was developed further by Sacré (1975) by re-examining the assumptions made and using a numerical analysis solution to cope with hills of any shape. The aim of the numerical method was not to give an accurate explanation of the phenomenon, but to predict correctly for engineering applications, the magnitude and extent of the region where speed-up effects occurred over any smooth hill shape.

In a neutrally stable boundary-layer, it was shown that the surface shear stress, τ_s over the hill was related to the A_Z value at the ground by

$$A_{(Z=0)} \approx \sqrt{\frac{\tau_s}{\tau_o}} \qquad 3.15$$

Typical distributions of shear stress and amplification factor taken from Sacré (1975) for a rounded escarpment shape are shown in Fig.3.8 and show a close similarity in behaviour to the more simple solutions in Figs.3.3 and 3.4. However Sacré's solution situated the maximum speed-up value on the upstream slope of a symmetrical hill contrary to other theoretical solutions such as Taylor and Gent (1974) and Jackson and Hunt (1975). A consistent trend of greater influence on the flow from a short obstruction characterised by an isolated symmetrical ridge, compared with a long obstruction of the same height and upwind slope such as an escarpment or plateau was evident.

Fig.3.9 shows Sacré's results on the influence of the hill shape and upstream velocity-height profile on the maximum speed-up values close to the ground. Quite good agreement with equation 3.12 was obtained considering that significant surface roughness was included in Sacré's results. However, Sacré noted that apart from the average gradient (Fig.3.9a), the less significant but nevertheless important effects of hill height (Fig.3.9b) surface roughness (Fig.3.9c) and the local geometry of the summit should also be considered.

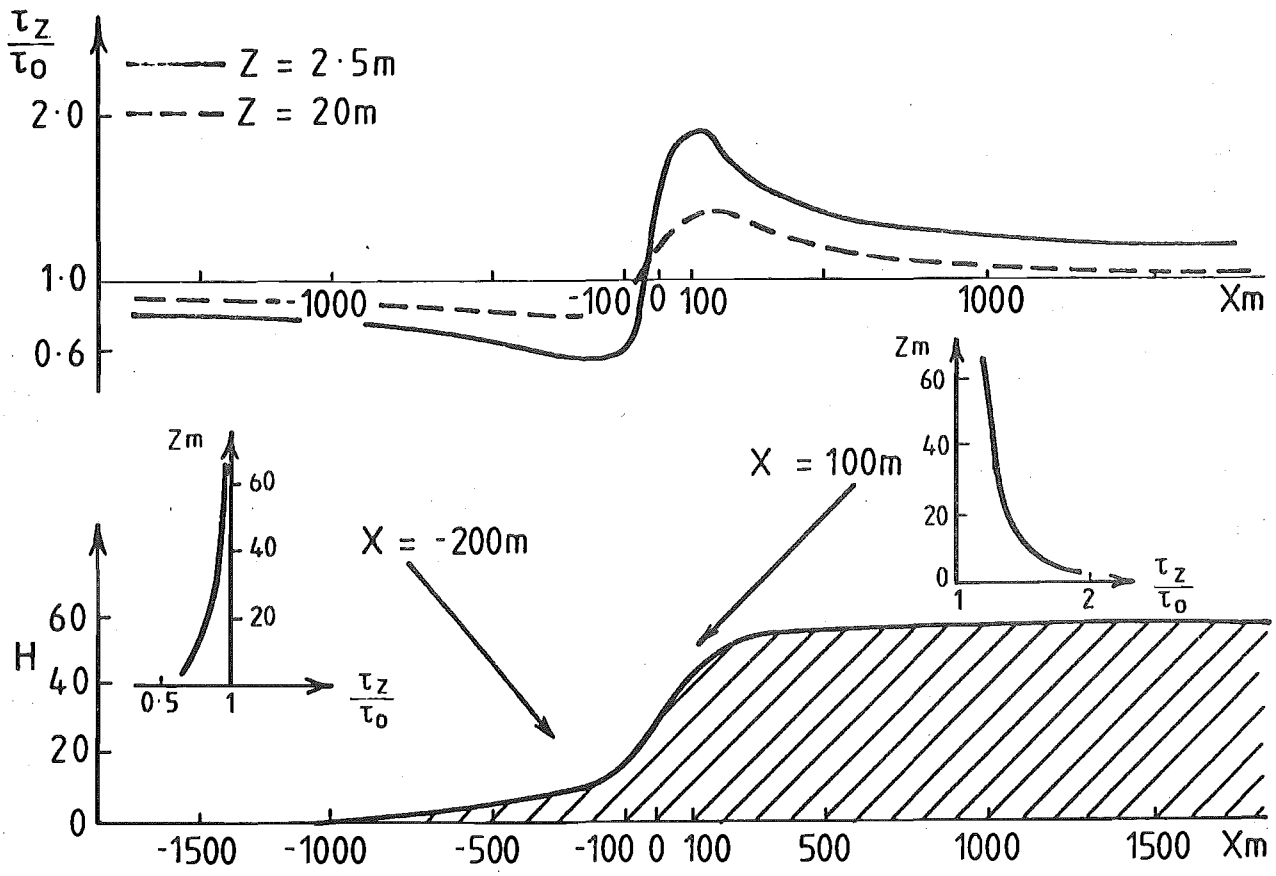

(a) variation of shear stress

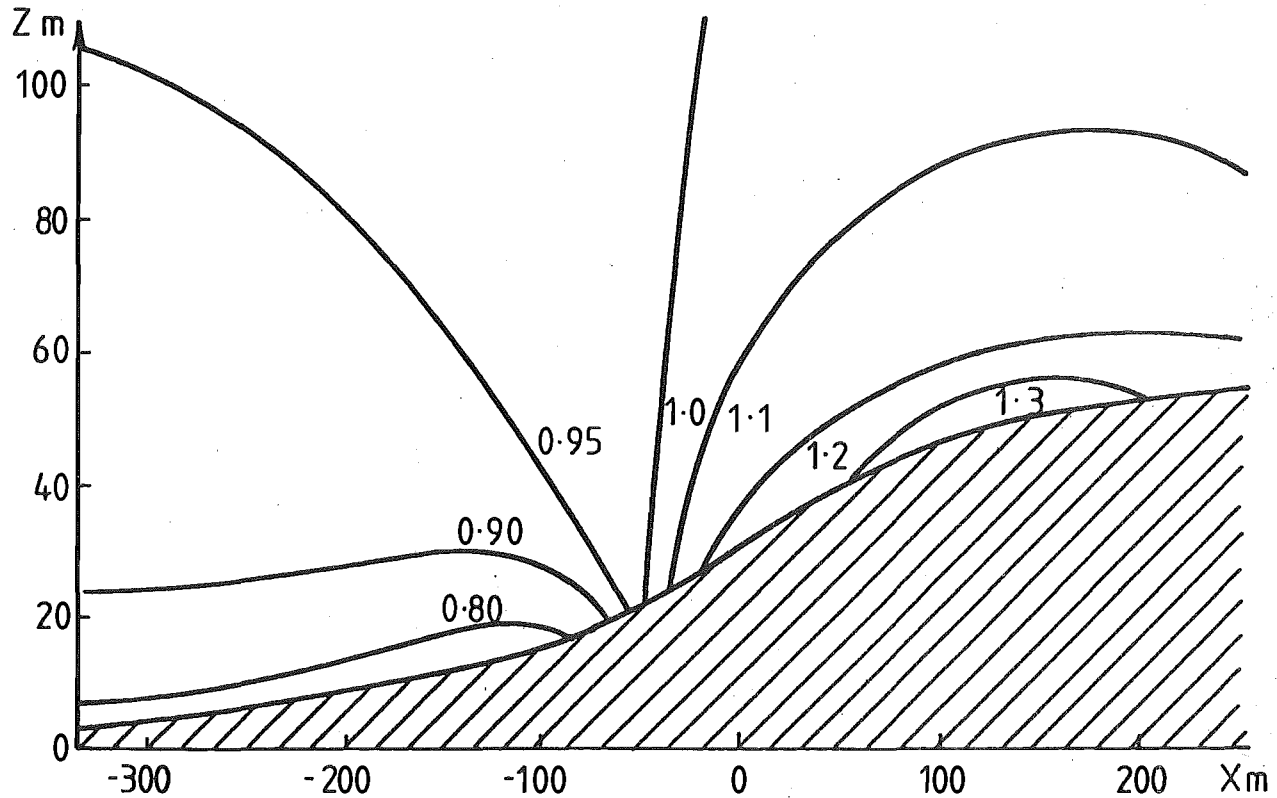

(b) lines of constant amplification factor

FIG 3·8 VARIATION OF SHEAR STRESS AND AMPLIFICATION FACTOR OVER A ROUNDED OBSTRUCTION. (Sacré, 1975)

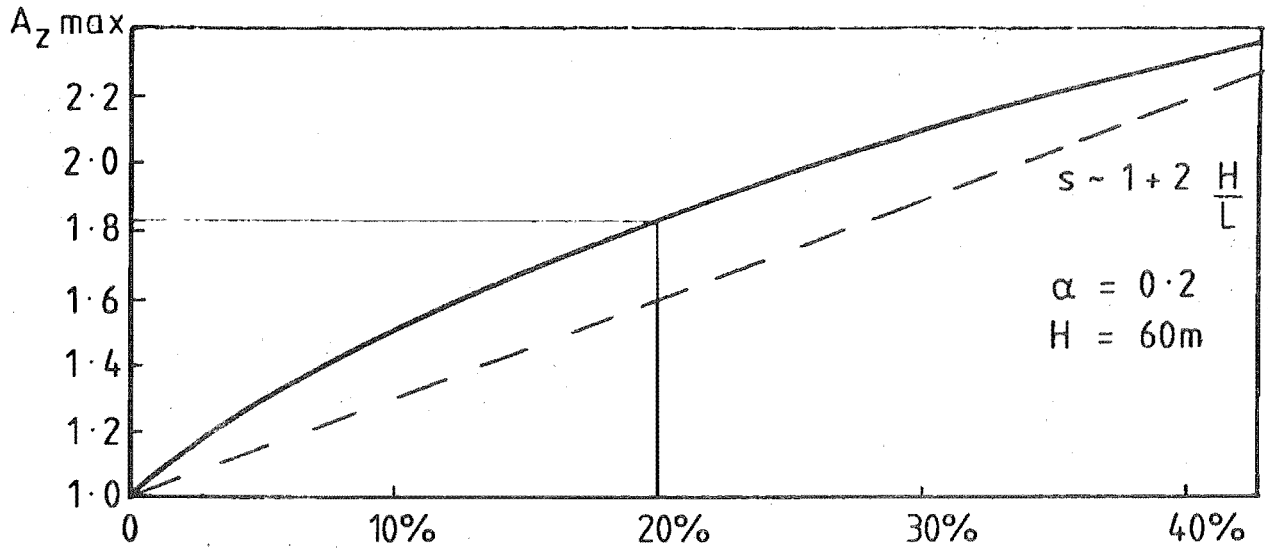

(a) maximum gradient of windward slope

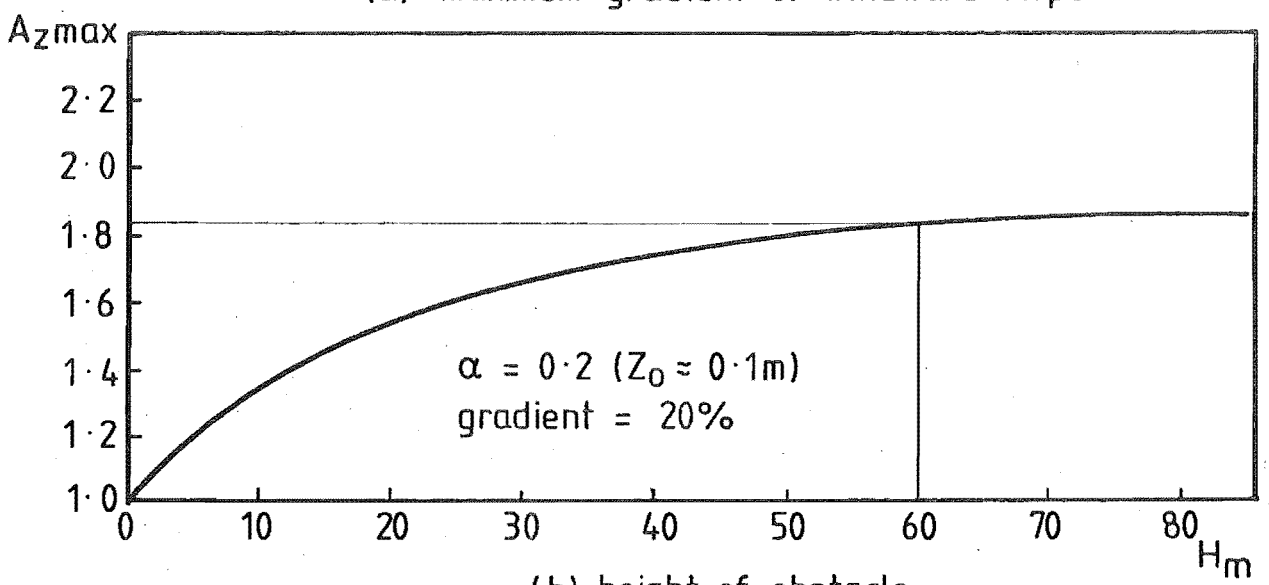

(b) height of obstacle

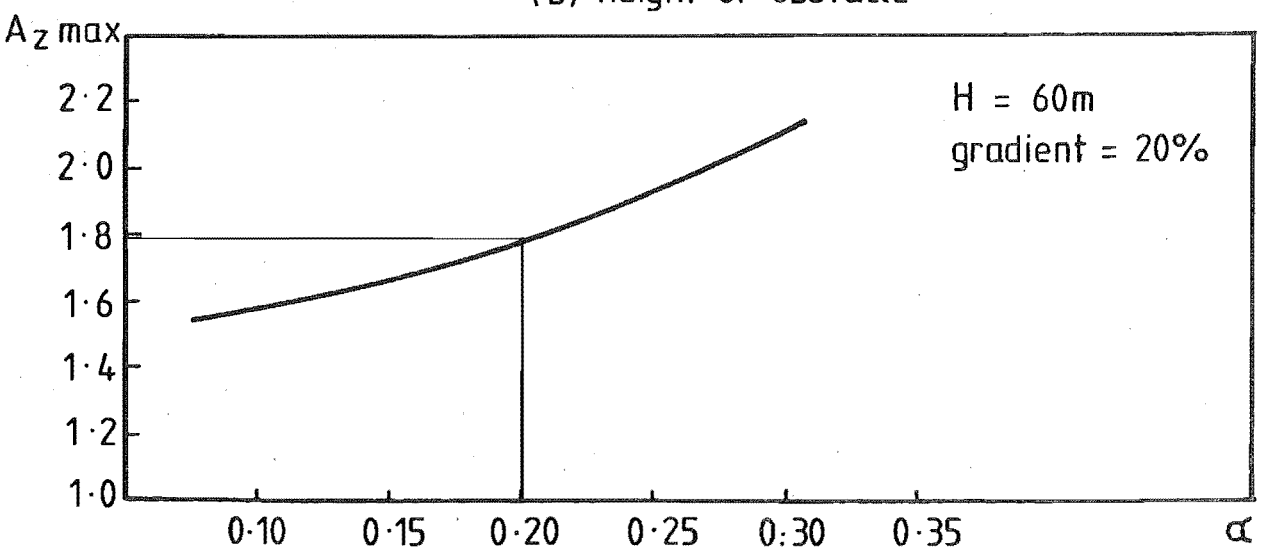

(c) average ground roughness (α = upstream velocity power law exponent)

FIG 3·9 INFLUENCE OF THE FLOW AND OBSTACLE SHAPE ON THE AMPLIFICATION FACTOR AT Z = 2·5m. (Sacré, 1975)

It was shown that the $^{H}/_{L}$ parameter had the most significant role. The obstruction height, H only seemed to be significant for low hills less than about 40 m in height for the particular upstream roughness considered. It was also concluded that an increase in surface roughness and accompanying change in upstream velocity-height profile, could increase the speed-up effects by about 30%. The amplification factor close to the ground was very sensitive to local changes in gradient just upstream of the measurement site, but rather insensitive to changes downwind.

Deaves (1975/1976) solved the equations of motion of atmospheric flow in a finite difference form using numerical techniques. In this way, hills of any shape could be investigated provided that the maximum gradient of hill, $^{H}/_{L} < {}^{1}/_{3}$, $H \leqslant 100$ m and no separation of the flow occurred. Singularities at the ground were avoided by using a variable consisting of the product of flow vorticity and the scalar eddy viscosity. Closure of the equations was accomplished using an adaptation of Prandtl's mixing-length hypothesis. In agreement with Sacré (1975), the equation 3.15 was proven showing the intimate connection of the speed-up close to the ground and the change in surface shear stress.

Jackson and Hunt (1975) presented a very useful analytical solution for the flow of a neutrally stable turbulent boundary-layer over a two-dimensional hill of small curvature. Their findings gave a better understanding of the mechanics of such flows and formed a basis for the formulation of velocity prediction rules for design purposes and for the comparison of experiments. Jackson (1975) extended the theory to include hills of greater slope and investigated the case of a two-dimensional escarpment in detail.

Jackson and Hunt showed that the Reynolds stress variation was negligible in the main part of the boundary-layer where the disturbance due to the hill was almost irrotational. However, close to the surface in an inner region, the eddy viscosity distribution for equilibrium flow near a wall was used to determine the variation in Reynolds stress. The increase in surface stress was found to be surprisingly large, the total stress being doubled on a gently sloping hill where $^{H}/_{L} \approx 0.2$. The pressure perturbation in the outer region was driven by the vertical displacement of the flow in the inner region due to the hill. It was of the same order as that in an inviscid flow driven by a uniform velocity upwind equal to the velocity in the boundary-layer flow at a height equal approximately to the half length of the

hill, L. The pressure perturbation was significantly larger than the pressure change calculated using the velocity at the height of the obstacle, H. This externally generated pressure gradient was used as the main driving force on the inner region flow.

The maximum increase in velocity occurred at the top of the obstacle at a small height above the summit equal to the depth of the inner region, ℓ. This maximum velocity was shown to be approximately equal to the velocity at the same elevation above level ground upwind of the hill, so that $S \approx 1.0$. However S was shown to be highly dependent on the height above ground and the upstream slope. Use of the fractional speed-up ratio, ΔS was preferred which had a maximum occurring at a height of approximately $\ell/10$ at the top of the hill and was not so sensitive to the height above ground. Its magnitude increased slowly with roughness length and was approximately proportional to H/L. From several observations from hills in the range applicable to their theory, it was shown that $\Delta S_{max}/(H/L) \approx 2.0$. compared with potential flow which predicted $\Delta S_{max}/(H/L) = 1.0$.

Jackson (1977) stated that his series solution for the mean velocity outside an inner layer of depth ℓ, described in Jackson (1975) could be written as,

$$\bar{V}_Z = \frac{V_*}{k} \left[\log_e \left(\frac{\tilde{Z}}{Z_o} \right) + H(\tilde{Z}) \cdot \frac{H}{L} \cdot P(\tilde{x}) + \ldots \right] \qquad 3.16$$

for $L/Z_o \to \infty$ and $H/L \ll 1$ where $\tilde{x} = x/L$, the nondimensional horizontal position and

$\tilde{Z}$ = $Z - Hf(\tilde{x})$, local height above hill surface

H = hill height

$Hf(\tilde{x})$ = hill shape.

Also $H(\tilde{Z}) = \log_e \left(\frac{L}{Z_o} \right) - \log_e \left(\frac{\tilde{Z}}{L} \right) + A_2$ 3.17

where A_2 is a constant = +1 from theory but -2.0 from comparison of results quoted by Taylor and Gent (1974).

For an escarpment, $P(\tilde{x}) = \frac{\tilde{x}}{1+\tilde{x}^2}$ 3.18

so that $P_{max} = \frac{1}{2}$ at $\tilde{x} = 1$

($\tilde{x} = 0$ at half hill height position on the upwind slope)

For an embankment, $P(\tilde{x}) = \frac{1-\tilde{x}^2}{(1+\tilde{x}^2)^2}$ 3.19

so that $P_{max} = 1$ at $\tilde{x} = 0$

($\tilde{x} = 0$ at the crest)

Caution was expressed as to the difficulty of defining L as there was no obvious and unique choice, but it had been assumed by Jackson in the above account to be the distance in which the hill fell to half its height. Typical values of the height of the inner layer, ℓ in which the theoretical predictions did not apply were given by Jackson (1975) using

$$\frac{\ell}{L} \log_e \left(\frac{\ell}{Z_o}\right) \approx 2k^2 = 0.32 \qquad 3.20$$

L m	Z_o m	ℓ m
10	0.001	0.5
10	0.01	0.7
100	0.01	5
1000	1	70

TABLE 3.1 TYPICAL VALUES OF THE HEIGHT OF THE INNER LAYER FROM JACKSON (1975)

Typical limits on the hill length were also quoted as :

If Z_G = 400 m and Z_o = 1 m then L << 7,500 m

If Z_G = 100 m and Z_o = 0.0001 m then L << 4,300 m

Using equation 3.16, the most convenient form to express the velocity speed-up would be in terms of ΔS so that

$$\Delta S = H(\tilde{Z}) \cdot P(\tilde{x}) \cdot \log_e^{-1} \left(\frac{\tilde{Z}}{Z_o}\right) \cdot \frac{H}{L} \qquad 3.21$$

The maximum calculated value of ΔS would occur at the minimum height for which the theory holds (being $Z = \ell$) and is therefore very sensitive to the conditions and assumptions that determine the value of ℓ. On the other hand in practice, ΔS_{max} will be shown to occur at the surface making the discussion of ΔS_{max} rather hazardous when comparing field, model and theoretical data.

The prediction method outlined by Jackson (1977) was utilised for the escarpment slopes 2:1, 4:1, 6:1 and 8:1 that had been tested in the wind tunnel (see Chapter 8). It should be noted that the two steepest slopes did not fall within the theoretical restriction $H/L \ll 1$, but were incorporated to allow a comparison with the field tests of the 2:1 escarpment (Chapter 6) using an H = 13 m and Z_o = 0.05 m. The fractional speed-up factors shown in Fig.3.10 were calculated using

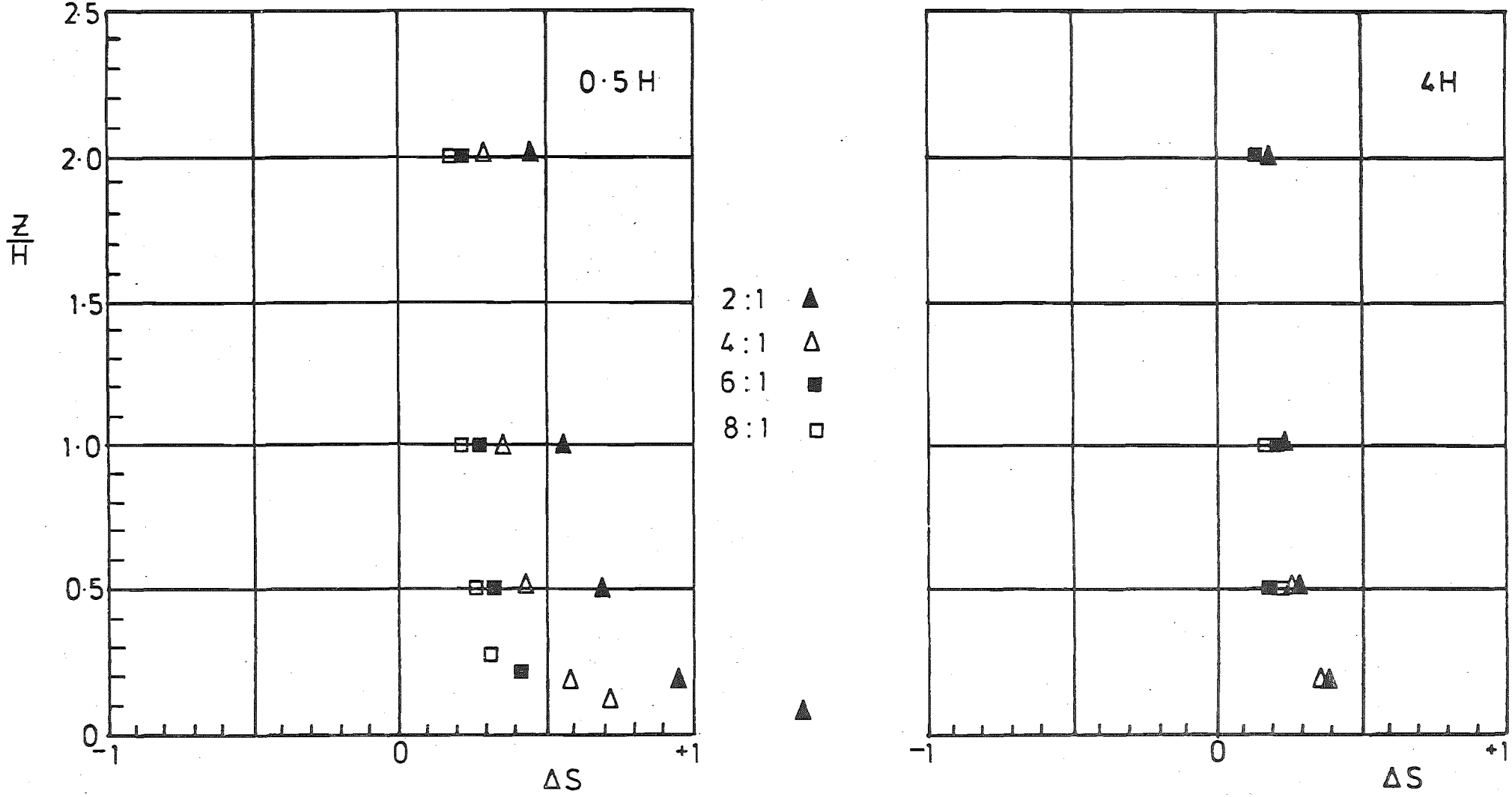

FIG 3·10 PREDICTED FRACTIONAL SPEED—UP RATIOS CALCULATED FOR VARIOUS ESCARPMENT SHAPES AT 0·5H AND 4H USING THE METHOD OFFERED BY JACKSON (1975). (H=13m, Z_o=0·05, ϕ=0°)

equations 3.17, 3.18 and 3.21 and will be compared later with the model and field data in Chapter 9. During the calculations, the height of the inner layer ranged from 1.3 m for the 2:1 escarpment to 3.8 m for the 8:1 slope. The function $H(\tilde{Z})$ ranged between 5 and 10 depending on the height Z in contrast to the recommended value of 2.0 offered by Jackson (1977), but this discrepancy may partly be due to the choice of the constant A_2. For the escarpment slopes considered above, the ratio $\Delta S_{max}/(H/L)$ varied slightly within 1.25 and 1.42 being somewhat smaller than the value of 2.0 suggested by Jackson and Hunt (1975), which may have been partly due to the height at which the values of ΔS_{max} were calculated ($Z = \ell$ cf: $Z = \ell/10$).

3.1.4 Stratified Flows

Until recently most of the theoretical work on wind over surface obstructions had been concerned in the effects of stratified air flow over mountain barriers to explain such phenomena as mountain lee waves (Scorer, 1949), atmospheric diffusion and transient phenomena such as effect of diurnal temperature variations in the air flow (Mahrer and Pielke, 1975). However these solutions did not describe the air flow close to a low hill under strong wind conditions which is the concern of the present project. Nevertheless, they would be useful in understanding the behaviour of the high winds in the mountains that are often subjected to strong thermal effects.

3.2 MODEL TESTS

Although there have been a number of recent wind tunnel investigations involving the flow over complex terrain, the majority of these have been concerned in a unique site and problem from which very little may be gleaned as to the behaviour of flow over hills in general. For instance, the Fluid Dynamics and Diffusion Laboratory of the University of Colorado has completed over ten investigations of the wind flow over mountainous terrain under various conditions of thermal stability. These tests were done in the course of investigating potential problems concerning the diffusion of atmospheric pollutants or changes in local climate. Investigations to enable the classification of hilly terrain into exposed and sheltered areas suitable for forestry have been carried out by Booth et al (1976) and others. The effects of high winds on the Advanced Passenger Train, UK whilst travelling along an embankment have been reported by Everett et al (1976) and concern about the wind loading of electricity

transmission pylons in exposed sites prompted the work reported by Counihan (1973,1974). Meroney et al (1978) have compared model and field measurements in complex hilly terrain and noted good agreement although somewhat limited by the day to day variation in the field conditions.

There remained only six recent model investigations at the time of writing which have set out explicitly to record the individual effects of some of the major parameters associated with an isolated obstruction that would affect the flow of air close to the ground. The conclusions from these tests are discussed separately below in order to isolate any definite trends that might apply to the flow over escarpments and to obtain an idea of the scatter in results. However, because of the large number of variables and hill shapes encountered in these tests and because of the limited number of tests involving escarpments, a direct comparison of actual ΔS or A_z height profiles at various positions over a range of escarpment shapes was thought to be fruitless.

3.2.1 Variation in Mean Velocity Over a 2D Hill

One of the earliest model tests involving escarpments was reported by Serra (1949) for a sharp edged and rounded cliff and 2:1 slopes using an upwind velocity profile of approximately $\alpha = 0.23$ ($^H/\delta$ unknown), although the turbulence characteristics were not measured. Maximum velocity increases were marginally higher for the rounded cliff due to less violent separation behind the crest but the converse was true for the 2:1 slopes. The contours of equal amplification factor showed some dependence on Reynolds number, an effect which was later disproved by Bouwmeester et al (1978). Rough estimates of variation of A_z ($\approx$ 1.35 - 1.4 maximum) with position behind the 2:1 slope crest showed that peak values occurred along a line stretching downwind from the crest with a gradient of 0.5 and did not occur on the surface, except at the crest.

Counihan (1973) reported mean wind speed and turbulence measurements over a series of sinusoidal hills and escarpments ($^H/\delta$ = 0.125, 0.083 and 0.042) normal to a simulated rural boundary-layer. Diagrams giving isovents and isoturbs over the models were given but little information on the speed-up near the crest was evident. However, it was stated that the mean velocity peaks were consistently less than $1.2\ \bar{V}_G$.

Measurements of mean wind speed and surface static pressures were reported by de Bray (1973) and Freeston (1974) over a series of smooth straight ramps, and sine and source ramps in a simulated open country profile, although $^{H}/\delta$ was not reported. The 20° slope ($^{H}/L = 0.73$) showed attached flows and high A_Z values close to the ground ($A_Z \approx 1{\cdot}4$ max. at $^{Z}/H = 0.25$ $\therefore$ $\Delta S/(^{H}/L) = 0.55$), whilst the 40° and 60° ramps ($^{H}/L = 1.68, 3.46$) showed lower speed-up values and detached flows. The smooth source and sine ramp showed higher velocities further downstream than the sharp crested escarpments due to the less severe separation.

Sacré (1973) reported some model tests of rough escarpments with slopes of 10,20 and 30% ($^{H}/L = 0.2$, 0.4 and 0.6) with the approach flow modelled with $\alpha = 0.18$ and $^{H}/\delta \approx 3$. The reference velocity was however measured rather too close to the escarpments and insufficient positions were investigated immediately behind the crest to enable an accurate estimate of the variation in A_Z with height and position. The attempt to fit power law profiles to the velocity profiles near the crest where there is no justification for the flow to behave in this way is of doubtful value and met with limited success close to the ground. However, the zone of maximum amplification factor moved further behind the crest for the steeper slopes (> 1 H behind the crest for the 30° slope) but remained at a similar height of about $^{1}/3$ H above the ground. Below this level the value of A_Z decreased rapidly.

The only other data available at the time of writing which offered ΔS values over several differently shaped smooth obstructions have been presented by Rider and Sandborn (1977) and are shown in Fig.3.11. Maximum values of ΔS were shown in this case to occur close to the ground which was smooth as opposed to Sacré's rough models. It should however be noted that these obstructions had a short length and the ΔS profiles were not taken at the crest. The upstream profile was not defined in the report.

3.2.2 Detailed Hill Shape

As mentioned earlier, consistently higher velocities close to the ground had been noted by Sacré (1973), Freeston (1974) and Rider and Sandborn (1977) over hill shapes that did not cause separation of the flow behind the crest. The criteria for separation in which the detailed shape of the hill has a major influence will be discussed later. Rider and Sandborn (1977) considered a number of differently

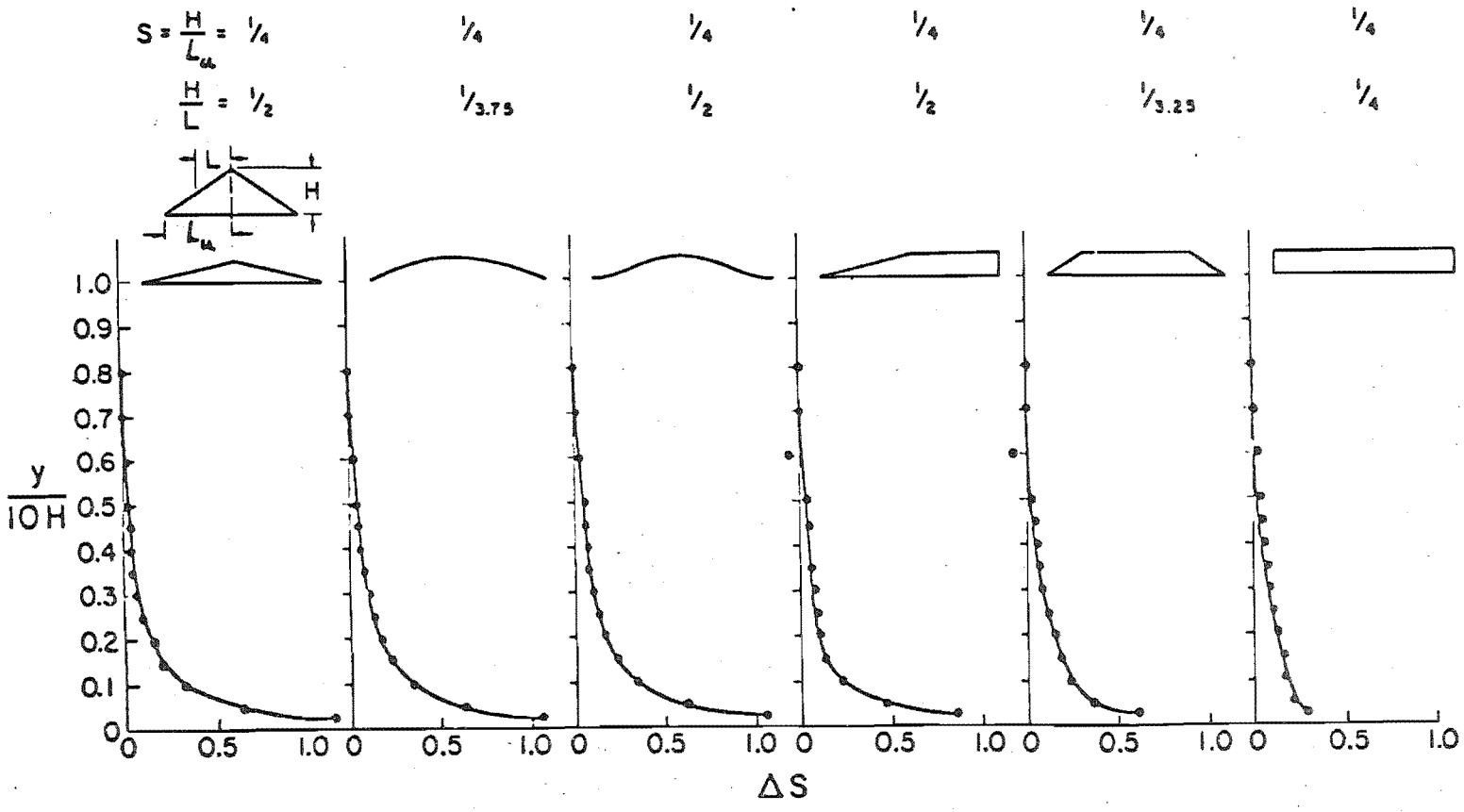

FIG. 3·11 FRACTIONAL SPEED-UP RATIOS FOR VARIOUS HILL SHAPES WITH THE SAME H/L_u RATIO. (RIDER AND SANDBORN, 1977)

shaped obstructions having the same $^{H}/L_{u}$ but different $^{H}/L$ ratios as shown in Fig.3.11. The speed-up effects over the crest varied significantly close to the ground indicating that the base length L_{u} was not a good characteristic length with which to define the hill shape. The results also showed that the detailed geometry of the hill and particularly the slope near the crest has a significant effect on the flow close to the ground. However the influence of the detailed hill shape decreases rapidly with height above the ground.

3.2.3 Characteristic Hill Shape, $^{H}/L$

The peak amplification factor near but not necessarily directly above the crests of various escarpments were recorded by Sacré (1973) and have been replotted in Fig.3.12 against the parameter $^{H}/L$. Sacré noted the limit in ΔS_{max} (or $A_{Z_{max}}$) of about 0.4 at $^{H}/L \approx 0.4$ and suggested that for steeper slopes ($^{H}/L > 0.8$ was quoted) separation behind the crest would have occurred, thus seriously modifying the flow. Additional data from Freeston (1974) at the crest has been added to Fig.3.12 which confirmed this trend, but higher values may have been missed due to the sparse measurement locations. The data in Fig.3.12 for escarpment flows suggested that $\Delta S_{max}/(^{H}/L) \approx 1$ for $^{H}/L \lesssim 0.4$ compared with a value of 2 for the ratio suggested by Jackson and Hunt (1975). However this discrepancy in proportionality may only be due to the incorrect definition of the characteristic hill length L for escarpments, as the theoretical prediction of ΔS_{max} by Jackson (1977) agrees more closely with the model data. Bouwmeester et al (1978) showed a similar limit at $^{H}/L \approx 0.4$ ($^{H}/L_{u} = 0.2$) for unsymmetrical triangular hills ($^{1}/2 > {}^{H}/L_{d} > {}^{1}/4$) when considering the crest amplification factor at Z = H.

3.2.4 Flow Separation

Large changes in mean velocities, static pressures and longitudinal turbulence intensities were noted by Bouwmeester et al (1978) when discussing the flow over various symmetrical triangular hills. A slope of $^{H}/L = 0.25$ ($^{H}/L_{u} = 0.12$) was found to be close to the steepest hill which sustained non-separated flow and coincided with the slope giving the highest velocity amplification. Counihan (1973) showed that for sinusoidal hills, the flow was separated for $^{H}/L > 0.42$ to 0.54 ($^{H}/L_{u} > 0.21$ to 0.27). The limits depended on the value of $^{H}/\delta$, unlike Bouwmeester who concluded that $^{H}/\delta$ had no effect. The extent of the wake was found to be proportional to the $^{H}/L$ ratio and

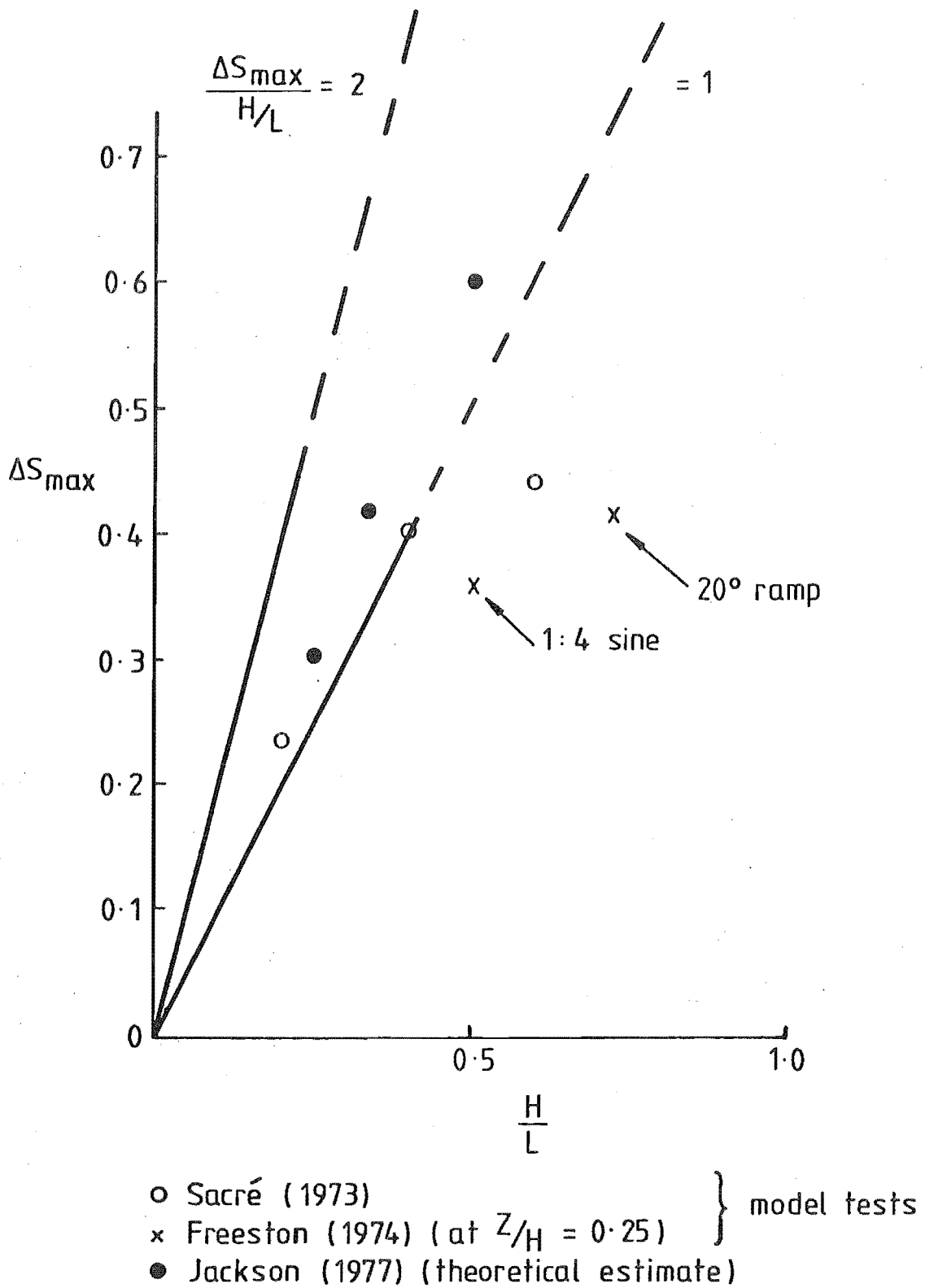

FIG 3·12 MAXIMUM FRACTIONAL SPEED-UP FACTORS ABOVE THE CRESTS MEASURED FROM MODEL AND THEORETICAL STUDIES OF ESCARPMENTS AND PLOTTED AGAINST THE CHARACTERISTIC HILL SHAPE PARAMETER, H/L.

the flow was not yet in equilibrium immediately after re-attachment.

Bouwmeester et al (1978) showed by using a series of unsymmetrical triangular hill models, that the downwind slope also affected the onset and extent of the separation. A graph showing his empirical envelope of upwind and downwind slopes indicating the onset of separation behind a sharp edged ridge is shown in Fig.3.13. Flow separation would presumably be delayed for a smooth hill crest of the same $^{H}/_{L}$. Bouwmeester also showed that the onset of flow separation was delayed until steeper slopes if the upwind surface roughness was greater than that near the ridge and if the turbulence levels in the approaching flow were higher. It is generally accepted though that an increase in surface roughness towards the ridge introduced higher shear stresses in the flow. This in turn would cause a larger total head loss in the flow close to the ground and consequently more likelihood of separation.

In contrast however, Counihan (1973) found no evidence of flow separation behind the crest of his sand coated cliff escarpment and reported that the flow returned to its upstream condition after 6 to 8 H downstream. The escarpment models having the steeper ramp angles were found to require the shorter distance for wake recovery.

Upwind separation was found by Bouwmeester for the steeper slopes $^{H}/_{L} > 1$ ($^{H}/_{L_u} > \frac{1}{2}$) with the separation extending no further than 2 H upwind, but this should only occur for near normal flow directions.

3.2.5 Hill Height, H

No reports are available in the literature which have investigated the influence of this parameter using model studies but tests are currently being conducted at the University of Canterbury by Pearse. Bouwmeester et al (1978) suggested from a theoretical solution that the ΔS ratio at a certain height should decrease with increasing hill height in contrast with the theoretical predictions of Sacré (1975).

3.2.6 Wind Direction, ϕ

The oblique flow ($\phi = 10°$) over a 20% slope ($^{H}/_{L} = 0.4$) was measured by Sacré (1973) who reported a reduction in ΔS_{max} of about 5%. No other test data was available in the literature. This parameter is however a very important one as it is very rarely the case that a prevailing wind is normal to the slope. However, for

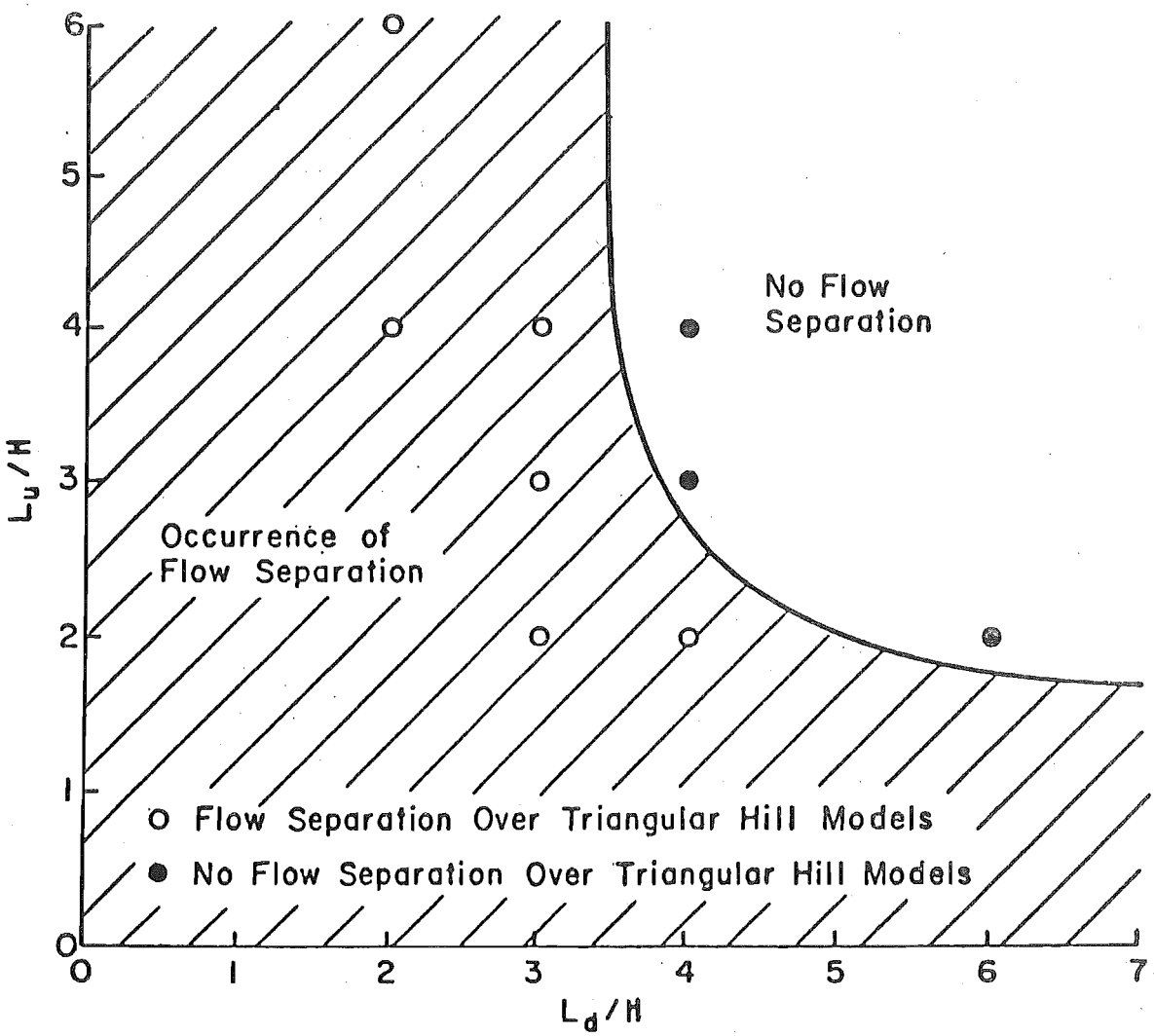

FIG 313 CRITERION FOR FLOW SEPARATION OVER RIDGES. (BOUWMEESTER ET AL., 1978).

maximum loading, the worst case when $\phi = 0$ may be the important design consideration.

3.2.7 Upstream Terrain Roughness, Z_o

A comparison of velocities over two smooth, rounded ramps by de Bray (1973) showed significant increases in ΔS values below a height of 2 H with a change from uniform flow to shear flows with $\alpha = 0.11, 0.14$. Bouwmeester et al (1978) also showed increases of up to 70% in ΔS with a change from smooth to rough surface boundary-layers. His empirical relation to allow for different upstream power law profiles is described in Chapter 10.

3.2.8 Three Dimensional Effects

The effect of finite ridge length was considered briefly by Bouwmeester et al (1978) during his model test programme who showed that for the ridge lengths tested (9 H and 18 H), the flow was very close to the two-dimensional case under neutrally stable flow conditions. The velocities at low levels near the centre of the ridge were slighly less than for the two-dimensional case, especially if a large separated flow existed downwind. In contrast, the velocities near the ends of the ridges were slightly higher than the two-dimensional case, apparently due to the reduced separated flow region at the sides of the downwind slope.

3.2.9 Stratified Flows

The effects of a stably stratified flow on the extent of a separated region behind model hills was reported by Bouwmeester et al (1978). Speed-up factors over the crest were not strongly affected and the small increase detected was thought to be due to the change in the approach flow profile. However the downwind separated region was much longer under stable conditions than under neutral conditions as the heavier air in the separated region resisted reattachment. A further reduction in longitudinal turbulence intensity over that originally observed for the neutral flow case was also detected.

However speed-up factors over a finite ridge width in a stable stratified boundary-layer were found to be significantly less than those over the same ridge under neutral conditions, particularly near the ends of the ridge, due to the air tending to by-pass the ridge rather than flow over it.

3.2.10 Turbulence

Rider and Sandborn (1977b) noted that significant changes in the flow turbulence over a series of model triangular hills were confined to a layer close to the ground in which the behaviour of the turbulence was found to be consistent with theoretical results for a flow through a contraction. However no inner layer characterised by large changes in Reynolds stress was found with the steeper hills. The longitudinal turbulence, $\sqrt{\overline{u}^2}$ increased towards the foot of the hill and then decreased as the flow passed over the hill. The decrease was found to be greater ($\approx$ 12%) for flows with greater turbulence. Conversely, the vertical turbulence, $\sqrt{\overline{w}^2}$ decreased as the flow approached the hill and increased again towards the summit. The shear stress, $\sqrt{\overline{uw}}$ was found to decrease towards the base of the hill and increase rapidly over the hill crest coinciding with the increase in mean velocity. Probability density and spectral measurements reported by Bouwmeester et al (1978) showed that the differences in structure were quite small as the flow negotiated the triangular model hills outside the separated regions.

Contours of equal turbulence intensity were also presented by Counihan (1973) for three different escarpment shapes and it was noticed that the wake behind the crest returned quickly to the upstream condition within about 6 to 8 escarpment heights.

3.3 FULL SCALE INVESTIGATIONS

Reported field measurements of the wind flow close to the ground are very scarce due to the inherent difficulties of full scale investigations. The early and energetic field investigations of Putnam (1948) and Golding (1955) for wind energy conversion purposes, accumulated a good deal of data. However application of this information to the general problem of flow over hills is difficult due to the inevitable unique shape and situation of the hills considered and the lack of upwind data on the undisturbed mean velocity-height profile and atmospheric stability.

The WMO report #63 (1964) reviewed the site data offered by Golding (1955) and Frenkiel (1962,63) and endeavoured to fit power law exponents to the summit velocity profiles, but the values of the exponents varied widely and seemed to be of little use in defining those situations. However it was noted that a slope of about 8:1 was not steep enough to cause a significant change in the wind profile

shape (but speed-up effects could still be significant). Slopes of about 1:3 to 1:5 caused very flat profiles ideal for wind power generation, but these slopes could also cause a reduction of wind speed with height. The possibilities of velocity speed-up over locally elevated sites was discussed and it was noted that as the factor depended markedly on the continually changing atmospheric conditions such as atmospheric stability and upwind slope insolation, over a long period of time the average speed-up factor may not be significant for wind power purposes. However the situation may occur in windy conditions when the velocity amplification is unusually high, causing unusually high winds close to the ground with the attending extreme structural loadings. Experimental evidence was said to show that the greater the atmospheric stability, the greater the speed-up factor in contrast with the conclusions from model tests using 2D ridges. In addition, insolation on the windward slopes modified the stability of the air stream close to the ground and could have a large influence on the speed-up factor at the crest. Warming of the windward slopes exposed to the sun would decrease the stability thus increasing turbulent mixing and thereby it was said, causing a decrease in the speed-up factor at the crest.

3.3.1 Mountains

Several mountain groups have received close attention from field wind studies such as Gibralter (Scorer, 1952 and Cook et al, 1978) and Hawaii (Hardy,1977). However apart from noting general large scale effects, difficulty in defining quantitatively the upwind velocity-height profile and stability conditions and in categorising each site with respect to hill shape characteristics, ground cover and local stability changes, makes the application of the data to our problem very difficult. Scorer (1952) noted that in regions where the air below mountain top level was characterised by strong stability, it was common to find unusually strong winds in the lower layers when shallow masses of cold air found their way through mountain gaps and along steep coastlines. Cook et al (1978) studied model and field data concerning the persistent downwind vortices in a similar situation behind the sharp edged topographical feature of the Rock of Gibralter.

Shellard (1963) quoted from accumulated meteorological experience in the U.K. stating that on hill tops which rose rather abruptly from more or less level terrain or sea, maximum wind speeds were not much different from those at the same elevation in the undisturbed air flow upwind. In other words, $S \approx 1.0$. This is the same principle on which

the escarpment rules of the U.K.,Australian and New Zealand building codes (discussed in Chapter 10) were based. To substantiate this principle, Shellard (1963) took two sets of mountain top sites and compared them with the nearest low level recording sites for days when the mountain top wind speeds exceeded 20 m/s. The mean hourly wind speeds on the mountain tops at around 750 m A.M.S.L. were some 80 to 90% stronger than those recorded near sea level. The peak one minute gust speeds were also 60 - 75% stronger. The ratio of gust speed to mean speed averaged only 1.4 for the mountain top sites compared with the higher values of 1.67 and 1.46 for the low level sites, even though the latter were very open and exposed. Shellard illustrated his principle by showing that a reasonable estimate of the mean wind speed on the mountain top could be made if the free air speed at the same elevation was used by applying the power law velocity gradient with $\alpha = 0.17$ up to a height of 365 m with a constant velocity above that height, corresponding to the gradient wind speed. The similar application of a $\alpha = 0.085$ power law for gust speeds which was known to hold approximately for flat terrain, underestimated the mountain top gust speed by 20%.

Further evidence was reported by Elliott (1977) who quoted data from E.W. Wahl (U.S. Air Force, Cambridge Research Laboratories). Wahl had evaluated the wind speed records from six European mountain summits ranging in elevation from 800 m to 3000 m. The values for each individual summit ranged from less than 30% of the estimated free air wind speed at the same elevation to 80% or more for the very exposed summits. On the average, the summit wind speeds were 60 to 70% of the free air speed for wind speeds greater than 8 m/sec and were reasonably independent of the summit elevation. The results confirmed that Shellard's estimate based on $S = 1$ may in fact be close to the truth for only the very exposed summit situations.

However conflicting information has appeared in the data obtained from the wind-energy resource survey of New Zealand reported by Cherry (1976,77). Cherry (1977) discussed the accuracy of extrapolating low level readings over flat terrain to summit sites using the power law as discussed above. As an example,using radar balloon data over the Christchurch area characterised by flat open farmland, the measured power law exponent was 0.173 between 14.3 m and 900 m altitudes. The ratio of measured mean wind speed at approximately 10 m in strong wind conditions on two separate days between the summit of Hilltop at 700 m A.M.S.L. and nearby flat open terrain at 22.5 A.M.S.L.

was 3.32 (low level S wind, $\bar{V}_{10}$ = 5.6 m/s) and 2.16 (low level NE wind, $\bar{V}_{10}$ = 2.16 m/s). These ratios corresponded to an equivalent power law exponent of 0.33 and 0.224 respectively. Cherry concluded that the velocity ratio varied considerably with wind direction (effect of local terrain) and atmospheric conditions and were in general, greater than that indicated by the undisturbed profile over flat ground. In other words, S was usually greater than 1.0. However additional data accumulated over the Otago region of New Zealand by Dawber and Edwards (1978) suggested a strong trend of increasing mean velocities with altitude over terrain which is largely rounded and exposed elevated plateaux. Under these conditions it is thought that S would probably be less than 1.0.

The use of high level wind data may also be used to estimate windy areas in complex terrain as described by Cherry (1978), although the available data is not sufficiently detailed to predict local terrain effects accurately.

3.3.2 Low Isolated Hills

Using cup anemometers about 6 m above ground level, Mitsuta (1971) measured the mean wind speeds at a dozen sites across a 1.2 km wide strait and adjacent narrow ridges of between 60 and 100 m in height during a typhoon under presumably near neutral, very strong wind conditions. The amplification factors using a reference site in an open situation varied from 1.1 on a 90 m conical summit to 1.7 and 2.1 on the level ridge near the straits. Further measurements of winds between 13 and 47 m/s were recorded from eight anemometers at 40 m intervals along a ridge of a 700 m hill. Corresponding turbulence intensities varied from 0.09 to 0.48 within 40 metres distance showing that the turbulence characteristics and mean wind speeds were greatly influenced by small scale changes in the local topography. Gust factors for peak gusts averaged over one second varied between 1.2 and 3.0 with a strong correlation with the standard deviation of velocity.

Field measurements in Russia reviewed by Berlyand (1972) showed amplification factors at a height of 1 to 2 metres above the crests of various relief forms compared with some model test results of similar situations and are reproduced in Table 3.2.

Relief forms	Slope angle θ	Microclimatic observations ΔS	Slope Angle θ	An experiment in a wind tunnel ΔS
The summits of the open elevations.	> 10°	1.4-1.5	15° 18°	1.3 1.55
The summits of the small sloping elevations . . .	< 10°	1.1-1.2	6°	1.1
The middle parts of the windward open slopes . .	> 10°	1.0-1.1	15°	1.1
The leeward slopes of the elevations	> 10°			
- upper part		1.0-0.9		
- lower part		0.6	18°;15°;12°	0.5;0.65;0.75
The leeward slopes of the elevations	< 10°	0.6-0.7	6°	0.8

TABLE 3.2 FIELD AND MODEL TEST RESULTS OF ΔS OVER VARIOUS HILL SHAPES (BERLYAND 1972)

Fitting the correct $^{H}/_{L}$ parameter to each result is difficult as the hill form is unknown but if the hills are assumed to be triangular in cross-section then $\Delta S \approx (0.5 \text{ to } 0.8)\ ^{H}/_{L}$ for the summit data.

Perhaps the most detailed full scale investigation of the airflow over a hill has recently been reported by Sacré (1978). The hill at Pouzauges near Nantes, France was situated with its long ridge normal to the prevailing SW winds in open farmland. The summit was quite broad (350 m), at about 60 m above the upwind flat country. The upwind slope was about 9% which carried several minor surface irregularities and the downwind slope was about 3%. Measurements were taken using orthogonal arrays of Gill propeller anemometers scanned at 2 Hz during strong winter SW wind conditions in 1975-76. An accuracy within 5% was claimed for the mean statistical parameters and 10-15% for the measured Reynolds stress component, $\tau = -\rho\overline{uw}$.

The ratio of measured Reynolds Stress divided by the friction velocity, V_* taken from the mean velocity-height profile, was used as an indication of the logarithmic character of the velocity-height profile at that particular site. It was inferred from the report that

due to the low solar radiation intensities of the winter season and the strong wind situations, the atmospheric stability had been assumed to be neutral and the function $\psi(Z/L)$ of equation 2.16 was insignificant. Thus any changes in the ratio $\sqrt{-\overline{uw}}/V_*$ could be attributed to terrain effects and would be manifested by a change in the value of Z_o to an apparent value. This approach relied on a further assumption that the modification to the velocity-height profile was sufficiently gentle that a straight line could still be fitted to the logarithmic velocity plot. (It was noticed that the ratio $\sqrt{-\overline{uw}}/V_*$ had values generally between 1.0 and 1.8 which if they had been measured over flat homogeneous terrain, would have indicated unstable atmospheric conditions as noted in Chapter 6.) It was explained that if the ratio $\sqrt{-\overline{uw}}/V_*$ was less than one, then the apparent Z_o was greater than the real Z_o value and a general reduction in wind speeds was apparent compared with the flat homogeneous terrain case. Alternatively, if $\sqrt{-\overline{uw}}/V_*$ was greater than one, the apparent Z_o was less than the real Z_o value and speed-up effects would be apparent. Although the apparent or measured value of Z_o varied with the direction by up to a decade at each site, a strong linear relationship was noticed between $\sqrt{-\overline{uw}}/V_*$ and $\log {}^1/Z_o$. The true value of Z_o was taken as the value which yielded the ratio $\sqrt{-\overline{uw}}/V_* = 1$ from the accumulated data.

Analysis of the nearby slope at each measurement position showed that the apparent mean wind speed-height logarithmic exponent, α was smaller at the summit of an obstacle the greater the upwind slope in agreement with Frenkiel (1962). The proportionality between upwind slope and the factor ΔS_{max} suggested by Jackson and Hunt (1975), was shown to be correct with averaged values in this case of $\Delta S_{max}/({}^H/L) \approx 1.5$. However it was concluded that the local changes in topography such as whether or not the immediate upwind slope was convex or concave, also had a strong influence on the wind speed. The individual effects of change in ground roughness, local geometry and the overall hill shape were shown to have comparatively large influences on the mean wind speeds. However it was noticed that the wind direction within the range considered (about 45° to the ridge normal) had little effect on the fractional speed-up factor, ΔS. In addition, no systematic changes in the turbulence was noted and the measured values remained close to those offered by Counihan (1975) for rural terrain.

3.3.3 Escarpments

As a preliminary to the field tests reported later in Chapters 6 and 7, some measurements of the mean wind speed over the same two

escarpments (2:1 and cliff) were carried out by Bowen and Lindley (1974) using cup anemometers mounted on 10 m portable masts. The field results are reproduced in Fig.3.14 showing the mean velocity-height profiles compared with early wind tunnel results using a horizontal pitot tube sensor over smooth models (H = 50 mm) normal to the flow. Because the cup anemometers are sensitive to the longitudinal and lateral components of the flow regardless of sign and they tend to overestimate in turbulent flow, the readings close to the ground in the wake region are expected to be highly overestimated. The upstream profile for the sloping escarpment also indicates some measure of thermal instability, an impression which is further reinforced by the relatively low wind speeds, $\bar{V}_{10}$ = 4 m/s. In addition, the pitot tube which is sensitive only to the longitudinal flow component is rendered inaccurate in high turbulence and in regions such as near the crest where the streamwise pressure gradient is significant along the length of the pitot tube. However the conclusions showed that the amplification factor varied widely but were commonly within the range 1.1 to 1.4. Local peak values of up to 1.7 for the sloping escarpment ($\Delta S/(H/L) = 0.7$) and 2.1 for the cliff were recorded close behind the crests. The amplification factors decreased rapidly with height so that significant modifications to the wind speed were confined to below the first 2½ escarpment heights but extended beyond 12 escarpment heights downwind of the edge.

Jensen and Peterson (1978) discussed the wind speed measurements taken during a field investigation programme at Risφ, Denmark associated with an extensive study of the flow of wind from water to land. They showed that the increase in velocities noticed in a certain height range over the land could not be explained by a change in surface roughness but was due to the low escarpment profile of the coastal site. Using Jackson and Hunt's (1975) equation for the inner layer depth which marks the height of maximum speed-up effect, equation 3.20.

$$\frac{\ell}{L} \log_e\left(\frac{\ell}{Z_o}\right) = \text{constant}$$

they likened it to the growth of the lower boundary-layer depth, θ with distance x downwind from a change in roughness, as quoted in Chapter 2 equation 2.17 as

$$\frac{\theta}{x}\left[\log_e\left(\frac{\theta}{Z_o}\right) - 1\right] = \text{constant}$$

Jensen and Peterson then suggested a more simple relation for equation

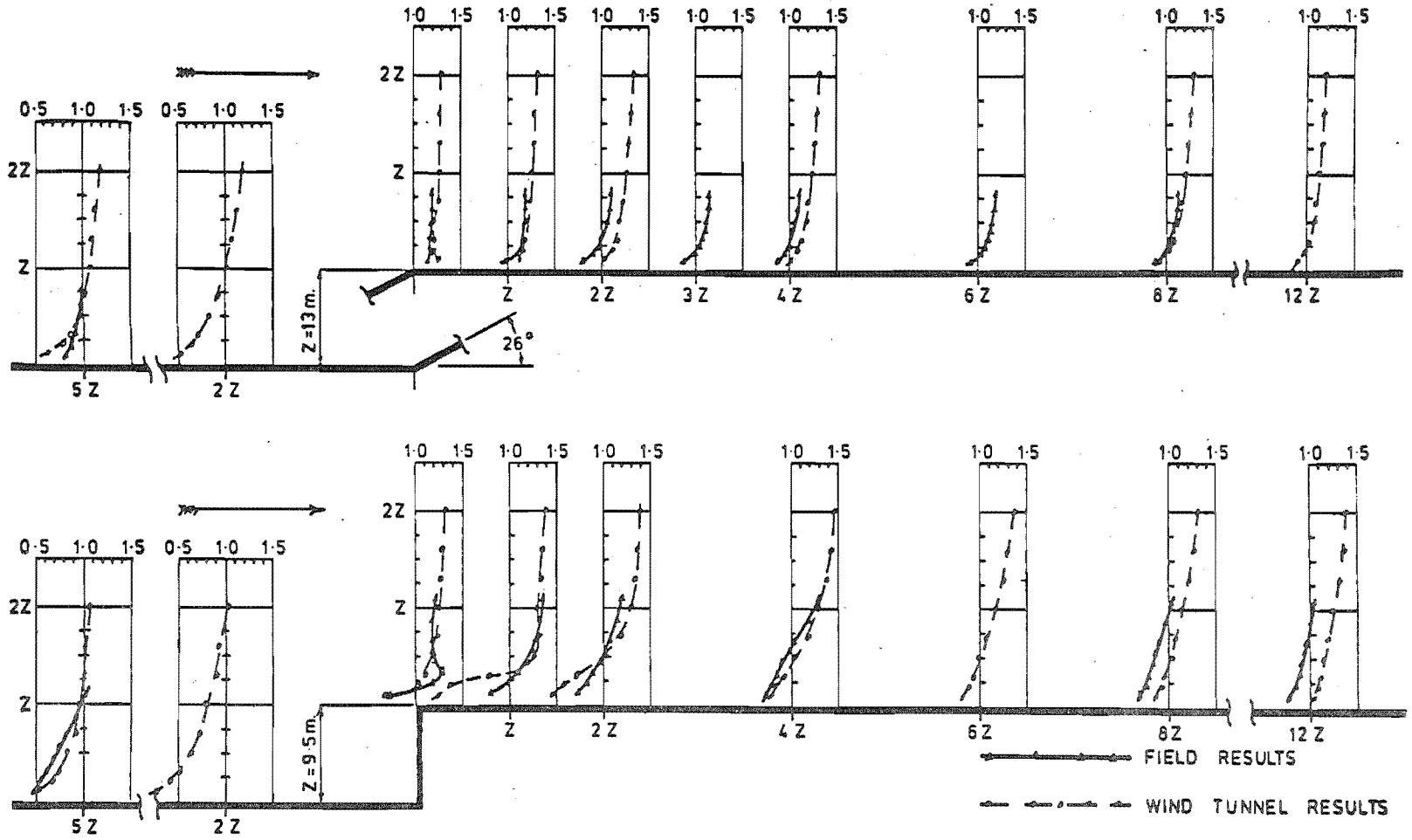

FIG 3·14 VARIATION OF MEAN WIND SPEED OVER A 2:1 AND CLIFF ESCARPMENT RELATIVE TO UPSTREAM WIND SPEED AT 10m ABOVE GROUND. FIELD RESULTS USING CUP ANEMOMETERS BY BOWEN AND LINDLEY (1974)

3.20 in just the same way as equation 2.19 was a simplified alternative to equation 2.17, as discussed in Chapter 2. Thus it was proposed that

$$\frac{\ell}{z_o} = C \left(\frac{L}{z_o} \right)^{0.8} \qquad 3.22$$

where C is a constant of the order 1 ($C \approx 0.5$ was assumed later).

The resulting inner layer depth, ℓ using L_u as the 'fetch' from the coast to the top of the escarpment and instrument mast (not the half length of the average slope proposed by Jackson and Hunt (1975)), coincided with the peak velocity changes (or kinks) in their velocity-height profiles for both towers. In addition, calculations of $\Delta S = 2(H/L_u)$ also coincided closely with their recorded values for the flow at the height of the inner layer, $Z = \ell$, thus showing that $\Delta S \approx H/L$. The velocities below this level were clearly dominated by the smooth to rough transition of the coastline. The instability of the atmosphere close to the ground due to the increased heat flux over the land was accepted as a factor unaccounted for. However it was stated that the influence of stability on the ΔS values would have been small under the circumstances prevailing during the tests. Nevertheless a significant variability in the ΔS values was noticed from one recording to the next which showed no systematic dependence on either the stability or the wind speed. It was not known to what degree the variability was associated with horizontal changes in the surface heat flux or any nonuniform vertical temperature structure.

Jensen and Peterson pointed out that for hills or escarpments with large values of L_u (and low H/L) the depth of the inner layer was quite large and the flow within it of some importance. Within this layer at the top of the hill, Jackson and Hunt's (1975) theory was shown to provide a logarithmic velocity profile with an apparent friction velocity that increased relative to the upstream value with increasing H/L such that

$$\bar{V}_Z = \frac{V_*}{k} \left[1 + \frac{H}{L} \left(\frac{\log_e(L/z_o)}{\log_e(\ell/z_o)} \right)^2 \right] \log_e(Z/z_o) \qquad 3.23$$

This equation offered a neat method of calculating the velocities over a hill within the inner layer region.

3.4 CONCLUSIONS

* The literature available on the flow of wind over complex terrain is very sparse but the recent revival of interest in wind energy has resulted lately in some useful reports concerned in the selection of wind turbine sites in hilly terrain. Various numerical solutions for the flow over simple hills and involving a wide range of complexity were described which relied on a variety of approximate closure assumptions and range of application. A potential flow solution to the flow over escarpments using a finite difference method was outlined which yielded contours of equal amplification factor over a range of slopes including those that were investigated in the field and described later in this report. A powerful analytical method was also available which indicated the importance and influence of the characteristic hill parameter, $^{H}/L$ and defined the flow velocity variation over a low, smooth hill in terms of the upwind flow conditions and the hill slope.

* However, the accuracy of all the theoretical solutions remained largely unconfirmed due to the lack of model and full scale data. The available model test results concerned entirely with two-dimensional hills were also reviewed and gave an indication of the effects of some of the main parameters as summarised below. However the coupling between each parameter and the inevitable complex three-dimensional nature of even the most simplest of field sites still make the prediction of wind speeds over complex terrain an inaccurate undertaking.

* The literature supported in general the concept of an inner layer close to the surface of a hill (provided it had low curvature and no separation) in which the increase in shear stress towards the top of the hill was the dominant feature. Outside this layer the shear stress variation was small and the flow behaved in an almost irrotational fashion as it negotiated the hill. The structure of the turbulence did not change significantly outside this layer unless a separated wake occurred.

* The peak value of the amplification factor occurred close to the ground at the crest of the hill and was closely related to the peak surface shear stress.

* The maximum fractional speed-up ratio, ΔS was shown to be proportional to the $^{H}/L$ ratio for $^{H}/L \leqslant 0.4$, but model tests showed that the constant of proportionality ranged from 1 to 3 depending

mainly on the local geometry of the upwind hill slope. Peak ΔS values occurred for the steepest hill which could sustain a non-separated flow.

* The onset of separation depended on both the upwind and downwind slopes and seriously modified the flow in that region. Separation in general reduced the peak ΔS values close to the crest. The limits of hill slope marking the onset of separation based on model tests of 2D triangular hills, was found to be approximately $H/L_u \approx 0.7$ and $H/L_d \approx 0.3$.

* Speed-up effects were thought to be reduced for a conical hill under stable atmospheric conditions due to the tendency for the air to move around the summit rather than over it. Model tests indicated that changes in speed-up over 2D hills due to changes in stability were small.

* Higher values of ΔS were noticed in the model tests with higher upstream velocity power law exponent, α or rougher upwind terrain. Local changes in surface roughness near the crest also had significant effects on the local mean wind speed and on the onset of separation at the crest.

* Theoretical studies suggested that speed-up effects were relatively insensitive to the angle of incidence of the wind up to about $\pm$ 45° from the normal to the crest line. Under oblique wind conditions the wind turned to strike the hill slope at an angle closer to the normal and reverted to its original direction behind the summit. Changes of up to 20 - 25° were predicted by theory.

* Theoretical predictions and model tests indicated conflicting trends in speed-up effects with increasing hill height and the effect of this parameter remains unresolved.

* Model studies suggested that ridges of finite length behaved in a similar manner to 2D hills for ridge lengths greater than about 9 H. Values of the speed-up factor, S would tend to 1.0 for steep conical hills.

CHAPTER 4

ANEMOMETER PERFORMANCE

Wind sensors in various forms have been used to measure the wind speed for many years. The pressure-tube anemograph mounted on a swinging vane and developed from W.H. Dines' design in 1890, is well established as a standard meteorological instrument in many countries. The more simple cup anemometer with origins over a century ago has developed into a robust, weather-proof instrument which is also widely used. The development of these instruments has been ably described by Mazzarella (1972) who has compiled an inventory of the performance specifications of the instruments currently in use in 1971. Further details of current instruments may also be found in The Handbook of Meteorological Instruments (HMSO, 1965).

Since the late 1920's when the first discussions by Shrenk (1929) and Giblett (1932)considered the dynamic performance of cup and pressure-tube anemometers, there has been a growing interest in the effects of turbulence on the output accuracy from the various designs of anemometers. In turbulent wind conditions, the slow dynamic response of a typical heavy and robust cup anemometer has been shown by authors such as Deacon (1951), MacCready (1966) and Busch and Kristensen (1976) to be directly responsible for the overestimation of the mean wind speed, commonly up to 10 or 15% depending on the turbulence intensity, and the inability to accurately record short term peak gust speeds. For instance, the common Dines pressure-tube anemograph is considered to record gusts accurately for averaging periods longer than about 5 seconds. [Giblett (1932)]. In addition, both instruments are restricted to the measurement of the horizontal wind speed regardless of wind direction and are unable to distinguish between the longitudinal and lateral components of the wind. McCready (1966) concluded that systematic wind speed measurement errors in turbulent winds can be 'extremely large' when large or slow sensors are used at low elevations over rough terrain. This fact is well illustrated in Figs. 9.1 and 9.2 which shows some of the results from the early cup anemometer measurements of the wind flow over escarpments reported by Bowen and Lindley (1974) compared with the recent model and field tests. The RIMCO cup anemometers used in these tests have been described by Sumner (1968).

More recent interest in dynamic wind loading, diffusion and air pollution has prompted the development of high response instruments capable of providing accurate turbulence information. The Gill anemometer described by Gill (1975) is a good example and has prompted a wide discussion on its effective performance by authors such as Brook (1977), Hicks (1972), Horst (1973a) and Jackson (1976). When mounted in an orthogonal array, the instrument set allows the measurement of all three components of the turbulent wind flow.

The propeller anemometer used in the present field tests had a similar outside shape to that of the UVW Gill anemometer but the internal design and signal generating system was quite different. However, any discussion concerning the aerodynamic performance of the Gill anemometer may be directly applied to the University instrument, except for small differences that will be discussed later.

The mechanical design and development of the University propeller anemometer was carried out by the author using the signal generating and processing system developed by H. Anink of the Electronics Laboratory, Mechanical Engineering Department. The physical layout of the anemometer may be seen in Fig. 4.1 and more details may be obtained from Flay (1978), The shaft is supported by two ball bearings and drives a circular plate or 'light chopping disc' which has 32 slots cut in it. The rotating plate interferes with two light beams that are trained on to two light sensitive receivers. These receivers generate two pulse trains which are conditioned electronically in the anemometer housing into two out of phase, square-wave pulses of identical frequency. The processing of these signals is discussed in Chapter 5. The 10 cm diameter, 4 bladed helicoid propellers were made by the University from expanded polystyrene in a similar manner to the Gill propeller. A typical orthogonal array using the University propeller anemometers may be seen in Fig. 4.2.

In this chapter, the performance limits and expected errors of the propeller anemometers used in the field tests will be discussed in detail and will conclude with an estimate of their effect on the accuracy of the recorded turbulence data.

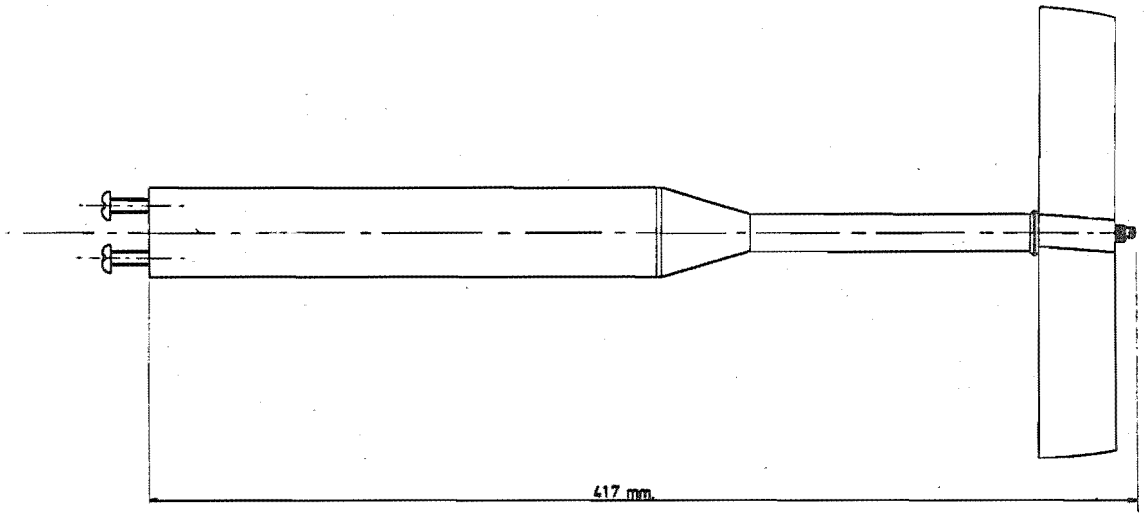

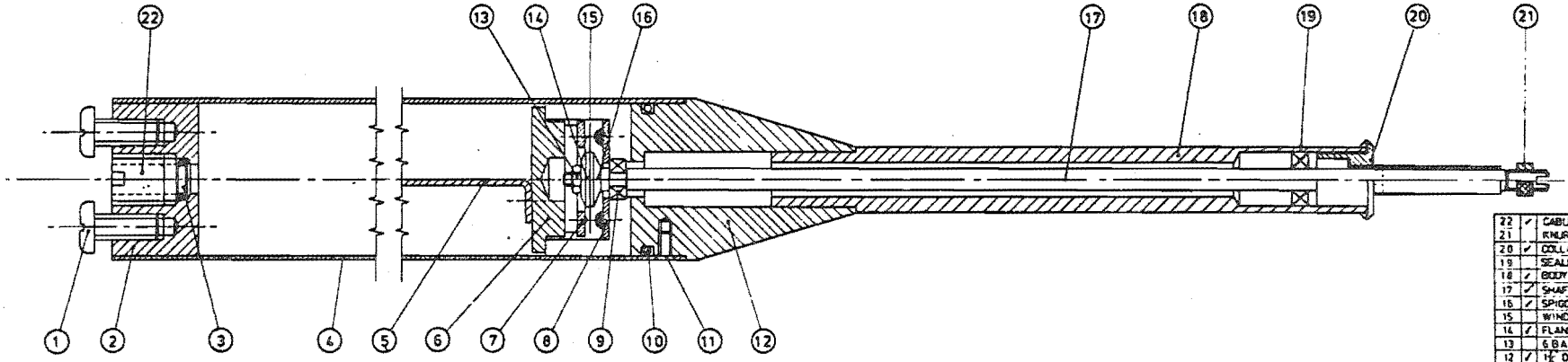

ITEM	Qty	DESCRIPTION	STOCK
22	✓	CABLE GLAND ¼" DIA.	AL ALLOY ROD
21		KNURLED 2BA NUT	" "
20	✓	COLLAR	" "
19		SEALED BALL BEARING	
18	✓	BODY ¼" DIA × 140 mm	AL ALLOY ROD
17	✓	SHAFT 7/32" DIA × 231mm	ST STEEL ROD
16	✓	SPIGOT ¼" DIA	AL ALLOY ROD
15		WINDOW DISC	
14	✓	FLANGE ¼" DIA	AL ALLOY ROD
13		6BA HEX NUT	CAD PLTD ST
12	✓	½" DIA × 74 mm	AL ALLOY RUL
11		5 BA × 6 mm C'SUNK SCREW	CAD PLTD ST
10		"GACO" R3116 O RING	RUBBER
9		¼" - ½" - ⅛" OPEN B BEARING	KLAJ ½
8	✓	PEP BASE	½" GL FIBRE SHT
7	✓	LED BASE	" "
6	✓	CAP 3" DIA × 10.5 mm	AL ALLOY ROD
5		CIRCUIT TRAY TO SUIT	⅛" AL ALLOY SHT
4	✓	1½" OD × 210 mm 17 SWG	AL ALLOY TUBE
3		¼" OD × 3/32" O RING	RUBBER
2	✓	BASE 3" DIA × 20 mm	AL ALLOY ROD
1		2 × M6 × 16 mm PAN HD SER	CAD PLTD ST

PROPELLER ANEMOMETER
MARK II

SCHOOL OF ENGINEERING
MECHANICAL DEPT

DRAWN - A J BOWEN APPROVED -
TRACED - J RITCHIE
DATE - NOV 1974
SCALE - 1 1 & Twice full size
DRG Nº 2A

FIG. 4·1 DESIGN OF PROPELLER ANEMOMETER

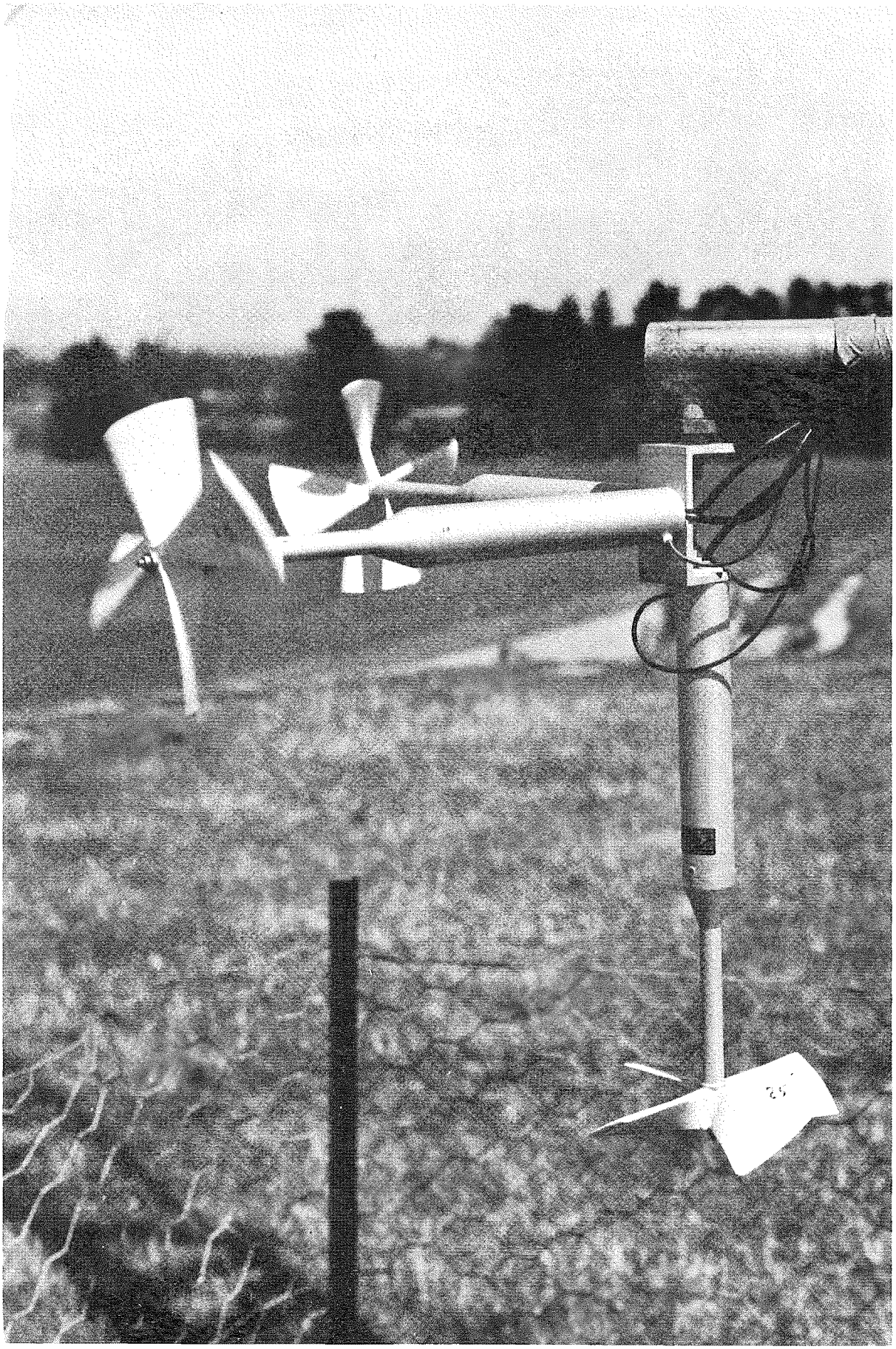

FIG.4.2 VIEW OF PROPELLER ANEMOMETERS ARRANGED IN A TYPICAL ORTHOGONAL ARRAY

4.1 AERODYNAMICS OF A HELICOID PROPELLER

The unique theoretical analysis by Jackson (1976) of the aerodynamics of the Gill helicoid propeller provided an approximate expression for the aerodynamic torque. This was then used to complete the equation of motion of the rotating anemometer in terms of parameters that could be found by experimentation. This approach is followed below as the equation of motion is a useful starting point for the discussion of anemometer performance and accuracy and it also highlights the important parameters involved.

Consider a wind flow with an instantaneous velocity V passing through the blades of a helicoid propeller at an angle θ to the axis of the shaft. It is reasonable to assume that for a gust frequency well below that of the blade passing frequency, the propeller would respond to the wind component $V_a = V.f(\theta)$ along the shaft axis. Ideally, $f(\theta) = \cos\theta$, as illustrated in Fig. 4.3. A helicoid propeller is designed to have a constant pitch P for any radius along the blade so that for each full turn of the propeller, the same amount of wind is passed at any position along the blades. The pitch P is the distance that the steady wind flow has moved along the axis of the anemometer during one revolution of the propeller, assuming ideal frictionless conditions. The pitch angle ϕ in Fig. 4.4, must necessarily increase with radius. A blade movement of d sin ϕ corresponds to the air moving a distance of d cos ϕ along the anemometer axis, so for one complete revolution of the propeller, the amount of air passed at a radius r is

$$d \cos\phi \cdot \frac{2\pi r}{d \sin\phi} \quad \text{metres}$$

so that

$$P = \frac{2\pi r}{\tan\phi} \quad \text{metres/revolution.}$$

It follows then that if the outer radius of the propeller is R_o with a pitch angle ϕ_o, then

$$\frac{r}{\tan\phi} = \frac{R_o}{\tan\phi_o} = R$$

so that

$$\frac{r}{R} = \tan\phi \qquad (4.1)$$

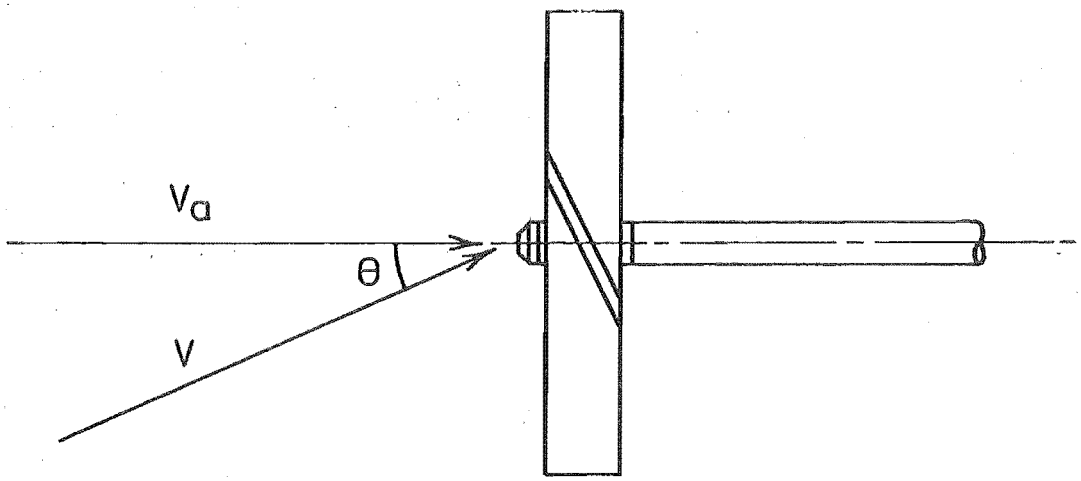

FIG. 4·3 FLOW GEOMETRY

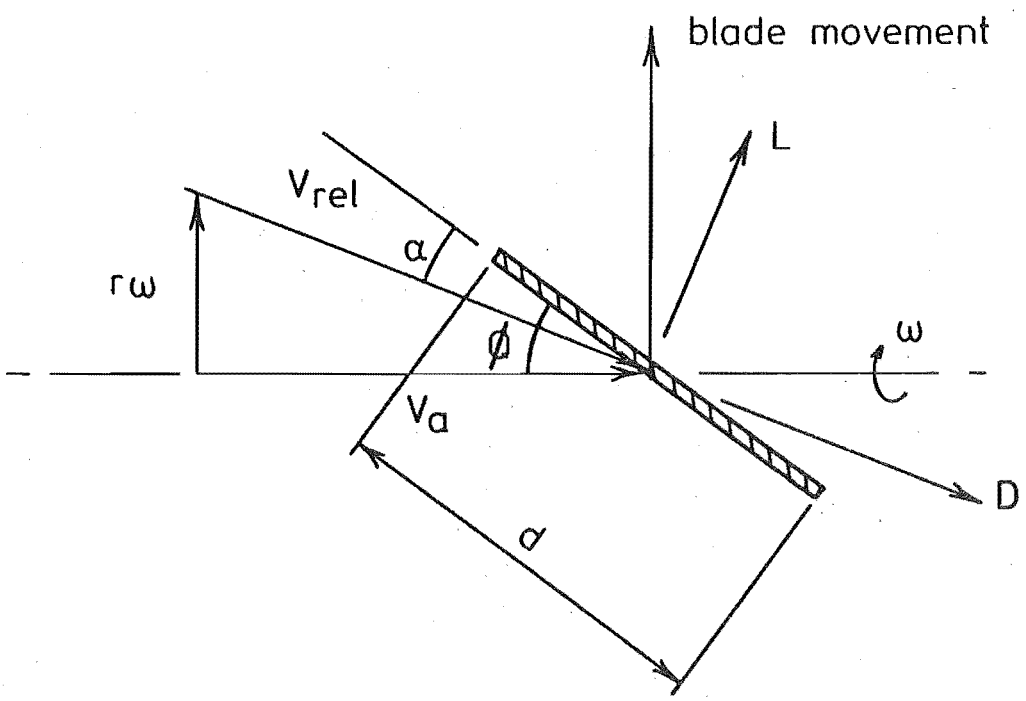

FIG. 4·4 COMPONENTS OF WIND VELOCITY AND FORCE.

If the angular velocity of the propeller is ω radians/second, then the wind velocity relative to the blade element is V_{REL} at an angle of incidence α to the blade element as shown in Fig. 4.4. It follows that

$$V_{REL}^2 = V_a^2 + r^2\omega^2 \tag{4.2}$$

also $$V_{REL}\cos\alpha = V_a\cos\phi + r\omega\sin\phi$$

and $$V_{REL}\sin\alpha = V_a\sin\phi - r\omega\cos\phi$$

$$\therefore \tan\alpha = \frac{V_a\sin\phi - r\omega\cos\phi}{V_a\cos\phi + r\omega\sin\phi}$$

$$= \frac{V_a\tan\phi - r\omega}{V_a + r\omega\tan\phi}$$

Using equation 4.1,

$$\tan\alpha = \frac{r(V_a - R\omega)}{V_aR + r^2\omega} \tag{4.3}$$

The aerodynamic forces on the blade elements are the lift, ΔL and drag, ΔD directed normal and along the direction of V_{REL} respectively and are assumed to be the same as for a flat plate for small angles of incidence.

Hence $$\Delta L = \frac{1}{2}\rho V_{REL}^2 C_L\, d\Delta r$$

For small α, C_L is proportional to α

so that $$\frac{dC_L}{d\alpha} = \text{constant, } C_L'$$

$$\therefore C_L = C_L'\alpha$$

and $$\Delta L = \frac{1}{2}\rho V_{REL}^2 C_L'\alpha\, d\Delta r \tag{4.4}$$

However for small α, C_D is independent of α

so that $\Delta D = \frac{1}{2} \rho V_{REL}^2 C_D \, d\Delta r$ (4.5)

The torque provided by the element is therefore

$$\Delta T = [\Delta L \cos(\phi-\alpha) - \Delta D \sin(\phi-\alpha)]\, r$$

or $$\Delta T = \frac{1}{2} \rho V_{REL}^2 [C_L' \alpha \cos(\phi-\alpha) - C_D \sin(\phi-\alpha)]\, r \, d\Delta r$$

The total aerodynamic torque on the propeller, T_A is then given by integrating the contribution ΔT from the blade element at radius r for r = 0 to r = R_o which results in a complicated expression. However the integration may be approximated to yield a more simple form of solution by evaluating $\frac{\Delta T}{d\Delta r}$ at r = R (so that $\phi = \frac{\pi}{4}$) and multiplying by an effective area A.

Since $$\frac{\Delta T}{d\Delta r} = \frac{1}{2} \rho V_{REL}^2 r[C_L' \alpha \cos(\phi-\alpha) - C_D \sin(\phi-\alpha)]$$

it follows then that for b number of blades and r = R,

$$T_A = \frac{\Delta T}{d\Delta r} A b$$

$$\therefore \quad T_A = \frac{1}{2} \rho V_{REL}^2 R A b[C_L' \alpha(\cos\phi \cos\alpha + \sin\phi \sin\alpha) - C_D(\sin\phi \cos\alpha - \cos\phi \sin\alpha)]$$

For small α which would occur in practice, $\tan\alpha = \sin\alpha = \alpha$ and $\cos\alpha = 1$,

also from equation 4.3 as r = R,

$$\alpha = \frac{V_a - R\omega}{V_a + R\omega} \tag{4.6}$$

and from equation 4.1,

$$\frac{r}{R} = \tan\phi = 1 \therefore \phi = \frac{\pi}{4} \text{ and } \cos\phi = \sin\phi = \frac{1}{\sqrt{2}}$$

$$\therefore \quad T_A = \frac{1}{2\sqrt{2}} \rho b R A V_{REL}^2 \left(C_L' \alpha(1+\alpha) - C_D(1-\alpha)\right) \tag{4.7}$$

In practice $C_D << C_L$ so the term C_D may be omitted together with all α^2 terms so that

$$T_A \approx \frac{1}{2\sqrt{2}} \rho b R A V_{REL}^2 C_L' \alpha$$

This relation may be expanded using equations 4.2 and 4.6 such that

$$T_A = \frac{1}{2\sqrt{2}} \rho\, b\, R\, A\, C_L' \left(V_a^2 + R^2\omega^2\right) \frac{(V_a - R\omega)}{(V_a + R\omega)}$$

$$= \frac{\rho\, b\, R\, A\, C_L'}{2\sqrt{2}} \left[\frac{V_a^3 + V_a R^2\omega^2 - V_a^2 R\omega - (R\omega)^3}{V_a + R\omega} \right]$$

Rearranging,

$$T_A = \frac{\rho\, b\, R\, A\, C_L'}{2\sqrt{2}} \left[V_a(V_a + R\omega)\left(\frac{V_a - R\omega}{V_a + R\omega}\right) - R\omega(V_a + R\omega)\left(\frac{V_a - R\omega}{V_a + R\omega}\right)^2 \right]$$

but as $\alpha = \dfrac{V_a - R\omega}{V_a + R\omega}$ and is small, the $\left(\dfrac{V_a - R\omega}{V_a + R\omega}\right)^2$ term may be neglected

so that $T_A \approx \dfrac{1}{2\sqrt{2}} \rho\, b\, R\, A\, C_L' \left|V_A\right| (V_a - R\omega)$ (4.8)

The restriction on the sign of the V_a term has been added to ensure the correct sign of T_A.

The equation of motion of the propeller may be written as

$$I\frac{d\omega}{dt} = T_A + T_s$$

where I is the moment of inertia of the rotating parts of the anemometer and T_s represents the effects of bearing friction, induced drag and changes in C_L due to air turbulence and secondary flows. Assuming that $T_s \alpha\, V_s^2\ (\theta)$, the sign of T_s depending on the direction of rotation and $V_s(\theta)$ being a function depending only on θ having the dimensions of velocity, then the equation of motion may be written as

$$L\, R\, \frac{d\omega}{dt} = \left|V\, f(\theta)\right| \left(Vf(\theta) - R\omega\right) - V_s^2(\theta) \operatorname{sign} \omega \qquad (4.9)$$

where

$$L = \frac{2\sqrt{2}\ I}{\rho\, b\, R^2\, A\, C_L'} \qquad (4.10)$$

a length characterising the dynamic response of the anemometer.

Thus the response of a propeller anemometer $\omega(t)$ to a wind velocity input (V,θ) can be predicted once the four parameters R, $f(\theta)$, $V_s(\theta)$ and L are known.

4.2 CALIBRATION FOR STEADY FLOWS

Under steady flow conditions, equation 4.9 reduces to

$$\bar{V}^2 f^2(\theta) - R\,\bar{\omega}\,\bar{V}\,f(\theta) - V_s^2(\theta) = 0$$

so that

$$\frac{R\bar{\omega}}{\bar{V}f(\theta)} = \frac{\bar{V}^2 f^2(\theta) - V_s^2(\theta)}{\bar{V}^2 f^2(\theta)} \qquad (4.11)$$

This expression relates the actual flow velocity $\bar{V}$ with the indicated velocity $R\bar{\omega}$ given by the rotational speed of anemometer shaft and its form is shown in Fig. 4.5.

It should be noted at this stage that :

If R is expressed in metres/radian then ω has the units rads/sec.

If R is expressed in metres/revolution then ω has the units revs/sec.

The latter combination is used in the following discussion.

4.2.1 High Speed Calibration

The calibration constant R may be found by testing the anemometer in a steady high speed wind tunnel flow so that $\bar{V}f(\theta)$ tends to $R\bar{\omega}$. With the shaft aligned into the flow then the equation 4.11 simplifies still further to

$$R = \frac{\bar{V}}{\bar{\omega}} \qquad (4.12)$$

Jackson (1976) noted that a small departure from equation 4.12 of around 4% could be expected due to the aerodynamic drag term that was neglected during the earlier analysis.

The propellers used in the present field tests were made by the University from expanded polystyrene and were designed to be similar in shape to the 19 cm (7½") diameter, 4 bladed Gill propeller. However, due to difficulties arising from the mould design, the blade thickness was somewhat greater than that of the Gill propeller and they did not have the dimensional accuracy and smoothness of the commercial product.

The manufacturer of the Gill anemometer reported (R.M. Young Co.,1972) that the calibration was linear with a value of R = 0.317 metres/rev. for all wind speeds over 1.2 m/sec and Jackson reported a similar calibration reading of 0.31.

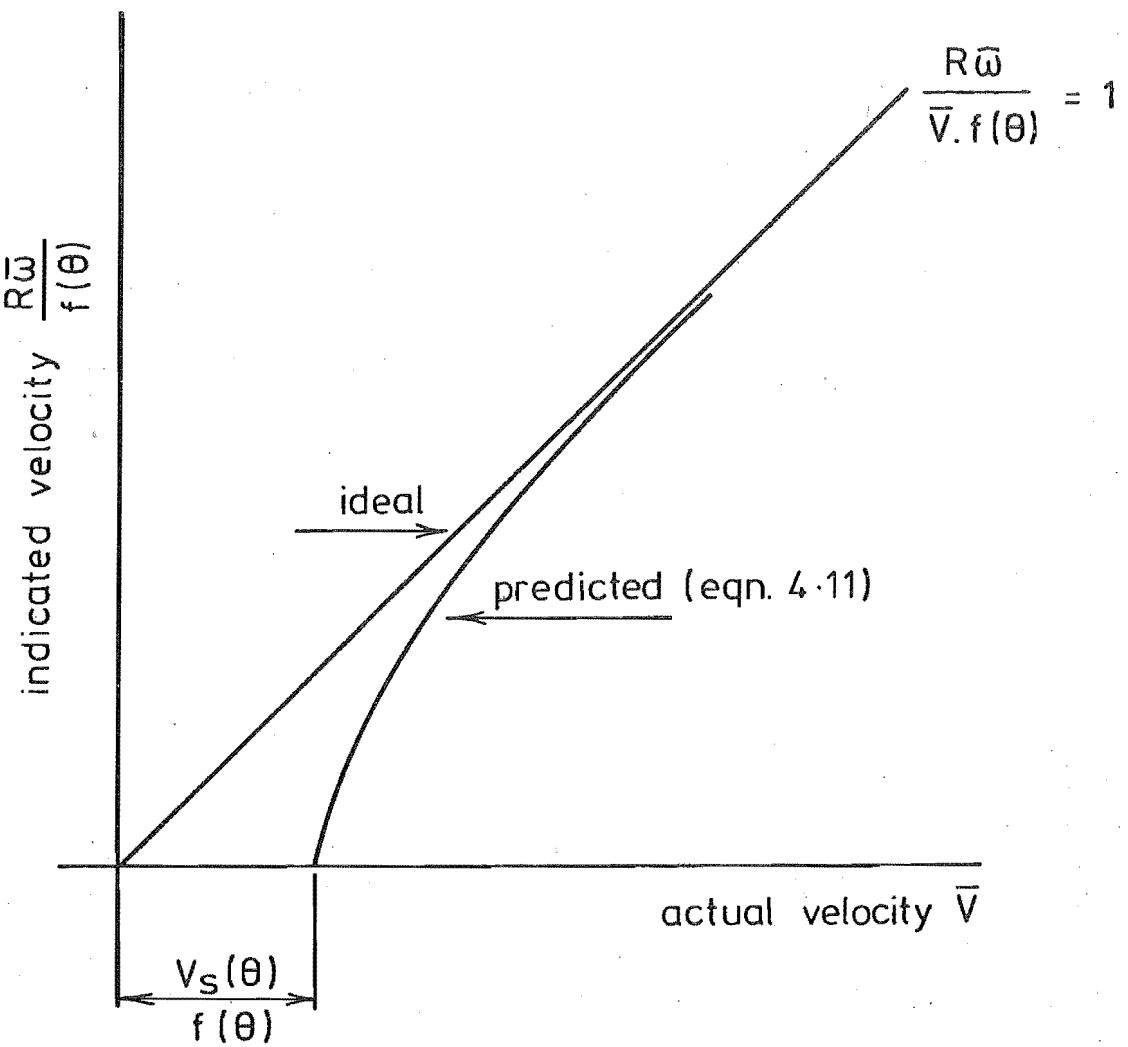

FIG. 4·5 PREDICTED VARIATION OF ANEMOMETER CALIBRATION FROM THE IDEAL CASE AT LOW VELOCITIES

The design of the University anemometer had developed through several models and with each design change, a difference in bearing type or method of support may have introduced changes in bearing friction. In addition, various batches of propellers had been made with varying degrees of dimensional accuracy and surface finish and it was shown by Milsom (1978) that the calibration could be changed by up to 8% by altering the surface finish and trimming the edges of the propeller. These factors make the earlier calibration tests such as those reported by Lindley et al (1974) (R = 0.290) inapplicable to the present instruments. In general, however, the often repeated calibration of the University anemometers have consistently produced lower values of R than with the Gill for the reasons just mentioned.

The propeller anemometers were calibrated by Flay (1978) in March 1977 and again just before the present tests as part of his field research programme and it was decided to use his results for the present test series. Flay obtained a best fit line of 0.277 and 0.271 respectively with a spread of approximately ± 5% amongst the 36 instruments at 10 m/s mean velocity. It was then evident that each instrument and propeller possessed its own characteristics and the calibration accuracy could only be improved by using individual values of R for each instrument-propeller combination. It was also noticed that the bearing friction could change during long periods in the field due to 'running in' processes lowering the friction or moisture and dust raising it. However, in view of the formidable task of keeping track of each instrument and propeller through propeller breakages and instrument replacement, it was decided to use a calibration value of R = 0.274 for all instruments and accept an expected error of about ± 0.5% per m/s velocity. As all the velocity data would be nondimensionalised, the scatter in the calibrations were considered to be more significant than a common error in the absolute value of R itself.

4.2.2 Stall Velocity

At low steady flow speeds illustrated in Fig.4.5, the linear calibration with velocity, $\frac{\bar{V}f(\theta)}{R\bar{\omega}} = 1$ no longer holds true and must then be predicted by equation 4.11. The anemometer just starts to turn when $Vf(\theta) = V_s(\theta)$, so $V_s(\theta)$ is called the stall velocity for a certain angle of incidence θ.

Low speed calibration tests have been conducted by Jackson (1976) using the Gill anemometer and later by Milsom (1978) under the supervision of the author using the University anemometers. Both tests used the technique of towing the anemometer at a known speed through still air.

Sample low speed calibration curves from Milsom are shown in Fig.4.6 for $\theta = 0$ and 75°. Difficulty was experienced in fitting the best value of $V_s(\theta)$ to fit all the test points which would easily explain the difference between Jackson's and Milsom's results shown in Table 4.1. At $\theta = 75°$ for instance, an average of all the test data indicated a value of $V_s(75) = 0.1$ m/s and a corresponding ratio $V_s^2(\theta)/V_s^2(0) = 0.28$ adopted by Milsom, whereas if only the data for the two lowest velocities were taken, a value of 0.066 m/s was obtained (and used in Fig.4.6 by the author). This latter approach yielded a $V_s^2(\theta)/V_s^2(0)$ ratio of 0.12 which was close to Jackson's 0.1. However the strong decrease in $V_s(\theta)$ was evident in both sets of results with θ. Other factors such as the interference from the mounting system would affect the results for incident angles close to 180°. It was also realised that the stall velocity would depend very much on the condition of the anemometer bearings. For increasing velocity, the actual calibration fell short of the ideal more than predicted by equation 4.11 which was probably due to the higher values of aerodynamic drag, especially at higher incident angles θ.

The information contained in Table 4.1 enables an estimate of the effect of stall velocity on the indicated velocity from an anemometer which is arranged at a certain angle to the flow in any wind velocity. Using equation 4.11 it follows that the necessary correction factor that should be applied would be

$$\frac{\bar{V}f(\theta)}{R\bar{\omega}} = \frac{1}{1 - \left[\frac{V_s(\theta)}{\bar{V}f(\theta)}\right]^2}$$

This expression is best rearranged as

$$\frac{\bar{V}f(\theta)}{R\bar{\omega}} = \frac{1}{1 - \left[\frac{V_s(0)}{\bar{V}}\right]^2 \left[\frac{V_s(\theta)}{V_s(0)}\right]^2 \left[\frac{1}{f(\theta)}\right]^2} \qquad (4.13)$$

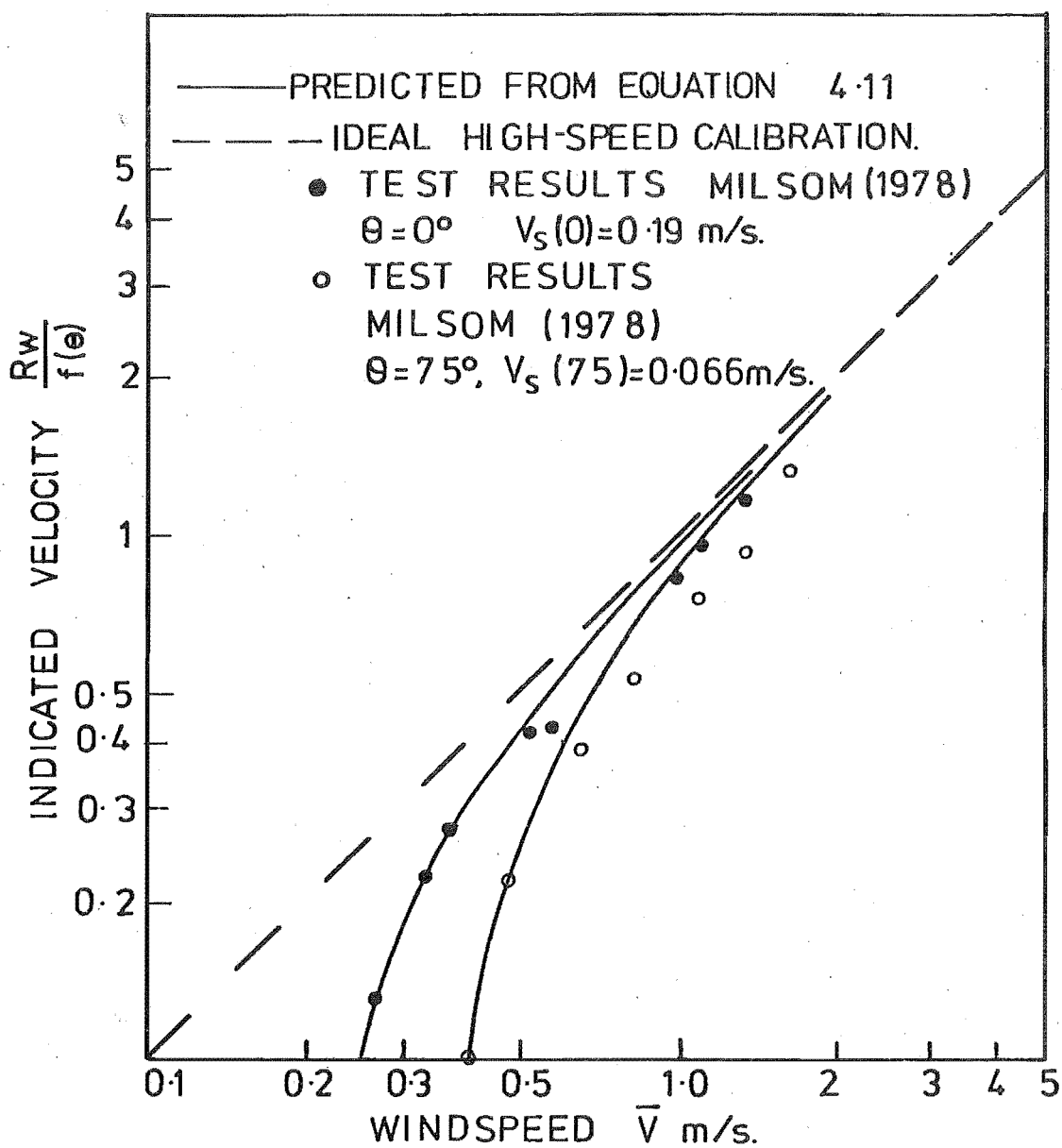

FIG. 4·6 PREDICTED AND ACTUAL VARIATION IN ANEMOMETER CALIBRATION FROM THE IDEAL CASE FOR θ = 0°, 75°.

ANGLE OF INCIDENCE θ	$V_s^2(\theta)/V_s^2(0)$	
	JACKSON (1976)	MILSOM (1978)
0	1.0	1.0
15	0.8	1.0
30	0.6	0.6
45	0.3	0.5
60	0.2	0.34
75	0.1	0.28
105	0.07	0.34
120	0.3	0.28
135	0.3	0.60
150	0.2	0.7
165	-0.2	1.1
180	0.2	1.2

$V_s(0)$:- JACKSON 0.27 m/s

MILSOM 0.19 m/s

TABLE 4.1 COMPARISON OF STALL VELOCITY WITH THE ANGLE OF INCIDENCE OF THE ANEMOMETER SHAFT

θ	$\left[\frac{V_s(\theta)}{V_s(0)}\right]^2$	f(θ)	Correction factors at certain velocities, m/s				
			$\bar{V}$ = 0.5	1	2	5	10
0	1.0	1.0	1.17	1.04	1.01	1	1
15	0.8	0.95	1.15	1.03	1.01	1	1
30	0.6	0.81	1.15	1.03	1.01	1	1
45	0.5	0.58	1.27	1.06	1.01	1	1
60	0.3	0.39	1.40	1.08	1.02	1	1
75	0.2	0.19	5.00	1.25	1.05	1.01	1
82	0.1	0.09	-	1.80	1.13	1.02	1
90	0	0	-	-	-	-	-

TABLE 4.2 EFFECT OF STALL VELOCITY ON THE ANEMOMETER OUTPUT

Using smoothed approximate data from Table 4.1 in conjunction with equation 4.13, the data in Table 4.2 was generated which indicates the approximate effect of velocity and angle of incidence on the anemometer accuracy. It is evident that for velocities below 2 m/s the stall velocity has a significant influence, especially for large angles of incidence. For normal high speed wind flows with the anemometers about 45° to the mean flow, this error would be insignificant. However, the accuracy of the vertical anemometer is seriously questioned but the data is insufficient to predict with sufficient accuracy the error at angles within a few degrees to the normal, so that this error could not be corrected for in the present tests.

4.2.3 THRESHOLD VELOCITY

The wind speed required to just start the propeller turning from rest is termed the Threshold Velocity, V_t. This velocity does not correspond to the stalling speed, V_s because parts of the propeller may be stalled when $\omega = 0$ and $V \neq 0$ whereas V_s is given by the backward extrapolation of measurements taken from a rotating unstalled propeller. The average value of V_t at $\theta = 0$ was found by Jackson (1976) to be 0.26 m/s for the Gill anemometer. Horst (1973) suggested that the threshold response effect would be minimised for the v and w components by orientating the array so that the mean wind bisected the angle between the U, V and W anemometers. However further testing suggested that there was little to be gained from tilting the W component away from the vertical due to the more involved analysis and loss of resolution in the horizontal and vertical components. Horst concluded that by arranging for the angle between the U, V anemometers to be bisected by the wind, the threshold response error (presumably incorporating the error due to the stall velocity also) would be eliminated and the non-cosine error discussed in Section 4.3 would be minimised.

The present discussion has indicated that the measured turbulence characteristics relying on the w component could be seriously affected by the threshold response and the resulting periods when the propeller was in a stalled, stationary state. It appears to be impossible to apply a correction factor to modify the apparent zero reading from a stalled anemometer. However, the error from the vertical anemometer due to stalling was shown by Horst to be surprisingly small for a power

spectra of the vertical wind component below a frequency of 0.3 Hz by comparing the output of a Gill array with a sonic anemometer. The adequacy of the vertical anemometer for horizontal wind speeds greater than 2 m/s was also confirmed by Hicks (1972).

4.2.4 Directional Response

Careful comparative experiments using an orthogonal array of Gill anemometers and a sonic anemometer as a reference prompted Horst (1973a) to conclude that the most serious error in the Gill anemometer at frequencies below about 0.3 Hz was the inability of the propeller to respond to the component of the wind parallel to the axis of rotation, i.e. V cos θ. This non-cosine response represented by $f(\theta)$ may be found by repeating the high speed calibration tests for various angles of incidence, θ. Horst (1973a), Jackson (1976) and Flay (1978) amongst others, have carried out these tests and have obtained similar values of $f(\theta)$ to the manufacturers of the Gill anemometer, R.M. Young and Co. A comparison of the $f(\theta)$ values recently obtained by Flay for the University anemometers and the ideal cosine response is shown in Fig.4.7. The reported correction factors computed from $\frac{\cos\theta}{f(\theta)}$ are shown as an integer$\times$100 in Fig.4.8 from the work of Horst, Jackson and Flay for comparison. The factors used in the present tests were a somewhat smoothed version of those recorded by Flay and are recorded in Table 4.3.

Any small differences in the reported correction factors for $-90° < \theta < +90°$ would be due to the difference in anemometer characteristics. Outside this range, the interference of the anemometer body or that of other anemometers in the array can cause large deviations from the $-90 < \theta < +90$ values, revealed by the asymmetry of the correction factors about 90° in Fig.4.8. Because the present tests involved the measurement of winds from one direction only, the anemometers were arranged so that the wind approximately bisected the angle between the two horizontal anemometers and correction factors for $0 < \theta < +90$ only (listed in Table 4.3) were incorporated in the correction procedure. The positive and negative flows expected in the vertical plane would be small compared with the horizontal component for strong, nearly horizontal flows so that the interference in this case would also be negligible and consequently was not accounted for in the correction procedure. A modification suggested by Hicks involving the addition of a shaft extension 'outboard' of the propeller could have improved the symmetry of the non-cosine response and decreased the stall region but was not attempted due to the development work involved.

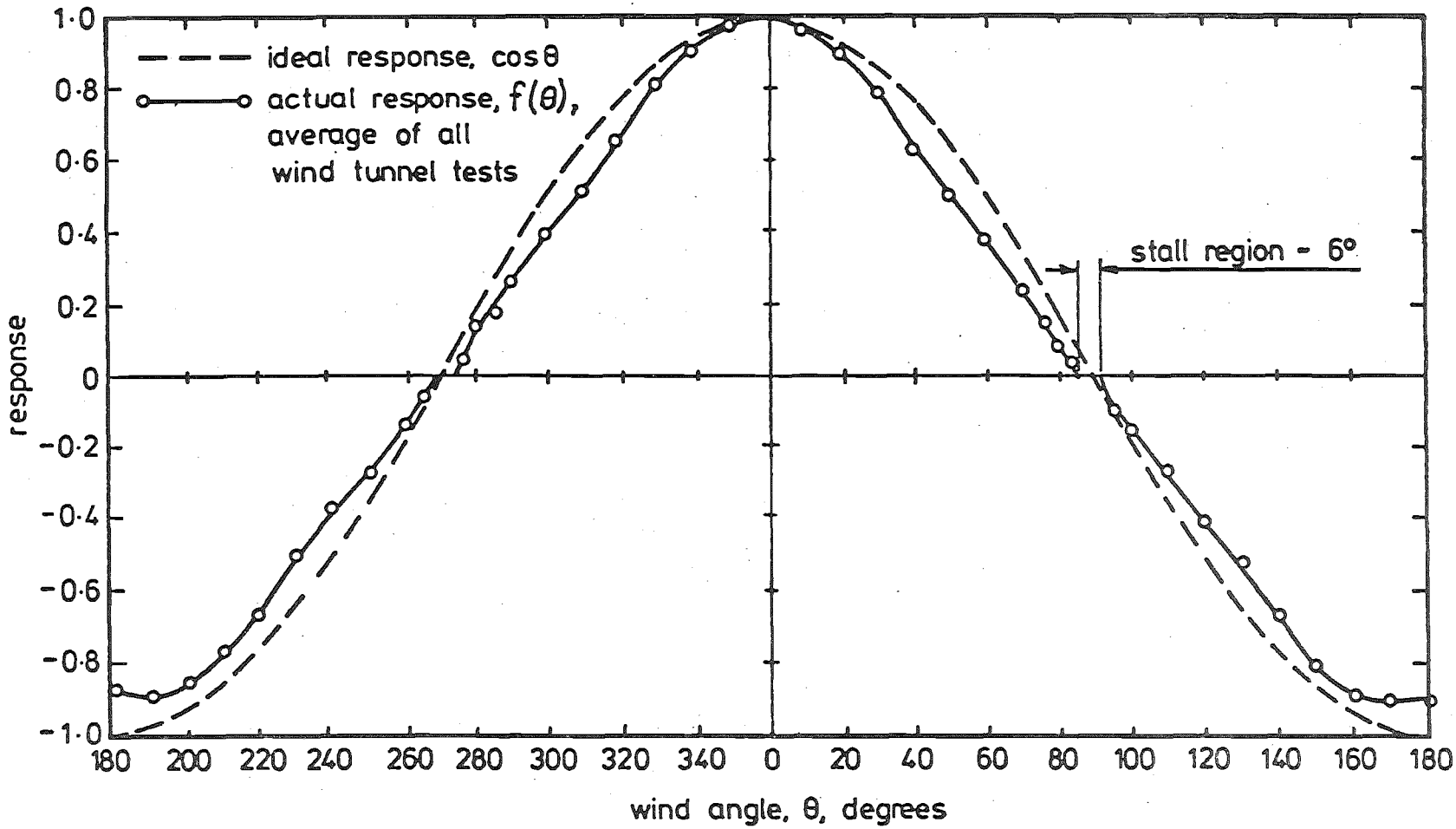

FIG 4·7 COMPARISON OF THE ACTUAL AND IDEAL DIRECTIONAL RESPONSE OF THE ANEMOMETER WITH WIND INCIDENCE ANGLE.

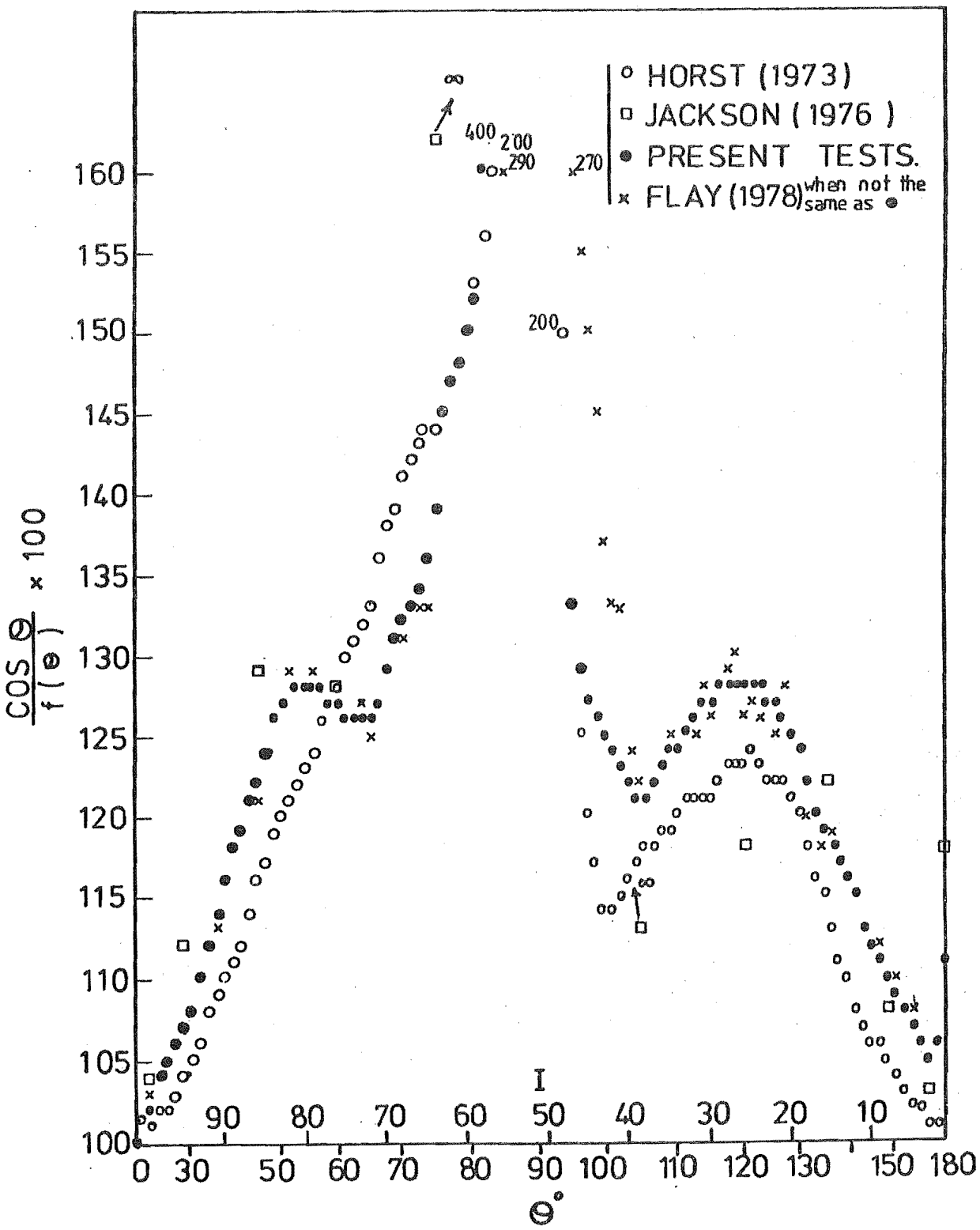

FIG. 4·8 NON COSINE RESPONSE FACTORS WITH ANGLE OF INCIDENCE.

I	cos θ	θ	$\frac{\cos\theta}{f(\theta)}$ x 100	I	cos θ	θ	$\frac{\cos\theta}{f(\theta)}$ x 100
1	-1.00	180	111	101	+1.00	0	100
2	-0.98		106	100	0.98		101
3	-0.96		105	99	0.96		102
4	-0.94		106	98	0.94		104
5	-0.92		107	97	0.92		105
6	-0.90	154	108	96	0.90	26	106
7	-0.88		109	95	0.88		107
8	-0.86		110	94	0.86		108
9	-0.84		111	93	0.84		110
10	-0.82		112	92	0.82		112
11	-0.80	143	113	91	0.80	37	114
12	-0.78		115	90	0.78		116
13	-0.76		116	89	0.76		118
14	-0.74		117	88	0.74		119
15	-0.72		118	87	0.72		121
16	-0.70	134	119	86	0.70	46	122
17	-0.68		120	85	0.68		124
18	-0.66		122	84	0.66		126
19	-0.64		124	83	0.64		127
20	-0.62		125	82	0.62		128
21	-0.60	127	126	81	0.60	53	128
22	-0.58		127	80	0.58		128
23	-0.56		127	79	0.56		128
24	-0.54		128	78	0.54		128
25	-0.52		128	77	0.52		127
26	-0.50	120	128	76	0.50	60	127
27	-0.48		128	75	0.48		126
28	-0.46		128	74	0.46		126
29	-0.44		128	73	0.44		126
30	-0.42		127	72	0.42		126
31	-0.40	114	127	71	0.40	66	127
32	-0.38		126	70	0.38		129
33	-0.36		125	69	0.36		131
34	-0.34		124	68	0.34		132
35	-0.32		124	67	0.32		133
36	-0.30	107	123	66	0.30	73	134
37	-0.28		122	65	0.28		136
38	-0.26		121	64	0.26		139
39	-0.24		121	63	0.24		145
40	-0.22		122	62	0.22		147
41	-0.20	102	123	61	0.20	78	148
42	-0.18		124	60	0.18		150
43	-0.16		125	59	0.16		152
44	-0.14		126	58	0.14		160
45	-0.12		127	57	0.12		171
46	-0.10	96	129	56	0.10	84	204
47	-0.08		133	55	0.08		267
48	-0.06		200	54	0.06		400
49	-0.04		400	53	0.04		400
50	-0.02		400	52	0.02		400
51	-0.00	90	400				

TABLE 4.3 HORIZONTAL NON-COSINE RESPONSE CORRECTION FACTORS

The correction factors for the vertical anemometer when the wind flow fluctuates about an angle close to 90°, are large compared with those associated with small angles close to $\theta = 0°$ (see Fig.4.9). As θ moves away from 90°, the correction factors tend to a value of + 1.25 over the range $50 < \theta < 130$ due to the almost linear variation of cos θ and $f(\theta)$ as shown in Fig.4.9. It has been suggested by Horst (1973a) and Gill (1975) that the iterative correction procedure for non-cosine response described later under Chapter 5 may be expedited by applying a correction factor of + 1.25 to all the vertical anemometer readings beforehand and using correspondingly lower correction factors in the iterative correction procedure. This was in fact done in the present tests. However the small change in directional response with wind speed noticed by Hicks (1972) was not accounted for in the present tests as it was considered a small second order effect.

4.3 DYNAMIC PERFORMANCE

The extent to which the propeller anemometer can faithfully record the variation of wind velocity in the turbulent atmosphere must be appreciated if any confidence is to be placed in the recorded data. A useful indication of their accuracy under such conditions may be obtained from a comparison of their output with a sonic anemometer, but the number of tests reported such as Horst (1973a) have been very few. The University has so far not attempted this exercise due to the expense and as yet unproven performance of the few available commercial sonic anemometers. However an indication of the likely dynamic performance and pertinent factors may be obtained from a study of the first order system response. A logical extension to this analysis is to estimate the aerodynamic admittance function or frequency response of the anemometer from simple wind tunnel experiments and apply it to the known likely power spectra in the atmosphere to estimate the inherent errors from the instrument's response. Such an analysis is described in the following section for the University propeller anemometer together with a discussion of the significant factors that determine its performance.

4.3.1 Distance Constant

The dynamic performance of the anemometer shaft and propeller is described by the equation of motion (4.9) which may be rearranged as

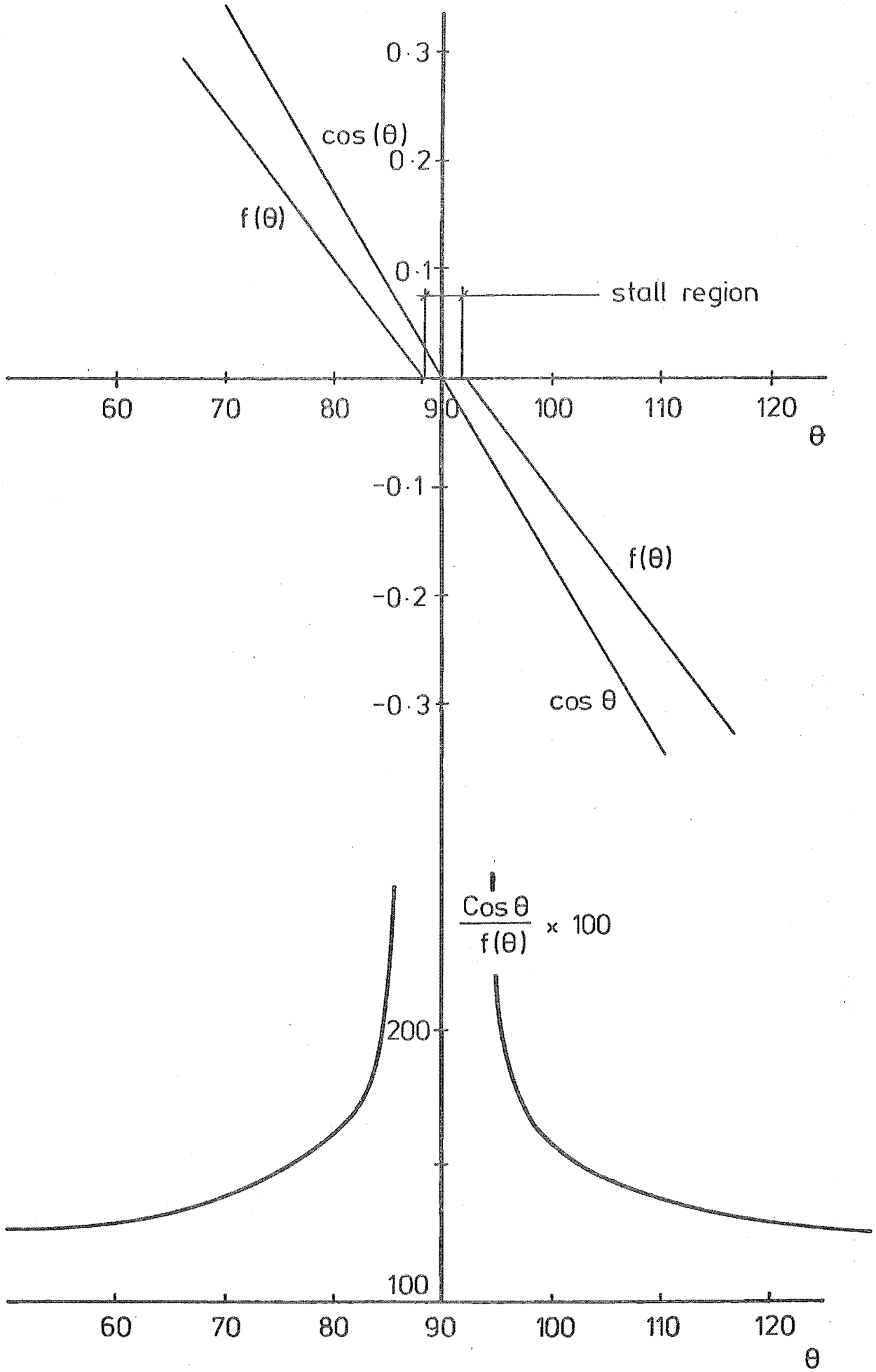

FIG 4·9 DIRECTIONAL RESPONSE FOR NEAR PERPENDICULAR FLOW DIRECTIONS.

$$\frac{L}{Vf(\theta)} \cdot \frac{d(R\omega)}{dt} + (R\omega) = \frac{V^2 f^2(\theta) - V_s^2(\theta)}{Vf(\theta)} \qquad (4.14)$$

Equation 4.14 describes the response of a first order system with time and may be compared with the standard form

$$T_c \frac{d\omega}{dt} + \omega = A$$

which has a solution of the form, $\omega = A\left(1 - e^{-t/T_c}\right)$ (4.15)

Consider the case when A is a constant, describing a step input at time t = 0 so that

$$A = \frac{V^2 f(\theta) - V_s^2(\theta)}{Vf(\theta)}$$

If the step input in velocity V is sufficiently large compared with the stall velocity $V_s(\theta)$, then $A \rightarrow Vf(\theta)$.

The response time constant $T_c = \frac{L}{Vf(\theta)}$ varies with flow velocity whereas the characteristic length, L predicted by equation 4.10 does not and is therefore a more useful anemometer characteristic and for this reason, L is termed the distance constant.

i.e. $L = Vf(\theta)\ T_c$ (4.16)

The dynamic behaviour of the instrument to a step change in wind speed may be recorded from wind tunnel tests by releasing the anemometer from rest in a flow of known velocity and recording the analogue output trace with time. A typical response is shown in Fig.4.10 from which the distance constant may be calculated. The response is not adequately described by equation 4.15 for small t when the propeller is stalled but this may be overcome by measuring the time taken $\Delta t = T_c$ for ω to change from ω_1 to ω_2 so that

$$\frac{\omega_2 - \omega_1}{\omega_3 - \omega_1} \approx 1 - \frac{1}{e} = 0.632$$

A more accurate method would be to somehow provide a step input in flow velocity on a rotating unstalled propeller but is fraught with practical difficulties. The manufacturers of the Gill anemometer R.M. Young, quote a value of L = 0.82 m for the 7½" four bladed propeller in the Gill anemometer whilst Jackson (1976) reported L = 0.95 m for a $6\frac{1}{8}$" diameter propeller. Recent tests on the University anemometer and propeller estimated L = 0.89 m but found variations of

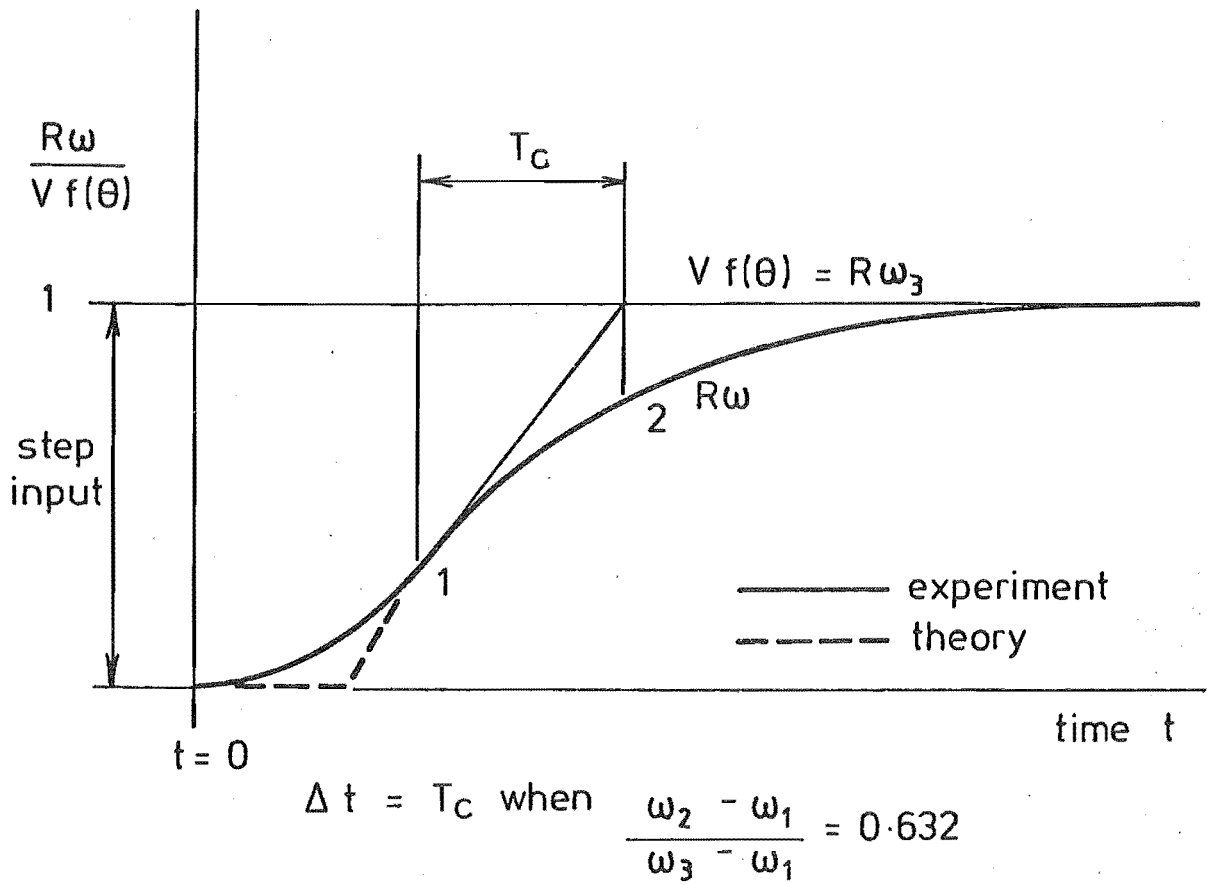

FIG. 4·10 RESPONSE OF A STOPPED ANEMOMETER AFTER RELEASE IN AN AIR FLOW

± 6% depending on the type of bearings employed. It therefore seemed reasonable to adopt a value of $L \approx 0.9$ m for the distance constant (at $\theta = 0°$) of the University anemometer system. It should be noted that the University design utilises a light chopping disc instead of the small generator in the Gill anemometer, but the performance has not been improved significantly. This insensitivity of the performance to the shaft inertia would be due to the propeller which has a dominating polar moment of inertia of the order of 100 times that of the shaft, together with aerodynamic damping effects which have not been investigated.

The response length has been observed by Hicks (1972), Gill (1975), Jackson (1976) and others to have a strong dependence on the angle of incidence and their results are shown together in Fig.4.11 for comparison. Hicks suggested that especially for values of θ close to 90°, $L(\theta) = L(0) \cos^{\frac{1}{2}} \theta$ which appears from Fig.4.11 to be a reasonable approximation of what has been observed. For an orthogonal array, the horizontal anemometers would be consistently about 45° away from the wind flow so that a more realistic distant constant would be $L(45) = 0.90/0.85 = 1.06$ or close to 1 metre. In view of these findings and the level of accuracy involved, an effective value of $L = 1$ metre has been adopted for the dynamic response estimates that follow. It can be seen however, that the equivalent distance constant for the vertical anemometer would be typically 4 or 5 metres at least, depending on the degree of turbulence and mean vertical component of wind velocity occurring.

4.3.2 Frequency Response of a First Order System

Let us consider the case when $\theta = 0$ and the anemometer is subjected to small fluctuations in a high speed flow so that $V >> V_s$ and $T_c = \frac{L}{\bar{V}}$. In this case, the equation of motion described by equation 4.14 reduces to

$$T_c \frac{d\omega}{dt} + \omega = \frac{V}{R} .$$

Consider now a sinusoidal velocity fluctuation of frequency $f = 2\pi n$ radians/sec,

$$V = \bar{V} + \Delta V \sin ft$$

so that

$$V = \bar{V} \left(1 + \frac{\Delta V}{\bar{V}} \sin ft\right)$$

and

$$T_c \frac{d\omega}{dt} + \omega = \frac{\bar{V}}{R} \left(1 + \frac{\Delta V}{\bar{V}} \sin ft\right) \qquad (4.17)$$

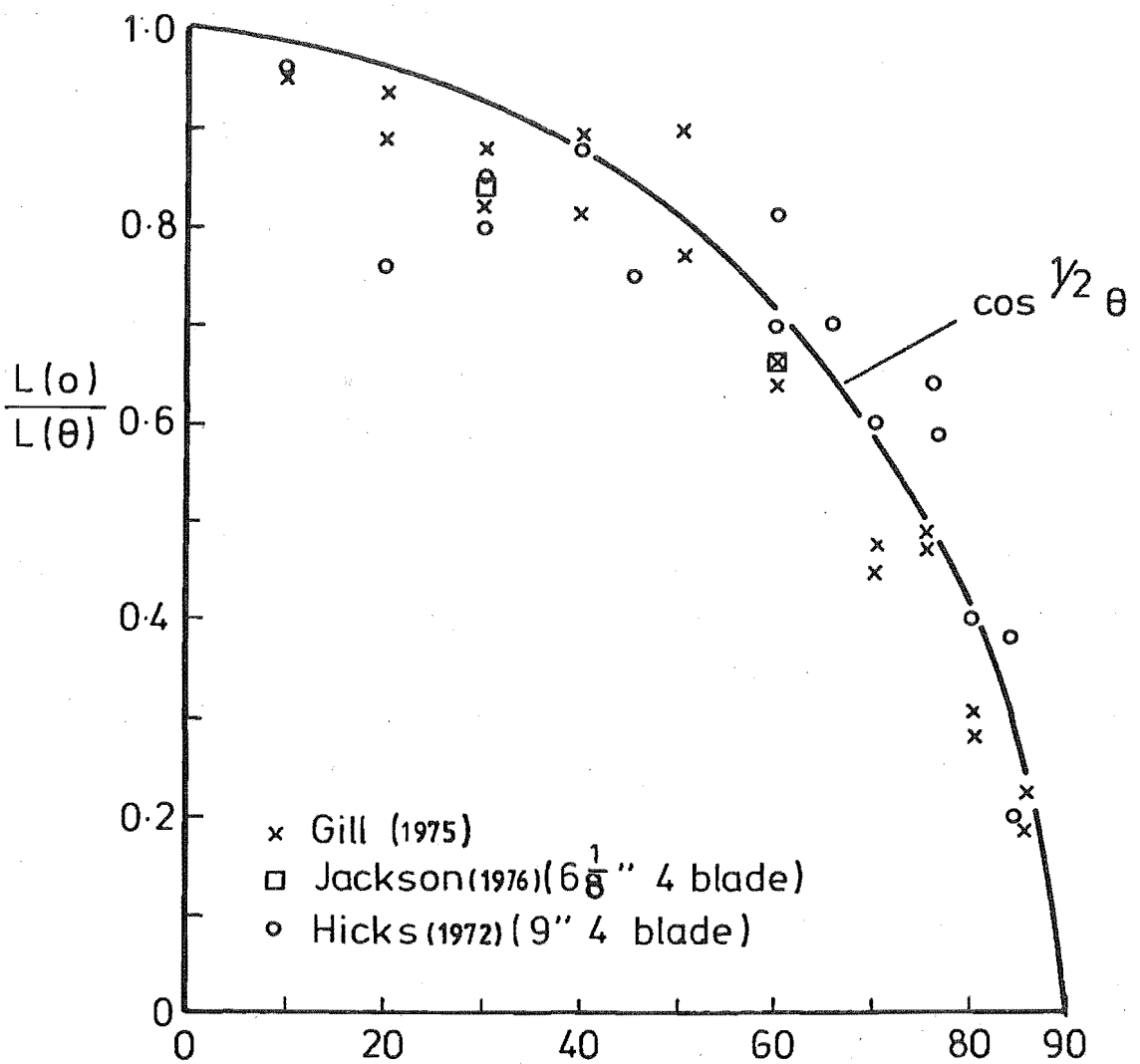

FIG 4·11 VARIATION OF DISTANCE CONSTANT WITH ANGLE OF INCIDENCE.

The steady state solution to the equation of motion under these conditions will be of the form

$$\omega = B \sin ft + C \cos ft + D$$

The coefficients may be found by comparing terms according to classical theory,

so that $\frac{d\omega}{dt} = Bf \cos ft - Cf \sin ft$

$$\therefore \quad T_c \frac{d\omega}{dt} + \omega = BfT_c \cos ft - CfT_c \sin ft + B \sin ft + C \cos ft + D$$

$$= (BfT_c + C) \cos ft + (B - CfT_c) \sin ft + D$$

by comparing terms with equation 4.17,

$$BfT_c + C = 0, \quad B - CfT_c = \frac{\Delta V}{R} \text{ and } D = \frac{\bar{V}}{R}$$

$$\therefore \quad B = \frac{\Delta V}{R} \frac{1}{[1+(fT_c)^2]} \text{ and } C = -\frac{\Delta V}{R} \frac{fT_c}{[1+(fT_c)^2]}$$

so that $\omega = \frac{\Delta V}{R} \frac{1}{[1+(fT_c)^2]} (\sin ft - fT_c \cos ft) + \frac{\bar{V}}{R}$

which may be arranged so that

$$\omega = \frac{\bar{V}}{R} + \frac{\Delta V}{R} \frac{1}{[1+(fT_c)^2]^{\frac{1}{2}}} \left[\frac{\sin ft}{[1+(fT_c)^2]^{\frac{1}{2}}} - \frac{fT_c \cos ft}{[1+(fT_c)^2]^{\frac{1}{2}}} \right]$$

Let $\phi = \tan^{-1} fT_c$

$$\therefore \quad \sin \phi = \frac{fT_c}{[1+(fT_c)^2]^{\frac{1}{2}}} \text{ and } \cos \phi = \frac{1}{[1+(fT_c)^2]^{\frac{1}{2}}}$$

$$\therefore \quad \omega = \frac{\bar{V}}{R} + \frac{\Delta V}{R} \frac{1}{[1+(fT_c)^2]^{\frac{1}{2}}} \left[\cos \phi \sin ft - \sin \phi \cos ft \right]$$

$$= \frac{\bar{V}}{R} + \frac{\Delta V}{R} \frac{1}{[1+(fT_c)^2]^{\frac{1}{2}}} \sin (ft - \phi)$$

The indicated velocity $V_i = R\omega$ is then given by

$$V_i = \bar{V} + \Delta V \frac{1}{[1+(fT_c)^2]^{\frac{1}{2}}} \sin (ft - \phi) \qquad (4.18)$$

The output of an anemometer behaving as a first order system with a sinusoidal velocity input of frequency $f = 2\pi n$, is given by equation 4.18. The equation predicts that the anemometer would indicate the correct mean velocity but the magnitude of the indicated oscillation would be less by a factor $[1+(2\pi nT_c)^2]^{-\frac{1}{2}}$ and lag by a phase angle $\phi = \tan^{-1} fT_c$. In other words,

$$\frac{\Delta V_i}{\Delta V} = [1+(2\pi n T_c)^2]^{-\frac{1}{2}} \qquad (4.19)$$

where ΔV_i is the indicated amplitude of the fluctuating velocity.

The sinusoidal gust of frequency n will possess a wavelength $\lambda = \frac{\bar{V}}{n}$. Remembering that $T_c = \frac{L}{\bar{V}}$, then

$$2\pi n T_c = 2\pi n \frac{L}{\bar{V}} = 2\pi \frac{L}{\lambda}$$

Rearranging equation 4.19 ,

$$\frac{\Delta V_i}{\Delta V} = \left[1+\left(2\pi \frac{L}{\lambda}\right)^2\right]^{-\frac{1}{2}} \qquad (4.20)$$

The ratio of indicated to true velocity for an anemometer with a distance constant of L metres is predicted by equation 4.20 for various gust wavelengths λ m. This equation has been commonly used to predict instrument responses and Fig.4.12 taken from Gill (1967) indicates this theoretical effect on the accuracy of various anemometers showing different distance constants. The response of the Gill anemometers to sinusoidal fluctuations have been recorded experimentally by Ng (1972) using a gust generator and the results are shown in Fig.4.13. The consistently low experimental values of $\frac{\Delta V_i}{\Delta V}$ even at large $\frac{\lambda}{L}$ indicates a consistent 8% experimental error rather than a significant deviation from the first order prediction, as the experimental values tend to $\frac{\Delta V_i}{\Delta V} = 0.92$ as $\frac{\lambda}{L} \to \infty$ and not 1.0 as expected.

4.3.3 Admittance Function

The first order response described by equation 4.20 may be used to indicate the accuracy of the recorded velocity power spectra at different frequencies. It is convenient for this purpose to use an aerodynamic admittance factor $|\chi(n)|$ such that

$$|\chi(n)|^2 = \left[\frac{\Delta V_i}{\Delta V}\right]^2$$

and

$$S(n) = \frac{S(n)_i}{|\chi(n)|^2}$$

where $S(n)_i$ is the indicated variance at a frequency n.

Due to the constantly varying angle of incidence θ, the distance constant $L(\theta)$ will vary and affect the instantaneous value of $\chi(n)$. The effect of turbulence intensity on the response of a vertical Gill anemometer has been investigated by Fichtl and Kumar (1974) and found

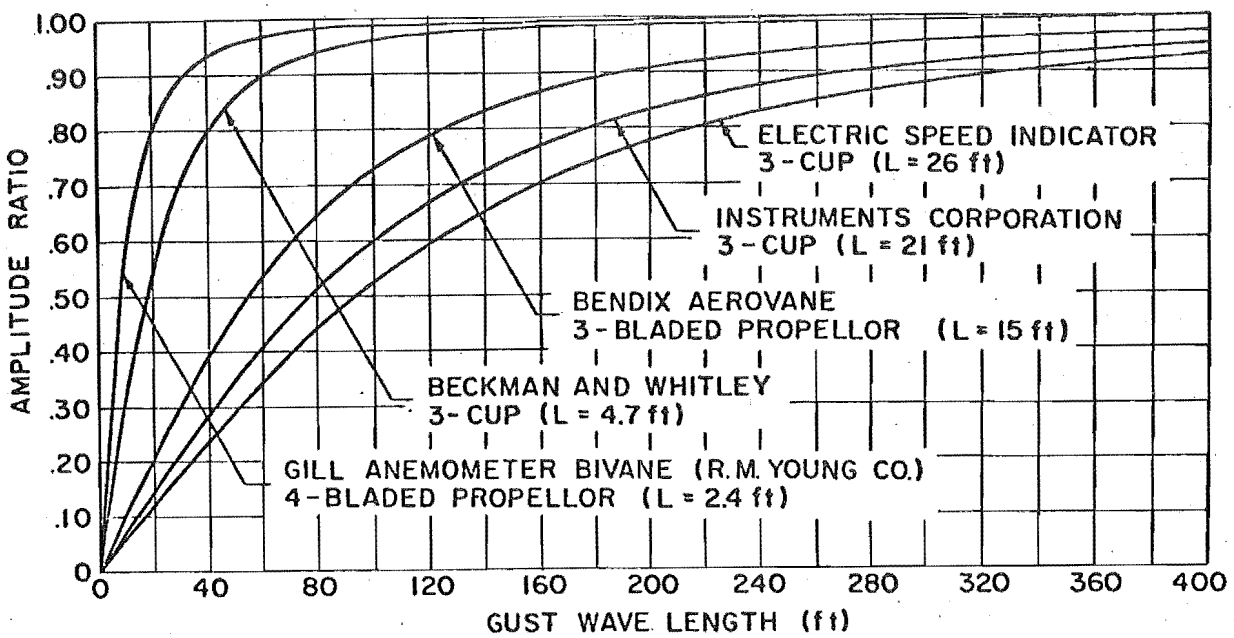

FIG 4·12 RESPONSE OF SEVERAL TYPICAL WIND SENSORS TO SINUSOIDAL WIND SPEED FLUCTUATIONS OF VARYING GUST WAVELENGTH (GILL, 1967)

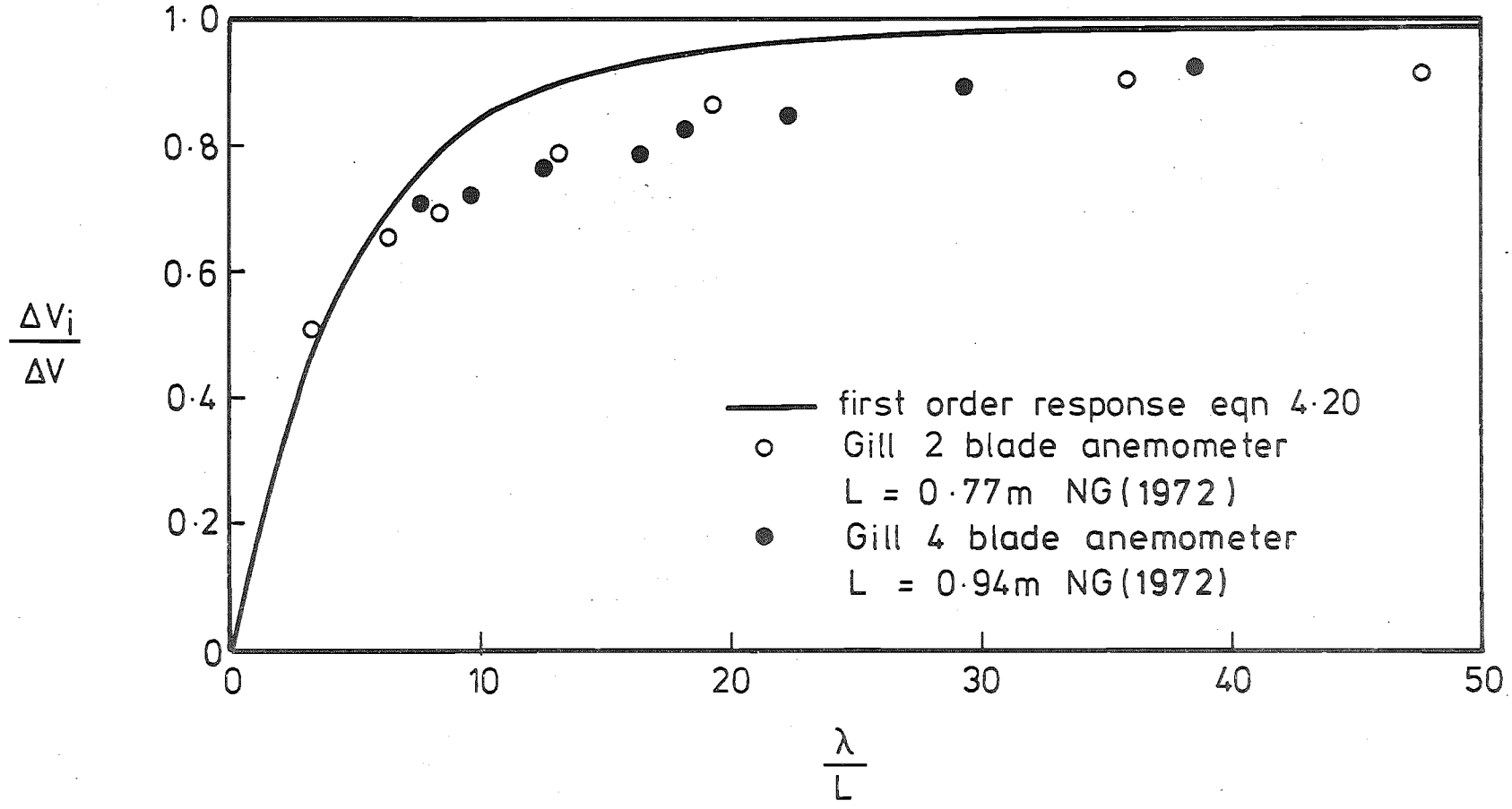

FIG. 4·13 RESPONSE OF GILL ANEMOMETERS TO SINUSOIDAL WIND VELOCITY

to be significant but this correction has not been attempted in the present tests. They concluded that although the vertical anemometer behaved as a first order system the phase angle was not as predicted. In fact, the anemometer became more responsive to a step change in increasing vertical turbulence intensities $\frac{\sigma w}{\bar{V}}$. However, using a constant average distance constant and equation 4.20 then

$$|\chi(n)|^2 = \left[1+(2\pi L)^2 \left(\frac{n}{\bar{V}}\right)^2\right]^{-1} \qquad (4.21)$$

The resulting Admittance functions for the horizontal anemometers using L = L(45) $\approx$ 1 m and the vertical anemometers using L $\approx$ 5 m (see Section 4.3.1) are plotted against gust frequency in Fig.4.14. For less than a 1% error in $\frac{\Delta V_i}{\Delta V}$ when L = 1 m, $\frac{n}{\bar{V}} \leq 0.023$. The corresponding maximum frequency limit of the instrument for 99% accuracy in recorded velocity is dependent on velocity as shown in the following table :

$\bar{V}$ m/s	1	2	5	7	10	15	20
n_{max}	0.02	0.05	0.11	0.16	0.23	0.34	0.46

The effect of the aerodynamic admittance function may be illustrated by applying it to the standard velocity power spectral density functions from ESDU (1974) for the wind conditions similar to those recorded in Amberley run #5. The three components of the velocity power spectral density functions are shown in Fig.4.15 as standard data and also as predicted by the anemometer, taking regard to its first order response. It can be seen that the longitudinal and lateral components are affected very little, with frequencies below about 0.25 Hz (for $\bar{V}$ = 7.88 m/s) being recorded without error. However, due to the higher frequency content of the vertical component and the longer distant constant for flows nearly normal to the anemometer shaft, the vertical power spectral density is severely affected even at the peak frequency. However, the peak frequency and distant constant for the vertical component are not as reliable as for the other components, so the indicated vertical spectrum must only be taken as approximate.

By comparing the square root of the area under each spectrum, the ratio of indicated to actual turbulence intensity may be obtained. In the case of the u and v components the error in indicated turbulence intensity is less than 1.5%, but for the w component this analysis indicates an error of about 33% below that expected.

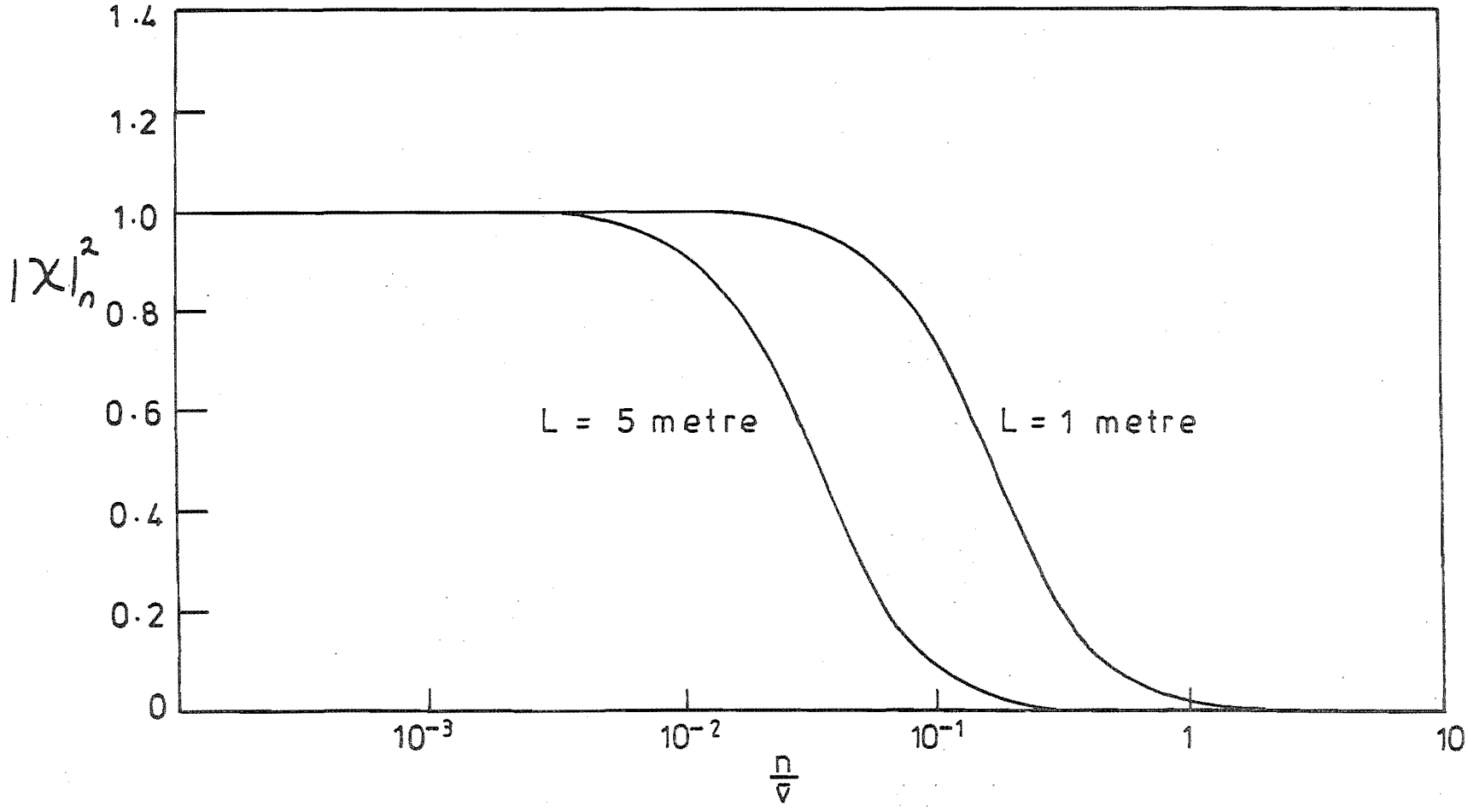

Fig. 4.14 VARIATION OF AERODYNAMIC ADMITTANCE FUNCTION WITH GUST FREQUENCY.

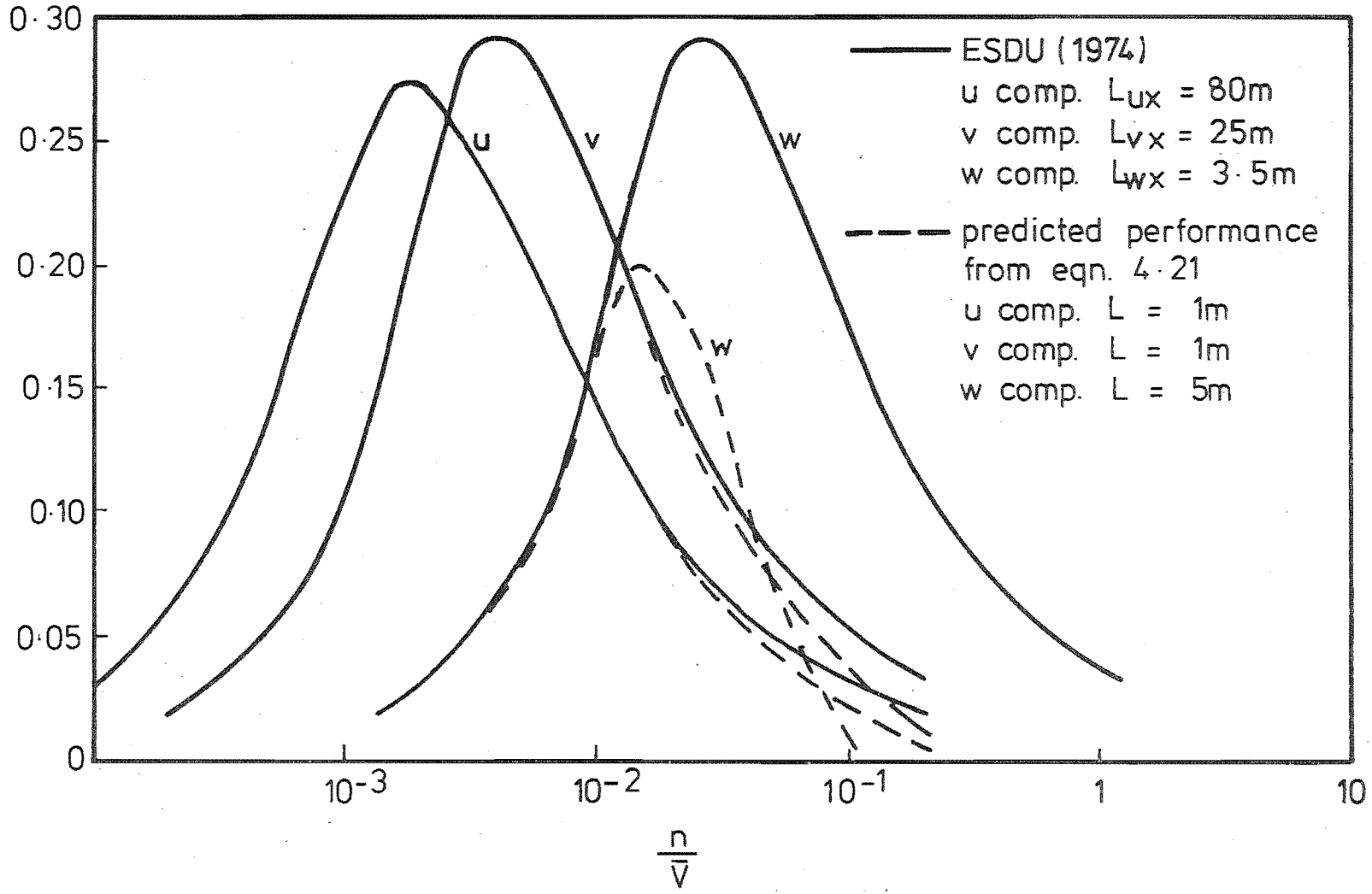

FIG. 4·15 PREDICTED ANEMOMETER FREQUENCY RESPONSE ON THE THREE COMPONENTS OF VELOCITY POWER SPECTRAL DENSITIES TAKEN FROM ESDU (1974) Z_o=0·05, Z=10m, V=7·88 m/s.

The effects of friction and inertia were investigated theoretically by Jackson (1976) who also showed that the values of $\bar{U}$ and σu for high wind speeds were relatively unaffected by the inclusion of friction and inertia terms in the equation of motion. However, the vertical component suffered considerably with corrections of up to 25 to 30% estimated as necessary for the σw and $\sqrt{\overline{uw}}$ terms. In addition, direct field test comparisons between propeller and sonic anemometers by Hicks (1972) and Horst (1973a) reported that the performance of the vertical anemometer was accurate for frequencies below about 0.2 Hz but due to the higher frequency content, the underestimation of the Reynolds stress and the variance could be considerable. On the other hand, the Reynolds stress co-spectrum is constituted mainly from the lower frequencies (Kaimal et al 1972), thus increasing the probable accuracy of the result and reducing its dependence on the anemometer performance at higher frequencies.

Jackson concluded that the proper approach was to solve the three equations of motion for each anemometer at each time step to take account of the nonlinear forcing function, including the effects of inertia and friction. However this was considered beyond the scope of the present test programme and was therefore not attempted. The large possible underestimation of the vertical variance and Reynolds stress was left uncorrected and the results must therefore be treated as an indication of their approximate value only.

4.3.4 Overestimation

Although a good deal has been published on the performance of propeller anemometers in turbulent flows as indicated in the preceding discussion, most of the attention has been directed to their frequency response and resulting accuracy in determining power spectra, Reynolds stresses and turbulence intensities. However very little information is available on their overestimation of the mean velocity which is an established characteristic of the less responsive cup anemometers.

Tieleman and Tavoularis (1977) compared the performance of a pair of othogonal propeller anemometers against a TSI split film anemometer system and noted that the propeller anemometers overestimated the mean velocity by up to 7% in a flow with a turbulence intensity of 22%. However, conflicting evidence from Horst (1973) showed that the Gill UVW anemometer system yielded mean velocities after correcting for non-cosine response, which were consistently within the 5% scatter indicated by the two reference sonic anemometers.

Laboratory tests using 'sinusoidal' gusts generated in a wind tunnel by Lindley and Bowen (1974) indicated that for normal turbulence levels encountered (say $\sigma u/\bar{V} = 0.22$ giving the parameter $\frac{1}{2}(\frac{\Delta V}{\bar{V}})^2 \simeq 0.05$), the overestimation of the mean wind speed would be small. Consequently, in the light of these tests and the scant and indecisive field evidence available, the effect of overestimation was ignored in the present tests.

4.4 TOWER EFFECT

It is well known that the proximity of the anemometer to its supporting tower may affect the accuracy of its recordings and there have been a number of experimental investigations of this problem such as Gill et al (1967) and Cermak and Horn (1968). The magnitude of the tower influence varies considerably with the design of the tower, the distance of the anemometer away from the tower and the wind direction. The effect is worst of course when the anemometer lies in the wake of the mast but a 5% reinforcement has been noted by Gill when positioned about one tower width upwind of an open lattice tower.

In the present tests, the direction of the wind was known beforehand and the anemometers were placed upwind of the towers at a distance between 1.7 and 17 tower widths from the edge of the tower. (Flay (1978)). Consequently the tower effect was considered to be negligible.

4.5 CONCLUSIONS

* The preceding discussion indicated that the propeller anemometers used in the present tests were adequate for the longitudinal and lateral turbulence measurements in the atmosphere provided that the mean wind bisected approximately the angle between the two horizontal instruments.

* For anemometers in good order and mean wind speeds over 2 m/s, the mean wind speed would be accurate to within ± 0.5% per m/s provided that the readings were corrected for non-cosine response.

* Gusts with frequencies up to approximately 0.25 Hz at 10 m/s mean wind speed would be accurately followed, but the frequency limit would decrease with decreasing velocity. For gust frequencies above the limit, the error would increase but the overall effect on the turbulence intensities would be about 1.5% or less for the longitudinal component.

* The accuracy of the vertical anemometer appeared to fall far below that of the horizontal pair due to the generally low vertical velocities encountered and the frequent stopping and starting.

* The vertical turbulence intensity and Reynolds stress were predicted as being about 30% low coupled with a significant effect on the vertical power spectral density functions above a frequency of about 0.1 Hz. However indications from comparative field tests were that the performance of the w component was poor but may be better than that anticipated from a theoretical study.

* Improvements to the quality of the surface finish and dimensional accuracy of the helicoid propellers could improve their accuracy significantly. Better bearing design to reduce friction could improve the dynamic performance, but the distance constant could not be improved significantly without a reduction in the propeller inertia. Any improvement may be limited by the aerodynamic damping which has so far, received very little attention in the literature.

CHAPTER 5

FIELD DATA ACQUISITION AND PROCESSING

The digital data acquisition system used in the field test programme was designed and built at the University for use with the University propeller anemometers as a result of an M.E. project by Morfee (1973) during 1972-73. Following construction and initial tests, further development by H. Anink of the Electronics Laboratory, Mechanical Engineering Department improved the robustness and reliability of the wiring and also incorporated a direction sensitive system, thus completing the unit in its present state. The design and operation of this unit has been fully described by Flay (1978) so that only the principles of operation of this acquisition system have been summarised in Section 5.1 of this chapter. Section 5.2 follows with a description of the data collection techniques used to maintain the integrity of the information from the anemometers and justifies the choice of the important parameters involved. Section 5.3 briefly describes the computer programs that were developed and utilised in order to read off the recorded data from the magnetic tape, check for recording errors, calibrate and then process into the required statistical results. The chapter concludes with an assessment of the integrity of the data acquisition system.

5.1 DATA ACQUISITION SYSTEM

The field data acquisition unit has the capacity to accept and record on magnetic tape any number of triplets or groups of three anemometer channels up to a total of 36 anemometers. A typical triplet may be seen in Figure 4.2. The anemometer which has been described in Chapter 4, generated two identical but out of phase square wave pulse trains. The frequency of the two pulse trains was proportional to the speed of rotation of the anemometer shaft whilst the sign of the phase difference indicated the direction of shaft rotation. As the light-chopping disc in the anemometer had 32 windows, the frequency of each pulse train was 32 times that of the shaft.

One of the square wave signals and a positive or negative voltage indicating the direction of rotation were relayed via multi-core cables to the data unit where the pulse train was fed to an 8 bit counter, there being one counter for each anemometer channel. Although

the maximum binary count using 8 bits was 256 (0-255), half of this range was used to indicate negative values as illustrated in Table 5.1. Each channel had an overload display light which operated if an absolute count of 124 or higher occurred.

Each counter was scanned at a predetermined scan rate selected from the range 8, 16, 32, 64 and 128 Hz. The counters were allowed to count the pulses for a period of exactly T seconds, termed the sampling interval which was the inverse of the scan rate. At the completion of a T second period, each set of three counters or triplet was isolated from their input signals whilst their individual pulse counts were transferred to a buffer memory. While this transfer was taking place, the three counters did not function and therefore created a gap in the data stream from each channel equal to $^{T}/15$ seconds. There were 16 triplets to have data transferred sequentially during each scan. With reference to Figure 5.1 it follows that the effective time taken for each scan was actually $\left(1 + \frac{1}{15}\right)$ or $\frac{16}{15}$ T and two triplets may be out of phase by up to $\frac{11}{15}$ T seconds per scan. The maximum possible phase difference was therefore 0.09 seconds which was considered to be insignificant and the scans from all channels may be considered to be simultaneous. The data from all channels were then recorded periodically onto the magnetic tape in blocks of 512 words after being multiplexed in groups of three from 3 x 8 bit characters to 4 x 6 bit characters to match the computer compatible 7 track magnetic tape.

In order to identify the correct data with the correct channel, three code numbers were inserted onto the tape before the data from each scan was recorded. The first number was 127 which served to mark the commencement of each scan cycle and allowed synchronisation when reading off the tape. The second code number had a value between x = 1 to 5 indicating the chosen scan rate from 8 - 128 Hz mentioned previously so that :

$$\text{Scan Rate} = 2^{(x+2)}\ \text{Hz}.$$

The third code number which was the number of channels in question, was then followed by the recorded data in the form of sequential binary counts for each channel 1,2,3 etc. until the last channel. This cyclic process was then repeated for the next scan cycle and so on until the end of the recording.

ORIGINAL PULSE COUNT	CORRECTED PULSE COUNT FOR ANALYSIS	REMARKS
	CHANNEL FAIL = 128	
127	+ 127	MAX +VE COUNT
126	126	
125	125	NORMAL LIMIT
124	124	IS 124 COUNTS
'	'	
'	'	
'	'	+VE COUNTS
'	'	
'	'	
1	+1	+1
0	0	ZERO COUNT
255	-1	-1
'	'	
'	'	
'	'	-VE COUNTS
'	'	
'	'	
132	-124	NORMAL LIMIT IS 124 COUNTS
131	-125	
130	-126	
129	-127	MAX -VE COUNT

TABLE 5.1 ANEMOMETER PULSE COUNT CODE TO INDICATE DIRECTION OF ROTATION

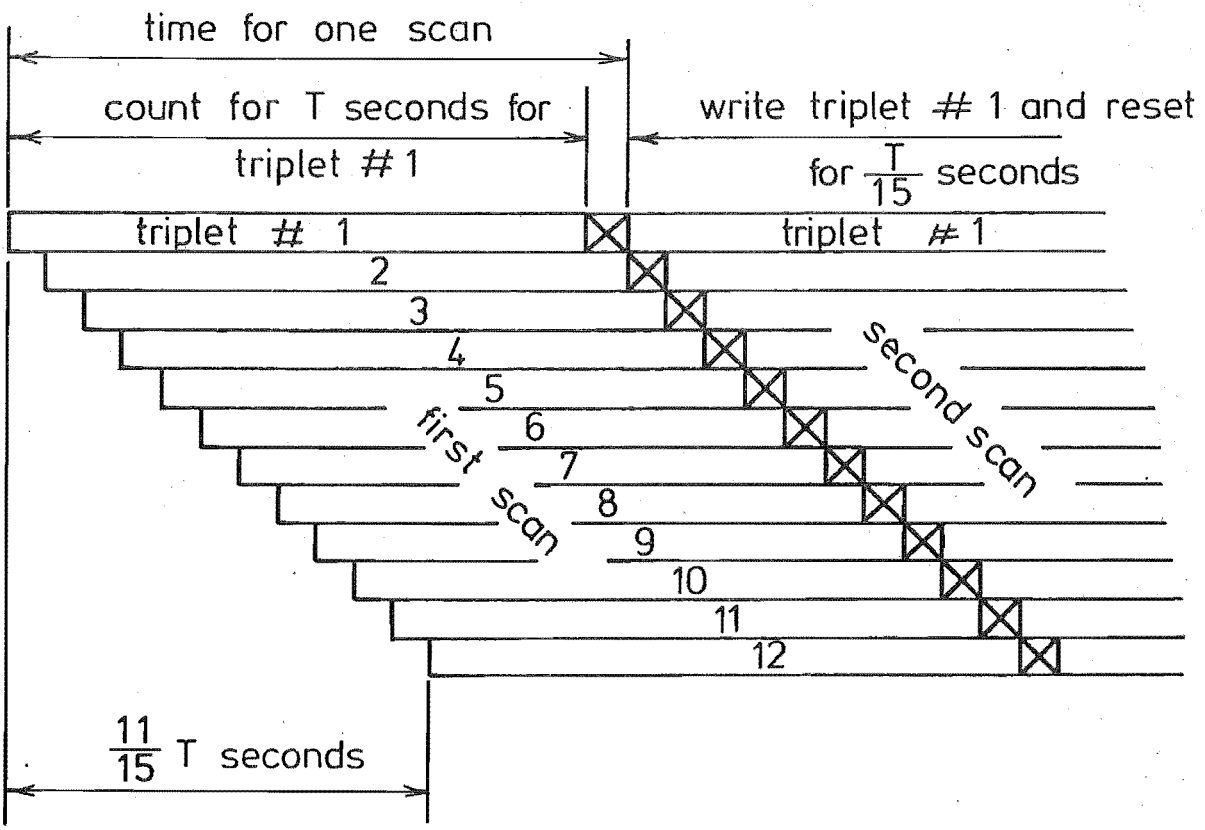

Recording time T_o = No. of scans $\times \frac{16}{15} T$

FIG 5·1 RELATIONSHIP BETWEEN RECORDING TIME T_o AND SAMPLING INTERVAL T.

5.2 DATA COLLECTION

5.2.1 Input Signal

The horizontal anemometers were predicted in Figure 4.14 to respond correctly to all fluctuating velocities of frequency below $\frac{n}{\bar{v}} = 0.025$ and with increasing error for higher frequencies up to $\frac{n}{\bar{v}} = 0.20$, above which the output signal would be negligible. The performance of the vertical anemometer was somewhat inferior but due to the higher frequency content of the vertical wind component, the higher frequency limit of $\frac{n}{\bar{v}} = 0.20$ mentioned above still holds true. Noting that the typical mean wind speeds in the tests were somewhat less than 10 m/s but anticipating perhaps an absolute limit of 50 m/s, the normal maximum frequency contained in the output signal would be of the order of 2 Hz with an absolute maximum of 10 Hz. These frequencies should not be confused with the pulse frequency generated by the light chopping disc. The scanning rates used in the field tests were mostly 16 Hz except for one high speed case when 32 Hz was used.

5.2.2 Pulse Resolution Error

The number of pulses accepted by a counter after a sampling period of T seconds is a discrete integer which will introduce an error if the size of the total count is low.

The number of pulses per shaft revolution = 32

$\therefore$ number of pulses per second, = $32\,\omega$

number of pulses per scan = $32\,\omega\,T$

but $\bar{v} = R\,\bar{\omega}$

$\therefore$ number of pulses per scan = $32.\frac{\bar{V}}{R}.T$ (5.1)

but from Chapter 4, the calibration constant R = 0.274

and remembering that the scan rate = $1/T$

then the number of pulses per scan, N = $\frac{116.8\,\bar{V}}{\text{scan rate}}$ (5.2)

The maximum possible resolution error is 1 count in N

so that the Percentage Resolution error = $\frac{\text{scan rate}}{1.168\,\bar{V}}$

The percentage resolution error is tabulated in Table 5.2 for the various scan rates and flow velocities. It may be concluded that the resolution error is small for a scan rate of 16 Hz if the velocity component along the anemometer axis is greater than 5 m/s, which was the case for the horizontal anemometers in the tests. However the error involved in the vertical anemometer readings is large, probably $\sim$ 10%, but it is difficult to estimate as the RMS velocity is only an indication. One method of reducing this error would have been to increase the number of windows in the light chopping disc, but the present number is close to the physical limit imposed by the disc diameter and the accuracy in alignment of the light-emitting diode and pick-up.

5.2.3 Counter Overflow

In order to keep the pulse resolution error to a minimum, the number of counts per scan must be maintained at a high level but overloading the counters must be avoided as loss of information on the actual peak gust would then occur. The capacity of the counters was arranged at 127 counts so that using equation 5.2, the maximum peak velocity along the axis of the anemometer is given by V_{max} = 1.087 x SCAN RATE. The resulting peak axial velocities that may be recorded without error due to counter overflow are accordingly :-

SCAN RATE	8	16	32	64	128
VELOCITY m/s	8.7	17.4	34.8	89.6	139

A short term overload would not appreciably affect the mean velocity recorded but would affect any subsequent gust factor analysis.

5.2.4 Scan Rate

It was shown in the preceding two sections that careful selection of the scan rate was necessary to avoid overflowing the counters and yet maintain a low pulse resolution error. However further consideration of the choice of scan rate or sampling interval is given here in relation to the maximum frequency content of the incoming signal. If the scan rate is too high, the consecutive data would yield highly correlated and redundant data and unnecessarily increase the labour and necessary computer memory for subsequent calculations. On the other hand, a too low a scan rate might lead to aliasing with confusion between low and high frequency components of the original data. It may be shown as in

SCAN RATE Hz / VELOCITY m/s	8	16	32	64	128
1	6.8	13.7	27.4	54.8	-
2	3.4	6.8	13.7	27.4	54.8
5	1.4	3.4	6.8	13.7	27.4
10	0.7	1.4	3.4	6.8	13.7
20	0.3	0.7	1.4	3.4	6.8
50	0.1	0.3	0.7	1.4	3.4

TABLE 5.2 PULSE RESOLUTION ERRORS IN PERCENT FOR DIFFERENT WIND VELOCITIES AND SCAN RATES

in Bendat & Piersol (1971), that the maximum frequency which can be defined by sampling at a scan rate of $^1/_T$ Hz is $\frac{1}{2T}$ Hz. Frequencies above this Nuyquist frequency would be folded back into the frequency range from 0 to $\frac{1}{2T}$ and be confused with data in the lower range.

The Nuyquist frequency in our case is 8 Hz corresponding to the scan rate of 16 Hz utilised in the present tests. It has been shown earlier that a typical maximum frequency in the incoming signal would be about 2 Hz with this limit rising to 10 Hz in very strong winds but containing a very small contribution to the overall signal. Consequently no significant aliasing would occur during normal wind measurements. One may also conclude that scan rates over 16 Hz are unnecessary and extravagent for wind measurements unless it is raised to avoid counter overflow.

5.2.5 Length of Recording

The mean velocity is usually accepted to represent the mean hourly wind speed, but recordings of one hour duration are tedious and accumulate a large volume of data. There is also a greater chance of a significant trend appearing in the mean data if the weather situation begins to change. However, it was generally considered [Flay (1978) and ESDU (1972)] that recording lengths between 30 minutes and one hour would produce stationary data. However ESDU (1972) concluded that for recording lengths of less than 45 minutes, the maximum T second gust speed occurring in a particular period would generally decrease as the record length T_o decreases. For T_o = 30 minutes the probable reduction in peak wind speed was shown to be still small and consequently the field tests were conducted using 30 minute recordings whenever possible.

5.2.6 Statistical Effects of Finite Sampling and Averaging Times

For a finite duration of sampling or record length T_o, the contribution of low frequency variations would be partially excluded from the turbulent motion quantities, such as the mean square velocity or turbulence intensity and power spectra. At the other end of the scale, some of the high frequency structure would be smoothed out by the effective sampling intervals, T due to the use of a finite scanning rate $^1/_T$.

Pasquill (1974) described these effects by considering the process of averaging over a time interval s about a time origin t', of a contribution from a single frequency, n represented by $y = a \sin(2\pi n t)$

so that $$\bar{y}_s = \frac{1}{s}\int_{t'-s/2}^{t'+s/2} y.dt$$

By evaluating this integral the expression for the mean value of y was obtained as

$$\bar{y}_s = \left[\frac{a}{\pi.n.s}\sin(\pi ns)\right]\sin(2\pi nt')$$

It was pointed out that the original sinusoidal variation was replaced by a variation of the same form but with an amplitude which was reduced to $\frac{\sin(\pi ns)}{\pi ns}$ of the original value. Consequently the variance σ^2 was reduced by $\left[\frac{\sin(\pi ns)}{\pi ns}\right]^2$.

Now considering the time interval s to be the sampling interval T, then the reduction of the variance containing a certain frequency n would also be $\left[\frac{\sin(\pi nT)}{\pi nT}\right]^2$. It should be noted that the contribution to the variance would be negligible for $n > {}^{1}/T$ and virtually 100% for $n < {}^{0.1}/T$.

Thus generalising for the whole spectrum for a record length $T_o = \infty$ and sampling interval T, and using the notation σ_{T,T_o},

$$\sigma^2_{T,\infty} = \int_o^\infty S(n).\left[\frac{\sin(\pi nT)}{\pi nT}\right]^2 dn \qquad (5.3)$$

Pasquill went on to explain that the complimentary effect of sampling over a record length of T_o while maintaining $T \to 0$ may be expressed in terms of the true variance $\sigma^2_{o,\infty}$ as

$$\sigma^2_{o,\infty} = \sigma^2_{T_o,\infty} + \left[\sigma^2_{o,T_o}\right]_\infty$$

The square bracket with the subscript ∞ implies averaging the variances from consecutive periods T_o over infinite time.

$\therefore$ Using equation 5.3, it follows that

$$\left[\sigma^2_{o,T_o}\right]_\infty = \sigma^2_{o,\infty} - \int_o^\infty S(n)\left[\frac{\sin(\pi nT_o)}{\pi nT_o}\right]^2 dn$$

but by definition, $$\sigma^2_{o,\infty} = \int_o^\infty S(n)\,dn$$

$\therefore$ $$\left[\sigma^2_{o,T_o}\right]_\infty = \int_o^\infty S(n)\left[1 - \left[\frac{\sin(\pi nT_o)}{\pi nT_o}\right]^2\right] dn \qquad (5.4)$$

If the fluctuating quantity was observed over a record length T_o, the variance apparent in this sample would on the average, be equal to the variance of the whole spectrum modified by the function in equation 5.4 which has a complementary shape to the previous one in equation 5.3. In contrast with the previous function, contributions to the variance would be negligible for $n < \frac{1}{T_o}$ and virtually 100% for $n > {}^{10}/T_o$. Combining the two effects,

$$\left[\sigma^2_{T,T_o}\right]_\infty \text{ or } \overline{\sigma^2_{T,T_o}} = \int_o^\infty S(n)\left[\left[\frac{\sin(\pi nT)}{\pi nT}\right]^2 - \left[\frac{\sin(\pi nT_o)}{\pi nT_o}\right]^2\right] dn \qquad (5.5)$$

The effect of using finite values of T and T_o may be considered to be a filter on the spectrum described by the function

$$\psi_{T,T_o} = \left[\frac{\sin(\pi nT)}{\pi nT}\right]^2 - \left[\frac{\sin(\pi nT_o)}{\pi nT_o}\right]^2 \qquad (5.6)$$

as $T \to 0$ and $T_o \to \infty$ this function $\psi \to 1$ and $\sigma^2_{T,T_o} \to \sigma^2_{o,\infty}$ or σ^2.

Equation 5.5 may also be written in the form

$$\int_{-\infty}^{+\infty} \frac{nS(n)}{\sigma^2} \cdot \psi_{T,T_o} \cdot d(\log_e n) = \frac{\sigma^2_{T,T_o}}{\sigma^2} \qquad (5.7)$$

The effect of the function ψ_{T,T_o} is shown in Figure 5.2 and ESDU (1974) provides graphical data based on this theory which may be used for convenience to estimate the effects of T and T_o using values utilized in the field tests. In our own case, $T = {}^1/16$ and $T_o = 1800$ seconds with a typical mean velocity of say 7 m/s. For open country spectra, it may be concluded from the ESDU graph that the adopted values of T and T_o would not affect the variance values in the u and v direction, but would reduce the vertical component by 7% due to its high frequency content. The vertical turbulence intensity would thus be $\tilde{\sim}$ 3.5% low under these conditions. The 30 minute record length would have no effect on the recordings for frequencies above $^1/T_o$ or 5.5×10^{-4} Hz.

However the function ψ_{T,T_o} would have an effect on the spectrum for frequencies greater than $\frac{0.1}{T} = 1.6$ Hz for a scan rate of 16 Hz. The scan rate of 16 Hz is therefore ideally suited to the performance of the anemometer used which also attenuates frequencies over about

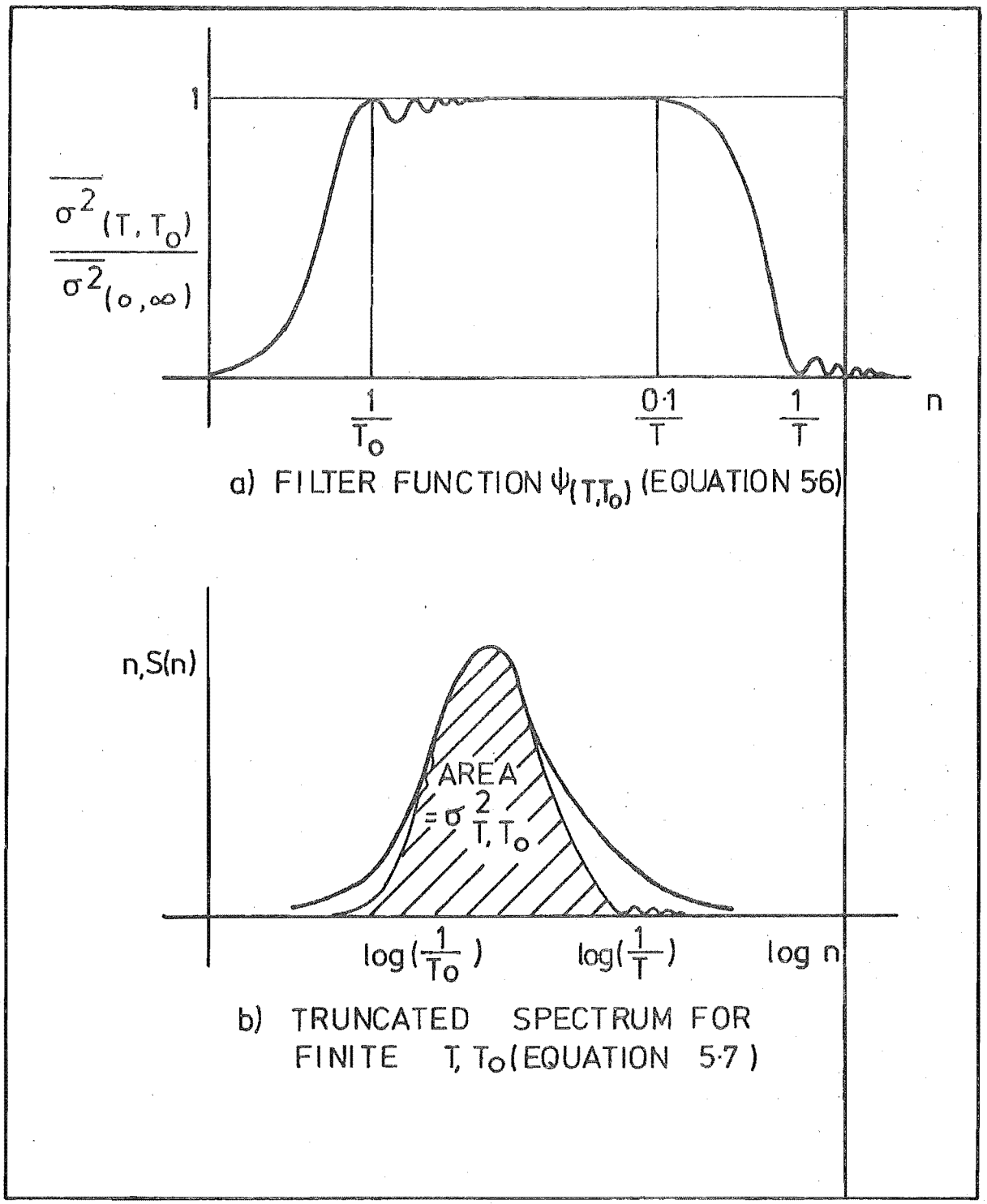

FIG 5·2 EFFECT OF SAMPLING INTERVAL, T AND RECORD LENGTH, T_o

2 Hz as discussed earlier. Flay (1978) confirmed the practical frequency limit of about 2 Hz in his study of the effect of sampling frequency on the turbulence data.

To allow efficient computer processing of the data during the power spectra calculations, the effective sampling frequency was reduced to 2 Hz during these calculations. Flay (1978) concluded after comparing the effect of T on the spectra, that the 2 Hz sampling frequency would have only a minimal effect on the longitudinal power spectra and is close to the response limit of the anemometer.

5.2.7 Stationarity

The importance of removing trends in the mean and mean square values of random data has been confirmed by Flay (1978) who made a detailed study of their effects on a field recording. The removal of significant trends in the mean velocity was shown to be particularly important for reliable velocity power spectra, correlation functions and their associated length scales. The effect on the turbulence intensities was to reduce their values slightly but a greater reduction effect on the absolute values of the Reynolds stresses was noted. It is anticipated that the removal of a trend in the mean data would reduce the apparent peak gust velocity by a value of somewhat less than one half of the total trend. Flay also conducted stationarity checks on the mean square values throughout the recording but found an acceptably small long term fluctuation.

The trend in mean values recorded during the present tests were monitored by printing out the cumulative mean values of the first array every 16 seconds throughout the recording. All but one recording (with 14%) showed a variation of less than 10% and one further recording was discarded due to its large trend in mean velocity. As the majority of the trends recorded appeared to be small compared with the example studied by Flay and the fact that his mean square values were still stationary, no trend removal was attempted on the present data. The power spectral density analyses were confined to the recordings with no significant trends in the mean velocity.

5.3 DATA PROCESSING

The digital data recorded on the 7 track magnetic tape were processed by the University's Burroughs B6718 computer using a set of Algol programs. This section describes each program briefly and high-

lights the major processing steps undertaken to indicate how the statistical wind data were obtained.

5.3.1 Program CHECKDATA

This program was written by Flay (1978) for a similar application but it was utilised with the present test recordings in a somewhat simplified form with all references to the special channels omitted. As this program checked but did not process the recorded data in any way, a repeated description was felt unnecessary and reference to Flay (1978) should be made for a full description of this program.

Each data file held on magnetic tape and representing one field recording was first processed by the program CHECKDATA to test for and identify any serious recording faults. The data was read off the magnetic tape in convenient blocks and any errors in recording sequence identified before decoding the data into time sequence binary pulse counts for each channel. Unlike Flay's field arrangement, each triplet did not represent an orthogonal array of anemometers.

Provided that the bit pattern on the tape was as expected for that number of channels and decoding could be done, then various tests were made to check the integrity of the data and error messages were printed out identifying the error, scan number and channel involved. The individual counts from each anemometer channel were checked at each scan to make sure that they had not reached the capacity of the counters and the difference between consecutive counts was noted if it exceeded a predetermined value. This difference check enabled malfunctioning anemometers and data unit channels to be recognised. The difference limit was raised to a value of 9 or 12 depending on the flow turbulence encountered until the majority of the channels showed no evidence of exceeding the limit. However, faulty channels usually exceeded the limit quite frequently and the number of occurrences which were printed out clearly indicated the faulty channels. A mean value for each channel was also printed out and compared to see if the values were reasonably near those expected from field observations at the time the data were recorded. Depending on this program check, the data file could be rejected or accepted for further processing.

During the present tests no data file was rejected as a result of this scrutiny, but the results from several anemometer channels indicated faulty anemometers and the data from those channels were not

used in the later analysis. It appeared that the majority of channel errors were due to loose or distorted light-chopping discs in the anemometers which generated erratic square wave output signals.

5.3.2 Program CORRECTDATA

After the data files had been checked for recording errors, they were processed by the program CORRECTDATA which was written by the author to suit the unusual anemometer arrangement (see Chapter 6) and to accomplish the tasks described below. The principal aim of this program was to convert the raw digital field data to a set of time series, corrected orthogonal velocity components for each array position and to write these on to a library tape for further analysis. Turbulence parameters were also computed and printed out together with speed-up factors for each array. The main steps in the program which is listed in Appendix I are described briefly below.

The first input data card contained the following information: (The numbers in parenthesis are typical values used in the present tests.)

NOCH	Number of data channels	(36)
NARR	Number of anemometer arrays	(14)
SR	Scan rate in Hz	(16)
IKK	Number of scans in recording	(27,000)
R	Calibration constant in metres/rev x 100 $= \frac{\bar{v}}{\omega} \times 100$	(274)

The other 4 input data cards were grouped to contain the non-cosine correction factors as HORCOR[I] $= \frac{\cos\theta}{f(\theta)} \times 100$ which are listed in Table 4.3. The angle θ refers to the angles of incidence with each anemometer $\theta_a, \theta_b, \theta_c$ as in Figure 5.3.

The data were read off the magnetic field tape in blocks of 384 characters until the array D[I,J] was full. This array was dimensioned so that each row (I = 1 to NOCH) represented a data channel containing 256 consecutive data points (J = 0 to 255) which had been allocated the correct sign representing the direction of rotation.

The next stage was to introduce the missing vertical channels containing zero velocities to the arrays which only had two horizontal anemometers so that all arrays could then be treated in a similar fashion. Whilst this was done the counts were converted to velocity in metres/second and stored in array UCCD[I,J] with I = 1 to 3 x NARR, J = 0 to 255. For the present tests the calibration factor was the same for all instruments.

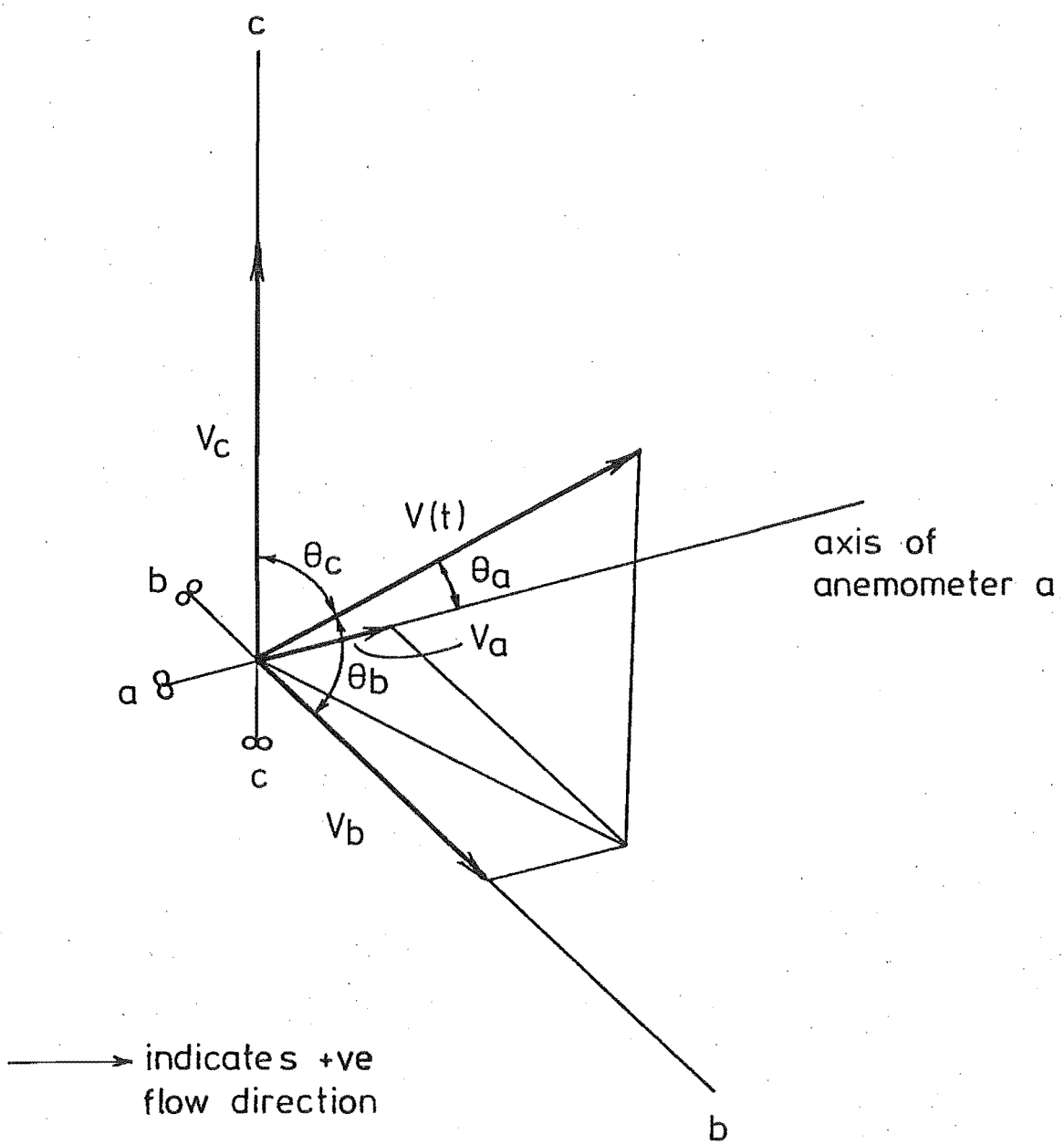

FIG 5·3 ANEMOMETER AXES AND INSTANTANEOUS WIND FLOW, V(t)

The velocity data were then corrected for non-cosine response using the iterative method developed by Horst (1973b) and placed in a new array CCD[I,J]. The vertical velocity readings were first multiplied by $^5/_4$ (see Chapter 4.2.4) to expedite the iteration and the correction factors applied to this component were reduced by a corresponding amount. Because it was noted that the iteration occasionally did not converge but oscillated between two similar values in the vertical direction (probably due to the large correction factors near 90^o), the iteration was only allowed to proceed for 6 cycles. The corrected velocities were taken from the results of the last iteration except for the vertical component which was averaged over the last two. However in most cases the iteration converged within two or three cycles.

The data block computations concluded with the calculation of the culmulative mean velocities along each anemometer axis using the general relation

$$\bar{V}_n = \left(\frac{n-1}{n}\right) \bar{V}_{n-1} + \left(\frac{1}{n}\right) V_n \qquad (5.8)$$

where n is the number of data blocks processed, V_n is the mean velocity for the data block number n and $\bar{V}_n$ is the culmulative mean velocity of the record including the last data block. The corrected velocity component data along each anemometer axis was then transferred to a temporary disk file TEMPFILE, to make way for the next data block of raw data. The computations just described were repeated for the next block of data until all the data were corrected and written onto TEMPFILE.

Because of the expected change in mean wind direction, $\bar{\beta}$ (Figure 5.4) with array position and the probable presence of a mean vertical component causing a significant value of $\bar{\alpha}$, it was necessary to convert the velocity components from the V_a, V_b, and V_c axes to one aligned along the mean wind direction u, v and w. The value of $\bar{\alpha}$ and $\bar{\beta}$ were calculated for each array position using the computed values of $\bar{V}_a$, $\bar{V}_b$, and $\bar{V}_c$ as in Figure 5.4. Calculations could then proceed to convert each set of data to the new coordinates using equations 5.11, 5.12 and 5.13, with reference to Figure 5.5, showing the general case of an instantaneous wind recording. By considering the elevation sketch,

$$w \cos \bar{\alpha} + u \sin \bar{\alpha} = V_c \qquad (5.9)$$

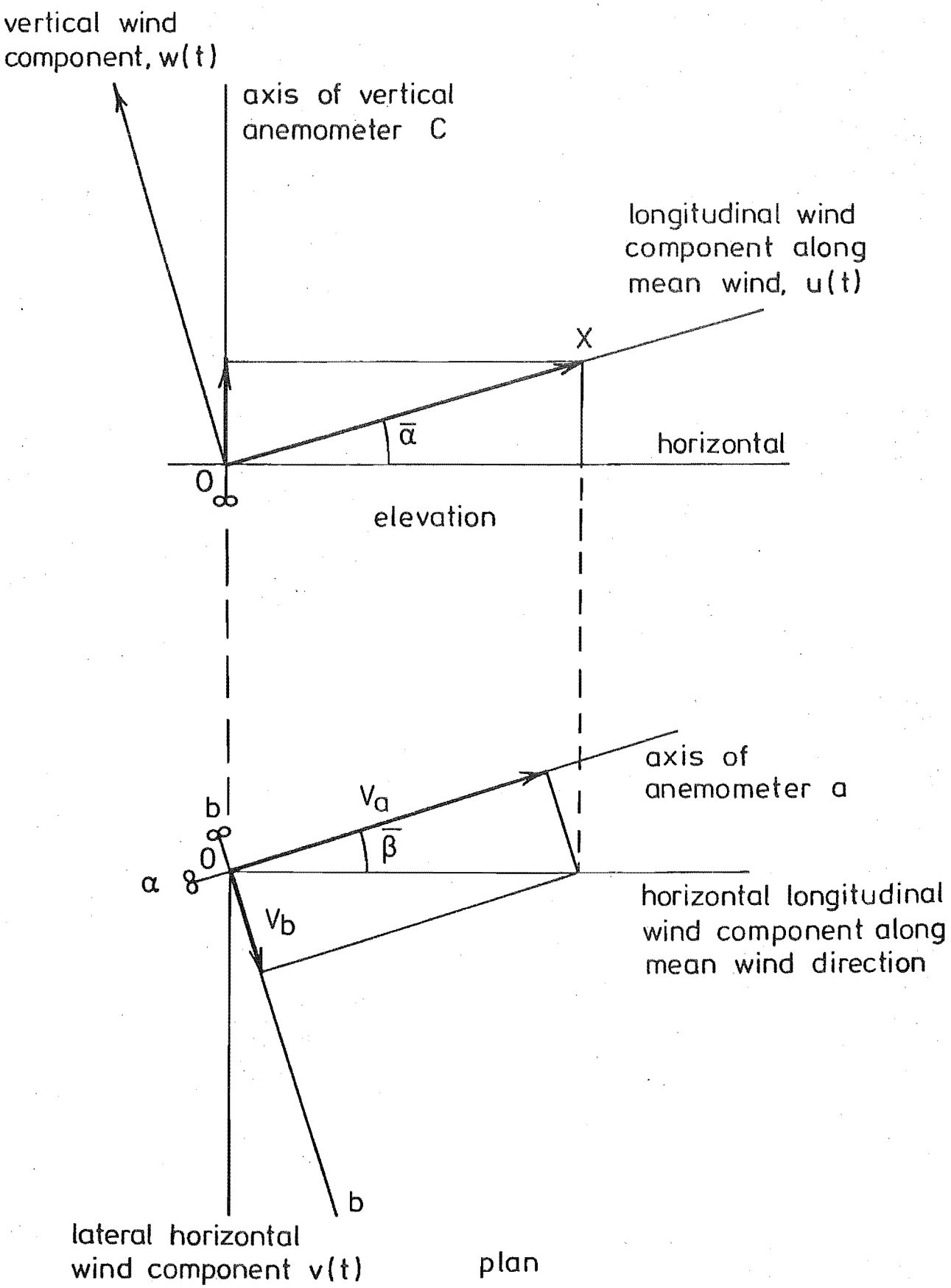

FIG 5·4 MEAN WIND DIRECTION AND ORTHOGONAL COMPONENTS, u, v, w(t)

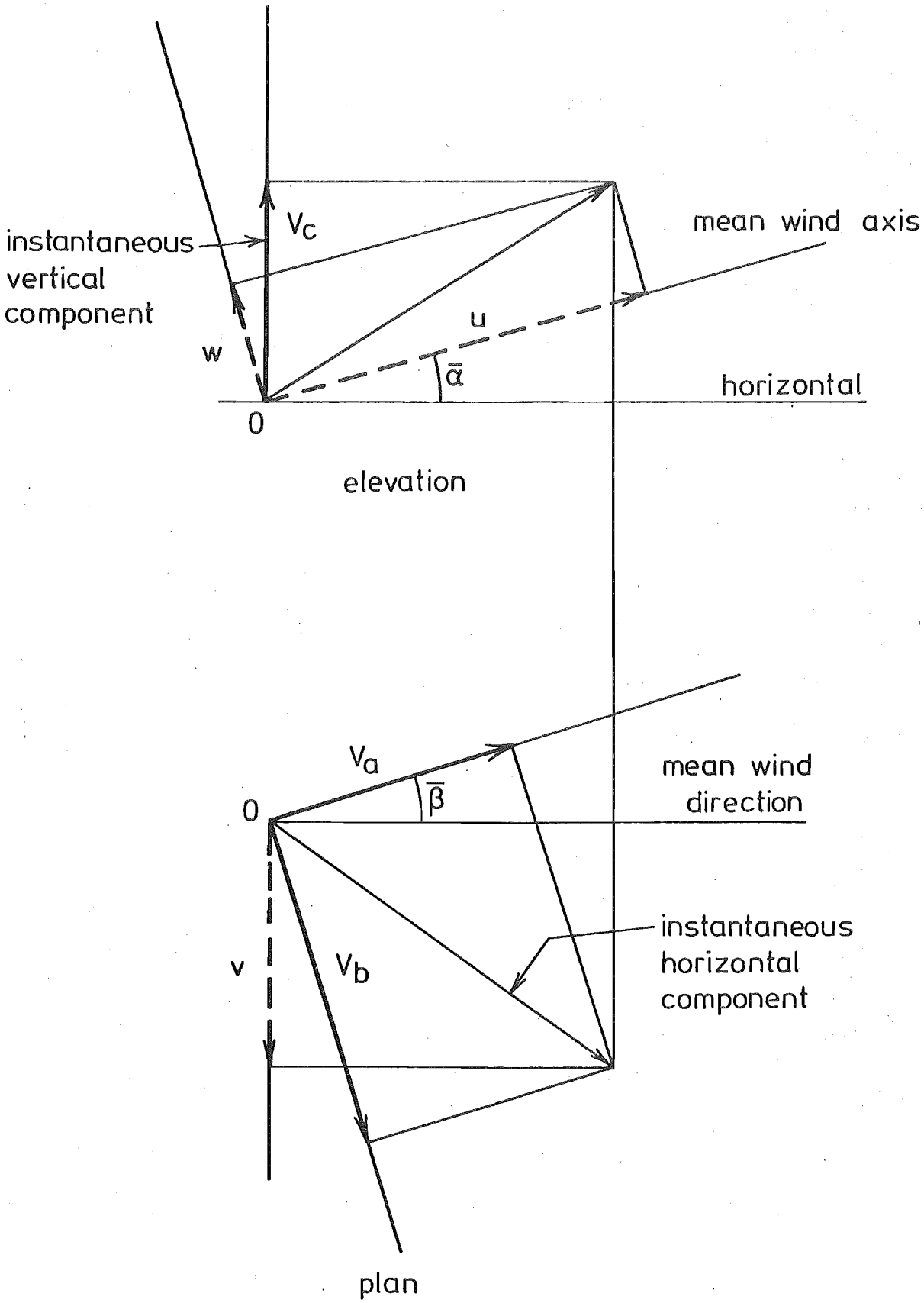

FIG. 5·5 INSTANTANEOUS WIND DIRECTION AND ORTHOGONAL COMPONENTS

and $$u \cos \bar{\alpha} - w \sin \alpha = V_a \cos \bar{\beta} + V_b \sin \beta \quad (5.10)$$

By combining 5.9 and 5.10 to eliminate w,

$$u = (V_a \cos \bar{\beta} + V_b \sin \bar{\beta}) \cos \bar{\alpha} + V_c \sin \bar{\alpha} \quad (5.11)$$

Also by considering the plan sketch it follows that

$$v = V_b \cos \bar{\beta} - V_a \sin \bar{\beta} \quad (5.12)$$

By combining 5.9 and 5.10 to eliminate u, it follows that

$$w = V_c \cos \bar{\alpha} - (V_a \cos \bar{\beta} + V_b \sin \bar{\beta}) \sin \bar{\alpha} \quad (5.13)$$

Calculations to convert the axes as described were carried out on the data from TEMPFILE and placed in array VEL[I,J] in blocks. The three components of turbulence intensity and Reynolds stress were also calculated from the data in the VEL[I,J] array before returning to TEMPFILE for another block of data. Any error in Reynolds stress due to misalignment of the vertical anemometer would be corrected for by the change in axes described above. The turbulence data from each block were combined using culmulative means as in equation 5.8 and printed out.

The corrected velocity readings in the VEL[I,J] array were stored on a temporary disc file, TEMPFILE 2 until the whole record had been processed. At the completion of the program the disc file was copied onto a 9 track magnetic library tape for further analysis in the same format used by Flay (1978). This format consisted of a series of 256 consecutive pieces of data from each channel with the channels recorded in numerical order and the cycle repeating itself until all the data was recorded. Each data sample was allocated one word for convenience.

5.3.3 Program PEAKGUSTS

This program was written by the author to provide more information on the behaviour of the longitudinal velocity component in the form of the probability density function and maximum and minimum velocities averaged over various sampling times for each array. The main steps in the program which is listed in Appendix I, are described briefly below.

The input data card contained the following information. (The numbers in parenthesis are typical values used in the present tests.)

NOCH	Number of data channels	(36)
NARR	Number of anemometer arrays	(14)
SR	Scan rate in Hz	(16)
N	Number of scans in recording	(27,000)
NCL	Number of frequency increments or classes for the probability density function	(25)

The field data used for this program was in the form produced by the preceding program, CORRECTDATA and was first read off the corrected library tape onto a temporary disc file, TEMPFILE 2. The longitudinal velocity component u(t) was read off the disc file, TEMPFILE 2 over the whole length of the recording for one anemometer position at a time and placed in the array u[Z,J], J = 0 to 255 and Z = 1 to $^{N}/_{256}$. The data was laid out along consecutive rows 256 long, but it was later discovered that a long one-dimensional array (J = 0 to N) could have been utilised and thereby simplifying the complicated but necessary address and retrieval system used in the peak value analysis.

The accumulated data for this particular instrument position was searched for the maximum and minimum values and their time addresses recorded. These peak velocities were then averaged with their neighbouring values, with equal numbers of data points on either side of the peak occurrence, to obtain peak velocities averaged over a range of approximate periods, between 0.5 and 5 seconds. The process loop was then repeated for the next anemometer position. The main assumption implied by this approach is that the peak values averaged over a range of relatively short time periods all occur near the same event and are located symmetrically in time about the peak velocity occurrence. This assumption is open to doubt as there may be a further and unrelated event with a slightly smaller but flatter peak which could have yielded higher averaged peak velocities but did not have the 'instantaneous' peak velocity data point of sufficient magnitude to identify it. This undoubtedly would have occurred if the peak velocity located was due to a recording error, characterised by a high peak velocity at one data point and low adjacent values. In this case however the error was easily detectable from the tails of the probability density functions

and were subsequently rejected. The alternative method requiring a good deal more computation time would have been to regroup all the data of the recording into sets representing a selected sampling period and then to locate the peak values and repeating for different sampling periods. It is doubtful if this latter method would have yielded more accurate results as it is still open to chance how the data near a peak occurrence is distributed in the adjacent data sets and thereby affecting their individual averages. It was pointed out in Chapter 2 that the peak values exhibited their own random distribution anyway and it was thought that the method adopted was sufficiently accurate to yield useful results about the peak value behaviour.

The probability density functions were computed for each instrument position in turn. First of all, the size of the velocity increment or class width was calculated by dividing the velocity range encountered by the number of classes, NCL (usually a convenient value such as 25 was used for NCL). Following the definition of the class mid points and boundaries, the number of data samples within each class was totalled and the distribution printed out as a normalised function described by equation 2.40 together with the cumulative probability function.

5.3.4 Program PSAUTCORS

Although the principal information sought from the field tests was obtained from the preceding two programs, advantage was taken of the recently developed program PSAUTCORS by Flay (1978) which enabled the calculation of velocity power spectra and auto correlation coefficients using a Fast Fourier Transform library package. Sample calculations using a sampling frequency, T=2 Hz were undertaken using one recording from each test site which exhibited no significant trends in the mean velocity. A full description of the program with the essential theory involved may be found in Flay (1978).

Although the theoretical low frequency limit to the velocity power spectra was defined in Section 5.2.6 as being $\frac{1}{T_o}$ Hz, Flay (1978) found from repeated spectral measurements of the same turbulent flow that the random variation in the spectral density due to the random nature of the input signal became very significant for frequencies below $^{16}/T_o$ Hz. This low frequency limit was adopted in the present project as the anemometer data handling and processing was very similar to Flay's and the limit has been included on all spectra presented in order to define the low frequency limit to the reliable data in a

conservative manner.

5.4 CONCLUSIONS

* The main features and principles of operation of the data acquisition system which was designed and built by the University were described. It was shown that the system was adequate for the purpose of wind turbulence measurements provided that the correct scan rate was chosen to ensure a reasonable count per scan.

* The data acquisition system was shown to match the performance of the propeller anemometers closely and record the undistorted data successfully on magnetic tape in a form which could be read by the University's computer.

* The accuracy of the vertical anemometer channels was reduced due to the high frequency content and the typically lower velocities in the vertical component of turbulence. A random error of about 10% could occur due to the poor count resolution and an additional 3.5% reduction in the turbulence intensity was predicted for a scan rate of 16 Hz.

* A recording period of 30 minutes was considered an adequate minimum to ensure stationary data provided that there were no significant long term trends in the mean and variance of the velocity.

* The Algol programs utilised in the processing of the field data were described. The main features in the data processing sequence were:

(1) Read off raw binary data from the field magnetic tape and check for recording errors.

(2) Sort data into groups of three representing each anemometer array and calibrate data to metres/second.

(3) Correct data for non-cosine response.

(4) Convert the three component axes from along the anemometer shafts to a set aligned to the mean wind direction.

(5) Calculate the three components of turbulence intensity, Reynolds stresses and the mean wind speed at each array.

(6) Write corrected data recordings on a library tape.

(7) Calculate maximum and minimum gust speeds averaged over a series of sampling intervals from $\frac{1}{2}$ to 5 seconds.

(8) Calculate the probability distribution function and culmulative probability function for each longitudinal velocity.

(9) Calculate sample power spectra and auto correlation coefficients.

CHAPTER 6

THE SLOPING ESCARPMENT FIELD TEST

The 13.0 m high, 2:1 sloping escarpment near Amberley, was the first site investigated between early January and mid February, 1978 and resulted in 4 half-hour and one 15 minute recording in mean wind speeds at 10 m above the ground ranging between 7.1 and 9.7 m/s.

This chapter describes the site in some detail, the weather conditions prevailing at the time of the recordings and then presents the results obtained from the recording analyses.

6.1 SITE DESCRIPTION

The location of the site in relation to the sea and the nearby township of Amberley, 40 km north of Christchurch, is shown in Fig. 6.1 which has been taken from a 1 inch to the mile, Lands and Survey Department topographical map. The nearest significant hills were 7 km NE along the coast and 8 km NW of the site and were considered to be far enough away not to affect the results. The site area has been boxed in on the map and is shown on an enlarged scale in Fig. 6.2 to indicate the important site features and local roughness. The recorded winds came in off the sea at a mean angle of 60 ± 5 degrees to the normal from the escarpment crest.

Apart from two eroded gullies shown on the map, the crest lay in a straight line along the NE-SW axis. The escarpment was separated from the open sea by 1.3 km of ploughed land, low scrub and the occasional group of trees. The general layout and nature of the site is shown in Figs. 6.3 to 6.6. The top of the escarpment was flat and smooth and together with the slope, was covered in well cropped grass. The profile of the escarpment along the tower centre line was measured using a theodolite and staff and is shown in Fig.6.7. The crest was close to 13 metres above the base of the slope from which the ground sloped very gently towards the sea. The average angle of inclination of the escarpment was approximately 26° making it very close to a 2:1 slope ($\tan^{-1} 1/2$).

The ground upwind of the site could be categorised as open farmland with numerous small obstructions and an expected Z_o range

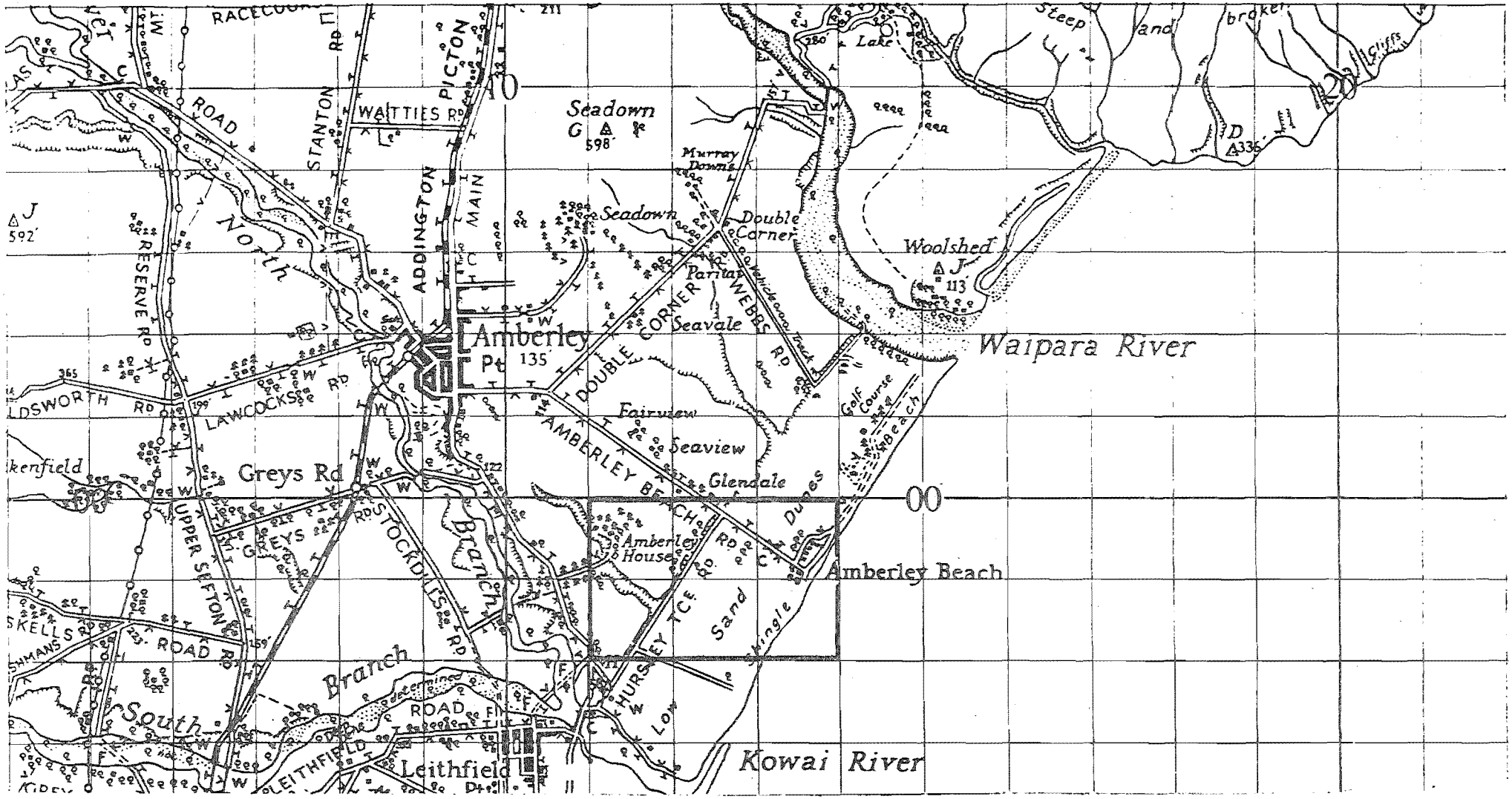

FIG 6·1 LOCATION OF AMBERLEY SITE (SCALE 1inch = 1 mile.)

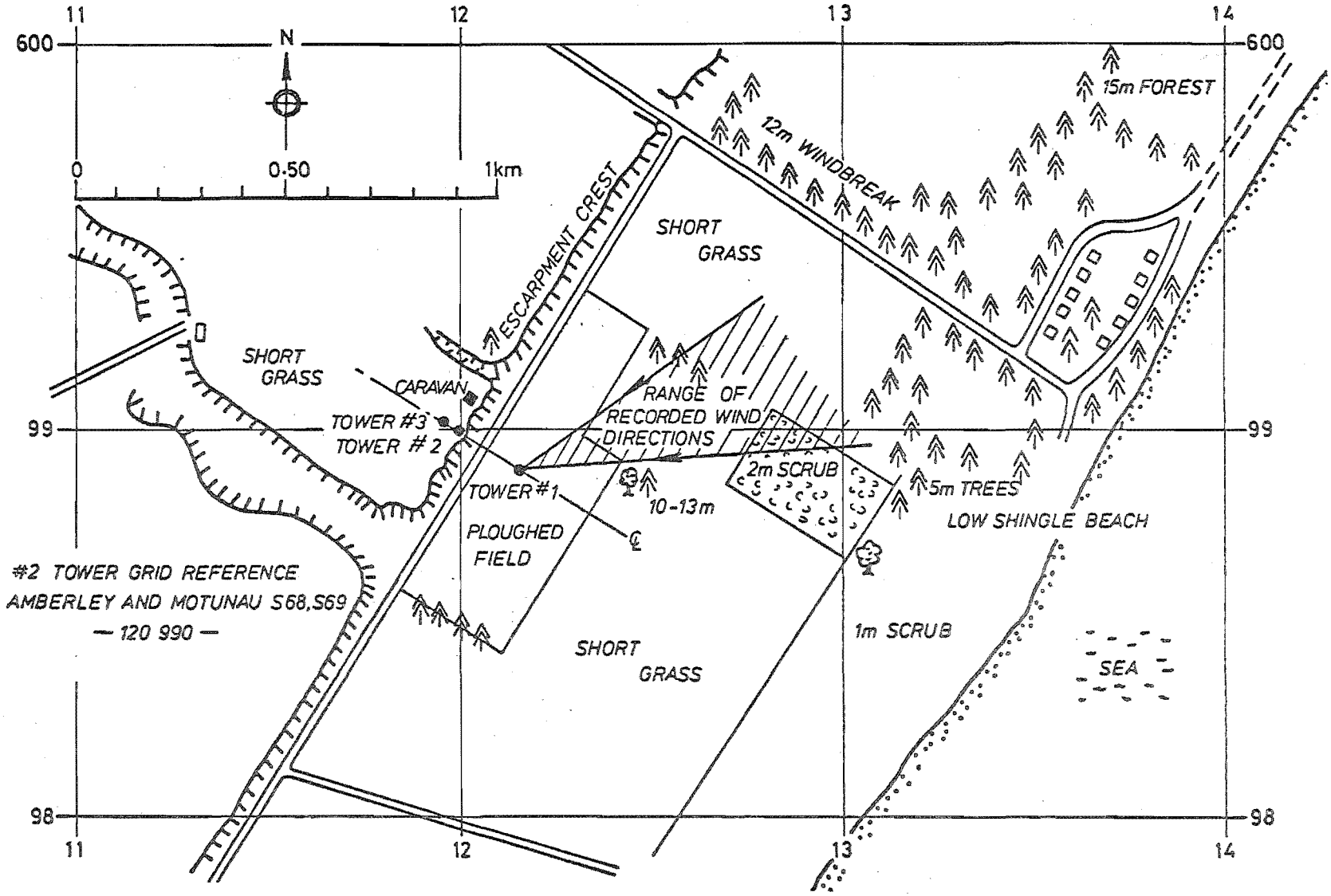

FIG 6·2 MAP OF AMBERLEY SITE AREA AND TOWER POSITIONS

FIG.6.3 VIEW LOOKING NE ALONG THE CREST AND SHOWING THE CARAVAN AND #2 TOWER AT THE AMBERLEY SITE

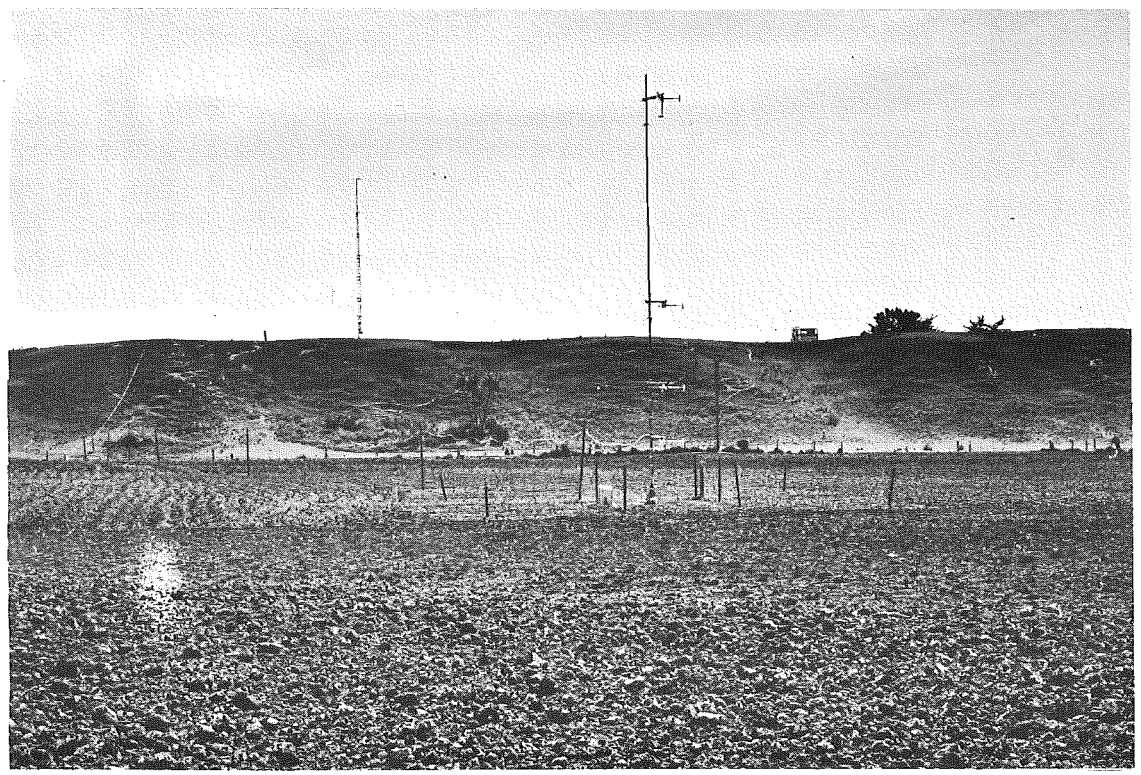

FIG.6.4 VIEW LOOKING NW FACING THE SLOPE AND SHOWING ALL THREE TOWERS AT THE AMBERLEY SITE

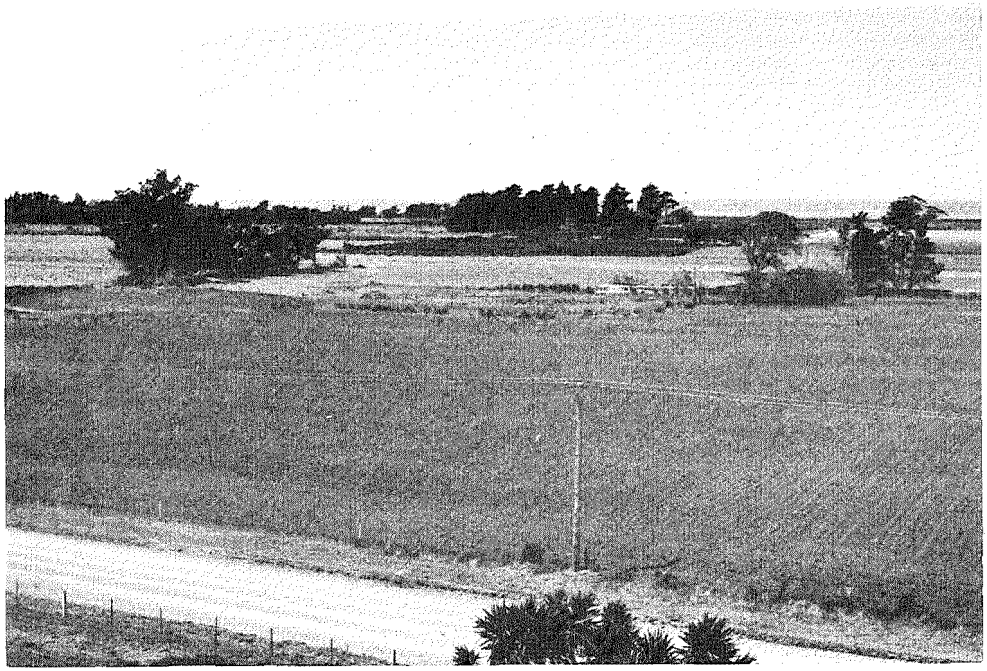

FIG.6.5 VIEW DUE EAST INTO THE WIND LOOKING FROM THE TOP OF THE CREST AT THE AMBERLEY SITE

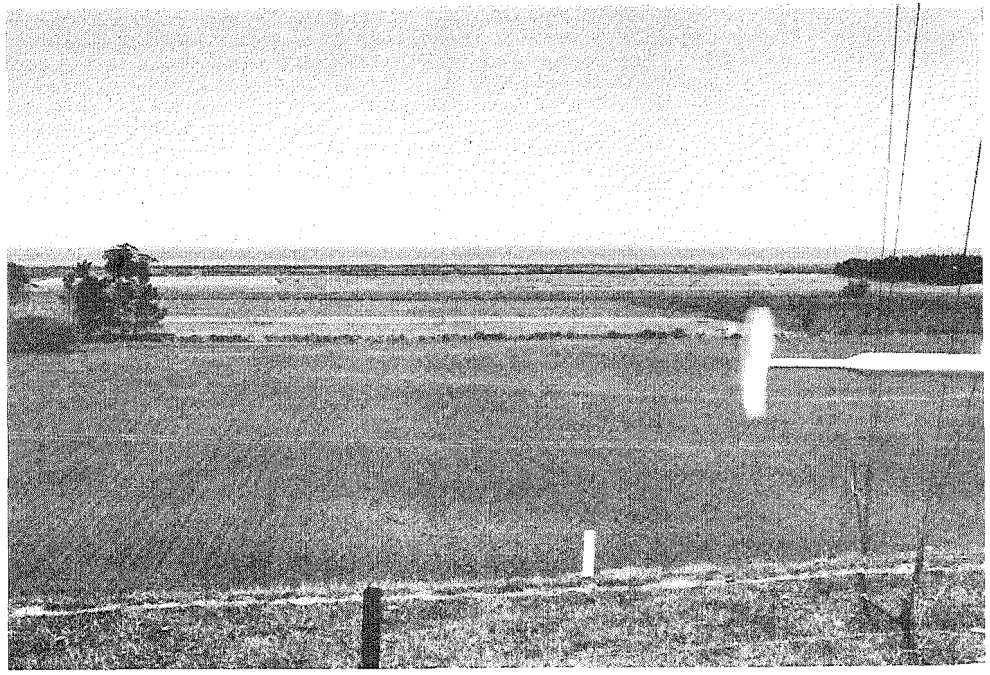

FIG.6.6 VIEW LOOKING FURTHER TO THE RIGHT AND SHOWING TOWER #1 AT THE AMBERLEY SITE

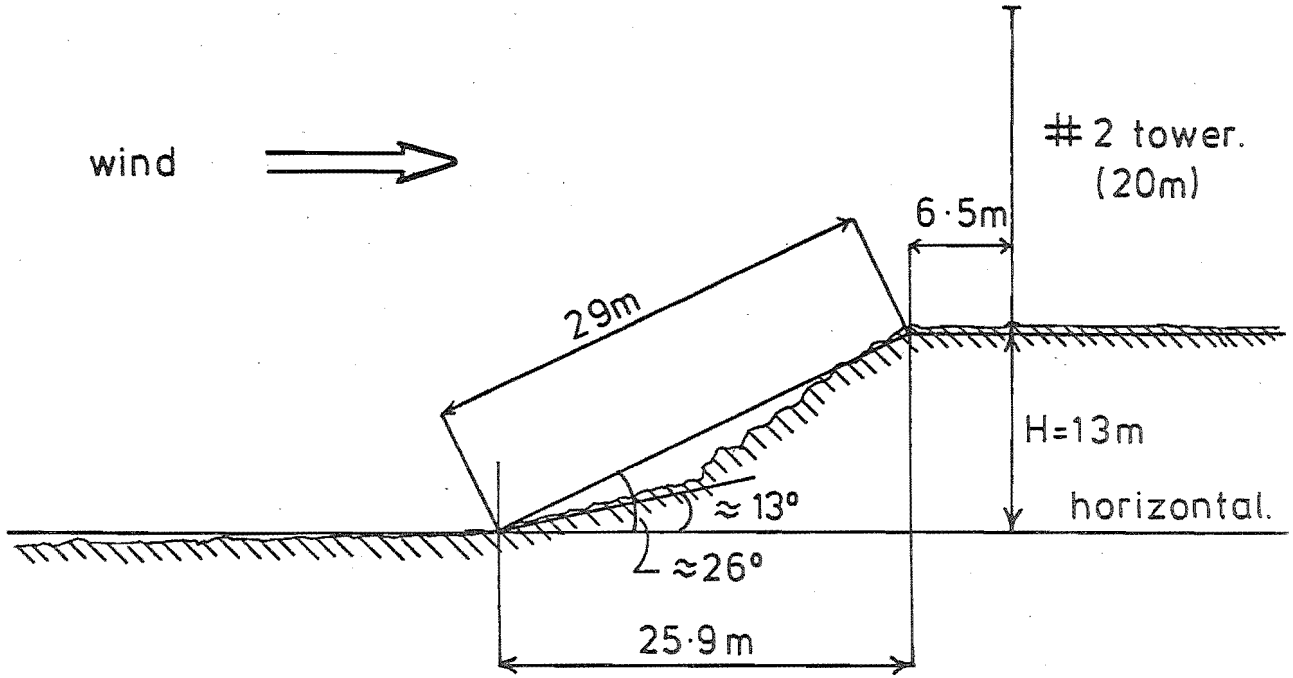

FIG. 6·7 PROFILE AND DIMENSIONS OF THE SLOPING ESCARPMENT AT AMBERLEY.

between 0.01 and 0.1 [Counihan (1975) and ESDU (1972)]. However, the adjacent ploughed field extending upwind some 0.3 km could be sufficient to influence the lower 20-30 m of boundary layer and create a lower Z_o, perhaps between 0.005 and 0.02 in that height range.

6.2 INSTRUMENT LAYOUT

Three towers were erected to support the anemometer arrays. A 10 m high, guyed aluminium pole (tower #1) was placed on the lower level at a distance of 130 m (10 H) from the foot of the escarpment to monitor the oncoming wind conditions before they were modified by the escarpment. It was noted from previous wind tunnel tests (Bowen and Lindley (1977)) that a distance of 10 H upstream was sufficient to find the undisturbed boundary-layer. Tower #1 was fitted with instruments at four levels. A guyed 20 m high, telescopic steel-lattice mast (tower #2) was placed as close as possible to the crest on the upper level which was conveniently 6.5 m (0.5 H) from the crest, with instruments at six levels. A further 10 m pole (tower #3) was placed on the upper level at a distance of 52 m (4 H) behind the crest with instruments at four levels. All three masts may be seen in Fig.6.4 and a closer view of the lattice mast seen in Fig.6.3.

The lower four instrument levels on all three masts were the same at 9.87 m ($^{Z}/H = 0.759$), 4.90 m (0.377), 2.88 m (0.222) and 1.56 m (0.12) with two extra levels on the #2 tower at 18.78 m (1.445) and 14.87 m (1.144). Three propeller anemometers were set up in an orthogonal array for each instrument level on the #2 tower and the top level only on the other two towers. All the anemometer arrays were aligned in the same direction using a magnetic compass to within about ±2°. All other positions were fitted with a pair of horizontal anemometers only and in this way, the 36 anemometers were distributed over 14 positions. It was felt necessary to fit the #2 tower with vertical anemometers overall as a significant mean vertical component was expected close to the crest. The vertical anemometers near the 10 m level on the other two masts were intended to provide sample Reynolds stress data.

All the instruments were permanently wired to the data acquisition unit in the caravan by means of multicore, twisted pair cables which also provided power to the anemometers in a similar arrangement

to Flay (1978). The cables were slung overhead to avoid damage from the sheep and cattle. A portable diesel generator provided power to the data acquisition unit in the caravan.

6.3 SITE RECORDINGS

The tape recordings were initiated by hand when the weather conditions were appropriate and after each data channel had been checked for a sensible output. It was intended to take recordings during conditions of neutral stability which normally could be expected during strong winds and cloudy weather and consequently no temperature profile measurements were attempted. Unfortunately the Summer during which the recordings were taken was unusual for its lack of wind and cloud. Over a period of six weeks only three days were suitable and five recordings were taken under rather similar weather conditions, characterised by strong winds off the sea and cloudless, sunny skies. The details of the five recordings are summarised in Table 6.1. Unfortunately two of the recordings had to be terminated before the half hour was reached due to problems with the tape recorder.

The synoptic weather conditions recorded by the New Zealand Meteorological Service for the three days when the wind recordings were taken are shown in Appendix II. It may be inferred from these charts that on all three days similar conditions of strong local sea to land winds prevailed, rather than a strong air stream over the whole country. The recorded winds came in off the sea from a surprisingly Northerly direction making a larger angle with the normal to the escarpment crest than was hoped for. The non-stationary trends in the mean velocity at Z = 10 m were indicated by the variation in the cumulative mean velocity at the 10 m level on tower #1. The range of its variation which was typically nonlinear, is given as a percentage in Table 6.1 and was not compensated for in the data processing.

6.4 UPWIND REFERENCE CONDITIONS

A knowledge of the conditions prevailing in the boundary-layer upwind and beyond the influence of the escarpment is of prime importance if the field results are to be of any signifiance, as their behaviour would be greatly influenced by these reference conditions.

RECORD #	DATE	TIME OF START	LENGTH T_o MINUTES	AIR TEMP. C°	$\bar{\phi}$[a]	$\bar{V}_{10}$ m/s	TREND LIMITS[b] %
1	31 JAN	11.56	30.15	19	57	8.14	10
2	8 FEB	15.17	25.32	21	57	(9.59)[c]	9
3	8 FEB	17.04	14.51	19	57	(8.50)	6
4	12 FEB	11.11	30.15	20	66	7.14	9
5	12 FEB	12.58	30.15	22	62	7.88	NIL

NOTES:-

All records scanned at 16 Hz

a. Angle between mean wind direction and normal to crest

b. Percentage variation of cumulative mean velocity, tower #1

c. Values in parenthesis contain small recording error

TABLE 6.1 DETAILS OF THE AMBERLEY SITE RECORDINGS

Unfortunately the reference tower #1 was only 10 m high corresponding to a $^{Z}/H = 0.759$ and a small fraction of the total boundary-layer depth. This tower provided velocity data from four levels which was considered a bare minimum to define the prevailing conditions, thus releasing the rest of the instruments to record the velocity variations over the escarpment itself. An attempt to analyse the velocity data from the reference tower #1 and to come to some conclusion as to the stability of the prevailing boundary-layer is described in this section.

6.4.1 Mean Velocity-Height Profile

The five recordings provided very similar normalised velocity-height profiles which have been plotted in Figs.6.8 and 6.9 as averaged values to compare them with the established power and logarithmic law behaviour. It is not known why the #3 instrument array (top array was #1) consistently yielded higher velocities than expected although the variation is within the ±5% calibration range discussed earlier.

The power law profile in Fig.6.8 corresponded to a low value of exponent $\alpha = 0.13$ equivalent to very smooth open country ($Z_o \tilde{} 0.005$ m), although it may be indicative of the ploughed field in which the tower was situated. However the power law is probably quite misleading over such a small range of boundary-layer depth.

The logarithmic profile in Fig.6.9 yielded a surface roughness parameter of approximately 0.003 m assuming neutrally stable conditions, which agreed with the indication given by the power law plot of the influence from the adjacent smooth field.

6.4.2 Turbulence Data at 10 metre Height

The turbulence intensities and Reynolds stress data at the $\tilde{}$ 10 m height on tower #1 are summarized in Table 6.2 from recordings 1,4 and 5. Consistent results have been obtained in the longitudinal direction, but the variations between recordings have increased markedly for the lateral component. The variations are somewhat greater for the vertical component as predicted by the error analyses in Chapters 4 and 5. The wind direction was such that the right-hand anemometer was subjected to about one quarter of the velocity recorded by the left-hand instrument, so that the lateral component may be expected to have a larger error than the optimum situation when the

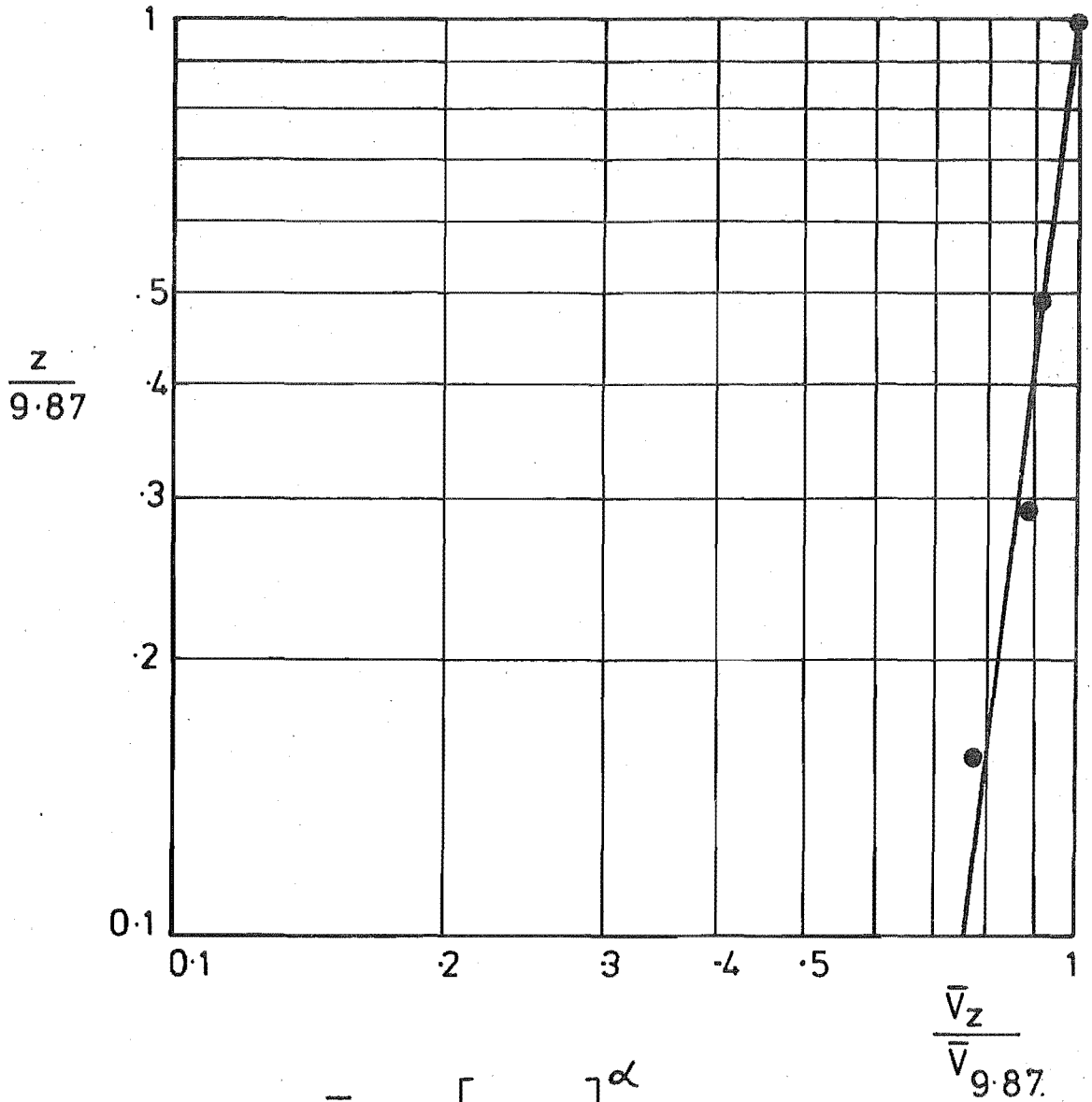

$$\frac{\bar{V}}{\bar{V}_{9\cdot87}} = \left[\frac{z}{9\cdot87}\right]^{\alpha}$$

$$\alpha = \frac{1\cdot6}{12\cdot7} = \frac{1}{7\cdot9} \approx 0\cdot13$$

FIG. 6·8 AVERAGED UPWIND MEAN VELOCITY-HEIGHT PROFILE AS POWER LAW: AMBERLEY TEST SITE.

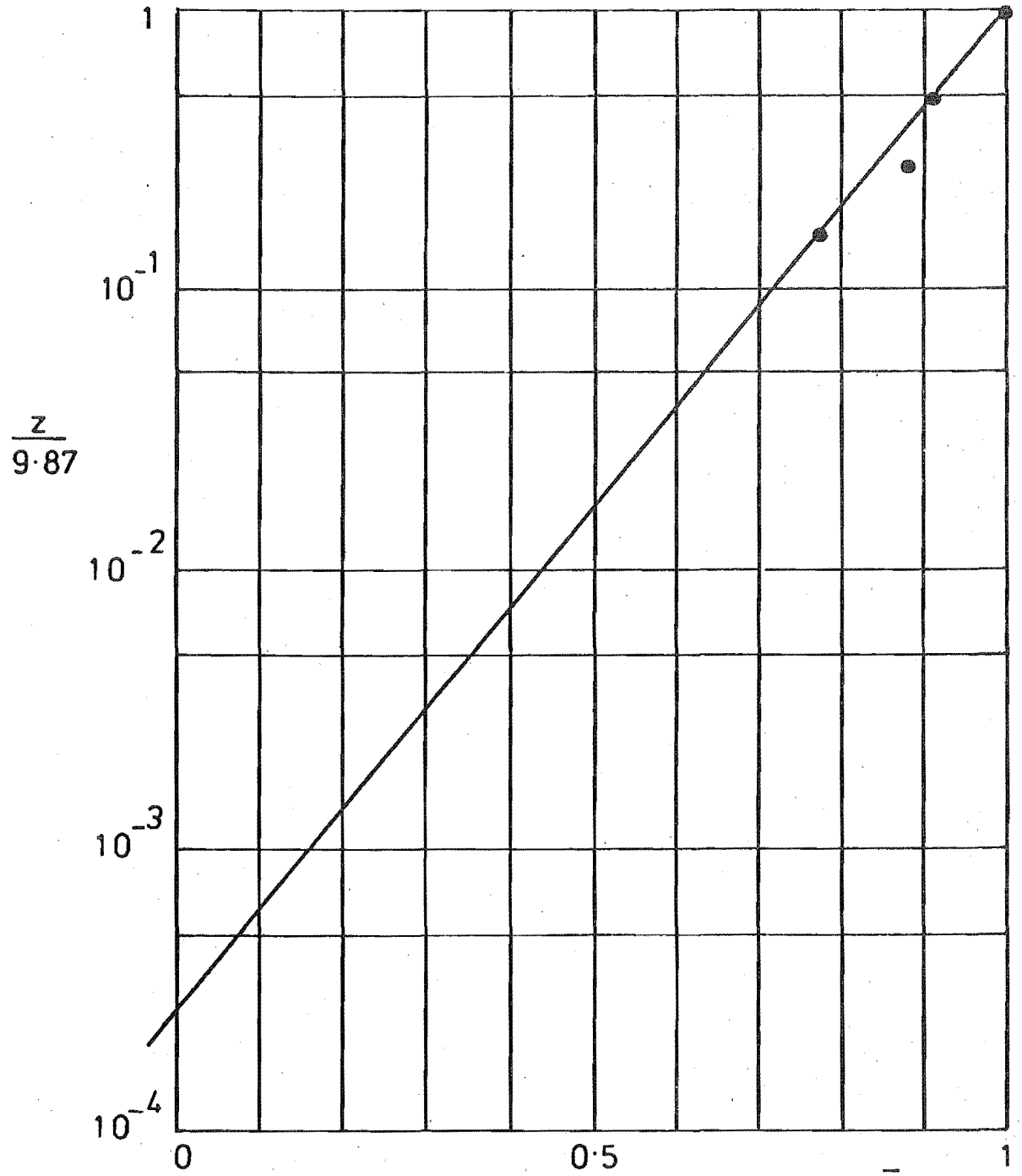

$$\frac{\bar{V}_z}{\bar{V}_{9{\cdot}87}} = \frac{\log[\,^{z}/_{z_o}\,]}{\log[\,^{9{\cdot}87}/_{z_o}\,]}$$

$z_o \approx 3\text{mm}$

FIG. 6·9 AVERAGED UPWIND MEAN VELOCITY–HEIGHT PROFILE AS LOGARITHMIC LAW. AMBERLEY TEST SITE.

RECORD #	$\bar{V}_{10}$ m/s	$\frac{\sigma_u}{\bar{V}_{10}}$	$\frac{\sigma_v}{\bar{V}_{10}}$	$\frac{\sigma_w}{\bar{V}_{10}}$	$\frac{\overline{uw}}{\sigma_u \cdot \sigma_w}$	$\frac{\overline{vu}}{\sigma_v \cdot \sigma_u}$	$\frac{\overline{wv}}{\sigma_w \cdot \sigma_v}$
1	8.14	0.207	0.145	0.094	-0.372	-0.110	0.045
4	7.14	0.226	0.181	0.122	-0.320	+0.219	-0.024
5	7.88	0.214	0.164	0.103	-0.245	+0.089	-0.060
AVERAGED DATA		0.22	0.16	0.11	-0.31	(+0.07)	(-0.01)
$\frac{\text{STD. DEV.}}{\text{MEAN}}$ %		4	9	11	17	(205)	(335)

$$\sigma_u : \sigma_v : \sigma_w = 1 : 0.73 : 0.50$$

TABLE 6.2 UPWIND TURBULENCE DATA AT $\approx$ 10 m HEIGHT ON TOWER #1, AMBERLEY TEST SITE

wind bisects the angle between the two horizontal anemometers. Recordings #2 and 3 showed a significant recording error in the right-hand horizontal anemometer which due to their alignment with the mean wind just described, would not have altered the mean wind data by more than 2 or 3 percent. However the lateral component of turbulence would be significantly in error and therefore these two recordings were omitted from Table 6.2.

The three components of turbulence intensity yielded the ratios of $\sigma_u : \sigma_v : \sigma_w$ as 1 : 0.73 : 0.50 which compared with standard data, were close to the expected values of 1 : 0.75 : 0.50 from Counihan (1975) and 1 : 0.69 : 0.43 from ESDU (1974). The values obtained corresponded to a surface roughness length Z_o in neutrally stable conditions of between 0.06 m and 0.10 m taken from ESDU (1974), compared with the low value of 0.003 m from the mean velocity-height profile. This large discrepancy was thought to be due to the instability of the boundary-layer and is discussed in the next section.

A satisfactory value of the principal Reynolds stress component

$$\frac{\overline{uw}}{\sigma_u \cdot \sigma_w} = -0.31$$

was obtained compared with -0.29 and -0.26 for Z_o = 0.06 m and 0.003 m respectively, taken from ESDU (1974). The low and highly variable values of the other two components were in accordance with ESDU and Flay (1978) who concluded that both components were small and may be ignored. The larger errors expected in the vertical component velocities as discussed in Chapters 4 and 5 however, cast a doubt on the accuracy of these Reynolds stress parameters.

A longitudinal velocity power spectrum taken from the field recording #5, which exhibited no trends, is shown in Fig.6.10 and is compared with the standard spectrum from ESDU (1974) for open country terrain at 10 m height. Close agreement is indicated if due regard to the anemometer response and to the sampling frequency of 2 Hz is taken as described in Chapters 4 and 5.

6.4.3 Atmospheric Stability

The discrepancy noted during the previous section in the value of Z_o indicated by the turbulence parameters and the value indicated by the mean velocity profile under neutrally stable conditions, indicated

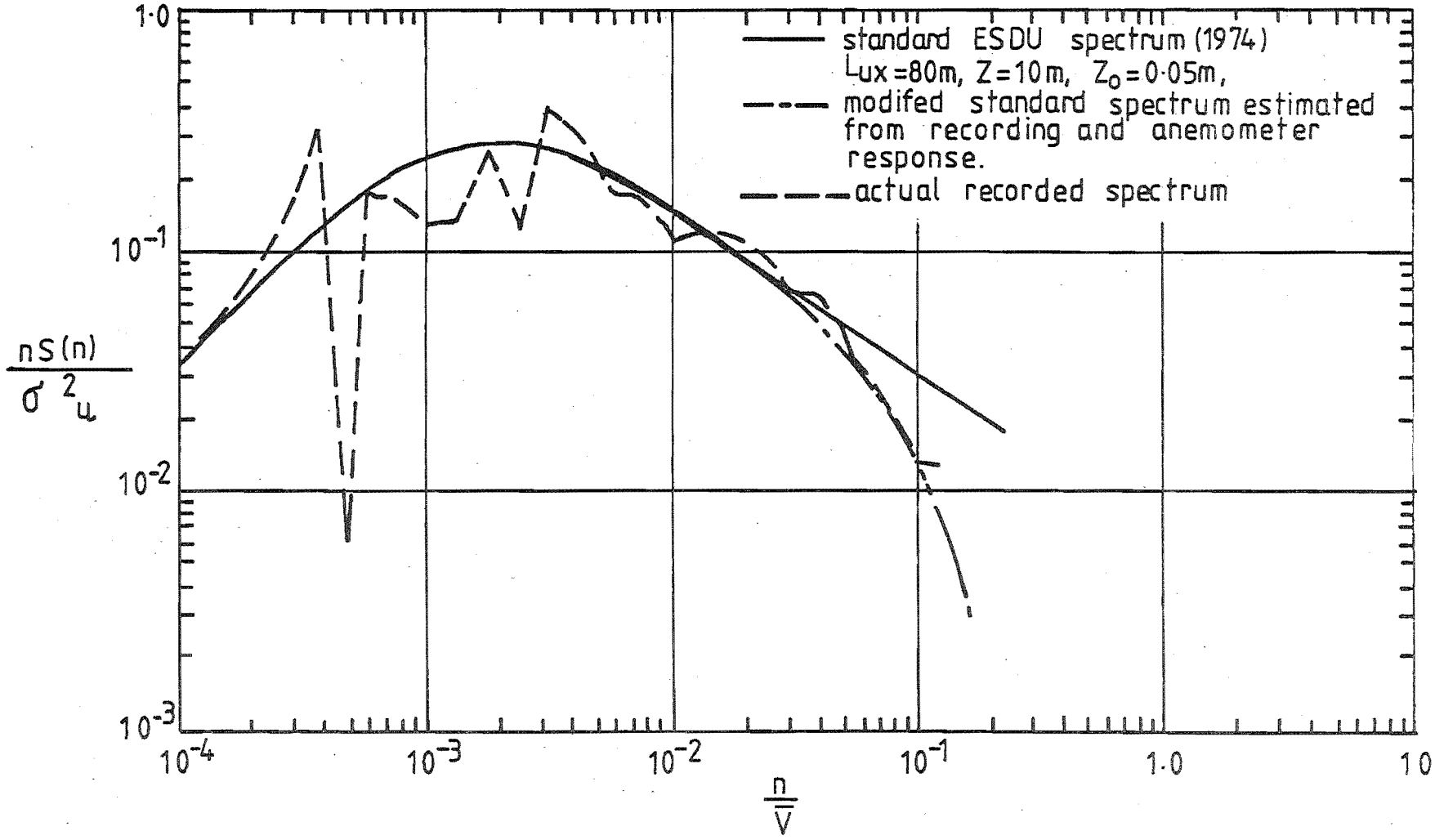

FIG 6·10 EFFECT OF ANENOMETER FREQUENCY RESPONSE ON A TYPICAL LONGITUDINAL VELOCITY POWER SPECTRAL DENSITY FUNCTION: A COMPARISON OF PREDICTED AND ACTUAL RECORDING. (L=1m, $\bar{v}$ = 7·88m/s, Z=10m, Z_o=0·05m)

that the atmospheric boundary-layer could not be assumed to be neutrally stable. However the weather conditions and the mean velocity profile measured during each recording were quite consistent and it was assumed that similar atmospheric conditions prevailed during each field recording.

An indication of the average atmospheric stability existing during the tests may be drawn from the influence of the stability term $\psi\left(\frac{Z}{L}\right)$ on the turbulence data normalised by the friction velocity V_*. It was established in Chapter 2, equation 2.16 that

$$\bar{V}_z = \frac{V_*}{k}\left[\log_e\left[\frac{Z}{Z_o}\right] - \psi\left(\frac{Z}{L}\right)\right]$$

Case 1) Under neutrally stable conditions, the $\psi\left(\frac{Z}{L}\right)$ term may be ignored and the recorded turbulence data presented as in Table 6.3, column #1. The value of Reynolds stress obtained was considered to be reasonable for the type of terrain so that the high value of $\sqrt{-\overline{uw}}\ /V_*$ compared with the expected value of unity, indicated an unusually low value of friction velocity. This low value due to the incorrect assumption on the stability of the boundary-layer, has in turn raised the turbulence parameters σ_u/V_* etc. well above those suggested by Counihan (1975). The low value of Z_o indicated from the mean profile and discussed earlier, would also have been caused by this incorrect stability assumption.

Case 2) By using Panofsky's (1977) method (described in Chapter 2) for estimating the effects of atmospheric stability, and assuming a Pasquill stability class C/D for the strong sun and medium wind speeds encountered, the data in Table 6.3, column #2 were generated. The intermediate steps in this iterative process are summarised in Fig.6.11. The turbulence parameters, σ_u/V_* have been reduced in value somewhat but were still higher than that expected. The value of friction velocity was still 20% lower than that indicated from the measured Reynolds stress.

Case 3) It was also possible to obtain an idea of the value of friction velocity from the measured Reynolds stress by assuming that $\sqrt{-\overline{uw}} = V_*$. By using Panofsky's method summarised in Fig.6.12, a more appropriate value of $Z_o = 0.05$ m was obtained with a class C stability. Realistic values of σ_u/V_* were also indicated using these assumptions. The resulting data are listed in Table 6.3, column #3.

It may be concluded that the upwind boundary-layer was consist-

PARAMETER	STANDARD RURAL DATA COUNIHAN (1975) ESDU (1974)	AMBERLEY 2:1		
		ASSUME 1 NEUTRAL STABILITY	2 CLASS C/D STABILITY	3 $V_*\sqrt{-\overline{uw}}$
α	0.14 -0.17	0.13[a]	0.17[b]	0.19[b]
Z_o m	0.01 -0.15	0.003[a]	0.025	0.050
$V_*/\bar{V}_{10}$		0.049	0.072	0.087
$V_*/\bar{V}_G$		0.029[e]	0.042[e]	0.050[e]
$\sigma u/\bar{V}_{10}$	0.18 -0.25	0.22[a]	0.22[a]	0.22[a]
$\sigma v/\bar{V}_{10}$	0.12 -0.20	0.16[a]	0.16[a]	0.16[a]
$\sigma_w/\bar{V}_{10}$	0.08 -0.12	0.11[a]	0.11[a]	0.11[a]
$-\overline{uw}/\sigma u.\sigma w$	0.29 -0.31	0.31[a]	0.31[a]	0.31[a]
$\sqrt{-\overline{uw}}/V_*$		1.77	1.20	1[c]
$-\overline{uw}/\bar{V}_G^2$	0.002-0.003	0.0026	0.0026	0.0026
$A=\sigma u/V_*$	2.50	4.49	3.06	2.53
$B=\sigma v/V_*$	1.875	3.26	2.22	1.84
$C=\sigma w/V_*$	1.25	2.24	1.53	1.26
$\sigma v/\sigma u$	0.75	0.73[a]	0.73[a]	0.73[a]
$\sigma w/\sigma u$	0.50	0.50[a]	0.50[a]	0.50[a]
STABILITY CLASS	D	D	C/D	C[d]

NOTES:-

a MEASURED VALUE

b ESTIMATED VALUE FOR NEUTRALLY STABLE CONDITIONS

c THEORETICAL ASSUMPTION

d PREFERRED OPTION

e ASSUME $Z_G \approx 600$ m

TABLE 6.3 UPSTREAM TURBULENCE FIELD DATA AT ≈ 10 m HEIGHT SHOWING THE EFFECT OF VARIOUS ATMOSPHERIC STABILITY ASSUMPTIONS (AMBERLEY TEST SITE)

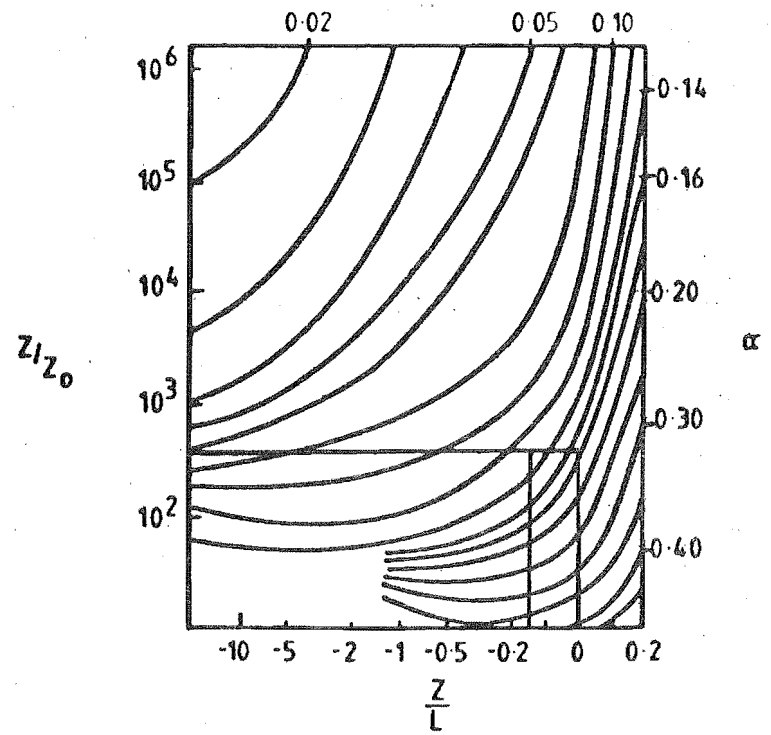

$$\psi\left(\frac{z}{L}\right) \approx 0.45$$

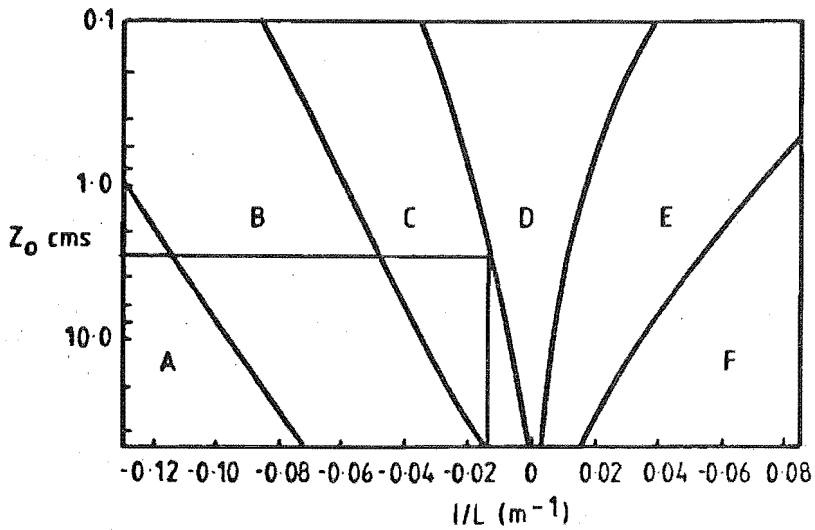

surface wind speed (at 10m) m sec^{-1}	Day: incoming solar radiation			Night: thinly overcast or ≥4/8 low cloud	Night: <3/8 cloud
	strong	moderate	light		
<2	A	A-B	B		
2-3	A-B	B	C	E	F
3-5	B	B-C	C	D	E
5-6	C	C-D	D	D	D
>6	C	D	D	D	D

The neutral class, D, should be assumed for thick overcast during day or night.

FIG. 6·11 ATMOSPHERIC STABILITY EFFECTS ON THE UNDISTURBED VELOCITY—HEIGHT PROFILE. PREDICTION METHOD, CASE 2

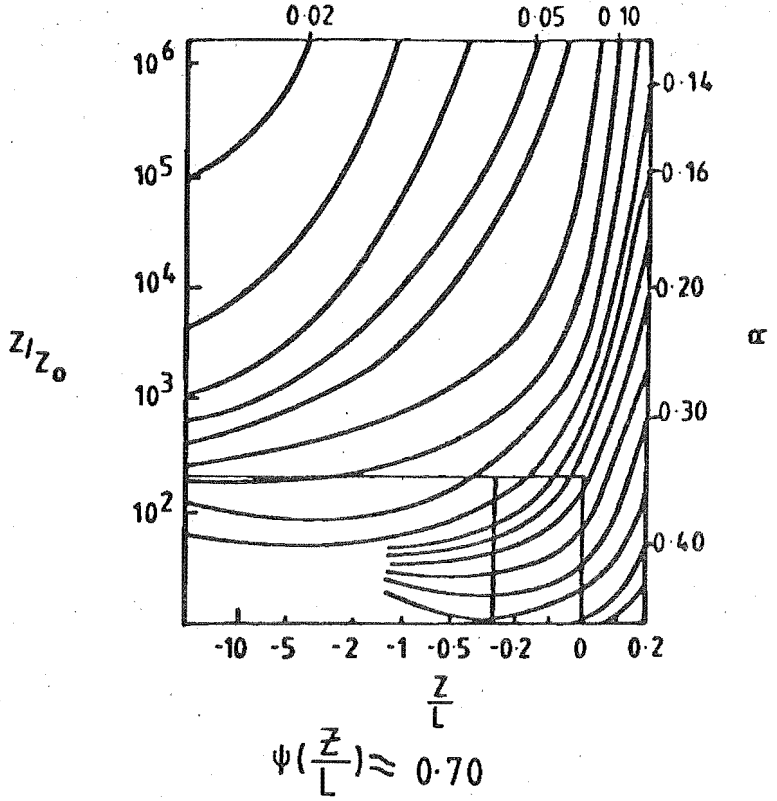

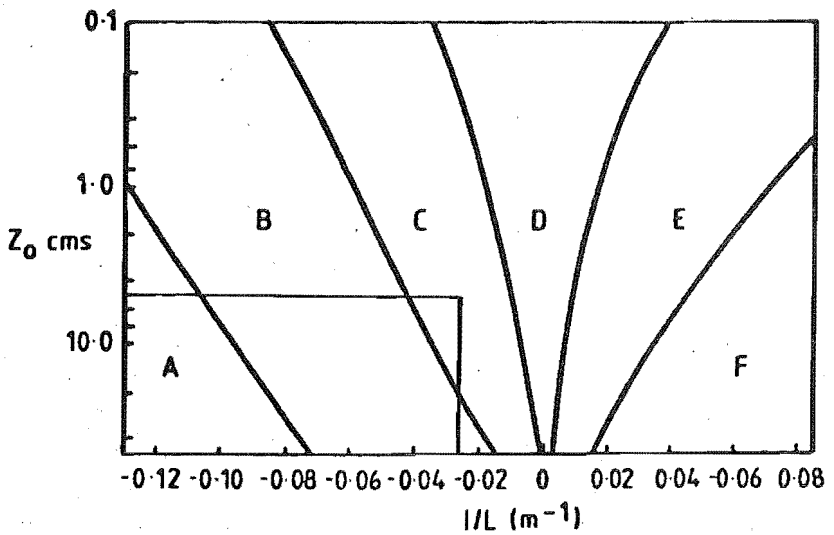

surface wind speed (at 10m) m sec^{-1}	Day			Night	
	incoming solar radiation			thinly overcast or ≥4/8 low cloud	<3/8 cloud
	strong	moderate	light		
<2	A	A-B	B		
2-3	A-B	B	C	E	F
3-5	B	B-C	C	D	E
5-6	C	C-D	D	D	D
>6	C	D	D	D	D

The neutral class, D, should be assumed for thick overcast during day or night.

FIG. 6·12 ATMOSPHERIC STABILITY EFFECTS ON THE UNDISTURBED VELOCITY — HEIGHT PROFILE, PREDICTION METHOD, CASE 3

ently unstable (class C), which may have been caused by the cold wind off the sea warming up in the lower levels of the atmosphere as it passed over the ground heated by the sun. The instability caused the unusually full velocity-height profile (α = 0.13) compared with that expected from a rural boundary-layer (0.14 - 0.17). When corrected for this instability by an appropriate choice of $\psi\left(\frac{z}{L}\right)$, the mean wind and turbulence data compared very well with the expected data presented by Counihan (1975) and ESDU (1974) for open rural terrain. However the unfortunate presence of the atmospheric instability in the field work makes close comparisons with other work and model tests more difficult.

6.5 FIELD RESULTS

The field results from the five recordings taken at the Amberley site are presented together as all the recordings were taken under similar atmospheric conditions. The scatter in results could have been due to small differences in stability from one recording to the other as the scatter was consistently high or low throughout a recording rather than randomly placed about the average. Results from channels associated with significant recording errors that were noticed during the processing of the results and discussed in Chapter 5, were omitted. The mean velocities measured over the escarpment were normalised by the estimated upwind velocity at the same height as the top of the escarpment ($^{z}/_{H}$ = 1) so that a direct comparison with the model tests described in Chapter 8 and other research work could be made. The alternative would have been to normalise by the measured velocity at 10 metres height, but the results would then be unique to that size of hill and a conversion to the previous format would have to be made before any serious comparisons could be made. The estimation of the upwind velocity at $^{z}/_{H}$ = 1 was made from an extrapolation of the velocity-height profile by about 5%, so that any error introduced into the results would have been quite small. Whenever possible the field results are shown with the model test results from Chapter 8, which were taken at the same angle of incidence to allow a direct comparison.

6.5.1 Mean Velocity

The variations in the mean flow velocity over the escarpment are presented in Fig.6.13 with the corresponding fractional speed-up ratios, ΔS in Fig.6.14. The scatter in ΔS values at each position was higher than for the mean velocity data as ΔS is a product of two

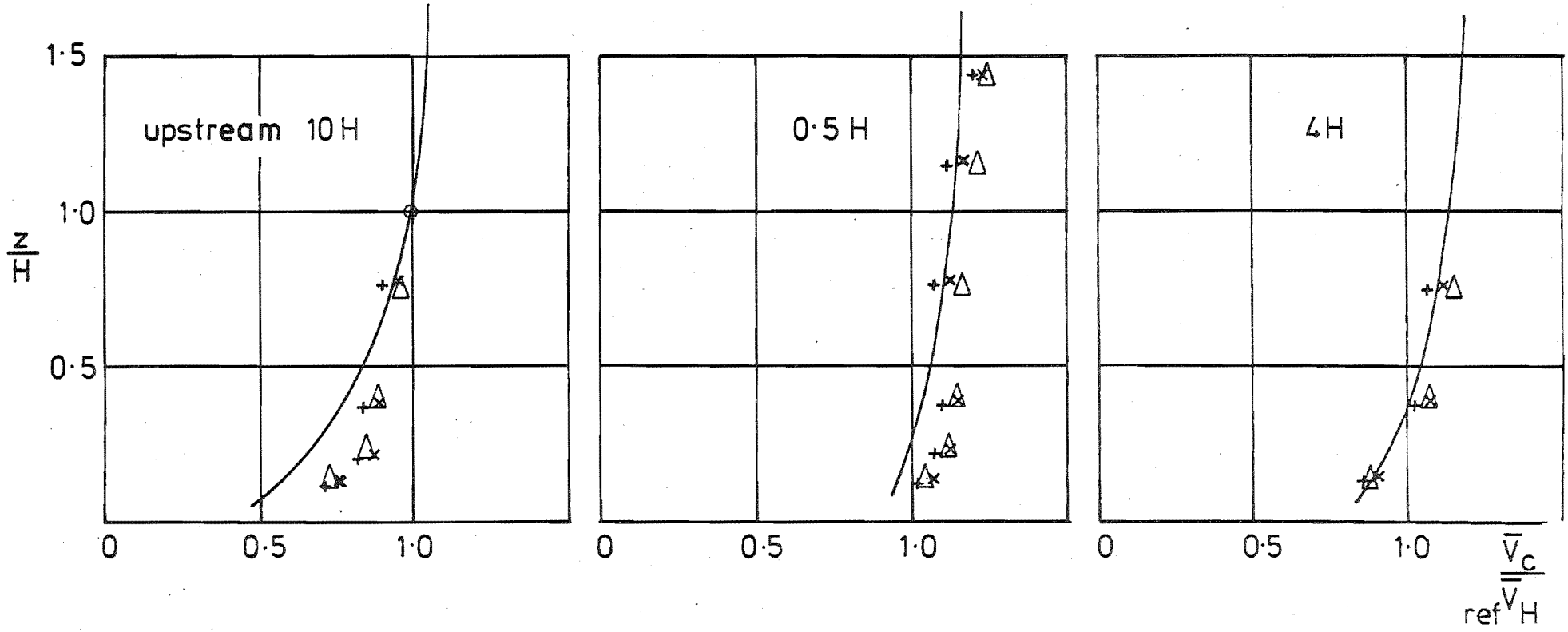

FIG. 6·13 MEAN VELOCITY–HEIGHT PROFILES OVER THE SLOPING ESCARPMENT AT THE UPSTREAM REFERENCE SITE, 0·5H AND 4H BEHIND THE CREST. ANGLE OF INCIDENCE TO CREST NORMAL, ϕ = 60°.

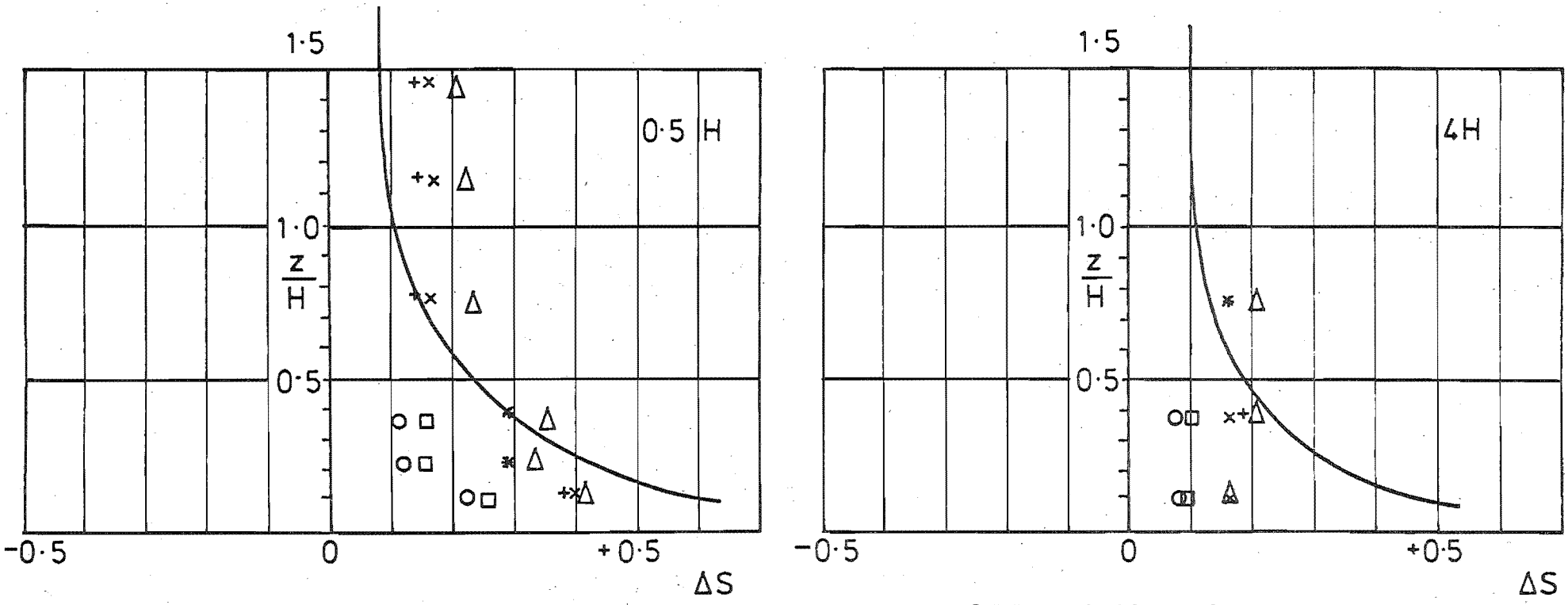

FIG 6·14 FRACTIONAL SPEED-UP RATIOS OVER THE SLOPING 2:1 ESCARPMENT. ($\Phi = 60°$)

independent measurements, whereas the mean velocities are normalised by the same reference velocity for each recording. The field ΔS values at the two highest levels on tower #2 at the 0.5 H position were calculated from estimated upwind velocities taken from the extrapolated upwind velocity-height profile. The data from recordings 2 and 3 were omitted from the normalised mean velocity data due to a suspected recording error affecting $_{REF}\bar{V}_H$. In addition, the values of ΔS from recordings 2 and 3 in Fig.6.14 were consistently lower than the others and as these recordings were taken on the same day, it suggests that the atmospheric conditions may have been somewhat different on that day.

The fractional speed-up ratios were commonly between 0.1 and 0.3 in the height range and distance behind the crest that were investigated and a peak value of 0.4 was obtained close to the ground at the 0.5 H tower position

6.5.2 Mean Flow Direction

The change in direction of the mean flow as it negotiated the escarpment is shown in Fig.6.15. The wind direction, ϕ at $^{Z}/_{H} = 1$ (Z = 13 m) was assumed to be the same as at Z = 10 m and remained within 60° ± 6° from the crest normal for all the five recordings. Despite a probable alignment tolerance of ±2° or 3°, a definite tendency to rise over the slope at a steeper angle by some 10° or 15° is indicated by the results.

The change in flow inclination with the horizontal was found to be insignificant at all positions even on the #2 tower at the 0.5 H position. The range in inclination encountered was typically less than 3° from the horizontal which was considered to be of a similar magnitude to the likely variation in anemometer alignment.

6.5.3 Turbulence Intensities

The variation of the three components of standard deviation, σ_u, σ_v, σ_w normalised by $_{REF}\bar{V}_H$ are presented in Figs.6.16, 6.17 and 6.18. Very little influence from the hill is evident in the results.

The corresponding three components of turbulence intensity, $\sigma_u/\bar{V}_z$ etc. are shown in Figs.6.19, 6.20 and 6.21 respectively. The major variation in these terms would be due to the variation in $\bar{V}_z$ over the escarpment rather than in the standard deviations themselves.

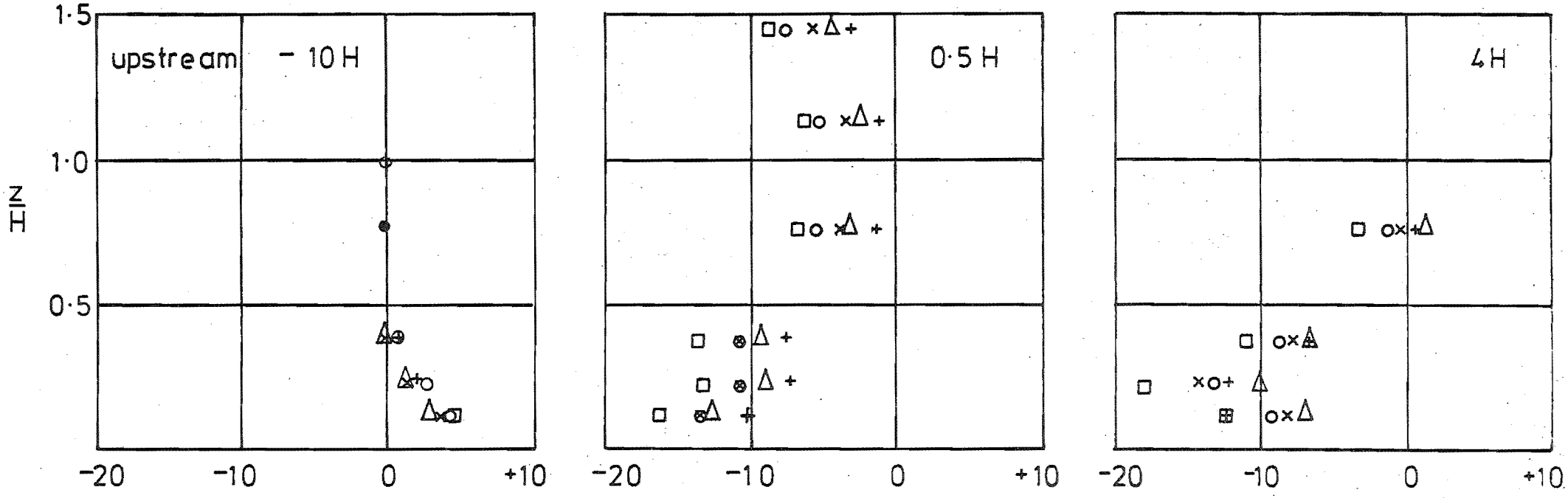

FIELD RECORDINGS:	SYMBOL	$REF\phi_{10}$
# 1	+	57
2	o	56
3	□	58
4	Δ	66
5	×	62

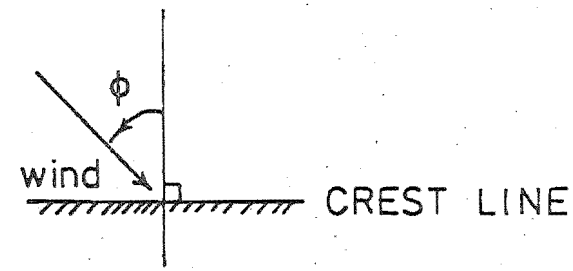

FIG. 6·15. CHANGE IN DIRECTION OF THE MEAN FLOW OVER THE SLOPING 2:1 ESCARPMENT ($\phi = 60°$).

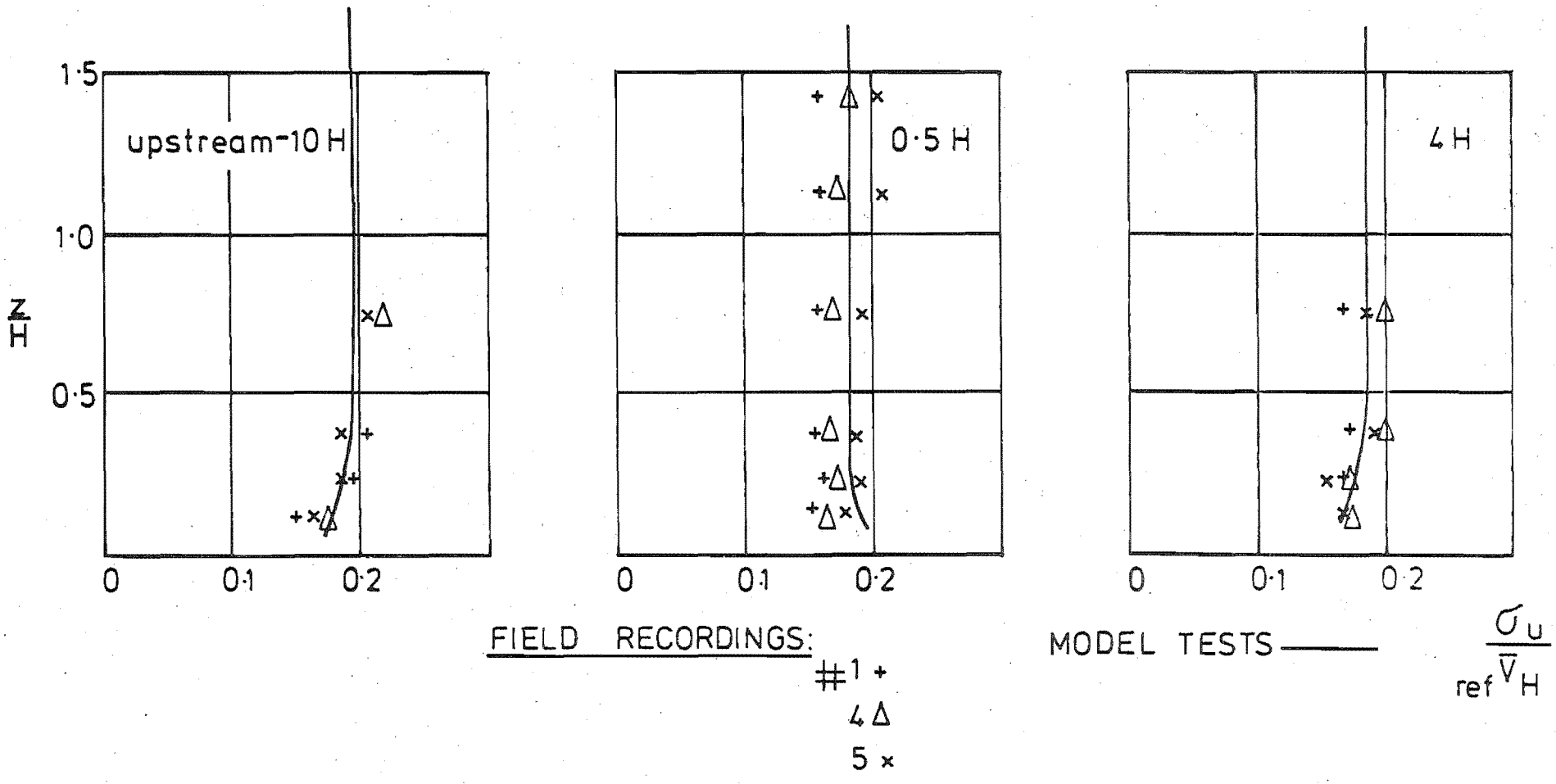

FIG. 6·16 VARIATION IN THE STANDARD DEVIATION OF THE LONGITUDINAL VELOCITY COMPONENT. (SLOPING 2:1 ESCARPMENT, $\phi = 60°$)

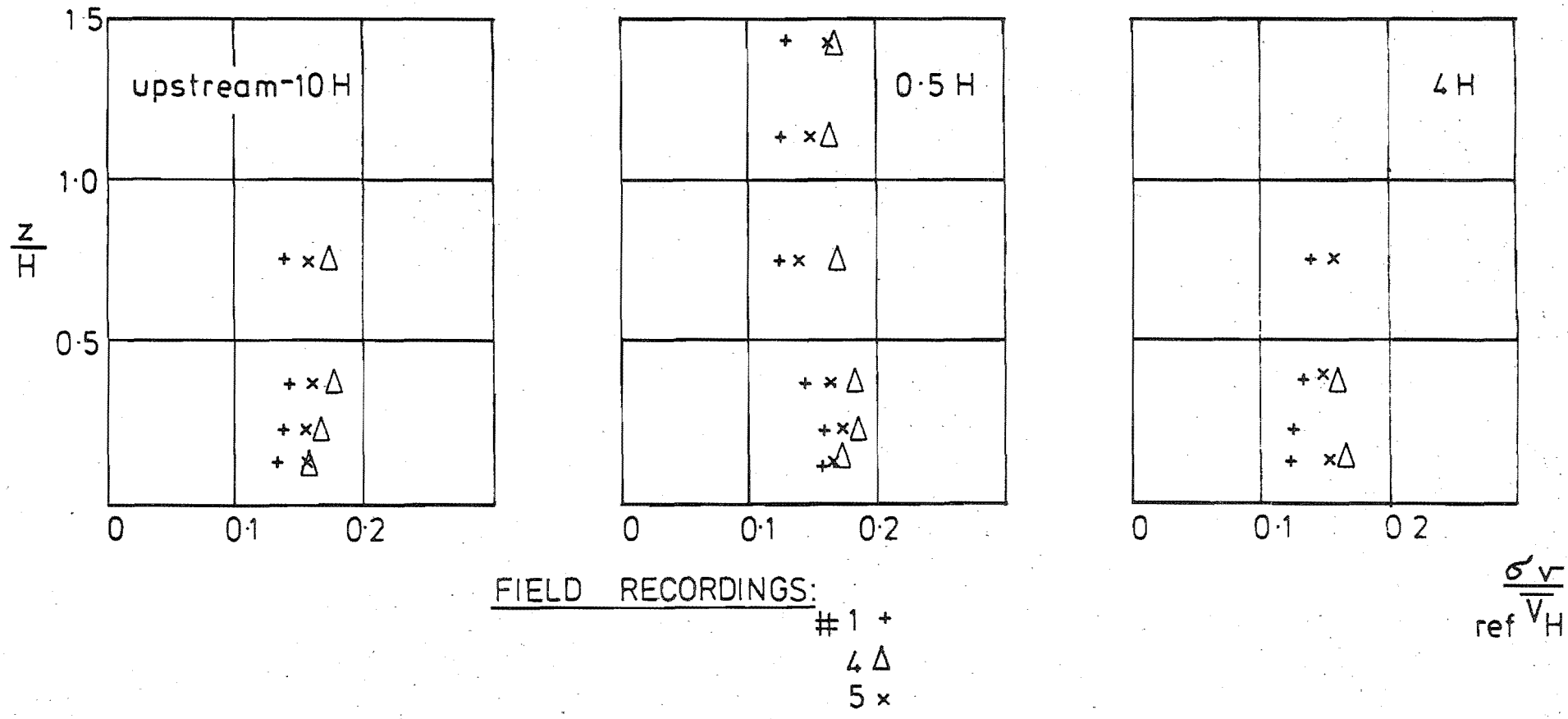

FIG. 6·17. VARIATION IN THE STANDARD DEVIATION OF THE LATERAL VELOCITY COMPONENT. (SLOPING 2:1 ESCARPMENT, $\phi = 60°$.)

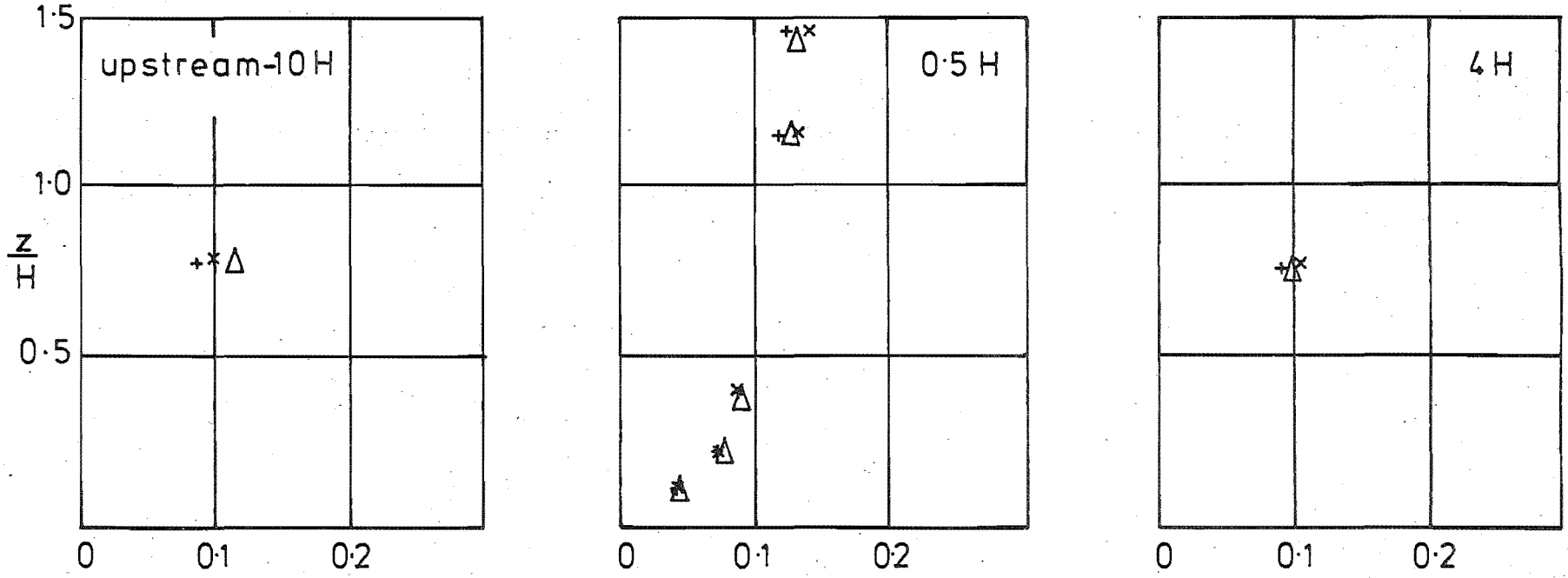

FIELD RECORDINGS:

#	
1	+
4	Δ
5	×

FIG. 6·18 VARIATION IN THE STANDARD DEVIATION OF THE VERTICAL VELOCITY COMPONENT. (SLOPING 2:1 ESCARPMENT, $\Phi = 60°$)

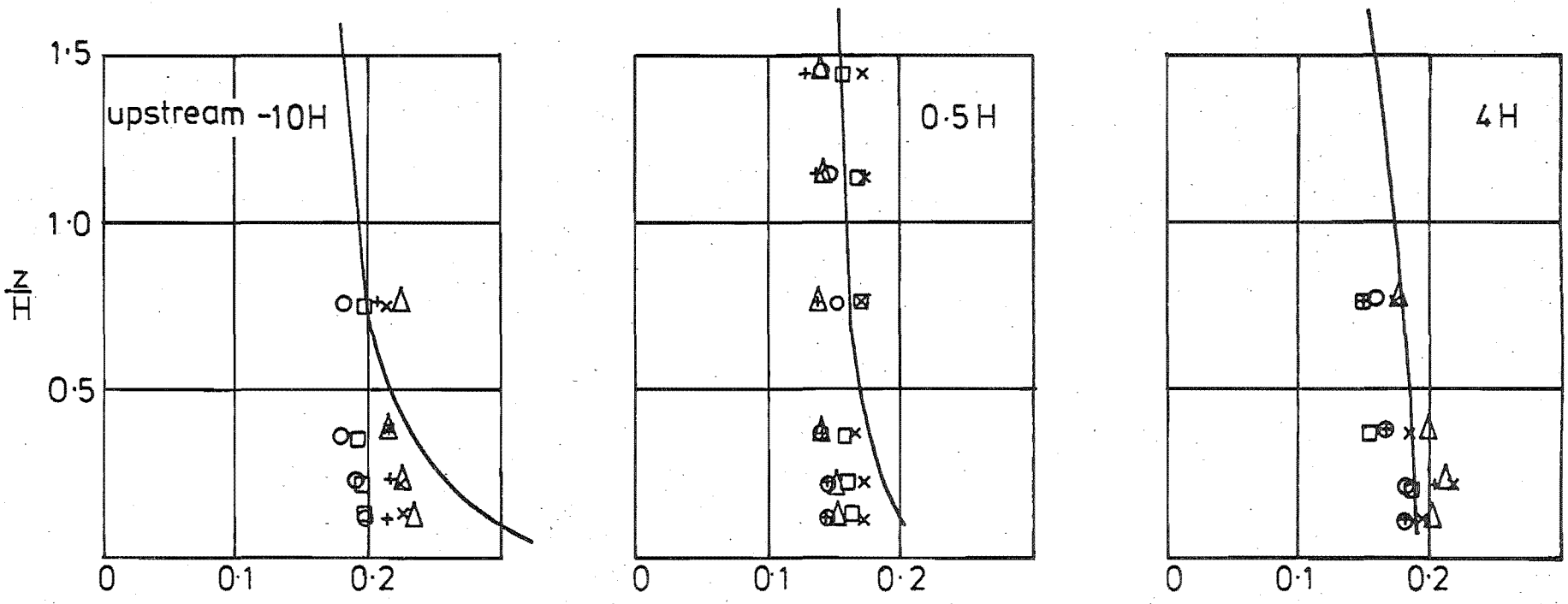

FIG. 6·19 VARIATION IN THE LONGITUDINAL TURBULENCE INTENSITY (SLOPING 2:1 ESCARPMENT. $\Phi = 60°$)

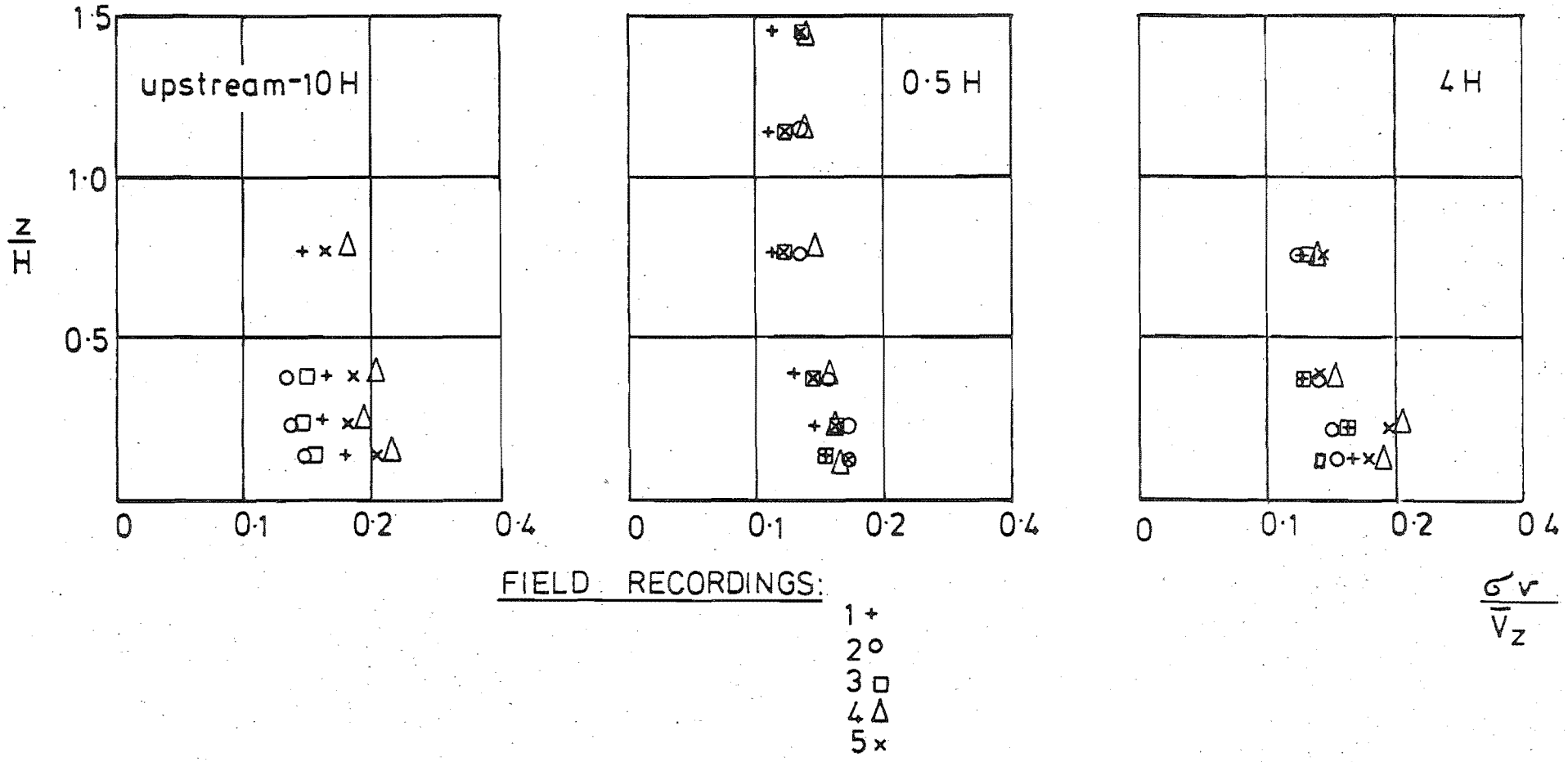

FIG. 6·20 VARIATION IN THE LATERAL TURBULENCE INTENSITY. (SLOPING 2:1 ESCARPMENT, $\phi = 60°$)

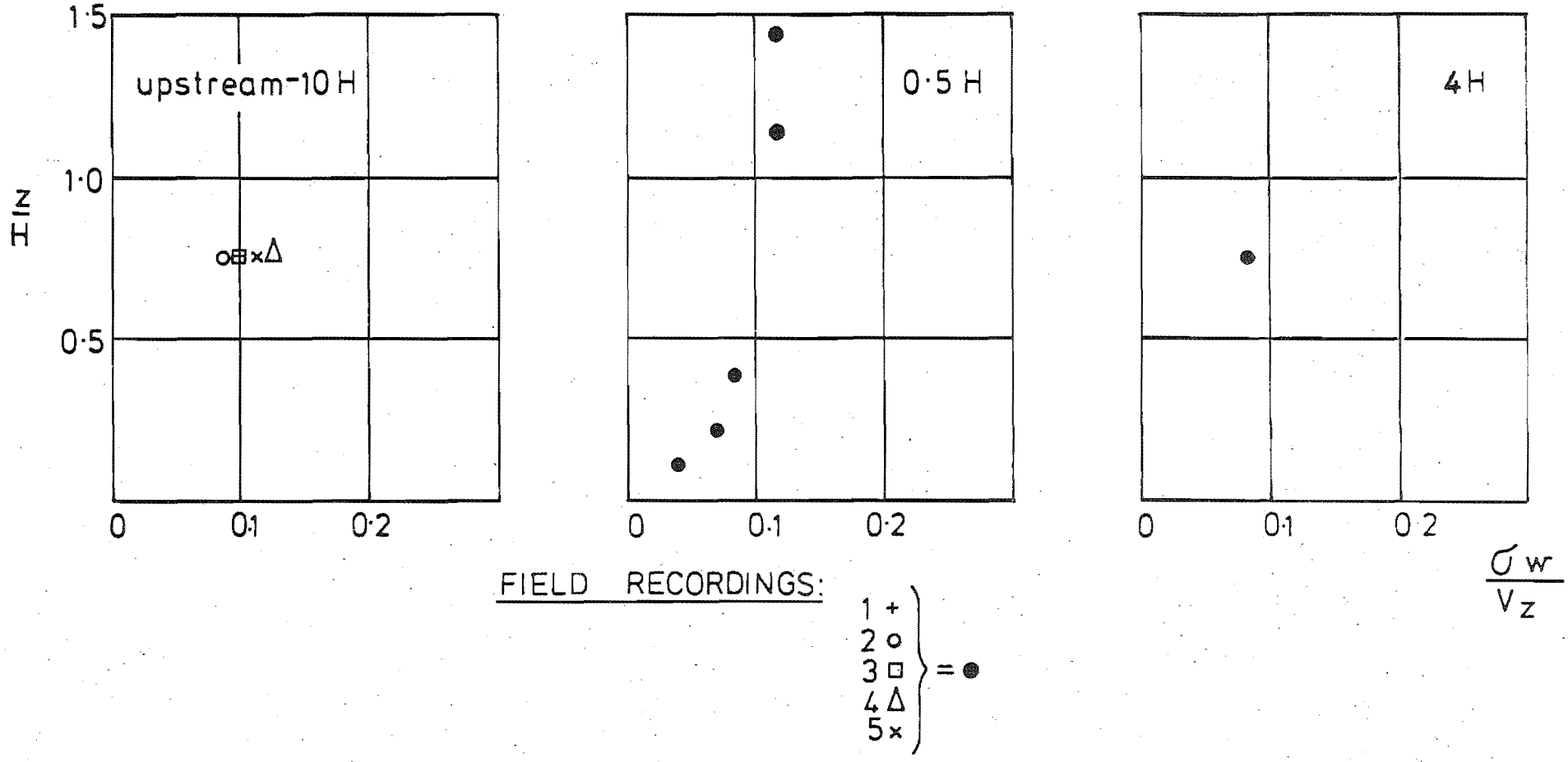

FIG. 6·21. VARIATION IN THE VERTICAL TURBULENCE INTENSITY. (SLOPING 2:1 ESCARPMENT, $\phi = 60°$).

6.5.4 Reynolds Stresses

The principal Reynolds stress term $\frac{\overline{uw}}{\sigma_u \cdot \sigma_w}$ is shown in Fig.6.22 which showed a significant reduction in absolute value close to the ground behind the crest if one assumed that there was little variation with height at the upstream position,ESDU (1974). The other two components are shown in Figs.6.23 and 6.24 which rose to similar magnitudes as the $\overline{uw}$ component but were less consistent, especially the $\overline{uv}$ component. They changed sign occasionally in a similar manner to those recorded by Flay (1978).

6.5.5. Longitudinal Velocity Power Spectra

Sample power spectra calculated from the #5 field recording which contained no significant trend in the mean velocity, are shown in Figs. 6.25 and 6.26 for the 10 m and 1.56 m heights on the three towers. The spectra were calculated using an effective sampling frequency of 2 Hz. No change due to the presence of the hill is evident but the expected small shift to lower frequencies with increasing height above ground is visible between the two sets of spectra.

The longitudinal length scales of turbulence L_{ux} calculated by integrating the autocorrelation function until the correlation dropped to 5% and multiplying by the mean velocity, were typically about 100 m at Z = 10 m. They reduced somewhat with decreasing height as expected but little influence from the escarpment was evident. However the lateral length scales increased markedly behind the crest from 30-40 m upwind to almost double that value at the #2 tower (0.5 H). The ratio of L_{vx}/L_{ux} increased from about 0.35 to 0.6 from tower #1 to tower #2. The high L_{vx}/L_{ux} ratio was maintained at the #3 tower but the L_{ux} values were generally slightly smaller at this position especially close to the ground, indicating a slight rise in high frequency turbulence energy behind the crest.

6.5.6 Velocity Probability Distribution

The frequencies of occurrence of the longitudinal velocity component were analysed for all instrument positions and it was found that the probability distributions were always very close to Gaussian except for a variation in the peak gust magnitude or distribution tails. A sample plot is shown in Fig.6.27 for Z = 1.56 m, tower #3, 4 H behind the crest.

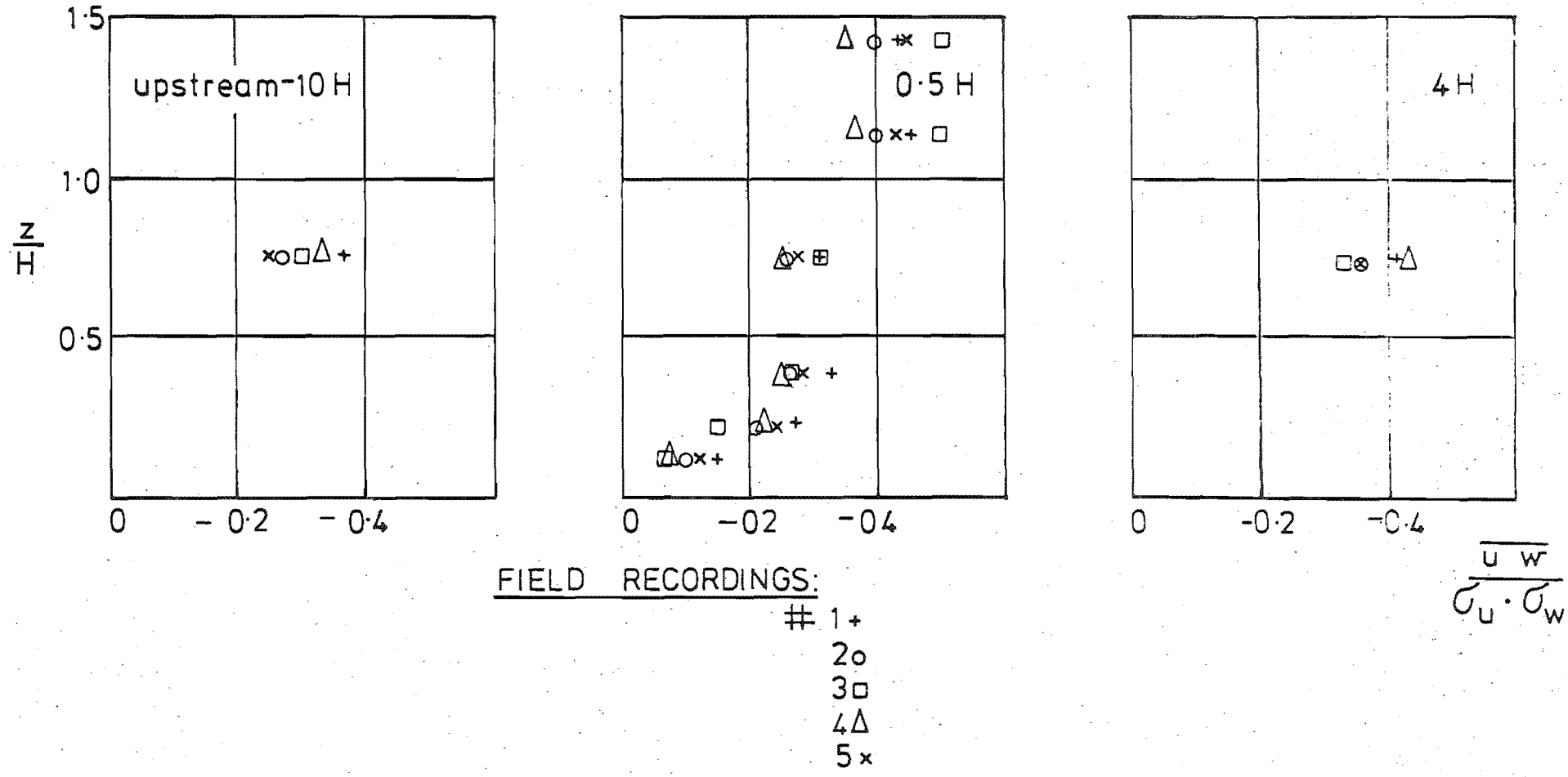

FIG. 6·22 VARIATION IN THE REYNOLDS STRESS, $\frac{\overline{u\,w}}{\sigma_u \cdot \sigma_w}$
(SLOPING 2:1 ESCARPMENT, $\phi = 60°$)

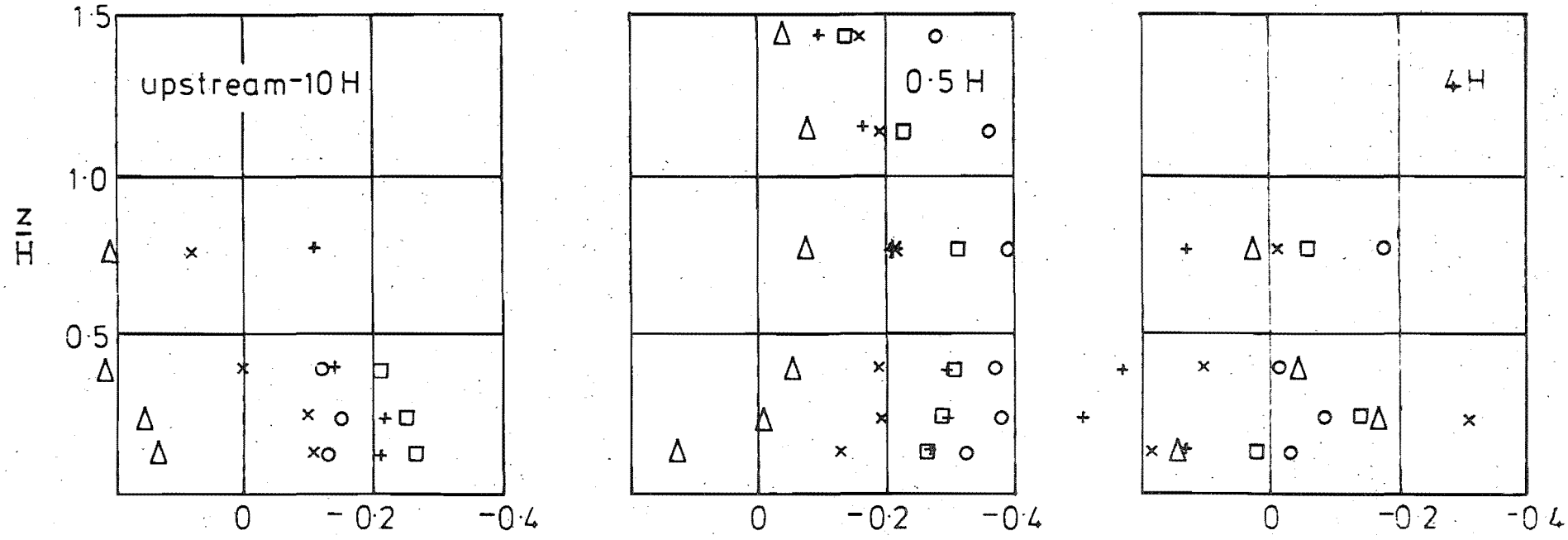

FIG. 6·23. VARIATION IN THE REYNOLDS STRESS $\frac{\overline{uv}}{\sigma_u \sigma_v}$ (SLOPING 2:1 ESCARPMENT, $\phi = 60°$).

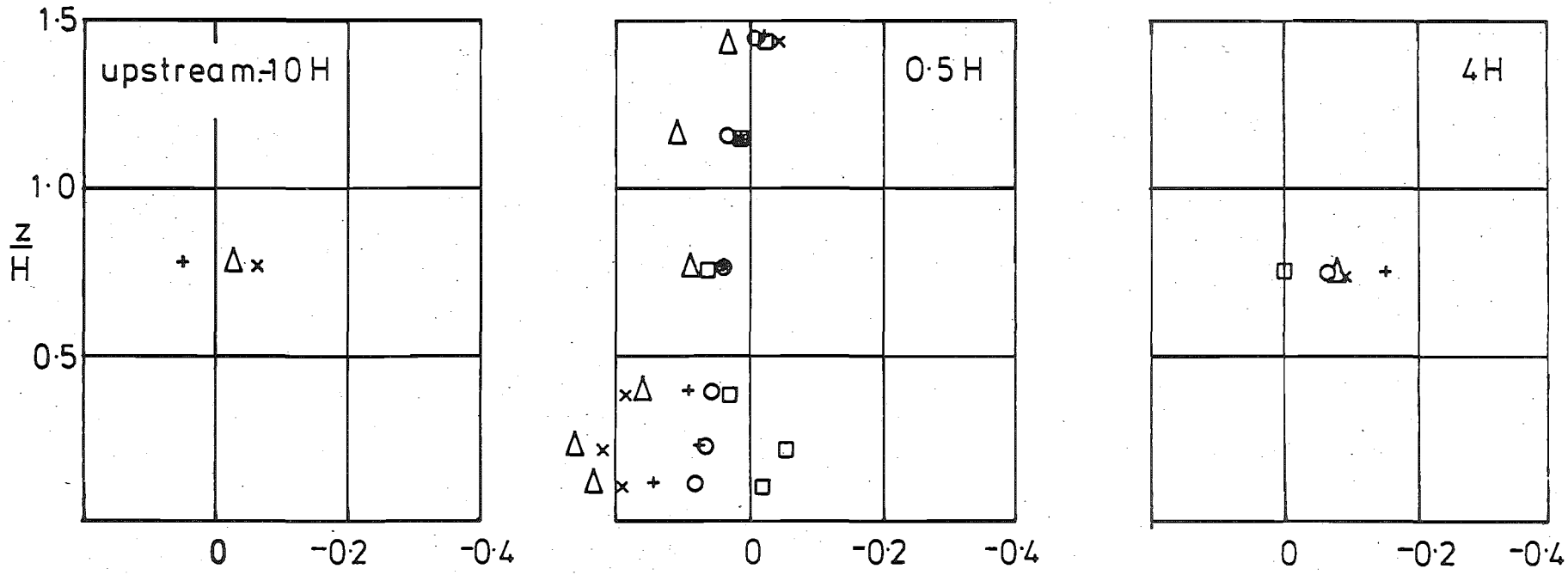

FIG. 6·24 VARIATION IN THE REYNOLDS STRESS. $\frac{\overline{vw}}{\sigma_v \sigma_w}$
(SLOPING 2:1 ESCARPMENT, $\bar{\phi} = 60°$)

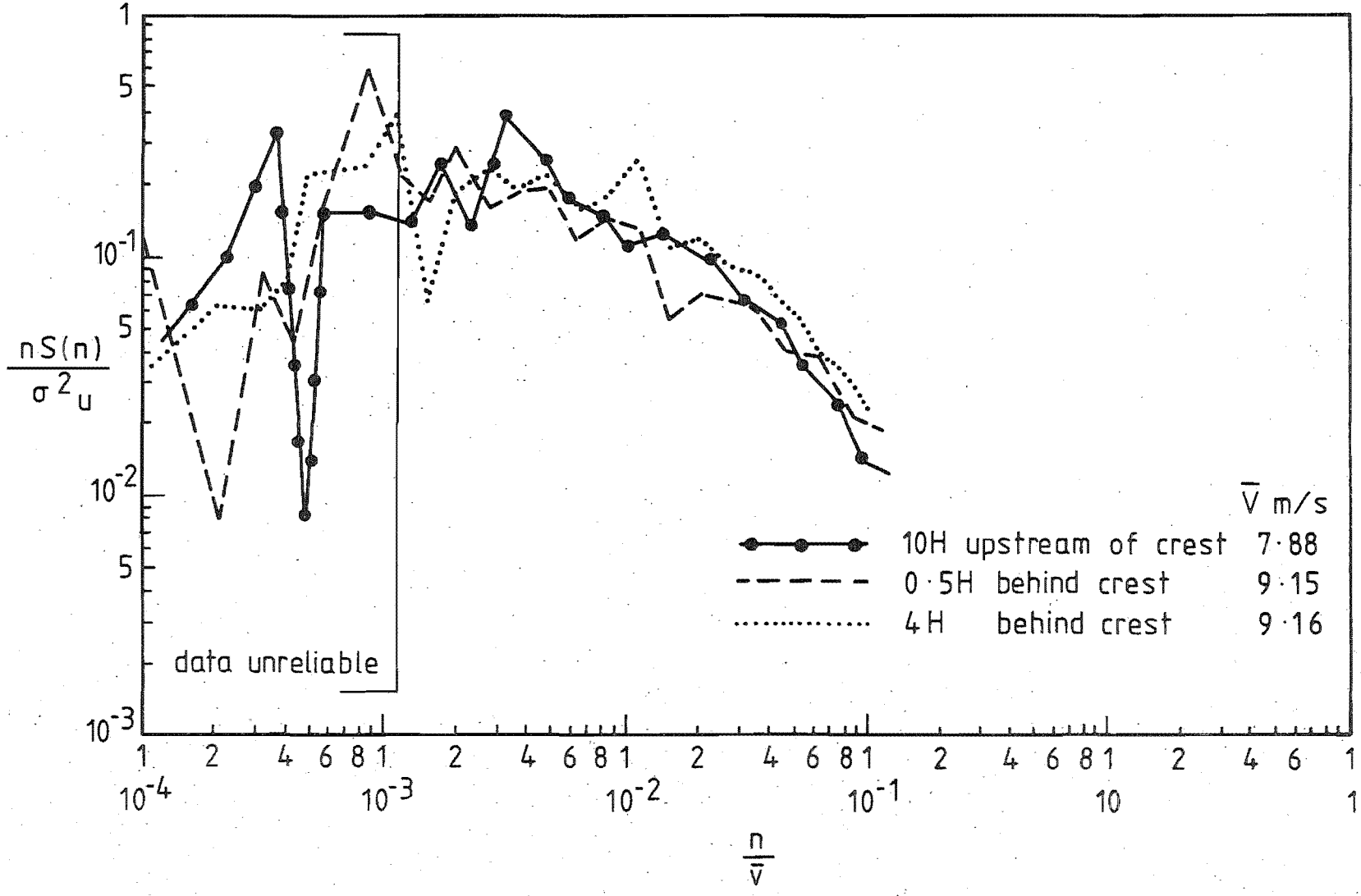

FIG 6·25 THE LONGITUDINAL VELOCITY POWER SPECTRA AT Z = 10m ($\frac{z}{H}$ = 0·76) AT DIFFERENT POSITIONS OVER THE 2:1 SLOPING ESCARPMENT. (ϕ = 60°)

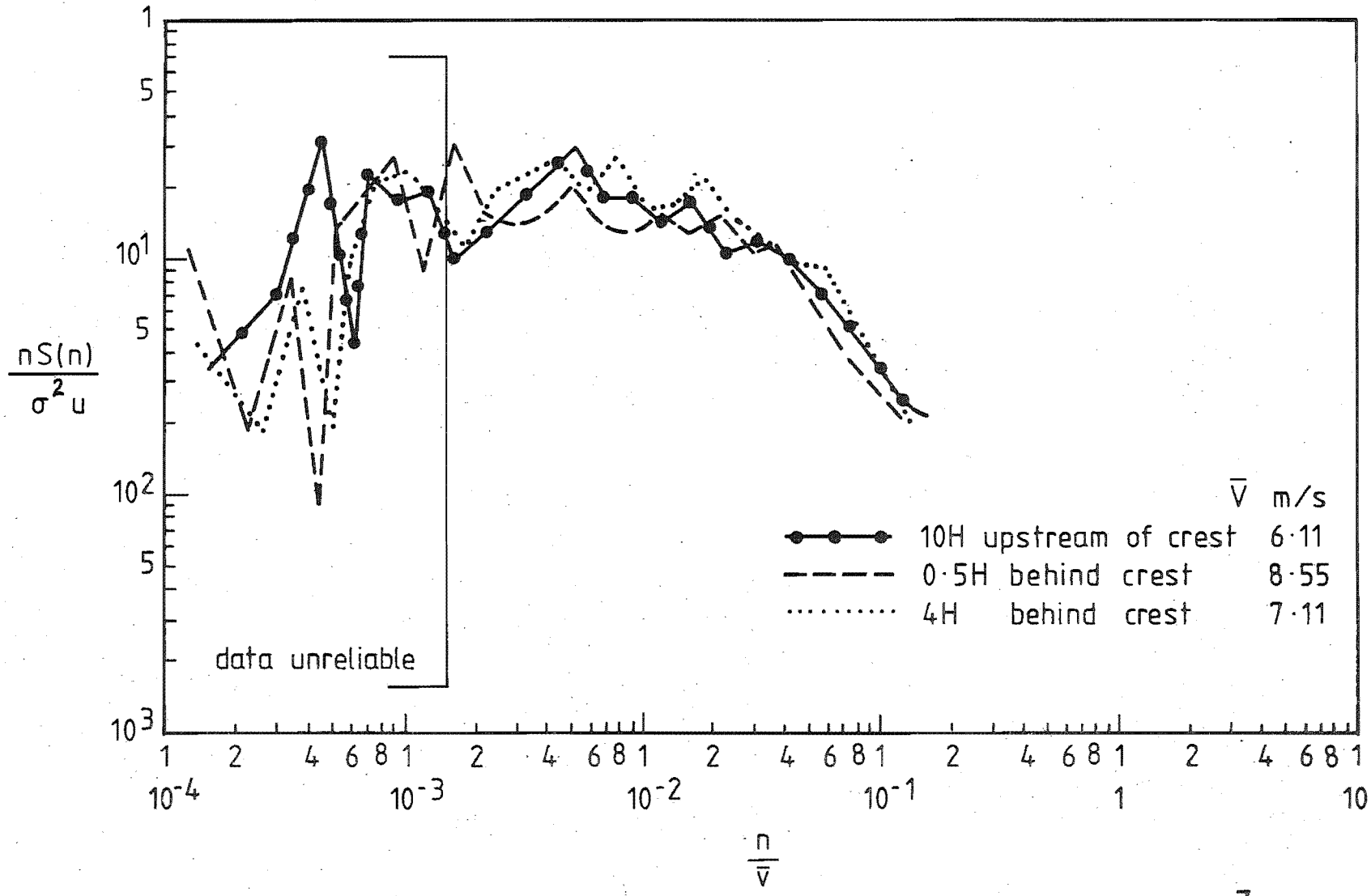

FIG 6·26 THE LONGITUDINAL VELOCITY POWER SPECTRA AT Z = 1·56m ($\frac{Z}{H}$ = 0·12) AT DIFFERENT POSITIONS OVER THE 2:1 SLOPING ESCARPMENT. (ϕ = 60°)

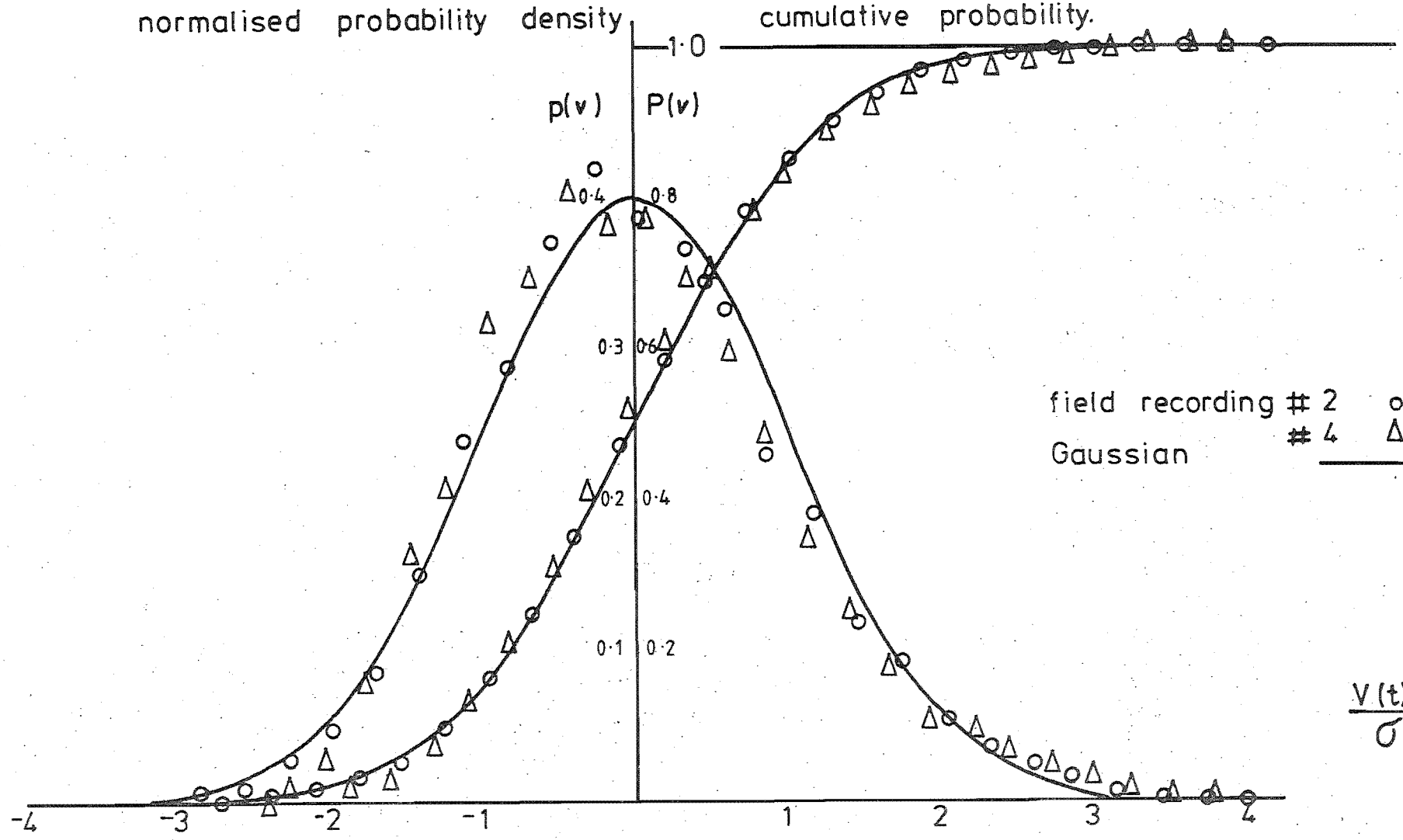

FIG. 6·27. VELOCITY PROBABILITY DISTRIBUTIONS FOR Z = 1·56m, TOWER #3 SLOPING 2:1 ESCARPMENT. ($\Phi = 60°$)

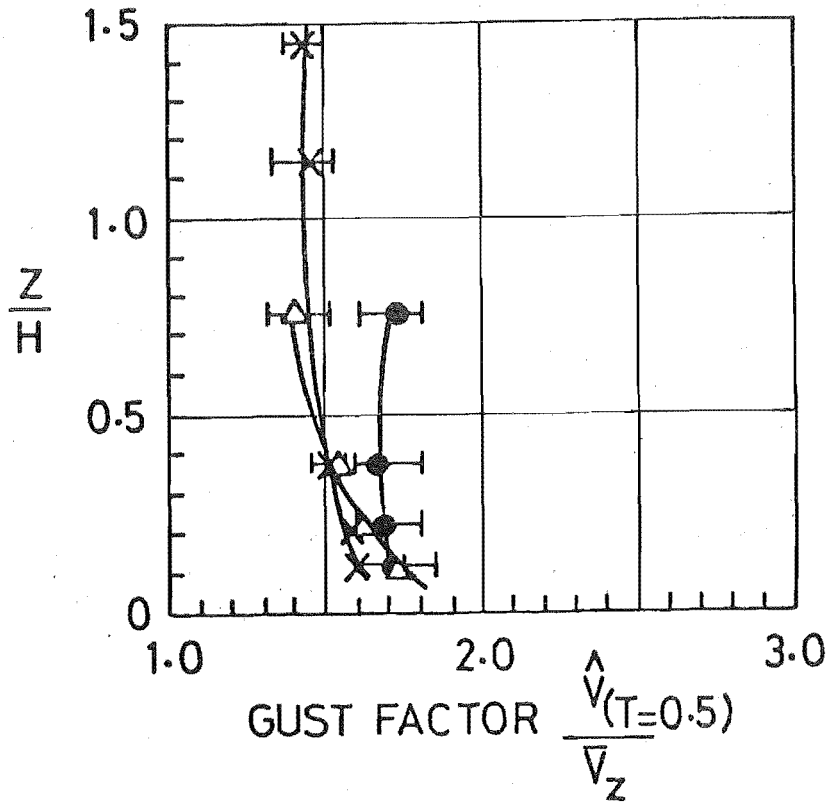

● 10 H upstream of crest
X 0·5H behind crest
Δ 4H behind crest
⊢⊣ range of results from 4 recordings.

FIG 6·28 VARIATION OF GUST FACTOR OVER THE SLOPING 2:1 ESCARPMENT ($T=0{\cdot}5s$, $T_o=1800s$, $\phi=60°$)

6.5.7 Peak Gust Velocities

The variation over the escarpment of the peak longitudinal gust velocity averaged over a period of T = 0.5 seconds and which was encountered during the period of one recording is shown in Fig. 6.28 as averaged values from the five recordings. A discussion on the previously observed (see Chapter 2) strong correlation between the gust velocity and the longitudinal turbulence intensity is described fully in Chapter 9 and confirmed that this relationship still held in the flow close to the escarpment. When considering the scatter in the results, it must be remembered that the peak velocity has a certain probability of occurrence with its own mean and standard deviation.

6.6 CONCLUSIONS

* The features of the 2:1, 13 m high sloping escarpment site near Amberley were described in detail and it was considered that the site was very suitable for the purpose of the test. Three masts were used with 14 instrument positions which provided data at 0.5 and 4 escarpment heights behind the crest to a height of 20 m and 10 m respectively, together with data from the undisturbed boundary-layer upstream.

* Four half-hour and one fifteen minute recording were taken in similar weather conditions. The mean wind speeds at 10 m height were between 7.1 and 9.7 m/s and blew off the sea with a mean angle of incidence to the crest normal consistently close to 60°. On all days, a strong sea breeze prevailed with clear skies which permitted strong sun radiation.

* By considering the mean flow and turbulence data at the 10 m height level upstream of the escarpment, it was evident that the atmospheric boundary-layer was consistently unstable during the recordings (Pasquill Stability Class C). The instability was attributed to the hot sun and the cool sea breezes flowing over the heated coastal areas. Satisfactory values of the three turbulence intensity components were obtained once correction for the atmospheric stability was made.

* The oblique mean flow velocities were significantly affected by the presence of the escarpment giving fractional speed-up ratios

commonly between 0.1 and 0.3 with a peak value of 0.4 close to the ground at the 0.5 H position.

* The presence of the escarpment had very little effect on the flow turbulence parameters that were measured and presented.

CHAPTER 7

THE CLIFF ESCARPMENT FIELD TEST

The 11.56 m high cliff escarpment on the banks of the Rakaia River was the second site investigated between mid February and mid April 1978. This field test resulted in three half-hour recordings and two shorter recordings with mean wind speeds at 10 m above the ground ranging between 6.76 and 13.27 m/s.

This chapter describes the site in some detail, the weather conditions prevailing at the time of the recordings and then presents the results obtained from the recording analyses. The deployment of equipment and anemometers and the experimental techniques used were very similar to the Amberley test site investigation which has been fully described in Chapter 6. Reference should be made to Chapter 6 for those common details as only the features unique to the Rakaia site are described below.

7.1 SITE DESCRIPTION

The cliff escarpment was located 70 km south of Christchurch on the south bank of the Rakaia River, 10 km west of the main south road. The location of the site is shown in Fig.7.1 which has been taken from a 1 inch to the mile, Lands and Survey Department map. The escarpment faced NE over the 2 km wide flat shingle riverbed which was partly covered by extensive patches of 0.5 - 1.0 m high lupin scrub. The countryside on both sides of the riverbed was flat open farmland with periodic rows of shelterbelt trees except for the opposite sloping riverbank. The site area has been boxed in on Fig.7.1 and is shown on an enlarged scale in Fig.7.2 to indicate the important site features and roughness and to locate the tower positions. The cliff was 11.56 m high on the tower centre line with a straight sharply defined crest and a flat open grass covered area downwind. The general layout and nature of the site is shown in Figs.7.3 to 7.6. The majority of the recorded winds came across the riverbed from the NE and over the escarpment at a mean angle of 24° ± 3° to the normal from the escarpment crest.

The ground upwind of the site in the riverbed could be categorised as an open plain with an expected Z_o value of about 0.02 (ESDU 1972).

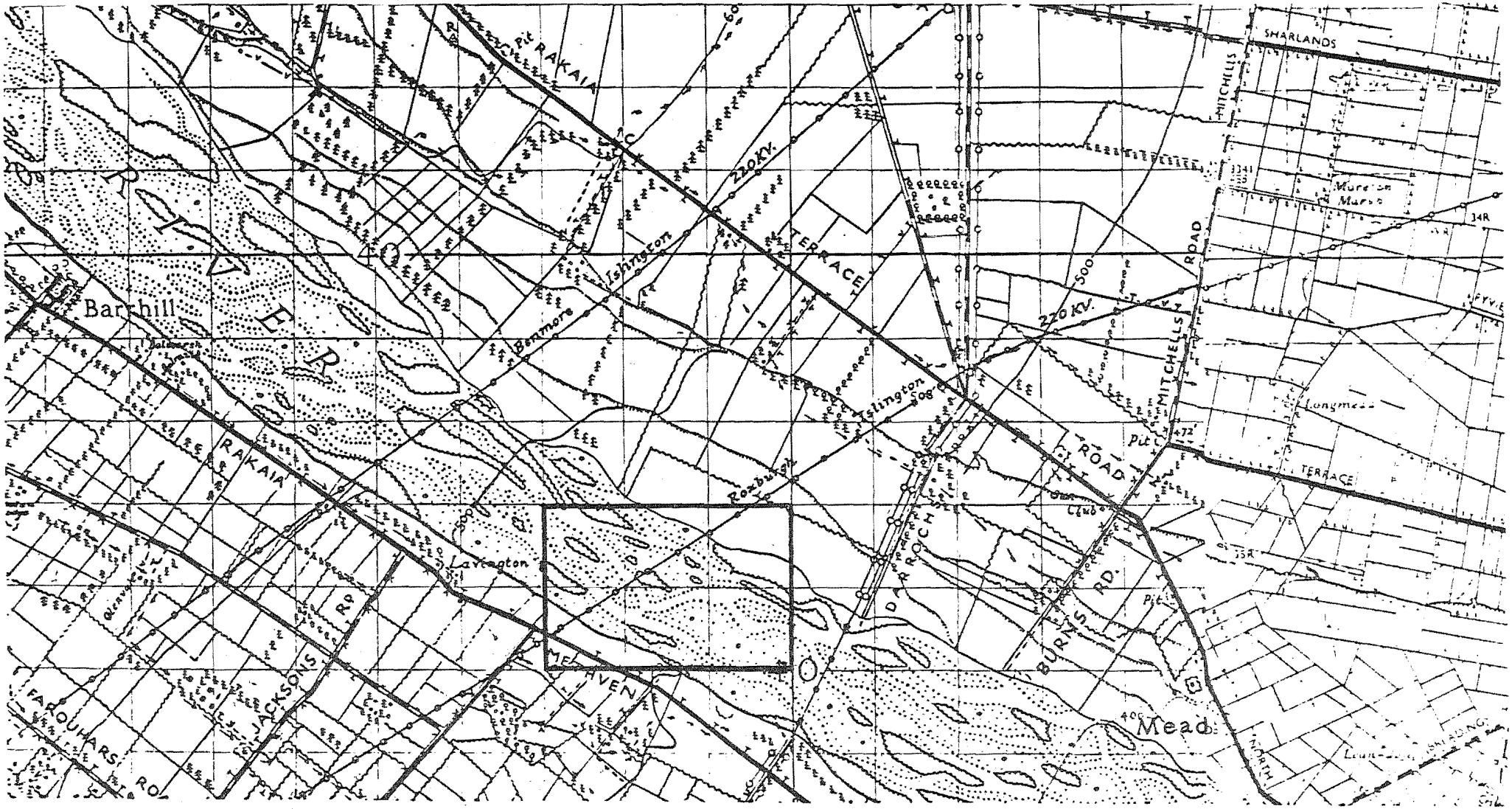

FIG 7·1 LOCATION OF RAKAIA SITE (SCALE 1inch = 1mile)

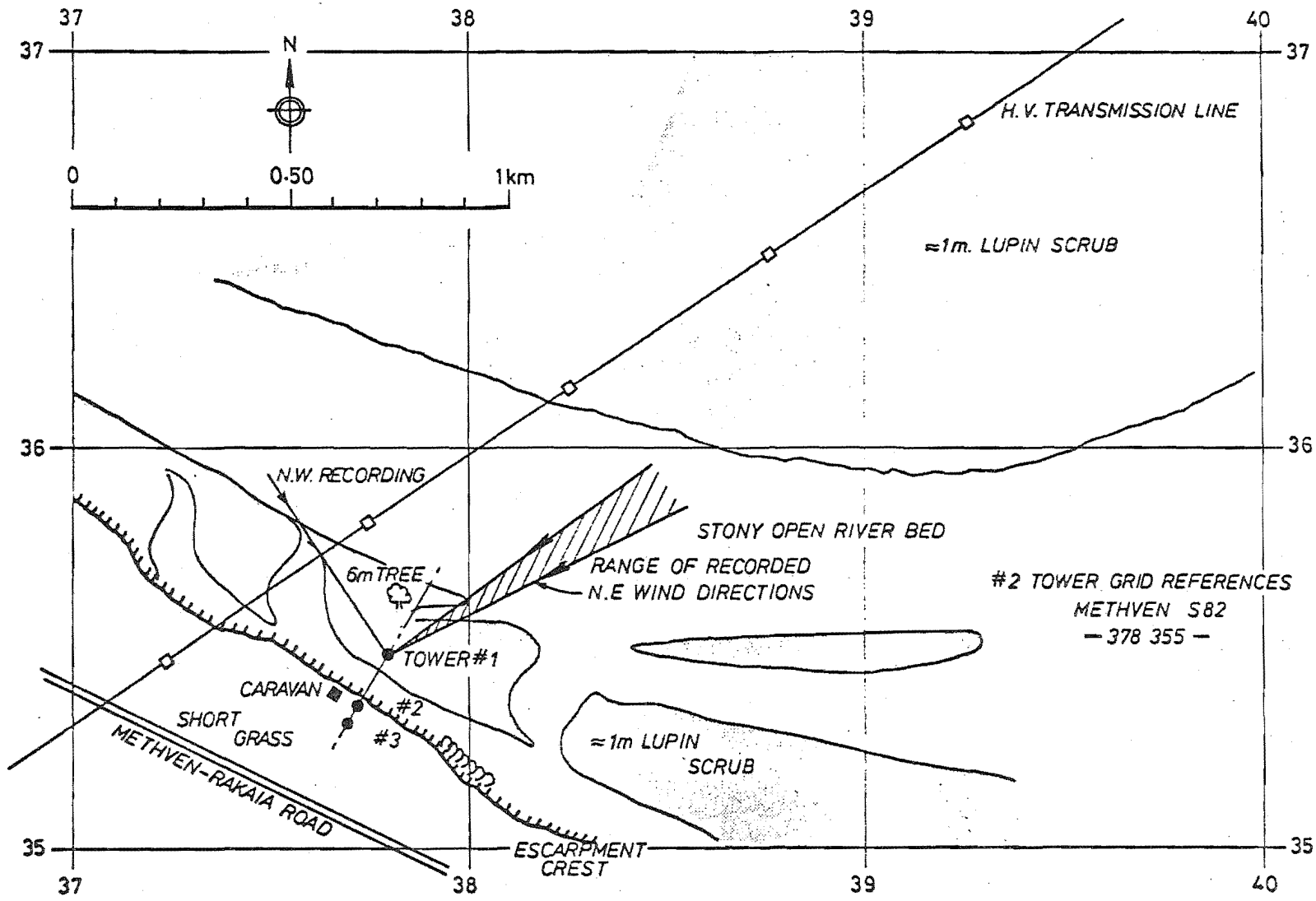

FIG 7·2 MAP OF RAKAIA SITE AREA AND TOWER POSITIONS.

FIG.7.3 VIEW LOOKING NW ALONG THE CREST AND SHOWING THE CARAVAN AND #2 TOWER AT THE RAKAIA SITE

FIG.7.4 VIEW LOOKING SE ALONG THE CREST AND SHOWING TOWERS #2 AND 3 AT THE RAKAIA SITE

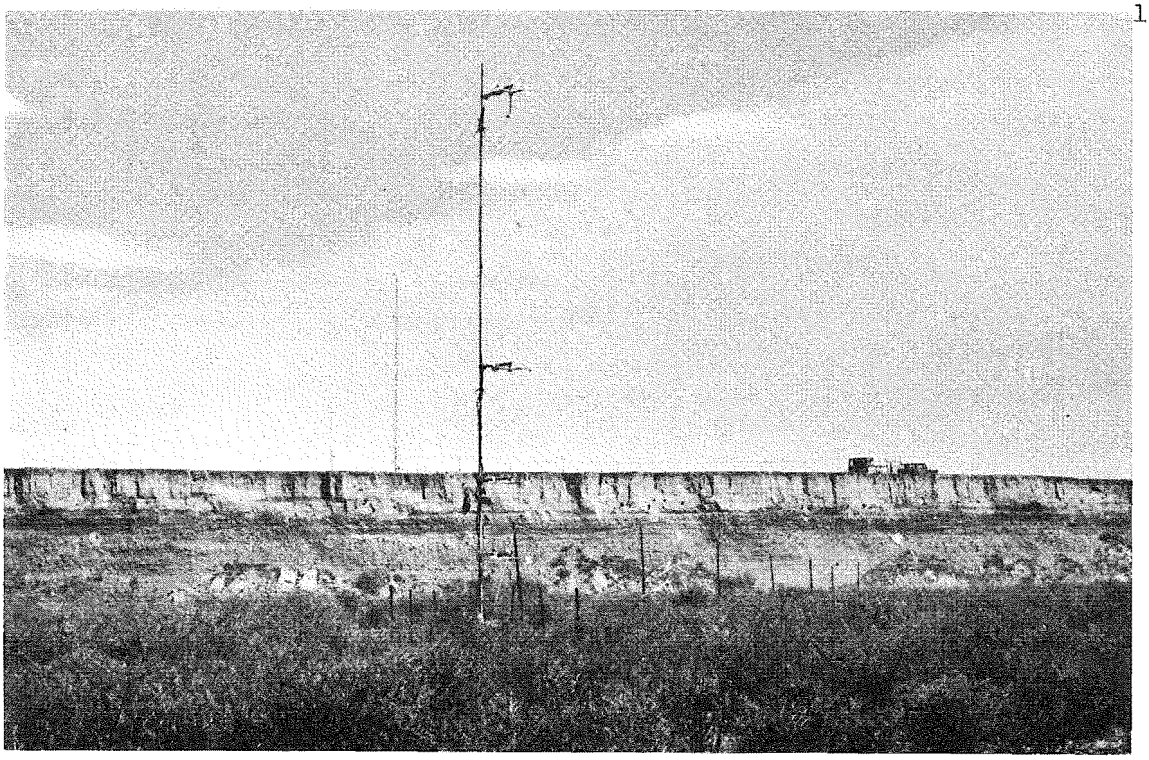

FIG.7.5 VIEW LOOKING SW FACING THE ESCARPMENT AND SHOWING THE THREE TOWERS AT THE RAKAIA SITE

FIG.7.6 VIEW LOOKING NE AND SHOWING TOWER #1 AND THE RIVERBED UP-WIND OF THE RAKAIA SITE

However the presence of the fairly open lupin scrub between 0.5 and 1 m high which surrounded the #1 reference tower, could have provided an effective displacement depth of about 0.5 metres.

7.2 INSTRUMENT LAYOUT

The three towers were erected to support the fourteen anemometer arrays in a similar manner to the Amberley site and may be seen in Figs.7.3 to 7.6. Only access by foot was available on to the riverbed and the equipment for the #1 tower had to be lowered over the cliff and positioned by hand at a distance of 116 m (10 H) upwind of the crest. Additional care was taken to reinforce the equipment on the riverbed against possible flooding which did occur on two occasions. The 20 m high #2 tower was situated on the upper level at a distance of 5.8 m (0.5 H) and tower #3 at 46.2 m (4 H) behind the crest. The lower four instrument levels on all three masts were the same at 9.87 m ($^{Z}/H = 0.854$), 4.90 m (0.424), 2.88 m (0.249) and 1.56 m (0.135) with two extra levels on the #2 tower at 18.99 m (1.643) and 15.05 m (1.302). The arrangement of anemometers amongst the fourteen arrays was the same as for the Amberley tests.

7.3 SITE RECORDINGS

The lack of strong winds and cloudy weather continued during the Rakaia tests and it took eight weeks to take four recordings from the NE and one from the NW direction. On all occasions the weather conditions appeared to be very similar with strong winds and cloudless sunny skies although recording #3 was taken just before sunset. The NW recording, #1 was taken during a strong, hot blustery wind off the mountains which raised clouds of dust off the riverbed visible in Fig.7.3. The anemometers were set up for recording winds from the NE direction so that the NW wind blew across the two horizontal anemometers making their readings rather unreliable. For this reason, only the mean wind speed data from this recording (#1) will be discussed to provide data for another angle of incidence to the crest. Details of the five recordings are summarised in Table 7.1 Unfortunately, two of the five recordings had to be terminated before the half-hour was reached due to problems with the tape recorder.

The synoptic weather conditions recorded by the New Zealand Meteorological Service for the five days when the wind recordings were

RECORD #	DATE	TIME OF START	LENGTH T_o MINUTES	AIR TEMP. C°	$\bar{\phi}^a$	$\bar{V}_{10}$ m/s	TREND LIMITS[b] %
1	22 FEB	12.41	20.34	30	64	13.27	4
2	8 MAR	15.22	30.15	23	23	7.03	NIL
3	30 MAR	18.30	29.01	18	21	7.16	16
4	4 APR	12.48	14.79	16	25	7.80	6
5	11 APR	14.53	30.15	19	28	6.76	NIL

NOTES:-

Recording #1 scanned at 32 Hz

Recordings #2-5 scanned at 16 Hz

a. Angle between mean wind direction and normal to crest

b. Percentage variation of cumulative mean velocity, tower #1.

TABLE 7.1 DETAILS OF RAKAIA SITE RECORDINGS

taken are shown in Appendix II. A strong north-westerly airstream prevailed over the whole of Canterbury on the day of the #1 recording. For the other four days it may be inferred from the charts that consistent conditions occurred with strong local sea to land winds from the NE prevailing. Although the site was some 30 km from the sea, the local sea winds often penetrated that far inland but conditions at higher altitudes may have been somewhat different and anything but stable.

7.4 UPWIND REFERENCE CONDITIONS

The velocity data from the reference tower #1 upwind of the escarpment are presented and discussed in this section in order to define the oncoming boundary-layer and its stability condition. The NW recording #1 was kept apart from the other four NE recordings which were averaged together as the weather conditions which occurred appeared to be quite similar.

7.4.1 Mean Velocity-Height Profile

The mean velocity data from the NW and NE recordings yielded very similar upwind mean velocity-height variations which are shown in Figs.7.7 and 7.8 as power law and logarithmic law profiles. A displacement depth of 0.5 m was used in both cases to allow for the surrounding low scrub.

The power law profiles in Fig.7.7 corresponded to a high value of $\alpha = 0.28$ for both wind directions which is equivalentto a surface roughness parameter $Z_o \tilde{\sim} 0.5$ m. This roughness is normally associated with somewhat rougher terrain than that which existed (Terrain class D: "Well covered by numerous obstructions e.g.:- suburbs of large towns and cities", ESDU (1972)). Omission of the displacement depth would have increased the value of α even further. The logarithmic profiles both yielded a $Z_o \tilde{\sim} 0.1$ m if neutral atmospheric stability was assumed.

The high effective surface roughness apparent from the velocity-height profiles may be due to the rough nature of the riverbed surface which would probably lose its influence on the boundary-layer if a deeper section of the boundary-layer was measured. The similarity between the NE and NW profiles reflected the similar upwind terrain in those two directions.

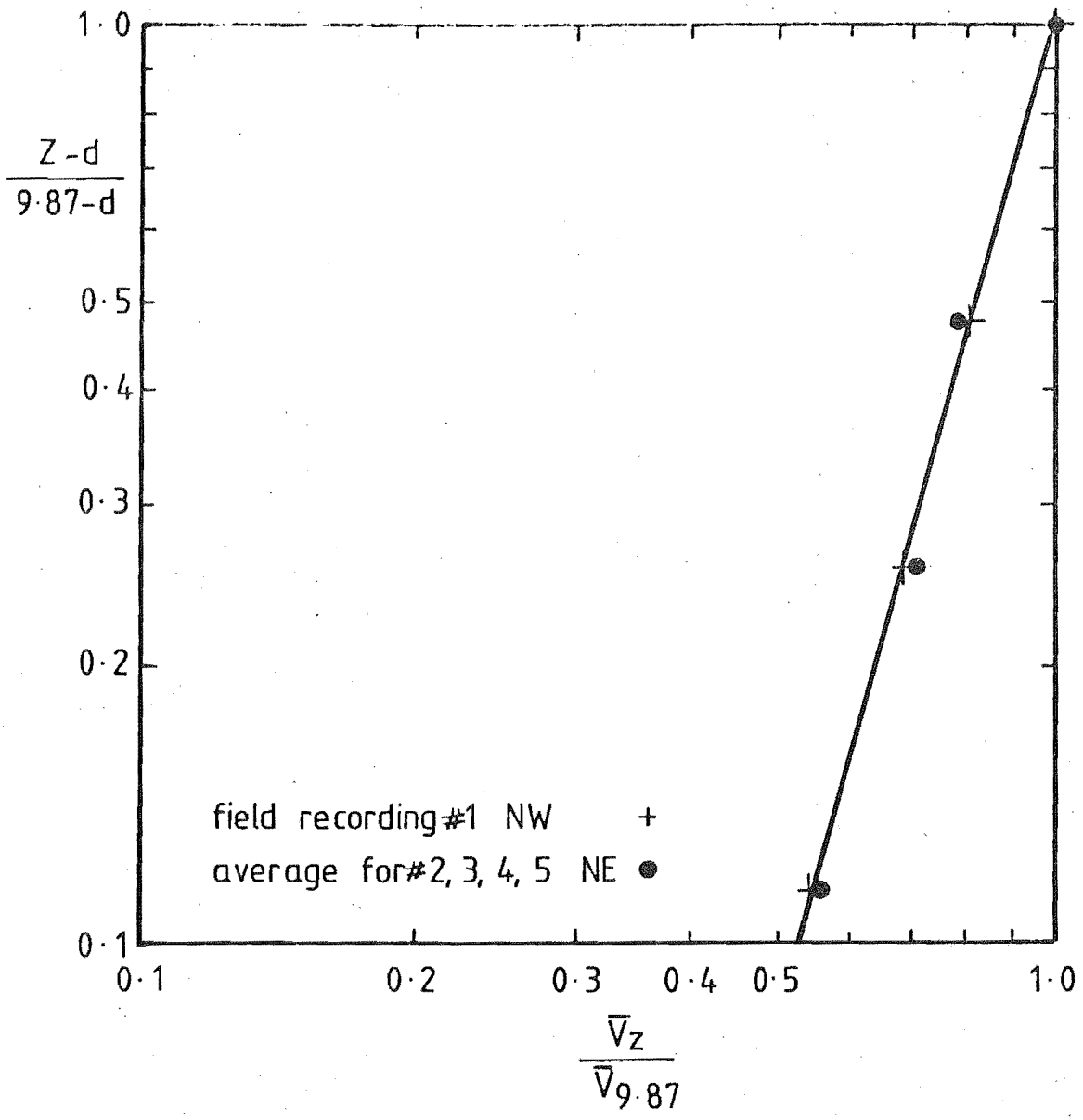

$$\frac{\bar{V}}{\bar{V}_{9\cdot87}} = \left[\frac{Z-d}{9\cdot87-d}\right]^{\alpha}$$

where $d = 0\cdot5\,m$

$$\alpha = \frac{3\cdot5}{12\cdot7} = \frac{1}{3\cdot63} \approx 0\cdot28 \text{ for all recordings}$$

FIG 7·7 UPWIND MEAN VELOCITY-HEIGHT PROFILES AS A POWER LAW FOR THE RAKAIA TEST SITE.

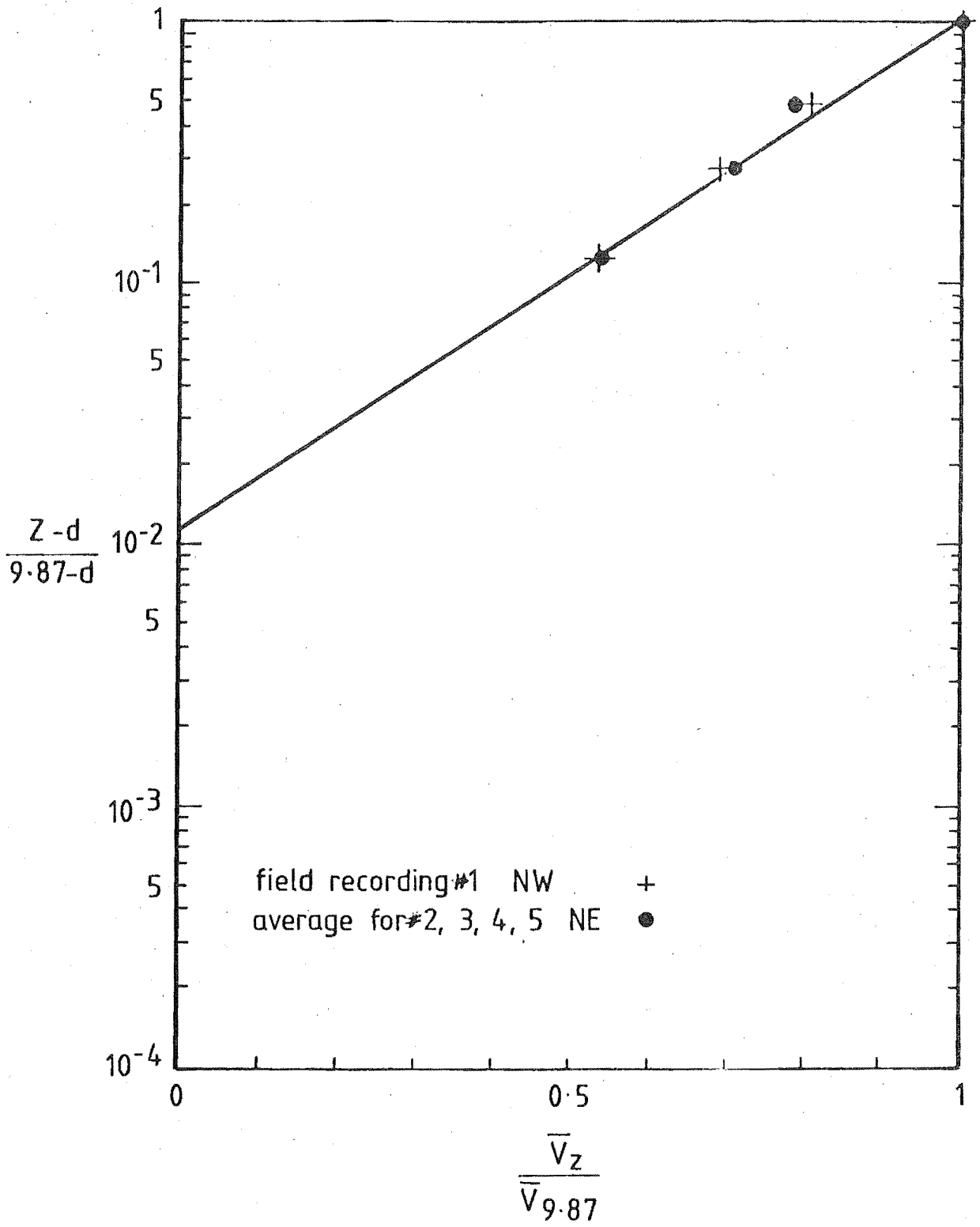

$$\frac{\bar{V}_z}{\bar{V}_{9\cdot87}} = \frac{\log\left[\frac{Z-d}{Z_o}\right]}{\log\left[\frac{9\cdot87-d}{Z_o}\right]}$$

$Z_o \approx 0\cdot1\text{m}$ for all recordings

FIG 7·8 UPWIND MEAN VELOCITY HEIGHT PROFILES AS A LOGARITHMIC LAW FOR THE RAKAIA TEST SITE.

7.4.2 Turbulence Data at 10 metre Height

Turbulence intensities and Reynolds stress data at the 10 m height on tower #1 are summarised in Table 7.2 for the NE wind direction. The variation in the data between the four recordings was satisfactory although the small range of $\sigma_w/\bar{V}_{10}$ encountered was surprising when the possible errors discussed in Chapters 4 and 5 were considered.

The three components of turbulence intensity yielded the ratios of $\sigma_u : \sigma_v : \sigma_w$ as 1 : 0.94 : 0.53 which when compared with Counihan (1975) with expected values of 1 : 0.75 : 0.50 or ESDU (1974) with 1 : 0.69 : 0.43, showed a somewhat large lateral component. The values of intensity obtained correspond to a surface roughness parameter Z_o in neutrally stable conditions of between 0.01 m and 0.08 m taken from ESDU (1974). The value of Z_o = 0.1 m taken from the mean velocity-height logarithmic profile is therefore rather high but is of the correct order of magnitude. A larger assumed displacement depth say d = 1 m could reduce this Z_o value into the desired range indicated from the turbulence intensities.

The Reynolds stresses obtained did not meet the expected values as well as the Amberley data, with a 60% lower value for the $\overline{uw}$ component of -0.18 and a rather high value for the $\overline{wv}$ component of 0.10. These discrepancies could have been due to a faulty vertical anemometer at that position but the recording integrity checks provided no evidence to substantiate this.

A longitudinal velocity power spectra taken from the field recording #5 which exhibited no trends, is shown in Fig.7.9 and compared with the standard spectra from ESDU (1974) for open country terrain at 10 m height. Like the Amberley results, close agreement is indicated if due regard to the anemometer response and to the sampling frequency of 2 Hz is taken as described in Chapters 4 and 5.

7.4.3 Atmospheric Stability

The effects of assuming different conditions of atmospheric stability on the calculated value of Z_o and the turbulence parameters σ_u/V_* etc. were investigated in a similar manner to the Amberley data. The data are presented in Table 7.3 with the intermediate steps in Panofsky's (1977) method illustrated in Figs.7.10, 7.11 and 7.12.

RECORD #	$\bar{V}_{10}$ m/s	$\frac{\sigma_u}{\bar{V}_{10}}$	$\frac{\sigma_v}{\bar{V}_{10}}$	$\frac{\sigma_w}{\bar{V}_{10}}$	$\frac{\overline{uw}}{\sigma_u \cdot \sigma_w}$	$\frac{\overline{vu}}{\sigma_v \cdot \sigma_u}$	$\frac{\overline{wv}}{\sigma_w \cdot \sigma_v}$
2	7.03	0.182	0.199	0.083	-0.218	0.098	0.124
3	7.16	0.195	0.123	0.096	-0.179	0.078	0.060
4	7.80	0.159	0.158	0.090	-0.109	-0.004	0.116
5	6.76	0.163	0.156	0.088	-0.208	-0.094	0.111
AVERAGED DATA		0.17	0.16	0.09	-0.18	0.02	0.10
$\frac{\text{STD.DEV.}}{\text{MEAN}}$ %		8	17	5	24	390	24

$$\sigma_u : \sigma_v : \sigma_w = 1 : 0.94 : 0.53$$

TABLE 7.2 UPWIND TURBULENCE DATA AT $\approx$ 10 m HEIGHT ON TOWER #1, RAKAIA TEST SITE, $\phi = 24°$

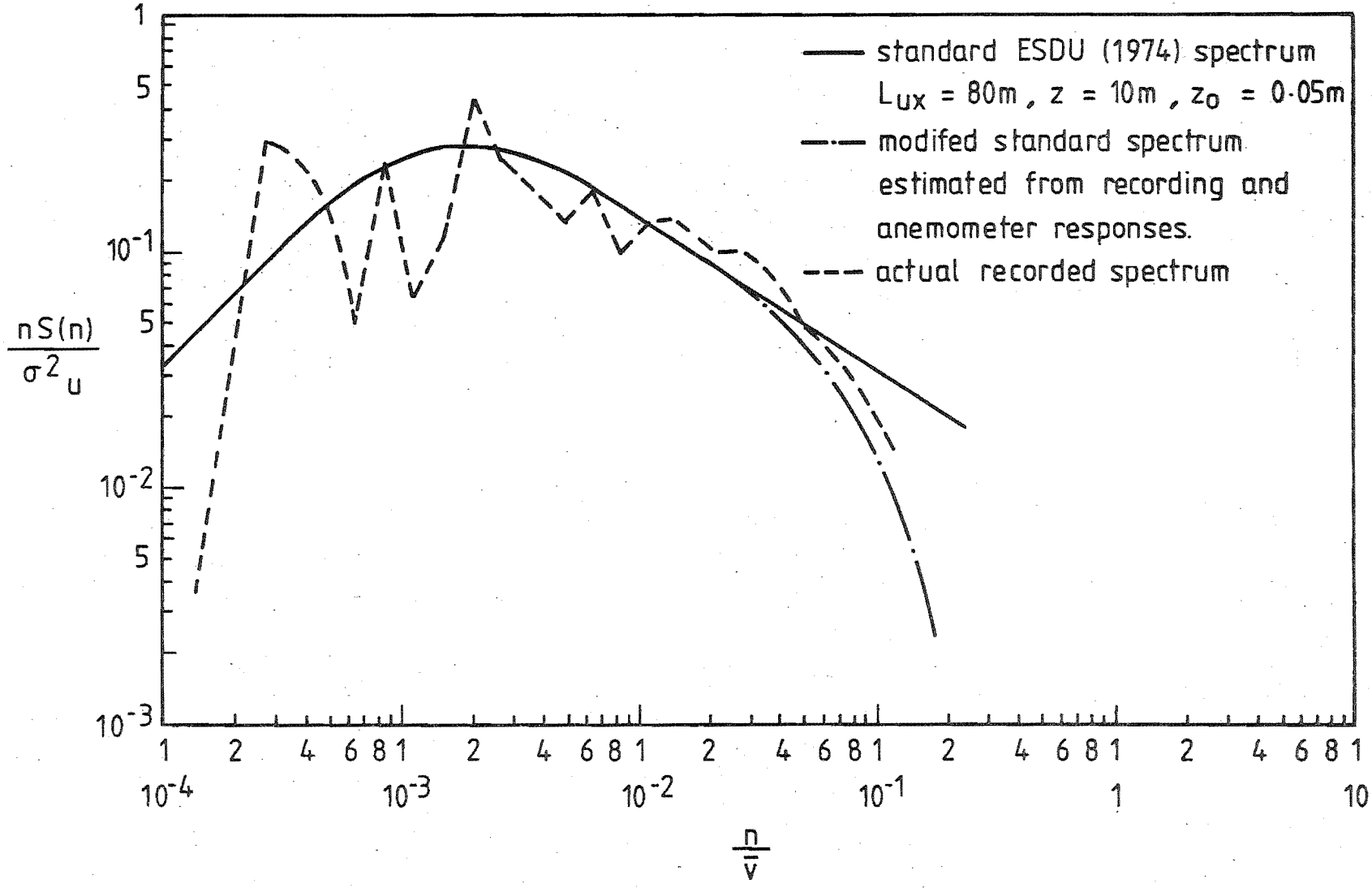

FIG 7·9 A RECORDED LONGITUDINAL VELOCITY POWER SPECTRUM AT Z = 10m UPSTREAM OF THE ESCARPMENT COMPARED WITH STANDARD DATA. (RAKAIA RECORDING #5)

PARAMETER	STANDARD RURAL DATA COUNIHAN (1975) ESDU (1974)	RAKAIA CLIFF			
		ASSUME 1 NEUTRAL STABILITY	2 CLASS C/D STABILITY	3 $V_* \equiv \sqrt{-\overline{uw}}$	4 CLASS D/E STABILITY
α	0.14 -0.17	0.28[a]	0.29[b]	0.16[b]	0.20[b]
Z_o m	0.01 -0.15	0.10[a]	0.25	0.013	0.067
$V_*/\bar{V}_{10}$		0.090	0.112	0.053	0.073
$V_*/\bar{V}_G$		0.028[e]	0.035[e]	0.017[e]	0.023[e]
$\sigma u/\bar{V}_{10}$	0.18 -0.25	0.17[a]	0.17[a]	0.17[a]	0.17[a]
$\sigma v/\bar{V}_{10}$	0.12 -0.20	0.16[a]	0.16[a]	0.16[a]	0.16[a]
$\sigma w/\bar{V}_{10}$	0.08 -0.12	0.09[a]	0.09[a]	0.09[a]	0.09[a]
$-\overline{uw}/\sigma u \cdot \sigma w$	0.29 -0.31	0.18[a]	0.18[a]	0.18[a]	0.18[a]
$\sqrt{-\overline{uw}}/V_*$		0.58	0.47	1[c]	0.72
$-\overline{uw}/\bar{V}_G^2$	0.002-0.003	0.00027	0.00027	0.00027	0.00027
$A=\sigma u/V_*$	2.50	1.89	1.52	3.21	2.33
$B=\sigma v/V_*$	1.875	1.78	1.43	3.02	2.19
$C=\sigma w/V_*$	1.25	1.00	0.80	1.70	1.23
$\sigma v/\sigma u$	0.75	0.94[a]	0.94[a]	0.94[a]	0.94[a]
$\sigma w/\sigma u$	0.50	0.53[a]	0.53[a]	0.53[a]	0.53[a]
STABILITY CLASS	D	D	C/D	E	D/E[d]

NOTES:-

a MEASURED VALUE (d = 0.5 m)

b ESTIMATED VALUE FOR NEUTRALLY STABLE CONDITIONS

c THEORETICAL ASSUMPTION

d PREFERRED OPTION

e ASSUME $Z_G \tilde{\sim}$ 600 m

TABLE 7.3 UPSTREAM TURBULENCE FIELD DATA AT 10 m HEIGHT SHOWING THE EFFECT OF VARIOUS ATMOSPHERIC STABILITY ASSUMPTIONS; RAKAIA TEST SITE

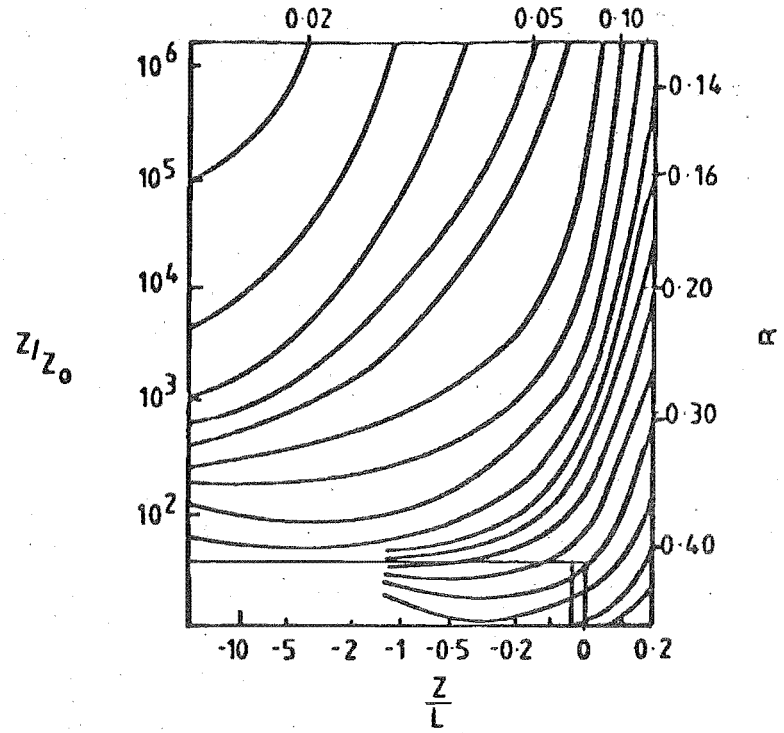

$$\Psi\left(\frac{z}{L}\right) \approx 0{\cdot}13$$

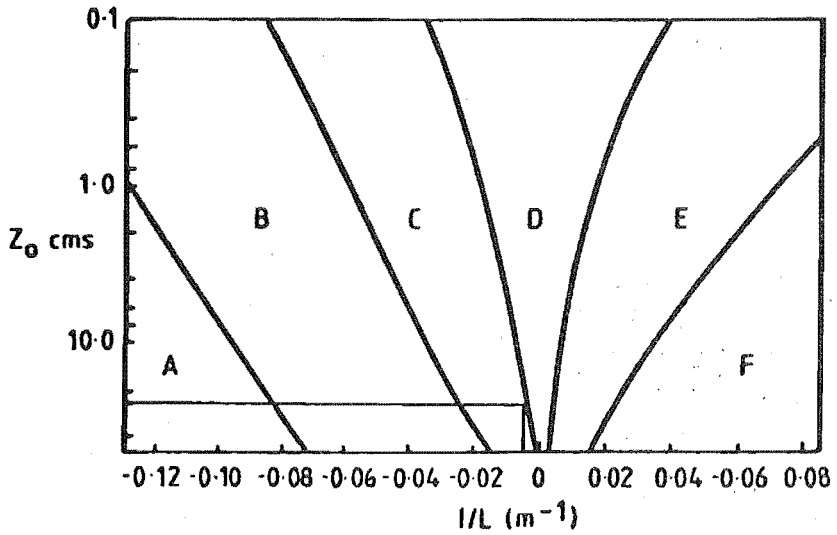

surface wind speed (at 10m) m sec^{-1}	Day			Night	
	incoming solar radiation			thinly overcast or ≥4/8 low cloud	<3/8 cloud
	strong	moderate	light		
<2	A	A-B	B		
2-3	A-B	B	C	E	F
3-5	B	B-C	C	D	E
5-6	C	C-D	D	D	D
>6	C	D	D	D	D

The neutral class, D, should be assumed for thick overcast during day or night.

FIG 7·10 ATMOSPHERIC STABILITY EFFECTS ON THE UNDISTURBED VELOCITY—HEIGHT PROFILE. PREDICTION METHOD, CASE 2

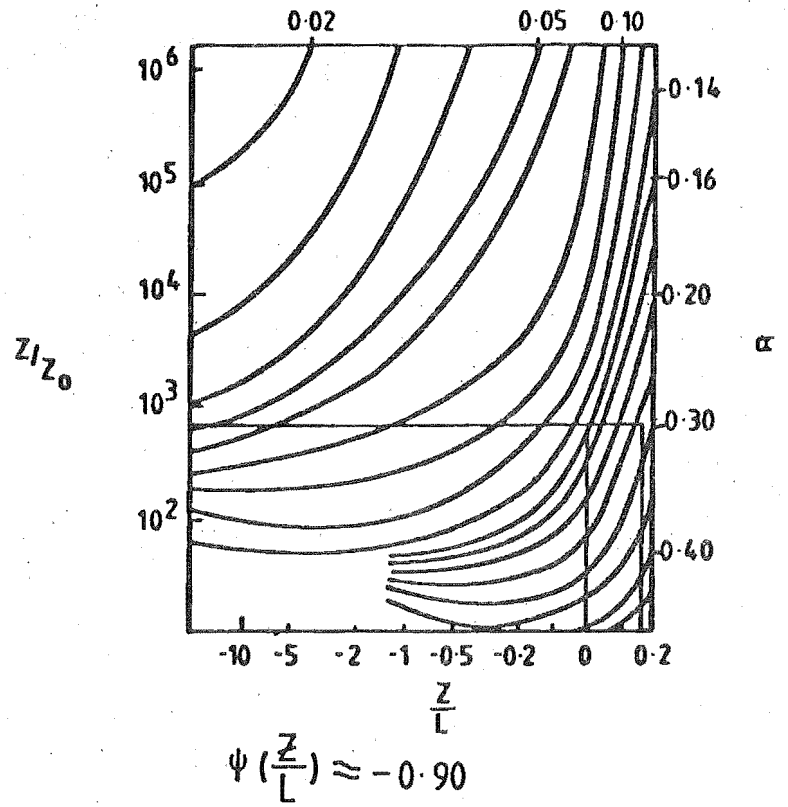

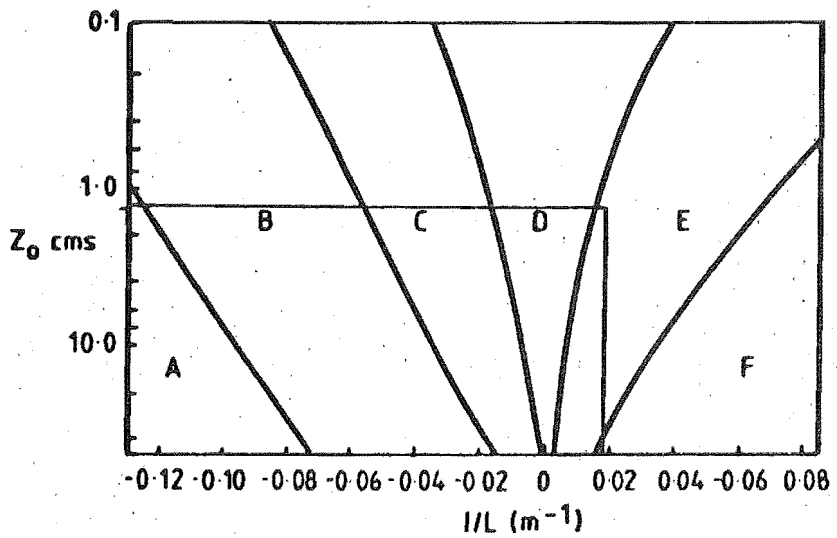

surface wind speed (at 10m) m sec^{-1}	Day: incoming solar radiation			Night: thinly overcast or ⩾4/8 low cloud	Night: <3/8 cloud
	strong	moderate	light		
<2	A	A-B	B		
2-3	A-B	B	C	E	F
3-5	B	B-C	C	D	E
5-6	C	C-D	D	D	D
>6	C	D	D	D	D

The neutral class, D, should be assumed for thick overcast during day or night.

FIG 7·11 ATMOSPHERIC STABILITY EFFECTS ON THE UNDISTURBED VELOCITY–HEIGHT PROFILE. PREDICTION METHOD, CASE 3

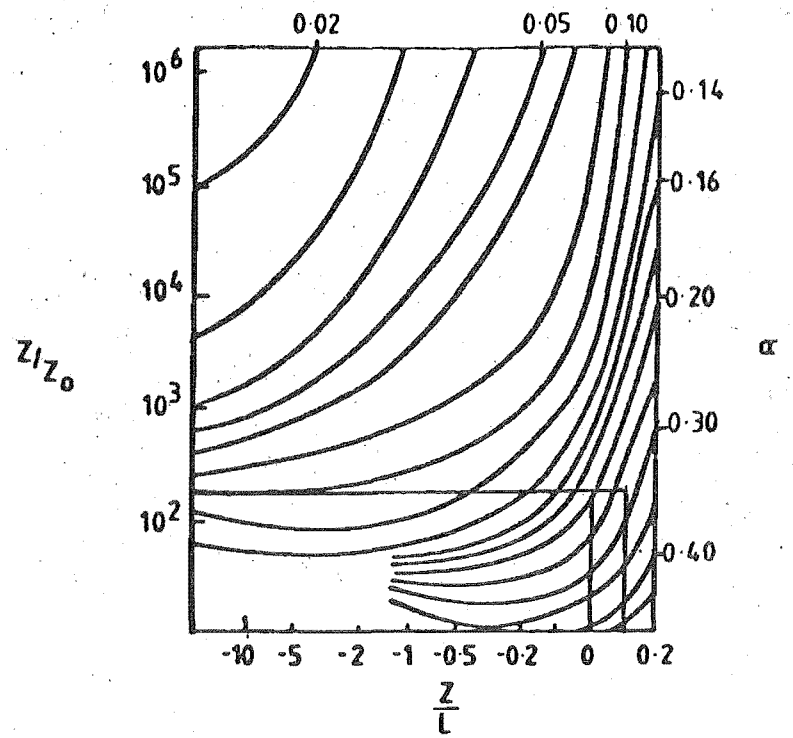

$$\psi\left(\frac{z}{L}\right) \approx -0{\cdot}5$$

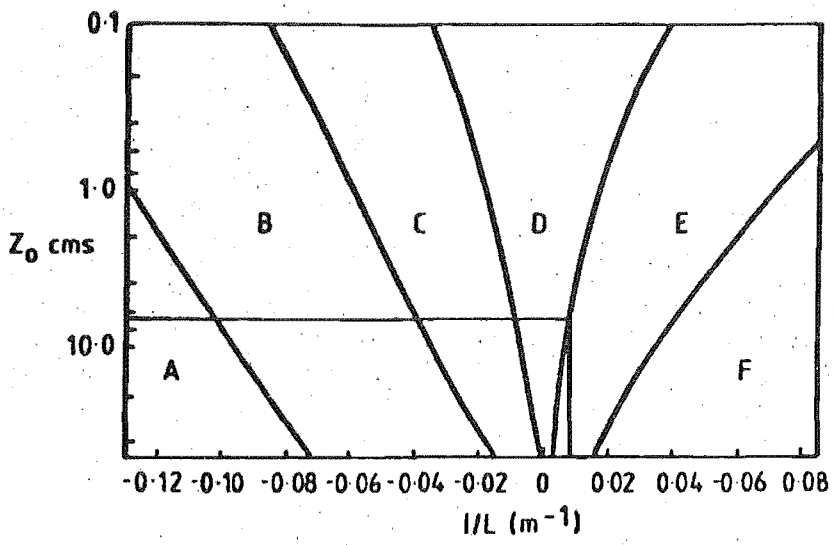

surface wind speed (at 10m) m sec^{-1}	Day: incoming solar radiation			Night: thinly overcast or ⩾4/8 low cloud	Night: <3/8 cloud
	strong	moderate	light		
<2	A	A-B	B		
2-3	A-B	B	C	E	F
3-5	B	B-C	C	D	E
5-6	C	C-D	D	D	D
>6	C	D	D	D	D

The neutral class, D, should be assumed for thick overcast during day or night.

FIG 7·12 ATMOSPHERIC STABILITY EFFECTS ON THE UNDISTURBED VELOCITY — HEIGHT PROFILE. PREDICTION METHOD, CASE 4.

(Case 1) Under neutrally stable conditions with the $\psi\left(\frac{Z}{L}\right)$ term assumed to be small, the recorded turbulence data may be presented as in column #1 of Table 7.3. The turbulence parameters σ_u/V_* etc. generally appeared to be too low indicating that the estimated friction velocity was too high. This conclusion was also borne out by the very low value of the $\sqrt{-\overline{uw}}/V_*$ ratio. The value of Z_o corresponding to the measured power law exponent $\alpha = 0.28$ would have been 0.25 m under neutrally stable conditions which was high for the Rakaia terrain.

(Case 2) The data were made worse by assuming a stability class C/D shown in Fig.7.10 and column #2 of Table 7.3.

(Case 3) If the measured $\sqrt{-\overline{uw}}$ term was equated with the friction velocity, the data were transformed to a set of turbulence data which was generally too high, (Fig.7.11) indicating a low value of estimated friction velocity. These parameters represented a stable atmosphere of class E.

It therefore became apparent that the conditions could be somewhere between case (1) and (3) and an assumed stability state of D/E was next attempted.

(Case 4) Assuming a Pasquill stability class D/E, the conditions in column #4 of Table 7.3 were obtained with the intermediate steps shown in Fig.7.12. A reasonably good compromise was realised with a somewhat high value of Z_o (=0.067 m) and α (=0.2) for the terrain, but this could have been due to the small range of the boundary-layer investigated as mentioned earlier. The turbulence parameters were of the correct order of magnitude although the lateral component still remained rather high. The Reynolds stress value is also lower than expected.

It may be concluded that the upwind boundary-layer was consistently slightly stable (class D/E) with an unusually high Z_o value apparent from the velocity profile in the restricted height range investigated. The turbulence data were reasonably close to that expected from open rural terrain except for the Reynolds stress which was too low.

7.5 FIELD RESULTS

The field results from the Rakaia cliff site were normalised in an identical manner to those from the Amberley site and are presented

below with the relevant wind tunnel model results. The single recording with winds from the NW was utilised to provide data for mean velocities only, due to the inappropriate anemometer alignment for that wind direction.

7.5.1 Mean Velocity

The variations in the mean flow velocity over the escarpment are presented in Figs.7.13 and 7.14 for the two wind directions recorded and the corresponding fractional speed-up ratios ΔS are shown in Figs.7.15 and 7.16.

A displacement depth of d = 0.5 m was used in the nondimensional height $^{Z-d}/_{H-d}$, for the field mean velocity results from the upstream tower #1 to compensate for the surrounding scrub visible in Figs.7.5 and 7.6. However d was omitted when presenting the field results in Figs.7.3 onwards for the following reasons. There was no significant displacement around the other two towers and the ΔS values were calculated directly by comparing velocities from the instrument arrays which were mounted at the same height Z as those on tower #1. As the value of d = 0.5 m for tower #1 was rather uncertain it was therefore felt better to omit it altogether in the data presentation that follows. By comparing velocities at the same height Z-d rather than Z, a beneficial small lowering of the plotted points would have occurred for the values close to the ground, say for the lower two heights, but it would be insignificant for velocities at higher positions. However the inclusion of a displacement depth was made in the model test results and is discussed and justified in Chapter 8.

The fractional speed-up ratios had a wider range than the Amberley data due to the strong wake evident behind the cliff crest which severely limited the velocities close to the ground. The wake effect was less obvious for the wind flow from the NW (Fig.7.16) which blew onto the escarpment at a larger angle of incidence ψ to the crest normal.

A low velocity, reverse flow was recorded at the bottom level of tower #2 but was observed nowhere else. This region of separation was probably restricted in size due to the oblique angle of incidence.

7.5.2 Mean Flow Direction

The change in direction of the mean flow as it negotiated the escarpment is shown in Fig.7.17 for the NE wind recordings. Apart from

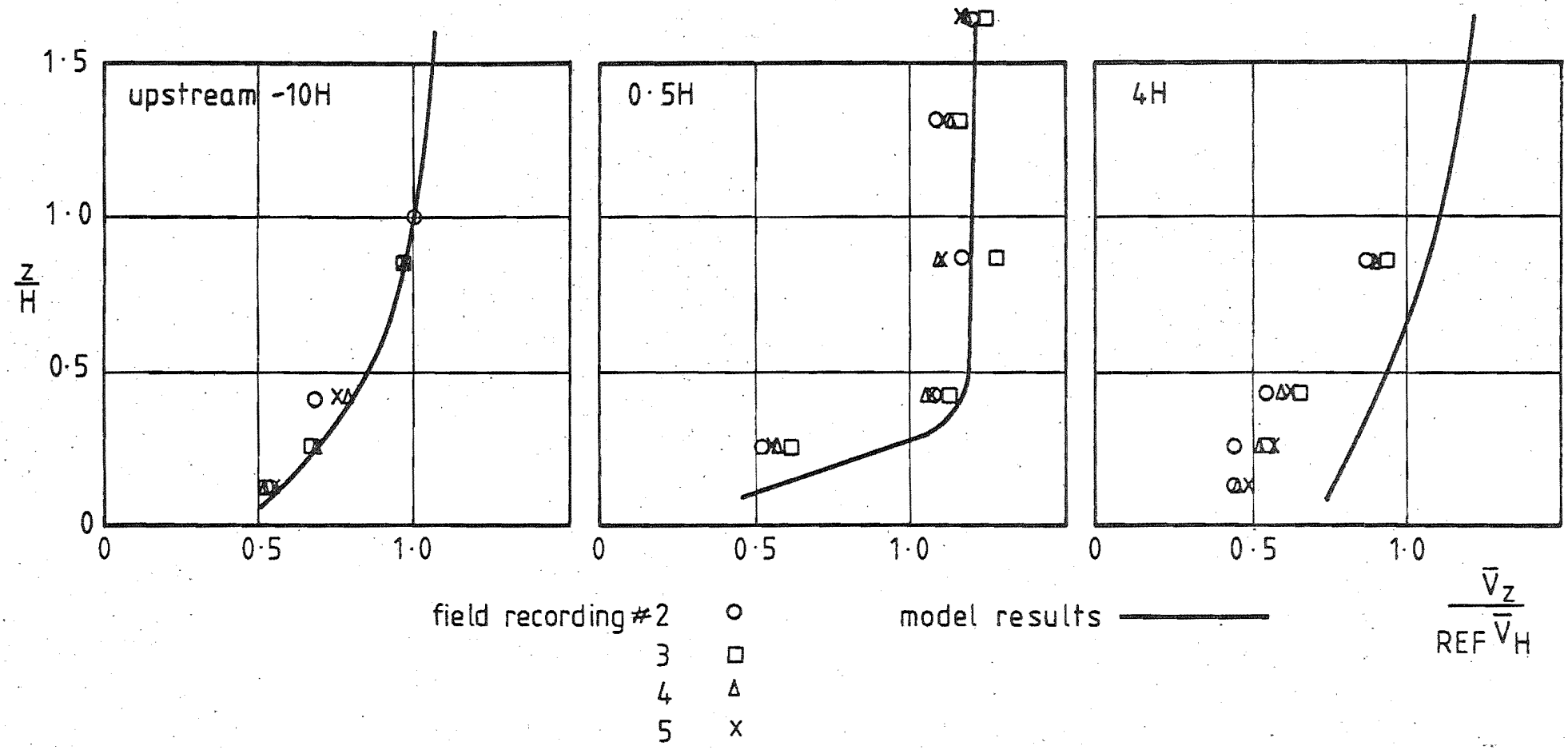

FIG 7·13 MEAN VELOCITY PROFILES OVER THE CLIFF ESCARPMENT AT THE UPSTREAM REFERENCE SITE, 0·5H AND 4H BEHIND THE CREST. WIND DIRECTION FROM THE NE WITH AN ANGLE OF INCIDENCE TO CREST NORMAL, Φ = 24°.

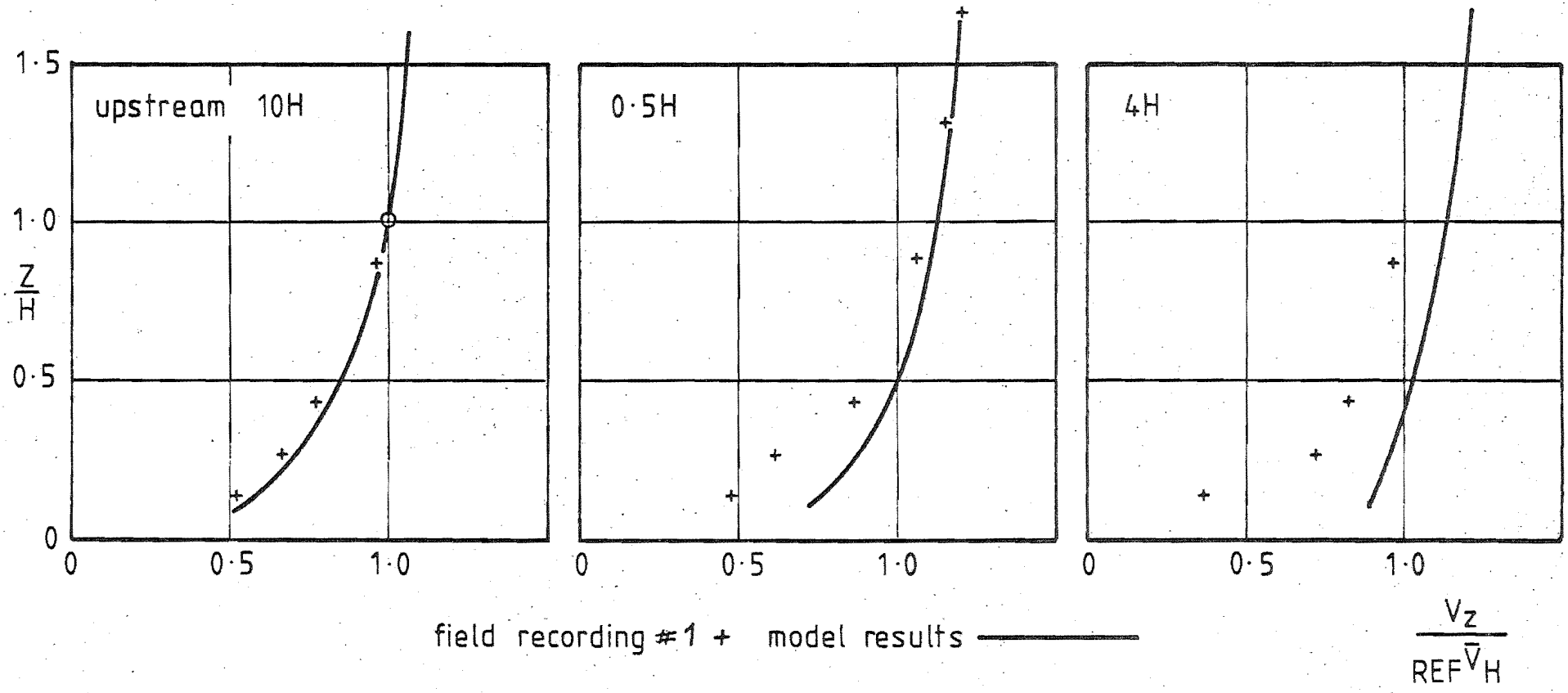

FIG 7·14 MEAN VELOCITY-HEIGHT PROFILES OVER THE CLIFF ESCARPMENT. WIND DIRECTION FROM THE NW WITH AN ANGLE OF INCIDENCE TO CREST NORMAL, ϕ = 65°.

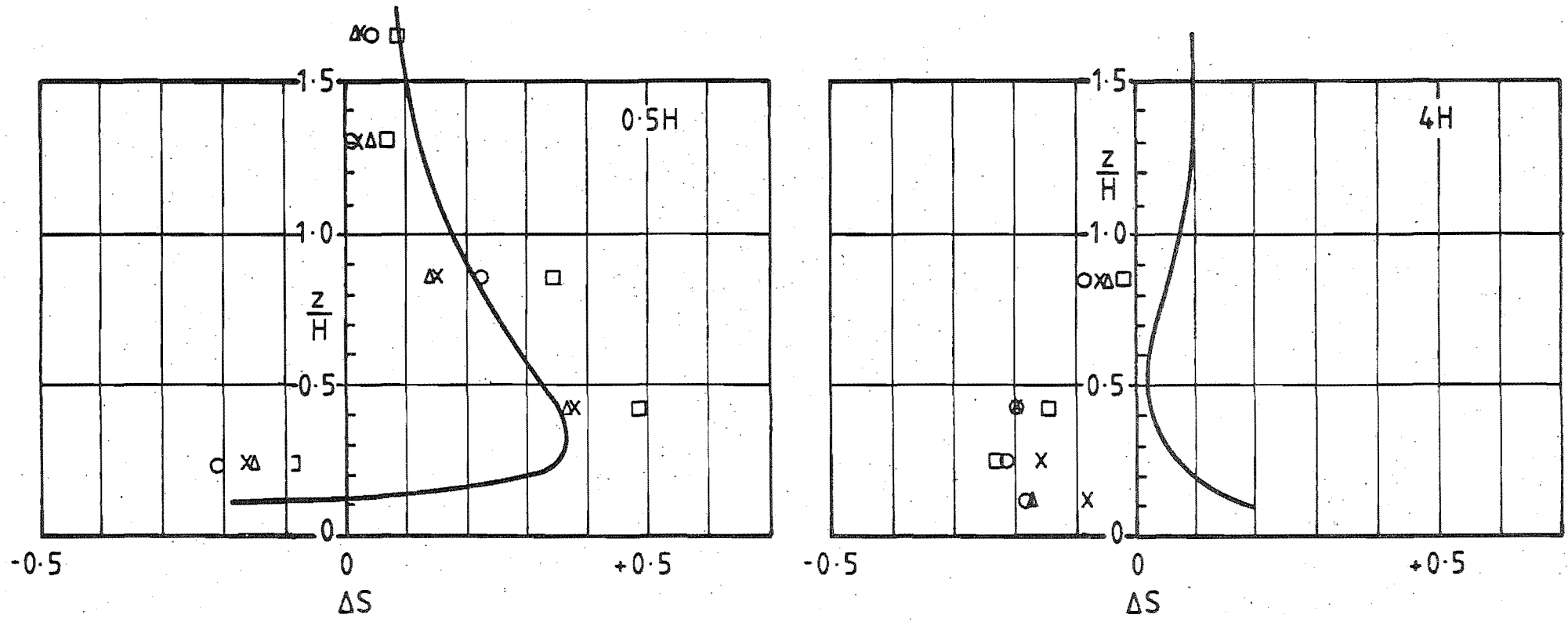

FIG 7·15 FRACTIONAL SPEED-UP RATIOS OVER THE CLIFF ESCARPMENT (NE, $\Phi = 24°$)

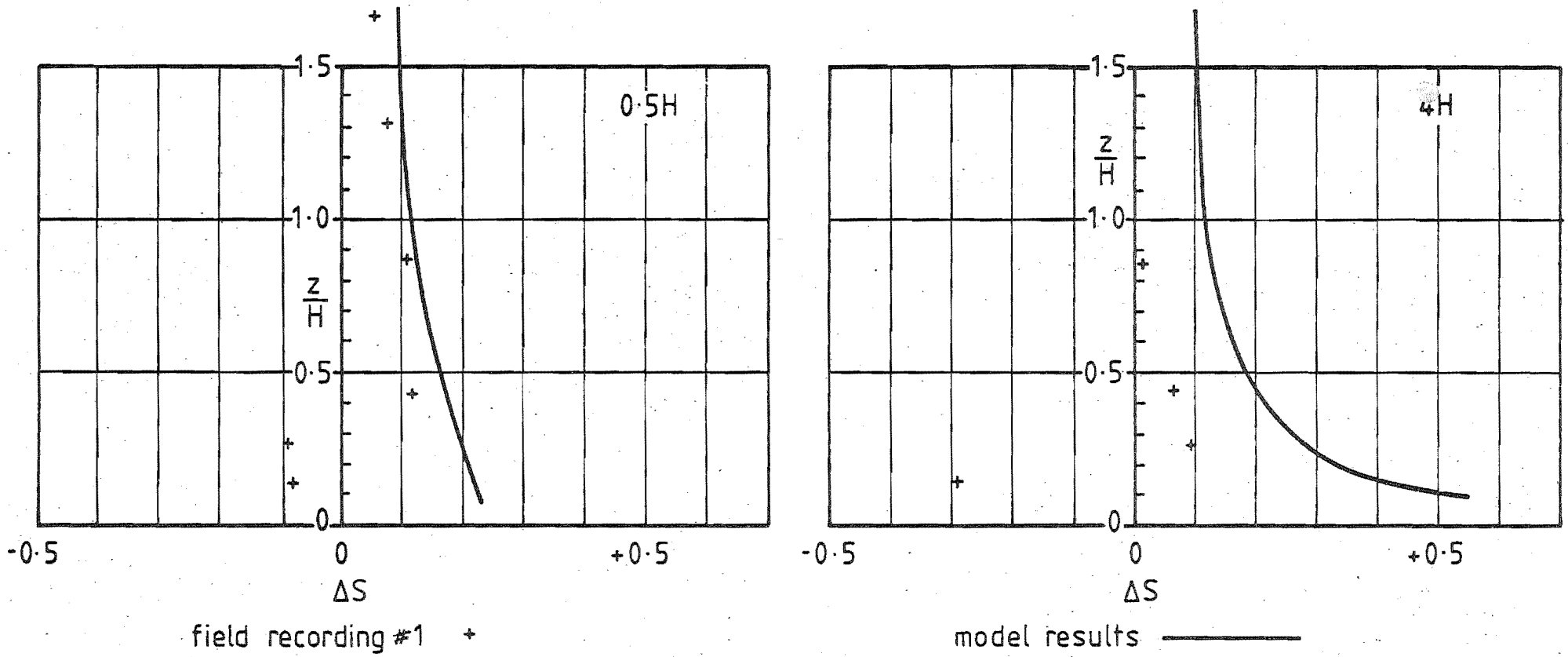

FIG 7·16 FRACTIONAL SPEED-UP RATIOS OVER THE CLIFF ESCARPMENT (NW, Φ = 65°)

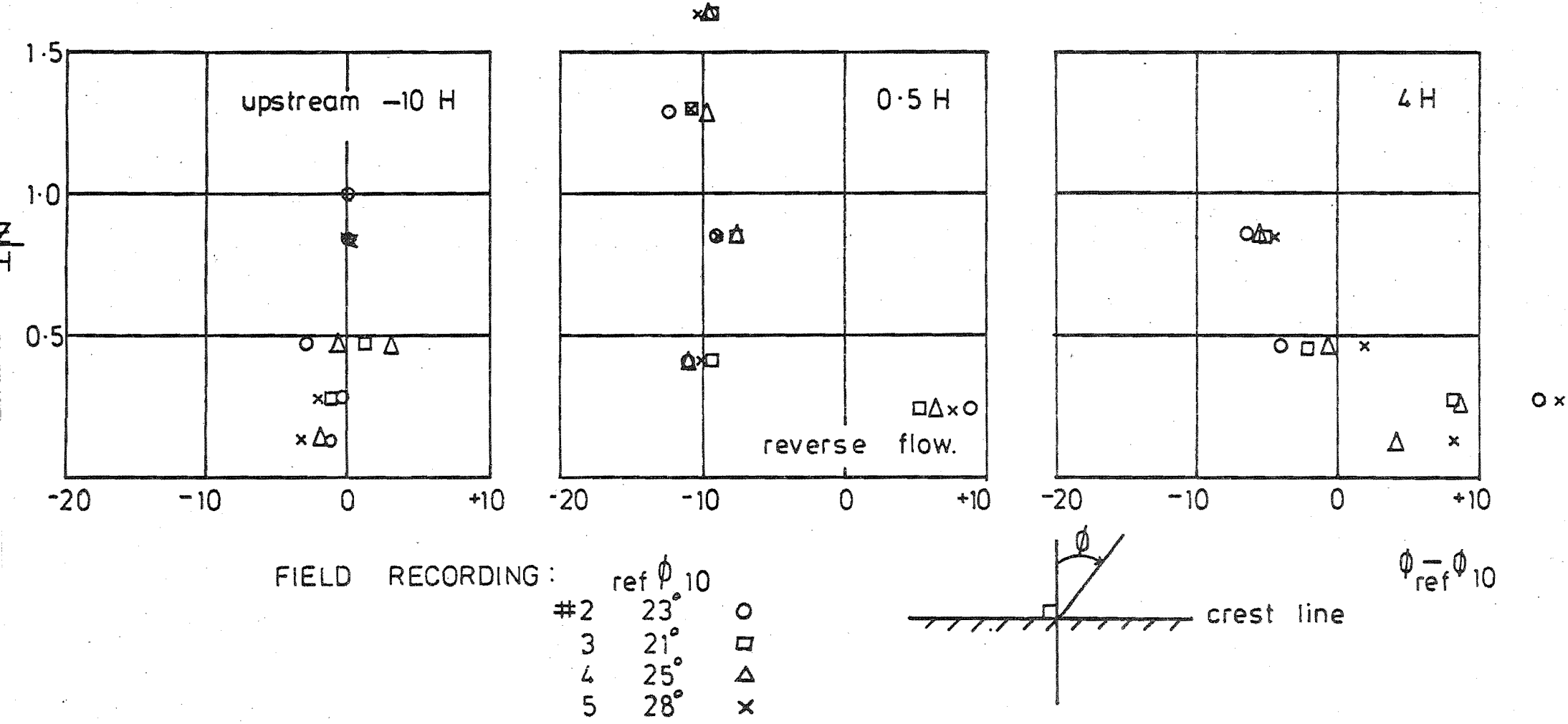

FIG 7·17 CHANGE IN DIRECTION OF THE MEAN FLOW OVER THE CLIFF ESCARPMENT (NE, ϕ =24°)

the low reverse flow recorded at the lowest level on tower #2, the flow was largely unaffected by the cliff. One further exception however was the tendency for the flow to run more closely to the crest direction at the lower levels. The flow from the NW direction remained generally within ±4° of the upwind direction except close to the ground behind the crest where the flow ran approximately parallel with the crest line.

7.5.3 Turbulence Intensities

The variation of the three components of standard deviation σ_u, σ_v, σ_w normalised by $_{REF}\bar{V}_H$ are presented in Figs.7.18, 7.19 and 7.20. Large increases in the longitudinal and lateral components were evident behind the crest in the wake area. The effect was greatest near the ground and below 0.5 H on the tower #2 and decreased in magnitude at the tower #3, but its influence extended over a greater depth. The vertical component appeared to be unchanged if a constant value with height at the upwind tower was assumed.

The corresponding components of turbulence intensity are shown in Figs.7.21, 7.22 and 7.23. The trends noticed in the standard deviations are repeated here but are accentuated due to the general decrease in local velocity in the turbulent wake region.

7.5.4 Reynolds Stresses

The three Reynolds stress components are presented in Figs.7.24, 7.25 and 7.26. The $\overline{uw}/\sigma_u.\sigma_v$ component appeared to increase in absolute value from tower #1 to tower #2 but the magnitudes of the other two components were small and their variation over the escarpment insignificant.

7.5.5 Longitudinal Velocity Power Spectra

Sample power spectra calculated from the #5 field recording which contained no significant trend in the mean velocity are shown in Figs.7.27 and 7.28 for the 10 m and 2.88 m heights on the three towers. The lowest height was not utilised due to the reverse flow evident at the #2 tower and the consequential errors in the anemometer recordings.

Apart from the expected shift to higher frequencies as the height above ground was reduced, a shift was also evident for tower

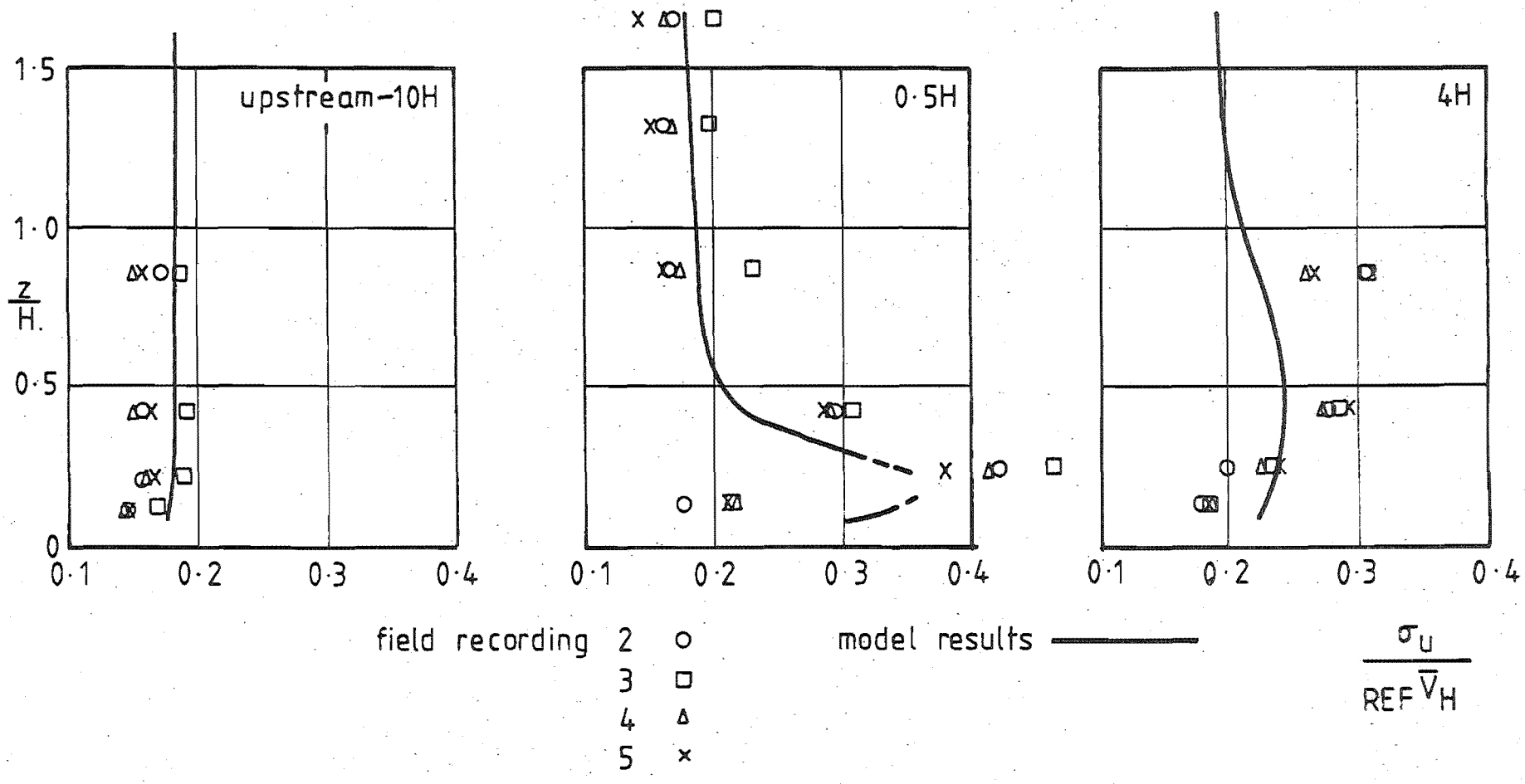

FIG 7·18 VARIATION IN THE STANDARD DEVIATION OF THE LONGITUDINAL VELOCITY COMPONENT (CLIFF ESCARPMENT, NE, ϕ = 24°)

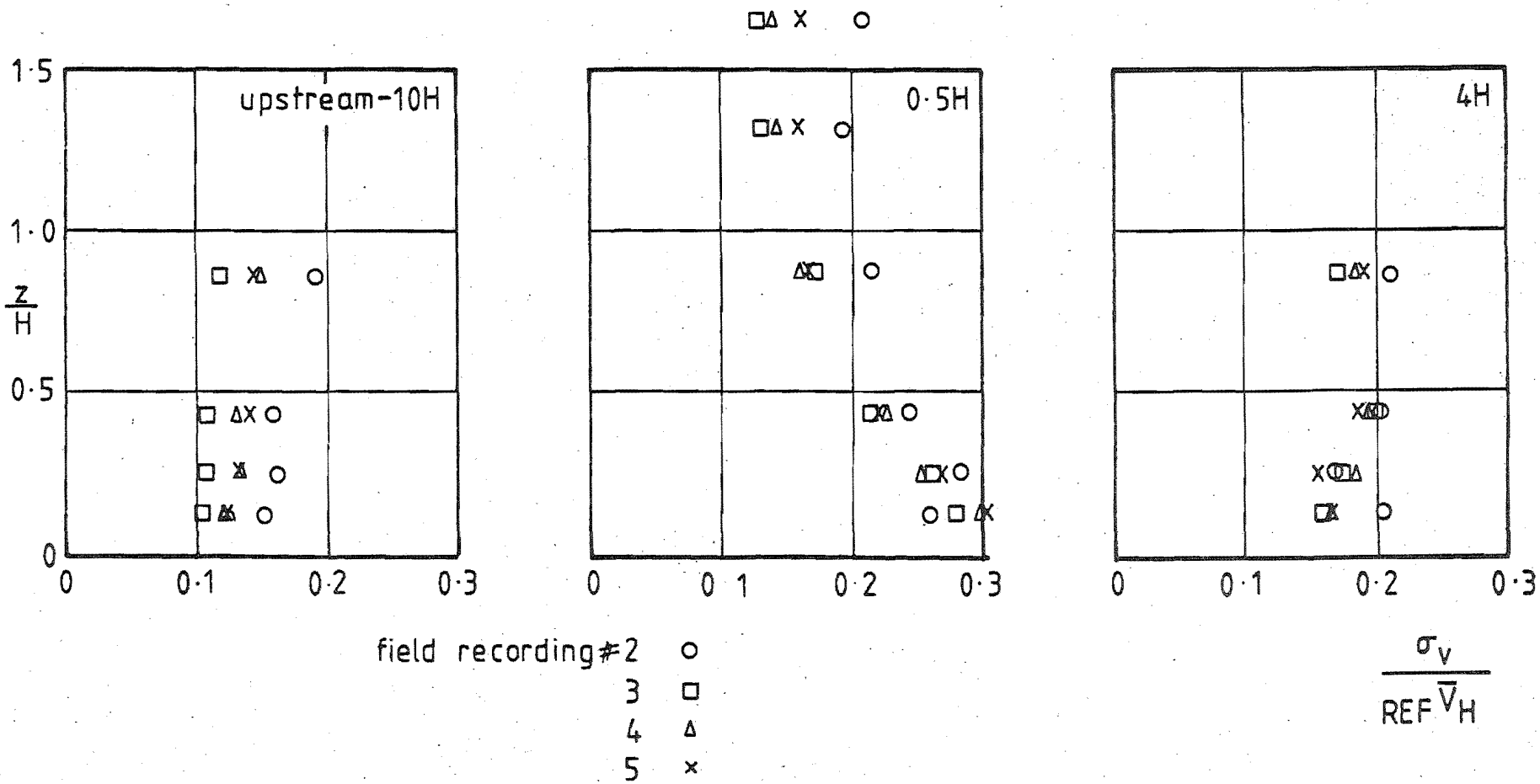

FIG 7·19 VARIATION IN THE STANDARD DEVIATION OF THE LATERAL VELOCITY COMPONENT. (CLIFF ESCARPMENT, NE, ϕ = 24°)

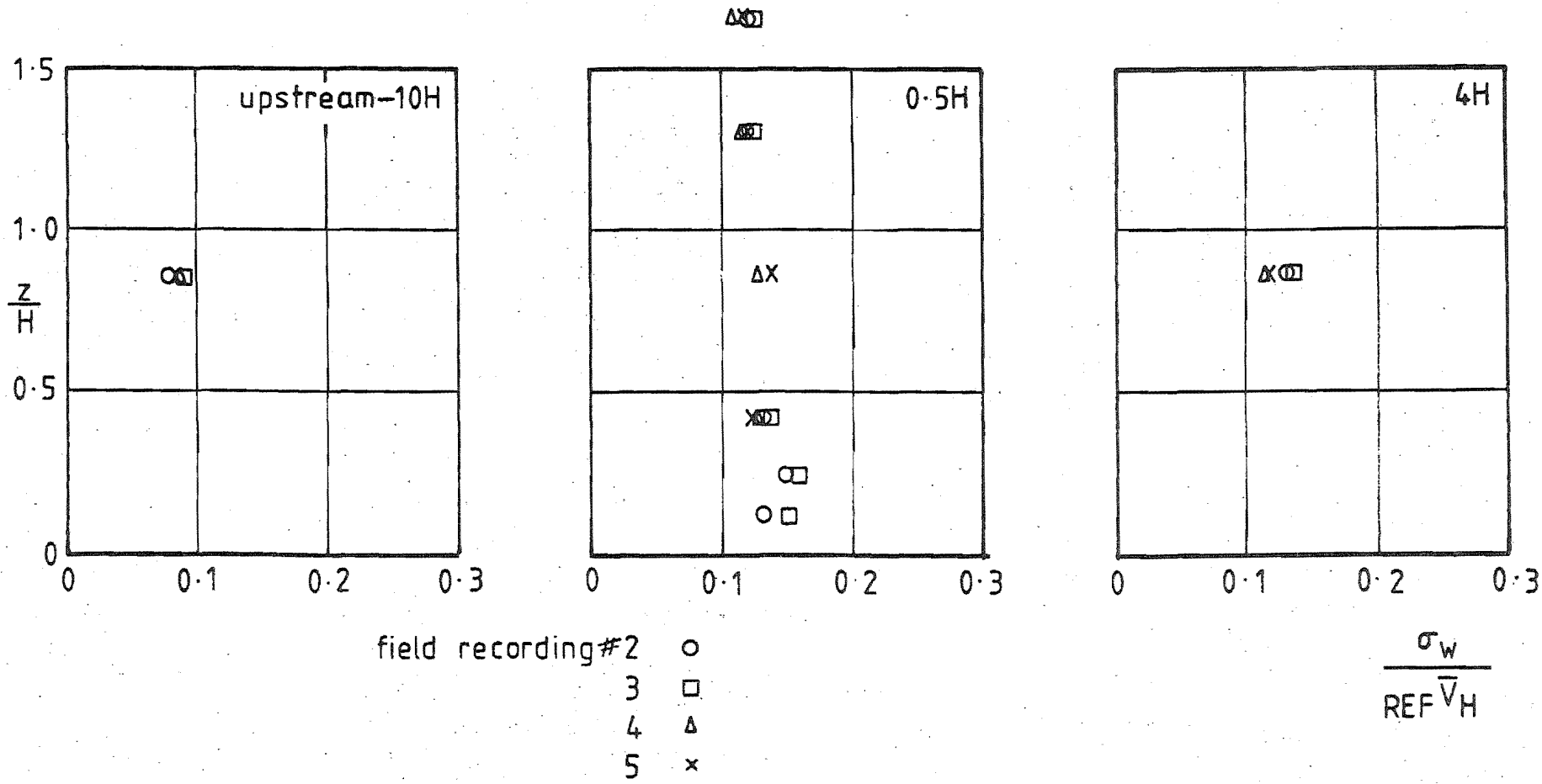

FIG 7·20 VARIATION IN THE STANDARD DEVIATION OF THE VERTICAL VELOCITY COMPONENT.
(CLIFF ESCARPMENT, NE, ϕ = 24°)

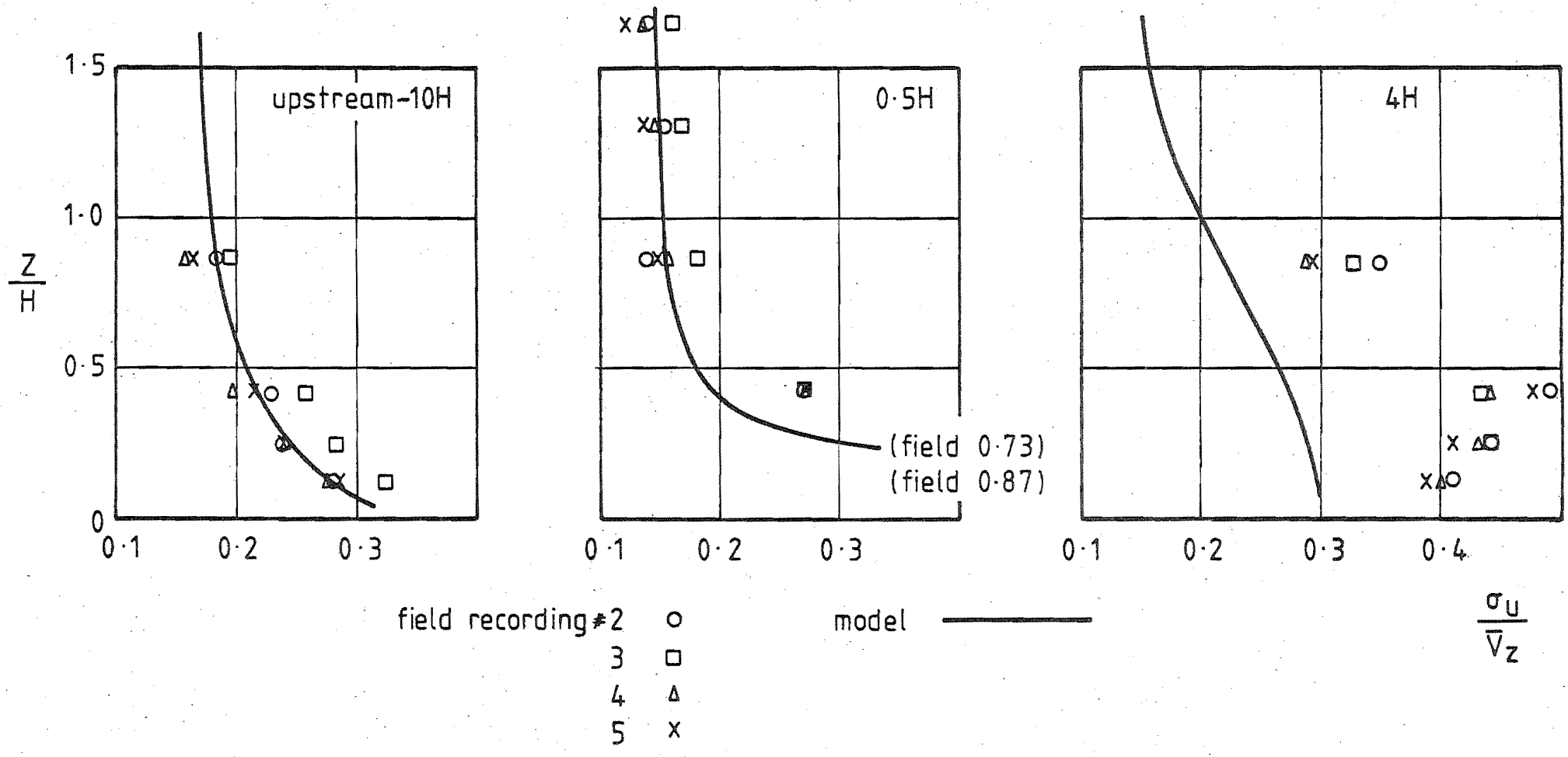

FIG 7·21 VARIATION IN THE LONGITUDINAL TURBULENCE INTENSITY (CLIFF ESCARPMENT, NE, ϕ = 24°)

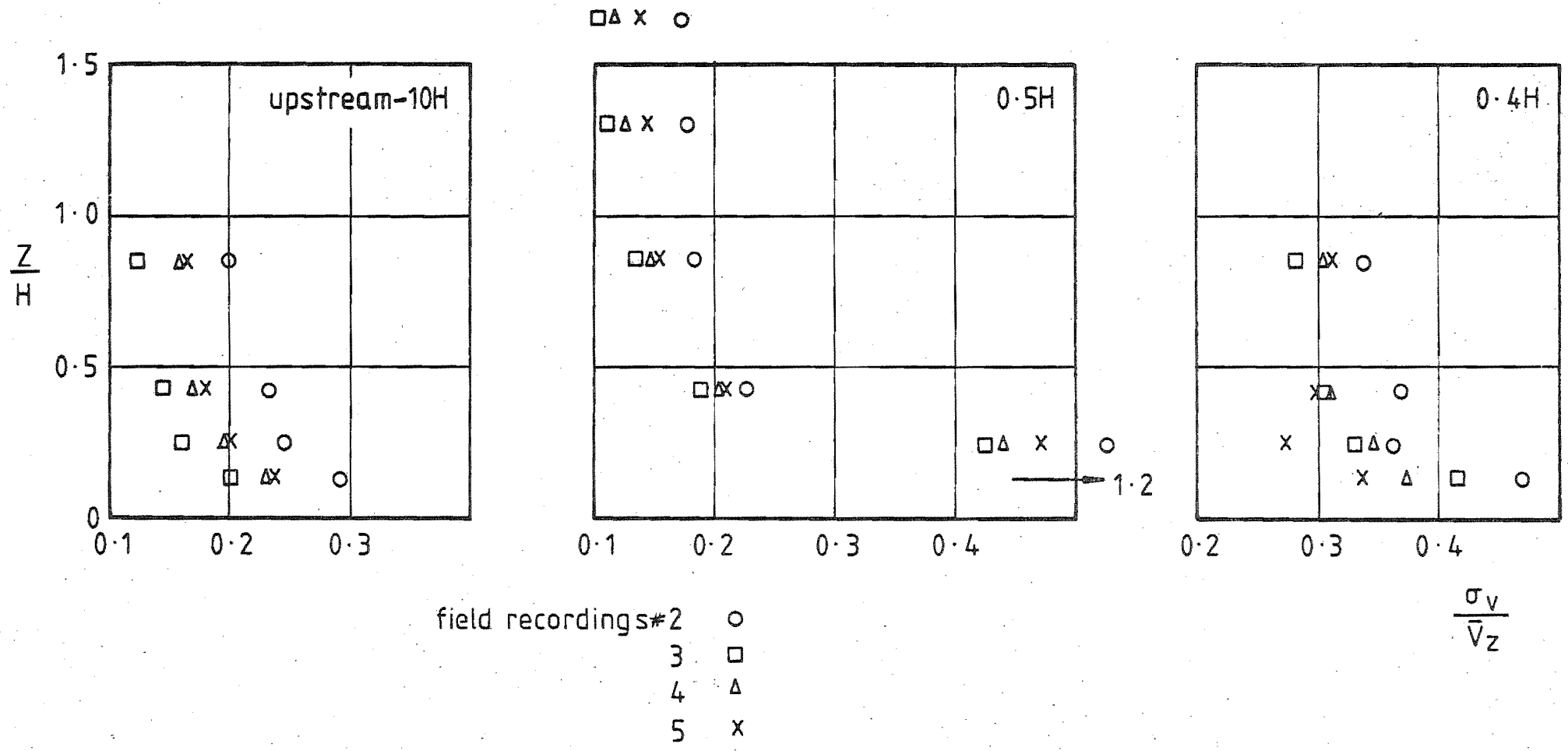

FIG 7·22 VARIATION IN THE LATERAL TURBULENCE INTENSITY (CLIFF ESCARPMENT, NE, $\phi = 24^{\circ}$)

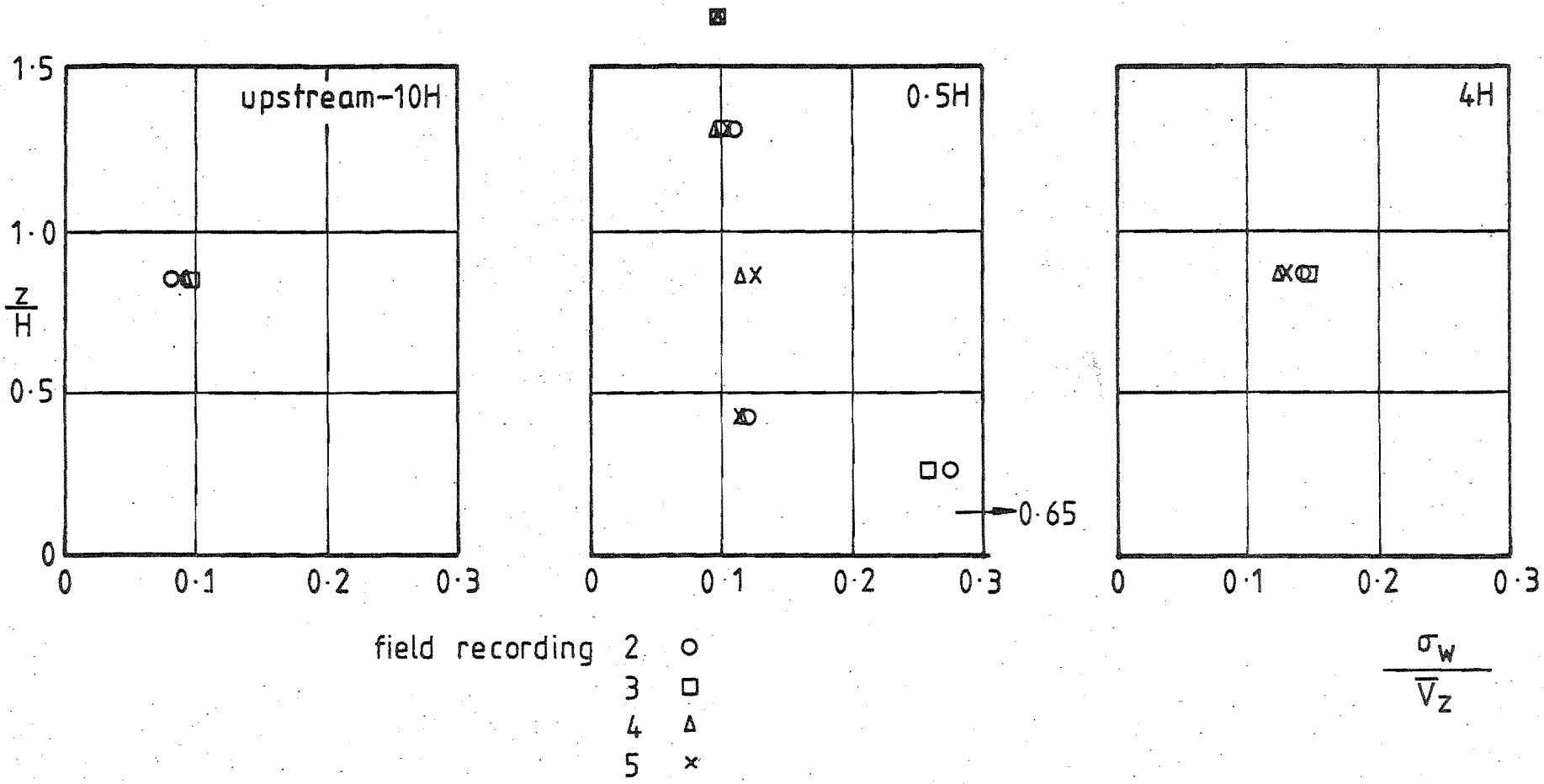

FIG 7·23 VARIATION IN THE VERTICAL TURBULENCE INTENSITY (CLIFF ESCARPMENT, NE, Φ = 24°)

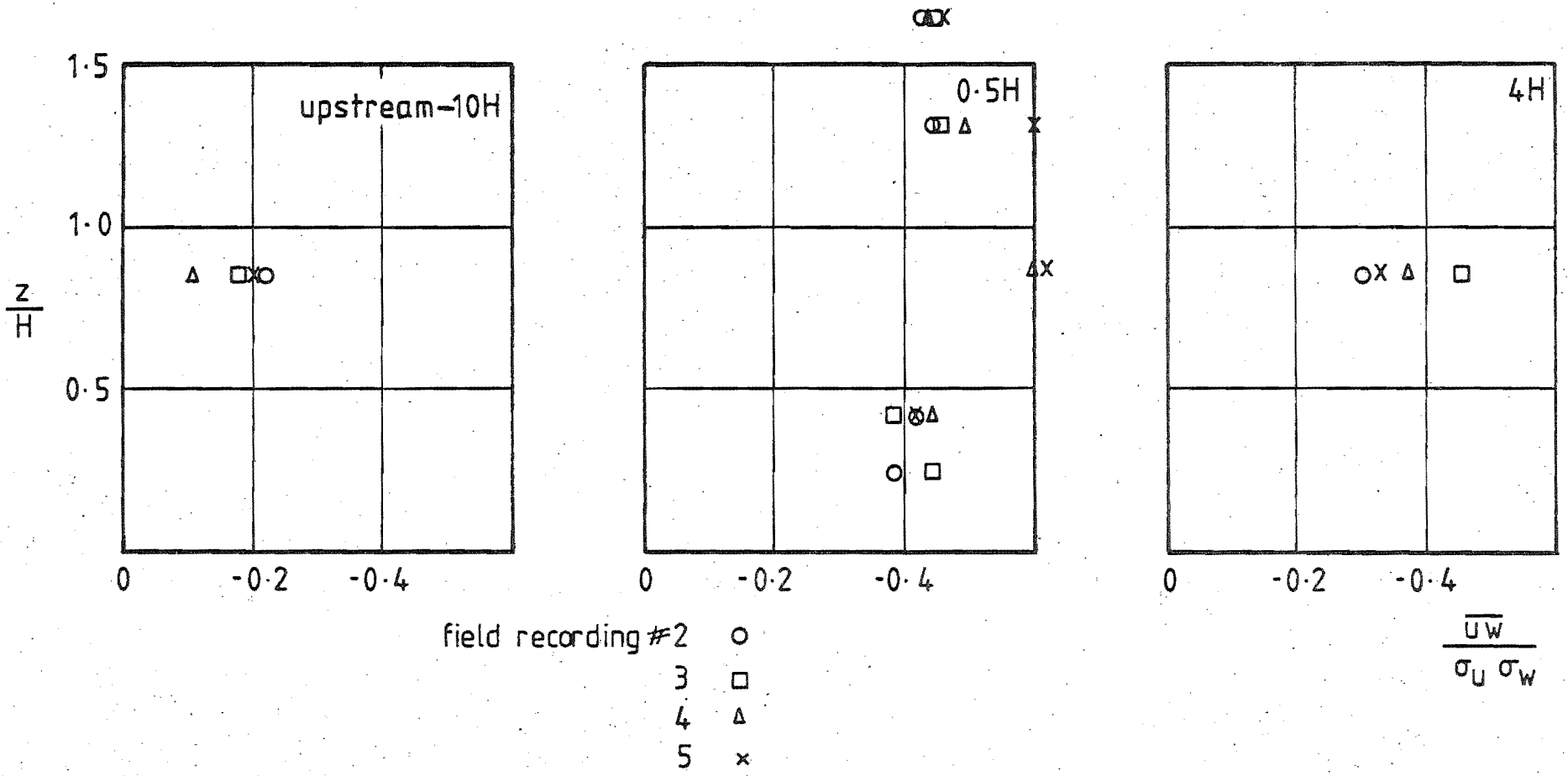

FIG 7·24 VARIATION IN THE REYNOLDS STRESS, $\frac{\overline{uw}}{\sigma_u \sigma_w}$ (CLIFF ESCARPMENT, NE, ϕ = 24°)

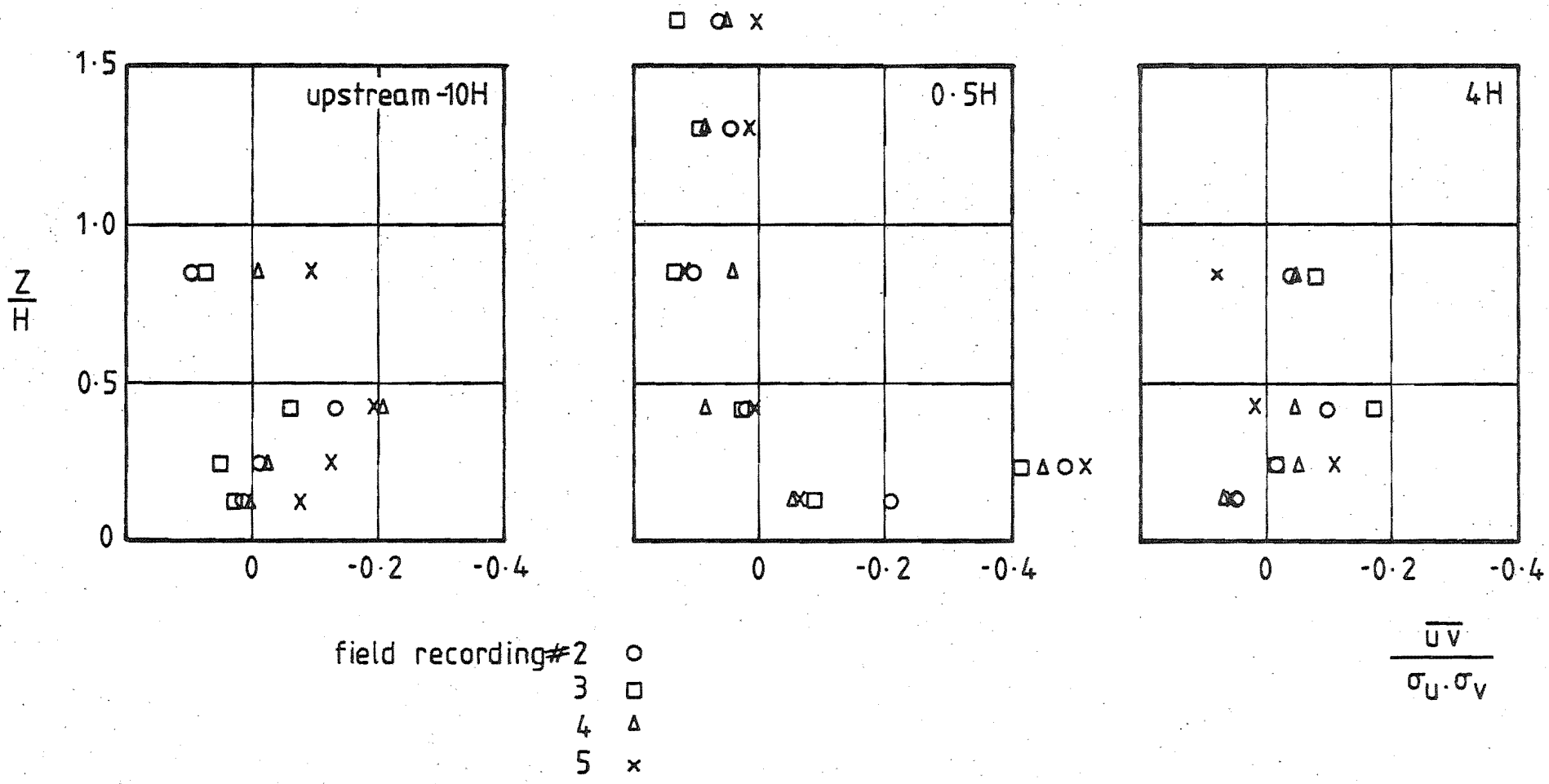

FIG. 7·25 VARIATION IN THE REYNOLDS STRESS, $\frac{\overline{uv}}{\sigma_u \cdot \sigma_v}$ (CLIFF ESCARPMENT, NE, $\phi = 24^\circ$)

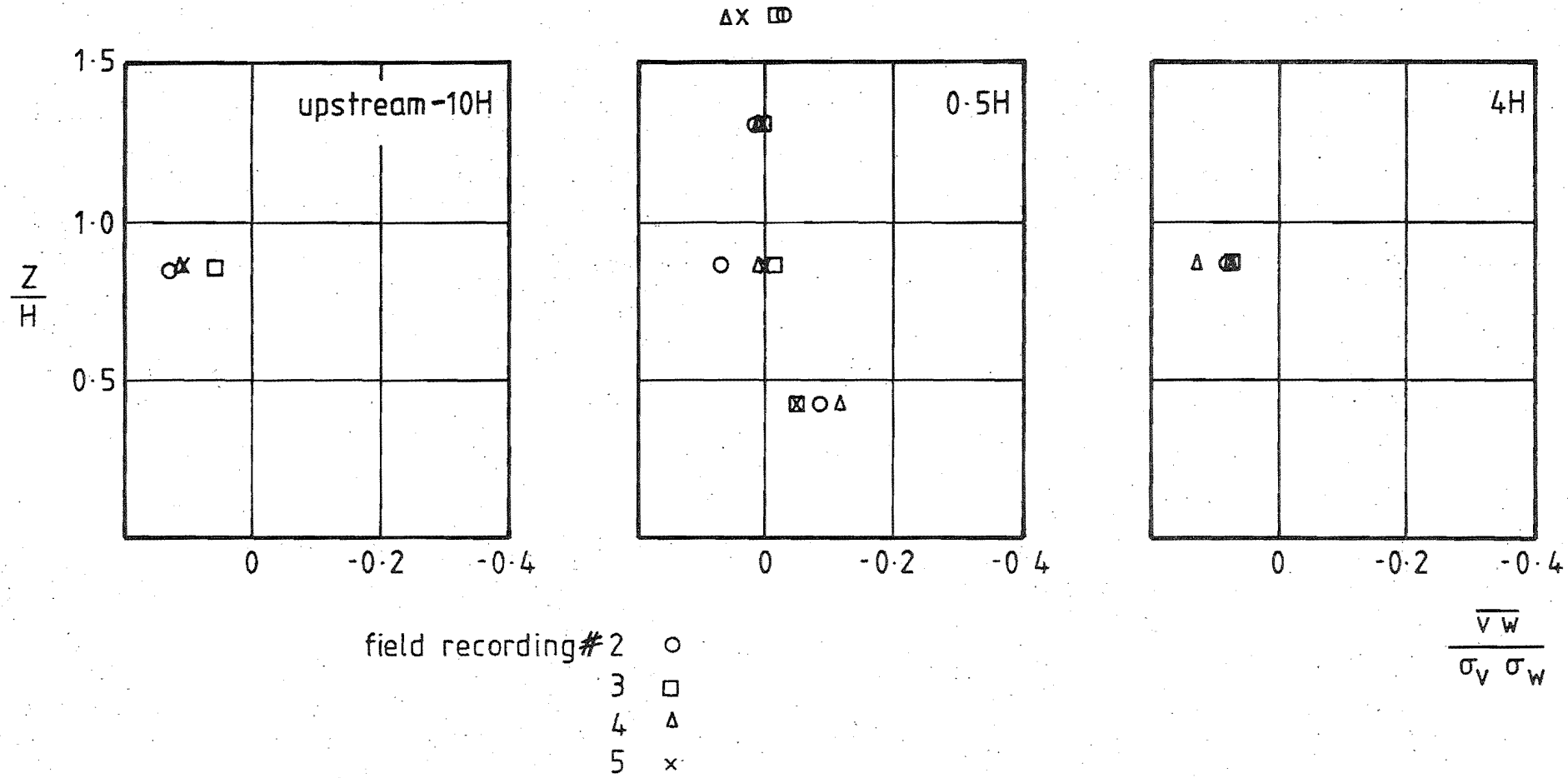

FIG 7·26 VARIATION IN THE REYNOLDS STRESS, $\frac{\overline{v\,w}}{\sigma_v \sigma_w}$ (CLIFF ESCARPMENT, NE, ϕ = 24°)

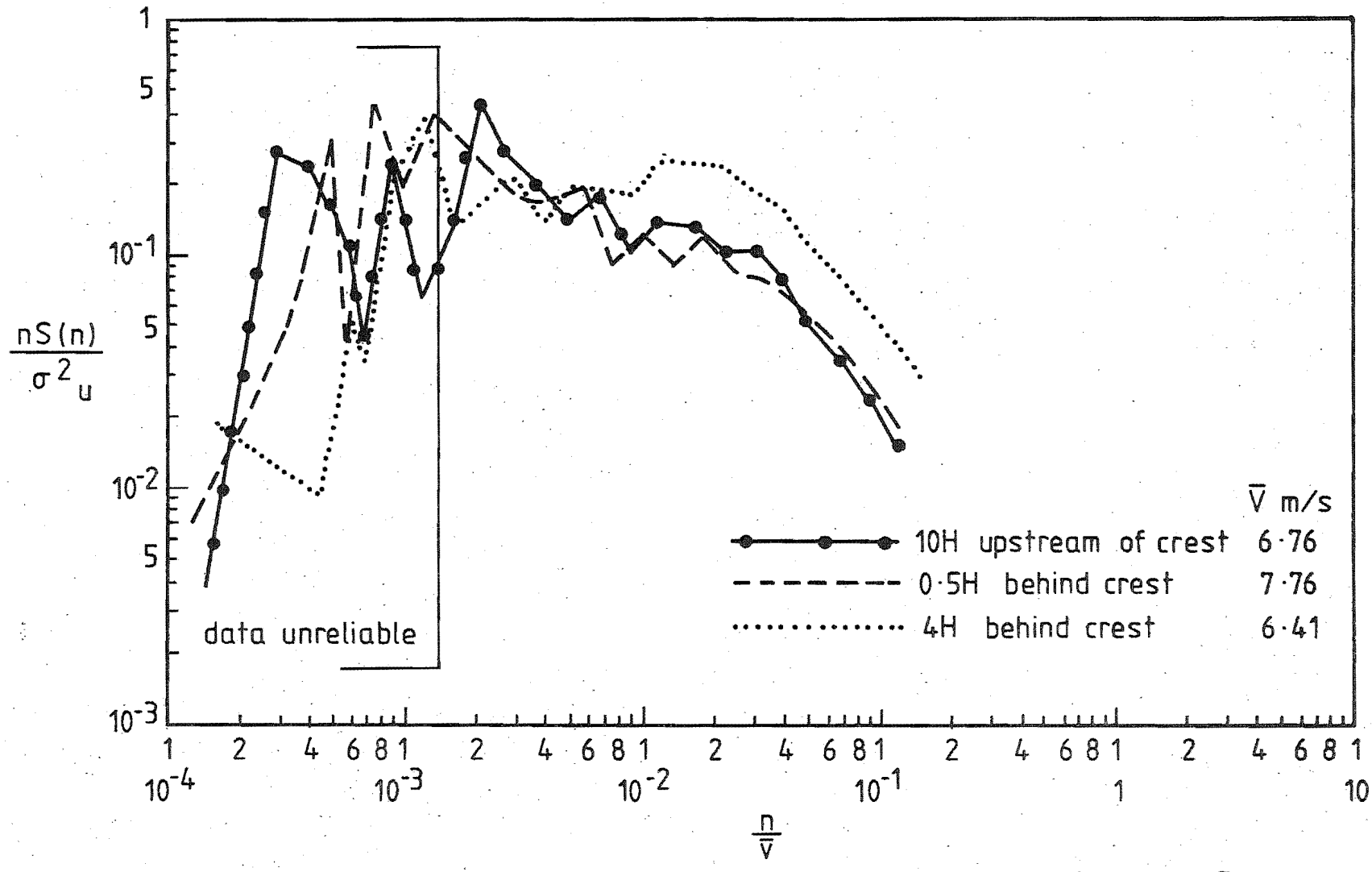

FIG 7·27 THE LONGITUDINAL VELOCITY POWER SPECTRA AT Z = 10m ($\frac{Z}{H}$ = 0·85) AT DIFFERENT POSITIONS OVER THE CLIFF ESCARPMENT, NE, $\phi = 24^{\circ}$.

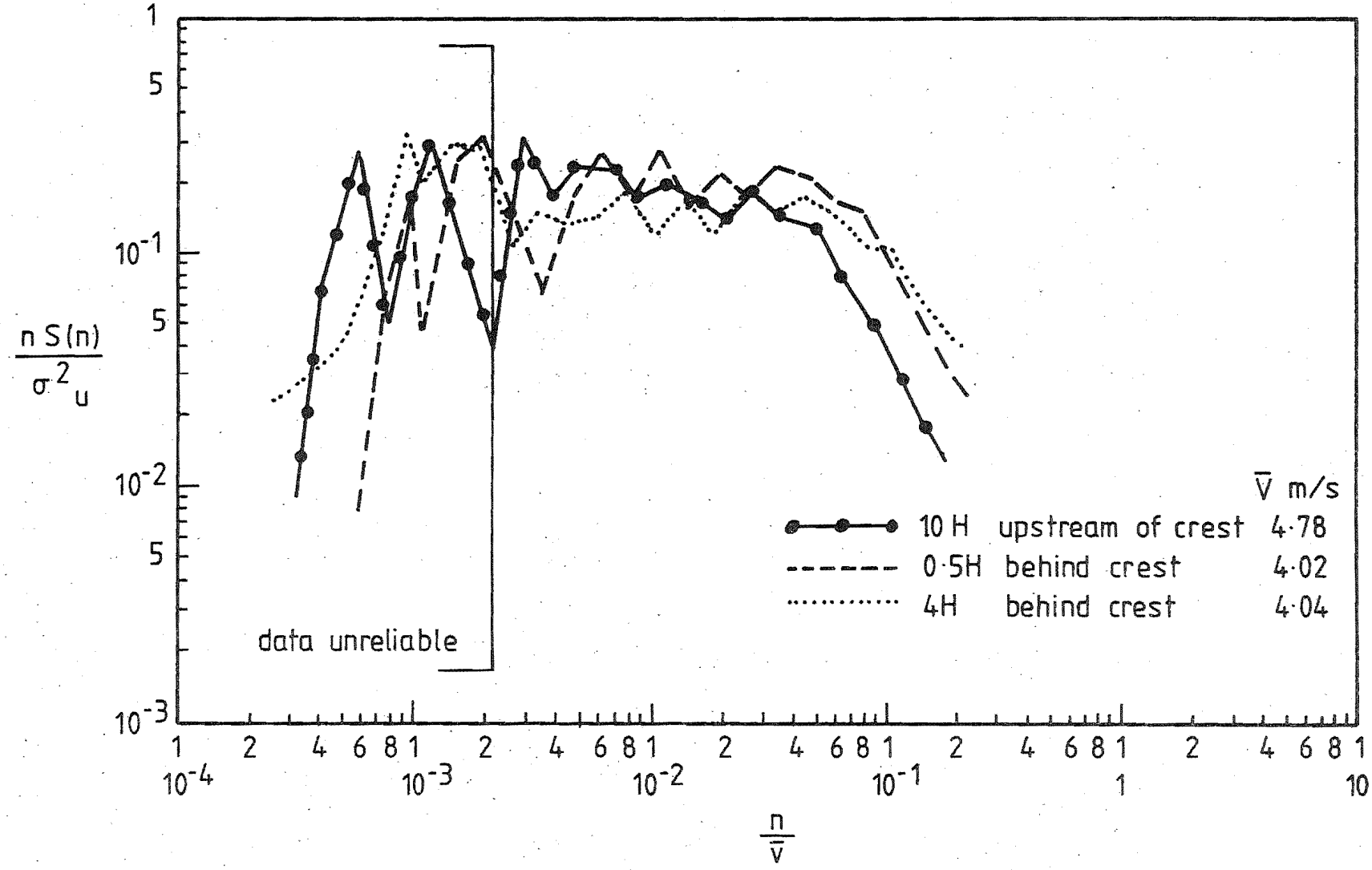

FIG 7·28 THE LONGITUDINAL VELOCITY POWER SPECTRA AT $Z = 2·88m$ ($\frac{Z}{H} = 0·25$) AT DIFFERENT POSITIONS OVER THE CLIFF ESCARPMENT, NE, $\Phi = 24°$.

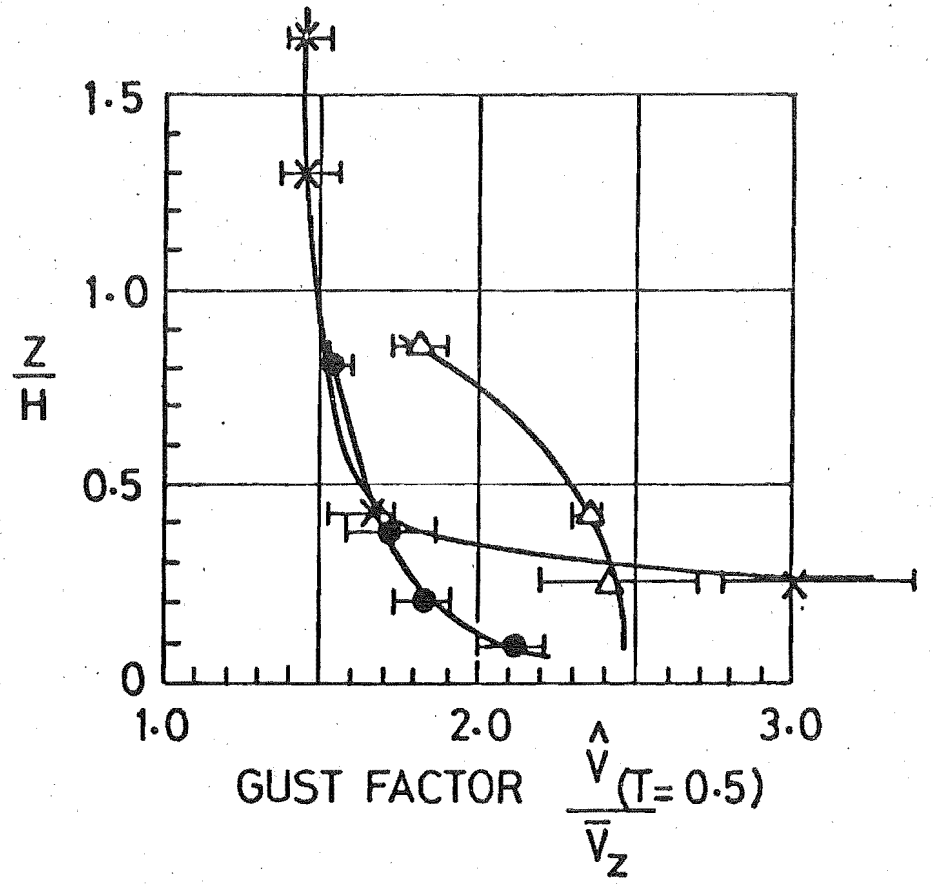

● 10 H upstream of crest
X 0·5H behind crest
Δ 4H behind crest
⊢⊣ range of results from 4 recordings.

FIG 7·29 VARIATION OF GUST FACTOR OVER THE CLIFF ESCARPMENT ($T=0.5s$, $T_o=1800s$, NE, $\phi=24°$)

#3 at 10 m (Fig.7.27) and towers #2 and #3 at the 2.88 m level (Fig.7.28). The instrument arrays affected would have been immersed in the turbulent wake which spread vertically as the flow moved downstream of the crest.

The power spectra exhibited a very flat peak especially for the positions close to the ground (see Fig.7.28), which suggested rather indefinite length scales associated with their peak frequencies. However the longitudinal length scales of turbulence, L_{ux} calculated from the autocorrelation function, gave a consistent decrease in value with decreasing height. The length scales measured varied from a value of about 100 m at 10 m height to 20 m at 1.56 m at the upstream tower, in a similar fashion to the Amberley data. A decrease at all levels from tower #1 to #2 was evident in agreement with the trend noticed in the power spectra. However the lateral length scales showed a general decrease as the flow moved over the escarpment in contrast with the Amberley data. The ratio L_{vx}/L_{ux} at the upstream tower was high (0.70-1.4) compared with the Amberley flow (0.35) and their trend over the escarpment was inconclusive. More recordings would need to be analysed before any firm conclusions could be drawn.

7.5.6 Velocity Probability Distribution

The frequencies of occurrence of the longitudinal velocity component were analysed for all instrument positions and it was found that the probability distributions were without exception, very close to Gaussian. A typical example is shown in Fig.6.27, taken from the Amberley data.

7.5.7 Peak Gust Velocities

The variation over the escarpment of the peak longitudinal gust velocity averaged over a period of T = 0.5 seconds and which was encountered during the period of one recording, is shown in Fig.7.29 as averaged values from the four NE recordings. The strong correlation between the gust velocity and the longitudinal turbulence intensity was again confirmed and will be discussed fully in Chapter 9.

7.6 CONCLUSIONS

* The features of the 11.6 m high cliff escarpment site on the banks of the Rakaia River were described in detail and it was considered that the site was very suitable for the purpose of the test. Three

masts were used with 14 instrument positions which provided data at 0.5 and 4 escarpment heights behind the crest to a height of 20 m and 10 m respectively, together with data from the undisturbed boundary-layer upstream.

* One twenty minute recording was taken of winds from the NW at 64° to the crest normal ($\bar{V}$ = 13.27 m/s). Three half hour and one fifteen minute recordings were taken of winds from the NE at 24±3° to the crest normal. The NE wind recordings were all taken during clear sunny skies with wind speeds at 10 m height of between 6.76 and 7.8 m/s.

* By considering the mean flow and turbulence data at the 10 m height level upstream of the escarpment, it was evident that the atmospheric boundary-layer was consistently slightly stable during the recordings (Pasquill Stability class D/E). Reasonably satisfactory values of the three components of turbulence intensity were obtained once correction for the atmospheric stability was made. However the resulting surface roughness parameter of Z_o = 0.067 m was considered rather high for the upwind terrain which may have been due to the small range of the boundary-layer investigated.

* The oblique mean flow velocities were significantly affected by the presence of the escarpment, giving fractional speed-up ratios of between 0.4 and -0.8. The presence of a strong wake behind the crest reduced the mean velocities and increased the turbulence close to the ground and was responsible for the negative values of fractional speed-up ratios encountered for the NE wind flows. The values of fractional speed-up ratios encountered for the more oblique NW wind flow direction were significantly less than for the more normal NE wind direction.

* Large increases in the longitudinal and lateral components of turbulence intensity were evident behind the crest in the wake area. The wake area was confined below 0.5 H at the tower #2 (0.5 H behind crest) but spread to cover a depth of about 1.0 H at tower #3 (4 H). The high values of turbulence intensity decreased somewhat as the flow proceeded downstream and the wake diffused upwards.

* The turbulence in the wake area generally contained energies at higher frequencies than the flow at the same height upstream.

CHAPTER 8

THE WIND TUNNEL MODEL TESTS

A wind tunnel investigation of the flow over escarpments was carried out as a subsidiary programme to complement the field tests. Although the field work was intended to be the principal contribution of this project, it was felt that the model tests could quickly and relatively easily provide information that would have been very difficult and impossibly time consuming to obtain in the field.

The contribution and benefits from the model test programme were seen as those listed below.

(a) Information from model tests would assist in the planning for the field test programme by indicating the best places for the three towers and the range of values that might be encountered. For instance, it was necessary to find out the minimum distance upstream of the escarpment that the #1 tower should be placed in order to be fully immersed in the undisturbed boundary-layer.

(b) Test results from model investigations were not dependent on the uncertanties of the weather and often frustrating and long periods of waiting for the correct wind conditions to occur. As a result, information may be gathered with far greater efficiency by way of model test investigations.

(c) A greater range of positions relative to the crest and height above the ground surface could be reached over the models than in the field tests which were severely limited by the short towers and their lack of mobility. The model results could then be used to fill in and extend the range of positions covered by the field tests.

(d) The opportunity to test models at other slopes and wind incidence angles and thereby study their effects on the flow was available. The possibility of finding a convenient set of slope angles and wind directions in the field was too much to expect, so that work of this sort had to be undertaken in the wind tunnel to obtain a suitable range of results from which to draw conclusions.

(e) By using accurate models of the escarpments that were actually tested in the field together with similar simulated flow

directions and properties, a direct comparison between the model and field results could be made. Important conclusions on the relevance of the model tests and their accuracy in predicting the full scale situation could then follow.

(f) The investigation of other significant parameters which would have an influence on the flow such as the upwind velocity-height profile, hill height to boundary-layer height and hill shape, would have extended the model test programme well beyond its intended subsidiary role in the present project. These other essential factors however, were the subject of a further study in the Department by J. Pearse and would be reported in due course.

The present wind tunnel investigation may be divided into two quite distinct series of tests. The first test series was conducted during the period from December 1975 to February 1976 before the field tests were undertaken. The wind tunnel was then in its original state with the two fans upstream of the working section and the four models (cliff, 1:1, 2:1 and 4:1 slope, where 2:1 indicates a slope of $\tan^{-1} 1/2$) were investigated at zero incidence angle (flow normal to the forward facing slope) at many positions upwind and downwind of the crests. Because the models were relatively long in the streamwise direction, it was felt that a smooth ground surface over the escarpment in contrast with the 3 mm roughness elements on the tunnel floor upwind of the models, would have introduced a rough to smooth transition with the associated speed-up effects in the flow over and above the effects of the hill itself. Consequently the same roughness elements that were used in the upwind tunnel floor were utilised on the surfaces of the model escarpments for the first test series. These models are referred to as rough models. This first series of model tests was the subject of the paper Bowen and Lindley (1977) and the results are reproduced in Section 8.4 as part of the project programme.

The second series of model tests was conducted during the period from May to July, 1978 after the field tests had been completed. By this time the wind tunnel had been extensively altered although the working section remained unchanged, and the flow conditions just upstream of the model turned out to be slightly different. The second test series was undertaken to provide information on the effect of wind incidence angle, ϕ described in Section 8.4. The field tests were conducted at quite considerable wind incidence angles and a means was needed to relate these field results to the results of the first model test series which were conducted at normal incidence ($\phi = 0$). The

ground positions where readings were taken were confined to the three tower positions adopted in the field tests. It was also felt that an increase in the range of slope angle investigated to 6:1 and 8:1 would be a useful addition, as the lowest slope of 4:1 in the first series still showed a very significant influence on the flow.

The original roughness elements on the model surfaces that were used for the first series corresponded to a $^{z}/_{H}$ of 0.06. In terms of a 13 m escarpment they represented full scale roughness elements that were 0.78 m high which was felt to be excessive and unrealistic. The models used in the second series of tests were therefore tested with smooth ground surfaces more representative of a smooth grassy field, but sufficient repetition of the rough model tests was also made to provide a comparison (described under Section 8.3.3) between the results of both test series.

In addition, the two field test situations were modelled as accurately as possible with similar wind incidence angles and the site terrain details accurately reproduced. The comparison between the model tests and the field results are described under Section 8.5 and during the field data presentation of Chapters 6 and 7.

8.1 DESCRIPTION OF TEST FACILITIES

The wind tunnel model tests were undertaken in the atmospheric boundary-layer wind tunnel situated in the Department of Mechanical Engineering laboratories, University of Canterbury.

8.1.1 Wind Tunnel

The design, operation and performance of the wind tunnel in its original 'blower' configuration has been fully documented by Raine (1974 a,b) and was used in this form for the first series of the present tests in 1975-76. Immediately following the completion of these tests, the fans were relocated on the mezzanine floor, downwind of the working section. Although the working section remained unchanged, the modifications resulted in the tunnel operating at a negative gauge pressure. The modifications had the desired effect of improving the uniformity of the flow and in particular, reducing the tendency for the flow to swirl through the working section. The second test series was conducted in the tunnel after these modifications had taken place which together with a slightly different utilisation of trip fences and the upstream

grid, resulted in small differences in the flow characteristics which are discussed in the next section.

The 1.22 m square working section had a streamwise length of 12 m in which the boundary-layer was developed over the rough floor surface. The 'Torro' baseboard roughness elements that were used were 3 mm high by 4.5 mm diameter and situated on a square 8 mm grid pattern, parallel with the flow. The first test series was conducted using the wind tunnel arrangement developed and finally adopted by Raine (1974a) who described it as Layout #14. A nonuniform grid across the flow preceded the working section roughness elements which had four additional trip fences to reinforce the large scale turbulence in the upper part of the boundary-layer. The second test series used a similar nonuniform grid layout and ground roughness elements but utilised only one trip fence at the beginning of the working section. This second layout was developed by Pearse (1978) during his model hill study programme.

8.1.2 Upstream Flow Conditions

The undisturbed mean velocity-height profiles measured during the two model test series close to the 9.0 m position in the tunnel working section, are present in Figs.8.1 and 8.2. The free stream velocity during both series of tests varied between 18 and 20 m/s. A displacement depth of d = 3 mm, equal to the depth of the surface roughness, was used in plotting the velocity-height profiles. The arrangement of roughness elements described in the previous section was very dense and little flow would have occurred below the height of the roughness elements. The two profiles yielded similar surface roughness lengths, Z_o of 0.2 and 0.35 mm but different boundary-layer depths of 0.7 and 1.5 metres approximately. The power law exponent, α in both cases was close to $^1/_6$. The difference in boundary-layer depth would have had little effect on the model scale as the flow properties at the escarpment level were considered to be the most important. The longitudinal turbulence intensity profiles are shown in Fig.8.3 and the values at $^Z/_H = 1$ differed by about 5% between the two test series.

Raine (1974) discussed the scaling of his similar boundary-layer (Layout #14, Z_o = 0.2 mm, $\alpha = {}^1/_6$) in detail by comparing model and expected full scale values of the surface roughness length, turbulent length scales and scaled profiles of mean velocity and turbulence

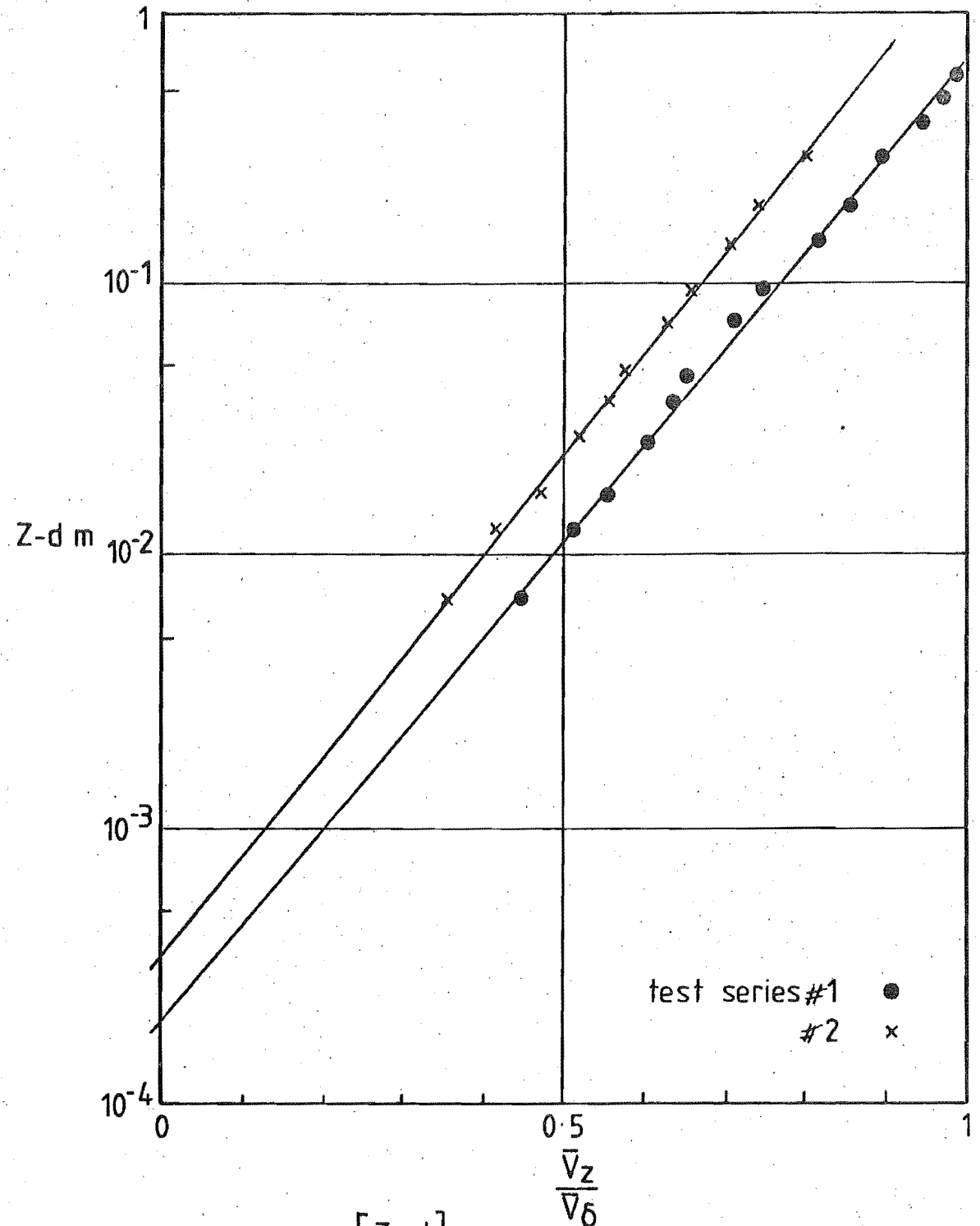

$$\frac{\bar{V}_z}{\bar{V}_\delta} = \frac{\log\left[\frac{Z-d}{Z_o}\right]}{\log\left[\frac{\delta-d}{Z_o}\right]}$$

	$Z_o \times 10^{-3}$ m	δm	dm
test series#1	0·2	0·7	0·003
test series#2	0·35	1·5	0·003

FIG 8·1 UNDISTURBED MEAN VELOCITY-HEIGHT PROFILES MEASURED DURING THE TWO MODEL TEST SERIES

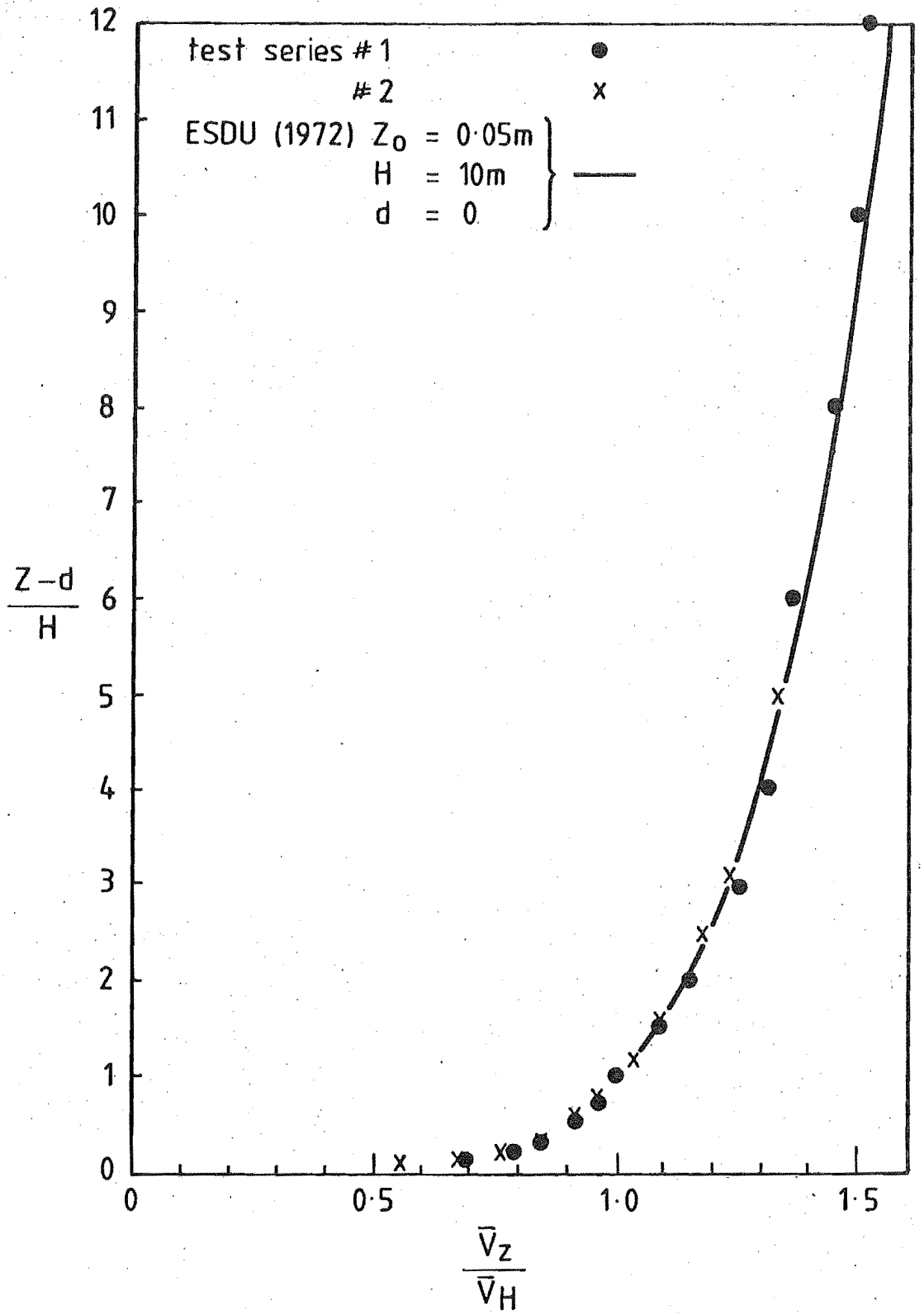

FIG 8·2 MODEL MEAN VELOCITY–HEIGHT PROFILES COMPARED WITH STANDARD OPEN COUNTRY DATA

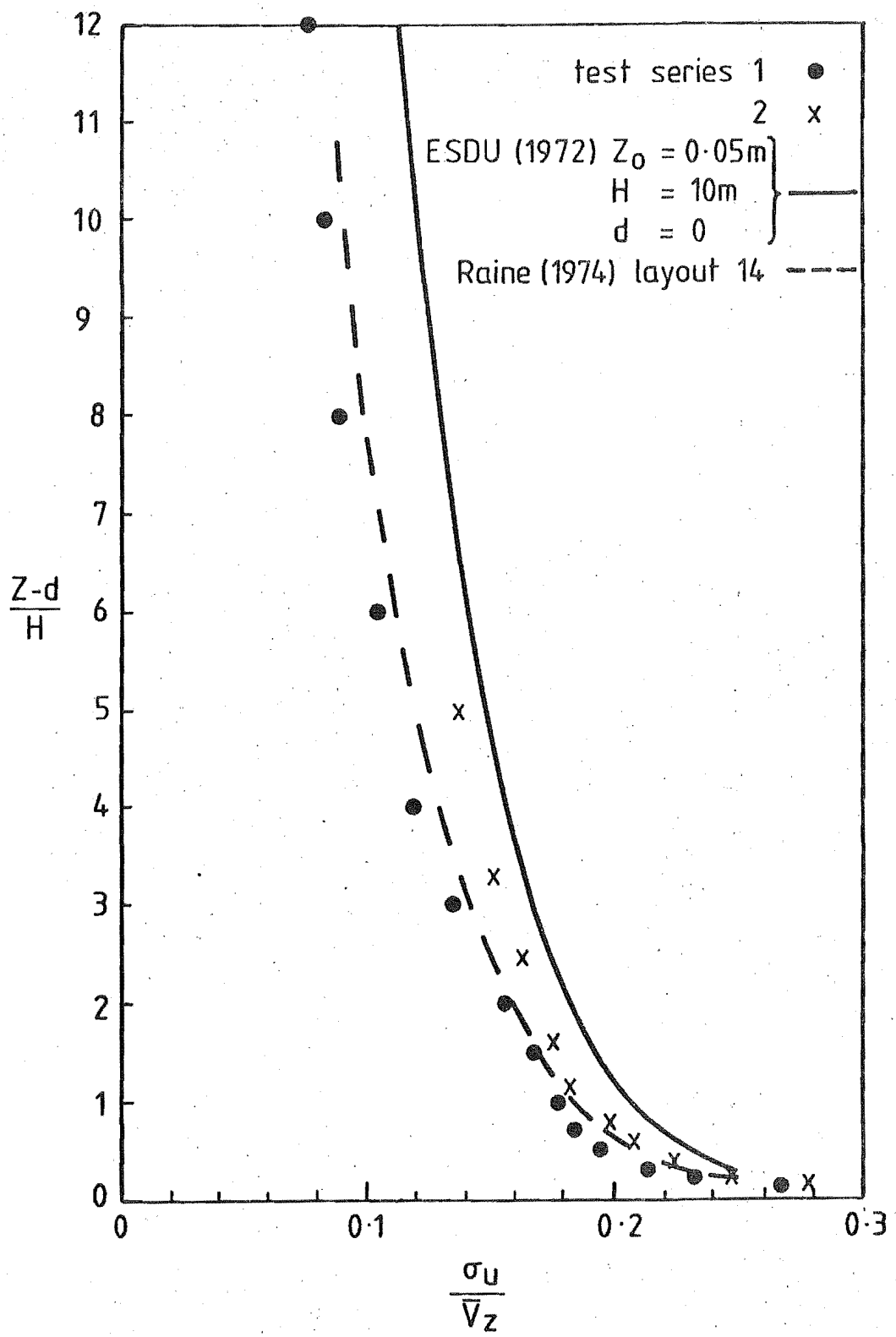

FIG 8·3 MODEL LONGITUDINAL TURBULENCE INTENSITIES COMPARED WITH STANDARD OPEN COUNTRY DATA.

intensity. He concluded that the model conditions encountered best suited a model scale of 1:300. As the roughness layout, tunnel conditions and the resulting mean velocity and turbulence profiles were reasonably close to those observed by Raine, the same scaling factor of 1:300 was adopted for both series of the present test programme. The 50 mm and 60 mm models used in the present tests therefore represented full size escarpments of 15 and 18 m in height. The standard mean velocity and turbulence intensity-height profiles for open country terrain with a Z_o = 0.05 m (ESDU 1974) may now be compared against the wind tunnel data as shown in Fig.8.2 and 8.3 using H = 10 m, a convenient value close to the field escarpment heights. Although the model turbulence intensities were about 12% lower than the expected standard data, the mean velocities compared very well. It was observed by Flay (1978) that the ESDU turbulence intensities were significantly higher than the standard data from other sources as well as his own field measurements. Velocity power spectral measurements taken upstream during the two model test series and shown in Fig.8.12 (Test series #1) and Fig.8.18 (Test series #2) confirmed Raine's conclusion that the modelled turbulence was close to that expected for a rural boundary-layer to that scale, especially at $^{Z}/H$ = 1. At the lower height of $^{Z}/H$ = 0.25 the agreement was not so close with the apparent scaling out by a factor of about 1.5. A displacement depth of 3 mm was used when estimating the appropriate standard length scale from ESDU (1974).

The presented test data therefore confirmed that the model boundary-layer during the two test series satisfactorily represented open country, neutrally stable conditions to a scale of about 1:300. In addition, the data showed that the model escarpments were a suitable size to simulate the actual escarpments investigated in the field. The differences between the modelled boundary-layer conditions and the actual field conditions encountered are discussed in Chapters 6 and 7 during the presentation of the field data.

Raine (1974) observed that the boundary-layer at the 9.0 m position was not yet in equilibrium and the conditions were a little different to the 11.0 m position where self-preservation of the boundary-layer was thought to exist. However the differences were small and the presence of the models would have dominated the development of the flow beyond the 9.0 m position. The roof panel positions were altered to achieve a constant static pressure along the working section during the

growth of the boundary-layer but they were too long to accommodate the solid blockage expected from the models. However the blockage from the models is shown in the next section to have been insignificant.

8.1.3 The Models

The height of the two-dimensional model escarpments was conveniently chosen as 50 mm which corresponded to a full scale value of 15 metres when scaled by the adopted boundary-layer scale factor of 1:300. However during the investigation of the wind incidence effects, the models were laid on top of the floor roughness elements which raised the model height to 60 mm. This change in model height between tests was accommodated in the non-dimensional height $\frac{Z-d}{H}$ and the 20% change in scale was considered to have had a negligible effect on the flow behaviour.

The model height was large enough to enable the hot wire probe to be positioned with reasonable accuracy down to a height of $Z/H = 0.1$ of the surface. The accuracy in probe position estimated as ±0.5 mm, gave the worst percentage accuracy at this lowest position (Z = 5 mm) of ±10%.

Conversely, the model height was small enough to keep the model : wind tunnel cross-sectional area ratio down to 4% in order to avoid significant blockage effects. The problem of blockage effects from the presence of a body in the flow of a closed wind tunnel and subject to the constraining effect of the tunnel walls can be a serious one. However its effect on the flow near a surface mounted body that is immersed in a turbulent boundary-layer is not well documented. Various theories such as Maskell's reported in recent texts (Pope and Harper, 1966), deal satisfactorily with the effect of solid blockage on the drag coefficient measured on bodies suspended in a wind tunnel air stream. However very little has been reported on its effects on the flow close to a surface mounted body. McKeon and Melbourne (1971) and later Modi and El-Sherbiny (1975) have dealt experimentally with the blockage effects on the pressure distribution around a surface mounted bluff body that was immersed in a turbulent boundary-layer, but the attendant changes in the flow close to the body are still not clear. However Pope and Harper stated that the increase in effective velocity around a free body was much less (about one fourth) than the increment obtained from the direct area reduction. Consequently the cross-sectional

area ratio was kept as low as possible and it was assumed that the 4% area ratio adopted would have caused very little change to the flow, especially close to the escarpment surface. This assumption was confirmed by the essentially constant static pressures that were measured in the free stream flow above the escarpments.

The models were constructed with a timber frame, lined with particle board and Torro baseboard in the case of the 'rough' models, to within ±0.5 mm of the required dimensions. The models extended completely across the tunnel and at least 1 metre downstream of the crest before tapering gradually back to the floor level. The wind incidence angle was altered by trimming the edges of the model to fit against the wind tunnel walls. A general view of a model escarpment and the wind tunnel is shown in Fig.8.4.

In addition, an accurate 'smooth' model shown in Fig.8.5 was made of the Amberley site with the few trees and unevenness in slope modelled as closely as possible. The Rakaia cliff escarpment was sufficiently close to the bare 2D step and so devoid of any unusual features that a more accurate model was considered unnecessary.

8.2 FLOW MEASURING EQUIPMENT

The flow measurements were taken with a DISA hot wire anemometer system in a similar manner for both test series. However, during the 2½ years that separated the two test series, the laboratory equipment had been extensively upgraded. As a result, the techniques used in the calibration of the probe and in the analysis of the probe output to obtain the velocity power spectra differed between the test series and are therefore discussed separately below. The common details covering the well established and proven DISA anemometer system are only briefly referred to as the details are well covered by the DISA instruction manuals and information periodicals.

8.2.1. Hot Wire Anemometer System

Measurements in the flow were made with a linearised DISA 55D00 constant temperature anemometer system with a single horizontal probe normal to the flow in a similar manner to the work described by Raine (1974).

The single wire probe is sensitive only to the flow movement perpendicular to the wire which in this case was comprised of the

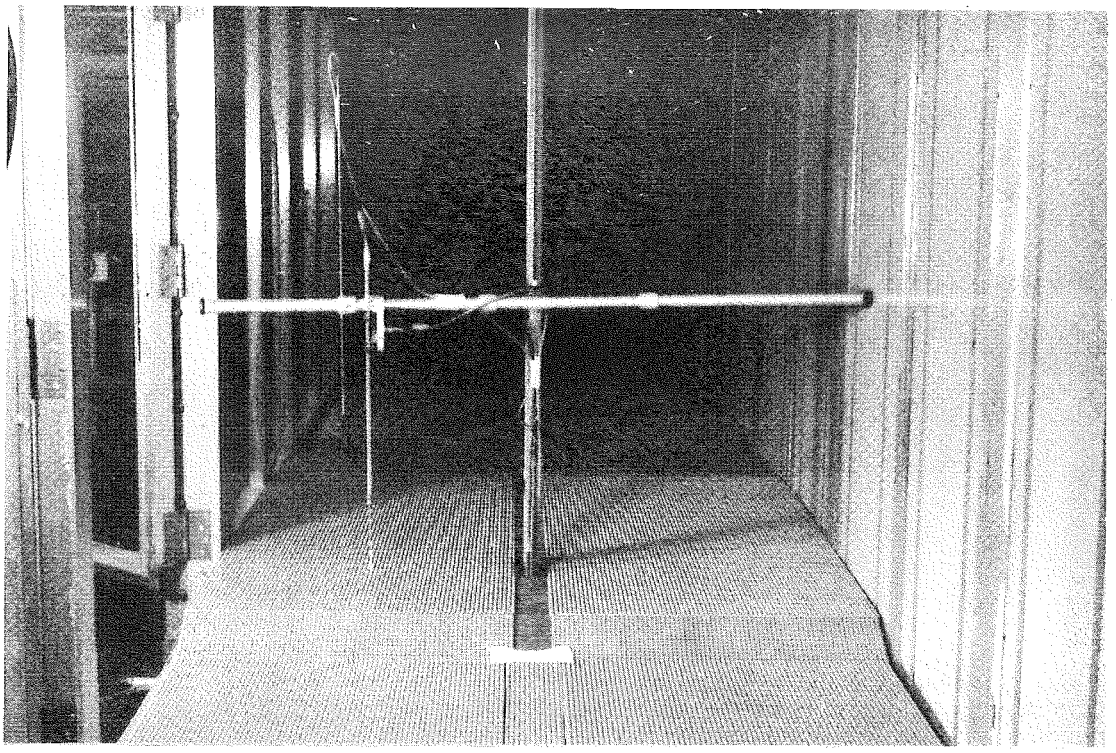

FIG.8.4 VIEW OF THE ROUGH 2:1 SLOPING ESCARPMENT MODEL IN THE WIND TUNNEL LOOKING DOWNSTREAM AND SHOWING THE HOT WIRE PROBE SUPPORT AND THE SURFACE ROUGHNESS

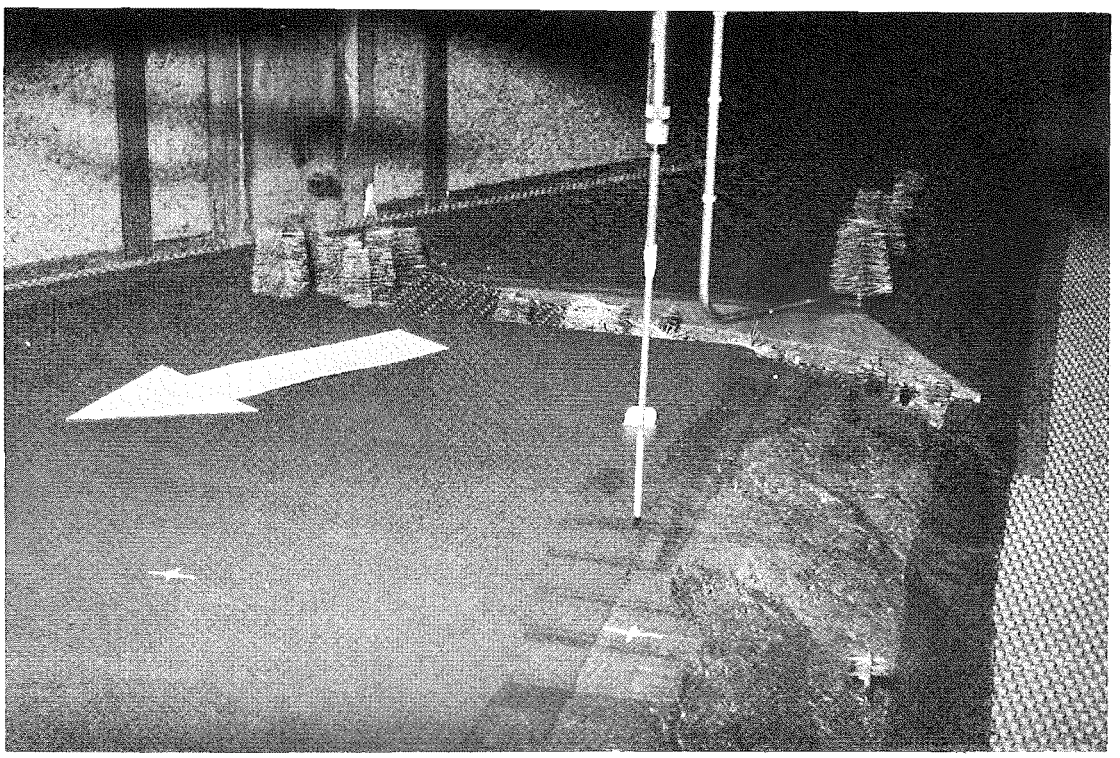

FIG.8.5 VIEW OF ACCURATE MODEL OF THE AMBERLEY FIELD TEST SITE IN THE WIND TUNNEL AND SET OBLIQUELY TO THE FLOW. THE TWO WHITE CROSSES INDICATE THE POSITIONS OF TOWERS #2 AND 3

longitudinal and vertical components of the flow. The instantaneous flow velocity sensed by the probe was therefore

$$U(t) = \left((\bar{U} + u)^2 + w^2 \right)^{\frac{1}{2}} .$$

In some cases the mean flow may have had a significant vertical component near the model slopes for instance, which would have been incorporated into the velocity sensed by the probe. However any lateral deviation caused by the oblique model slopes would have been ignored. Field measurements (Fig.6.15) indicated lateral deviations in the mean flow of no more than 15° which would not have caused a serious error in the total mean velocity by its omission in the model tests.

The theory describing the performance of a hot wire in a turbulent flow field is very extensive and has been well documented by Hinze (1975), Bradshaw (1971) and others. The more practical aspects have been discussed in the DISA information periodicals and particularly for our application, by Rasmussen (1966) and will not be repeated here. It is generally accepted that the output voltage of the constant temperature anemometer may be written as

$$V^2 - V_o^2 = BU^n$$

where V_o is the output voltage at zero velocity and B,n are experimental constants. However using a correctly adjusted lineariser, the output is converted to one which is linear with velocity so that $V = CU$. Assuming that u and w are small compared with $\bar{U}$, then the mean and standard deviation of the voltage output are directly proportional to the mean and standard deviation of the velocity component directed along the mean streamwise velocity, $\bar{u}$ and $\sqrt{\bar{u}^2}$. Rasmussen (1966) maintains that the DISA hot wire system normally yields an accuracy within 2% for $\bar{u}$ and 5% for $\sqrt{\bar{u}^2}$ for flows with a turbulence intensity below 20%. The accuracy is known to deteriorate for higher turbulence intensities but information on this aspect is very scarce. High turbulence intensities were encountered in both model and field tests in the wake region behind the crest and in this region, the hot wire measurements should only be relied on to indicate trends due to their serious limitations in such flow conditions.

Major errors in the anemometer output could accrue from inaccurate linearizing and calibration and for this reason great care was taken when carrying out these adjustments in accordance with the DISA instructions.

The techniques employed in the two test series were quite different and are discussed separately in the following two sections. Fluctuations in the ambient temperature can also cause considerable thermal drift in the calibration and was minimised by frequent calibration checks against a pitot tube in the undisturbed flow high above the model. Calibration checks were normally done before each profile traverse which usually took 15 to 20 minutes to accomplish. The probe was cleaned regularly once a day to prevent the build-up of dirt on the wire.

The hot wire probe was supported by a DISA 55H01 traversing unit which was in turn mounted on the wind tunnel traversing gear described by Raine (1974). The wind tunnel traversing gear was used only for coarse adjustments of the probe which was accurately located before a vertical traverse was accomplished using the DISA rack unit. Due to various problems in the rigidity of the support system and difficulty in positioning the probe at the beginning of each traverse, it was estimated that the accuracy in position could only be considered as ±0.5 mm although for the majority of cases the accuracy would have been significantly better.

The accuracy of the results involving additional errors from other sources are discussed later but sample repeated measurements on independent days indicated that the results were repeated within 6%. The majority of the differences between results were found to be biassed and not random, indicating that the predominating error was in the calibration and linearisation of the anemometer.

8.2.2 First Test Series

The horizontal probe used for the velocity measurements was a DISA 55A36 general purpose single wire probe. This probe had a 90° bend in the supporting prongs so that the sensor wire was mounted perpendicular to and upstream of the probe support axis. Due to the aerodynamic interference from the probe holder and supports, the use of this probe was recommended only for low turbulence intensities below 5% but the lack of the more suitable but expensive gold plated probes at the time prevented the use of the latter type until later. However it was considered that the resulting error from its use in higher turbulence would have been tolerable when considered with the errors already discussed. The standard miniature probes which have the same frequency restriction as the general purpose series are used extensively for wind tunnel work elsewhere.

The probe was linearised in the wind tunnel by measuring the output voltage from the anemometer at a dozen or so flow velocities measured by a pitot tube as no calibration unit was available. The range of velocity was achieved by raising or lowering the probe and the adjacent pitot tube through the boundary-layer. However fluctuations in the tunnel flow, difficulties in the accurate positioning of both instruments at exactly the same height and the large changes in turbulence intensity over the velocity range, caused significant errors in the readings and doubt as to the accuracy of this method. The results were plotted as log $[(V/V_o)^2 - 1]$ versus log $[\bar{U}]$.

The exponent taken from the gradient of the resulting straight line was used to set the linearizer. The linearised anemometer was then checked against the pitot tube for error over as large a velocity range as possible (usually 2:1) and readjusted if necessary. A suitable calibration factor was then chosen and the voltage output set at a known flow velocity. This latter calibration setting was checked repeatedly throughout the investigation.

Following the velocity measurements, a number of power spectra and autocorrelation measurements were accomplished. A DISA 55F95 gold plated, single horizontal wire probe which had a similar configuration to the general purpose probes used previously but designed for use in high turbulence, was used to drive the DISA analogue correlator and time delay unit together with a Bruel and Kjaer $1/3^{rd}$ octave bandwidth analyser and recorder. The anemometer was linearised and calibrated in the same manner as before. Autocorrelation coefficients - time delay curves were then plotted from the recorded data and the turbulent length scale associated with each data set calculated from the area under the curve multiplied by the mean velocity. Normalised power spectra from 2-20,000 Hz were plotted from the recorded frequency spectra using equations 2.31 and 2.32 and the turbulent length scale estimated from the peak frequency calculated using equation 2.38. The equipment layout and individual instrument settings were similar to those reported by Raine (1974).

8.2.3 Second Test Series

The horizontal single wire probe used in the second test series was a DISA 55F35 miniature probe with the same configuration and performance as the general purpose probe used in the first series, but

with slimmer prongs and probe supports. The linearisation and initial calibration adjustments this time were carried out with a Thermo-Systems Inc.Model 1125 Calibrator which provided a closely controlled flow with low turbulence. In this way the anemometer was adjusted far more accurately than was previously possible. However repeated calibration checks during the experiments were maintained using the pitot tube in the wind tunnel to minimise the thermal drift in the calibration.

At this stage, the data acquisition system which could take two channels of hot wire signals and process them digitally on the adjacent laboratory HP 2100A computer had been commissioned. In addition, the programs for the calculation of mean velocity, turbulence intensity and power spectra had been written and proven.

Advantage was taken of this recent facility which has been fully reported by Pearse et al (1978), to obtain a number of power spectra and turbulence length scales which are reported later. Agreement of usually well within 10% occurred between the mean and standard deviation of velocity calculated digitally and that indicated from the mean and RMS meters. Although the RMS meter was set to a long averaging time (usually 100 seconds) a slow variation in output always occurred due to the variation in tunnel conditions. In comparison, the digital data was obtained over a relatively short period of time so that it was inevitable that the data from the two systems would have varied somewhat. With that in mind, the agreement between the digital and analogue systems was considered to be quite satisfactory.

8.3 EFFECT OF SLOPE GRADIENT

Information regarding the effect of slope gradient on the flow over the escarpments facing normal to the flow have been collected in this section from both test series. A comparison between the results from rough and smooth models then follows.

8.3.1 Rough Models (First Test Series)

The following results were obtained during the first test series using models with rough surfaces situated normal to the wind tunnel centreline, ($\phi = 0$). The free stream velocity, $\bar{V}_\infty$ throughout the test series was close to 20 m/s. Data for Fig.8.9 were normalised by the free stream velocity, $\bar{V}_\infty$ but may be converted to $\bar{V}_H$ by using the ratio $\bar{V}_H/\bar{V}_\infty = 0.652$. No displacement depth was used in the presentation of

this test series data except in Fig.8.6 to allow a direct comparison between rough and smooth models.

Typical mean velocity-height profiles over the escarpments tested are presented in Fig.8.6 and the almost linear profile near the crest with only a small increase in velocities for increasing slope may be seen for the range of slopes considered. The profiles at ½ H were very similar to the profiles at the crest except for the wake effect below $\frac{Z-d}{H} = 0.15$ in the former. The resulting fractional speed-up ratios are shown in Fig.8.7 as height profiles for each position. Only the two extreme cases of slope considered are shown to indicate the range of values encountered. These profiles then established the contours of equal fractional speed-up ratio which are presented in Fig.8.8 for the four escarpment models.

A certain degree of shelter was apparent up to 5 H upstream of the slopes where ΔS was negative, although the strength of the upstream vortex in front of the cliff face was not investigated. About one third of the way up the slope in the rapidly accelerating flow, ΔS turned positive and rapidly increased in value towards the crest. The velocity-height profiles at the crest (Fig.8.6) were nearly uniform which caused the value of ΔS to increase very quickly towards the ground. An overall maximum value of ΔS of about 0.7 was found for all four slopes at the lowest height ($^{Z}/_{H} = 0.2$) above the crest that was investigated. The behaviour of the flow closer to the displacement depth was not known. Care must be taken when comparing ΔS values close to the ground as the $^{Z}/_{H} = 0.2$ represents a more realistic $\frac{Z-d}{H}$ ratio of 0.14. The major region of influence from the escarpments defined say by $\Delta S > 0.1$, was confined to below a height of 3 H above the local ground level. This region persisted beyond 10 H downstream of the crest for all the four slopes considered. Downstream of the crest, a wake region of high shear and lower mean velocities grew from the crest and extended to a height of about 1 H for the cliff and 0.4 H for the 4:1 slope, before becoming insignificant at about 10 H downstream. ΔS profiles at sites in this wake region tended to change their shape from that near the crest to one with a maximum value somewhat above the ground level. The peaks in the ΔS profiles rose from ground level at the crest to approximately $^{Z}/_{H} = 1$ at between 5 to 10 H downstream. Surprisingly, the peak values of ΔS at sites well downstream tended to be greater for the more gradual slopes where the wake was not so strong and the possibility of separation less likely.

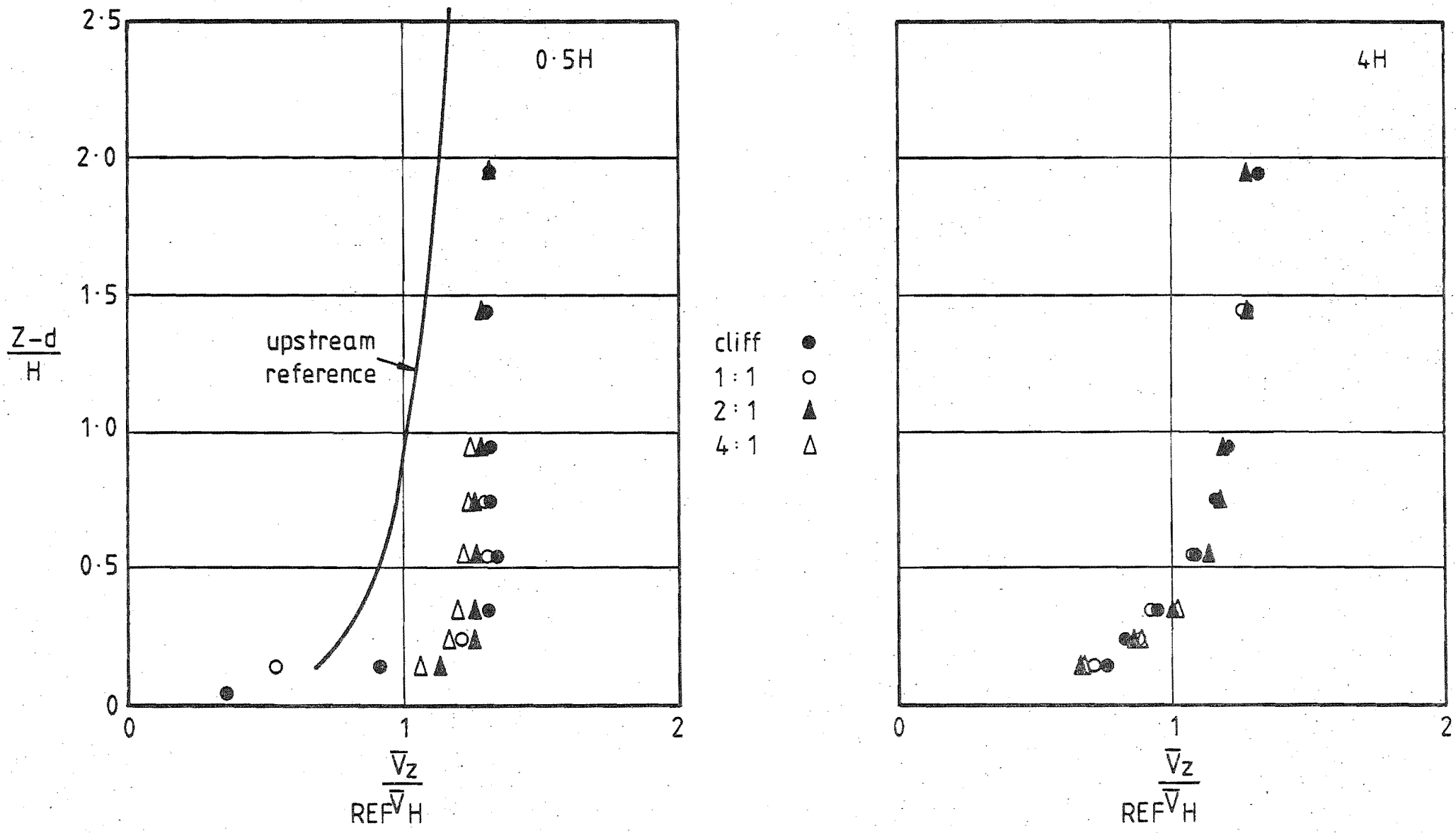

FIG 8·6 SAMPLE MEAN VELOCITY-HEIGHT PROFILES OVER THE ROUGH MODEL ESCARPMENTS AT 0·5H AND 4H DOWNSTREAM OF THE CREST (WIND INCIDENCE ANGLE, ϕ = 0° TO CREST NORMAL)

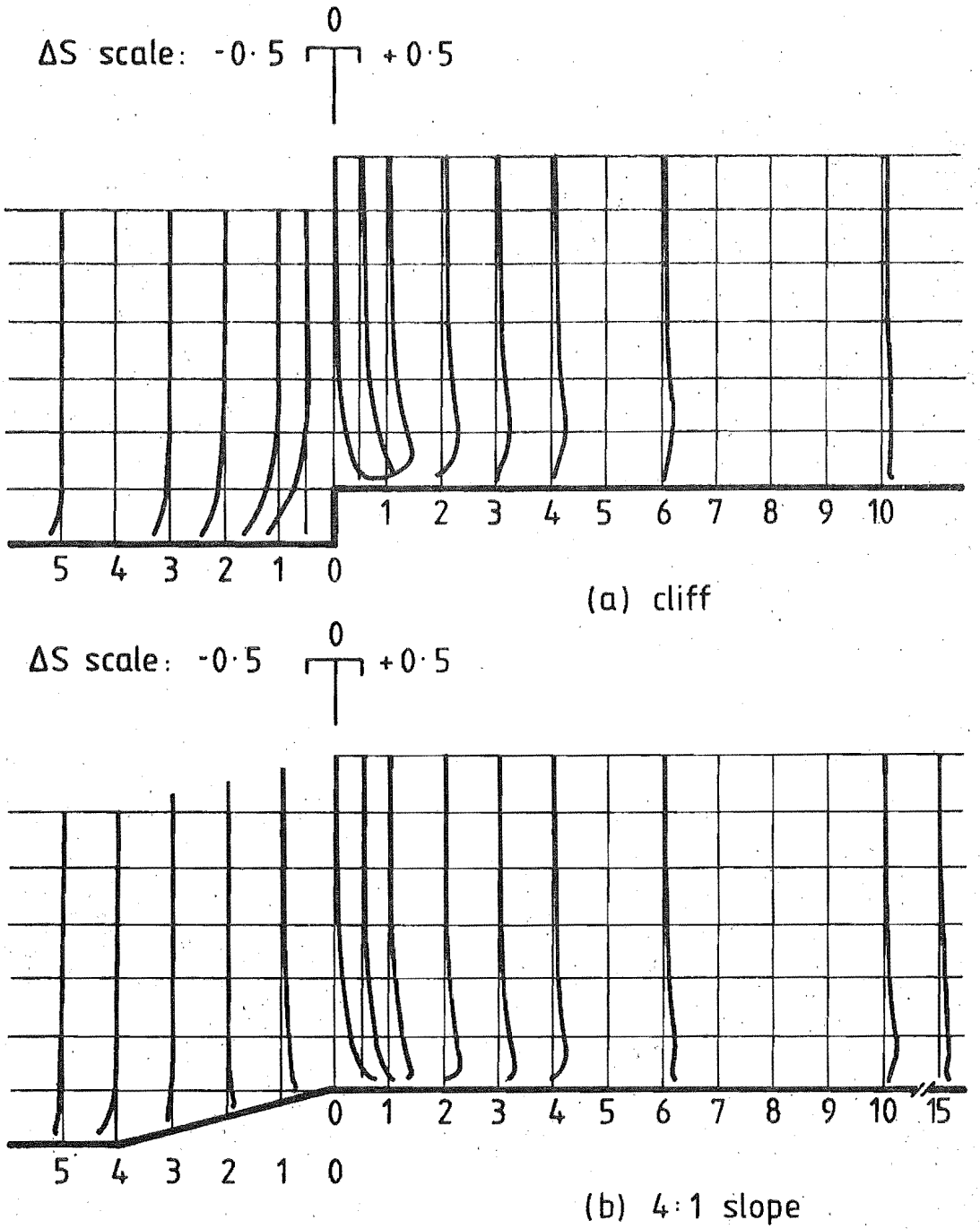

FIG 8·7 FRACTIONAL SPEED-UP RATIOS OVER THE ROUGH MODEL CLIFF AND 4:1 ESCARPMENTS, (ϕ = 0°)

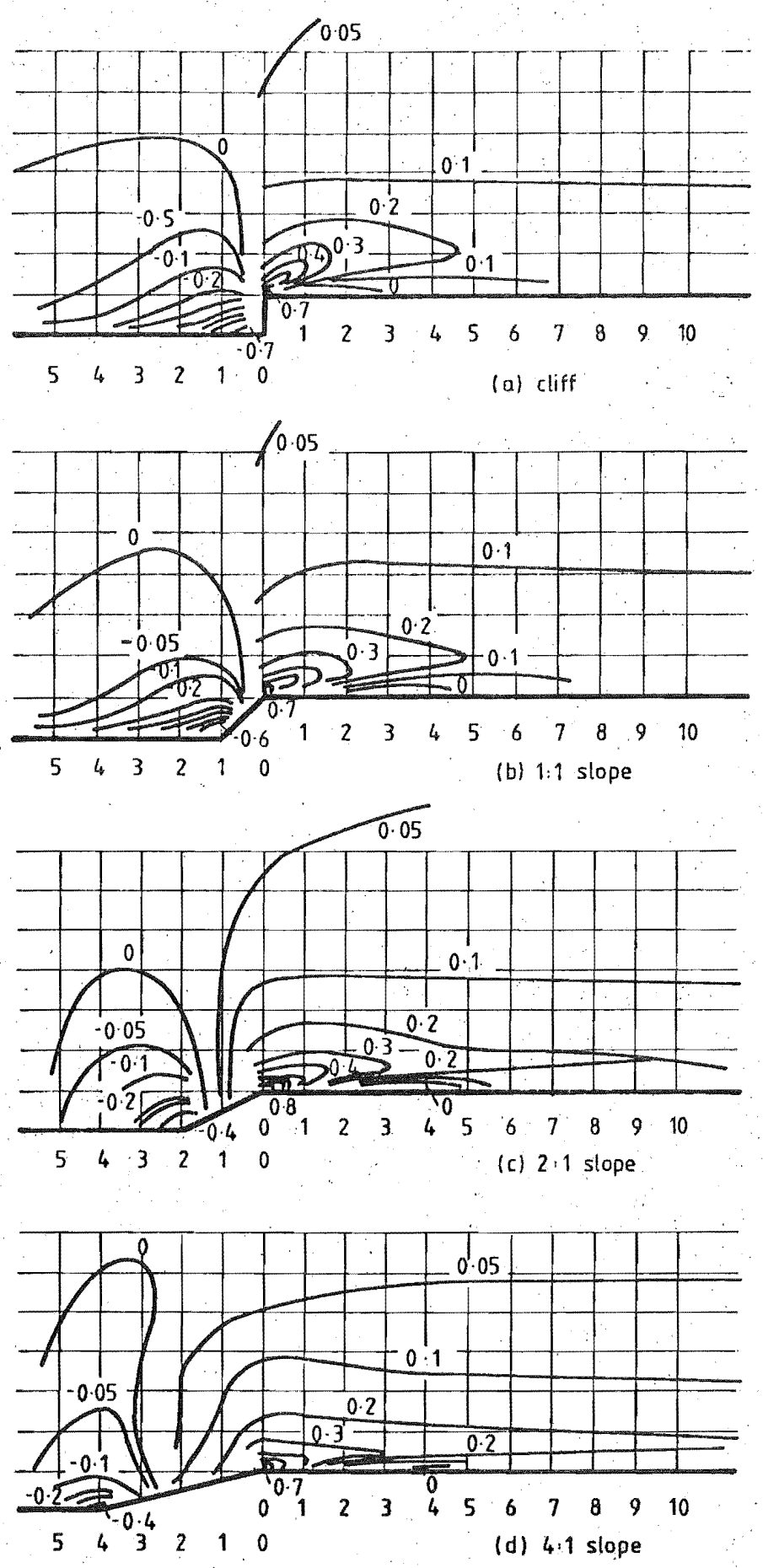

FIG 8·8 CONTOURS OF EQUAL FRACTIONAL SPEED-UP RATIO OVER VARIOUS ROUGH MODEL ESCARPMENT SLOPES ($\phi = 0°$)

The variation in the standard deviation of longitudinal velocity is presented in Fig.8.9 for the cliff and 4:1 escarpment. The extent of the wake generated behind the crest was evident in the large increase in turbulence which dissipated as the flow proceeded downstream. Very little modification to the turbulence in the flow was evident outside this wake region.

The variation in turbulence intensity is shown in Figs.8.10 and 8.11 and was accentuated by the generally higher σu values occurring in the regions of lower mean velocity. The turbulence intensity and the extent of the wake region increased with the slope angle of the escarpment. Outside the wake region, the small increase in flow speeds caused the longitudinal turbulence intensity to be reduced slightly.

Close upstream of the cliff and immediately downwind of the crests of all the models close to the ground, there were regions where separated flows and high turbulence levels were normally to be expected. Because of the inaccuracies of the hot wire anemometer in these conditions, the data in these regions must only be taken as an indication of trends.

Sample longitudinal velocity power spectra for a number of sites over the escarpments are shown in Figs.8.12 and 8.13. A trend to slightly higher frequencies was evident as the flow passed into the turbulent wake at the $^{Z}/_{H} = 0.2$ height behind all the models where presumably, smaller scale turbulence was generated. This modification was lost as the flow continued further downstream and was not evident at a height of $^{Z}/_{H} = 1$ at any position. The variation in the turbulence length scale, L_{u_x} over the escarpments is indicated in Fig.8.14 and indicated the same trend at low heights. The length scales were derived from the auto-correlation-time delay curves up to 100 m secs. However the increase in length scale for larger $^{Z}/_{H}$ values would have been due to the streamline compression convecting turbulence from a higher elevation upstream to a lower position over the escarpments. As the length scales generally increase with height, then the longer length scales would have been brought closer to the ground.

8.3.2 Smooth Models (Second Test Series)

The following results were obtained during the second test series using models with smooth surfaces situated normal to the wind tunnel centreline. The free stream velocity, $\bar{V}_{\infty}$ in these tests was close to 18.3 m/s with a $\bar{V}_H / \bar{V}_{\infty}$ ratio of 0.576 (H = 50 mm).

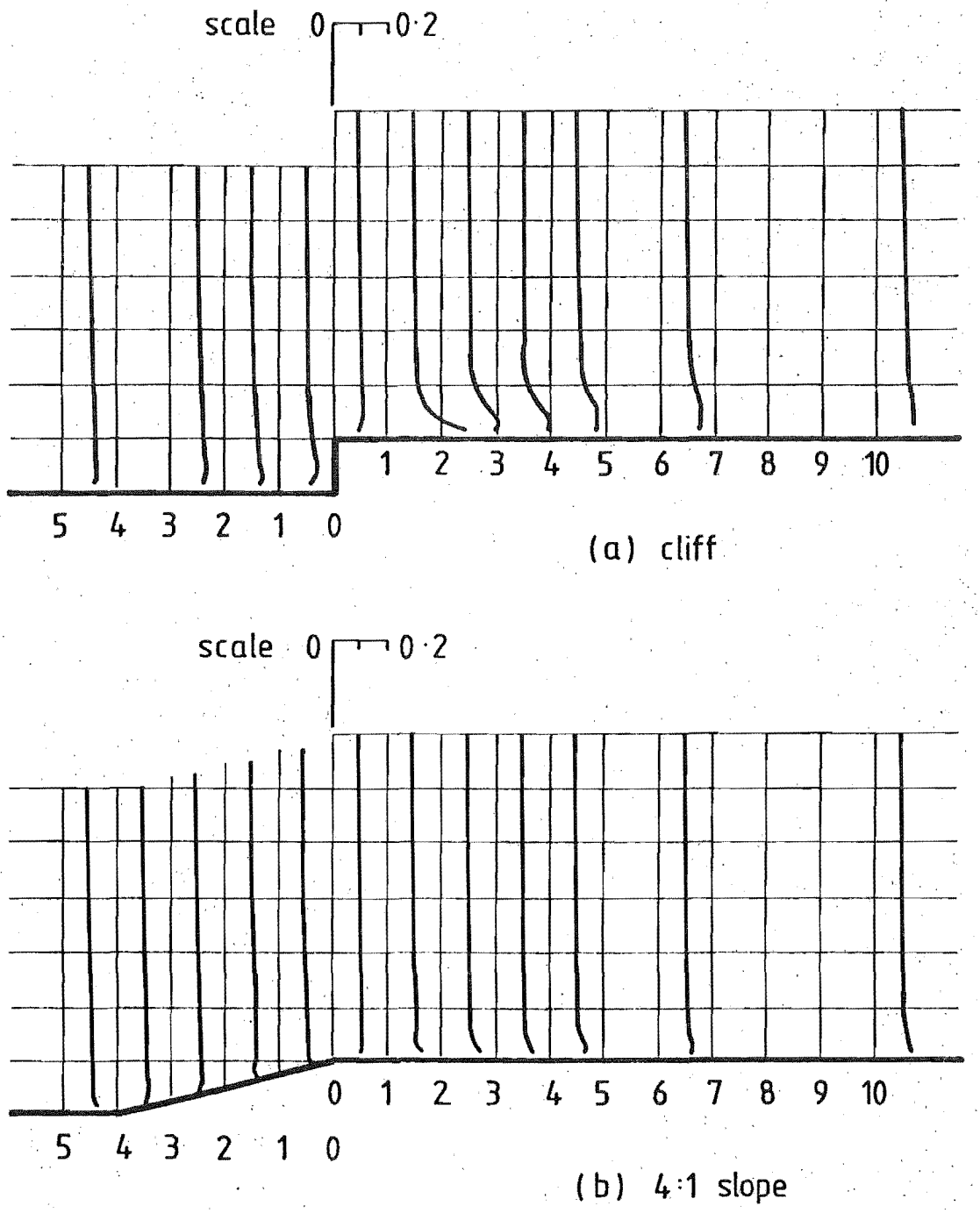

FIG 8·9 VARIATION OF $\sigma_u / \bar{V}_\infty$ OVER THE ROUGH MODEL CLIFF AND 4:1 ESCARPMENTS WITH $\bar{V}_\infty$ = 20m/s (ϕ = 0°)

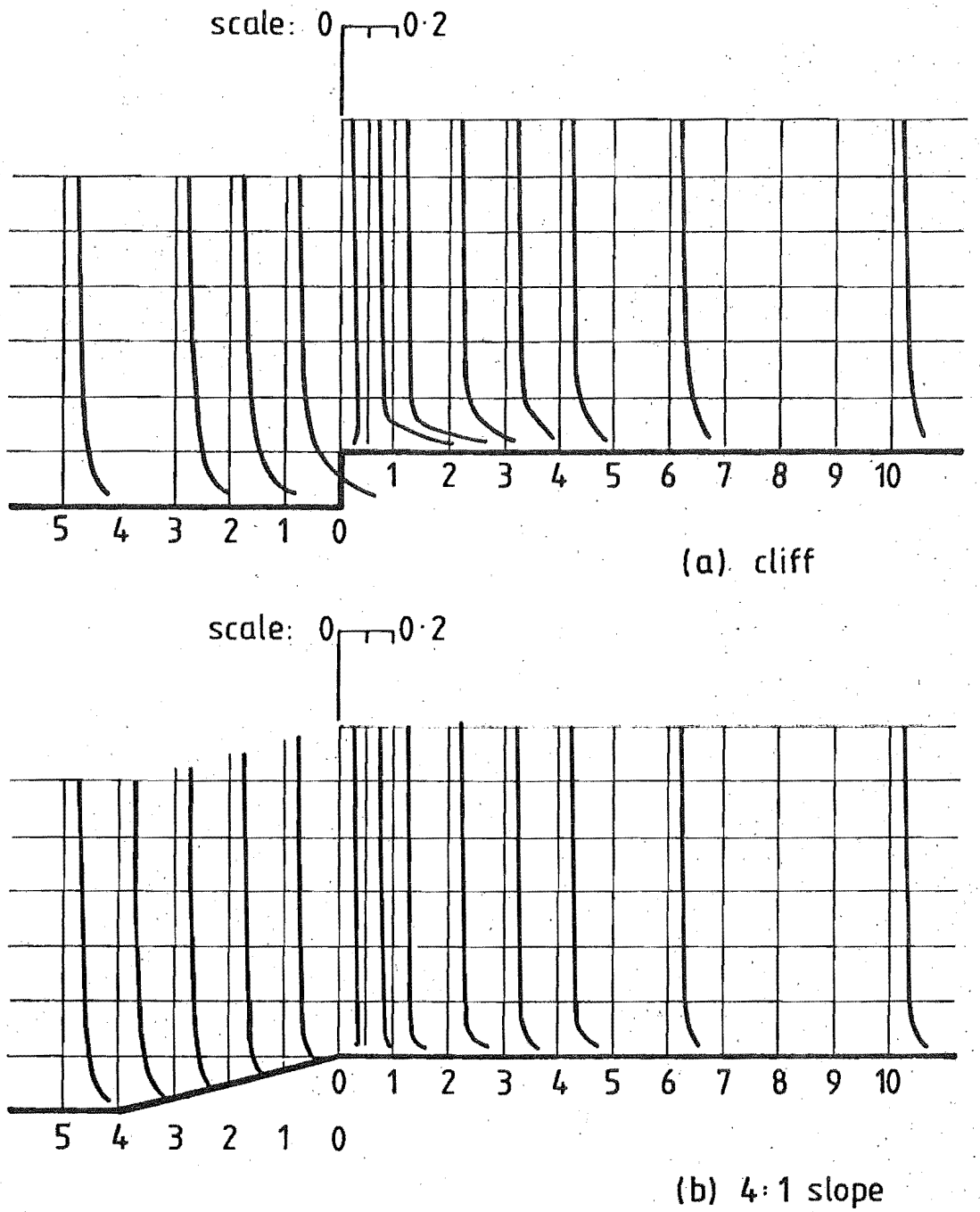

FIG 8·10 VARIATION OF LONGITUDINAL TURBULENCE INTENSITY OVER THE ROUGH MODEL CLIFF AND 4:1 ESCARPMENTS ($\phi = 0°$)

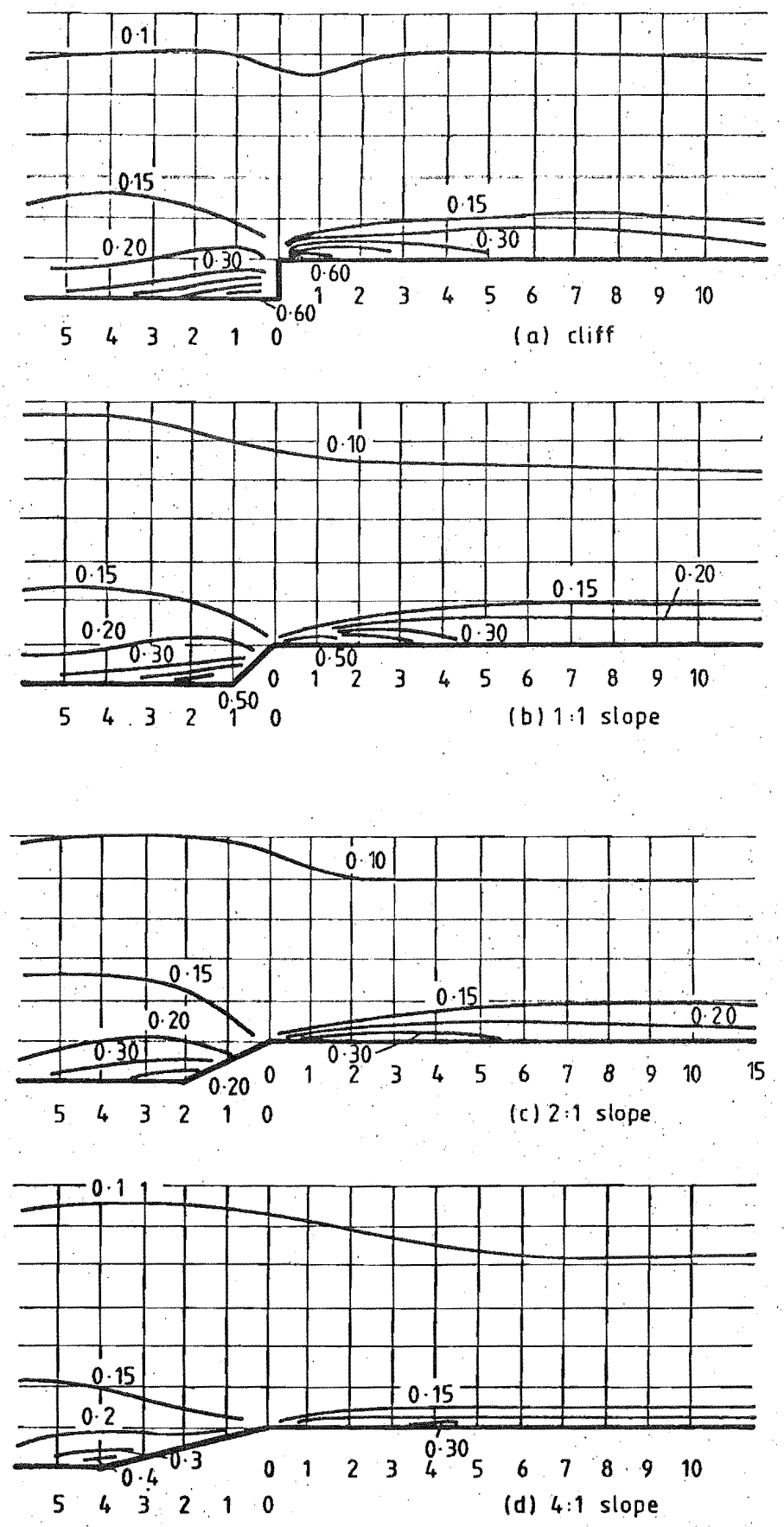

FIG 8:11 CONTOURS OF EQUAL LONGITUDINAL TURBULENCE INTENSITY $\sigma_u / \bar{V}_z$ OVER VARIOUS ROUGH MODEL ESCARPMENTS (ϕ = 0°)

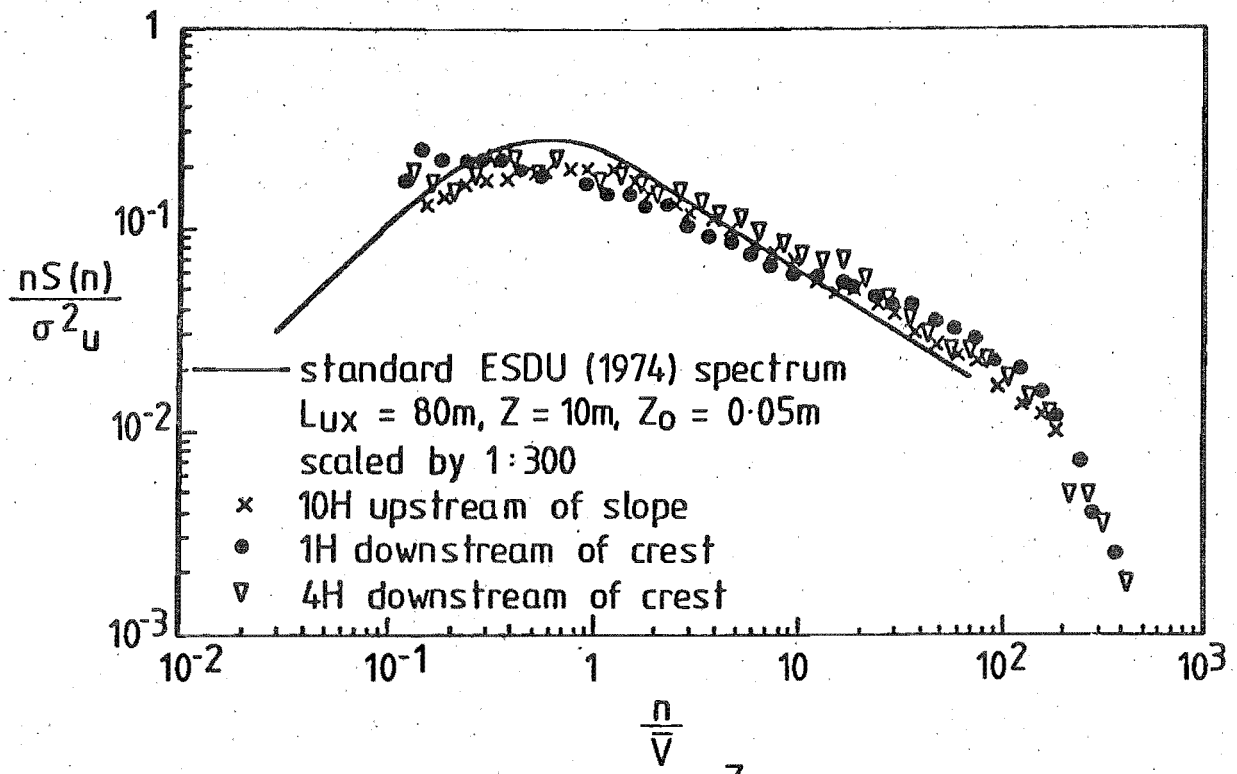

(a) cliff height $\frac{Z}{H}$ = 1

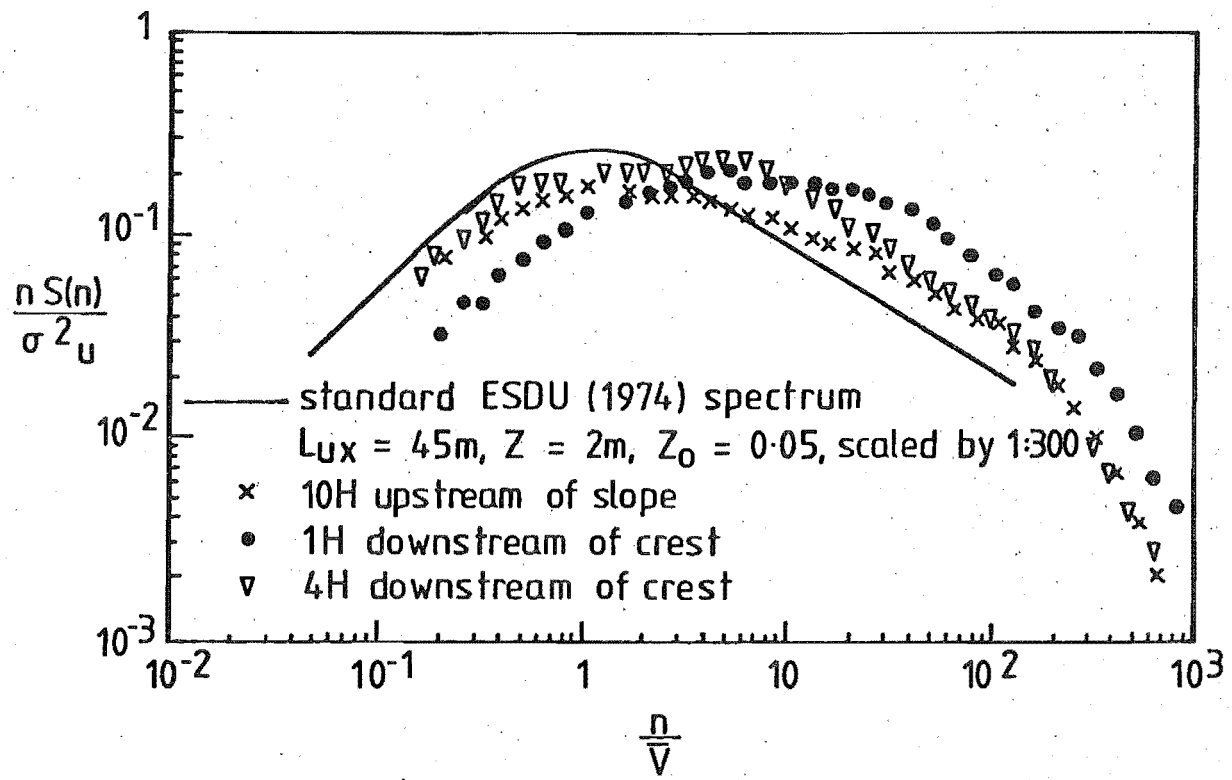

(b) cliff height $\frac{Z}{H}$ = 0·2, or $\left(\frac{Z-d}{H} = 0·14\right)$

FIG 8·12 LONGITUDINAL VELOCITY POWER SPECTRA FOR VARIOUS POSITIONS OVER THE ROUGH CLIFF MODEL ESCARPMENT AT TWO HEIGHTS a) Z/H = 1, b) Z/H = 0·2. (ϕ = 0°)

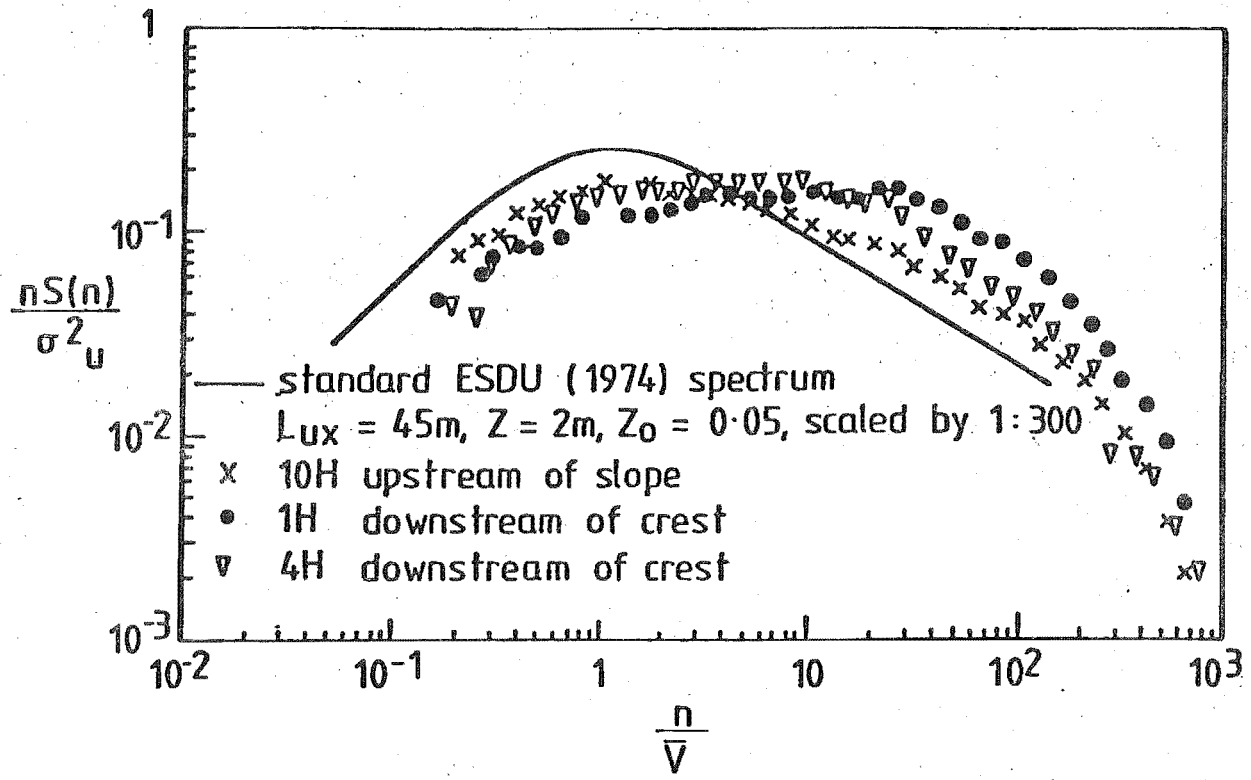

(a) 2:1 slope, height $\frac{Z}{H}$ = 0·2

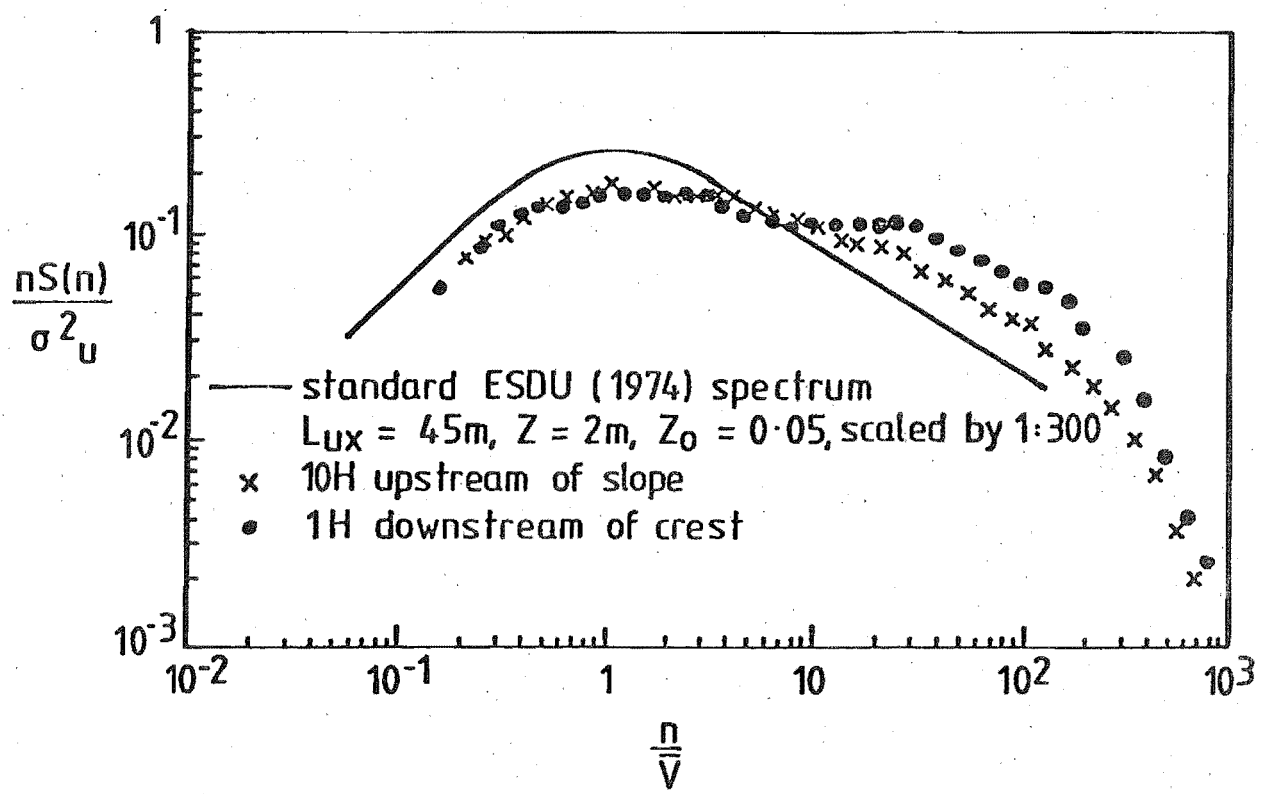

(b) 4:1 slope, height $\frac{Z}{H}$ = 0·2

FIG 8·13 LONGITUDINAL VELOCITY POWER SPECTRA FOR VARIOUS POSITIONS OVER THE ROUGH 2:1 AND 4:1 MODEL ESCARPMENTS AT Z/H = 0·2 OR $Z-d/H$ = 0·14 (ϕ = 0°)

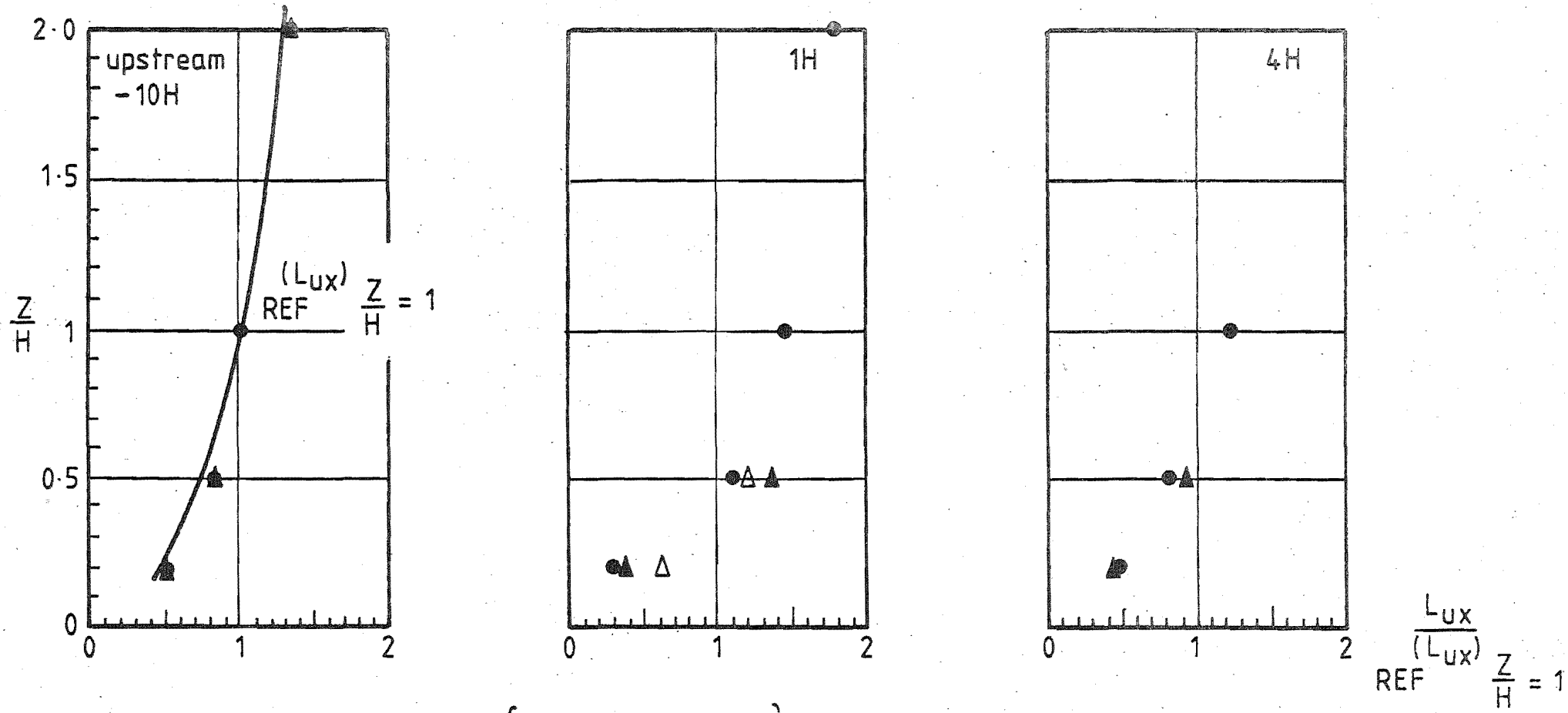

FIG. 8·14 VARIATION OF THE LONGITUDINAL TURBULENCE LENGTH SCALES, L_{ux} WITH POSITION OVER THE ROUGH ESCARPMENT MODELS ($\phi = 0°$)

A displacement depth of 3 mm was used for the presentation of the upstream flow velocities over the rough tunnel floor and the fractional speed-up ratios over the escarpments were calculated using velocities at the same distance Z-d above the roughness (d=3 mm upstream and d=0 downstream).

Typical mean velocity-height profiles at 0.5 H and 4 H behind the escarpment crests are presented in Fig.8.15 compared with the upstream reference profile in the tunnel. The profiles at the 0.5 H position were very similar for all the slopes tested except close to the ground in the expected wake region. In this region, the large deficit in velocity for the cliff and 1:1 slope was evident. This wake deficit covered a depth of 0.3 H at the 0.5 H position and increased to 1 H at the 4 H position for the cliff and 1:1 slope. The other profiles were very similar to each other and indicated no wake at all above a height of $^{Z}/H = 0.14$. These levels were repeated in the fractional speed-up ratios presented in Fig.8.16. However there was a slight trend at the 0.5 H position and outside the wake region, for the steeper slopes to yield a higher ΔS value. This trend was reversed however at the 4 H position.

The turbulence intensities shown in Fig.8.17 were very similar for all slopes considered except for the cliff and 1:1 slope in the wake region. Apart from these exceptions the turbulence intensities were somewhat lower than upstream due to the higher local mean flow velocities.

The power spectra behind the cliff are shown in Fig.8.18 and were very similar to those taken earlier by the spectral analyser over the rough models (Fig.8.12). The increase in turbulence at higher frequencies noted previously in the wake region behind the cliff was not so evident with these smooth models. However the spectra in this region exhibited a flatter profile and sample turbulence length scales measured at these positions were markedly lower than for the other more gradual slopes. The power spectra for the other slopes are not shown as they were very similar to the upstream reference spectra.

8.3.3 Discussion

The effect of slope angle on the flow parameters may be seen from the results that have been presented and discussed in the preceding two sections. Generally speaking for regions outside the wake, the

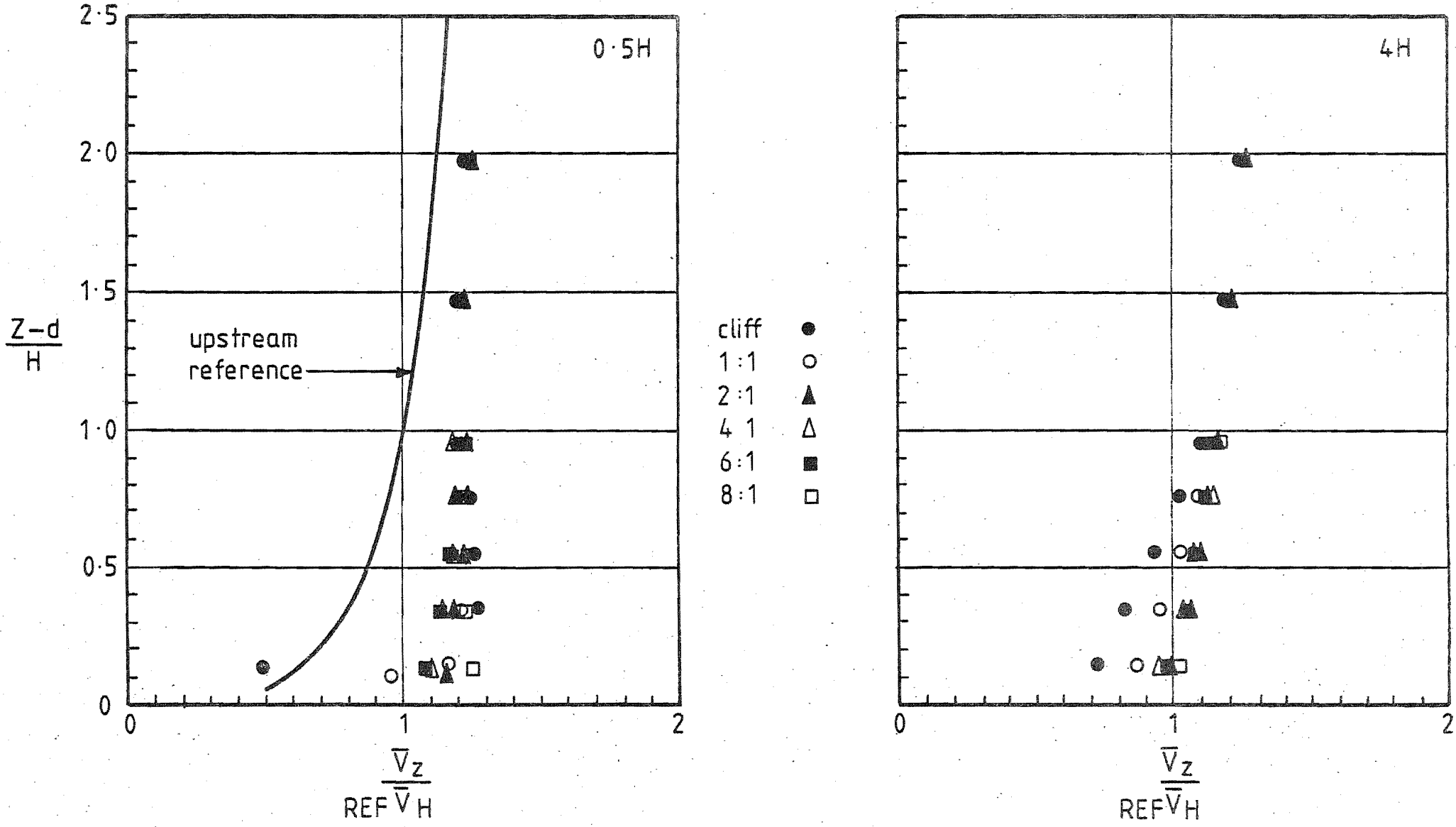

FIG 8·15 MEAN VELOCITY-HEIGHT PROFILES OVER THE SMOOTH MODEL ESCARPMENTS AT 0·5H AND 4H DOWNSTREAM OF THE CREST (ϕ = 0°)

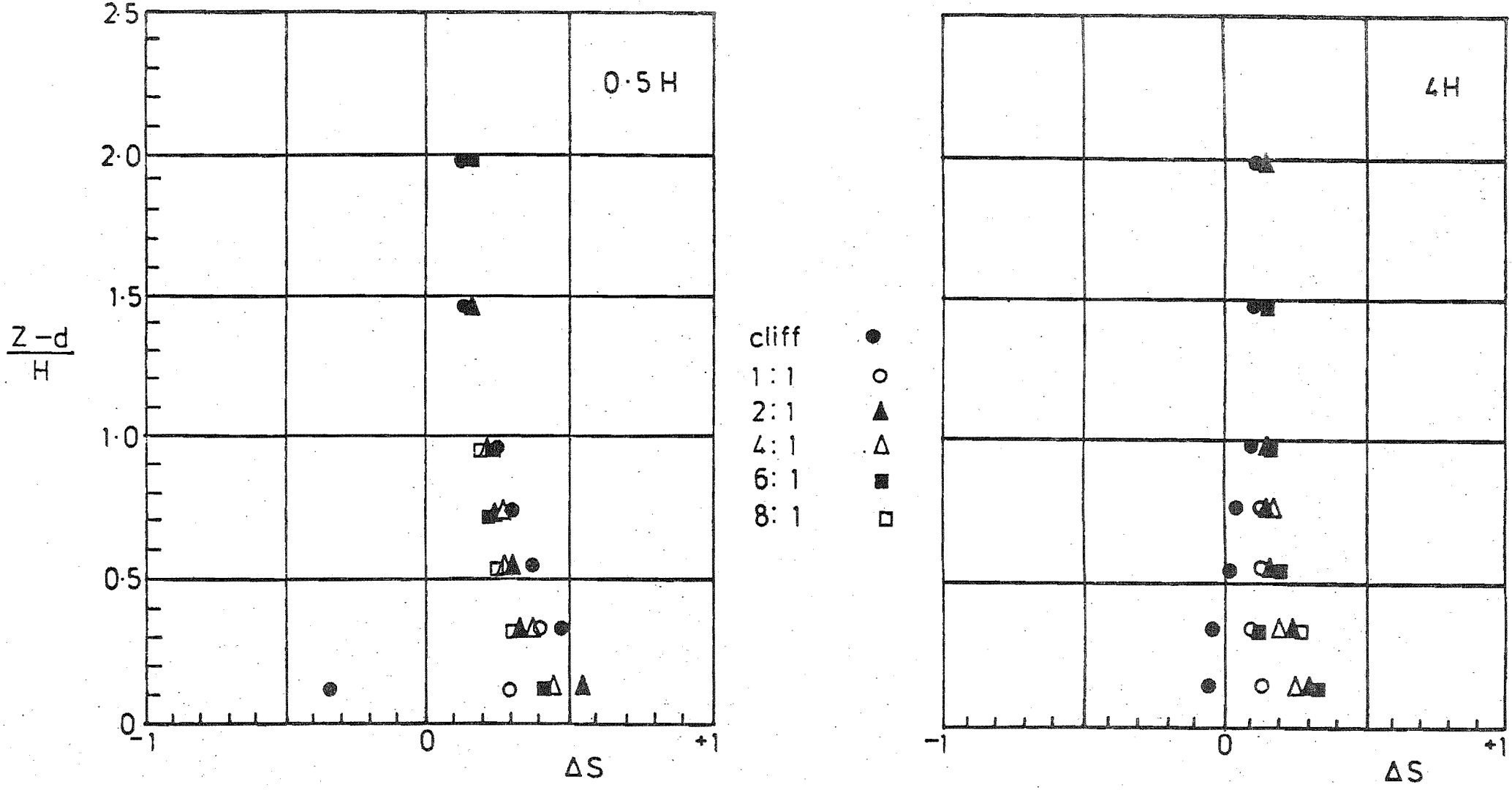

FIG 8·16 FRACTIONAL SPEED—UP RATIOS OVER THE SMOOTH MODEL ESCARPMENTS AT 0·5H AND 4H DOWNSTREAM OF THE CREST. (ϕ=0°).

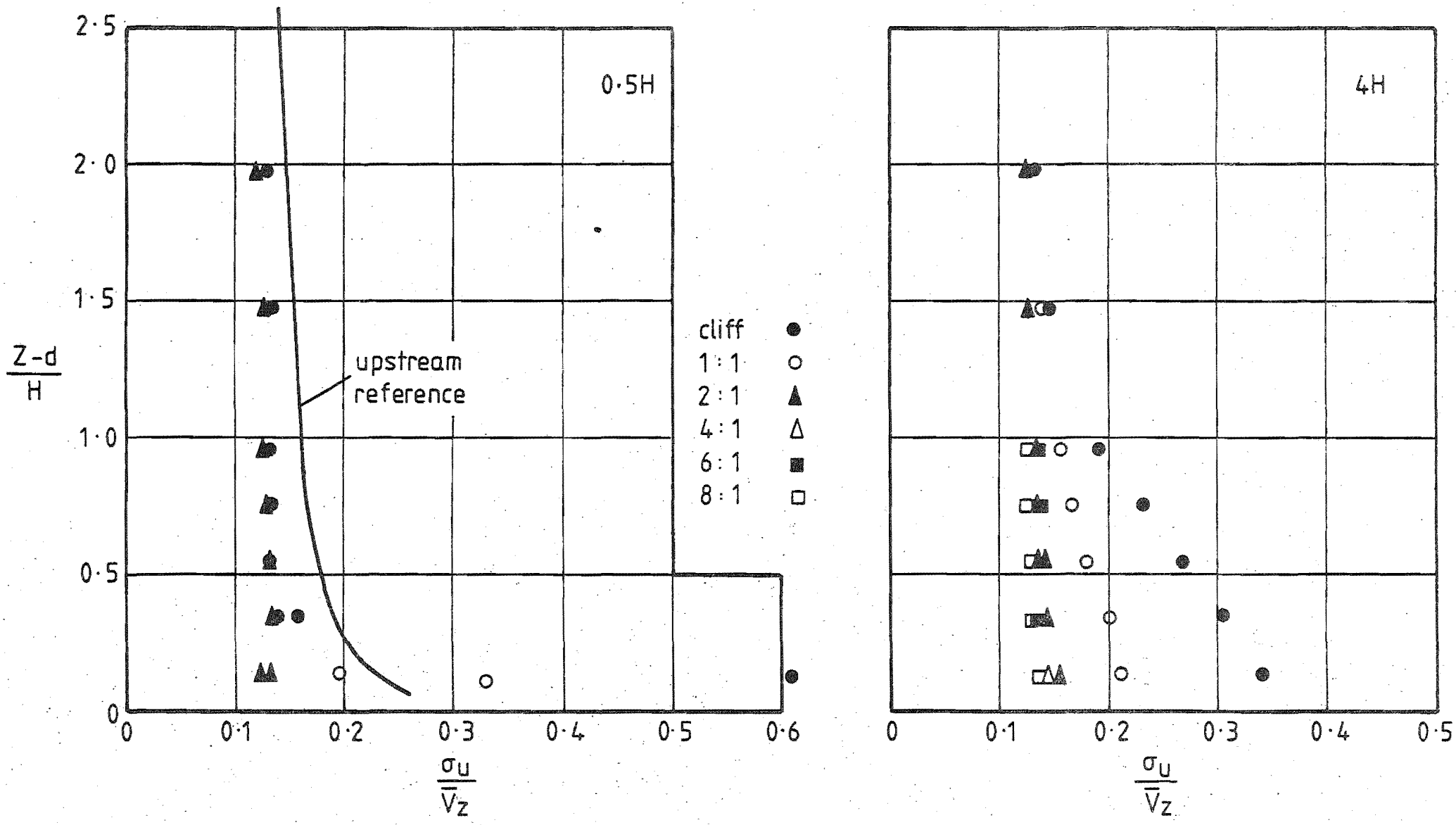

FIG 8·17 VARIATION OF LONGITUDINAL TURBULENCE INTENSITY OVER THE SMOOTH MODEL ESCARPMENTS AT 0·5H AND 4H DOWNSTREAM OF THE CREST (ϕ = 0°)

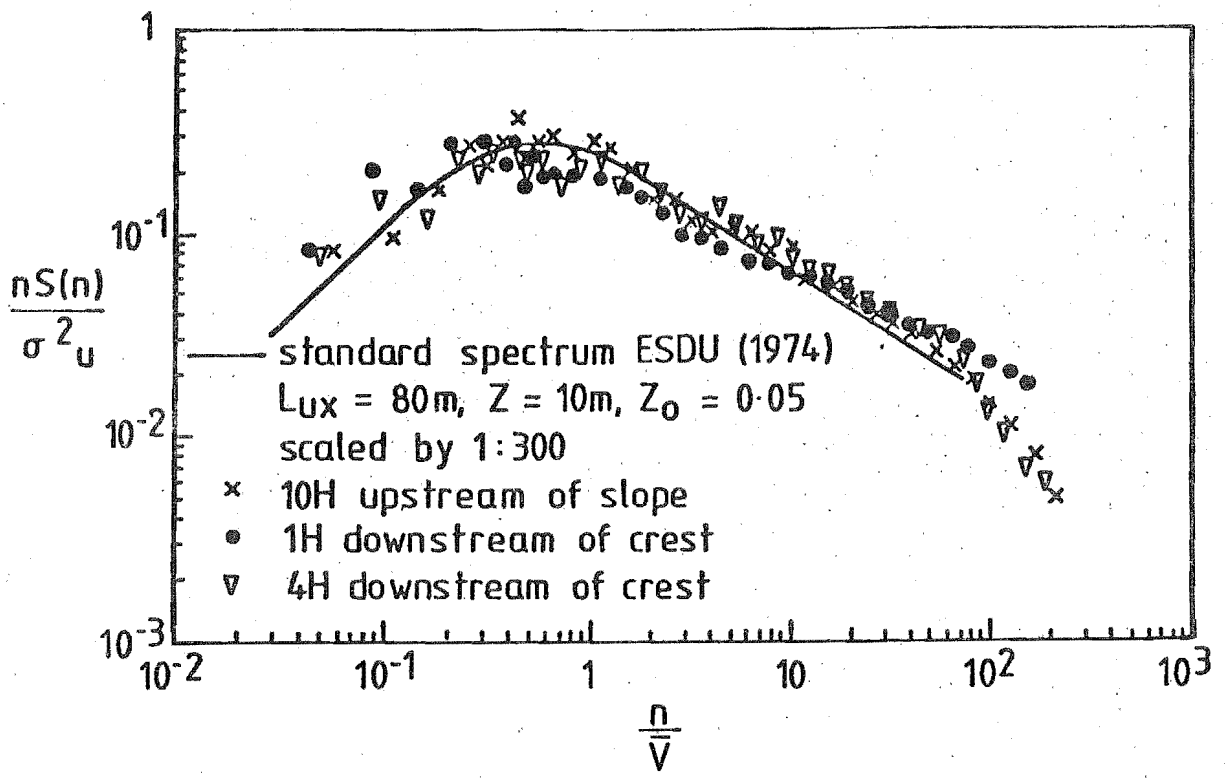

(a) cliff height, $\frac{Z}{H}$ = 1

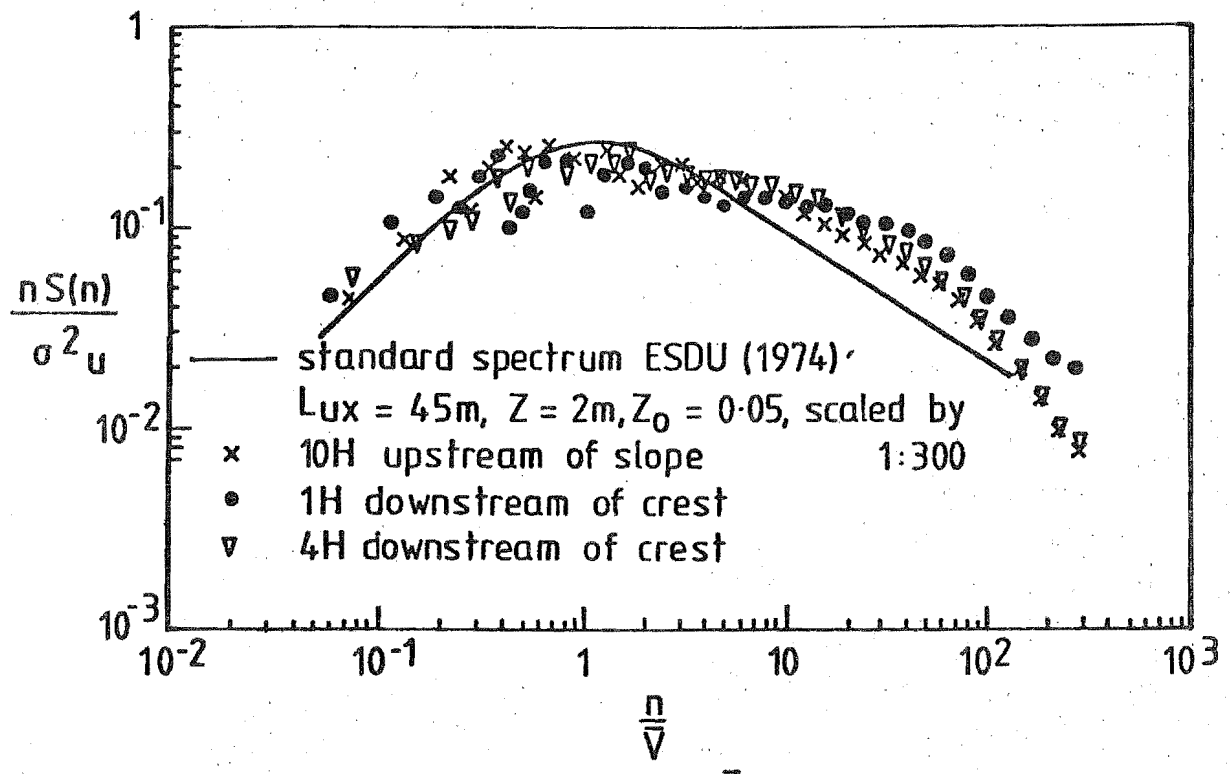

(b) cliff height, $\frac{Z}{H}$ = 0·25

FIG 8·18 LONGITUDINAL VELOCITY POWER SPECTRA FOR VARIOUS POSITIONS OVER THE SMOOTH CLIFF ESCARPMENT MODEL AT TWO HEIGHTS a) Z/H = 1, b) Z/H = 0·25 (ϕ = 0°)

effect of slope angle has been shown to be rather slight on both the mean velocity and turbulence intensity. However the trends have been somewhat obscured by the utilisation of various boundary-layer conditions, flow measuring techniques and the rough and smooth sets of models throughout the two test series.

A comparison of results in the form of the variation in fractional speed-up ratio, ΔS from the various tests has therefore been compiled and is illustrated in Figs.8.19 and 8.20. The effect of slope angle noted earlier as being slight, does in fact show a definite trend of increasing ΔS with increasing slope gradient close behind the crest at the 0.5 H position (Fig.8.19). It is also notable that significant ΔS values would have occurred for slope angles below the 8:1 (7.12°) gradient. The horizontal axes are not a linear scale of slope angle (1:1 represents 45°) which highlights the observation that only a small change in ΔS occurred for slope angles, θ between 45 and 90°. However the noted increase of ΔS with increasing θ did not occur at all positions. Firstly, in regions where separation or strong wake effects were evident (see Fig.8.19c) for the cliff and 1:1 slopes, the ΔS values were very much lower than expected. Secondly, close to the ground at the 4 H position over the smooth models (see Fig.8.20c), a reverse trend of decreasing ΔS with increasing slope gradient was evident. This latter deviation was likely due to the weaker wakes that existed behind the more gradual slopes, coupled with the expected flow acceleration due to the rough to smooth surface transition at the upstream edge of the models.

The ΔS data compared reasonably well between the smooth and rough tests of the second test series which was due in part to the great care exercised in the positioning of the probe and the use of the displacement depth where necessary when locating the correct velocities for the ΔS parameter calculation. However the results from the first test series for the steeper slopes were up to 15% higher than the second test series, but it must be remembered that the ΔS parameter was a result of four experimental readings ($\bar{V}_z$, $\bar{V}_\infty$ both on position and upstream), all with their encumbent errors. In addition, the region investigated was characterised by high velocity shear and turbulence especially close to the ground, which together with systematic errors in the probe position mentioned earlier, could have been responsible for these differences in the velocity and resulting ΔS discrepancies.

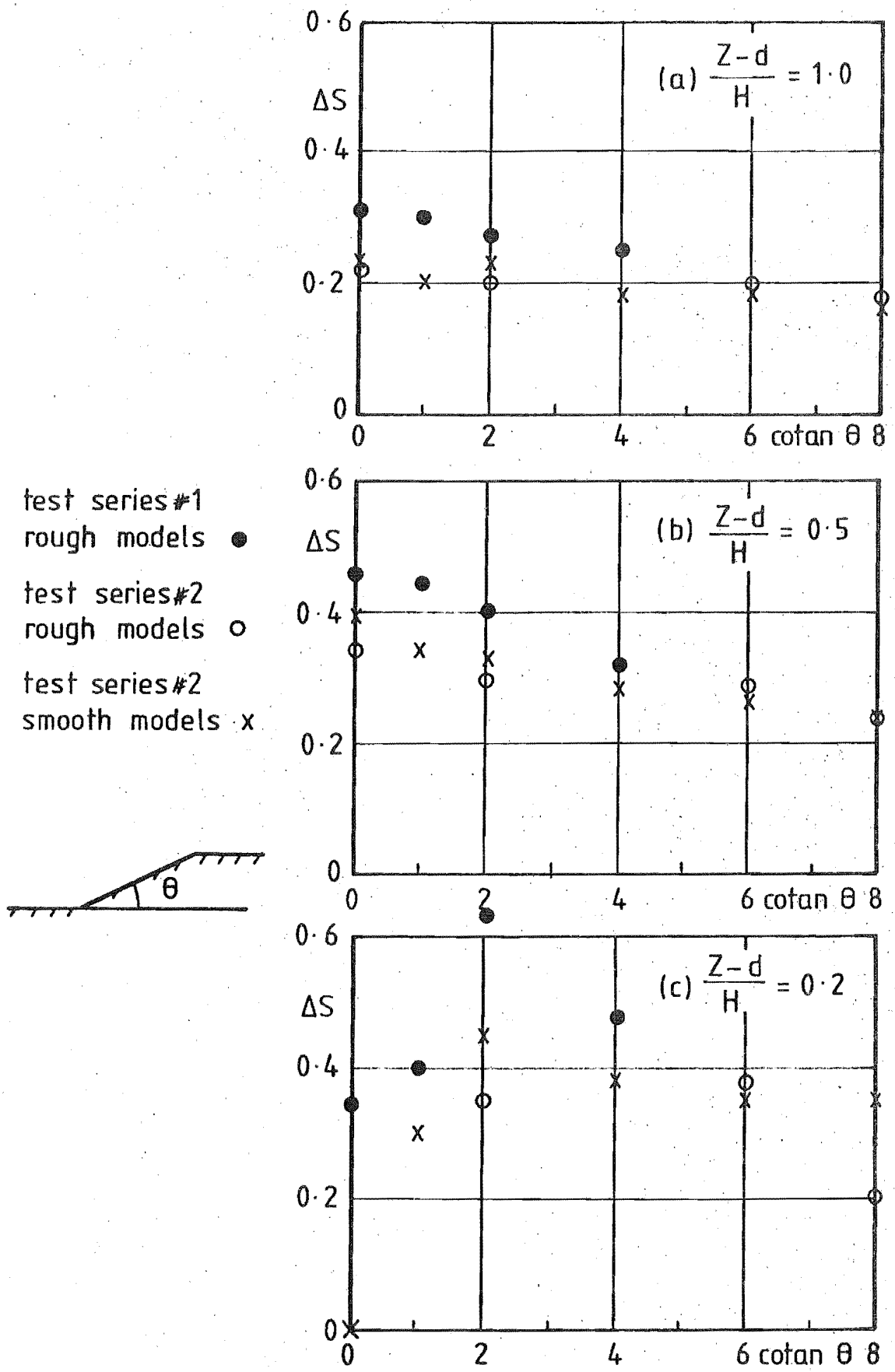

FIG 8·19 COMPARISON OF THE FRACTIONAL SPEED-UP RATIOS TAKEN FROM THE VARIOUS MODEL TEST SERIES AT 0·5H BEHIND THE CREST FOR VARIOUS SLOPE GRADIENTS (ϕ = 0°)

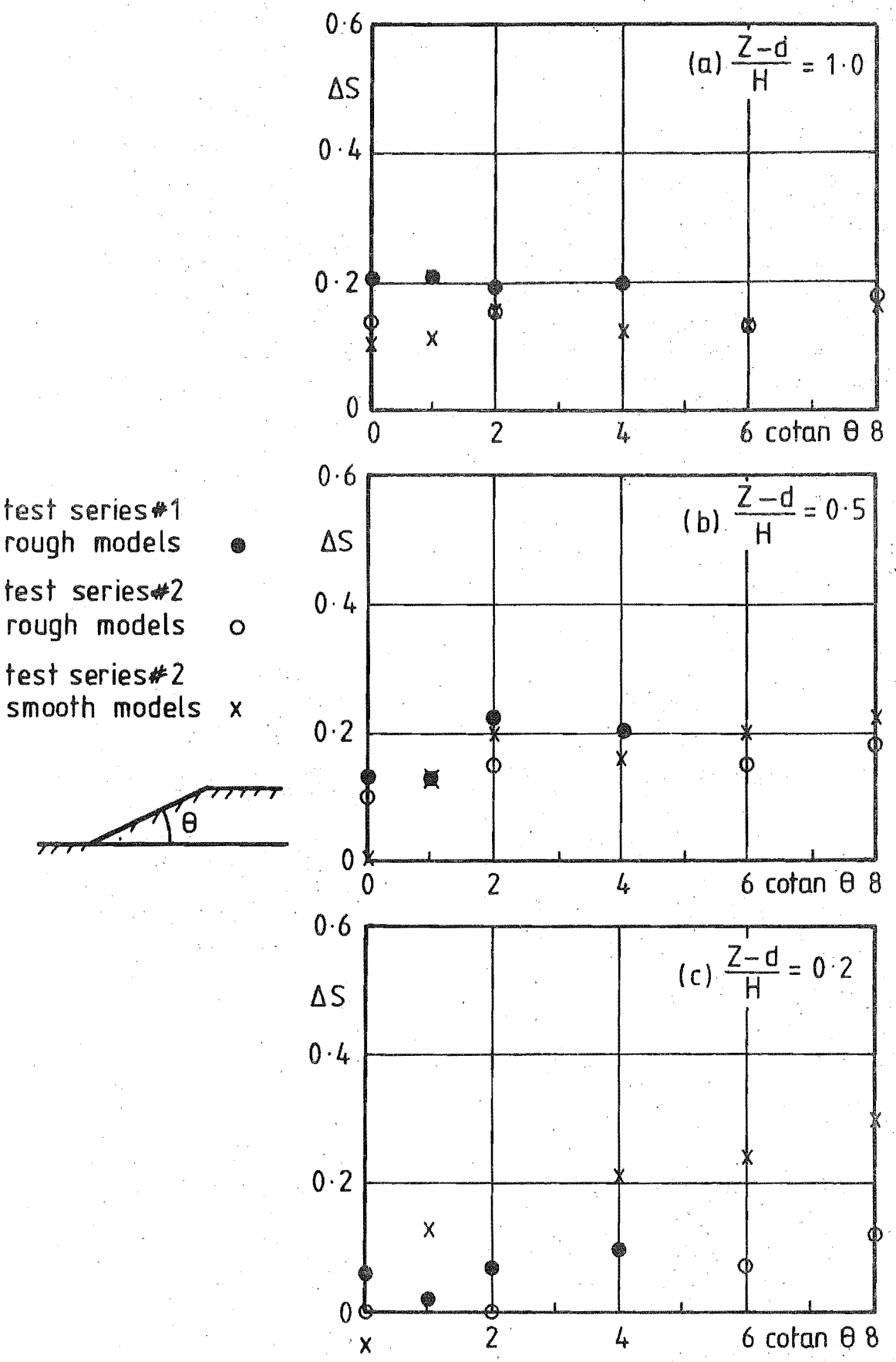

FIG 8·20 COMPARISON OF THE FRACTIONAL SPEED-UP RATIOS TAKEN FROM THE VARIOUS MODEL TEST SERIES AT 4H BEHIND THE CREST FOR VARIOUS SLOPE GRADIENTS.
(Φ = 0°)

It was also evident that the smooth models created less wake effects behind the crest and correspondingly higher velocities close to the ground and downstream of the crest. Wake effects were only evident for the cliff and 1:1 slopes of the smooth models whilst the rough models created significant wakes even with the 4:1 slope.

8.4 EFFECT OF WIND INCIDENCE ANGLE

The smooth cliff and 2:1 slope models were tested at various wind incidence angles and the resulting fractional speed-up ratios, ΔS were plotted in Figs.8.21 and 8.22 for these heights at the 0.5 H and 4 H positions. Close behind the crest a general decrease in ΔS was evident for increasing incidence angles for both slopes investigated. However, at the 4 H position which had a significant length of smooth surface upstream, the effect of the rough to smooth transition has predominated. This effect was strongest at positions close to the ground and at higher incidence angles where the smooth fetch upstream was the longest. Without this trend the value of ΔS would be expected to have reached zero for flows parallel to the crest when $\phi = 90°$.

8.5 MODELLED FIELD TESTS

The accurate model of the Amberley site shown in Fig.8.5 and the cliff model were tested at the same wind incidence angles as in the field to allow a direct comparison between field and model data. The results are presented throughout Chapters 6 and 7 with the field data and will therefore not be repeated here.

However it was thought worthwhile to compare the results obtained from the plain 2:1 model and the accurate Amberley model at the same wind incidence angle of 57°. The resulting fractional speed-up ratios, ΔS and the longitudinal turbulence intensities are presented in Figs. 8.23 and 8.24 from which it is evident that the greater accuracy in modelling made very little difference to the results. Perhaps there was a slight increase in turbulence at the 4 H position from the few trees and the eroded gully which were almost upwind at that wind direction. The similarity in the results did not prove that accuracy in the model details was unnecessary but did suggest that the Amberley site was indeed close to a 2:1, two-dimensional sloping escarpment, even at the large wind incidence angle that occurred.

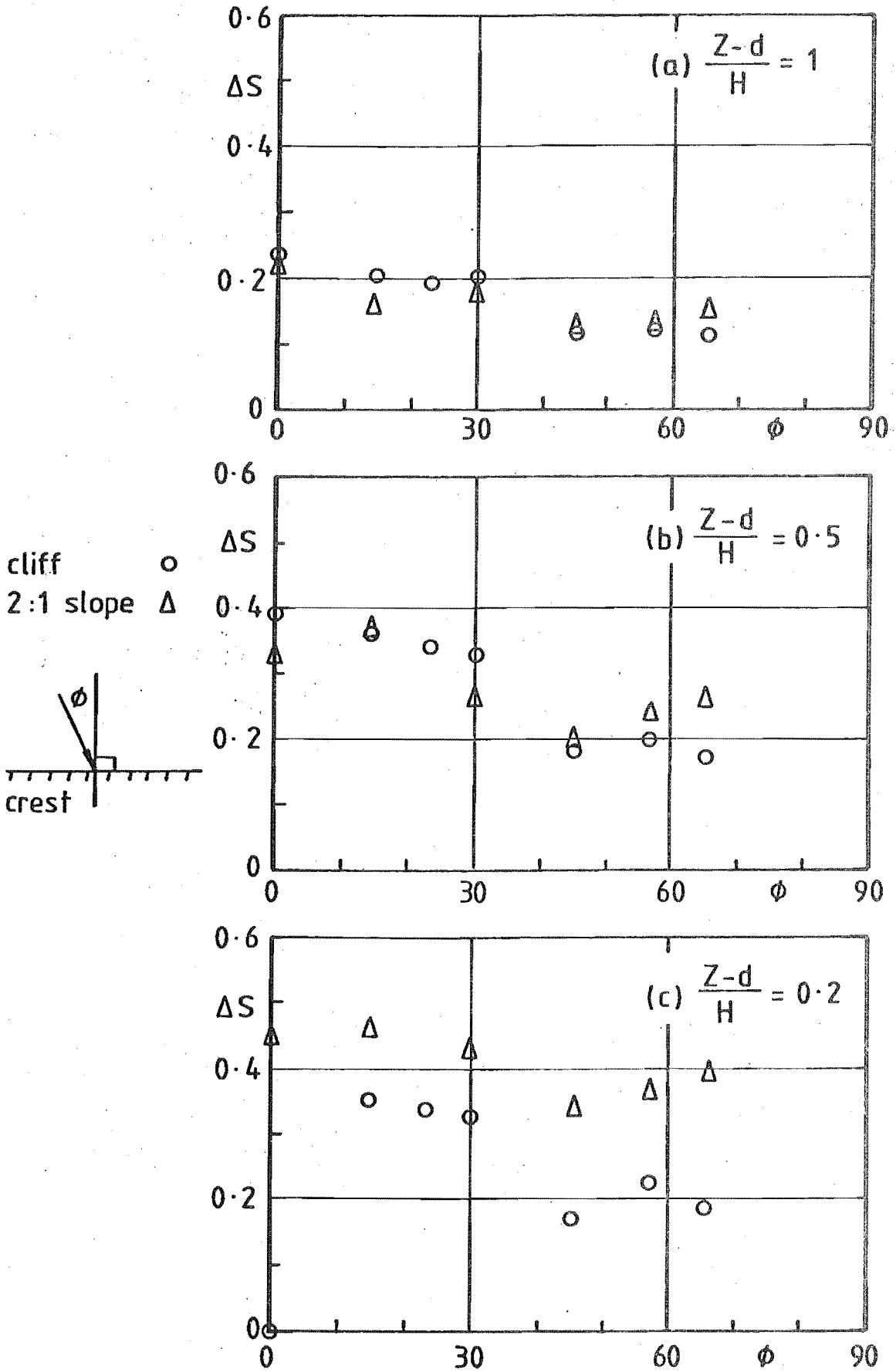

FIG 8·21 COMPARISON OF THE FRACTIONAL SPEED-UP RATIOS TAKEN FROM THE SMOOTH MODEL TEST SERIES AT 0·5H BEHIND THE CREST FOR VARIOUS WIND INCIDENCE ANGLES

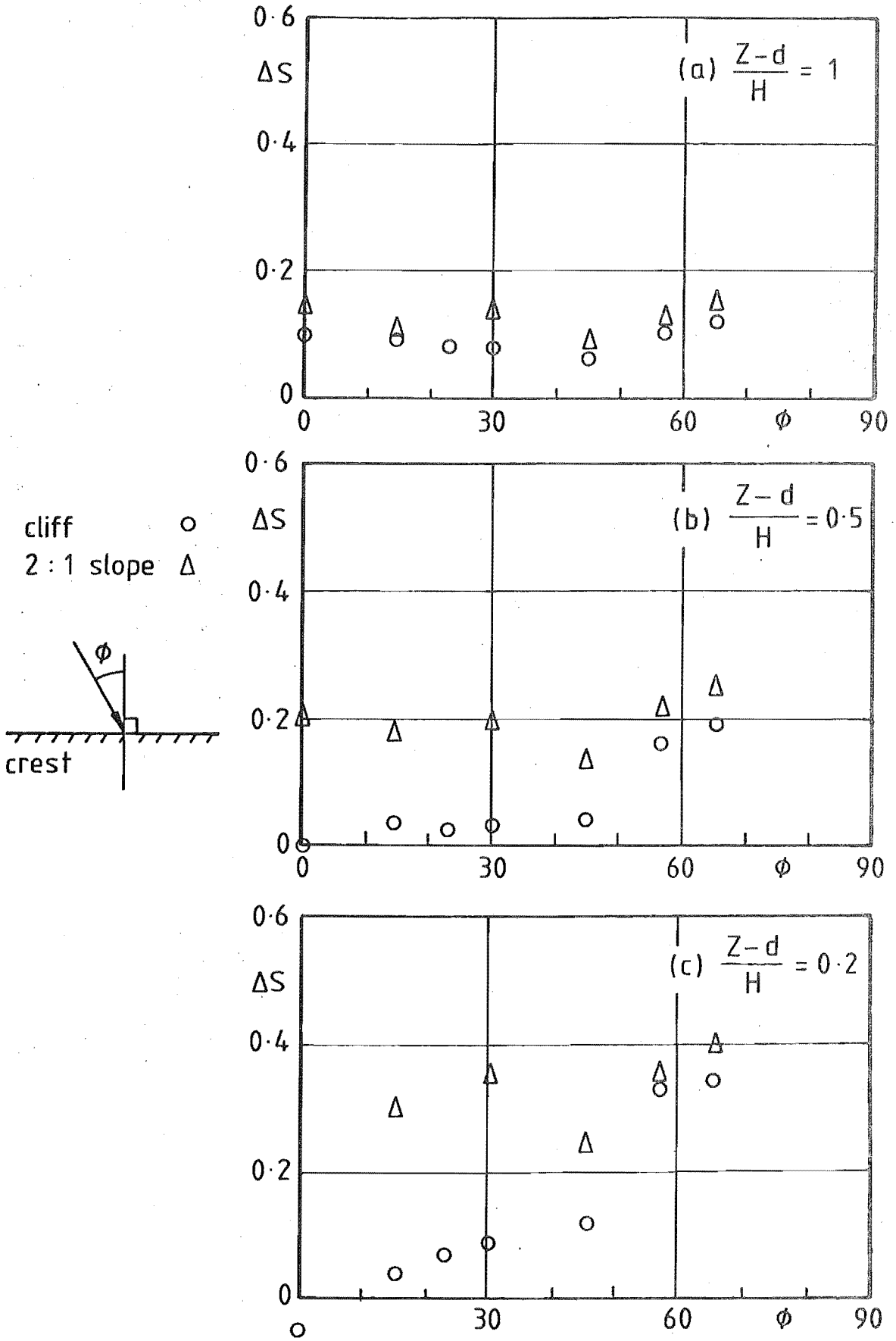

FIG 8·22 COMPARISON OF THE FRACTIONAL SPEED-UP RATIOS TAKEN FROM THE SMOOTH MODEL TEST SERIES AT 4H BEHIND THE CREST FOR VARIOUS WIND INCIDENCE ANGLES.

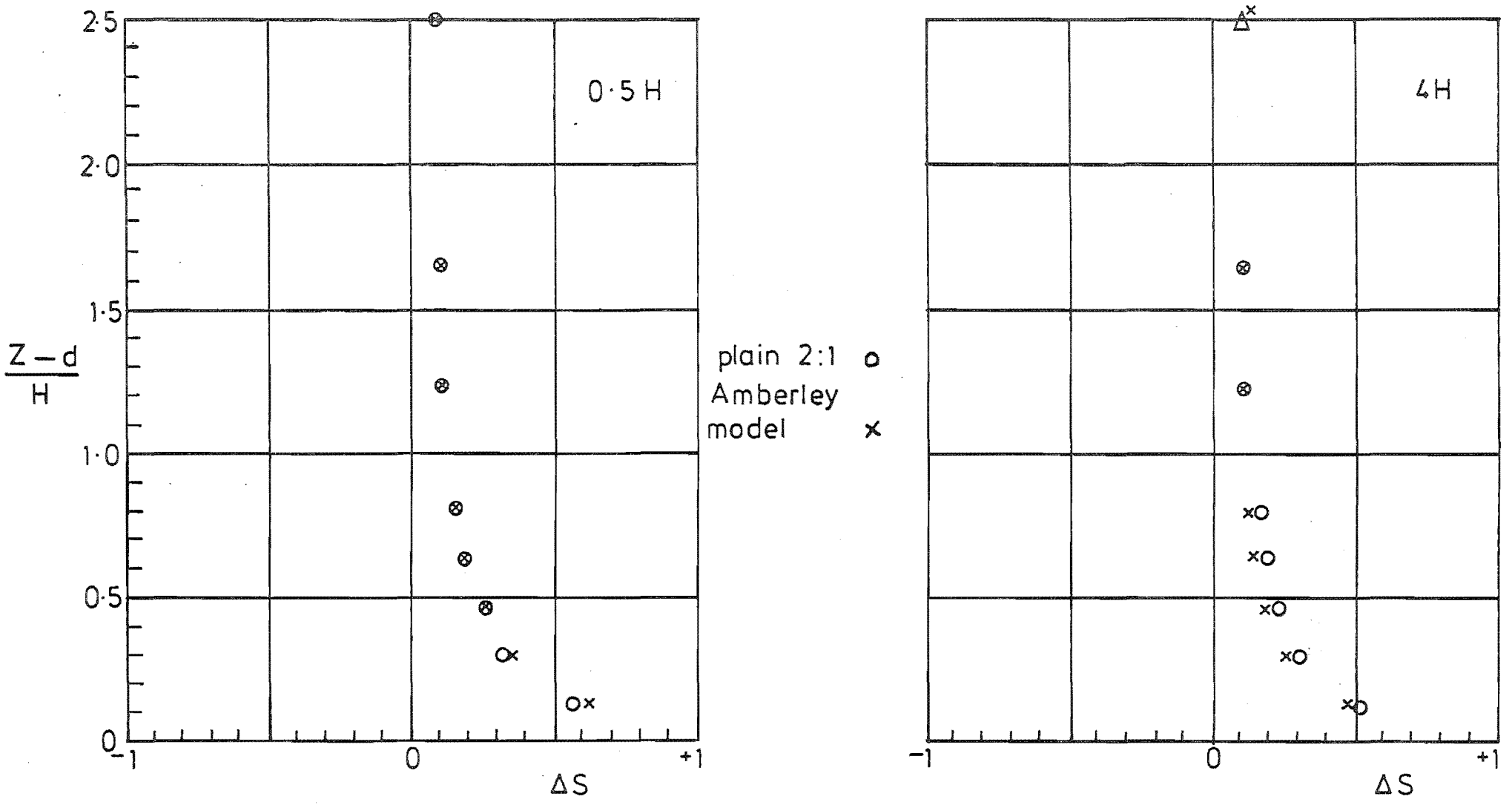

FIG 8·23 COMPARISON OF FRACTIONAL SPEED-UP RATIOS OBTAINED FROM AN ACCURATE MODEL OF THE AMBERLEY SITE AND A PLAIN 2D, 2:1 ESCARPMENT ($\phi = 57°$).

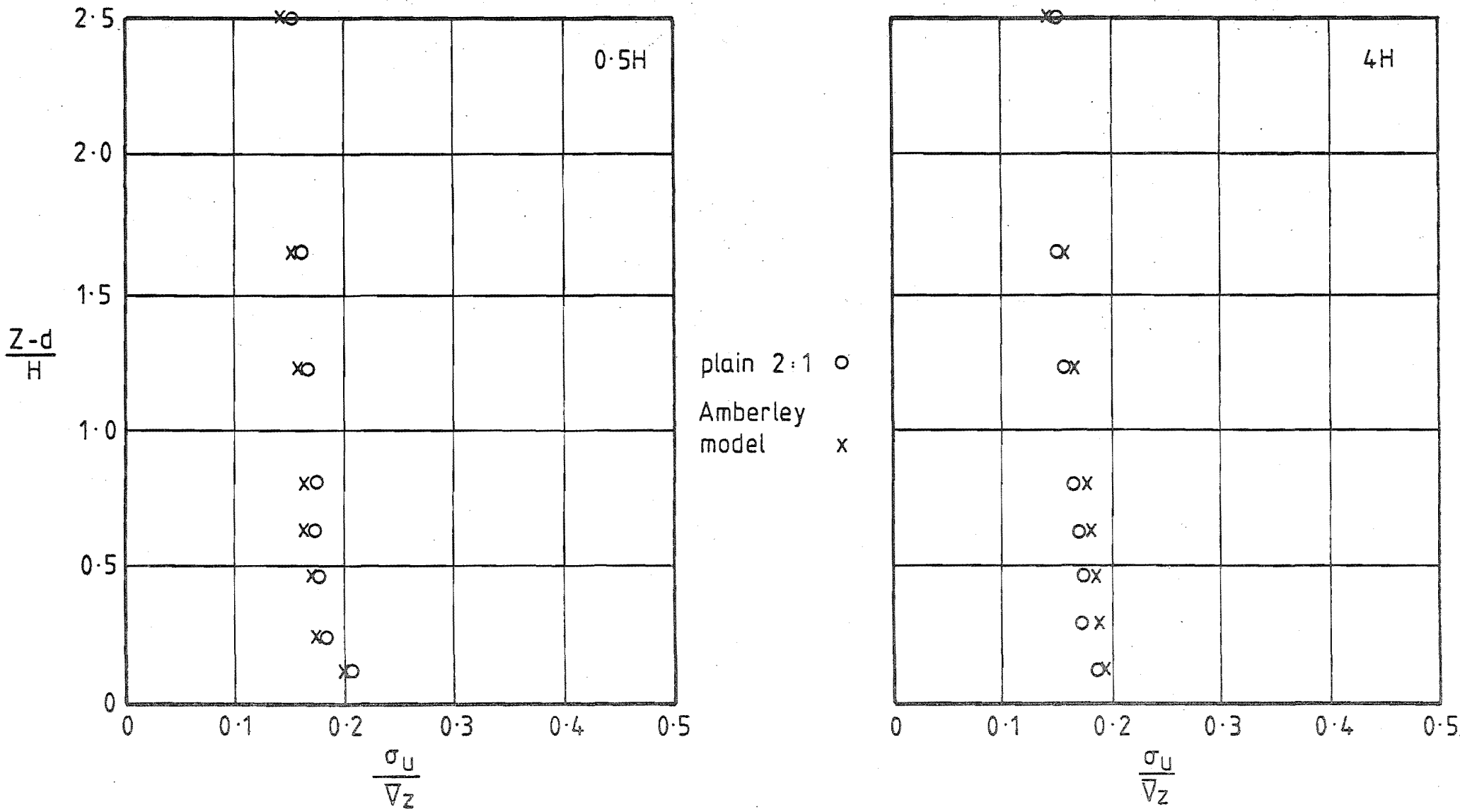

FIG 8·24 COMPARISON OF THE LONGITUDINAL TURBULENCE INTENSITIES OBTAINED FROM AN ACCURATE MODEL OF THE AMBERLEY SITE AND A PLAIN 2D 2:1 ESCARPMENT (ϕ = 57°)

8.6 CONCLUSIONS

* The model test programme involving rough and smooth surfaced models and the investigation of the effects on the flow of slope gradient and wind direction was discussed and justified.

* A brief description of the wind tunnel and the boundary-layer roughness elements was given. The undisturbed boundary-layers during the two test series were shown to be quite similar and adequately modelled the standard neutrally-stable open-country wind flow to a scale of 1:300.

* The models were shown to be of a suitable size for the wind tunnel boundary-layer and represented escarpments of a similar height to those investigated in the field without creating significant solid-blockage effects.

* The hot wire anemometer system was described briefly with its major errors and limitations. Sample repeated measurements on independent days indicated that the results were generally within 6%. The support and traversing unit was estimated to be accurate within ±0.5 mm or better. The calibration and linearisation of the anemometer against a pitot tube in the wind tunnel boundary-layer as done during the first test series, was shown to be less accurate than the use of the calibration unit that was utilised in the second test series.

* Model tests using rough surfaced escarpments normal to the wind flow indicated that the region where ΔS was greater than 0.1 was confined within the first three escarpment heights above the ground. The modification to the flow decreased rapidly with height from a maximum of ΔS near the crests of about 0.8 (at $\frac{Z-d}{H} = 0.14$) but persisted beyond ten heights downstream of the crests. A degree of shelter was evident within five escarpment heights upstream of the slope. The variation in slope angle within 90° and 14° had only a small effect on the mean flow behaviour.

* A wake region characterised by higher turbulence and lower mean flow speeds was noticed close to the ground, downstream of each crest. The turbulence intensity and the extent of the wake region increased with slope angle but weakened quickly in all cases to merge with the main flow after about ten escarpment heights downstream. A shift of the peak frequency in the longitudinal velocity power spectra towards higher frequencies corresponding to a decrease in the turbulence

length scale L_{u_x}, was noticed for the flow entering the wake region close behind the crest, but this modification was lost as the wake developed. Outside the wake region there was little change in the flow turbulence.

* Tests using smooth surfaced models yielded similar results to those using rough models except that the wake region was only evident behind the cliff and 1:1 slope. A trend was evident close behind the crests and outside the wake region for values of ΔS to increase with slope angle, but this trend was reversed further downstream where acceleration from the rough to smooth surface transition predominated. The influence from the slope angle was strongest for the more gradual slopes and very little effect was noticed above 45°.

* Close behind the crest a general decrease in ΔS was evident for increasing wind incidence angles but the effect was again lost further downstream due to the accelerating flows over the smooth surface.

* The accurate model of the Amberley field site yielded results that were very similar to those from the plain 2:1 escarpment model which suggested that the Amberley site truly represented a two-dimensional escarpment, even at the large wind incidence angle of 57°.

CHAPTER 9

DISCUSSION OF RESULTS

The results from the two field investigations of the 2:1 and cliff escarpments have been presented in Chapters 6 and 7 and followed by the supplementary model tests in Chapter 8 which covered a wider range of slopes and wind directions. The purpose of this chapter is to compare the results and implied trends evident in these three chapters with those contained in the existing literature reviewed earlier in Chapter 3. The following discussion however has been confined to only the escarpment shapes and flow conditions encompassed by the project. Extrapolation to other situations such as regular hill shapes has been avoided due to the difference in downwind hill shape which has been identified as a parameter of major significance.

9.1 PROPELLER AND CUP ANEMOMETER TEST RESULTS

The measurement of the mean wind speeds by Bowen and Lindley (1974) over the same two escarpments as those of the present tests provided a unique opportunity for a direct comparison with the present field data as no other field data of a similar situation were known to exist. The tests by Bowen and Lindley described in Chapter 3 were conducted under very similar conditions as those of the present tests except for the lower wind speeds and the smaller wind incidence angle, ϕ encountered during the 2:1 escarpment investigation at Amberley. However the major significant difference between the two tests was in the use of cup anemometers by Bowen and Lindley which as explained in Chapter 3, were capable of high over-estimation of the mean wind speeds in turbulent flows.

The normalised mean wind speeds from the present field tests and those from Bowen and Lindley (1974) are shown in Figs. 9.1 and 9.2 for a direct comparison of the flow data over the 2:1 and cliff escarpment. Good agreement is apparent between the two data sets for the 2:1 slope but in regions of high turbulence behind the cliff, the cup anemometers have indicated unusually high readings as predicted. Correspondingly high values of ΔS in the turbulent wake regions would have occurred and the region of influence downwind of the crest would have been somewhat over-estimated in extent.

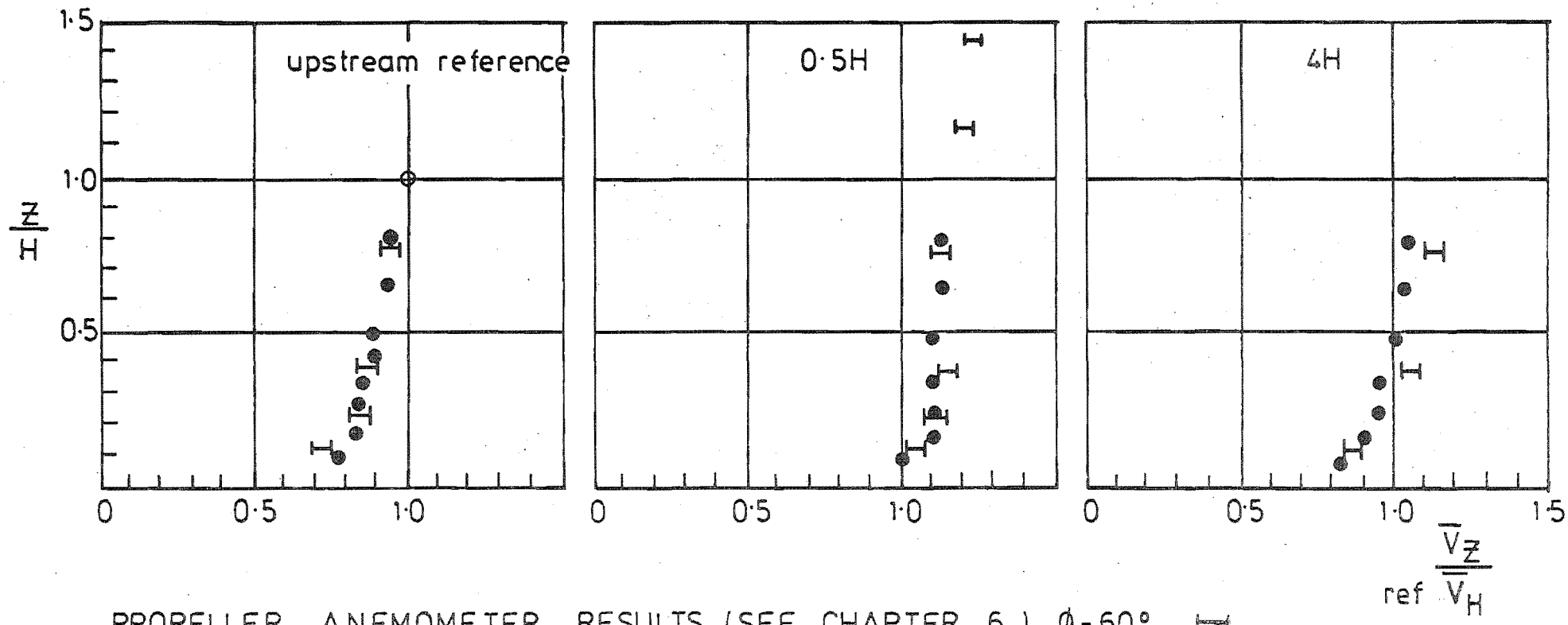

PROPELLER ANEMOMETER RESULTS (SEE CHAPTER 6), $\phi = 60°$
CUP ANEMOMETER RESULTS (BOWEN AND LINDLEY, 1974) $\phi \approx 20°$

FIG. 9·1 COMPARISON OF THE FIELD MEASUREMENTS WITH CUP ANEMOMETER READINGS OF THE MEAN WIND SPEED OVER THE 2:1 SLOPING ESCARPMENT AT AMBERLEY FOR AN OBLIQUE WIND INCIDENCE.

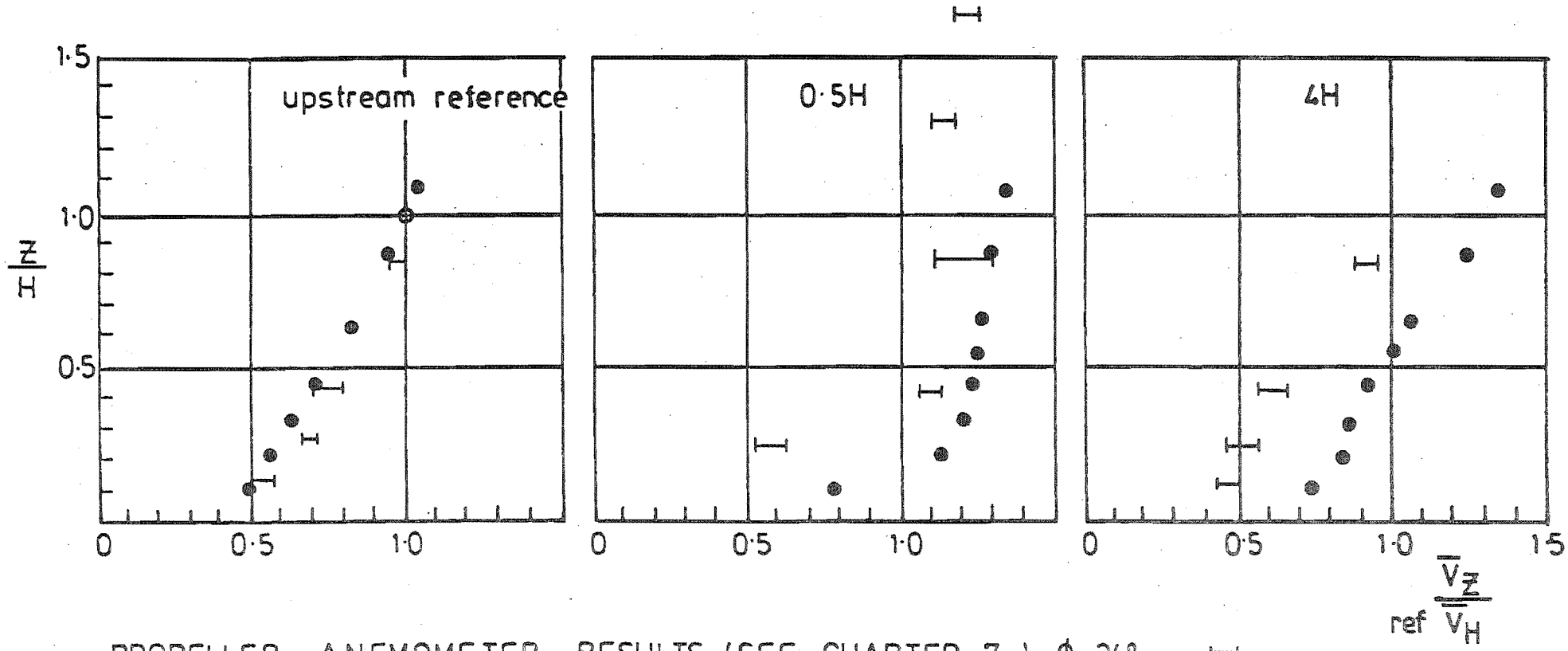

PROPELLER ANEMOMETER RESULTS (SEE CHAPTER 7). $\phi = 24°$
CUP ANEMOMETER RESULTS (BOWEN AND LINDLEY, 1974) $\phi \approx 0°$

FIG. 9·2 COMPARISON OF THE FIELD MEASUREMENTS WITH CUP ANEMOMETER READINGS OF THE MEAN WIND SPEED OVER THE CLIFF ESCARPMENT AT RAKAIA FOR APPROXIMATELY NORMAL WIND INCIDENCE.

9.2 MODEL AND FIELD TEST RESULTS

The field recordings presented in Chapters 6 and 7 were plotted together with the model test results from Chapter 8, which utilised accurately reproduced models with similar test conditions and wind incidence angles as in the field. A direct comparison of model and field data is therefore possible and any significant discrepancies evident between the two are discussed below.

The model and field velocity-height profiles over the 2:1 escarpment shown in Fig.6.13, behaved in a similar fashion except for the fuller field profile at the reference upwind position. Correspondingly higher values of ΔS have resulted with the model tests, especially at the 4 H site (Fig.6.14). This excess velocity noted in the model tests is also very marked in both the model cliff data sets (Figs.7.13, 7.14). The discrepancy is greatest at the 4 H position which implies that a further influence is present which decreases with increasing height. In the case of the NW wind (ϕ = 65°, Fig.7.14) the discrepancy is also significant at the 0.5 H position.

Several factors may be responsible for this common discrepancy between the model and field tests. The models that were tested had smooth ground surfaces which contrasted with the 3 mm roughness elements used to create the upstream boundary-layer. As a result, the flow close to the ground would not have been in equilibrium and would have been subjected to accelerations due to the rough to smooth transition. This effect would, in the same manner as the observed discrepancies, have increased in magnitude with distance downwind of the roughness transition or in other words, increased with decreasing slope, distance behind the crest and increasing wind incidence angle. An additional small speed-up effect due to the 4% blockage from the model in the wind tunnel may also have contributed.

A further factor that would have enhanced the observed discrepancy would have been due to the field results representing the mean local longitudinal velocity, whereas the horizontal hot wire would have been sensitive to the horizontal plus vertical component in a plane parallel with the mean flow direction. However the vertical component at both positions behind the crest was shown in the field tests to be insignificant and the deviation of the local wind vector from the mean wind direction was mostly less than 10° (Figs.6.15 and 7.17). In addition, the hot wire is known to have

increased error in highly turbulent flow as mentioned in Chapter 8 and would not be reliable in the highly turbulent wake areas which coincided with the major discrepancies between the model and field test data. In the wake areas especially behind the crest of the cliff, flow reversals may have occurred for a certain fraction of the time and the hot wire would have been insensitive to this change in sign and thus over-estimated the mean flow speeds. The propeller anemometers on the other hand, would have subtracted these reversed flow readings thus yielding a more correct mean wind speed.

The separation point was fixed at the crest of the sharp edged escarpments for the Reynolds numbers associated with the model and field tests. However Bouwmeester (1978) reported that a decrease in surface roughness near the crest of a hill decreased the onset of separation. In the case of the smooth escarpments, the change from rough to smooth ground surface may have reduced the extent of the separated area thus increasing the flow velocities close to the ground. It was in fact noticed in Chapter 8 that the smooth models produced less wake effects and higher flow velocities close to the ground than the 'rough' models.

Better agreement was evident in the variation of the longitudinal velocity variance shown in Figs.6.16 and 7.18 but the turbulence intensities (Figs.6.19 and 7.21) showed significant discrepancies which would have been almost entirely due to the influence of the mean velocity used in its calculation.

9.3 THE INNER LAYER

The inner layer which was defined and discussed in Chapter 3 may have been applicable to the most gradual slope considered in the model tests (8:1) but the 2:1 slope studied in the field was definitely beyond the scope of the theoretical explanation offered by Jackson and Hunt (1975). However as a matter of interest these two slopes were considered using this concept and yielded (equation 3.20) an inner layer depth, ℓ of approximately 1.3 m ($\ell/H \approx 0.1$) for the 2:1 field escarpment and 3.8 m ($\ell/H \approx 0.3$) for the 8:1 model with the same H/Z_o.

In the case of the 2:1 data, the lowest anemometer array and model test position was above the estimated inner layer depth and no unusually high Reynolds stresses or a local peak in the ΔS profiles

were evident. For the 8:1 model test, the lowest measurement position should have been immersed in the inner layer but no ΔS peak was recorded. Reynolds stress measurements were not taken in the model test series which could have identified the extent of this inner region. The relatively steep slopes of the escarpments considered and the sharp crests with resulting strong wake effects, may have been sufficient to destroy any evidence of an inner layer. Bouwmeester et al (1978) also noted a lack of evidence for an inner layer with their model hill test results.

9.4 FRACTIONAL SPEED-UP FACTOR

The variation with height above the crest of the fractional speed-up factor, ΔS in the model test series was compared with the limited data in the literature and the results presented in Figs. 9.3 and 9.4. In all cases a rural boundary-layer was used but with varying and sometimes unspecified depth. The model test data from the present tests were plotted with a displacement depth.

The model test results from Freeston (1974) (20° slope or $H/L = 0.73$) and Pearse (1978) showed good agreement with the present test data for the smooth model, $H/L = 1$ (2:1 slope), but the data from Serra (1949) was consistently high and of unspecified accuracy. The analytical approach formulated by Jackson (1977) showed very good agreement for the 8:1 slope which was within the slope range of his theoretical analysis but when applied outside the range for steeper slopes, the results over-estimated ΔS significantly. The finite element method of Astley (1977) yielded consistently good agreement for all slopes considered. The significant variation in results between the rough and smooth model test series has already been discussed in Chapter 8. However the influence of the rough to smooth transition over the smooth models is clearly evident in the 8:1 slope data of Fig.9.4 close to the ground, where the smooth model data exceeded the rough model data significantly.

9.5 UPSTREAM SLOPE GRADIENT

The effect of slope angle evident in the model test results which were presented in Chapter 8, varied with height and position and were largely influenced by the extent and intensity of the wake area. Increasing ΔS values were noted with slope gradient outside

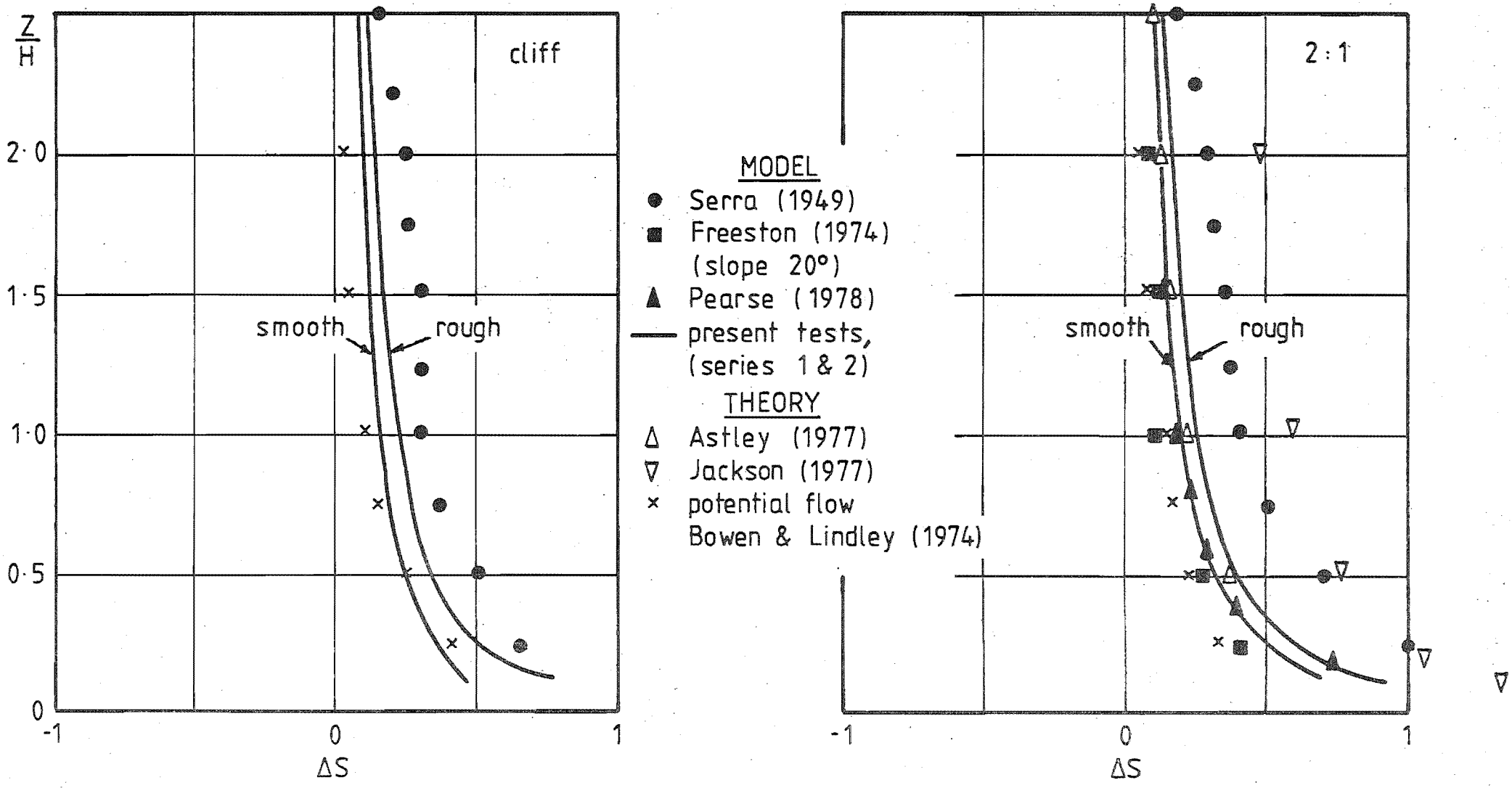

FIG 9·3 COMPARISON OF EXISTING FRACTIONAL SPEED-UP DATA FROM MODEL TESTS AND THEORY ABOVE THE CREST OF A CLIFF AND 2:1 ESCARPMENT NORMAL TO THE FLOW IN A RURAL BOUNDARY-LAYER.

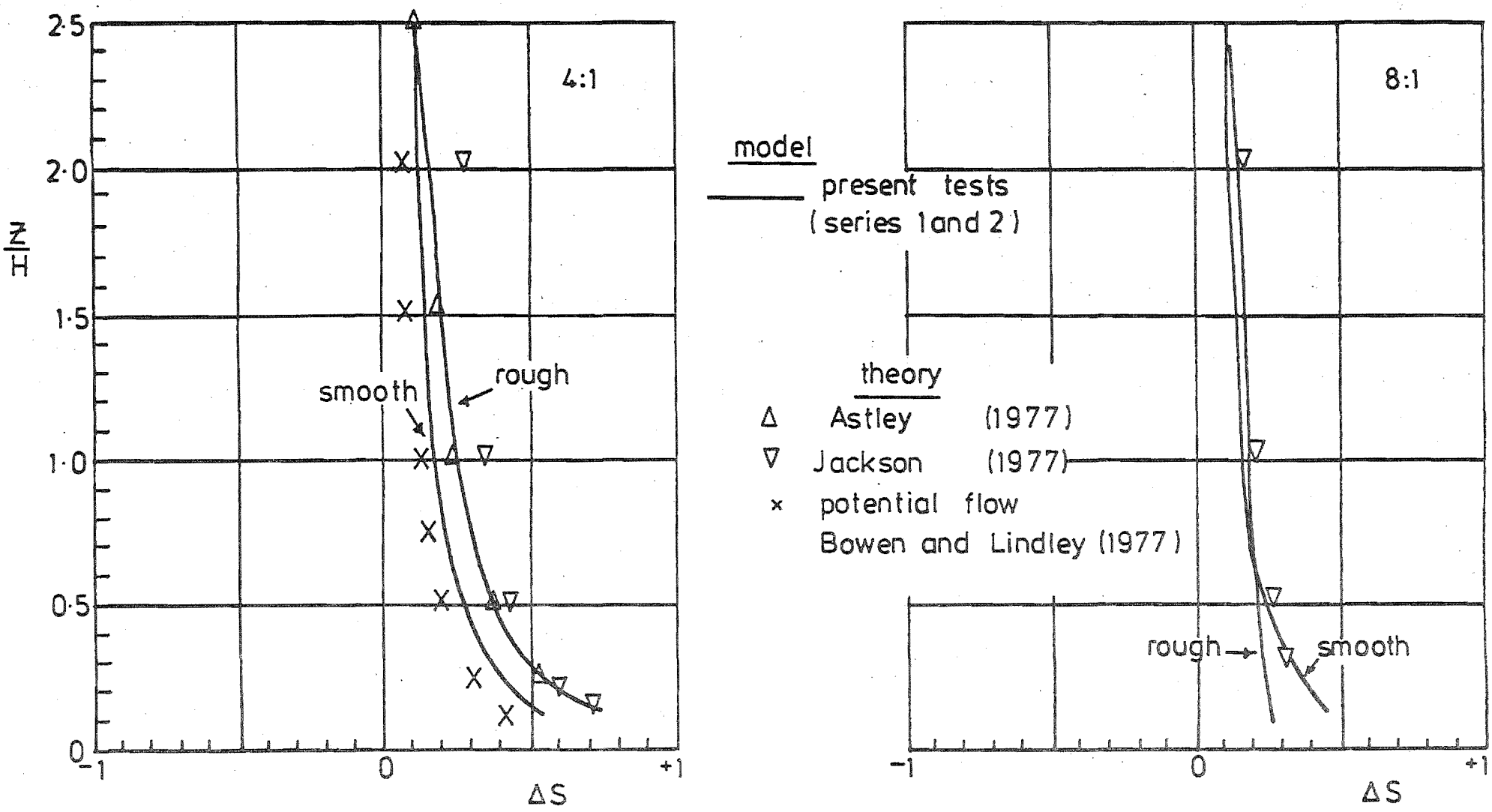

FIG 9·4 COMPARISON OF EXISTING FRACTIONAL SPEED-UP DATA FROM MODEL TESTS AND THEORY ABOVE THE CREST OF A 4:1 AND AN 8:1 ESCARPMENT NORMAL TO THE FLOW IN A RURAL BOUNDARY-LAYER.

the wake area up to a limit corresponding to an H/L of approximately 1.0, although linearity with H/L was limited to slopes below $H/L \approx 0.4$.

Jackson's (1977) analytical method suggested that the maximum ΔS occurred above the crest at a small height in the inner layer. Consequently the value of ΔS increased rapidly towards the ground reaching a well defined maximum at $Z = \ell/10$ with the velocity decreasing through the inner layer in perhaps, a logarithmic profile (Jensen and Peterson, 1978). However the present model tests and those of Bouwmeester et al (1978) have been unable to locate this maximum position and the ΔS values continued to increase rapidly towards the ground. It was therefore thought to be quite misleading to compare maximum values of ΔS using model test data. However it was thought worthwhile to compare ΔS values measured at a small defined height above the crest, which has been done in Fig.9.5 for $Z/H = 0.2$ and zero wind incidence angle for the model and field test data together with available results from the literature. Where a maximum value of ΔS was clearly defined at a height above $Z/H = 0.2$ then this value was used, otherwise the ΔS value at 0.2 was utilised. For the 10 - 15 m escarpment heights investigated in the field, the height corresponding to $Z/H = 0.2$ was just above head level. In most applications, the flow below this level would be dominated by local terrain or vegetation and would be of little general interest. The field results were also incorporated in Fig.9.5 after modifying the values using trends shown by the model data, to allow for the oblique wind incidence angles encountered.

The influence of the wake and subsequent separation for the steeper slopes is evident and suggests that the maximum values of ΔS lie between 0.5 and 0.7 depending on the flow and local terrain conditions and occur for slopes close to $H/L = 1.0$ when separation is absent. This behaviour confirms the conclusions of Bouwmeester et al (1978) and Sacré (1973. However it should be noted that higher ΔS values may be obtained if a lower height was adopted and the envelope in Fig.9.5 would then change its vertical disposition but retain its general shape.

For gradual slopes where $H/L \leq 0.4$ say, the increase in ΔS_{max} with H/L was most significant and the data accumulated in Fig.9.5 suggested that for the plain forward facing escarpment

$$\frac{\Delta S_{max}}{H/L} \approx 1.0 \text{ for } H/L \leq 0.4 \qquad 9.1$$

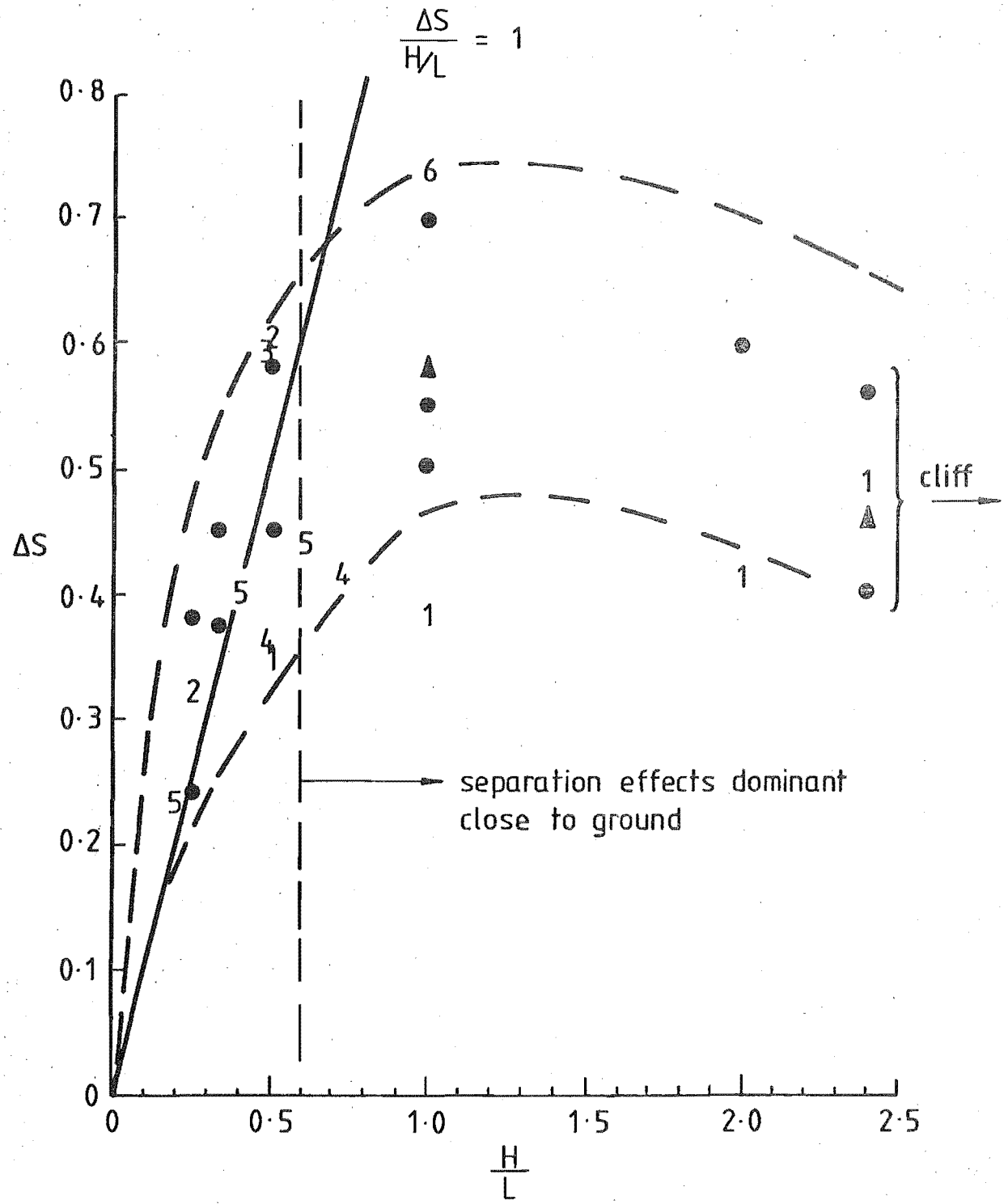

FIG 9·5 VARIATION OF FRACTIONAL SPEED-UP FACTOR, ΔS WITH H/L AT THE ESCARPMENT CREST. VALUES TAKEN FROM PRESENT TESTS AND LITERATURE AT Z/H = 0·2 WHERE POSSIBLE. (φ = 0°)

9.6 WIND DIRECTION

9.6.1 Effect of Wind Incidence on the Velocity Speed-up

The results of the model tests showing the effect of the wind incidence angle on the fractional speed-up factor, ΔS were presented in Figs.8.21 and 8.22 for the 2:1 and cliff escarpments. The results provided a means of converting the field data obtained under quite oblique incidence angles to effective data at normal incidence for a comparison of ΔS results in Fig.9.5.

The values of ΔS in Figs.8.21 and 8.22 showed an expected decrease with increasing incidence angles away from the normal for situations unaffected by the rough to smooth transition, although little change was noted for angles of less than 30°. It is logical to expect the ΔS factor at 90° incidence to have a value of zero. No other data was available in the literature to allow a comparison of these results.

9.6.2 Change in Flow Direction Over the Slope

As predicted by Taylor (1977b), the flow over the 2:1 escarpment below a height of about 0.75 H was measured in the field (Fig.6.15) to change direction over the slope by about 10° so as to negotiate the slope at a steeper angle. However this behaviour was not evident in the cliff field data (Fig.7.17) which indicated a weak trend in the opposite direction. This apparent contradiction may be attributed to the strong flow of air that was noticed to flow along the cliff face for the oblique wind angles encountered and which could have affected the air flow close to the ground behind the crest.

9.7 FLOW TURBULENCE

The predicted performance of the anemometers from Chapter 4 appeared to be close to that observed in the field. This agreement is illustrated in Fig.6.10 showing the velocity spectrum from the Amberley array #1 at the Z = 10 m reference position in which the drop off in high frequency accuracy was well predicted.

The characteristics of the turbulence observed in the model and field tests were compared and discussed in detail in Chapters 6, 7 and 8 and coincided reasonably well where a comparison was available. However the presence of the escarpments had very little

effect on the turbulence of the flow outside the wake regions behind the crest, which was confirmed by the conclusions from the model test results of Bouwmeester et al (1978). The turbulence appeared to be convected along the streamlines with no significant change except by virtue of the fact that the streamlines were compressed near the crest which brought the upstream turbulence closer to the ground. The large changes in turbulence intensity were invariably due to the changes in mean wind speed unless the position was immersed in the wake region.

The wake region was characterised by highly turbulent flows and lower mean velocities. In the field tests a return flow was detected close to the ground behind the cliff, but the hot wire measurements were not able to detect an equivalent flow in the model tests. No evidence of flow separation was noticed by Counihan (1973) with his cliff model either. The turbulence in the wake region contained increased energies of higher frequencies. The extent and intensity of the wake region increased significantly with slope angle as shown also by Counihan (1973), as well as with the surface roughness of the models.

9.8 GUST VELOCITIES

The peak gust velocities recorded during the field tests have been presented in Figs.6.28 and 7.29 and showed a strong dependence with the local turbulence intensity. This dependence was confirmed by the various empirical relationships put forward in the literature which were discussed in Chapter 2. With the field test results now available, the opportunity was taken in this chapter to test these relationships and any systematic influence from the terrain would then become evident by unusual departures from the predicted behaviour.

9.8.1 Effect of Averaging and Recording Times

As described in Chapter 5, the longitudinal velocity recorded every $^{1}/_{16}^{th}$ s at each instrument array position was scanned over the whole length of the recording time, T_o and the peak velocity reading located. The data situated symmetrically on either side of this peak reading was then averaged over different periods to produce effective peak velocities with T = $^{1}/_{16}$, 0.5, 1, 1.5 etc. up to 5 seconds averaging time. In order to check the empirical equation 2.48 namely

$$\frac{\hat{V}(T,T_o)}{\bar{V}} = 1 - A \log_{10}\left[\frac{T}{T_o}\right] ,$$

the peak velocities were averaged over the number of recordings available for each averaging time. Three examples representing conditions of different turbulence intensities are shown in Fig.9.6 as gust factor, $\frac{\hat{V}}{\bar{V}}$ against averaging time, T. The plots confirmed the accuracy of equation 2.48 for $T \geqslant 0.5$ s and revealed no obvious influences from the local terrain, even in the wake region. The value of A is in fact represented by the gradient x(-1) of each line drawn in Fig.9.6.

It was also evident that the gust factor averaged over T = 0.5 s behaved in the same predictable manner as those averaged over longer periods, despite the upper frequency limit of about 0.25 Hz estimated for the anemometers in Chapter 4. The relationship between the averaging time of the highest peak gust capable of being recorded within a certain limit of accuracy and the upper frequency limit of the anemometer subjected to single frequency sinusoidal gusts has still not been adequately defined. However it is logical to expect an improved dynamic performance in strong wind conditions as noted in the results above. The gust peak is invariably preceded by lower but nevertheless significant velocities which would make the gust periods large compared with the response time of the instrument for a significant frequency range above the assumed limit of the anemometer.

9.8.2 Effect of Turbulence Intensity

Having established that the 0.5 s gust factors were accurately recorded for each position over the two escarpments, they were used in Fig.9.7 to define the factor A in equation 2.48. When considering the scatter in the results, it must be remembered that the peak velocity has a certain probability of occurrence with its own mean and standard deviation. In addition, the different mean velocities encountered at each array would alter the dynamic response accuracy of the anemometers from one position to the other. The results showed a compromise between the two empirical estimates of Mackey (1970) and ESDU (1972) given in equations 2.49 and 2.50. No significant effects from the local terrain was noticed as the disposition of the points showed no systematic change with position over the escarpments. The value of A would increase with a decrease in the distance constant of the anemometer. The upper limit suggested by

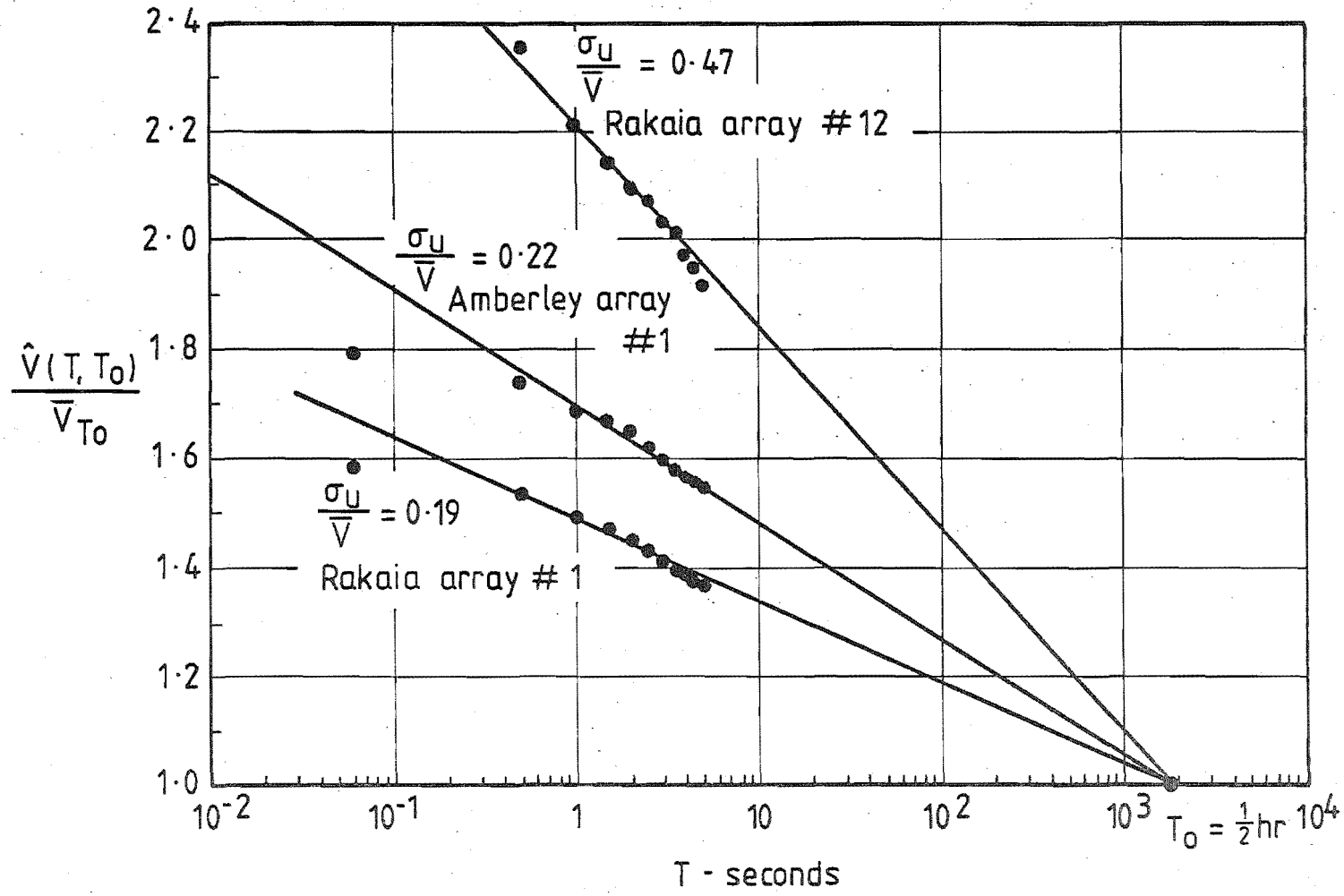

FIG 9·6 THE VARIATION OF GUST FACTOR WITH AVERAGING TIME, T FOR THREE TYPICAL TURBULENCE INTENSITIES (T_o = 1800s)

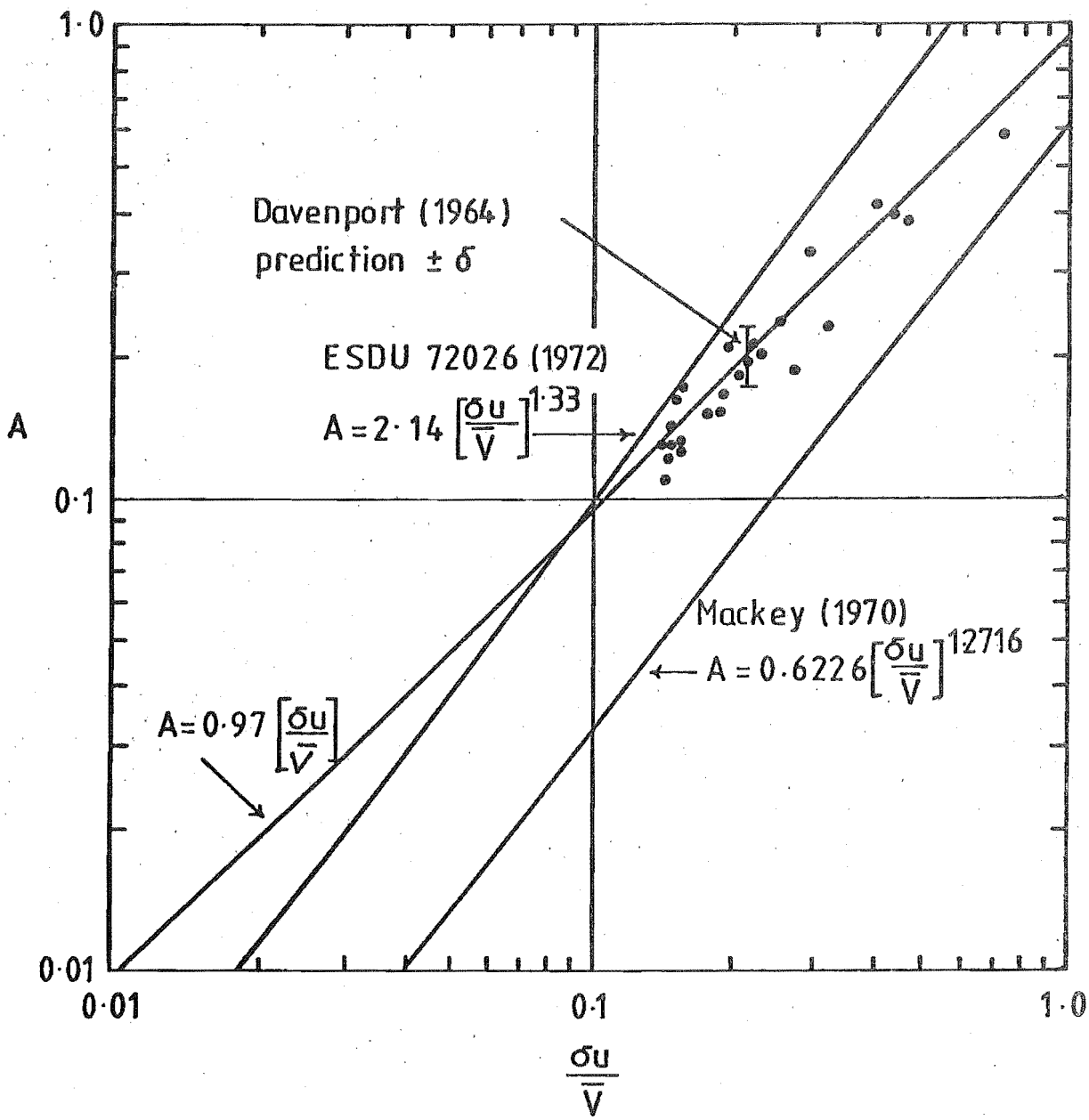

FIG 9·7 VARIATION OF GUST FACTOR CONSTANT, A (EQUATION 2·48) WITH TURBULENCE INTENSITY ($T = 0 \cdot 5s$, $T_o = 1800s$)

ESDU (1972) may be close to the actual situation in the atmosphere whereas Mackay's data was obtained using a number of different instruments of unrecorded but presumably lower dynamic performance than the propeller anemometers used in the present tests. Little difference was obtained in the distribution of the points in Fig.9.7 using gust factors of different averaging times due to the already proven accuracy of equation 2.48 used in the calculation of A.

9.8.3 Extreme Value Analysis

An alternative analytical approach by Davenport (1964) using the longitudinal velocity power spectra and extreme value analysis was explained in Chapter 2 and the expressions for the average gust velocity and its standard deviation were given in equations 2.45 to 2.47, namely

$$\text{Mean } \hat{\eta} = (2 \log_e \nu T_o)^{\frac{1}{2}} + 0.577 (2 \log_e \nu T_o)^{-\frac{1}{2}}$$

$$\sigma(\hat{\eta}) = 1.283 (2 \log_e \nu T_o)^{-\frac{1}{2}}$$

where $\eta = (V - \bar{V})/\sigma_u$

and $$\nu^2 = \frac{\int_0^\infty n^2 S(n)\, dn}{\int_0^\infty S(n)\, dn}$$

These expressions were used to predict the gust factor using data from the Amberley recording #5, reference array #1 at 10 m height above ground by way of example. Converting to a logarithmic frequency scale in terms of the wave number, $n/\bar{V}$

$$\nu^2 = \frac{\bar{V}^2 \int_{-\infty}^{+\infty} \left(\frac{n}{\bar{V}}\right)^2 \left[\frac{nS(n)}{\sigma^2}\right] d\left[\log_{10}\left(\frac{n}{\bar{V}}\right)\right]}{\int_{-\infty}^{+\infty} \frac{nS(n)}{\sigma^2} d\left[\log_{10}\left(\frac{n}{\bar{V}}\right)\right]} \qquad 9.2$$

The bottom line is the area under the power spectrum taking into account the instrument response, whereas the top function is a frequency weighted spectrum which may be directly calculated from the original spectrum. Both functions have been plotted out in Fig.9.8 and their areas measured by a planimeter in order to define the function, ν. The spectrum used was the smooth standard ESDU (1974) spectrum set to the correct wave number for the Amberley array #1 (Fig.4.15) which was shown in Fig.6.10 to be close to the spectrum obtained from the field recording, but not so irregular. It was found that $\nu = 0.015\ \bar{V}$ which

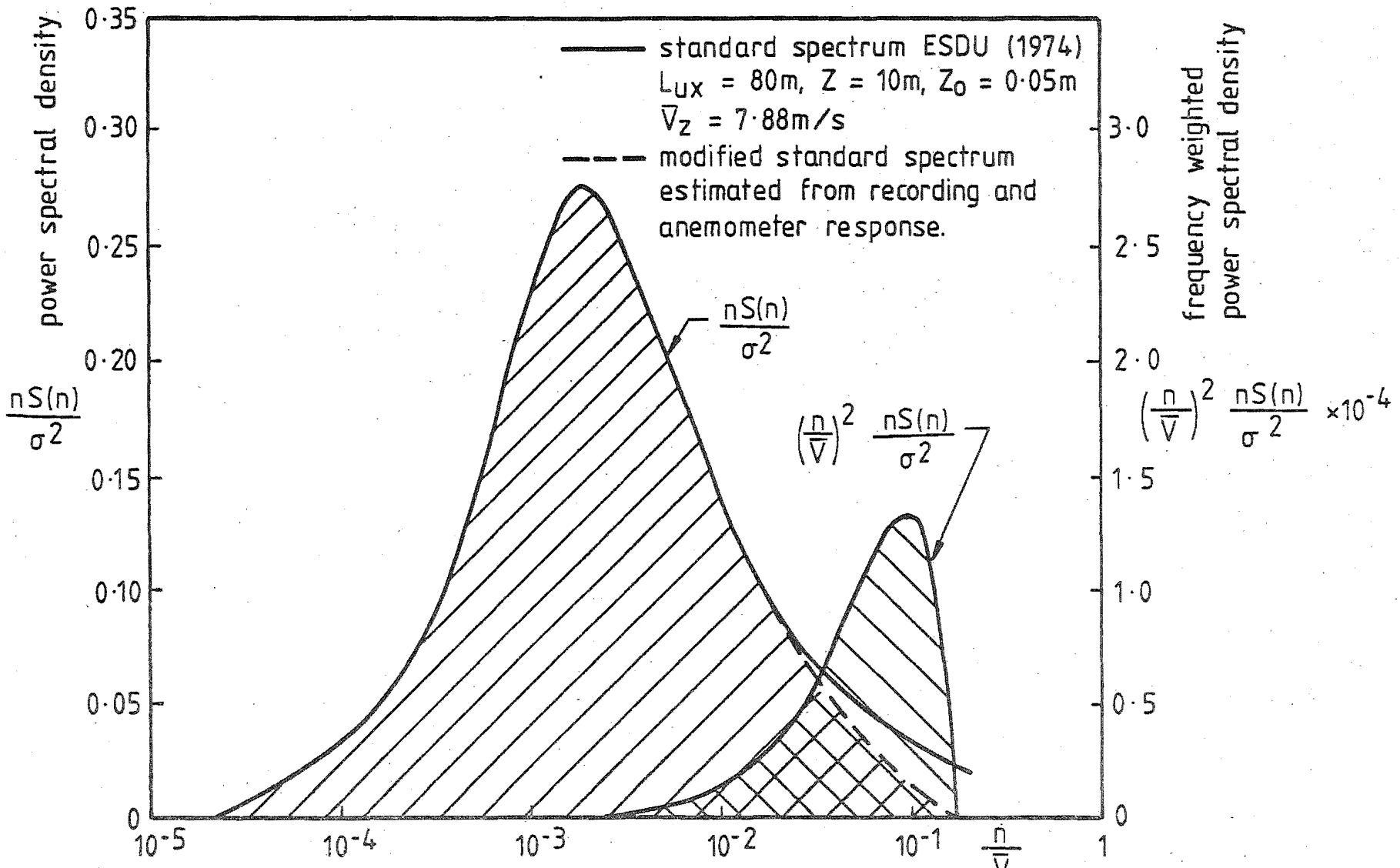

FIG 9·8 CALCULATION OF GUST FACTOR FOR AMBERLEY ARRAY #1, 10m HEIGHT UPSTREAM.

for $\bar{V}$ = 7.88 m/s and T_o = 1800 s, yielded the following values :

$$\nu T_o = 210$$

Mean peak factor $\hat{\eta} = 3.45$

$$\sigma(\eta) = 0.392$$

Mean gust factor $\frac{\hat{V}}{\bar{V}} = 1.74$ (For a turbulence intensity, $\frac{\sigma_u}{\bar{V}} = 0.214$)

The estimated value for the mean gust factor and its standard deviation (1.74 ± 0.08) coincides with the value obtained from the field recording analysis shown in Fig.6.28. The corresponding value of A may be plotted on Fig.9.7 confirming the reasonable agreement with the field data. However the choice of averaging time is open to question as it yields a value of A which is slightly on the high side.

It is interesting to note that if a constant peak factor is assumed to exist over a wide range of turbulence intensities, then a straight line may be drawn in Fig.9.7 which appears to fit the field data better than the empirical predictions discussed earlier. In other words,

$$\text{if } \hat{V} = \bar{V} + 3.45\,\sigma_u \qquad 9.3$$

$$\text{and as } \hat{V} = \bar{V} + A \log_{10}\left(\frac{T_o}{T}\right) \cdot \bar{V} \text{ from equation 2.48}$$

$$\text{then } A = 3.45\,\frac{\sigma_u}{\bar{V}} \log_{10}^{-1}\left(\frac{T_o}{T}\right)$$

which for T = 0.5 s, T_o = 1800 s becomes

$$A(0.5,1800) = 0.97\,\frac{\sigma_u}{\bar{V}} \qquad 9.4$$

Consequently, for T ⩾ 0.5 s

$$\frac{\hat{V}}{\bar{V}} \approx 1 + \frac{\sigma_u}{\bar{V}} \log_{10}\left(\frac{T_o}{T}\right) \qquad 9.5$$

The above expression is more simple than the previous relationships put forward by Wieringa (1973) and ESDU (1972) and coincides more closely with the field data from the present tests. However the scatter of the field data in Fig.9.7 indicates that equation 9.5 can only be considered as a first order approximation until further data becomes available.

The value of the mean peak factor, ≈ 3½ resulting from the present tests agreed with the generally accepted value given by

Davenport et al (1975) and the Canadian Building Code (1970).

9.9 CONCLUSIONS

* The present field test data were compared with previous data obtained with cup anemometers over the same escarpments. Although good agreement was noted in the flow outside the wake regions, large overestimation errors were evident in the cup anemometer data in regions of high turbulence.

* The model and field results obtained for the same wind incidence angles and similar upwind conditions were compared and showed reasonable agreement. However significant speed-up effects due to the rough to smooth surface transition at the leading edge of the smooth models were evident. In addition, the errors due to the inadequacy of the single horizontal hot wire to indicate the true longitudinal velocity component were considered to be significant, especially in regions of high turbulence.

* No inner region marked by large changes in the Reynolds stress variation with height above ground was identified in the model or field tests.

* The variation of the fractional speed-up factor with height above the crest were compared where possible with the limited literature available. A wide range of ΔS values were evident close to the ground due to a number of significant influences which were discussed. No maximum value close to the ground was evident in the experimental data and ΔS continued to increase rapidly as the ground was approached.

* The value of ΔS close to the ground above the crest increased with increasing upwind slope in such a way that $\Delta S/(H/L) \approx 1$ for $H/L \leq 0.4$. A wide range of ΔS values were encountered for steeper slopes but a peak value between 0.5 to 0.7 was evident near $H/L \approx 1.0$. Separation effects were dominant for slopes steeper than $H/L \approx 0.6$.

* The value of ΔS generally decreased with increasing wind incidence angles although little change was noted within $\pm$ 30° of the normal. An oblique wind flow tended to negotiate the slope at a steeper angle of up to 10° from the mean wind direction.

* The dynamic performance of the propeller anemometers was shown to be similar to that predicted from first order response considerations.

* Little change in the turbulence characteristics was noticed in the flow outside the wake region behind the crests. The changes in turbulence intensity were mainly due to changes in the mean velocity rather than the variance. The turbulence behaved as if convected along the streamlines.

* The extent and intensity of the wake turbulence increased with slope angle and surface roughness of the ground over the escarpments.

* The gust factors obtained from the field tests were discussed and no significant effect attributable to the presence of the escarpments was evident. The strong effect of the anemometer's dynamic performance, gust averaging time, record length and the flow turbulence intensity were adequately explained and the results compared with the literature. A peak factor of 3.5 was obtained which was identical to the generally accepted value for a high response instrument. This yielded a gust factor of 1.75 for open country conditions at a height of 10 metres.

CHAPTER 10

COMMENTS ON SOME PREDICTION METHODS FOR SITE EXPOSURE

A guide to the prediction of the wind conditions over hilly terrain for engineering purposes has so far only been provided by some of the national building codes in order to predict the wind loading on exposed structures. This chapter briefly reviews the empirical prediction methods contained in these codes and compares them with the present understanding and experimental results accumulated earlier in this report. Other prediction techniques currently being proposed in recent research papers are then reviewed. The chapter concludes with a brief discussion of the main features thought necessary in a code rule to cope with this problem.

10.1 CODE PROVISIONS

Although the variation of the wind speed-height profile with surface roughness appears to be adequately covered by the majority of the building codes, the important problem of exposure due to hill top or other exposed sites has been recognised but receives a far less rigorous treatment. Modification to the flow turbulence has been ignored and changes to the mean wind speed has normally been expressed as an exposure factor, similar to the amplification factor, A_z. For steeper hills, a modification to the effective height of the structure using a form of 'escarpment rule' has been specified. Both these methods are discussed below.

10.1.1 Exposure Factors

During a review of wind loading specifications throughout the world, Wyatt (1971) discussed the amplification factors that were used in some codes to account for hill exposure. The application of the factors was invariably very loosely defined and independent of hill shape and height above the ground. The range of factors noted varied between countries, with the widest scope given by the French Code which gave a 20% reduction for "saucer like" locations, to 25% - 35% increases specified for "narrow valleys and isolated hills". The British Code (1972) provided for a 10% reduction for "steep sided and enclosed valleys" to a 10% increase for "very exposed hills and valleys shaped to produce a funnelling of the wind". The Australian

code (1973) had no provision for exposure factors apart from their escarpment rule which will be discussed later, whilst New Zealand (1976) provided no shelter effects and "a 10 to 20% or higher increase for valleys and gorges shaped to produce funnelling of the wind; exposed hillsides, peaks and ridges where acceleration of the wind is known to occur; especially abnormal sites". ESDU (1972) recommended that a 30% increase could be applicable for extreme cases of exposed hill top sites assuming that the reference speed referred to flat, open terrain.

10.1.2 Escarpment Rules

The original escarpment rule used in the French code (1965) to cope with steep hill top sites was adopted by the British code BSCP3 (1972)which is shown in Fig.10.1. The escarpment rule was not intended to be used in addition to the exposure factors discussed earlier (Newberry and Eaton, 1974). The rule increased the effective height of the building by a fraction of the escarpment height, ΔZ which resulted in the choice of a higher design wind speed. However the effect of the escarpment or hill slope was restricted to within 4 H of the crest. Returning to the use of standard nomenclature, the effective amplification factor resulting from this rule at a height equal to the building, h is

$$A_{(Z=h)} = \frac{\bar{V}_{(Z+\Delta Z)}}{REF\bar{V}_Z} = \left(\frac{Z+\Delta Z}{Z}\right)^{\alpha}$$

$$\therefore A_Z = \left(1 + \frac{\Delta Z}{Z}\right)^{\alpha} \qquad 10.1$$

where ΔZ for sites within 1 H of the crest was defined as

$$\Delta Z = 0 \text{ for } \tan\theta \leqslant 0.3$$

$$\Delta Z = \left(\frac{\tan\theta - 0.3}{1.7}\right) H \text{ for } 0.3 < \tan\theta < 2$$

$$\Delta Z = H \text{ for } \tan\theta \geqslant 2$$

The Australian code AS1170:2 (1973) used a similar approach but adapted it in the light of the original test data from de Bray (1973) in order to simplify the procedure,(Fig.10.2). The limiting slope adopted this time was $\tan\theta \leqslant 0.2$ and the influence of the hill was extended to 5 H downstream. In contrast with BSCP3 (1972),

Appendix D

The effect of a cliff or escarpment on the height above ground H

Z_1 is the general level of the ground at the foot of the escarpment.
Z_2 is the general level of the top of the escarpment.
The difference of level $Z_2 - Z_1 = z$.
The artificial base from which H is measured is Z_e.
θ is the inclination of the mean slope of the cliff to the horizontal.

Three cases are considered as shown in Figs. 4, 5 and 6.

(1) The average slope $\tan\theta$ of the escarpment is $\leqslant 0.3$.

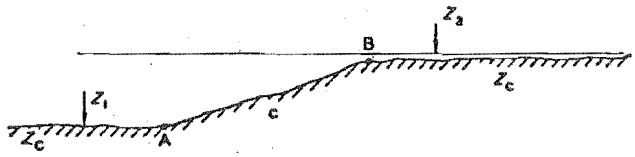

Fig. 4. Slope of escarpment (1)

The artificial base Z_e is that of the ground immediately around the building.

(2) $0.3 < \tan\theta < 2$.

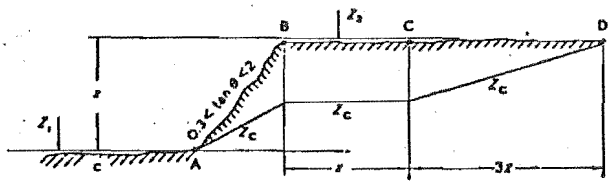

Fig. 5. Slope of escarpment (2)

The following points serve for reference:

A is the point of intersection of the level Z_1 and the mean slope of the escarpment,
B is the point of intersection of the level Z_2 and the mean slope of the escarpment,
C is such that $BC = z$,
D is such that $CD = 3z$.

Z_e is then taken such that:

in front of A, $Z_e = Z_1$;

from B to C, $Z_e = Z_1 + \dfrac{2-\tan\theta}{1.7} z$;

beyond D, $Z_e = Z_2$;

between A and B and between C and D, Z_e is obtained by linear interpolation.

(3) $\tan\theta \geqslant 2$.

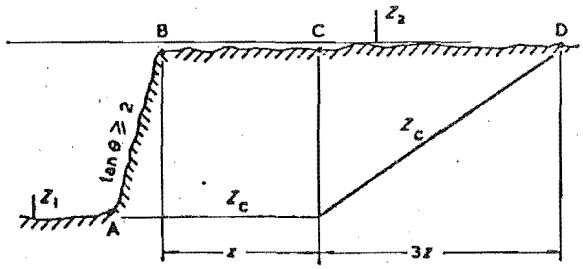

Fig. 6. Slope of escarpment (3)

A, B, C and D are as defined in case (2).

In front of A, $Z_e = Z_1$;
from A to C, $Z_e = Z_1$;
beyond D, $Z_e = Z_2$.

Between C and D, Z_e is obtained by linear interpolation.

NOTE. This method of defining the effective height of a building is taken from the French code of practice Règles N.V.65.

FIG 10·1 ESCARPMENT RULE FROM THE BRITISH CODE BSCP 3 (1972) CHAPTER 5, PART 2.

APPENDIX D

CALCULATION OF EFFECTIVE HEIGHT FOR STRUCTURES ON OR NEAR THE EDGE OF A STEEP RISE, CLIFF, BLUFF, OR ESCARPMENT

D1 PURPOSE. The wind loadings on structures on or near the edge of an escarpment or a relatively sudden change in ground level with a slope of $E/y \geq 0{\cdot}2$ shall be determined by applying the procedures given in the Rules of the Code using a modified regional basic design wind velocity V_M which is considered to apply at a height of 10 m above the actual ground surface in Category 2 conditions.

V_M shall be determined from an artificial ground datum Z_g established as shown in Fig. D1 such that:

$$V_M = V_{(z'+10)}$$

where

$V_{(z'+10)}$ is the design wind velocity at height $(z' + 10)$ m above the artificial ground datum for Category 2 as established from Table 4.

The value of z' adopted for this determination shall be the height above the artificial ground datum Z_g or 100 m, whichever is the less.

The derivation of the appropriate design wind velocity V_z for a particular terrain category and height z above the actual ground surface shall then be made using V_M as the regional basic wind velocity at a height of 10 m for Category 2 conditions by applying the velocity multipliers given in Table 4.

D2 NOTATION AND SYMBOLS.

G_1 = the general level of the ground at the top of the escarpment

G_2 = the general level of the ground at the bottom of the escarpment

$E = G_1 - G_2$, the rise of the escarpment

y = the horizontal dimension of the escarpment

Z_g = the artificial ground datum from which z' is measured

z = height above actual ground surface.

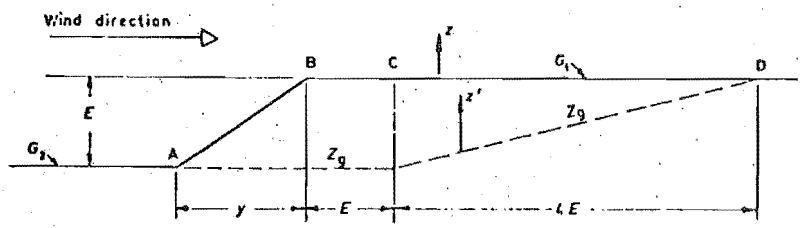

Fig. D1. ARTIFICIAL GROUND DATUM, Z_g

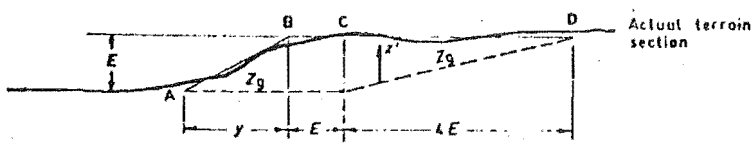

Fig. D2. TYPICAL CONSTRUCTION OF FIG. D1 ON ACTUAL TERRAIN SECTION

FIG 10·2 ESCARPMENT RULE FROM THE AUSTRALIAN CODE AS 1170 (1973), PART 2

APPENDIX A

CALCULATION OF HEIGHT ABOVE GROUND FOR BUILDINGS ON OR NEAR THE EDGE OF AN ESCARPMENT OR A RELATIVELY SUDDEN CHANGE IN GROUND LEVEL

For a building on or near the edge of an escarpment or a relatively sudden change in ground level, such that $E/y > 0.2$ as shown in Figs. 26 and 27, the height above ground shall be measured from an artificial ground datum as shown (dotted line marked z_g) in Figs. 26 and 27.

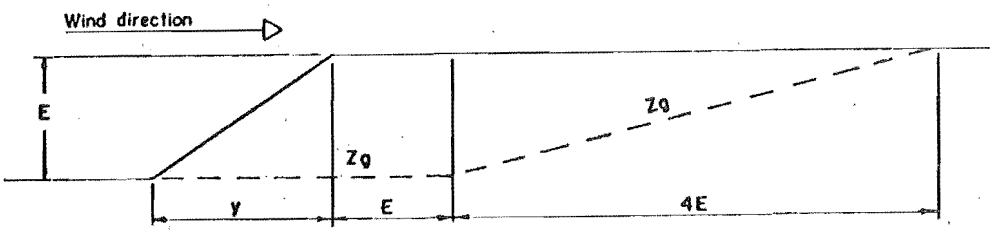

Fig. 26: Artificial ground datum z_g.

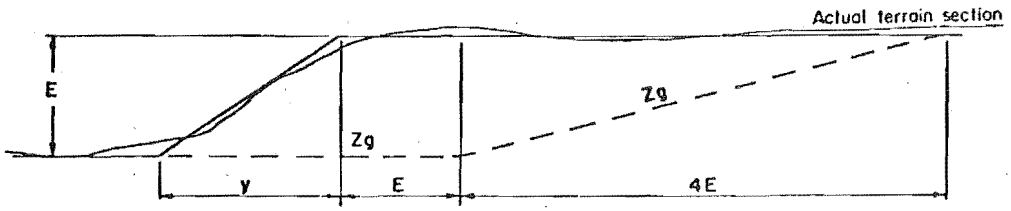

Fig. 27: Typical construction of Fig. 26 on actual terrain section.

FIG 10·3 ESCARPMENT RULE FROM THE NEW ZEALAND CODE NZS 4203 (1976), PART 4

the derived height correction, ΔZ was to be used to find a modified basic design wind speed at 10 m above ground level, making the amplification factor independent of the building height. Thus

$$A = \frac{\bar{V}_{(10+\Delta Z)}}{\bar{V}_{10}} \quad \text{for all } Z$$

$$\therefore \quad A = \left(1 + \frac{\Delta Z}{10}\right)^{\alpha} \qquad 10.2$$

The New Zealand Code NZS 4203 (1976) shown in Fig.10.3 used the same artificial ground datum as the Australian Code and the lower limit of $\tan \theta \leqslant 0.2$, but retained the height sensitive amplification factor described by equation 10.1 from the British Code.

It should be noted that within 1 H behind the crest, the amplification factor defined by equation 10.1 is equivalent to assuming that the speed-up factor, S = 1. The accuracy of this assumption for large hills as suggested by Shellard (1963) and Elliott (1977) has been discussed in Chapter 3. Under these conditions, values of S encountered were normally somewhat lower than S = 1 in contrast to the present model tests discussed below.

The predicted amplification factors for a 10 m high escarpment with various slopes and positions have been plotted in Figs.10.4, 10.5 and 10.6 against the model test results. An angle of incidence, $\phi=0°$ was used which is the wind direction providing the most onerous conditions. It is evident from these comparisons that all the code predictions fall significantly below the values obtained in the model tests. This model data normally gave values of S greater than one. However the trend with height has been correctly predicted by the British and New Zealand Codes. The limiting slope of $\tan \theta \leqslant 0.2$ or 0.3 appears to be far too steep, as even the 8:1 slope ($\tan \theta = 0.125$) yielded significant values of amplification factor whilst for steep slopes greater than 4:1, the slope gradient had only a minor effect. The limit on the affected region of 5 H downwind of the crest seems insufficient as substantial speed-up effects were noticed in the model tests beyond 10 H downstream. However the behaviour of the flow would also be dependent on the nature and extent of the wake or separated flow region, which in turn may be influenced by the presence of any major obstruction in that area.

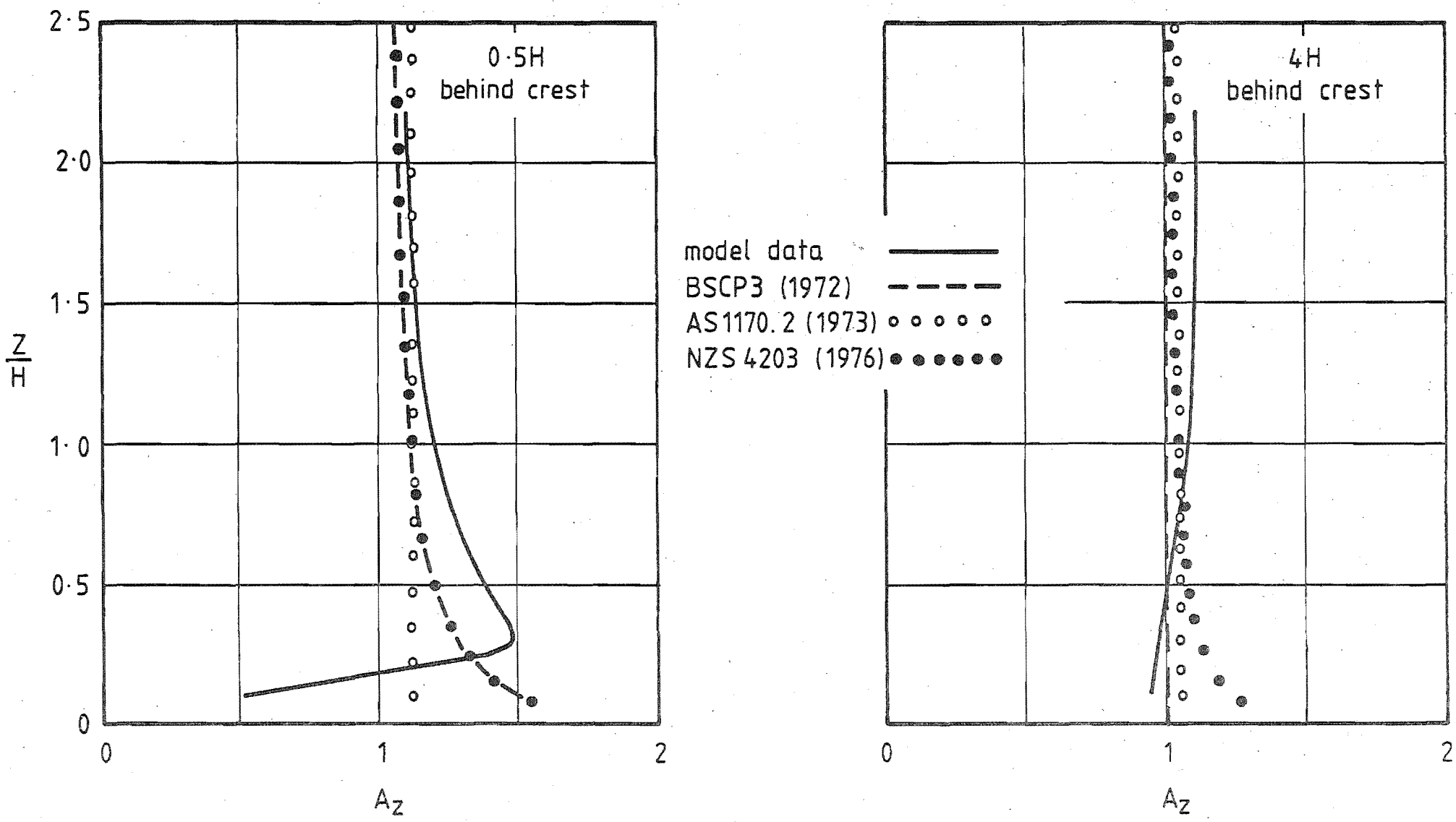

FIG 10·4 AMPLIFICATION FACTORS ESTIMATED FROM VARIOUS BUILDING CODES COMPARED WITH MODEL TEST DATA. (CLIFF ESCARPMENT, TAN $\theta = \infty$, H = 10m, OPEN COUNTRY TERRAIN, $\phi = 0°$)

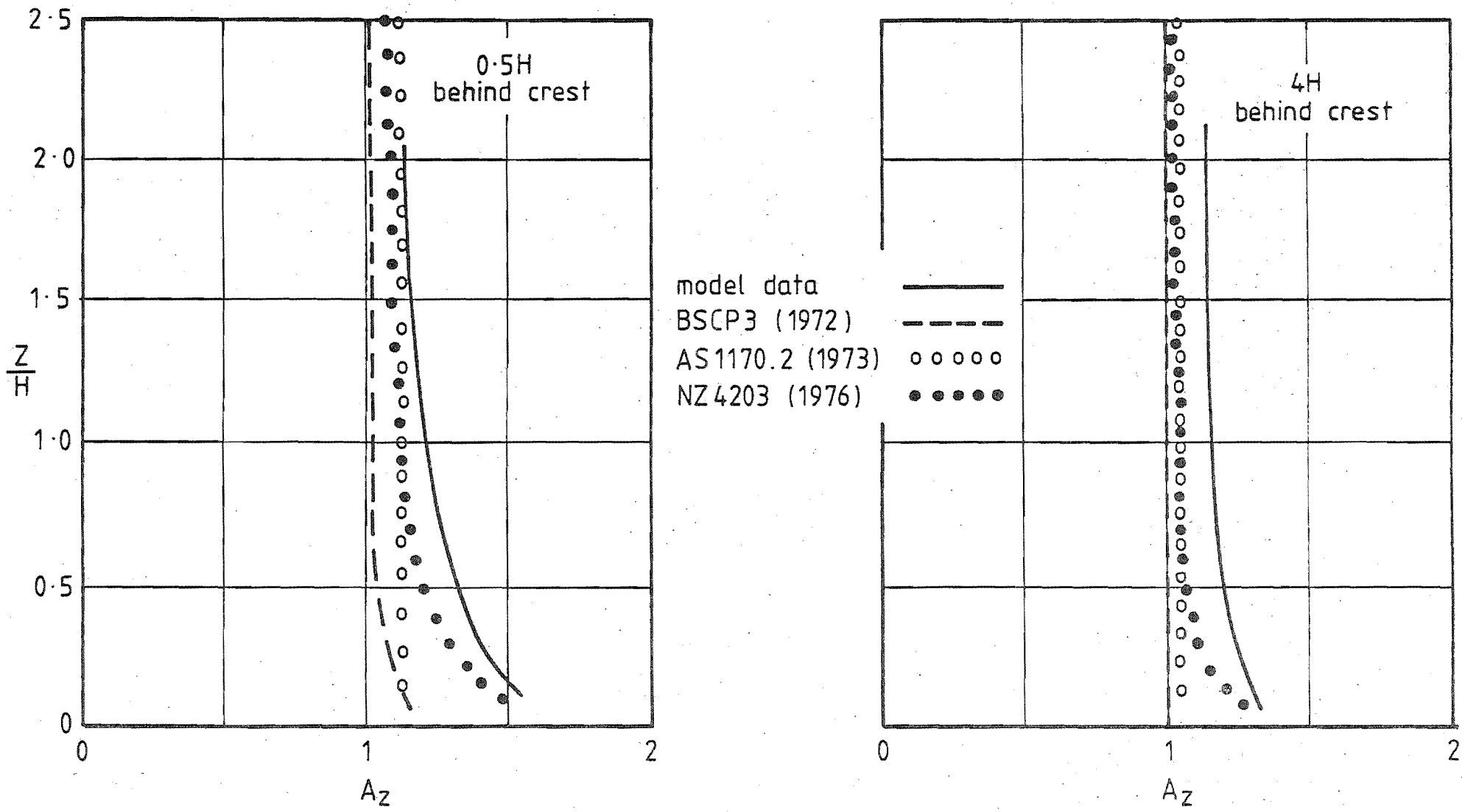

FIG 10·5 AMPLIFICATION FACTORS ESTIMATED FROM VARIOUS BUILDING CODES COMPARED WITH MODEL TEST DATA (2:1 ESCARPMENT, TAN θ = 0·5, H = 10m, OPEN COUNTRY TERRAIN, ϕ = 0°)

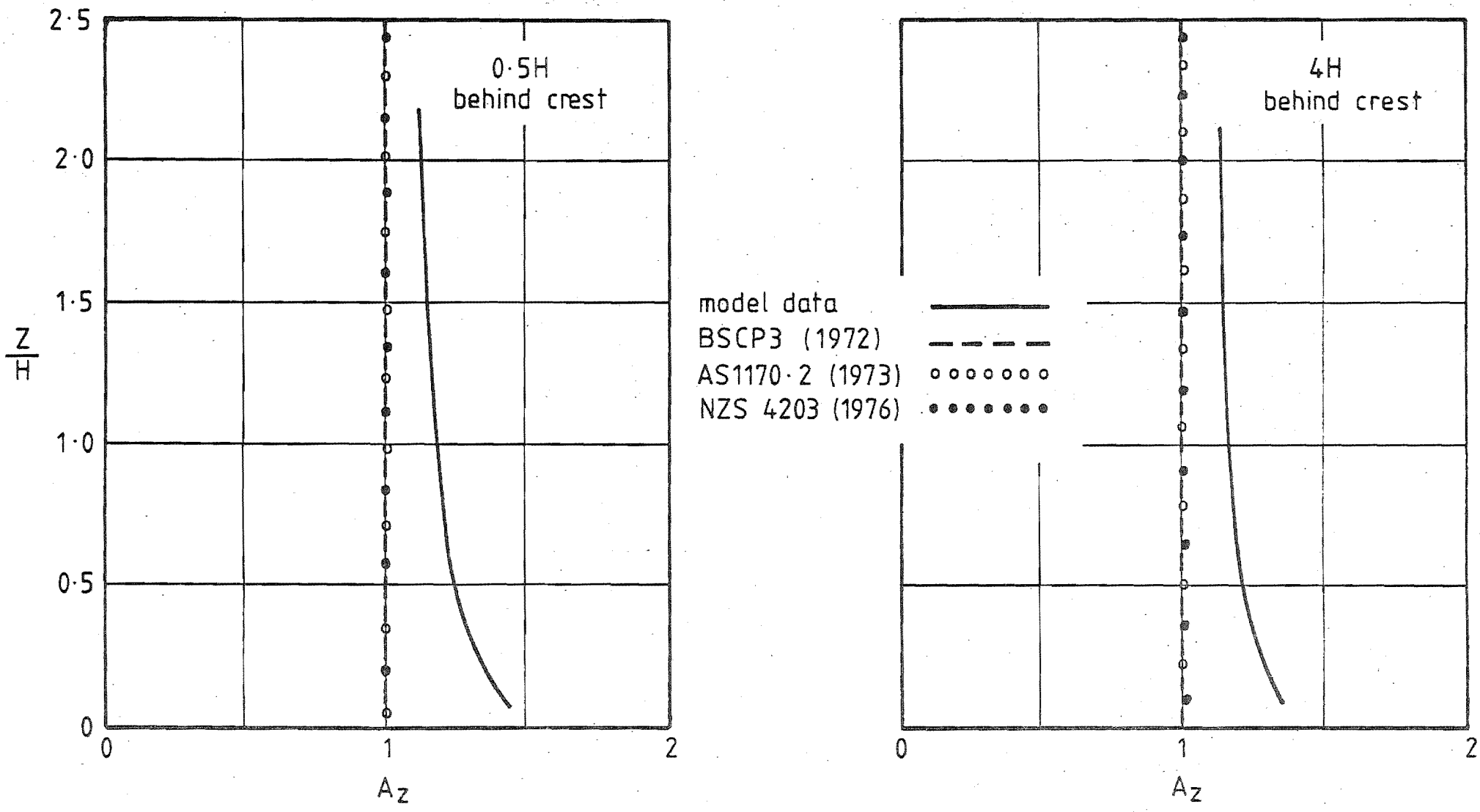

FIG 10·6 AMPLIFICATION FACTORS ESTIMATED FROM VARIOUS BUILDING CODES COMPARED WITH MODEL TEST DATA. (8 :1 ESCARPMENT, TAN θ = 0·125, H = 10m, OPEN COUNTRY TERRAIN, ϕ = 0°)

10.2 CURRENT PROPOSALS

The analytical theory put forward by Jackson and Hunt (1975) and Jackson (1975,1977) provided an accurate but complicated prediction method for the speed-up effects over low smooth hills with small slope gradients. However the necessary involved nature of the approach and its limitation to smooth gradual hills make it unsuitable for direct application to code design rules. Use could be made of the theory if the information was contained in graph form with suitable empirical extrapolations to cover the full range of likely hill shapes and wind conditions that are likely to be encountered. Such an approach was used for the estimation of dynamic loading in the Canadian Code (1970) and would presumably, be possible to accomplish for the hill flow problem, but was beyond the scope of this project. The discussion is therefore confined to simple empirical rules based on experimental data.

10.2.1 Bouwmeester et al (1978)

The above report proposed a prediction technique for the mean velocity profile at the crest of a ridge which was based on the assumption that the crest profile could be fitted to a power law. It was accepted that this would not be the case under some circumstances involving abrupt ridges which have been known to yield low level jets or almost linear profiles. However the assumption was thought to be justified as a means to an approximate solution.

If the power law exponent at the crest is α_c compared with that upstream, α_o then the amplification factor at a height, Z may be expressed in terms of known velocities at some reference height, Z_{REF} so that

$$A_Z = \frac{\bar{V}(Z)}{\bar{V}_{REF}(Z)}$$

$$= \frac{\bar{V}(Z_{REF})}{\bar{V}_{REF}(Z_{REF})} \cdot \frac{\bar{V}(Z)}{\bar{V}(Z_{REF})} \cdot \frac{\bar{V}_{REF}(Z_{REF})}{\bar{V}_{REF}(Z)}$$

$$= A_{(Z_{REF})} \cdot \left(\frac{Z}{Z_{REF}}\right)^{\alpha_c} \cdot \left(\frac{Z}{Z_{REF}}\right)^{-\alpha_o}$$

$$\therefore A_Z = A_{(Z_{REF})} \cdot \left(\frac{Z}{Z_{REF}}\right)^{\alpha_c - \alpha_o} \qquad 10.3$$

Selecting s so that $A_Z = 1$ when $s = \frac{Z}{H}$ (H = escarpment height) and a so that $a = \frac{Z_{REF}}{H}$

then

$$A_{(Z = sH)} = A_{(aH)} \left(\frac{sH}{aH}\right)^{\alpha_c - \alpha_o} = 1$$

$$\therefore \quad A_{(aH)} = \left(\frac{s}{a}\right)^{\alpha_o - \alpha_c} \qquad 10.4$$

It was shown using model test results that $\alpha_o - \alpha_c$ and A_H were highly correlated when a = 1 and s $\approx$ 8.5. From equation 10.3 then

$$A_Z = A_H \cdot \left(\frac{Z}{H}\right)^{\alpha_c - \alpha_o}$$

and from equation 10.4,

$$A_H = (8.5)^{\alpha_o - \alpha_c}$$

so that $$A_Z = \left(\frac{Z}{8.5\ H}\right)^{\alpha_c - \alpha_o} \qquad 10.5$$

and $$\alpha_c = \alpha_o - \frac{\log A_{(aH)}}{\log (8.5/a)} \qquad 10.6$$

However, from the experimental results, a more simple empirical relationship was obtained thus,

$$\alpha_c = \alpha_o - \frac{A_H - 1}{2.3} \qquad 10.7$$

which with equation 10.3 yielded,

$$A_Z = A_H \cdot \left(\frac{Z}{H}\right)^{\frac{1 - A_H}{2.3}} \qquad 10.8$$

Errors in prediction of less than 5% were claimed for equation 10.8 for positions above the inner layer compared with 15% from equation 10.5, once A_H was known. This information was provided by Figs.10.7 and 10.8 based on their model test data on triangular hills. The increase in speed-up effect with increasing H/L_u, together with the peak in speed-up near $H/L_u = 0.25$ ($H/L = 0.5$) both evident in Fig.10.8, are similar in behaviour to the trends observed in Fig.9.5 from the present tests. In general however, the escarpment data which were also plotted on Figs.10.7 and 10.8, consistently yielded lower values of A_H than the triangular hill data from Bouwmeester (1978). This anomoly suggests that the trends in A_H are too complicated to describe easily in such a way. The effect of hill shape, local geometry and surface roughness, are parameters which Sacré (1978) established as being equally important and must also be accounted for in some way.

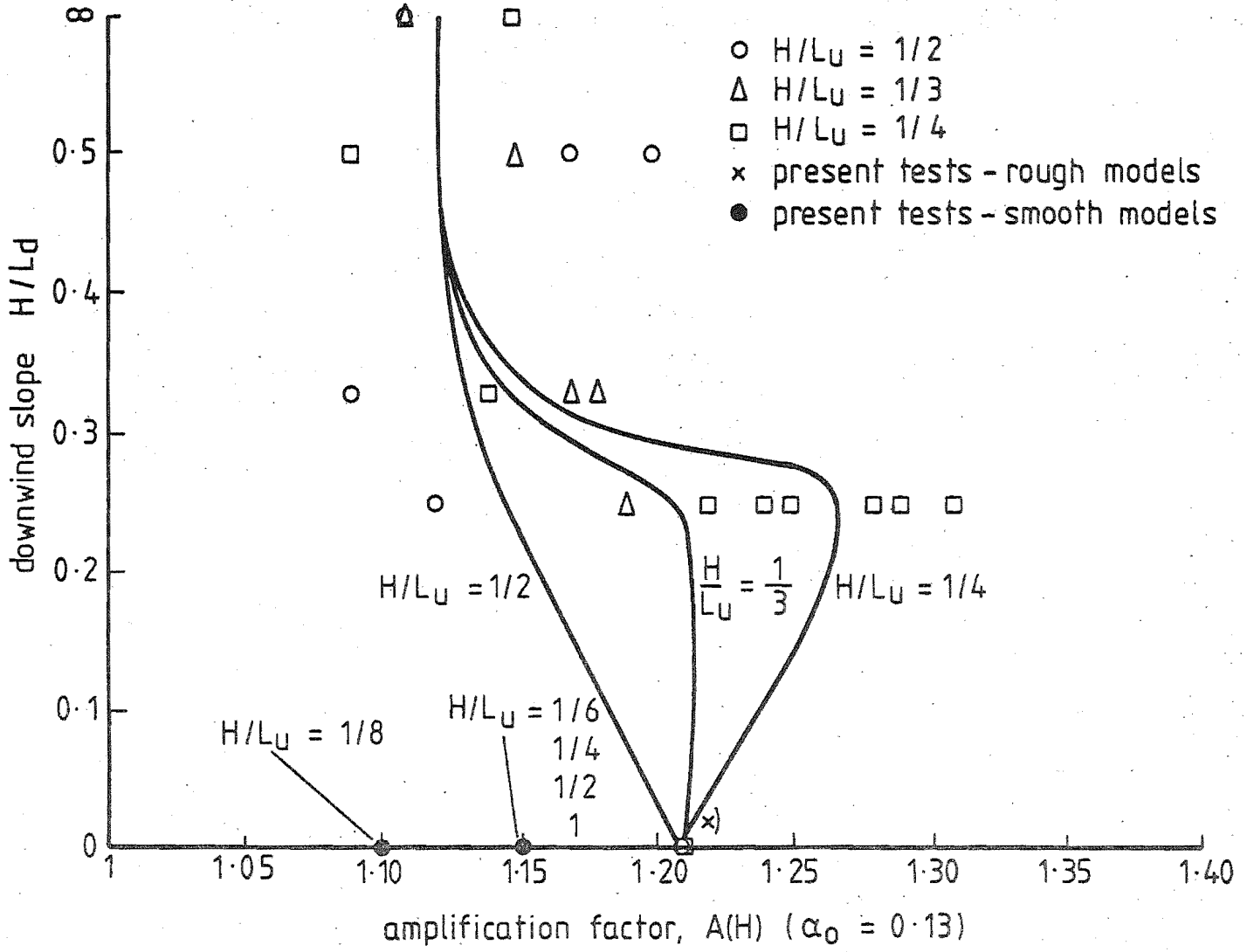

FIG. 10·7 DEPENDENCY OF CREST AMPLIFICATION FACTOR ON DOWNWIND SLOPE FOR H/L_u = 1/2, 1/3 AND 1/4. (α_o = 0·13) (Bouwmeester, 1978)

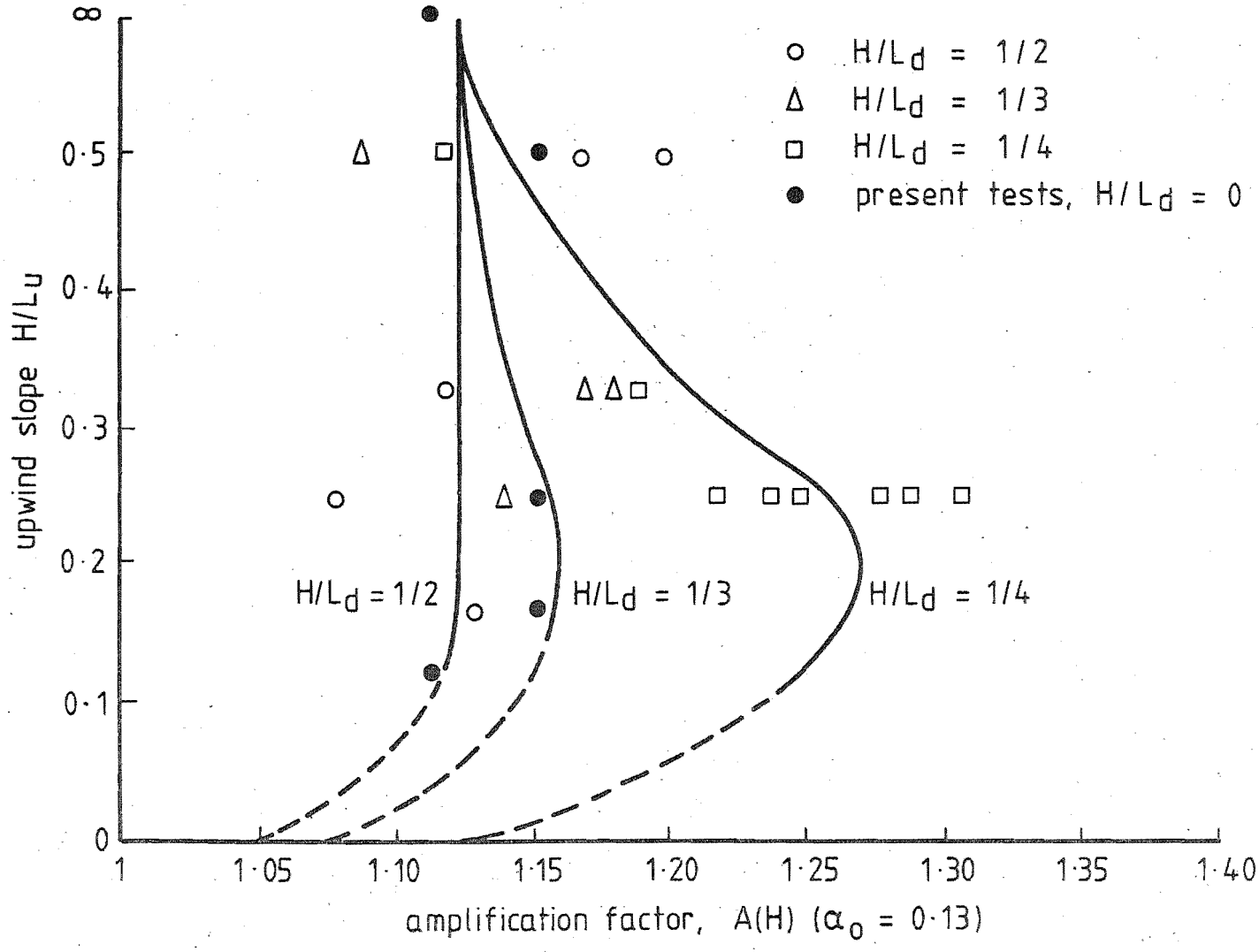

FIG 10·8 DEPENDENCY OF CREST AMPLIFICATION FACTOR ON UPWIND SLOPE FOR H/L_d = 1/2, 1/3, AND 1/4; (α_o = 0·13) (BOUWMEESTER, 1978.)

However the effect on A_H from different upstream velocity profiles was accounted for by the empirical relation,

$$A_{(\alpha_o)} = A_{(\alpha_o')} \cdot \frac{1.15 + \alpha_o}{1.15 + \alpha_o'} \qquad 10.9$$

10.2.2 Others

During a brief discussion of flow over hills in the course notes by Davenport et al (1975), a suitable expression was proposed for the variation of amplification factor with height above the crest which was based on unpublished theoretical and model test data. Thus

$$A_z = [1 + A_o]\, e^{-p(z/H)^q} \qquad 10.10$$

where $[1 + A_o]$ is the amplification factor near the ground on the hilltop

p = constant ≈ 1

q = constant ≈ 1 for peaked hills

and ≈ 2 for flatter hills.

Because of the typically large rates of change of A_z close to the ground, the accurate choice of $[1 + A_o]$ becomes a difficult task. In addition, the use of the exponential function is not very suitable for code rule applications and there was no provision for the effects of slope gradient which has been shown to be important for $H/L_u \leqslant 0.20$.

Recent development work on the British Draft Code of Practice for the loading of lattice towers has also involved the compilation of a promising prediction method which will be available shortly (B.W. Smith, Flint and Neill, Consulting Civil and Structural Engineers, London - private communication).

10.3 DISCUSSION

It has just been shown that some existing code rules for the estimation of the mean velocity speed-up over a hill were inadequate when compared with experimental evidence. The development of a more accurate rule is badly needed and although work is being carried out on this problem, no satisfactory rule has yet been published. Several important points have become evident as a result of the discussions in

previous chapters and these are summarised below in order to define the problem more clearly.

The purpose of a code rule is to define the envelope containing the worst possible conditions that could exist in simple terms. It is therefore reasonable to consider only the case of the wind blowing normal to the crest and to neglect any mitigation of exposure due to the wind incidence angle. In addition, any shelter effects due to separation should also be neglected for the same reason. It was suggested in Chapters 6 and 7, that the atmospheric stability could affect the behaviour of the flow over a hill significantly. However, conflicting evidence from model and theoretical analyses described in Chapter 3 make the estimation of stability effects impossible at this stage without further full scale experimental investigations. The most onerous wind conditions at a hilly site may well be a result of unusual atmospheric conditions.

The use of the amplification factor, A_z has been shown to be appropriate for the description of the mean velocity speed-up over a hill. If in fact the "T" second gust speed is to be defined, then the same amplification factors may be used providing that the turbulence intensity remains unchanged. However, if the hill site is situated within the turbulent wake area, then a further correction must be considered as discussed in Chapters 2 and 9, possibly assuming a constant peak factor which leads to the use of equation 9.5.

From the discussions in the previous chapters it is evident that any code rule must take into account the following significant parameters in order to define adequately the mean velocity over a hill.

a) Upwind Slope, H/L_u (or H/L) : The dependence of A_z on H/L is important for the lower slope gradients. However the definition of L still remains to be settled as the local geometry close to the crest is also an important factor.

b) Downwind slope, H/L_d : The variation of A_z downwind of the crest is important especially for the escarpment case when the influence of the escarpment extends beyond 10 H downwind.

c) Upwind velocity profile, α_o.

d) Local roughness changes near the crest.

e) Three-dimensional effects.

f) The height of the hill relative to the boundary-layer depth, H/Z_G. (The significance of this parameter has not yet been determined)

The longitudinal turbulence over a hill may be assumed to be approximately the same (or slightly less turbulence intensity) than that upstream unless the position is immersed in a wake behind the crest. In these cases large increases in the specified turbulence intensity would be necessary. The observed discontinuity in the established linear trend of increasing A_z with H/L for low slope gradients which occurs near the onset of separation should also be accounted for.

Due to the scarcity of data at this stage and the wide range of possible atmospheric conditions and hill slopes, any code rule cannot be expected to be accurate. Consequently any rule should reflect these deficiencies by being simple and conservative and there seems little point at this stage in developing a rule beyond one of a simple empirical nature. An additional unknown factor in the determination of structural loading is the change in pressure coefficient distribution over the face of the building due to the unusual velocity-height profiles often encountered on a hilly site.

10.4 CONCLUSIONS

* The prediction of exposure due to a hill site by several national building codes were compared with the model test data from the present project and all were shown to be inadequate.

* The parameters thought necessary for consideration in a satisfactory prediction method were listed.

* The accuracy of any method adopted could not be expected to be high as the existing experimental data was insufficient to adequately define the effects of atmospheric stability, hill height and local changes in hill shape.

CHAPTER 11

CONCLUSION

The principal features of the work carried out and the conclusions arising from each stage have been given at the end of each chapter and need not be repeated here. However, the main conclusions covering the most significant of the experimental observations are summarised below :

11.1 SUMMARY OF CONCLUSIONS

1) The dynamic performance of the propeller anemometers was shown to be similar to that predicted and together with the data acquisition system, was adequate for the measurement of the longitudinal turbulence characteristics.

2) The effect of atmospheric stability was shown to be a significant factor in the atmospheric boundary-layer at the moderate wind speeds encountered during the field tests.

3) The mean flow and turbulence close to the ground over the escarpments were dominated by the wakes generated behind the sharp crests.

4) The mean velocity fractional speed-up factor, ΔS had significant values beyond 10 escarpment heights downstream of the crest but decreased rapidly with height above the ground to a value below 0.1 at 3 escarpment heights above ground.

5) The value of ΔS close to the ground above the crest increased with increasing upwind slope in such a way that $\Delta S/(H/L) \approx 1.0$ for $(H/L) \leqslant 0.4$. A wide range of ΔS values were encountered for steeper slopes, but a peak value between 0.5 and 0.7 was evident near $H/L \approx 1.0$ Separation effects were dominant for slopes steeper than $(H/L) \approx 0.6$.

6) The value of ΔS generally decreased with increasing wind incidence angles measured from the crest normal, although little change was evident for angles less than $\pm 30°$.

7) Little change in the turbulence characteristics was noticed in the flow outside the wake region with the turbulence acting as if convected along the streamlines.

8) The extent and intensity of the strong turbulent wakes found behind the crest increased with slope angle and surface roughness of the escarpments.

9) No significant trends in gust factor were evident which could be attributed to the presence of the escarpments. The variation of gust factor over the escarpments was fully explained in terms of instrument response, gust averaging time, record length and turbulence intensity using established methods.

11.2 RECOMMENDATIONS FOR FUTURE WORK

11.2.1 Anemometer Development

Improvements to the quality of the surface finish and dimensional accuracy of the anemometer propellers would help to standardise their performance and reduce the scatter in their calibration. An improvement in the non-cosine response may also be possible by small changes in the blade profile, thus reducing or even eliminating the extent of the data correction required at present. Further testing of the non-cosine response for incidence angles close to 90° would improve the accuracy of the vertical anemometer correction factors. The poor dynamic performance of the vertical anemometers could be improved by increasing the pulse rate per revolution of the output signal from the anemometer so that the pulse count resolution is improved for each scan. Alternatively, the buffer storage capacity of the other two horizontal channels could be increased to allow a higher scan rate to be chosen for a given wind speed. In addition, a better understanding of the threshold velocity for large incidence angles would help in the prediction of the dynamic response of the vertical anemometer.

Improved bearing and housing design would help to reduce bearing friction and the corrosive effects from the weather, thus improving the dynamic performance and overall reliability. However the distance constant could not be reduced further without a reduction in the inertia of the propeller. Any improvement may also be limited by the aerodynamic damping which so far, has received very little attention in the literature. A more accurate mathematical description of the aerodynamic properties of the propeller anemometer system in turbulent conditions would indicate the parameters that would produce significant improvements in performance and serve to define any necessary correction factors. Further work is also necessary to establish the relationship between the 'averaging time' of the highest peak gust capable of being recorded within a certain limit of accuracy and the upper frequency limit of the anemometer subjected to single frequency sinusoidal gusts. The degree of over-estimation of the measured mean wind speed in

turbulent flow is also disputed in the literature and further comparisons with sonic or hot wire anemometers are necessary to obtain convincing evidence.

11.2.2 Effects due to Complex Terrain

During the present investigation it became abundantly clear that there was insufficient experimental information on the effects of the major parameters that influenced the wind flow over complex terrain. Consequently more model and field tests are necessary to rectify the deficiency. There seems little point in pursuing complex theoretical solutions to this problem unless there are sufficient experimental data to confirm the accuracy of their results.

Further model and full scale field tests of identical situations are also required to indicate the degree of accuracy and the limitations of wind tunnel investigations so that the conclusions from future model investigations may be considered in true perspective.

The parameters that require further experimental study to improve the understanding of this problem include the following :

1) The effect of different upwind slopes should be investigated for the more gradual slopes below 8:1 gradient which has been shown to still have a strong influence on the speed-up over the crest. The accuracy of the relation $\Delta S_{max} \alpha H/L$ still requires further confirmation together with the definition of the characteristic length, L for different hill shapes.

2) The profile of the upwind slope, whether straight, convex or concave and local changes in hill shape near the crest have been shown to be equally important as the average hill slope, but no details are yet available.

3) The existence of the inner layer predicted from theory has not yet been confirmed experimentally.

4) The effect of hill height to boundary-layer depth requires further investigation.

5) The prediction of separation near a hill top is important as the presence of separation dominates the flow over the steeper forward facing slopes.

6) Three dimensional effects require extensive experimental investigation but it may be that these effects are interrelated and too complex to isolate for even the most simple of the complex terrain situations. In that case, the only method of flow prediction would be to carry out model tests or measurements at the actual site.

7) The atmospheric stability effects on the speed-up over a hill of a certain shape are not understood as indicated by the conflicting statements in the literature. Extensive field measurements would be necessary covering a full range of stability conditions to determine whether or not stability had a strong effect, or only a secondary effect through its established modification of the approaching velocity-height profile.

   Field equipment for the measurement of the temperature gradient would be necessary together with higher masts (> 20 m) to cover a greater depth of the boundary-layer.

8) An improved prediction method for building code applications is long overdue and would be a very significant contribution to wind engineering.

REFERENCES

ALEXANDER, A.J. and COLES, C.F. (1971). A theoretical study of wind flow over hills. Proc. Third International Conference on Wind Effects on Buildings and Structures. Saikon Co.Ltd., Tokyo: 95-103.

ANTONIA, R.A. and LUXTON, R.E. (1971). The response of a turbulent boundary layer to a step change in surface roughness. Part I. rough to smooth. J.Fluid Mechanics, 48 part 4: 721-761.

ASTLEY, R.J. (1977). A finite element frozen vorticity solution for two dimensional wind flow over hills. 6th. Australasian Hydraulics and Fluid Mechanics Conference, University of Adelaide, South Australia: 443-446.

ASTLEY, R.J., BOWEN, A.J., LINDLEY, D. and PEARSE, J. (1977). The effect of some hill shapes on the atmospheric boundary layer near the ground. N.Z. Meteorological Service Symposium on Meteorology and Energy, Wellington, New Zealand: 93-108.

AUSTRALIAN STANDARD 1170 (1973) Part II, Wind forces: 52 p.

BARTKOWSKI, Z. (1965). Wind flow over small hills, Swiss Aero-Revue, 1: 2 p.

BAYNES, C.J. (1974). The statistics of strong winds for engineering applications. University of Western Ontario, Canada, BLWT-4-1974: 266 p (Thesis: Ph.D).

BENDAT, J.S. and PIERSOL, A.G. (1971). Random data: Analysis and measurement procedures. Wiley Interscience: 407 p.

BERLYAND, M.E. (1972). Atmospheric diffusion investigations in the USSR. Appendix to 'Dispersion and forecasting of air pollution.' W.M.O. Technical Note no. 121: 57-116.

BIETRY, J., SACRE, C. and SIMIU, E. (1978). Mean wind profiles and change of terrain roughness. J. Structural Div., ASCE, 104, ST 10, 1585-1593.

BOOTH, C., DANBY, N., EVERETT, T.W. and LAWSON, T.V. (1976). Wind conditions over the forest of Ae in South Scotland. University of Bristol, Dept.of Aeronautical Engineering Report, TVL/7620. 12 p.

BOUWMEESTER, R.J.B., MERONEY, R.N. and SANDBORN, V.A. (1978). Sites for wind-power installations: Wind characteristics over ridges. Draft final report, Part I, Colorado State University Research project No. CER 77-78 RJBB-RNM-VAS 51. Fort Collins, Colorado, U.S.A., 233 p.

BOWEN, A.J. and LINDLEY, D. (1974). Measurements of the mean wind flow over various escarpment shapes. Proc.Fifth Australasian Conference on Hydraulics and Fluid Mechanics, University of Canterbury, Christchurch, New Zealand: 211-219.

BOWEN, A.J. and LINDLEY, D. (1977). A wind tunnel investigation of the wind speed and turbulence characteristics close to the ground over various escarpment shapes. Boundary-Layer Meteorology, 12:259-271.

BOWEN, A.J. (1977). A review of current research relevant to the optimum siting of wind power installations in hilly terrain. Mechanical Engineering Dept., University of Canterbury report for the Institution of Mechanical Engineers (London) and the N.Z. Energy Research and Development Committee: 27 p.

BRADSHAW, P. (1971). An introduction to turbulence and its measurements. Pergamon Press (London): 218 p.

BRITISH STANDARD CP3 (1972). Basic data for the design of buildings. Chapter V, Part 2, Wind Loads: 48 p.

BROOK, R.R. (1977). Effective dynamic response of paired Gill anemometers. J.Boundary-Layer Meteorology, 11: 33-37.

BUSCH, N.E. and KRISTENSEN, L. (1976). Cup anemometer over-speeding. J.Applied Meteorology, 15: 1328-1332.

CANADIAN NATIONAL BUILDING CODE (1970). Canadian Structural Design Manual Supplement No. 4: 543-565.

CERMAK, J.E. and HORN, J.D. (1968). Tower shadow effect. J.Geophysical Research. 73, no. 6: 1869-1876.

CERMAK, J.E. (1974). Applications of fluid mechanics to wind engineering. Freeman Scholar Lecture, ASME Winter annual meeting, New York. 30 p.

CHERRY, N.J. (1976). Wind energy resource survey of New Zealand. Preliminary analysis of meteorological data. N.Z. Energy Research and Development Committee Report no. 8. April. 31 p. (NZERDC, University of Auckland, Auckland, N.Z.).

CHERRY, N.J. (1977). Wind energy resource survey of New Zealand. Annual Report, 1976-1977 to the N.Z. Energy Research and Development Committee. 15 p. (NZERDC, University of Auckland, Auckland, N.Z.).

CHERRY, N.J. (1978). Wind energy resource assessment using radar-wind observations. Wind Energy Resource Survey Publication WER-5. Dept. Agricultural Engineering, Lincoln College, Canterbury, N.Z.: 18 p.

COOK, N.J., COULSON, B.H. and McKAY, W. (1978). Wind conditions around the Rock of Gibralter. Building Research Establishment, U.K. Report CP27/78: 17 p.

COUNIHAN, J. (1973). Flow over two-dimensional hills and plateaux in simulated boundary layer flow. Central Electricity Research Laboratories Note no. RD/L/N277/73 UK. 18 p.

COUNIHAN, J. (1974). Flow over concatenated sinusoidal hills. Central Electricity Research Laboratories Note no. RD/L/N57/74, U.K.,14 p.

COUNIHAN, J. (1975). Adiabatic atmospheric boundary layers: A review and analysis of data from the period 1880-1972. Atmospheric Environment, 9: 871-905.

DAVENPORT, A.G. (1961). Applications of statistical concepts to the wind loading of structures. Proc. I.C.E., 19: 449-472.

DAVENPORT, A.G. (1964). Note on the distribution of the largest value of a random function with application to gust loading. Proc. I.C.E., 28: 187-196.

DAVENPORT, A.G. (1967). The dependence of wind loads on meteorological parameters. Proc.Second International Conference on Wind Effects on Buildings and Structures. Ottawa, Canada: 19-82.

DAVENPORT, A.G., VICKERY, B.J. and MELBOURNE, W.H. (1975). The structural and environmental effects of wind on buildings and structures. Post graduate course, Dept.Mechanical Engineering, Monash University, Melbourne, Australia: ch.2, 32-34.

DAWBER, K.R. and EDWARDS, P.J. (1978). Wind Energy resource in Otago. Wind Energy Resource Survey of New Zealand. Physics Dept., University of Otago, Dunedin, N.Z.: 53 p.

DEACON, E.L. (1951). The over estimation error of cup anemometers in fluctuating winds. J.Scientific Instruments, 28: 231-234.

DE BRAY, B.G. (1973). Atmospheric shear flows over ramps and escarpments. Industrial Aerodynamics Abstracts, 5: 1-4.

DEAVES, D.M. (1975/76). Wind over hills: A numerical approach. J.Industrial Aerodynamics, 1:371-391.

DURST, C.S. (1960). Wind speeds over short periods of time. Meteorological Mag., 89: 181-186.

ELDERKIN, C.E. (1966). Experimental investigation of the turbulence structure in the lower atmosphere. Battelle-Northwest Laboratory Report No. 329. Pacific Northwest Laboratory, Richland, Washington, U.S.A.

ELLIOTT, D.L. (1977). Synthesis of national wind energy assessment. Battelle Pacific Northwest Laboratories Report, BNWL 2220, WIND-5: Ibid: 47 p.

ESDU 72026 (1972). Characteristics of the wind speed in the lower layers of the atmosphere near the ground: Strong winds (neutral atmosphere). Engineering Sciences Data Unit, London, U.K., 35 p.

ESDU 74031 (1974). Characteristics of the atmospheric turbulence near the ground. Part II, Single point data for strong winds (neutral atmosphere). Engineering Sciences Data Unit. Ibid: 30 p.

EVERETT, T.W., FREESTON, D.H. and LAWSON, T.V. (1976). The wind tunnel simulation of the atmosphere for the study of the moving A.P.T. train. University of Bristol, Dept. of Aeronautical Engineering Report No. TVL 7610: 37 p.

FICHTL, G.H. and KUMAR, P. (1974). The response of a propeller anemometer to turbulent flow with the mean wind vector perpendicular to the axis of rotation. Boundary-Layer Meteorology, 6: 363-379.

FLAY, R.G.J. (1978). Structure of a rural atmospheric boundary layer near the ground. Dept. Mechanical Engineering, University of Canterbury, Christchurch, New Zealand. (Thesis: Ph.D.), 400 p + appendices.

FREESTON, D.H. (1974). Atmospheric shear flows over ramps and escarpments. Presented to Fifth Australasian Conference on Hydraulics and Fluid Mechanics, University of Canterbury, Christchurch, New Zealand. Available from Dept. Mechanical Engineering, University of Auckland, Auckland, N.Z.: 7 p.

FRENKIEL, J. (1962). Wind profiles over hills (in relation to wind power utilization). Quart.J. Royal Meteorological Soc., 88: 156-169.

FRENKIEL, J. (1963). Gusts over hills (in relation to wind power utilisation). Quart.J. Royal Meteorological Soc., 89: 281-283.

FRENCH RULES: Neige-Vent (1965). Revised 1967, reissued 1968.

FROST, W., MAUS, J.R. and FICHTL, G.H. (1974). A boundary-layer analysis of atmospheric motion over a semi-elliptical surface obstruction. Boundary-Layer Meteorology, 7: 165-184.

FROST, W., HARPER, W.L. and FICHTL, G.H. (1975). Analysis of atmospheric flow over a surface protrusion using the turbulence kinetic energy equation. Boundary-Layer Meteorology, 8: 401-417.

GIBLETT, M.A. (1932). The structure of the wind over level country. Meteorological Office Geophysical Memoranda, 51:20-35.

GILL, G.C. (1967). On the dynamic response of meteorological sensors and recorders. Dept. Meteorology and Oceanography, University of Michigan, U.S.A. Publication #90: 27 p.

GILL, G.C., OLSSON, L.E., SELA, J. and SUDA, M. (1967). Accuracy of wind measurements on towers and stacks. Bulletin American Meteorological Society, 48, No. 9: 665-674.

GILL, G.C. (1975). Development and use of the Gill UVW anemometer. Boundary-Layer Meteorology, 8: 475-495.

GOLDING, E.W. (1955). The generation of electricity by wind power. Philosophical Library, New York, 318 p.

HARDY, D.M. (1977). Wind studies in complex terrain. California University, Lawrence Livermore Laboratory report, May: 39 p.

HARRIS, R.I. (1968). Measurement of wind structure at heights up to 598 ft. above ground level. Proc.Symposium on Wind Effects on Buildings and Structures, Loughborough University of Technology, U.K.: 41 p.

HARRIS, R.I. (1970). The nature of the wind,CIRIA seminar, Modern Design of Wind Sensitive Structures, London. Paper no.3: 29-55.

HAUGEN, D.A. (ed)
(1973) Workshop on micrometeorology. American Meteorological Society, Boston, U.S.A.: 392 p.

HICKS, B.B. (1972). Propeller anemometers as sensors of atmospheric turbulence. Boundary-Layer Meteorology, 3: 214-228.

HINZE, J.O. (1975). Turbulence 2nd. Ed. McGraw-Hill Book Co., New York: 790 p.

HMSO (1965). Handbook of meteorological instruments. Air Ministry Meteorological Office, London. MO 557. 458 p.

HORST, T.W. (1973a). Corrections for response errors in a three component propeller anemometer. J.Applied Meteorology. 12:716-725.

HORST, T.W. (1973b). A computer algorithm for correcting non cosine response in the Gill anemometer. Battelle Pacific Northwest Laboratory report, BNWL-1651 Pt.1, Richland, U.S.A., 4 p.

JACKSON, P.S. and HUNT, J.C.R. (1975). Turbulent flow over a low hill. Quart.J.Royal Meteorological Soc. 101: 929-955.

JACKSON, P.S. (1975). A theory for flow over escarpments. Proc.Fourth International Conference on Wind Effects on Buildings and Structures, London, Cambridge University Press: 33-40.

JACKSON, P.S. (1976). Thorndon wind tower. Part I - Data collection. Ministry of Works and Development report No.3-76/4. MWD Central Laboratories, Gracefield, N.Z.: 61 p.

JACKSON, P.S. (1977). Aspects of surface wind behaviour. Wind Engineering, 1, No.1: 1-14.

JENSEN, N.O. and PETERSON, E.W. (1978). On the escarpment wind profile. Quart.J.Royal Meteorological Soc., 104: 719-728.

KAIMAL, J.C., WYNGAARD, J.C., IZUMI, Y. and COTE, O.R. (1972). Spectral characteristics of surface layer turbulence. Quart.J.Royal Meteorological Soc., 98: 563-589.

LAUNDER, B.E. and SPALDING, D.B. (1972). Lectures in mathematical models of turbulence. Academic Press: 169 p.

LINDLEY, D. and BOWEN, A.J. (1974). The response of cup and propeller anemometers to fluctuating wind speeds. Proc.Fifth Australasian Conference on Hydraulics and Fluid Mechanics. University of Canterbury, Christchurch, N.Z.: 269-277.

LINDLEY, D., BOWEN, A.J. and MORFEE, P. (1974). A propeller anemometer for a digital wind data acquisition system. Ibid: 258-268.

LUMLEY, J.L. and PANOFSKY, H.A. (1964). The structure of atmospheric turbulence. J.Wiley Interscience: 239 p.

MacCREADY, P.B. (1966). Mean wind speed measurements in turbulence. J.Applied Meteorology. 5: 219-225.

MACKEY, S. (1970). Wind studies in Hong Kong - some preliminary results. Industrial Aerodynamics Abstracts. 5: 1-16.

MAHRER, Y. and PIELKE (1975). A numerical study of the air flow over mountains using the two-dimensional version of the University of Virginia mesoscale model. J.Atmospheric Sciences. 32: 2144-2155.

MAZZARELLA, D.A. (1972). An inventory of specifications for wind measuring instruments. Bul.American Meteorological Soc., 53, No.9: 860-871.

McKEON, R.J. and MELBOURNE, W.H. (1971). Wind tunnel blockage effects and drag on bluff bodies in a rough wall boundary layer. Proc. Third International Conference on Wind Effects on Buildings and Structures, Tokyo: 263-272.

MERONEY, R.N. (1976). Wind characteristics and small WECS. Working group summary report, AMS-ERDA Workshop on Wind Characteristics for WECS. Boston U.S.A., CEP75-76RNM-41: 54 p.

MERONEY, R.N., SANDBORN, V.A., BOUWMEESTER, R. and RIDER, M. (1976). Wind tunnel simulation of the influence of two dimensional ridges on wind speed and turbulence. Proc.International Symposium on Wind Energy Systems. Cambridge, U.K.: 16 p.

MERONEY, R.N., BOWEN, A.J., LINDLEY, D. and PEARSE, J.R. (1978). Wind characteristics over complex terrain: Laboratory simulation and field measurements at Rakaia Gorge, New Zealand: Final report Part II, Colorado State University Research Report No. CER 77-78 RNM29: 219 p. (Also N.Z. Energy Research and Development Committee Report P5).

MILSOM, M.A. (1978). Low speed characteristics of the propeller anemometers. B.E. report no. 12/78. Mechanical Engineering Dept., University of Canterbury, Christchurch, N.Z.: 92 p.

MITSUTA, Y. (1971). Characteristics of air flow over the barriers in the storm. Proc.Third International Conference on Wind Effects on Buildings and Structures. Tokyo, Saikon Co.Ltd.: 33-44.

MODI, V.J. and EL-SHERBINY, S. (1975). Wall confinement effects on bluff bodies in turbulent flows. Proc.Fourth International Conference on Wind Effects on Buildings and Structures. London, U.K.: 121-132.

MORFEE, P.J. (1973). Data handling system. Dept.Mechanical Engineering, University of Canterbury, Christchurch, N.Z. (Thesis: M.E.):79 p.

MUNN, R.E. (1966). Descriptive Micrometeorology. Academic Press: 245 p.

NEWBERRY, C.W. and EATON, K.J. (1974). Wind loading handbook. Building Research Establishment Report, Dept.of the Environment, HMSO, LONDON, U.K.: 74 p.

NEW ZEALAND METEOROLOGICAL SERVICE (1975). Structure of the wind over New Zealand. Technical Information Circular No.147: 24 p.

NEW ZEALAND STANDARD 4203 (1976). Code of practice for general structural design and design loadings for buildings. Part 4; Wind Loads: 49-80.

NG, A. (1972). The performance of cup and propeller anemometers in steady and fluctuating wind streams. Dept.Mechanical Engineering, University of Canterbury, Christchurch, N.Z., (Thesis: M.E.): 160 p.

PANOFSKY, H.A. (1977). Wind structure in strong winds below 150 m. Wind Engineering, 1, No.2: 91-103.

PASQUILL, F. (1974). Atmospheric diffusion. C.E. Horwood Ltd., 2nd. Ed: 429 p.

PEARSE, J.R. (1978). (Private communication). Dept.Mechanical Engineering, University of Canterbury, Christchurch, N.Z.

PLATE, E.J. (1971). Aerodynamic characteristics of atmospheric boundary layers. U.S. Atomic Energy Commission, Office of Information Services. NTIS, Springfield Virginia 22151, U.S.A.: 190 p.

POPE, A. and HARPER, J.J. (1966). Low speed wind tunnel testing. J. Wiley and Sons: 457 p.

PUTNAM, P.C. (1948). Power from the wind. Van Nostrand Reinhold Co., New York: 224 p.

RAINE, J.K. (1974a). Modelling the natural wind. Dept.Mechanical Engineering, University of Canterbury, Christchurch, N.Z. (Thesis: Ph.D): 558 p.

RAINE, J.K. (1974b). Simulation of a neutrally stable rural atmospheric boundary layer in a wind tunnel. Proc.Fifth Australasian Conference on Hydraulics and Fluid Mechanics. University of Canterbury, Christchurch, N.Z.: 190-199.

RAINE, J.K. and STEVENSON, D.C. (1977). Wind protection by model fences in a simulated atmospheric boundary layer. J.Industrial Aerodynamics, 2:159-180.

RASMUSSEN, C.G. (1966). Measurement of turbulence characteristics. DISA Information, 3: 9-20.

RASMUSSEN, C.G. The DISA constant temperature anemometer. DISA Information Circular. DISA Electronik A/S, Herlev, Denmark: 9 p.

RIDER, M.A. and SANDBORN, V.A. (1977a). Measurements of the mean and longitudinal turbulent velocities over varying hill shapes. Colorado State University Research Memorandum No.28. CER 77-78 MAR-VAS28: 29 p.

RIDER, M.A. and SANDBORN, V.A. (1977b). Sites for wind power installations. Technical report. Boundary layer turbulence over two dimensional hills. Colorado State University Report. CER 77-78 MAR-VAS4: 125 p.

R.M. YOUNG CO. (1972). Instruction manual: Gill propeller anemometer. Traverse City, Michigan, U.S.A.: 19 p.

ROBERTSON, J.M. (1965). Hydrodynamics in theory and application. Prentice Hall: 141-145.

SACRE, C. (1973). Influence d'une colline sur la vitesse du vent dans la couche limite de surface. Centre Scientifique et Technique du Batiment, Nantes, France: 16 p.

SACRE, C. (1974). Estimation theorique des proprietes de l'ecoulement de l'air sur une colline bi-dimensionelle. Ibid: 30 p.

SACRE, C. (1975). Une methode numerique pour le calcul approche de la sur vitesse du vent sur une colline. Ibid. Report ENCL1-75-3: 26 p.

SACRE, C. (1978). An experimental study of the airflow over a hill in the atmospheric boundary layer. Submitted for publication to Boundary Layer Meteorology: 31 p.

SCHLICHTING, H. (1960). Boundary Layer Theory. McGraw Hill Book Co.: 647 p.

SCORER, R.S. (1949). Theory of waves in the lee of mountains. Quart. J.Royal Meteorological Soc., 75: 41-56.

SCORER, R.S. (1952). Mountain gap winds; a study of surface wind at Gibralter. Quart.J.Royal Meteorological Soc., 78: 53-61.

SERRA, L. (1949). Variations de la vitesse du vent au passage sur des obstacles de formes diverses. L'Institut Aerotechnique de St. Cyr. Paris: 7 p.

SHELLARD, H.C. (1963). The estimation of design wind speeds. National Physical Laboratories, U.K., Symposium 16: 30-51.

SHRENK, O. (1929). Errors due to inertia with cup anemometers in fluctuating winds. Zeitschrift fur Technischen Physik. 10: 57-66.

SMITH, G.D. (1975). Numerical solutions of partial differential equations. Oxford University Press: 179 p.

SUMNER, C.J. (1968). A low torque cup anemometer. Australian J. Instrumentation and Control. October: 39-40.

SUTTON, O.G. (1953). Micrometeorology. McGraw-Hill Book Co.: 333 p.

TAULBEE, D.B. and ROBERTSON, J.M. (1972). Turbulent separation analysis ahead of a step. Trans. ASME, J.Basic Engineering, Sept.: 544-550.

TAYLOR, P.A. and GENT, P.R. (1974). A model of atmospheric boundary-layer flow above an isolated two-dimensional 'hill'; an example of flow above 'gentle topography'. Boundary-Layer Meteorology, 7: 349-362.

TAYLOR, P.A. (1977a). Some numerical studies of surface boundary-layer flow above gentle topography. Boundary-Layer Meteorology, 11: 439-465.

TAYLOR, P.A. (1977b). Numerical studies of neutrally stratified planetary boundary-layer flow above gentle topography. I. Two dimensional cases. Boundary-Layer Meteorology, 12: 37-60.

TEUNISSEN, H.W. (1970). Characteristics of the mean wind and turbulence in the planetary boundary-layer. UTIAS Review No.32: 45 p.

TIELEMAN, H.W. and TAVOULARIS, S.C. (1977). An instrumentation system for the measurement of atmospheric turbulence. J.Industrial Aerodynamics, 2: 49-63.

TOWNSEND, A.A. (1965). The response of a turbulent boundary layer to abrupt changes in surface conditions. J.Fluid Mechanics, 22: 799-822.

WALKER, G.K. (1957). Rotational flow over a surface protrusion. Pennsylvania State University, U.S.A. (Thesis, M.Sc.): 75 p.

WIERINGA, J. (1973). Gust factors over open water and built-up country. Boundary-Layer Meteorology, 3: 424-441.

WIERINGA, J. (1976). An objective exposure correction method for average wind speeds measured at a sheltered location. Quart.J. Royal Meteorological Soc., 102: 241-253.

WMO (1964). Sites for wind power installations. World Meteorological Organisation Technical Note no.63: 38 p.

WYATT, T.A. (1971). A review of wind loading specifications. The Structural Engineer, 49, No.5: 227-234.

YIH, C.S. (1959). Two solutions for inviscid rotational flow with corner eddies. J.Fluid Mechanics, 5: 36-40.

APPENDIX I

ALGOL COMPUTER PROGRAMS DEVELOPED AND USED DURING THE PROJECT FOR THE PROCESSING OF THE FIELD DATA

- CORRECTDATA -

- PEAKGUSTS -

BURROUGHS B6700 ALGOL COMPILER, VERSION 2.9.190, WEDNESDAY, 07/26/78,

C O R R E C T D A T A

```
BEGIN
FILE DATA(KIND=TAPE7,FILETYPE=7,MAXRECSIZE=64,BLOCKSIZE=64,                    1
     LABELTYPE=STANDARD,UNITS=WORDS);
FILE TEMPFILE(KIND=DISK,MAXRECSIZE=256,BLOCKSIZE=256,AREASIZE=30,
     FLEXIBLE=TRUE,UNITS=WORDS);
FILE TEMPFILE2(KIND=DISK,MAXRECSIZE=256,BLOCKSIZE=256,AREASIZE=30,
     FLEXIBLE=TRUE,PROTECTION=SAVE,UNITS=WORDS);
FILE INFO(KIND=READER);
FILE FOO(KIND=PRINTER);
INTEGER NOCH,NARR,IKK;
REAL SR,R;
READ(INFO,<5I8>,NOCH,NARR,SR,IKK,R);
BEGIN
LABEL L1,L2,L3,L4,L5,L6,L7,L8,L9,L10,L11,L12;                                  2
INTEGER I,J,IA,Z,
     A,B,C,AA,BB,CC,NN,CH,
     MM,
     CHU,CHV,CHW;
REAL GU,GV,GW,ALFA,BETA,
     FU,FV,FW,VA,VB,VC,ZA,S,
     UM,UMS,
     CNVRTTORPS;
INTEGER ARRAY N[0:63],HORCOR[1:101],
          M[0:256*(NOCH+3)],D[1:NOCH,0:255],ISAVE[1:3*NARR];
REAL ARRAY CU,CV,CW,CUS,CVS,CWS[1:NARR],
     CUAV,CVAV,CWAV[1:NARR],
     CU2,CV2,CW2,CUV,CUW,CVW[1:NARR],
     SINALFA,COSALFA,SINBETA,COSBETA[1:NARR],
     US,U2S,V2S,W2S,UVS,UWS,VWS[1:NARR],
     UAV,RMSU,RMSV,RMSW,RUV,RUW,RVW[1:NARR],
     AMP[1:NARR],
     VEL[1:3*NARR,0:255],
     UFLUCT[1:NARR,0:255],UMEAN[0:NARR],
     UCCD[1:3*NARR,0:255],CORFCTR[1:3*NARR],CCD[1:3*NARR,0:255];
POINTER PA;
%
READ(INFO,<26I3>,FOR I:=1 STEP 1 UNTIL 101 DO HORCOR[I]);
WRITE(FOO,<X10,"NOCH= ",I2,X2,"NARR= ",I2,X2,"SR= ",I2,X2,"IKK= ",
     I8,X2,"R= ",I3>,NOCH,NARR,SR,IKK,R);
WRITE(FOO,<X5,"LENGTH= ",F6.2,X2,"MINUTES",/>,IKK*16/(SR*15*60));
WRITE(FOO[SPACE 2]);
WRITE(FOO,<X10,"HORCOR ARRAY",/>);
WRITE(FOO,<25I5>,FOR I:=1 STEP 1 UNTIL 101 DO HORCOR[I]);
WRITE(FOO[SPACE 2]);
CNVRTTORPS:=SR/32;
FOR I:=1 STEP 1 UNTIL 3*NARR DO
CURFCTR[I]:=R/1000;
FOR I:=1 STEP 1 UNTIL NARR DO
CUS[I]:=CVS[I]:=CWS[I]:=0;
%
%READ DATA BY BLOCKS AND PLACE IN D[I,J] ARRAY
%
WRITE(FOO,<X5,"CORRECTED MEAN VELOCITIES OF EACH DATA BLOCK IN METRES
PER SECOND ALONG EACH ANEMOMETER AXES FOR ARRAY NUMBER 1 ">);
WRITE(FOO,<X20,"DATA BLOCK MEANS",X24,"CULMULATIVE MEANS">);
WRITE(FOO,<X7,"Z",X9,"VA",X8,"VB",X8,"VC",X8,"VEL",X7,"VA",X8,"VB",X8,
"VC",X8,"VEL"/>);
MM:=0;
FOR I:=1 STEP 1 UNTIL NARR DO
BEGIN
ISAVE[I*3-2]:=ISAVE[I*3-1]:=86;                                                3
ISAVE[I*3]:=51;
END;
FOR Z:=1 STEP 1 UNTIL IKK/256 DO                                               3
BEGIN
FOR I:=0 STEP 1 UNTIL 2*(NOCH+3)/3-1 DO                                        3
BEGIN
PA:=POINTER(N[0],8);                                                           4
READ(DATA,64,N[*])[L1];
GO TO L3;
L1:
WRITE(FOO,<X10,"END OF 7 TRACK TAPE FILE BEFORE EXPECTED">);
WRITE(FOO,<X10,"BLOCK NO= ",I4,"I= ",I8>,Z,I);
GO TO L12;
L3:
FOR J:=0 STEP 1 UNTIL 383 DO
BEGIN
M[384*I+J]:=REAL(PA,1);                                                        5
PA:=PA+1;
END;
END;
IF M[0] NEQ 127 THEN GO TO L4;                                                 5
FOR I:=1 STEP 1 UNTIL NOCH DO                                                  4
BEGIN
FOR J:=0 STEP 1 UNTIL 255 DO                                                   4
BEGIN
D[I,J]:=M[(NOCH+3)*J+(I+2)];                                                   5
IF D[I,J]>128 THEN D[I,J]:=D[I,J]-256;
END;
END;
GO TO L2;                                                                      5
L4:                                                                            4
WRITE(FOO,<"SYNC LOST">);
WRITE(FOO,<"BLOCK NO= ",I4,"NO OF SCANS DONE= ",I6>,Z,(Z-1)*256);
```

```
GO TO L12;
L2:
%
%INTRODUCE MISSING CHANNELS TO MAKE UP ORTHOGONAL ARRAYS AND CONVERT TO
%METRES PER SECOND IN UCCD[I,J] ARRAY.
%
FOR J:=0 STEP 1 UNTIL 855 DO
BEGIN
FOR I:=1 STEP 1 UNTIL 5 DO
UCCD[I,J]:=D[I,J]*CNVRTTORPS*CORFCTR[I];
UCCD[6,J]:=0;
FOR I:=7 STEP 1 UNTIL 8 DO
UCCD[I,J]:=D[I-1,J]*CNVRTTORPS* CORFCTR[I-1];
UCCD[9,J]:=0;
FOR I:=10 STEP 1 UNTIL 11 DO
UCCD[I,J]:=D[I-2,J]*CNVRTTORPS*CORFCTR[I-2];
UCCD[12,J]:=0;
FOR I:=13 STEP 1 UNTIL 35 DO
UCCD[I,J]:=D[I-3,J]*CNVRTTORPS*CORFCTR[I-3];
UCCD[36,J]:=0;
FOR I:=37 STEP 1 UNTIL 38 DO
UCCD[I,J]:=D[I-4,J]*CNVRTTORPS*CORFCTR[I-4];
UCCD[39,J]:=0;
FOR I:=40 STEP 1 UNTIL 41 DO
UCCD[I,J]:=D[I-5,J]*CNVRTTORPS*CORFCTR[I-5];
UCCD[42,J]:=0;
END;
%
% CORRECT FOR NON COSINE RESPONSE AND PLACE IN CCD[I,J].
%
FOR CH:=1 STEP 1 UNTIL NARR DO
BEGIN
CHU:=CH*3-2;
CHV:=CH*3-1;
CHW:=CH*3;
FOR IA:=0 STEP 1 UNTIL 255 DO
BEGIN
NN:=0; % NN KEEPS TRACK OF THE NUMBER OF ITERATIONS
A:=ISAVE[CHU];
B:=ISAVE[CHV];
C:=ISAVE[CHW];
GU:=UCCD[CHU,IA]; %RAW DATA IN
GV:=UCCD[CHV,IA];
GW:=UCCD[CHW,IA]*1.25;
L5:
VA:=GU*HORCOR[A]/100;  %CORRECT DATA
VB:=GV*HORCOR[B]/100;
VC:=GW*HORCOR[C]/125;
S:=SQRT(VA**2+VB**2+VC**2)+0.001;
AA:=VA*50/S+51;
BB:=VB*50/S+51;
CC:=VC*50/S+51;
IF ABS(AA-A) GTR 1 THEN GO TO L8;
L6:
IF ABS(BB-B) GTR 1 THEN GO TO L8;
L7:
IF ABS(CC-C) GTR 1 THEN GO TO L8 ELSE GO TO L11;
L8:
NN:=NN+1;
IF NN GEQ 5 THEN GO TO L10;
L9:
A:=AA; % UPDATE COSINES FOR NEXT ITERATION
B:=BB;
C:=(C+CC)/2;
GO TO L5;
L10:
MM:=MM+1;
L11:
CCD[CHU,IA]:=VA;
CCD[CHV,IA]:=VB;
CCD[CHW,IA]:=(VC+GW*HORCOR[CC]/125)/2;
ISAVE[CHU]:=A;
ISAVE[CHV]:=B;
ISAVE[CHW]:=C;
END;
END; % END OF COSINE CORRECTION
%
%CALCULATE CUMULATIVE MEAN VELOCITY ALONG EACH ANEMOMETER AXIS.
%
FOR I:=1 STEP 1 UNTIL NARR DO
BEGIN
CU[I]:=CV[I]:=CW[I]:=0;
CHU:=I*3-2;
CHV:=I*3-1;
CHW:=I*3;
DO VECTORMODE (CCD[CHU,*],P=CU[I],FOR 256)
     BEGIN P:=*+CCD]INCREMENT CCD; END;
DO VECTORMODE (CCD[CHV,*],P=CV[I],FOR 256)
     BEGIN P:=*+CCD]INCREMENT CCD; END;
DO VECTORMODE (CCD[CHW,*],P=CW[I],FOR 256)
     BEGIN P:=*+CCD]INCREMENT CCD; END;
ZA:=(Z-1)/Z;
CUS[I]:=**ZA+CU[I]/Z;
CVS[I]:=**ZA+CV[I]/Z;
CWS[I]:=**ZA+CW[I]/Z;
END;
%      RECORD TREND IN MEAN VELOCITY OF CHANNEL #1
UM:=SQRT(CU[1]**2+CV[1]**2+CW[1]**2)/256;
UMS:=SQRT(CUS[1]**2+CVS[1]**2+CWS[1]**2)/256;
WRITE(FOO,<9F10.2>,Z,CU[1]/256,CV[1]/256,CW[1]/256,UM,
     CUS[1]/256,CVS[1]/256,CWS[1]/256,UMS);
%WRITE BLOCK ONTO TEMPFILE.
FOR I:=1 STEP 1 UNTIL 3*NARR DO
WRITE(TEMPFILE,256,CCD[I,*]);
END; % END OF DATA BLOCK PROCESSING
%
%
WRITE (FOO,<//X5,"MM= "I6/>,MM);
REWIND(TEMPFILE);
%
%CALCULATE MEAN WIND DIRECTION FOR EACH ARRAY.
%
WRITE(FOO,<//X5,"CORRECTED MEAN VELOCITIES IN METRES PER SECOND ALONG THE
 ANEMOMETER AXES">);

WRITE(FOO,<//X8,"I",X8,"VA",X8,"VB",X8,"VC",X6,"ALFA",X6,"BETA",X7,
```

```
"UMEAN"/>)$

FOR I:=1 STEP 1 UNTIL NARR DO
BEGIN
BETA:=ARCTAN2(CVS[I],CUS[I]))
SINBETA[I]:=SIN(BETA))
COSBETA[I]:=COS(BETA))
ALFA:=ARCTAN2(CWS[I],SQRT(CUS[I]**2+CVS[I]**2))$
SINALFA[I]:=SIN(ALFA))
COSALFA[I]:=COS(ALFA))
CUAV[I]:=CUS[I]/256)
CVAV[I]:=CVS[I]/256)
CWAV[I]:=CWS[I]/256)
UMEAN[I]:=SQRT(CUAV[I]**2+CVAV[I]**2+CWAV[I]**2))
WRITE (FOO(<7F10.2>,I,CUAV[I],CVAV[I],CWAV[I],ALFA*57.296,BETA*57.296,
      UMEAN[I]))
END)
WRITE (FOO[SPACE 2]))
%
%CHANGE AXES TO ALIGN WITH MEAN WIND DIRECTION
%
FOR Z:=1 STEP 1 UNTIL IKK/256 DO
BEGIN
% READ BLOCK OFF TEMPFILE AND PLACE IN CCD[I,J] ARRAY
FOR I:=1 STEP 1 UNTIL 3*NARR DO
READ(TEMPFILE,256,CCD[I,*])
% CONVERT AXES AND STORE IN VEL[I,J] ARRAY
FOR I:=1 STEP 1 UNTIL NARR DO
BEGIN
CHU:=I*3-2)
CHV:=I*3-1)
CHW:=I*3)
FOR J:=0 STEP 1 UNTIL 255 DO
BEGIN
VEL[CHU,J]:=(CCD[CHU,J]*COSBETA[I]+CCD[CHV,J]*SINBETA[I])*
      COSALFA[I]+CCD[CHW,J]*SINALFA[I])
VEL[CHV,J]:=CCD[CHV,J]*COSBETA[I]-CCD[CHU,J]*SINBETA[I])
VEL[CHW,J]:=CCD[CHW,J]*COSALFA[I]-
      (CCD[CHU,J]*COSBETA[I]+CCD[CHV,J]*SINBETA[I])*SINALFA[I])
UFLUCT[I,J]:=VEL[CHU,J]-UMEAN[I])
END)
END)
% CALCULATE MEAN TURBULENCE PARAMETERS
FOR I:=1 STEP 1 UNTIL NARR DO
BEGIN
CHU:=I*3-2)
CHV:=I*3-1)
CHW:=I*3)
CU[I]:=CU2[I]:=CV2[I]:=CW2[I]:=CUV[I]:=CUW[I]:=CVW[I]:=0)
DO VECTORMODE (VEL[CHU,*],P=CU[I],FOR 256)
      BEGIN P:=*+VEL INCREMENT VEL END)
DO VECTORMODE (UFLUCT[I,*],P=CU2[I],FOR 256)
      BEGIN P:=*+UFLUCT*UFLUCT INCREMENT UFLUCT END)
DO VECTORMODE (VEL[CHV,*],P=CV2[I],FOR 256)
      BEGIN P:=*+VEL*VEL INCREMENT VEL END)
DO VECTORMODE (VEL[CHW,*],P=CW2[I],FOR 256)
      BEGIN P:=*+VEL*VEL INCREMENT VEL END)
DO VECTORMODE (UFLUCT[I,*],Q=VEL[CHV,*],P=CUV[I],FOR 256)
      BEGIN P:=*+UFLUCT*Q INCREMENT UFLUCT,Q END)
DO VECTORMODE (UFLUCT[I,*],Q=VEL[CHW,*],P=CUW[I],FOR 256)
      BEGIN P:=*+UFLUCT*Q INCREMENT UFLUCT,Q END)
DO VECTORMODE (VEL[CHV,*],Q=VEL[CHW,*],P=CVW[I],FOR 256)
      BEGIN P:=*+VEL*Q INCREMENT VEL,Q END)
ZA:=(Z-1)/Z)
US[I]:=**+ZA*CU[I]/Z)
U2S[I]:=**+ZA*CU2[I]/Z)
V2S[I]:=**+ZA*CV2[I]/Z)
W2S[I]:=**+ZA*CW2[I]/Z)
UVS[I]:=**+ZA*CUV[I]/Z)
UWS[I]:=**+ZA*CUW[I]/Z)
VWS[I]:=**+ZA*CVW[I]/Z)
END)
%     WRITE BLOCK ONTO TEMPFILE2
FOR I:=1 STEP 1 UNTIL 3*NARR DO
WRITE(TEMPFILE2,256,VEC[I,*]))
END)
WRITE(FOO,<X5>"CORRECTED MEAN VELOCITY ALONG AXIS PARALLEL WITH MEAN WI
ND DIRECTION,TURBULENCE INTENSITIES AND REYNOLDS STRESSES"/>))

WRITE(FOO,<X5,"I",X8,"U",X8,"A",X8,"U2",X7,"V2",X7,"W2",X7,"UV",X7,
      "UW",X7,"VW"/>))

FOR I:=1 STEP 1 UNTIL NARR DO
BEGIN
UAV[I]:=US[I]/256+0.0001)
RMSU[I]:=SQRT(U2S[I]/256)+0.0001)
RMSV[I]:=SQRT(V2S[I]/256)+0.0001)
RMSW[I]:=SQRT(W2S[I]/256)+0.0001)
RUV[I]:=UVS[I]/(256*RMSU[I]*RMSV[I]))
RUW[I]:=UWS[I]/(256*RMSU[I]*RMSW[I]))
RVW[I]:=VWS[I]/(256*RMSV[I]*RMSW[I]))
END)
FOR I:=1 STEP 1 UNTIL 6 DO
AMP[I]:=0)
FOR I:=7 STEP 1 UNTIL 10 DO
AMP[I]:=UAV[I]/UAV[I-6])
FOR I:=11 STEP 1 UNTIL 14 DO
AMP[I]:=UAV[I]/UAV[I-10])
FOR I:=1 STEP 1 UNTIL NARR DO
WRITE(FOO,<9F9.3>,I,UAV[I],AMP[I],RMSU[I]/UAV[I],RMSV[I]/UAV[I],
      RMSW[I]/UAV[I],RUV[I],RUW[I],RVW[I]))
L12:
END)


END.
```

BURROUGHS 86700 ALGOL COMPILER, VERSION 2.9.190, WEDNESDAY, 08/02/78,

P E A K G U S T S

```
BEGIN
FILE TEMPFILE2(KIND=DISK,MAXRECSIZE=256,BLOCKSIZE=256,AREASIZE=60,                1
      FLEXIBLE=TRUE,PROTECTION=SAVE,UNITS=WORDS);
FILE INFO(KIND=READER);
FILE FOO(KIND=PRINTER);
INTEGER NOCH,NARR,N,NCL,SR;
READ (INFO,<SI8>,NOCH,NARR,SR,N,NCL);
BEGIN
LABEL L1,L2,L3,LEND;                                                             2
INTEGER Z,ZMAX,ZZMAX,ZMIN,ZZMIN,
      I,J,JMAX,JJMAX,JMIN,JJMIN,
      CV,IA,
      T,K,KK,M;
REAL KKA,ZA,CO,SI,CUM;
REAL ARRAY U[1:N/256,0:255],
      UMEAN,U2,RMS[1:NARR],
      UMEANS,U2S[1:NARR],
      UMAX,UMIN[1:NARR],
      T1,T2[1:NARR],
      FREQ[1:NARR,0:NCL+1],
      MOPT[1:NARR,1:NCL],GAUS[1:NARR,1:NCL],
      NORMGAUS[1:33],
      VELMAX,VELMIN[1:NARR,0:10];
%
% CONSIDERING EACH ARRAY IN TURN,READ OFF U VELOCITY
% COMPONENT(ALONG THE MEAN WIND DIRECTION) AND PLACE
% IN U[Z,*] ARRAY FOR WHOLE RECORD.
%
WRITE (FOO,<X5,"CHANNELS=",I2,X5,"ARRAYS=",I2,X5,"SCANS=",I6,X5,
"SCAN RATE=",I2,X5,"NCL=",I2//>,NOCH,NARR,N,SR,NCL);
WRITE (FOO,<X5,"I",X7,"UMIN",X5,"UMEAN",X4,"UMAX",X5,"RMSU",X5,
"G.F.",X5,"P.F."/>);
FOR I:=1 STEP 1 UNTIL NARR DO
BEGIN
FOR Z:=1 STEP 1 UNTIL N/256 DO                                                   3
READ (TEMPFILE2[(Z-1)*3*NARR+(3*I-3)],256,U[Z,*])[L1];
REWIND (TEMPFILE2);
GO TO L2;
L1:
WRITE (FOO,<X10,"END OF TEMPFILE2 BEFORE EXPECTED">);
WRITE (FOO,<X10,"BLOCK NO= ",I4,"I= ",I8>,Z,I);
GO TO LEND;
L2:
%
% FIND MAX AND MIN GUST SPEEDS AND THEIR COORDINATES IN ARRAY
%
UMIN[I]:=U[2,0];
FOR Z:=2 STEP 1 UNTIL N/256-1 DO
FOR J:=0 STEP 1 UNTIL 255 DO
BEGIN
IF ABS(U[Z,J]) GTR ABS(UMAX[I]) THEN                                             4
BEGIN
UMAX[I]:=U[Z,J];                                                                 5
ZMAX:=Z;
JMAX:=J;
END ELSE
IF ABS(U[Z,J]) LSS ABS(UMIN[I]) THEN                                             5
BEGIN
UMIN[I]:=U[Z,J];                                                                 5
ZMIN:=Z;
JMIN:=J;
END;
END;                                                                             5

%                                                                                4
% CALCULATE MAX AND MIN GUST SPEEDS OVER A RANGE OF AVERAGING TIMES
%
FOR T:=1 STEP 1  UNTIL 10 DO
BEGIN
M:=T*SR*15/64; % NUMBER OF DATA FOR HALF T/2 SEC. GUST                           4
KK:=0;
FOR K:=-M STEP 1 UNTIL M DO
BEGIN
KK:=KK+1;                                                                        5
KKA:=(KK-1)/KK;
%
IF JMAX+K LSS 0 THEN
BEGIN JJMAX:=JMAX+K+256;ZZMAX:=ZMAX-1;
END ELSE
IF JMAX+K GTR 255 THEN                                                           6
      BEGIN JJMAX:=JMAX+K-256;ZZMAX:=ZMAX+1;                                     6
      END ELSE
      BEGIN JJMAX:=JMAX+K; ZZMAX:=ZMAX;                                          6
END;                                                                             6
VELMAX[I,T]:=*+KKA+U[ZZMAX,JJMAX]/KK;                                            6
%
IF JMIN+K LSS 0 THEN
BEGIN JJMIN:=JMIN+K+256;ZZMIN:=ZMIN-1;
END ELSE
IF JMIN+K GTR 255 THEN                                                           6
      BEGIN JJMIN:=JMIN+K-256;ZZMIN:=ZMIN+1;                                     6
      END ELSE
      BEGIN JJMIN:=JMIN+K; ZZMIN:=ZMIN;                                          6
END;                                                                             6
VELMIN[I,T]:=*+KKA+U[ZZMIN,JJMIN]/KK;                                            6
END;
END;                                                                             5
%                                                                                4
% CALCULATE MEAN AND RMS VELOCITIES
%
```

```
FOR Z:=1 STEP 1 UNTIL N/256 DO
BEGIN
UMEAN[I]:=0;
U2[I]:=0;
DO VECTORMODE (U[Z,*],P=UMEAN[I],FOR 256)
    BEGIN P:=*+U;INCREMENT U;END;
DO VECTORMODE (U[Z,*],P=U2[I],FOR 256)
    BEGIN P:=*+U*U;INCREMENT U;END;
ZA:=(Z-1)/Z;
UMEANS[I]:=**ZA+UMEAN[I]/Z;
U2S[I]:=**ZA+U2[I]/Z;
END;
UMEAN[I]:=UMEANS[I]/256;
U2[I]:=U2S[I]/256;
RMS[I]:=SQRT(U2[I]-UMEAN[I]**2);
WRITE (FOO,<7F9.3>,I,UMIN[I],UMEAN[I],UMAX[I],RMS[I],
    UMAX[I]/UMEAN[I],(UMAX[I]-UMEAN[I])/RMS[I]);
END;
%
WRITE (FOO,</X10,"MAX GUST SPEEDS AVERAGED OVER T SECS FROM 0.5 TO 5 SEC
S",/>);

WRITE (FOO,<" AV. TIME",10F9.3/>,FOR T:=1 STEP 1 UNTIL 10 DO T/2);
FOR I:=1 STEP 1 UNTIL NARR DO
WRITE (FOO,<11F9.3>,I,FOR T:=1 STEP 1 UNTIL 10 DO VELMAX[I,T]);
WRITE (FOO,</X10,"MIN GUST SPEEDS AVERAGED OVER T SECS FROM 0.5 TO 5 SEC
S",/>);

WRITE (FOO,<" AV. TIME",10F9.3/>,FOR T:=1 STEP 1 UNTIL 10 DO T/2);
FOR I:=1 STEP 1 UNTIL NARR DO
WRITE (FOO,<11F9.3>,I,FOR T:=1 STEP 1 UNTIL 10 DO VELMIN[I,T]);
WRITE (FOO,</X10,"GUST FACTORS FOR PEAK VELOCITIES AVERAGED OVER T SECS"
,/>);

WRITE (FOO,<" AV. TIME",10F9.3/>,FOR T:=1 STEP 1 UNTIL 10 DO T/2);
FOR I:=1 STEP 1 UNTIL NARR DO
WRITE (FOO,<11F9.3>,I,FOR T:=1 STEP 1 UNTIL 10 DO VELMAX[I,T]/UMEAN[I]);
WRITE (FOO,</X10,"PEAK FACTORS FOR PEAK VELOCITIES AVERAGED OVER T SECS"
,/>);

WRITE (FOO,<" AV. TIME",10F9.3/>,FOR T:=1 STEP 1 UNTIL 10 DO T/2);
FOR I:=1 STEP 1 UNTIL NARR DO
WRITE (FOO,<11F9.3>,I,FOR T:=1 STEP 1 UNTIL 10 DO

(VELMAX[I,T]-UMEAN[I])/RMS[I]);
WRITE (FOO[SPACE 4]);
%
% CALCULATE AND PRINTOUT NORMALISED GAUSSIAN DISTRIBUTION
%
WRITE (FOO,<"THE NORMALISED GAUSSIAN DISTRIBUTION",//>);

FOR CV:=1 STEP 1 UNTIL 33 DO
BEGIN
NORMGAUS[CV]:=0.39894*EXP(-(((CV-17)/4)**2)/2);
WRITE (FOO,<"DISTANCE FROM MEAN IN STD. DEVS.= ",
F7.4,X3,"NORM. GAUSS. PROB.= ",F7.4>,(CV-17)/4,NORMGAUS[CV]);

END;
%
% CALCULATE VELOCITY PROBABILITY DISTRIBUTION FOR EACH ARRAY.
% FIND BIN WIDTH AND THEIR MID POINTS
%
WRITE (FOO[SPACE 2]);
WRITE (FOO,</X10,"VELOCITY PROBABILITY DISTRIBUTIONS FOR EACH CHANNEL
",//>);

FOR I:=1 STEP 1 UNTIL NARR DO
BEGIN
FOR Z:=1 STEP 1 UNTIL N/256 DO
READ (TEMPFILE2[(Z-1)*3*NARR+(3*I-3)],256,U[Z,*]);
REWIND (TEMPFILE2);
WRITE (FOO,<"THE BIN MID POINTS ARE AS FOLLOWS FOR ARRAY",I6/>,I);

T2[I]:=(UMAX[I]-UMIN[I])/NCL; % BIN WIDTH
T1[I]:=UMIN[I]+T2[I]/2; % LOWEST BIN MID POINT
FOR CV:=1 STEP 1 UNTIL NCL DO
BEGIN
MDPT[I,CV]:=T1[I]+T2[I]*(CV-1);
WRITE (FOO,<"BIN",I2,X2,"MID VALUE IS=",F9.3>,CV,MDPT[I,CV]);
END;
% CALCULATE FREQUENCIES OF OCCURRENCE
CO:=UMIN[I];
SI:=T2[I];
IF SI EQL 0 THEN GO TO L3;
FOR Z:=2 STEP 1 UNTIL N/256-1 DO
FOR J:=0 STEP 1 UNTIL 255 DO
BEGIN
IA:=INTEGERT((U[Z,J]-UMIN[I])/SI)+1;
FREQ[I,IA]:=*+1;
END;
FREQ[I,NCL]:=FREQ[I,NCL]+FREQ[I,NCL+1];
WRITE (FOO,</"NUMBER OF SAMPLES PER CLASS AND CUMULATIVE FREQUENCY FOR A
RRAY",I6/>,I);

CUM:=0;
FOR CV:=1 STEP 1 UNTIL NCL DO
BEGIN
CUM:=*+FREQ[I,CV]/(N-512);
WRITE (FOO,<"BIN",I2,X3,"NUMBER OF SAMPLES=",F6.1,X2,
"CUM. FREQUENCY=",F7.4>,CV,FREQ[I,CV],CUM);

% NORMALISE TO COMPARE WITH GAUSSIAN DISTRIBUTION
FREQ[I,CV]:=*/(SI*(N-512));
END;
WRITE (FOO[SPACE 2]);
% CALCULATE PROBABILITIES
FOR CV:=1 STEP 1 UNTIL NCL DO
WRITE (FOO,<"BIN",I2,X3,"DISTANCE FROM MEAN IN STD.DEVS.",F7.4,X3,
"PROB. DENSITY",F7.4,X3,"NORM. PROB. DENSITY",F7.4>,

CV,(MDPT[I,CV]-UMEAN[I])/RMS[I],FREQ[I,CV],FREQ[I,CV]*RMS[I]);
L3:
WRITE (FOO[SPACE 4]);
END;
END;
END;

END.
```

APPENDIX II

SYNOPTIC WEATHER CONDITIONS OVER THE SOUTH ISLAND OF NEW ZEALAND RECORDED BY THE N.Z. METEOROLOGICAL SERVICE ON THE DAYS OF THE FIELD TESTS

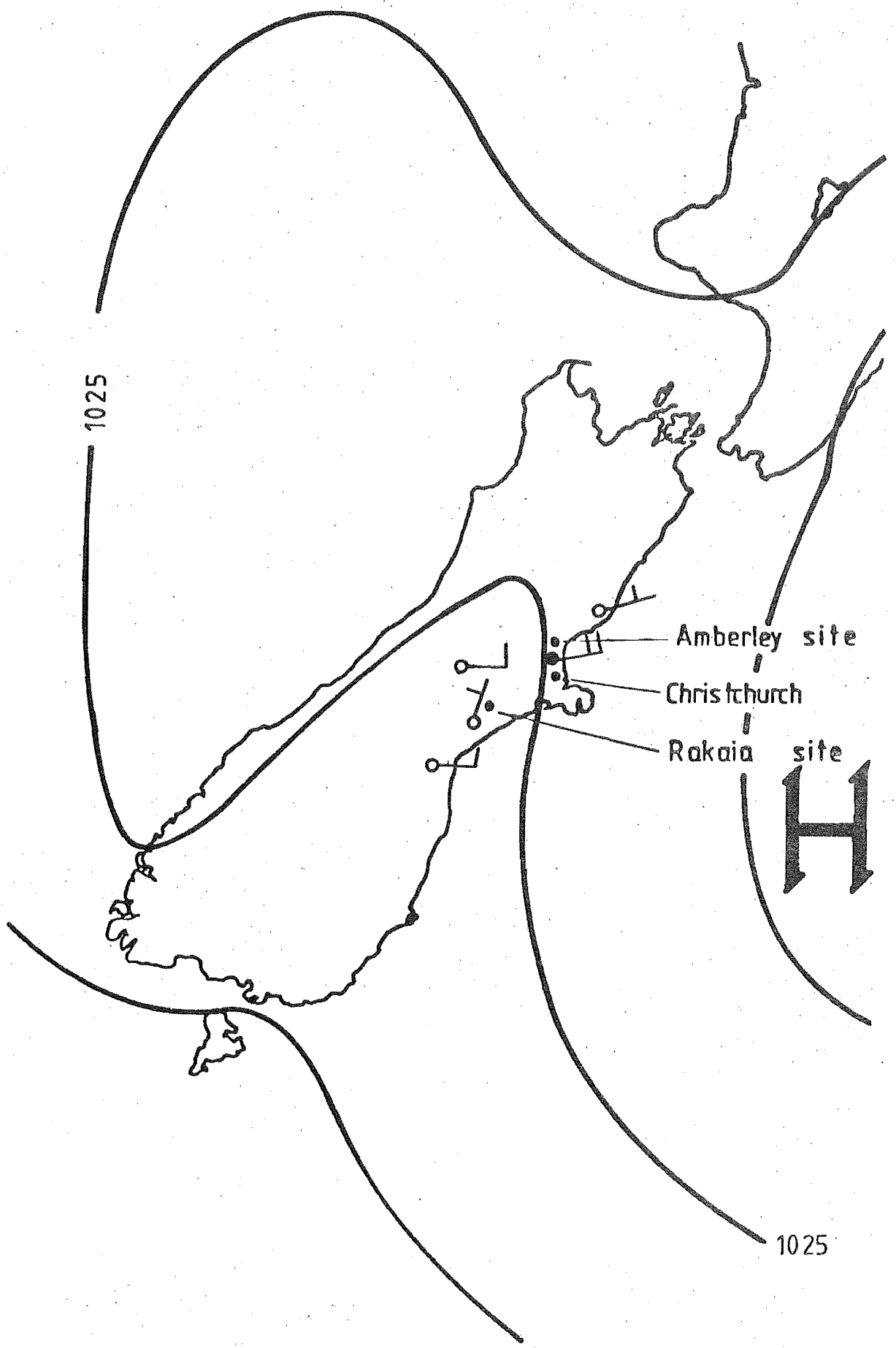

FIG1 AMBERLEY FIELD RECORDING #1, 1200 HRS 31/1/78

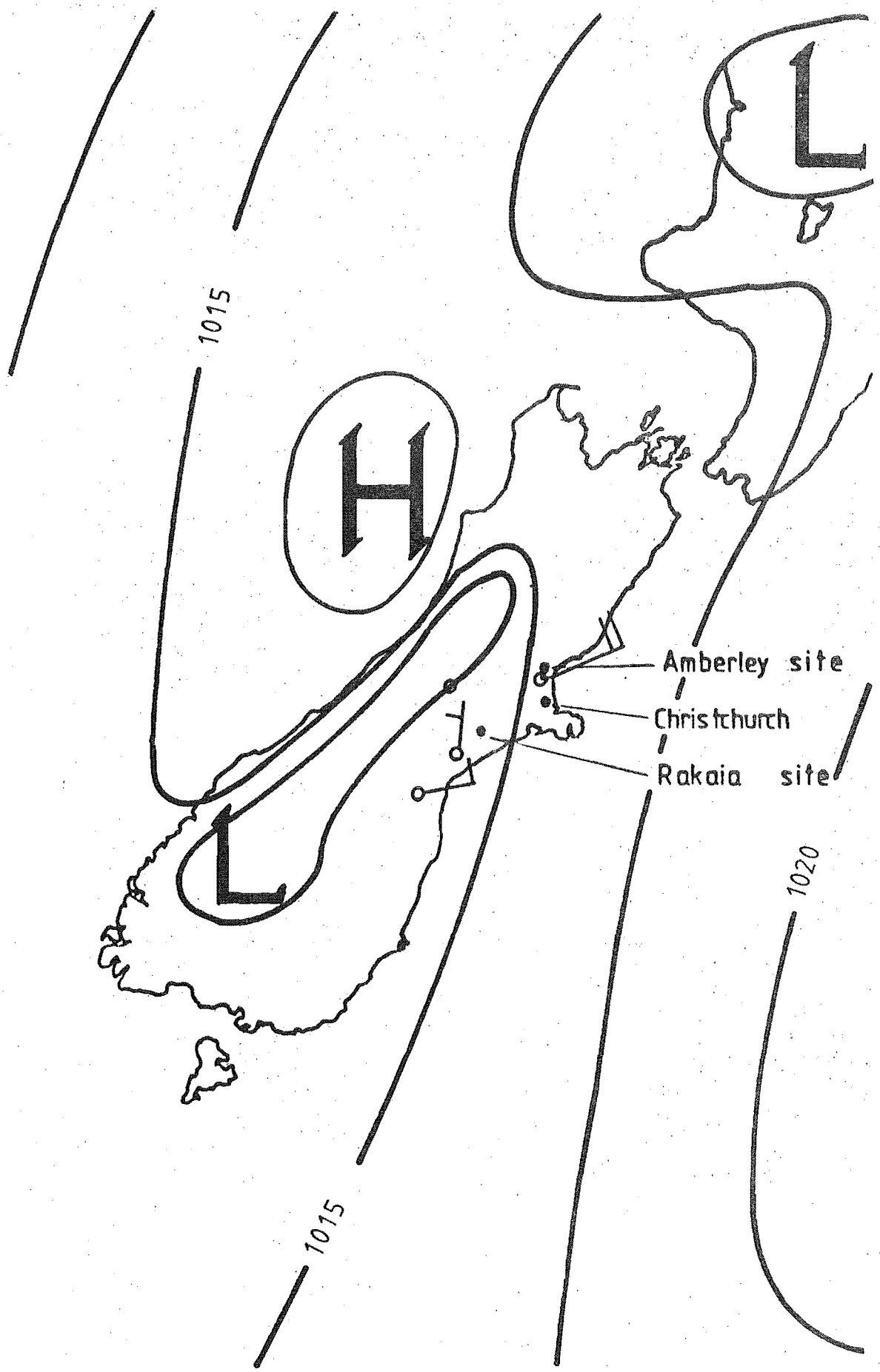

FIG 2 AMBERLEY FIELD RECORDING #23, 1500 HRS 8/2/78

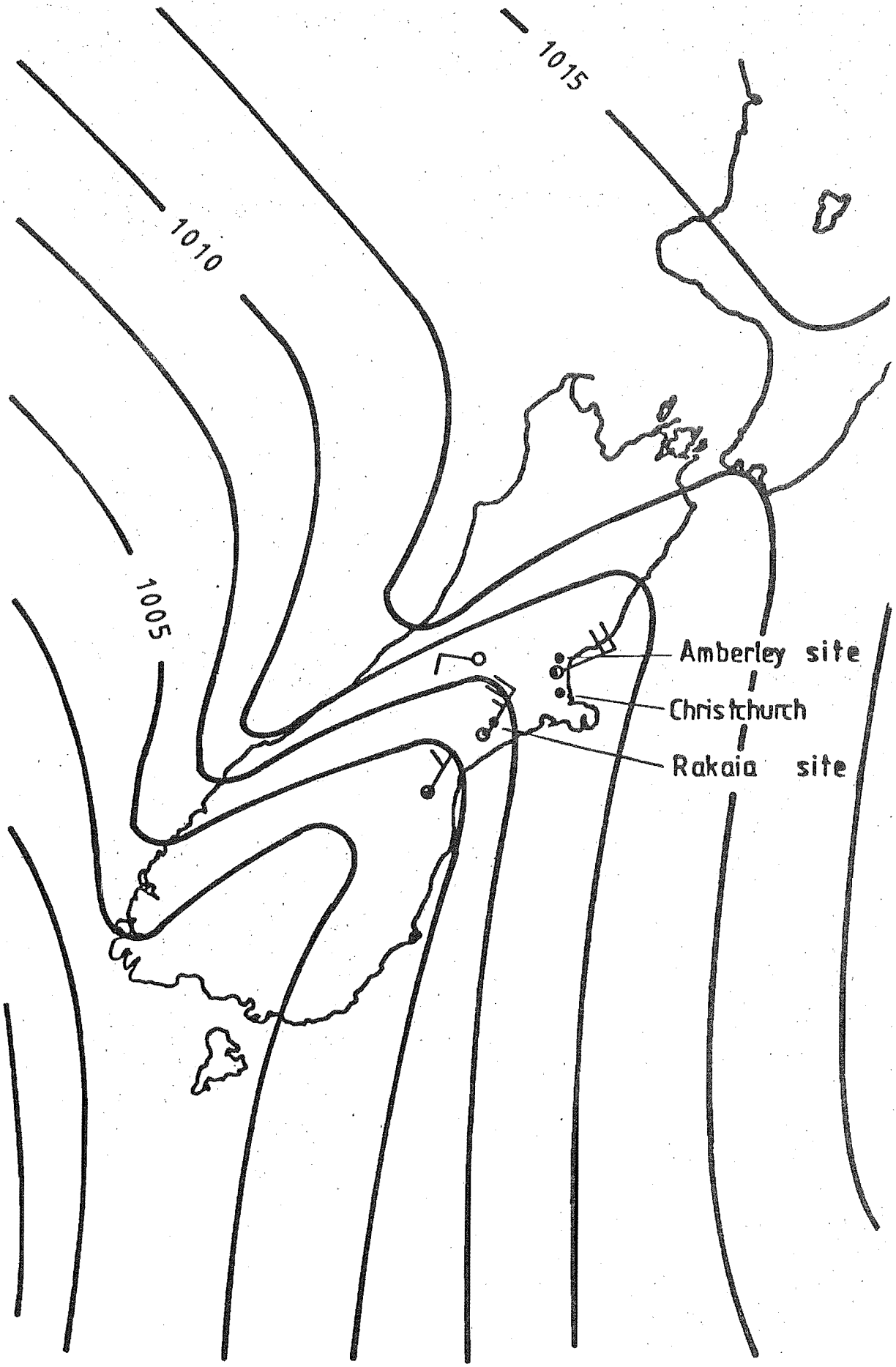

FIG 3 AMBERLEY FIELD RECORDING #4, 1200 HRS 12/2/78

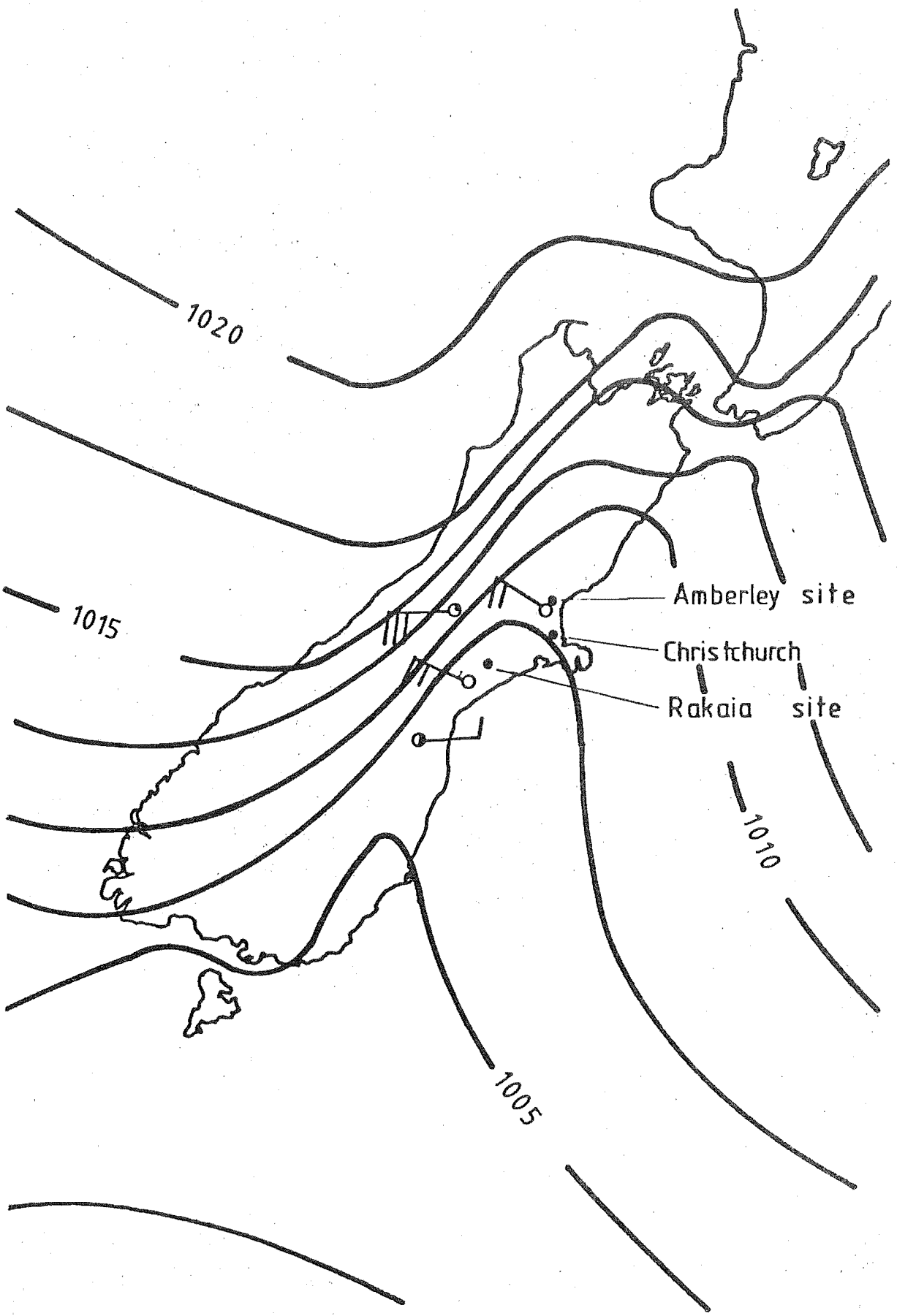

FIG 4 RAKAIA FIELD RECORDING #1, 1200 HRS 22/2/78

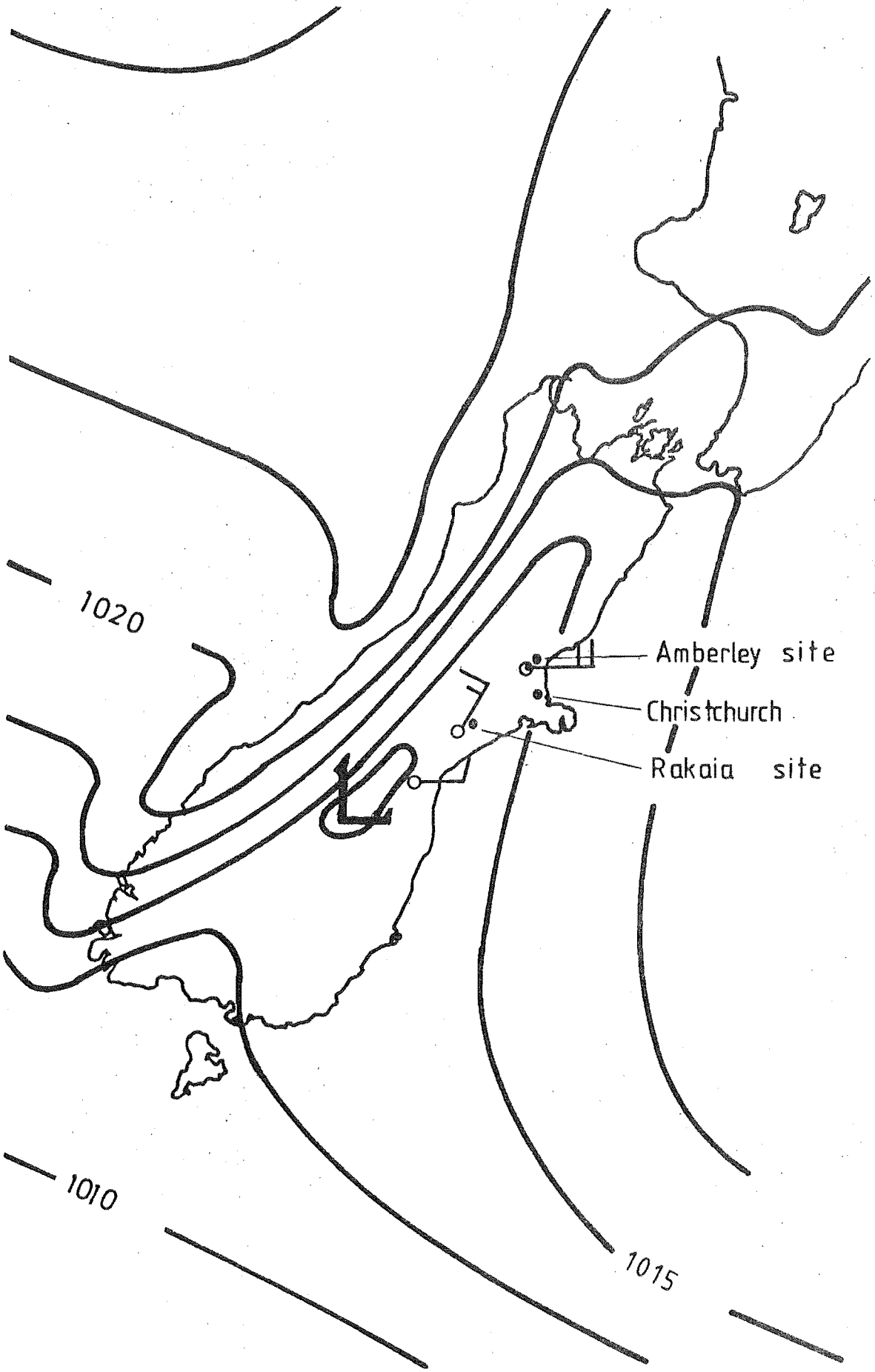

FIG 5 RAKAIA FIELD RECORDING #2, 1500 HRS 8/3/78

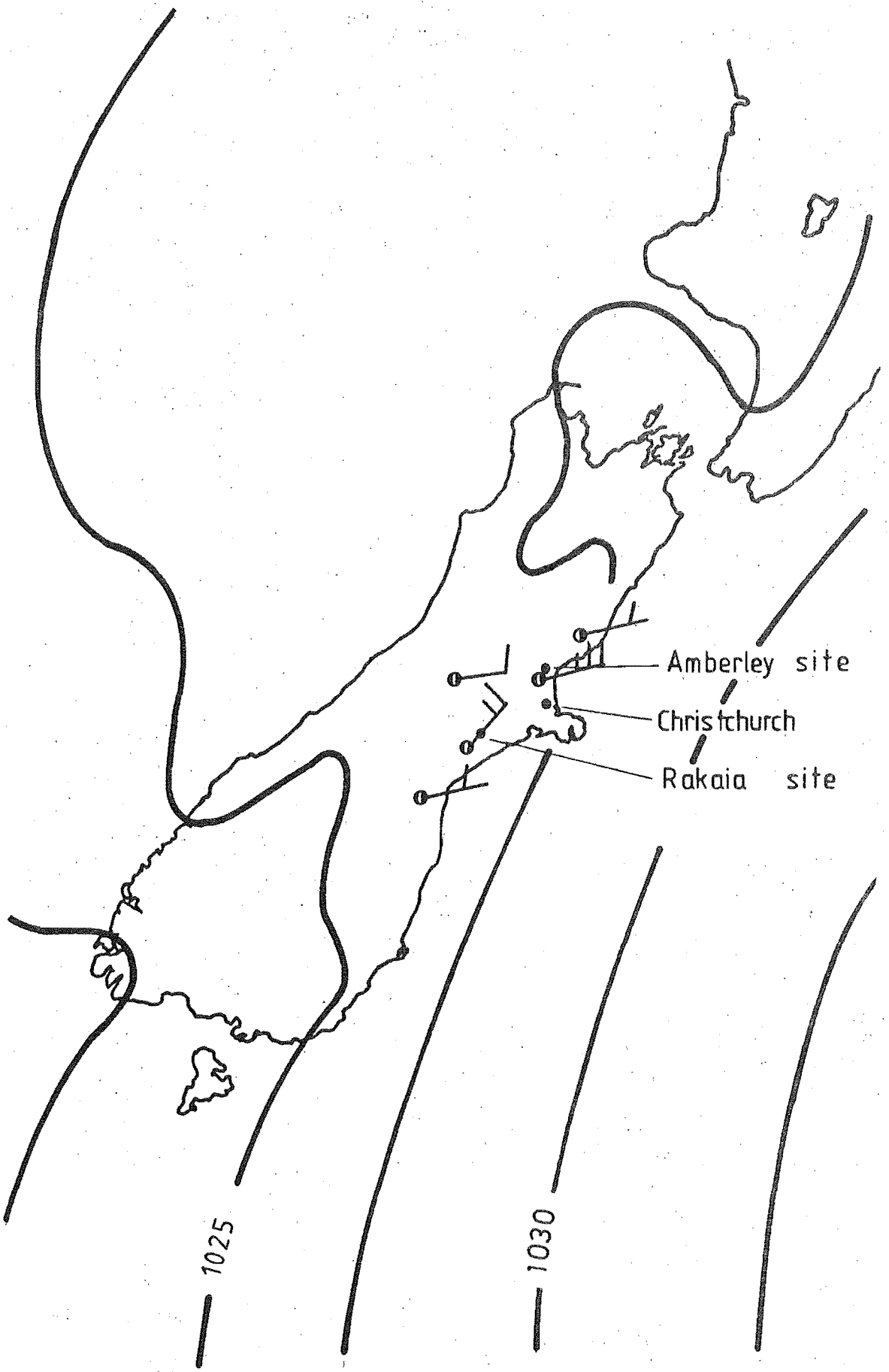

FIG 6 RAKAIA FIELD RECORDING #3, 1500 HRS 30/3/78

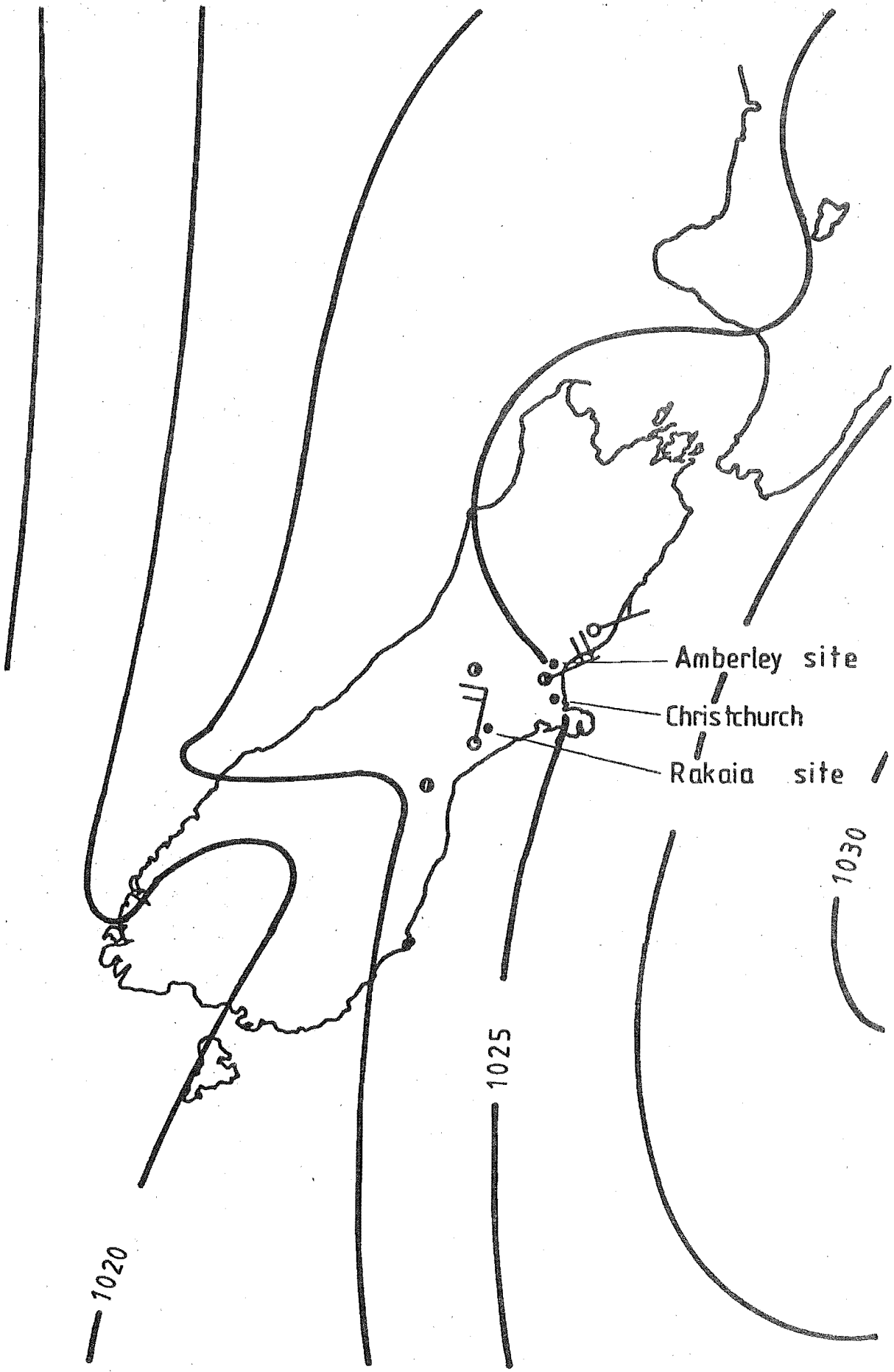

FIG 7 RAKAIA FIELD RECORDING #4, 1200 HRS 4/4/78

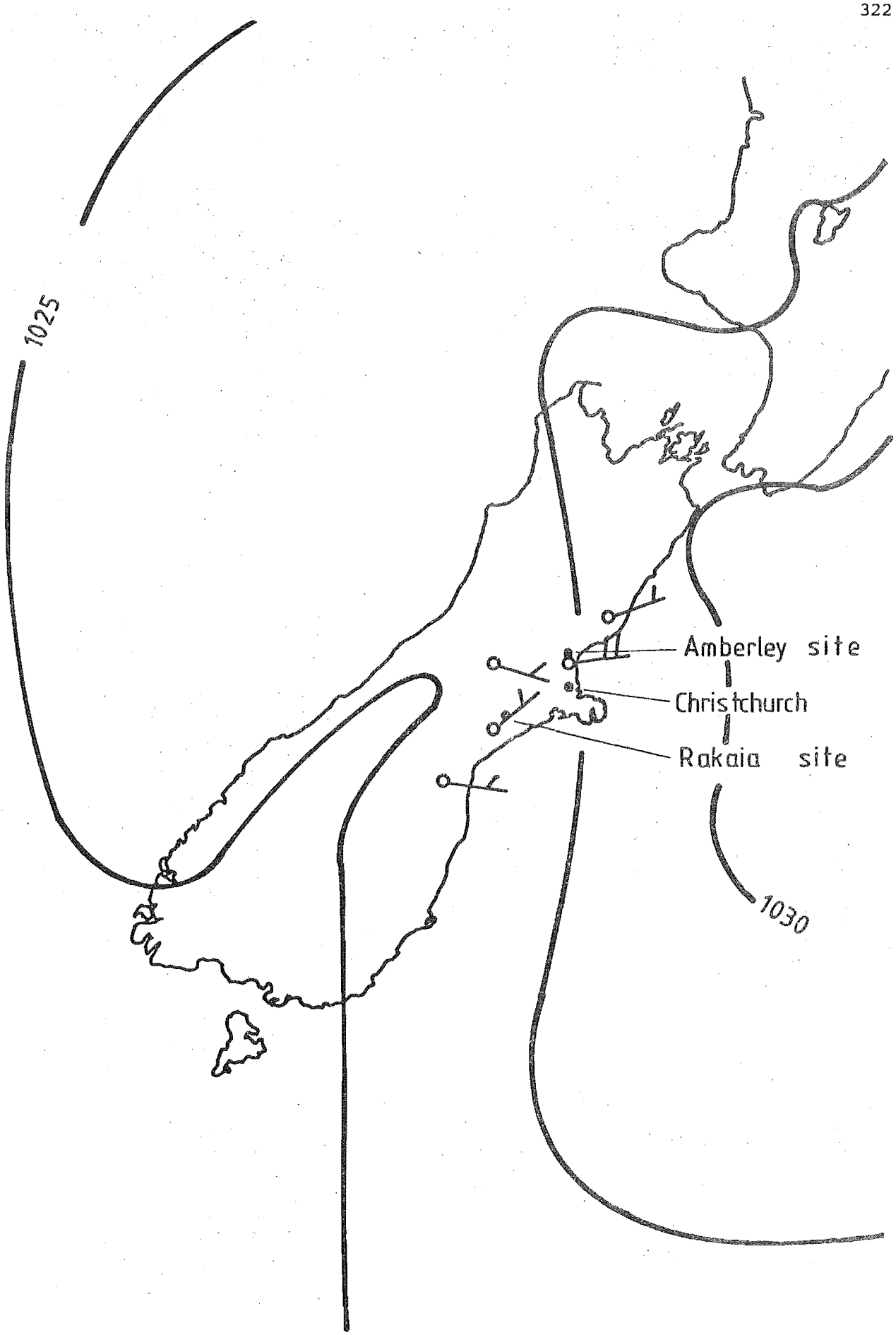

FIG 8 RAKAIA FIELD RECORDING #5, 1500 HRS 11/4/78